frontiers | Research Topics

Bioprocess designing towards clean energy production from industrial wastewater

Edited by
Mohd Nasrullah, Santhana Krishnan, Prabhu Saravanan and Mohd Fadhil Md Din

Published in
Frontiers in Chemical Engineering

ISSN 1664-8714
ISBN 978-2-8325-4560-7
DOI 10.3389/978-2-8325-4560-7

About Frontiers

Frontiers is more than just an open access publisher of scholarly articles: it is a pioneering approach to the world of academia, radically improving the way scholarly research is managed. The grand vision of Frontiers is a world where all people have an equal opportunity to seek, share and generate knowledge. Frontiers provides immediate and permanent online open access to all its publications, but this alone is not enough to realize our grand goals.

Frontiers journal series

The Frontiers journal series is a multi-tier and interdisciplinary set of open-access, online journals, promising a paradigm shift from the current review, selection and dissemination processes in academic publishing. All Frontiers journals are driven by researchers for researchers; therefore, they constitute a service to the scholarly community. At the same time, the *Frontiers journal series* operates on a revolutionary invention, the tiered publishing system, initially addressing specific communities of scholars, and gradually climbing up to broader public understanding, thus serving the interests of the lay society, too.

Dedication to quality

Each Frontiers article is a landmark of the highest quality, thanks to genuinely collaborative interactions between authors and review editors, who include some of the world's best academicians. Research must be certified by peers before entering a stream of knowledge that may eventually reach the public - and shape society; therefore, Frontiers only applies the most rigorous and unbiased reviews. Frontiers revolutionizes research publishing by freely delivering the most outstanding research, evaluated with no bias from both the academic and social point of view. By applying the most advanced information technologies, Frontiers is catapulting scholarly publishing into a new generation.

What are Frontiers Research Topics?

Frontiers Research Topics are very popular trademarks of the *Frontiers journals series*: they are collections of at least ten articles, all centered on a particular subject. With their unique mix of varied contributions from Original Research to Review Articles, Frontiers Research Topics unify the most influential researchers, the latest key findings and historical advances in a hot research area.

Find out more on how to host your own Frontiers Research Topic or contribute to one as an author by contacting the Frontiers editorial office: frontiersin.org/about/contact

Bioprocess designing towards clean energy production from industrial wastewater

Topic editors

Mohd Nasrullah — Universiti Malaysia Pahang, Malaysia
Santhana Krishnan — Prince of Songkla University, Thailand
Prabhu Saravanan — University of Concepcion, Chile
Mohd Fadhil Md Din — University of Technology Malaysia, Malaysia

Citation

Nasrullah, M., Krishnan, S., Saravanan, P., Din, M. F. M., eds. (2024). *Bioprocess designing towards clean energy production from industrial wastewater*. Lausanne: Frontiers Media SA. doi: 10.3389/978-2-8325-4560-7

Table of contents

frontiers | Frontiers in Chemical Engineering

TYPE Editorial
PUBLISHED 15 May 2024
DOI 10.3389/fceng.2024.1412081

OPEN ACCESS

EDITED AND REVIEWED BY
J. Paul Chen,
National University of Singapore, Singapore

*CORRESPONDENCE
Santhana Krishnan,
santhana.k@psu.ac.th

RECEIVED 04 April 2024
ACCEPTED 23 April 2024
PUBLISHED 15 May 2024

CITATION
Krishnan S, Nasrullah M, Saravanan P and Bin Md Din MF (2024), Editorial: Bioprocess designing towards clean energy production from industrial wastewater.
Front. Chem. Eng. 6:1412081.
doi: 10.3389/fceng.2024.1412081

Editorial: Bioprocess designing towards clean energy production from industrial wastewater

Santhana Krishnan[1]*, Mohd Nasrullah[2], Prabhu Saravanan[3] and Mohd Fadhil Bin Md Din[4]

[1]Department of Civil and Environmental Engineering, Faculty of Engineering, Prince of Songkla University, Songkhla, Thailand, [2]Faculty of Civil Engineering Technology, Universiti Malaysia Pahang, Kuantan, Pahang, Malaysia, [3]Department of Physical-Chemistry, Faculty of Chemical Sciences, University of Concepcion, Concepción, Chile, [4]Department of Water and Environmental Engineering, University of Technology Malaysia, Johor Bahru, Malaysia

KEYWORDS

bioenergy, biofuels, GHG reduction, bio-electrochemical systems, bioreactors, wastewater treatment

Editorial on the Research Topic
Bioprocess designing towards clean energy production from industrial wastewater

Highlights

This Research Topic received 12 submissions.
The best submissions were published after undergoing peer review assessment.
This Research Topic has enhanced understanding of fundamental scientific concepts addressed.

1 Introduction

The finite nature of fossil fuel-based energy sources, the significant rise in waste generation, and the growing requirement for alternative energy and chemicals have led to the necessity of a waste-derived bioeconomy. Due to the difficult decarbonization objectives, there has been a worldwide focus on the use of bioengineering and bioprocess technology in the past few decades. These technologies aim to replace fossil fuel-based technologies and promote clean energy, waste management towards environmental sustainability. Bioprocesses have significant implications in integrating environmental management methods, including biomass valorization, wastewater treatment, solid waste management, potential nutrient recovery and renewable energy production as depicted in Figure 1. In view of that, the current Research Topic, titled "*Bioprocess designing towards clean energy production from industrial wastewater*," aims to gather recent scientific advancements in the field of environmental bioprocess and sustainable alternative energy. The current Research Topic (RT) addresses areas such as emerging energy and environmental technologies, biorefinery, biomass valorization, microbial bioprocess design,

FIGURE 1
Sustainable environmental applications of bioprocess design.

bioconversions, biofuels, wastewater treatment, resource recovery, and energy storage. The manuscripts are chosen in the RT to cover an extensive choice of emerging themes in Bioprocess Engineering. The Editors believe that the outcome comprises a collection of highly intriguing papers that enhance understanding of the subject matter, and would be valuable for researchers and society as a whole.

2 Details of published articles on the Research Topic

Study 1: Due to the rising need for alternative fuels, microalgae have emerged as a feasible source that can provide high lipid content and a variety of other important chemicals. Therefore, Kumar et al. studied algae-based biodiesel production with an emphasis on its unit operations (both upstream and downstream) starting from strain selection, cultivation system, reactor operations, harvesting, and extraction of oil to biodiesel production. The strategies to enhance lipid accumulation by incorporating genetic, and metabolic engineering and harnessing bio-products nanoparticles, biofertilizers, biochar, and biopharmaceuticals have been addressed in detail.

Study 2: Microalgae is highly adaptable to the environment and has a high tolerance to various environmental stresses, however, their growth, Co_2 sequestration ability, and lipid accumulation are mainly influenced by the same stresses. To determine the physiological responses, Euglena gracilis was studied against environmental stresses (antibiotics, heavy metals, salinity), carbon resources (glucose and ethanol), potential for higher quality, yield of fatty acid with a high growth rate, and biodiesel properties were evaluated. Further, transcriptome analysis was used to investigate the regulation and production of fatty acids in various conditions to enhance biodiesel production. Treating TFA with glucose is very efficient and can be a good topic for detailed study in biodiesel synthesis. Transcriptome analyses indicate that optimal biodiesel production in E. gracilis can be attained through precise cultivation conditions that balance growth and photosynthesis (He et al., 2022).

Study 3: In recent days, herbicides such as glyphosates and chloroacetanilide classes have been extensively used in agricultural activities in the Indian nation to save crops from a variety of insects but their potential toxicity toward the non-target organisms, was equally reported to aquatic ecosystems. In this context, Mohanty and Jena (2022) investigated the biodegradation of the herbicide Butachlor belonging to the chloroacetanilide class using a synthetic microbial consortium, SMC1 embedded on ceramic raschig rings within a packed-bed bioreactor (PBBR). The authors used response surface methods to optimize the reactor's operational conditions. For the controlled biofilm-mediated reactions, they reported an optimal loading range (270–325 mg/l/d), COD removal (90%), flow rate (2.9 mL/min), herbicide concentration (454.63 mg/mL), nitrogen load (1,041 mg/L), for the maximal biodegradation of herbicides.

Study 4: Bioelectrochemical Systems (BES) are suggested as a substitute for traditional wastewater treatment, serving as either a main bioremediation method or for secondary wastewater treatment systems. Microbial fuel cells (MFCs) in bioelectrochemical systems (BES) utilize the metabolic ability of anodophilic (anode aspiring) bacteria to break down the organic material found in wastewater and simultaneous electricity production. In this perspective, Agudelo-Escobar et al. (2022) analyzed the capacity of indigenous microbial communities to break down organic substances in coffee industrial effluent and assessed its ability to generate electricity through an

MFC. MFC with 200 mL anodic chamber was operated in a fed-batch, open and closed-circuit conditions, for 60 days to bioremediate the coffee effluent and by measuring the physicochemical parameters, native microbial community characterization, and electrogenic potential of anodophilles. The proposed system was able to reduce 70% of the organic matter and 400 mV of open circuit voltages were recorded.

Study 5: Similarly, Babanova et al. (2022) reported a bioelectrochemical treatment technology (BETT) prototype system at a major brewery in Los Angeles, CA, United States. The system processes 0.6 m^3 per day of raw brewery effluent containing a significant amount of fruit pulp. Greenhouse gas emissions linked to power consumption, biomass production, and carbon dioxide release were calculated and contrasted with aerobic and anaerobic alternatives. BETT demonstrated a 33% reduction in total COD at 4 h s hydraulic retention time (HRT) and overall Co_2 emission reduction was estimated to be 85%–90% compared to aerobic and anaerobic alternatives.

Study 6: It is crucial to promptly develop and select appropriate cathode materials for the actual implementation of Microbial Fuel Cells (MFCs) in the current scenario. Therefore, Elangovan et al. (2023) reviewed the significant breakthroughs in oxygen reduction reaction (ORR) electrocatalysts including precious metals-based catalysts, non-precious metals-based catalysts, non-metals and carbon-based catalysts, and biocatalysts. Notable results for their application in microbial fuel cells (MFC), challenges, and prospects are critically discussed.

Study 7: Wastewater treatment technology based on the circular economy offers the most sustainable solutions for water pollution in developing nations. A new decentralized controller called Multi-Objective Decentralized Controller (MODC) is proposed for evaluating a Multi-Input Multi-Output (MIMO) activated sludge wastewater treatment plant (WWTP) to attain the highest effluent quality at the lowest cost (Subbian et al., 2023). A MIMO model was created for the activated sludge process (ASP). Relative gain array (RGA) analysis was conducted to assess loop interactions for selecting an appropriate control system. A MODC problem was defined to address the conflicting objectives of enhancing effluent quality and reducing operational costs through energy-efficient practices. Non-Dominated Sorting Genetic Algorithm II (NSGA-II) yielded several optimal solutions on the Pareto front. Enhancing effluent quality boosts active sludge generation, leading to increased methane output in the anaerobic digester.

Study 8: Lignin is regarded as a top substitute in future energy, fuel, and chemical industries. Exploring lignin's technical and economic potentials can unlock sustainable biorefineries and lead to a sustainable economy. In this context, Jassal et al. (2022) analyzed the potential of lignin as a developing substitute for petroleum and the current challenges in the commercialization process. The mini-review highlighted the need, potential, and emergence of lignin biopolymers, their extraction methods, and cost-reduction strategies were overviewed.

Study 9: Highly promising decarbonized fuels include hydrogen (H_2) with no pollutants released during direct combustion or fuel cell oxidation. Industrial production of H_2 relies on energy-intensive hydrocarbon reformation, which detracts from its environmental advantages and limits its use as a fuel. Hydrogen sulfide (H_2S) is an alternate source of H_2 that is often ignored. In this dimension, Velazquez-Rizo and Cavazos Sepulveda (2023) discussed the progress in the direct electrochemical separation of H_2S below the sulfur dew point, with a focus on the growing significance of sulfur poisoning. The review article explored several technologies, underlying mechanisms, and approaches employed to improve the energy efficiency and stability of H_2S electrolytic systems, including nanostructured electrodes and novel sulfur solvents utilized as electrolytes.

Study 10: Membrane distillation crystallization is an innovative technology that aims to recover water and minerals at the same time to address the difficulties encountered by the desalination sector. MDC continues to encounter obstacles in utilizing its industrial applications because of membrane fouling, scaling, and wettability issues. Hence, the study by Chimanlal et al. (2022) examined the occurrence of membrane fouling and wetness in MDC. Furthermore, parameter optimization, fouling control methods, and current advancements made to tackle these difficulties are thoroughly evaluated. Finally, the potential for the sustainability of this technology is emphasized.

Study 11: It is important to reassess energy security considerations and priorities in the context of climate change through the development of an economic model. In this analytical framework, Shayegh (2023) investigated how energy security policy and climate stability are influenced by imported natural gas, regional coal output, and potential direct air capture (DAC) deployment in the European Union (EU) under two intersections: full integration and full competitiveness among EU member states. The interesting findings indicated that full cooperation of the EU leads to increased dependence on imported energy but also creates a strong motivation for DAC adoption. Competition, however, could lead to increased dependence on domestic coal production and exacerbate climate change issues, even with the presence of DAC.

3 Perspectives for future

Study 1: Deployment of mass cultivation strategies, high-yielding algal strains, sustainable downstream processing, and commercial viability are some of the key areas to be focused on.

Study 2: It is recommended to utilize experimental validations such as gene knockdown or overexpression studies to confirm the functions of individual genes found through transcriptome analysis.

Study 3: Packed-bed bioreactor removal efficiency was mainly influenced by the retention period, initial loading rates, and substrate concentration. Integration of artificial intelligence (AI) mediated bioprocess optimization can enhance further yield and overall removal efficacy.

Study 4: Although microbial fuel cells (MFCs) hold potential, their application in large-scale wastewater treatment is hindered by the cost of electrode materials and other sustainable challenges. Current research must be aimed to overcome these obstacles to enhance the technology's efficiency and economic feasibility.

Study 5: It is recommended to conduct more large-scale pilot plants to validate the potential of coupling BES with carbon capture and utilization technologies beyond wastewater treatment.

Study 6: Improvements in the stability and effectiveness of the ORR electrocatalysts are essential for the practical application of

MFCs. Further experimental and theoretical study is needed to apply the successful performance of air-cathode MFCs in laboratory settings to practical applications.

Study 7: Before implementing, identify decision variables, establish communication protocols, and undertake thorough simulations to confirm the MODC's performance in several scenarios.

Study 8: Lignin extraction and purification are too intricate and expensive for large-scale application. Problem-solving requires accelerating technologies and cooperating across catalysis, chemical engineering, and analytics.

Study 9: Exploring sustainable and novel catalyst regeneration methods, such as subjecting the electrocatalysts to chemical or thermal treatment to revive their catalytic sites.

Study 10: Manufacturing membranes with eco-friendly reagents, refining membrane cleaning methods, and doing pilot-scale research to assess MDC applicability.

Study 11: Future studies could enhance this analysis by including additional stakeholders, exploring different energy alternatives, and utilizing more advanced climate change models.

4 Conclusion

The Guest Editors would like to extend their heartfelt gratitude to the Editor-in-Chief of Frontiers in Chemical Engineering, the Managing Editor, the Journal Managers, the Associate Publishing Content Specialist, and the entire team for their invaluable guidance and assistance, which greatly contributed to the success of this RT. The Guest Editors express their gratitude to all the authors for submitting their exceptional works and to the reviewers for their important remarks and suggestions. Devoid of these contributions, the complete completion of this RT would not have been possible. The articles in this RT are top-notch contributions that enrich scholarly understanding of the discussed Research Topic. The Editors of the current RT *Bioprocess designing towards clean energy production from industrial wastewater* aim to stimulate more research on the problem and facilitate the dissemination of new discoveries.

Author contributions

SK: Writing–review and editing, Writing–original draft, Visualization, Supervision, Project administration, Investigation, Formal Analysis, Data curation, Conceptualization. MN: Resources, Writing–review and editing, Validation, Formal Analysis. PS: Writing–review and editing, Validation, Formal Analysis. MB: Writing–review and editing, Validation, Formal Analysis.

Funding

The author(s) declare that no financial support was received for the research, authorship, and/or publication of this article.

Acknowledgments

This study was supported by the Postdoctoral Fellowship from Prince of Songkla University, Thailand.

Conflict of interest

The authors declare that the research was conducted in the absence of any commercial or financial relationships that could be construed as a potential conflict of interest.

Publisher's note

frontiers in Chemical Engineering

ORIGINAL RESEARCH
published: 28 February 2022
doi: 10.3389/fceng.2022.814987

A Bioelectrochemical System for Waste Degradation and Energy Recovery From Industrial Coffee Wastewater

Lina María Agudelo-Escobar[1]*, *Santiago Erazo Cabrera*[1] and *Claudio Avignone Rossa*[2]

[1]Biotransformation Research Group, School of Microbiology, University of Antioquia, Medellín, Colombia, [2]Department of Microbial Sciences, School of Biosciences and Medicine, University of Surrey, Guilford, United Kingdom

The primary production of coffee involves the extensive use of water resources, since it is not only used for irrigation of coffee plantations, but it is also required in large volumes for the processing of the coffee berry to obtain high quality green beans. It is calculated that for every kg of dry coffee grain produced, up to 40 L of water are consumed, and its disposal represents a significant environmental problem, since most coffee growers are small producers with no access to efficient technologies for wastewater treatment. This situation leads to these liquid wastes to be discarded untreated in natural water sources, generating environmental pollution and public health problems. Bioelectrochemical Systems (BES) have been proposed as an alternative to conventional wastewater treatments, either as a primary bioremediation strategy or for secondary wastewater treatment systems. Among BES, microbial fuel cells (MFCs) are designed to exploit the metabolic capability of andophilic microorganisms to degrade the organic matter present in the waste. Anodophilic microorganisms use electrodes as terminal electron acceptors, generating a flow of electrons that can be used in the generation of electricity. In this work, we evaluated the ability of native microbial communities to degrade the organic matter present in wastewater from the coffee agroindustry and its electrogenic potential for the co-generation of electricity was evaluated using an MFC device developed by the authors. Wastewater samples obtained at different stages of the coffee wet process were used as inoculum and feedstocks. The system was operated in fed-batch, in both open and closed-circuit conditions, for 60 days. The degree of decontamination or bioremediation of the wastewater was assessed by measurements of physicochemical parameters. For the characterization of the native microbial community, microscopic and molecular techniques were used and the electrogenic potential was established by assessing the electrochemical performance of the system. With the proposed bioelectrochemical system, a reduction of up to 70% of the initial content of organic matter of the residual water from the coffee benefit was achieved, and open circuit voltages of up to 400 mV were recorded, comparable to those reported for conventional air breathing cathode MFC.

Keywords: coffee wastewater, water treatment, microbial fuel cell (MFC), bioelectrochemical systems (BES), native microbial community, green energy, agro-industrial waste

OPEN ACCESS

Edited by:
Albert Guisasola, Universitat Autonoma de Barcelona, Spain

Reviewed by:
Marika Kokko, Tampere University, Finland
Elizabeth Susan Heidrich, Newcastle University, United Kingdom

***Correspondence:**
Lina María Agudelo-Escobar
lina.agudelo@udea.edu.co

Specialty section:
This article was submitted to Environmental Chemical Engineering, a section of the journal Frontiers in Chemical Engineering

Received: *14 November 2021*
Accepted: *21 January 2022*
Published: *28 February 2022*

Citation:
Agudelo-Escobar LM, Cabrera SE and Avignone Rossa C (2022) A Bioelectrochemical System for Waste Degradation and Energy Recovery From Industrial Coffee Wastewater. Front. Chem. Eng. 4:814987. doi: 10.3389/fceng.2022.814987

1 INTRODUCTION

By the year 2020, the global coffee market was USD 102.02 billion and an annual growth of 4.28% is estimated for the period between 2021–2026. Europe, North America and Asia are recognized as the main importing and consuming markets for coffee (Voora et al., 2020). Brazil ranks as the world's leading producer, with an estimated production of 56.4 million 60-kg sacks of green coffee, followed by Vietnam, Colombia, and Indonesia, countries that present ideal climate and environmental conditions for cultivation of this crop. In most coffee-producing countries, the primary production of "washed soft coffees" involves the use of the traditional wet processing method, resulting in large amounts of wastewater with high organic-content. This causes a severe negative environmental impact in the ecosystem of coffee farming areas, due to the large amount of lixiviates, drainage of pulp, and mucilage disposed onto the environment without treatment (Dankowska et al., 2017; Campos et al., 2021). These coffee wastes have a deleterious effect on the hydrographic basins around the coffee farms, resulting in severe contamination of soil and aquatic ecosystems as well as causing an increase in the transmission of waterborne illnesses (Didanna, 2014; Rodriguez et al., 2015).

The potential implementation of bioelectrochemical systems (BES) to reduce wastewater contamination and generate electricity represents an invaluable opportunity for small coffee farmers. BES technology is suitable in this case due to the high organic content in coffee waste and the possibility of bio-prospection of coffee-associated microbial communities. Chemical Oxygen Demand (COD) values between 13.0 and 29.5 g/L in coffee wastewater have been reported (Said et al., 2020; Campos et al., 2021), indicative of the need for efficient treatment processes. Leveraging and adding value to the coffee agroindustrial waste has a high impact from the environmental, social, and economic points of view. Reducing the polluting load of the residues by treatment in microbial fuel cells would generate environmental benefits in the coffee farming areas, lowering the high COD levels in the water systems and soils around the coffee production sites. The goal of this research was the evaluation of the bioelectrochemical performance of a native microbial community for the degradation of wastewater from the coffee agroindustry and the production of bioelectricity in a microbial fuel cell (MFC) prototype developed by the authors (unpublished data). We analyzed the characteristics and properties of the native communities in terms of their capacity to degrade the residues, and evaluated the degree of degradation achieved and the bioelectricity generated during the operation of the MFC using the native microbial community. This research is aligned with the existing global challenges of sustainable development. It includes aspects related to clean water and sanitation, affordable and clean energy, responsible consumption and production, life below water, life, and land and climate action.

2 MATERIALS AND METHODS

2.1 Microorganisms and Medium

Wastewater samples and native microbial communities from an agroindustrial coffee environment were obtained at one of the Coffee Processing Centers located in Andes, in the southwestern region of the Department of Antioquia, Colombia. Andes is located at 75°52′43.57″ W; 5°29′31.96″ N, at an atlitude of 1,360 m above sea level. The climate in Andes is classified as Tropical rainforest (Köppen climate classification Af), with high mean annual temperatures, small temperature ranges, very humid and wet, with rains throughout the year.

The scheme in **Figure 1** depicts the various stages involved in wet coffee processing. In this process, coffee cherries are subjected to an initial washing process to remove particulate matter and dirt (Stage 1). In Stage 2, they are subjected to the pulping process, in which the cherry seed (the bean) is released from the husk and pulp. The husk and pulp free bean is subjected to a fermentation process (Stage 3) to remove the mucilage layer. After this phase, the mucilage-free coffee bean is undergoes a drying step to obtain the dry bean (green coffee), the final product of the process. Solid pulp and husk waste are stored under cover for later use in other composting applications or for disposal. During this storage period, leachates are generated that are accumulated in a tank (Stage 4). Finally, the wastewater generated in each stage is collected and taken to the wastewater treatment plant. The points along the wet processing coffee method selected for collection of wastewater samples were: 1 Coffee cherry washing water; 2 Pulping water; 3 Fermentation tank water; 4 Leachate tank water; 5 Mixed water inlet to the water treatment plant. The samples were processed and stored under two different conditions. Water samples used as inocula of the microbial fuel cells were cryopreserved at −80°C. Water samples used as feedstock were stored either at 4°C or frozen at −20°C until use.

2.2 Bioelectrochemical System

2.2.1 Microbial Fuel Cells configuration

An air-breathing cathode MFC made of ABS polymeric material resistant to basic and acid chemical agents, with a 200 ml anodic chamber capacity was used in all the experiments. The cation exchange membrane used was a 5 mm thick earthenware plate (width: 40 mm; length: 70 mm). The anode was made of a carbon felt piece measuring 6.5 cm by 13.5 cm (projected anode area: 87.75 cm^2). Titanium wire was used as electron collector with a length of 45.0 cm for the anode and 25.0 cm for the cathode. The assembled MFC was characterised before the start-up of the experiments, by ensuring and establishing suitable anaerobic conditions, operating volume, substrate supply, sampling procedure, and adequacy of sensors for monitoring and recording physicochemical and electrochemical properties. **Figure 2** shows images of the MFC at diverse stages of the construction and operation.

2.2.2 Microbial Fuel Cells operation

The MFC was operated using as anodic feedstock the wastewater taken from different sampling points of the coffee processing plant. For the experimental setup MFC1, 170 ml of a 1:1 mixture of wastewater from leachate (sampling point 4) and fermentation (sampling point 3) were used. After open circuit operation for 58 days, the spent medium in the anode chamber was replaced with fresh wastewater mixture medium. The external circuit was

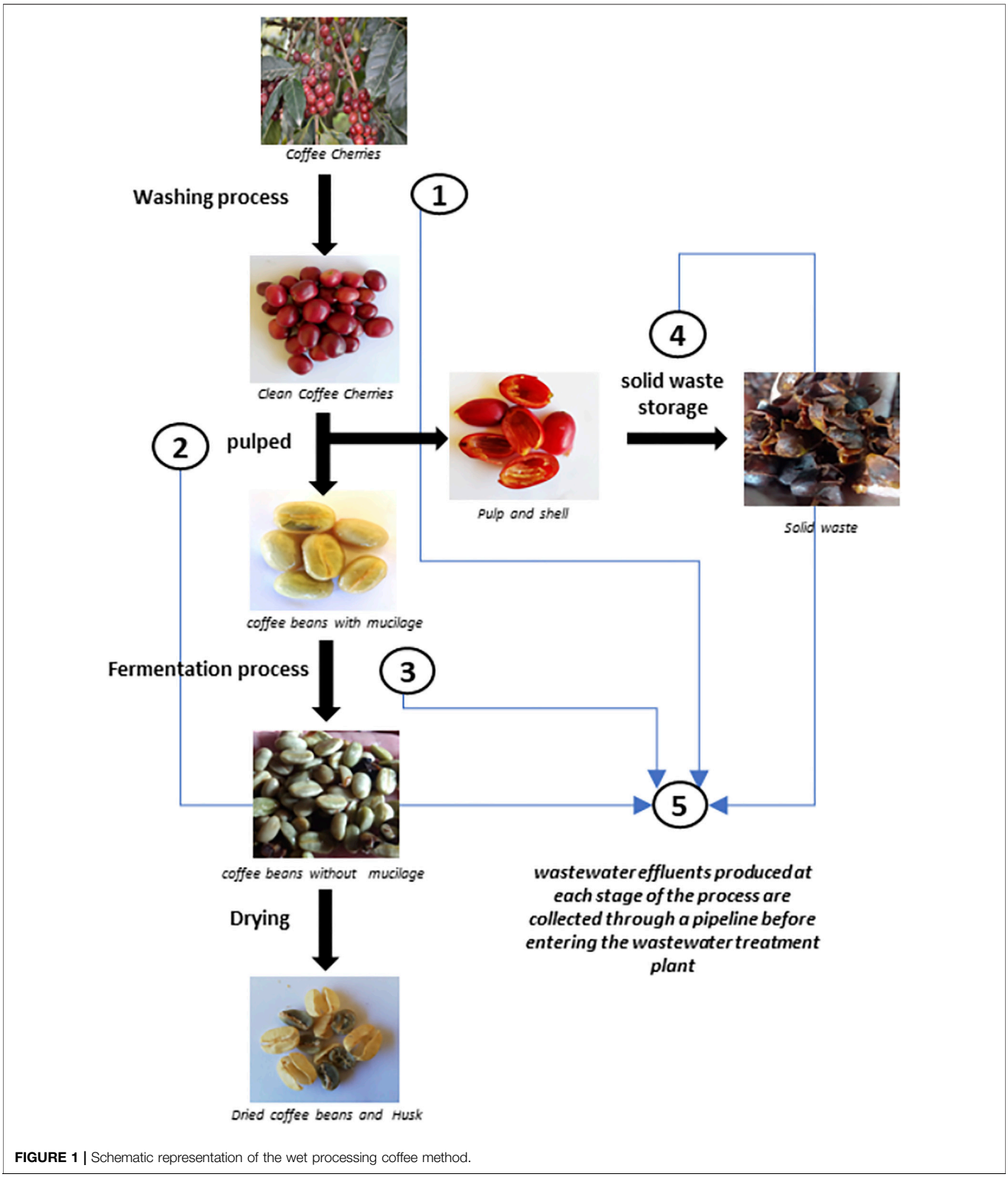

FIGURE 1 | Schematic representation of the wet processing coffee method.

closed with a 100 Ω resistance, and the system was operated for a further 37 days. During the entire operation, both in open and closed circuits, the liquid volume in the anodic chamber was maintained at a constant level by daily addition of medium to compensate for losses caused by evaporation or consumption of wastewater.

The acclimatised microbial community was used as inoculum for the study of the electrochemical performance of the microbial

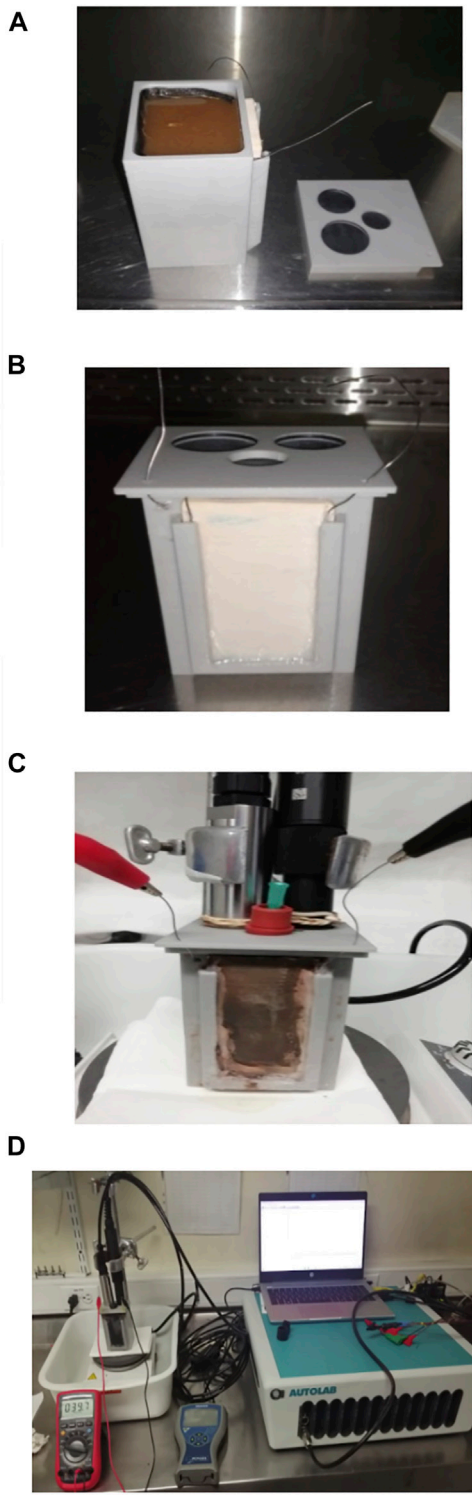

FIGURE 2 | Prototype Microbial Fuel Cell made of polymer and with ceramic membrane. **(A)** Detail of MFC assembly with the anode chamber filled with fresh coffee wastewater used as feedstock. **(B)** Front view of MFC prototype assembly showing the ceramic membrane. **(C)** MFC assembly with sensors and probes adapted. **(D)** Detail of MFC set up.

fuel cell (Experimental setup MFC2). 150 ml of the 1:1 mixture of fermentation wastewater and leachates were inoculated with 20 ml of the matured culture obtained in MFC1 and operated as open circuit system for 30 days. Subsequently, all the remaining liquid was replaced with 170 ml of fresh wastewater mixture. The external circuit was closed with a resistance of 100 Ω and the system was operated under these conditions for a further 30 days.

All experiments were carried out at an ambient temperature of 25°C and with magnetic stirring of 150 rpm to ensure good mixing. Liquid samples from the anode chamber were taken regularly to determine the concentration of organic matter, and samples from the anode were taken at the end of the open circuit stage of the MFC to evaluate the formation, evolution, and composition of the microbial community in the biofilm.

2.3 Chemical Analyses

The wastewater generated in the coffee wet process was analysed to determine the content of metals, phosphates, nitrogen, and organic matter, and using standardized quantification reference methods. For metals, SM 3030E, SM 30303F, and SM 3120B; for organic N, SM 4500B; for NH_3, SM 4500 NH3B (Standard Methods for the Examination of Water and Wastewater, APHA/AWWA/WEF, 2012a). Organic matter content was analysed by the standard protocol SM 5220 D for the determination of COD in wastewater samples of agricultural origin (Standard Methods for the Examination of Water and Wastewater, APHA/AWWA/WEF, 2012b). The protocol was modified by performing a 1:50 dilution of a 1.5 ml sample volume in distilled water. 0.65 ml of the diluted solution were mixed with 0.39 ml of the COD digestion solution and 0.91 ml of sulfuric acid mixed with silver. The samples were placed in micro-COD digestion tubes and incubated in a Spectroquant TR 420 thermoreactor at 150°C for 120 min. After digestion, the content was transferred to quartz cuvettes and the optical density was read at 600 nm in a spectrophotometer (Thermo Spectronic Genesys 2, Thermo Fisher Scientific). COD was calculated using a standard COD concentration curve, using distilled water as a blank.

Operational parameters (temperature, pH, dissolved oxygen (DO), and redox potential) were monitored and recorded continuously by an automatic data acquisition system with a multimeter (ODEON Portable meter pH-Conductivity, AQUALABO, France).

2.4 Electrochemical Measurements

Cell voltage monitoring was performed using a digital multimeter (UNI-T UT61C, Uni-Trend, Czech Republic). The electric current was calculated using Ohm's Law, $I = V/R$, where V is the voltage and R the external resistance. To determine the electrical power, equation $p = V\ x\ I$ was used, and the volumetric power and current densities were calculated by dividing the values of Power and Current by the volume of the anode chamber. Polarization curves were obtained using external resistances between the range of 1–15,000 Ω, with an

TABLE 1 | Chemical characterization of coffee wet processing wastewater from Sampling point 5.

Analysis	Sample 1	Sample 2
Total phosphorus (mg P/L)	28.9	30.2
Total Kjeldahl Nitrogen (mg N/L)	136.9	349.0
Iron (mg Fe/L)	8.2	5.8
Copper (mg Cu/L)	<0.2	0.3
Calcium (mg Ca/L)	56.1	96.5
Magnesium (mg/L)	17.3	25.0
Potasium (mg K/L)	270.6	703.0
Sodium (mg Na/L)	<1.5	5.4
Zinc (mg Zn/L)	<0.2	<0.2

interval of 10 min between each resistance change to achieve the registration of a stable value.

2.5 Microbial Community Analysis

Anode samples of 0.25 cm^2 were taken at the end of the open- and closed-circuit operations for analysis of the microbiological community. Samples of the biofilm were scraped off the carbon cloth using a sterile scalpel, and bacterial DNA was extracted using the GenElute Soil Extraction Kit. The molecular identification of the microorganisms present in the native community was carried out by Microbial amplicon sequencing-16S rRNA gene analysis of the V4 region with 515F and 806R primers. The analysis was carried out by Novogene Corporation (United Kingdom).

2.6 Electron Microscopy

Scanning electron microscopy (SEM) analyses were performed using a JEOL JSM 6490 LV electron microscope. The samples were fixed on a graphite tape, and coated with a thin gold coating of approximately 12.5 nm in a Denton Vacuum desk IV equipment. High resolution images were obtained by vacuum scanning electron microscope, and a secondary electron detector was used to analyse the morphology and topography of the samples. The analyses were carried out at the Advanced Microscopy Center (CAM) of the University of Antioquia.

3 RESULTS AND DISCUSSION

3.1 Characterization of Coffee Wastewater

Wastewater resulting from the wet processing of coffee was analysed to determine the content of organic matter, ions, and other components. **Table 1** shows the results of the analysis of samples taken from Sampling point 5 (see **Figure 1**) at two diferent times during the operation of the coffee wet process, labelled Sample 1 and Sample 2. The results of the analysis indicate the presence of nitrates, phosphates, iron, chromium, copper, potassium, zinc, magnesium, and sodium. These ions can act as co-factors for the development and evolution of microorganisms in the anodic chamber, and affect the electron transfer mechanisms in the MFC by changes in conductivity. Interestingly, Sample 1, and Sample 2 (obtained at different times during the process) present different concentrations of the measured components. This difference can be explained by the fact that coffee processing is not a standardized and controlled process, resulting in a highly variable composition. The amount of water used in the process depends on the initial load of processed coffee and operational conditions such as washing time, fermentation time, and pulp storage time for leachate decantation, among other variable conditions during the operation.

TABLE 2 | COD analysis results of the wastewater samples from the Coffee Wet Processing Plant.

Sampling point	Sample1	Sample2
	COD (g/L)	COD (g/L)
1 and 2—Washing and Pulped	36.39	19.51
3—Fermentation	24.17	27.99
4—Leached	53.06	59.01
5—Mixed	21.69	26.24

Table 2 shows the organic matter content, expressed as Chemical Oxygen Demand (COD), for the wastewater samples collected at different sampling points in the processing plant. The organic matter content of samples taken at early stages of the wet processing (sampling points 1 and 2, Washing and Pulped) show large differences in samples taken at different times (36.39 g/L for Sample 1 vs 19.51 g/L for Sample 2). The difference is smaller in samples taken from sampling points 2, 3, and 4, which show relatively similar values between Sample 1 and Sample 2.

The degree of contamination varies depending on the stage of the process being sampled (See scheme in **Figure 1**). The COD results indicate that the wastewater with the highest organic load is originated in sampling point 4–Leached, with values of 53.06 g/L and 59.01 g/L for Sample 1 and Sample 2, respectively. Sampling point 4 collects the leachate obtained from the husk and pulp waste. Those leachates are collected in tanks and stored for periods ranging from 12 to 24 h before being transferred to its final disposal outside the coffee processing plant. For Sample 1, the wastewater identified as Sampling point 1-2 (Washing and Pulped) with a COD value of 36.39 g/L has a higher load of organic matter than the wastewater from the Sampling point 3 (Fermentation), with a COD of 24.17 g/L. However, in Sample 2, the Fermentation wastewater has a higher organic load than the wastewater from Washing and Pulped, with COD of 24.17 g/L and 19.51 g/L, respectively. Finally, these variations in the concentrations of organic matter have an effect on the final concentration of the wastewater from Sampling point 5 (Mixture), which collects the mixture of all the wastewater from the different wastewater generation points in the wet coffee processing process. The COD values determined were 21.69 g/L and 26.24 g/L, for Sample 1 and Sample 2, respectively.

For illustration, images of the solid waste heaps of shell and pulp, the leachate storage tank, and the water treatment plant are presented in the **Supplementary Material**.

3.2 Performance of the Microbial Fuel Cells

3.2.1 Electrochemical activity

As indicated in the Methods section, the performance of the MFCs was evaluated during 60 days. Fresh substrate was added to

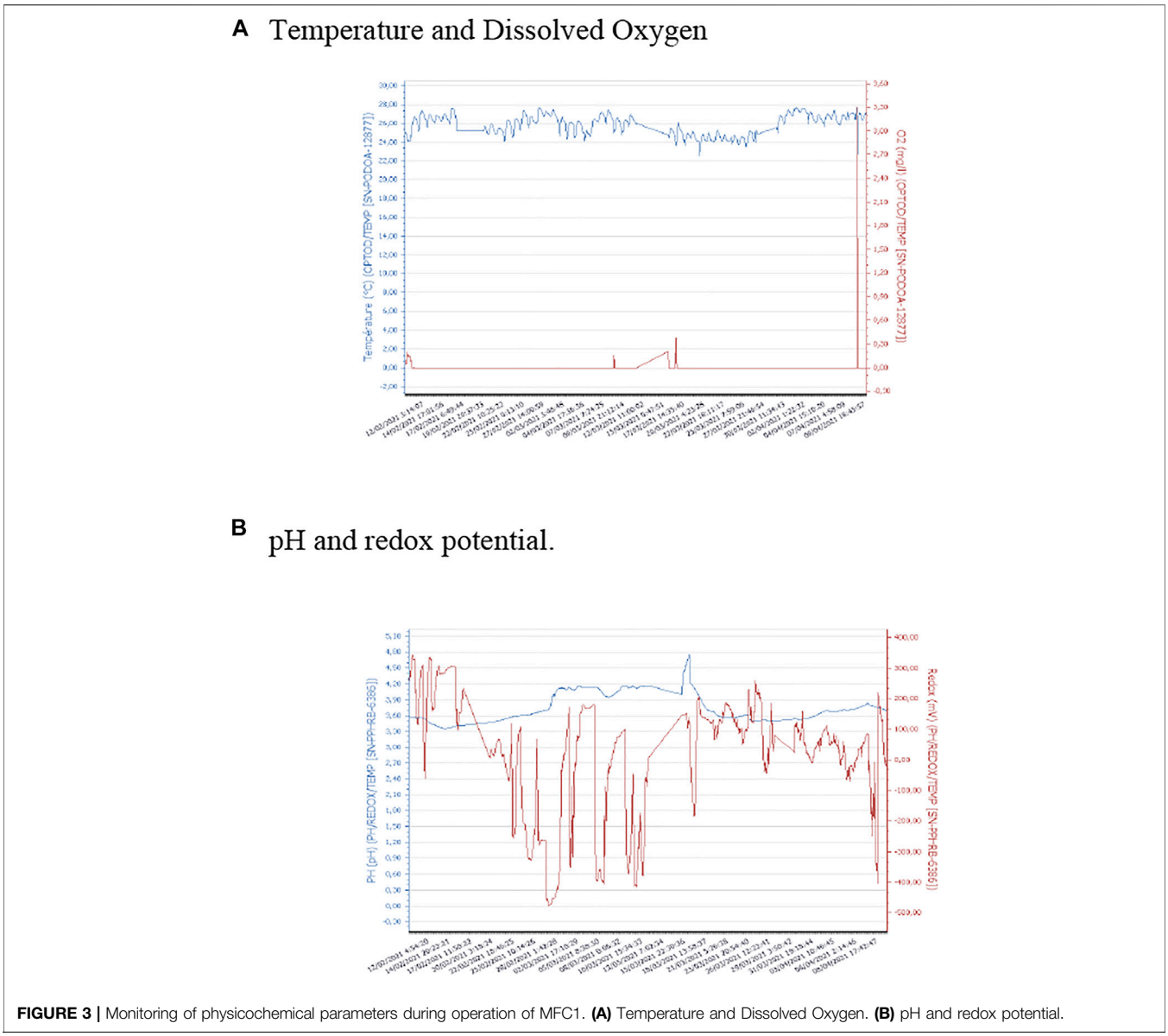

FIGURE 3 | Monitoring of physicochemical parameters during operation of MFC1. **(A)** Temperature and Dissolved Oxygen. **(B)** pH and redox potential.

the MFCs to maintain a constant volume in the anodic chamber. On average, the daily volume added for the cell identified as MFC1 was 12 and 28 ml for the cell identified as MFC2. This difference may be related to the physical changes observed in the substrate, such as the formation of a dense layer on the surface of the medium (**Figure 7A**). This phenomenon has been observed in other systems associated to foaming (Yang et al., 2021), probably caused by the biochemical transformation of the substrate. As the microbial community develops and specializes, its metabolic activity increases achieving a greater and faster transformation of the substrate, producing an increase in the amount of biomass and by-products such as extracellular polymeric substances and CO_2, which result in changes in the volume of the liquid substrate in the anode chamber. The evolution of pH, temperature, dissolved oxygen, and redox potential in MFC1 is presented in **Figure 3**. As it can be seen, all parameters remained stable during operation, except for the redox potential, which showed significant variations, without any clear trend during the entire operating time. The temperature remained constant, at an average value of approximately 25°C, and the pH showed some variations, but generally remained at a value of around 3.6. The concentration of dissolved oxygen was 0, indicating that the anode chamber remained anaerobic throughout the operation.

The open circuit voltage (OCV) was monitored during operation of both MFCs (**Figure 4**), 58 days for MFC1 and 30 days for MFC2. Although both cells were set up with the same configuration, materials, ceramic membrane, and anodic and cathode electrodes, and were fed with the same substrate, differences in the electrochemical behaviour were observed. For MFC1, a fast increase in voltage occurs approximately during the first 10 days of operation, reaching a value close to 300 mV at t =

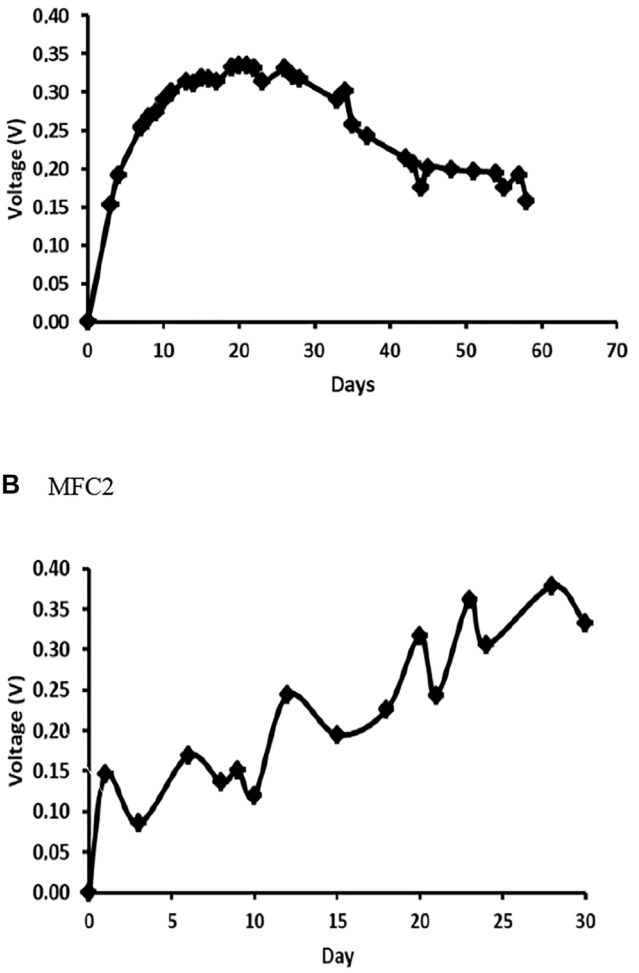

FIGURE 4 | Voltage tracking of MFCs. **(A)** MFC1 **(B)** MFC2

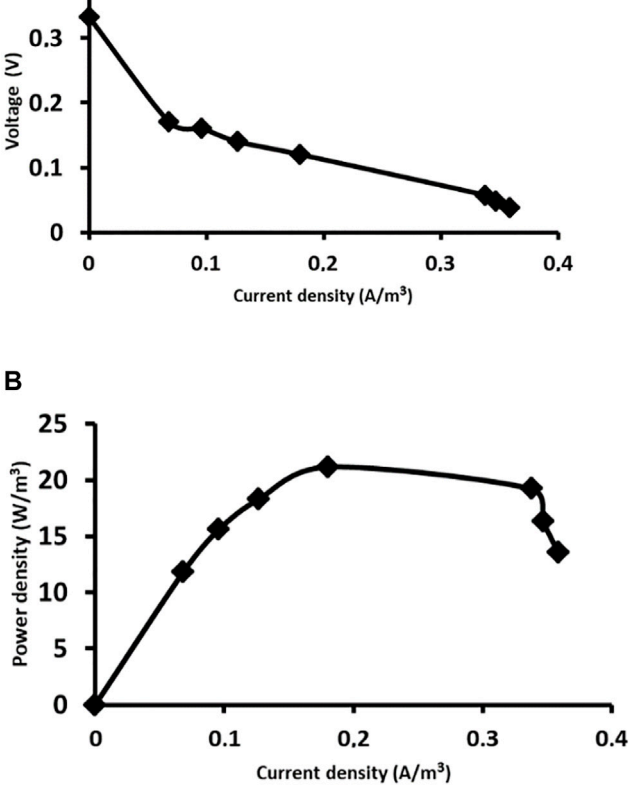

FIGURE 5 | Electrochemical performance of MFC2 at day 30: **(A)** Polarization curve; **(B)** Power density curve.

10 days, and slowly increasing thereafter to reach a maximum voltage of 335 mV at t = 21 days. The voltage remained at a relatively constant voltage of 330 mV until t = 30 days, decreasing thereafter down to 206 mV at t = 43 days, and from this day until the end of the operation (t = 58 days), when the recorded voltage is approximately 186 mV. A different behaviour was observed in MFC2: In this case, a slower increase in OCV is observed, reaching a maximum value of 378 mV at t = 28 days. In this set-up, no periods of stable voltage output are observed, with some oscillations but with a clear increasing trend.

The electrochemical performances of the MFCs operated at closed circuit voltage (CCV) were also different. Taking into account the low output voltage reached in MFC1 at day 58, the closed-circuit operation was performed with an external resistance of 100 Ω; however, no electrochemical response was obtained. On the contrary, the polarization curve determined in MFC2 operated at CCV by connecting an external resistance of 100 Ω at 30 days reached a maximum power density of 21.16 W/m^3 achieved with an external resistance of 3,800 Ω (**Figure 5**). The better electrochemical performance observed in MFC2 can be attributed to the use of a mature community as inoculum, indicating that the electrochemical behavior is directly related to the development and evolution of the microbial community colonizing the anode.

3.2.2 COD reduction

Together with the electrochemical performance, we evaluated the capacity of the MFCs to degrade the organic matter present in the wastewater. **Figure 6** shows the results of COD measurements in samples taken from MFCs at different times during the operation. In terms of COD concentration in the anodic chamber, MFC1 showed a constant decrease in COD until day 33, equivalent to a total COD reduction of 69%.

However, these measurements do not consider that the liquid in the chamber was replenished during operation by addition of fresh medium. Therefore, to calculate the consumption of organic matter, under these experimental conditions, and the calculation needs to be corrected to account for the daily addition of medium. Although the complexity of the system makes it difficult to obtain accurate values, approximate rates of COD reduction can be calculated to be approximately 4.5 gCOD/l/d for MFC1, assuming linearity and correcting for medium replenishment:

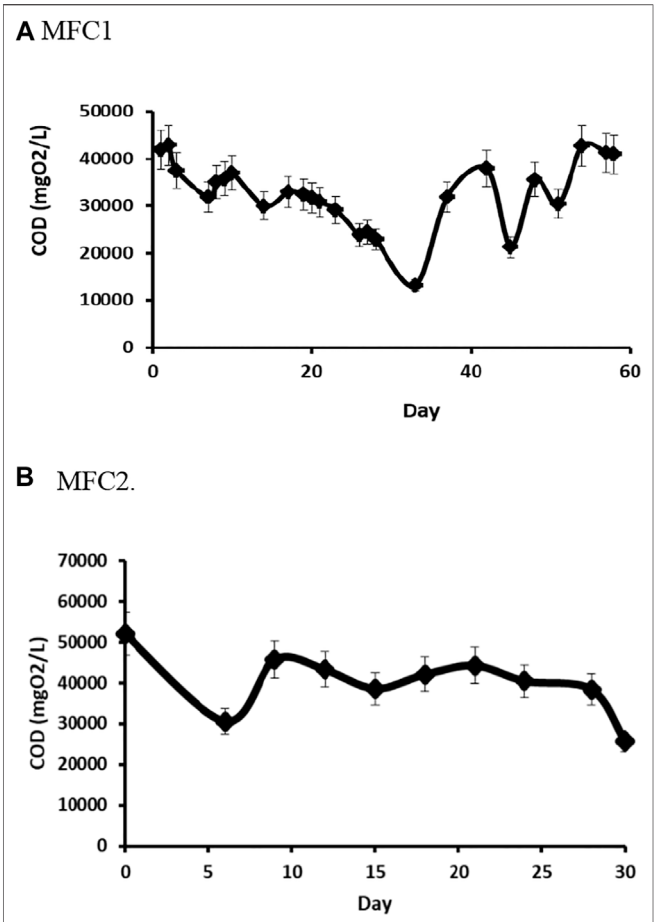

FIGURE 6 | Changes in COD during operation of MFCs. Anode chambers were replenished daily with fresh medium to compensate for decrease in liquid volume. The COD measured is the difference between the amount fed and the amount consumed. **(A)** MFC1 **(B)** MFC2

In this case, the consumption of COD is approximately 71%. Although the concentration of organic matter in the system (measured as COD) increases after day 33, reaching a value close to the initial value (41.3 gCOD/l), the calculation shows that the system is still able to consume COD at a rate of approximately 2.5 gCOD/l/d. This decrease in the capacity for COD consumption might be a result of diffusional limitations that could be eliminated by careful design of the process and adjustment of operational variables.

In MFC2, the COD was reduced by 41% during the first 5 days of operation, but between 10 and 28 days, the concentration of organic matter remained approximately constant at a value of 40.8 gO_2/l, which represents a reduction of 21.7%. Finally, by 30 days, a reduction of 49.4% was achieved. However, when a correction for the replenishment of medium in the system is taken into account, the reduction of COD is much larger. On day 5, the reduction is approximately 70%, reaching 80% by day 22 and 91% at the end of operation at day 30. The rate of decrease measured assuming linearity shows a very high rate of 11.57 gCOD/l/d at day 5, and decreasing to relatively constant values fluctuating between 8.5 and 9.0 gCOD/l/d.

The differences in electrochemical and biochemical behaviour could be associated with changes in physical properties of the liquid and the electrodes. Visual observation shows an increase in the viscosity of the medium, and the formation of a thick deposit on the surface of the anodes during the operation (**Figure 7**). This can be attributed to the increase in microbial biomass and the secretion of extracellular polymeric substances, as evidenced by the presence of a gelatinous material adhered to the walls of the anode chamber and suspended in the wastewater. A layer of a material with similar characteristics was observed on the surface of the anodes. As it can be seen in **Figure 7A** for the MFC1, despite the presence of gelatinous material, the wastewater in the centre of the chamber has a less viscous consistency and presents a slightly lighter colour, when compared to the fresh wastewater that was fed to the cell (**Figure 3A**).

The macroscopic changes in the development and evolution of the microbial community in MFC2 are more significant. As it can be seen in **Figures 7A,C** mycelial mat developed on the surface of the liquid in the anode chamber. Once this thick layer of microorganisms has been removed, it is possible to see the differences in viscosity and coloration of the treated wastewater compared to the initially observed characteristics. **Figure 7D** shows that the biofilm layer formed was thicker and more compact than that observed in MFC1 (**Figure 7B**). The development and evolution of microbial communities with different physical structures may account for the different results of bioelectrochemical performance and degradation of organic matter in the 2 MFCs. This issue needs to be carefully considered when designing a bioelectrochemical system to remediate wastewaters with high content of organic matter of variable and undefined composition.

3.3 Macroscopic and Microscopic Analysis of the Native Microbial Community

The macroscopic development and evolution of the microbial community in the MFC was evidenced as shown in **Figure 7** and discussed in the previous section. However, to confirm the evidence of the adaptation and colonization of the surface and internal structure of the anode electrodes, we performed a scanning electron microscopic analysis of anode samples. **Figure 8** shows micrographs of anode samples taken from MFC1. **Figures 8A,B** correspond to micrographs of the surface of the carbon felt used as an anodic electrode. As it can be seen in **Figure 8A**, the material has a structure composed of very different fibres randomly intertwined, with large spaces between them. **Figure 8B** shows details of one of the fibres, with a flat and smooth surface but a multi-layered configuration, which creates cavities and crevices along the fibre. In **Figure 8C**, the presence of microbial cells and biological material can be seen adhered to the surface of the fibres or embedded in the cavities of the material. Morphological structures corresponding to bacilli and cocci are observed, in addition to other amorphous structures that may correspond to components of the wastewater used as a substrate and to exopolysaccharides or other extracellular polymeric substances secreted by microorganisms to improve their adhesion to the surfaces of the material. **Figures 8D,E** show details of the microorganisms and deposits of substances that modify the surface structure, generating a rough and irregular layer of material to which cells may attach by means of structures (e.g.

A A thick deposit of a polymeric substance is observed on the walls of the anodic chamber of cell MFC1 on day 37.

B A thick biofilm developed on the carbon felt anode of MFC1 after 37 days of operation

C A thick layer of a mycelial structure was observed on the surface of the liquid in the anodic chamber of cell MFC2 on day 38.

D A thick biofilm developed on the surface of the anode of MFC2 showed a thick biofilm after 30 days of operation.

FIGURE 7 | Macroscopic changes observed in the anodic chamber of MFCs. **(A)** A thick deposit of a polymeric substance is observed on the walls of the anodic chamber of cell MFC1 on day 37. **(B)** A thick biofilm developed on the carbon felt anode of MFC1 after 37 days of operation. **(C)** A thick layer of a mycelial structure was observed on the surface of the liquid in the anodic chamber of cell MFC2 on day 38. **(D)** A thick biofilm developed on the surface of the anode of MFC2 showed a thick biofilm after 30 days of operation.

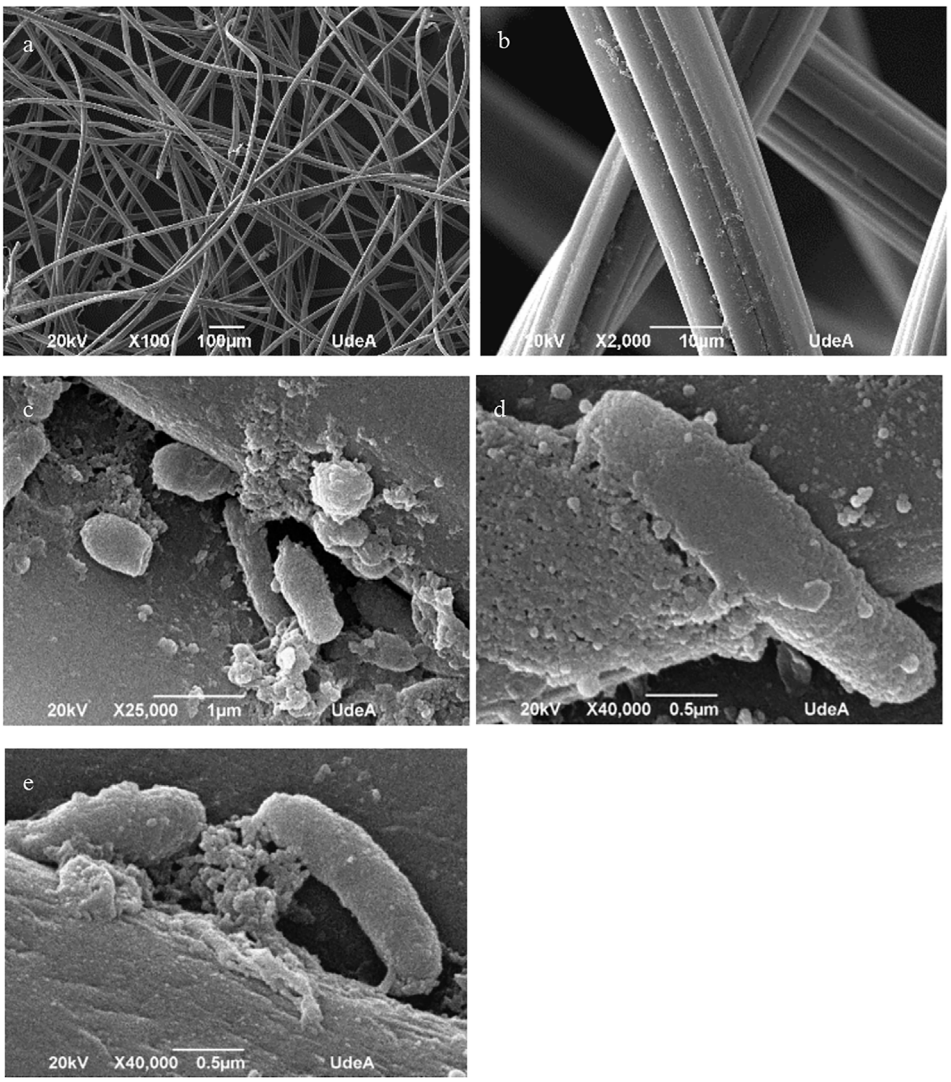

FIGURE 8 | Analysis by scanning electron microscopy of the anode of MFC1. The images show the microscopic changes observed in the carbon felt fibres after operation for 37 days **(A)** X100 magnification; **(B)** 2000X magnification. **(C)** Microbial cells embedded in polymeric substance can be observed attached to the carbon fibres; **(D,E)**. show details of the rough and irregular surface of the fibres caused by the deposits of polymeric substances.

pili). These structures have also been reported as being involved in mechanisms of electron transfer in electricity generation processes in bioelectrochemical systems (Shelobolina et al., 2007; Shelobolina et al., 2008).

Figure 9 shows the results of the SEM analysis carried out for the anode of MFC2. Here, the development and evolution of the microbial community present important differences with respect to the biofilm formation and anode colonization in the anode of MFC1. **Figures 9A,B** show regions of the anode where the fibres of the carbon felt are completely covered by a uniform layer of biological material. In the detail of **Figure 9B**, it is observed that the substance spreads in a regular way, covering completely the entire surface of the carbon fibre. However, in **Figure 9C** a large cluster of biological material is observed, which, unlike the thin layer in **Figure 9B**, presents a rather rough and amorphous structure with cavities and interstices, dispersed on the surface in an irregular manner. In **Figures 9D,E**, microorganisms with bacilli and cocci morphologies can be seen attached to this material with a different arrangement and configuration. In the case of the bacilli, membrane extension structures that may act as anchors for cell adhesion to surfaces and other cells can be observed. For the cocci, a very compact cluster of cells is observed. The differences in the structure of the biofilms could also be related to the significant differences on the electrochemical performance of the system.

3.4 Molecular Analysis of the Microbial Communities

In order to elucidate the taxonomic structure of the native and the evolved microbial communities developed in the MFCs, we

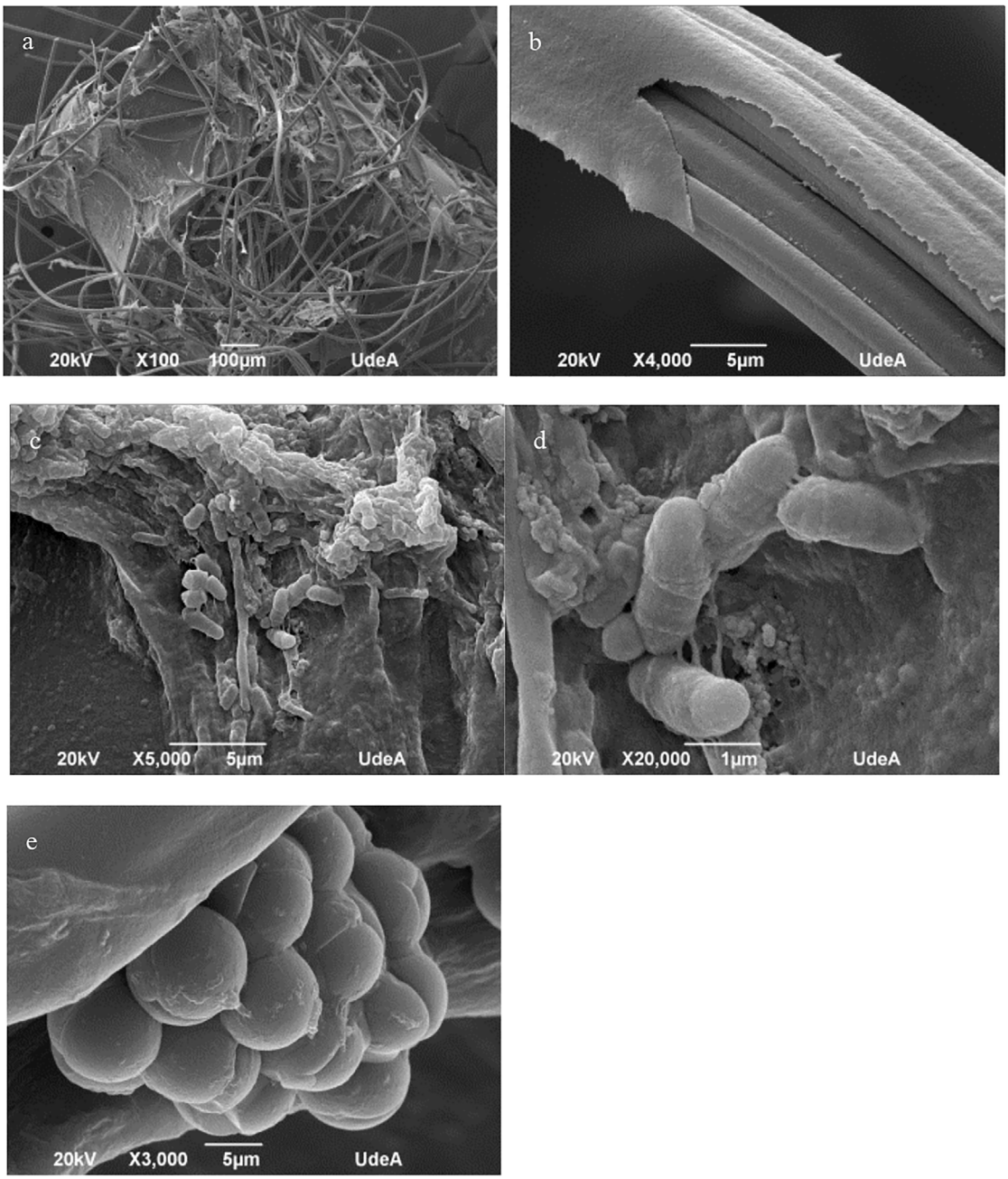

FIGURE 9 | Analysis by scanning electron microscopy of the anode of MFC2. The images show the microscopic changes observed in the carbon felt fibres after operation for 30 days **(A)** structure of the carbon felt at X100 magnification; **(B)** detail of the anode surface fibres covered by a layer of biological material at 4,000X magnification. **(C)** Microbial cells embedded in polymeric substance can be seen attached to the carbon fibres; **(D)** bacilli and **(E)** cocci can be observed attached to the carbon fibres.

performed a metataxonomic analysis of anodic biofilm samples. Some of the results of the molecular identification are presented in **Figures 10**, **11**. **Figure 10** corresponds to the results of relative abundance of the Phyla present in the analysed samples. Samples AR1, AR2, AR3, and AR4 correspond to the wastewater from the Washing, Fermentation, Leachate, and Mixed water sampling points. Samples SP1 corresponds to a soil sample from coffee plantations, and sample IM5 is the mixture of the wastewaters from the different sampling points. The samples identified as MFC1d30 and MFC1d37 correspond to samples of the microbial community present in the liquid of the anode chamber on days 30 and 37, respectively, after the start of the operation of MFC1. The sample identified as MFC1d37A corresponds to samples of the microbial community attached to the anode electrode of MFC1 at

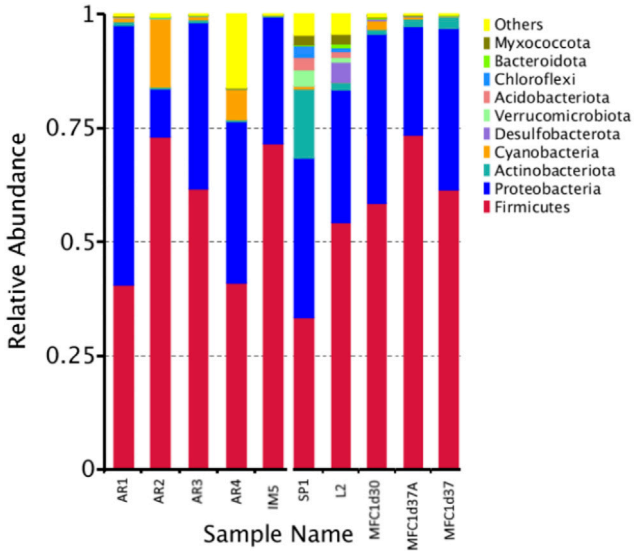

FIGURE 10 | Relative abundance at the level of Phylum from native microbial communities. Samples AR1–AR4 correspond to wastewater obtained at different stages of the process Washing, Fermentation, Leachate and Mixed, respectively, and as shown in the scheme in **Figure 1**. Sample IM5 is the mixture of the wastewater from all sampling points. Sample SP1 is a sample from soil associated to coffee plants. Sample L2 is a sample from soil not related to coffee farms, used as a comparison. Samples MFC1d30 and MFC1d37 are sample from the anolyte from MFC1 at 30 and 37 days of operation, respectively. Sample MFC1d37A is a sample form the anodic biofilm from MFC1 at 37 days of operation.

day 37. Samples L2, correspond to water samples taken in other environmental settings and regions other than the coffee agroindustry zone, and were included in the analysis for comparison purposes, to determine if the microbial communities associated to coffee present any functional characteristics specific to their natural environment.

In general terms, the results of relative abundance at the Phylum level indicate a higher abundance of *Firmicutes* and *Proteobacteria* in wastewater samples from the environment of the coffee region and, therefore, and in the communities present in the MFCs. The Phyla *Actinobacteriota, Cyanobacteria, Acidobacteriota, Desulfobacterota*, among others are also present at significant abundances. The sample exhibiting a higher diversity of Phyla corresponds to the microbial community obtained from the soil of the coffee plantation, sample SP1, which has a greater similarity to the diversity observed in the environmental samples identified as L2. The phyla with higher abundances in those samples are *Firmicutes* and *Proteobacteria*, while also *Actinobacteriotas*, *Desulfobacteriota*, *Bacteroidota, Chloroflexi,* and *Myxococcota* are detected.

In **Figure 11**, the genera identified in the native microbial community are presented. There are differences between the genera found in the different samples. For the SP1 sample, the genera *Clostridium, Cohnella, Aneurinibacillus,* and *Candida*, among others were identified, while the samples obtained in the different sampling points contain genera such as *Gluconacetobacter, Clostridium, Acetobacter, Bacillus, Weissella, Leuconostoc,* and *Lactobacillus*. However, the analysis of the samples from MFC1 show a significant proportion of unidentifiable genera. Besides the mentioned genera, the presence of *Tumebacillus* and *Bifidobacterium* is observed in anode sample MFC1d37, while the genus *Oenococcus* was identified in sample MFC1d30.

4 GENERAL DISCUSSION

Despite the fact that equipment and technology incorporated in wet processing coffee plants should allow the reduction of water consumption, large amounts of wastewater are released from coffee bean production process. In Colombia, the international recognition of the quality of its coffee is directly related to the category of "washed soft coffees", which makes the consumption of water essential in the process (Rodriguez et al., 2015). The COD results shown in **Table 2** are evidence of the degree of organic contamination carried by these wastewaters, before being subjected to conventional treatment in the water treatment plant. The COD values are above the levels allowed by the environmental authority, which establishes for the coffee agroindustry maximum CODs of 3.00 gO_2/l for the ecological coffee processing, and 0.65 gO_2/l for the traditional process that involves the wet processing of coffee (Resolution 631/2015, Ministerio de Ambiente y Desarrollo Sostenible, 2015). In addition to the need to treat the wastewater generated in large coffee processing units, the needs of small coffee producers, representing ca. 95% of the country's coffee growers, must also be considered. However, due to socio-economic factors and cultivation conditions (farm sizes not exceeding 2 hectares), these producers cannot access appropriate infrastructure to implement ecological technologies for coffee production, nor do they have the possibility of implementing wastewater treatment plants in their production processes (Federación Nacional de Cafeteros, 2021).

As evidenced in the results of the characterization of the wastewater from the wet processing coffee (**Table 1**), the differences in the concentration of the substances present are significant. These results are similar to those reported by other authors (Said et al., 2020), who determined concentrations of COD and Phosphorus and Nitrogen different from other reports, i.e., 137 mg N/L and 12 mg P/L. The differences in agroindustrial effluents can be attributed to variations in the harvesting processes (Lopes et al., 2014). In many cases, it is impossible to carry out controlled process, and the characteristics of the wastewater will depend on the amount of fruit processed, the amount of water used in washing and pulping the cherry, the fermentation times for the transformation of sugars, the storage times of the pulp and the peel, and the consequent generation of leachates, as well as other operational and environmental factors. The importance of the composition of wastewater lies in the fact that it affects the conditions required for its treatment, both in conventional wastewater treatment systems, as well as its potential for bioremediation through bioelectrochemical systems (Borjas et al., 2015).

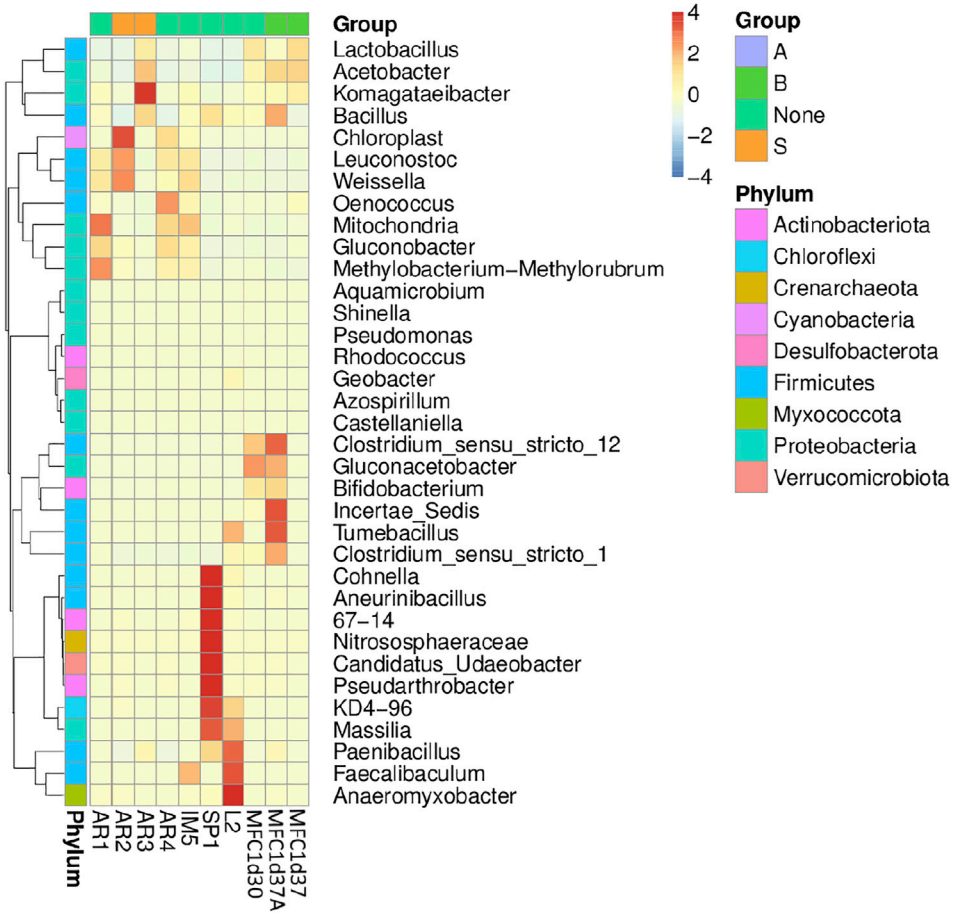

FIGURE 11 | Heat map with the bacterial genera of the samples of the native microbial communities and from the anode of MFCs, as described in **Figure 10**.

In the case of microbial fuel cells, these wastewaters are used as feedstock in the anode chamber so that microorganisms from native communities can degrade and transform organic matter through anaerobic processes of oxidation (Romero et al., 2012; Lovley, 1991). The wastewater from the coffee agroindustry contains Mg, Na, Ca, Zn, Cu, Fe, and other trace elements and co-factors essential for the growth and evolution of electrogenic microorganisms such as the reference electrogenic species *Geobacter sulfurreducens* (Lin et al., 2004; Romero et al., 2012; Echeverria and Nuti, 2017; Campos et al., 2021). Using native microbial communities ensures the metabolic adaptation of these microorganisms to the nutritional and environmental conditions of the wastewater, to degrade organic matter and to co-generate electricity (Logrono et al., 2015; Varanasi et al., 2017).

Regarding the performance of the MFC, the results indicate that the native microbial community present in the wastewater managed to carry out the transformation of the organic matter, achieving very high COD reductions. The COD reduction observed in MFC1 are close to those reported for degradation of wastewaters using microbial electrochemical systems, such as 64.9% COD reduction for urine (Zang et al., 2012), 58.6% for an integrated upflow wetland system coupled to a microbial fuel cell (Oon et al., 2015), or 63.5% COD reduction MFC fed with distillery wastewater (Samsudeen et al., 2015), while MFC2 showed COD reduction values similar to other systems fed with agroindustrial or domestic waste (Mansoorian et al., 2013; Firdous et al., 2018; Liang et al., 2018). Regarding the potential generation of electricity, the performance of the MFC under the evaluated conditions reached values of up to 378 mV in open circuit and power density values of 21.6 W/m^3, comparable to those reported by other authors (Mardanpour et al., 2012; Liang et al., 2018). These results provide clear evidence of the bioelectrochemical functioning of MFC, where a native microbial community exhibits bioremediation capacity to reduce water pollution, and while exhibiting potential for electricity co-generation.

However, it is important to indicate that the performance of microbial fuel cells is affected by different factors, such as the design of the system; the electrode and membrane materials; the environmental and operational conditions; the characteristics of the substrate used; and the microorganisms or microbial communities used as inoculum (Palanisamy et al., 2019). Therefore, the selection and evaluation of these factors is essential to achieve a better performance of the CFMs. In this study, the MFC evaluated was manufactured with inexpensive materials. The carcasse was constructed with ABS (acrylonitrile

butadiene styrene), a commercial material with multiple industrial and domestic applications (Perez, 2018). Similarly, the ceramic separation membranes evaluated were manufactured by an artisanal procedure from easily available local clays which present outstanding characteristics and properties for use in MFCs (Winfield et al., 2016; Yousefi et al., 2017). The maximum power achieved in the MFC was 21.6 W/m^3, higher than those reported by other authors who used MFCs of similar configurations, with open cathode and ion exchange membranes made of ceramic materials, e.g. 2.83 and 3.66 W/m^3 (Winfield et al., 2013); 6.57 W/m^3 (Jadhav et al., 2014); 4.21 W/m^3 (Chatterjee and Ghangrekar, 2014); 15 W/m^3 (Walter et al., 2016). The improved electrochemical performance of the MFC is probably due to the substrate and the microbial community used.

Nevertheless, despite these promising results, the performance of the MFC could be affected by the operational conditions under which the experimentation was carried out (Rabaey et al., 2011). As was observed in our long-term experiments, the formation of a thick biofilm on the anode electrode and the presence of exopolysaccharides in the liquid, a product of cell metabolism and the transformation of the substrate, could generate limitations in mass transfer. The negative effect of these limitations would be related to the high demand for fresh substrate due to the significant increase in biomass and the decrease in contact between the substrate and the cells. Both phenomena would cause a reduction in the anaerobic oxidation of organic matter, thus limiting the bioremediation capacity of the MFC. On the other hand, if the adaptation and evolution of the microbial community is achieved and an optimal amount of immobilized biomass is reached on the anode electrode, either by controlling biofilm formation, by implementing larger surface areas on the electrode anode, or by modification of the operational conditions (ie., Hydraulic Retention Time), an increase in the rate of bioremediation in the MFC, and therefore electricity generation, could be achieved (Li et al., 2014). The formation of a layer of biological material, shown in detail in **Figures 8C**, **9B**, may represent an advantage for survival and adaptation of microorganisms, which, taking advantage of the electron-accepting nature of the anode material, increase their metabolic activity (Li et al., 2010; Srivastave et al., 2015). However, this increase in biomass can also cause long-term plugging problems in the electrode and affect the performance of the MFC. As several authors have indicated, ideally a microbial community is expected to be synergistic, with microorganisms playing a specific role in the so-called "nutrient cycle ecosystem" (Costerton, 2007; Li et al., 2018).

The results of the molecular characterization carried out on the native microbial communities present in the coffee agroindustry and in the MFCs (see **Figures 10**, **11**) indicate the presence of Phyla such as *Proteobacteria, Firmicultes, Acidobacteria*, and *Actinobacteria*. These phyla are formed by multiple genera with metabolic capabilities for the biotransformation of the complex matrix of coffee wastewater. If the results of relative abundance in the samples of wastewater from the coffee agroindustry are compared with those obtained for samples from other non-coffee growing regions, important differences can be established in the composition of the microbial communities. In the case of environmental samples identified as R1 and R2, the community is composed mainly of the Phylum *Actinobacteriota*, followed by *Proteobacteria* and *Desulfobacterota*. However, the microbial community of the samples from coffee regions is composed mainly by microorganisms belonging to the Phyla *Firmicutes*, followed by *Proteobacteria*. The differences in the relative abundance of the microbial communities of the different sampling points in the processing plant, identified as AR1, AR2, AR3, and AR4, are not so significant, with only a greater abundance of the Phylum *Cyanobacteria* observed in the AR2 sample, and which corresponds to the wastewater from the fermentation stage. The metabolic capacity of *Cyanobacteria* in the production of methane has recently been reported (BižićKlintzsch et al., 2020). SP1, which corresponds to soil from coffee plantations, is the sample that exhibits the greatest diversity. Unlike the other samples, and a greater presence of the Phylum *Actinobacteriota* is observed. In environmental samples, the presence of the genus *Geobacter* is well-known, as members of this genus are recognized for their outstanding electrogenic characteristics, due to the ability to directly transfer electrons to different substances (Lovley et al., 2004; Holmes et al., 2006). For the samples from the coffee zone, the genus *Clostridium* stands out. *Clostridium* has been reported as possessing potential electrogenic capability (Jiang et al., 2016; Deng et al., 2017). Also, in these samples, the presence of the genus *Komagataeibacter* is evidenced. Within this genus, species with a wide metabolic capacity for the processing of glucose, glycerol, and cellulose have been reported. Their ability as producers of bionanocellulose and the synthesis of exopolysacatides is also highlighted (Ryngajłło et al., 2019). The genera *Bacteroides, Clostridium, Leuconostoc,* and *Lactobacillus* possess fermentative metabolism (Hodgson et al., 2016), while species of the genus *Bidifobacterium* present heterofermentative metabolism of glucose and lactose (Pokusaeva et al., 2011). It is possible to attribute an approximate metabolic function, taking into account the type of metabolic products present in the environment. However, it is not possible in a complex microbial community to identify the specific metabolic functions performed by each species (Hodgson et al., 2016). It is worth highlighting the importance of exploring different environments or specific environmental niches, since many species present in native microbial communities may present multiple metabolic capacities that can be used both for decontamination processes and for the co-generation of electricity in bioelectrochemical systems.

DATA AVAILABILITY STATEMENT

The datasets presented in this study can be found in online repositories. The names of the repository/repositories and accession number(s) can be found below: https://dataverse.harvard.edu/dataset.xhtml?persistentId=doi:10.7910/DVN/DTCR01. The research has the permission to access genetic resources contract No RGE156-10 issued by the Colombian authority Ministry of Environment and Sustainable Development.

AUTHOR CONTRIBUTIONS

All authors have made substantial direct and intellectual contribution to the work. Author contribution. SEC: Investigation, Data analysis, CA-R: Conceptualization, Data analysis, Writing (review and editing), Funding acquisition. LMA-E: Conceptualization, Experimental design, Data analysis, Project administration, Writing (original draft, review and editing), Funding acquisition. All authors approved the manuscript for publication.

FUNDING

This research was funded by the Colombia-UK Newton Prize Award 2018 "Valorisation of agro-industrial waste: A Bioelectrochemical System for waste degradation and energy recovery from industrial coffee waste" (Project number 1175).

ACKNOWLEDGMENTS

The authors would like to thank *Cooperativa De los Andes* for supplying wastewater samples and providing access to the coffee processing plants. CAR would like to thank the Biotechnology and Biological Sciences Research Council (BBSRC).

SUPPLEMENTARY MATERIAL

The Supplementary Material for this article can be found online at: https://www.frontiersin.org/articles/10.3389/fceng.2022.814987/full#supplementary-material

REFERENCES

APHA/AWWA/WEF (2012a). "5220 Chemical Oxygen Demand (COD)," in *Standard Methods for the Examination of Water and Wastewater*. Editors E.R.A. RiceBairdEaton and L. Clesceri. 22nd ed., 14–19. Available at: http://edgeanalytical.com/wp-content/uploads/Inorganic_SM5220.pdf.

APHA/AWWA/WEF (2012b). "Standard Methods for the Examination of Water and Wastewater," in *Standard Methods*. Editors E. Rice, R. Baird, A. Eaton, and L. Clesceri. 22nd ed.

BižićKlintzsch, M. T., Klintzsch, T., Ionescu, D., Hindiyeh, M. Y., Günthel, M., Muro-Pastor, A. M., et al. (2020). Aquatic and Terrestrial Cyanobacteria Produce Methane. *Sci. Adv.* 6, eaax5343. doi:10.1126/sciadv.aax5343

Borjas, Z., Ortiz, J., Aldaz, A., Feliu, J., and Esteve-Núñez, A. (2015). Strategies for Reducing the Start-Up Operation of Microbial Electrochemical Treatments of Urban Wastewater. *Energies* 8, 14064–14077. doi:10.3390/en81212416

Campos, R. C., Pinto, V. R. A., Melo, L. F., Rocha, S. J. S. S. d., and Coimbra, J. S. (2021). New Sustainable Perspectives for "Coffee Wastewater" and Other By-Products: A Critical Review. *Future Foods* 4, 100058. doi:10.1016/j.fufo.2021.100058

Chatterjee, P., and Ghangrekar, M. M. (2014). Design of Clayware Separator-Electrode Assembly for Treatment of Wastewater in Microbial Fuel Cells. *Appl. Biochem. Biotechnol.* 173, 378–390. doi:10.1007/s12010-014-0846-x

Costerton, J. W. (2007). *The Biofilm Primer*. Berlin-NewYork: Springer, 70.

Dankowska, A., Domagała, A., and Kowalewski, W. (2017). Quantification of *Coffea Arabica* and *Coffea Canephora* Var. Robusta Concentration in Blends by Means of Synchronous Fluorescence and UV-Vis Spectroscopies. *Talanta* 172, 215–220. doi:10.1016/j.talanta.2017.05.036

Deng, H., Xue, H., and Zhong, W. (2017). A Novel Exoelectrogenic Bacterium Phylogenetically Related toClostridium sporogenesIsolated from Copper Contaminated Soil. *Electroanalysis* 29, 1294–1300. doi:10.1002/elan.201600673

Didanna, H. L. (2014). A Critical Review on Feed Value of Coffee Waste for Livestock Feeding. *World J. Biol. Biol. Sci.* 2, 72–86.

Echeverria, M. C., and Nuti, M. (2017). Valorisation of the Residues of Coffee Agro-Industry: Perspectives and Limitations. *Towmj* 10, 13–22. doi:10.2174/1876400201710010013

Federación Nacional de Cafeteros (2021). Our Coffee Growers. Available at: https://www.cafedecolombia.com/particulares/our-coffee-growers/?lang=en (Accessed November 3, 2021).

Firdous, S., Jin, W., Shahid, N., Bhatti, Z. A., Iqbal, A., Abbasi, U., et al. (2018). The Performance of Microbial Fuel Cells Treating Vegetable Oil Industrial Wastewater. *Environ. Tech. Innovation* 10, 143–151. doi:10.1016/j.eti.2018.02.006

Hodgson, D. M., Smith, A., Dahale, S., Stratford, J. P., Li, J. V., Grüning, A., et al. (2016). Segregation of the Anodic Microbial Communities in a Microbial Fuel Cell cascade. *Front. Microbiol.* 7, 699. doi:10.3389/fmicb.2016.00699

Holmes, D. E., Chaudhuri, S. K., Nevin, K. P., Mehta, T., Methe, B. A., Liu, A., et al. (2006). Microarray and Genetic Analysis of Electron Transfer to Electrodes in *Geobacter Sulfurreducens*. *Environ. Microbiol.* 8, 1805–1815. doi:10.1111/j.1462-2920.2006.01065.x

Jadhav, D. A., Ghadge, A. N., Mondal, D., and Ghangrekar, M. M. (2014). Comparison of Oxygen and Hypochlorite as Cathodic Electron Acceptor in Microbial Fuel Cells. *Bioresour. Tech.* 154, 330–335. doi:10.1016/j.biortech.2013.12.069

Jiang, Y., Deng, H., Huang, X., Zhang, Y., and Zhong, W. (2016). Characterization of a Novel Electrogenic Clostridium Sporogenes Isolated from forest Soil. *Wei Sheng Wu Xue Bao* 56, 846–855. doi:10.13343/j.cnki.wsxb.20150335

Li, B., Zhou, J., Zhou, X., Wang, X., Li, B., Santoro, C., et al. (2014). Surface Modification of Microbial Fuel Cells Anodes: Approaches to Practical Design. *Electrochimica Acta* 134, 116–126. doi:10.1016/j.electacta.2014.04.136

Li, M., Zhou, M., Tian, X., TanMcDaniel, C. C. T., McDaniel, C. T., Hassett, D. J., et al. (2018). Microbial Fuel Cell (MFC) Power Performance Improvement through Enhanced Microbial Electrogenicity. *Biotechnol. Adv.* 36, 1316–1327. doi:10.1016/j.biotechadv.2018.04.010

Li, Z., Zhang, X., Lin, J., Han, S., and Lei, L. (2010). Azo Dye Treatment with Simultaneous Electricity Production in an Anaerobic-Aerobic Sequential Reactor and Microbial Fuel Cell Coupled System. *Bioresour. Tech.* 101, 4440–4445. doi:10.1016/j.biortech.2010.01.114

Liang, P., Duan, R., Jiang, Y., Zhang, X., Qiu, Y., and Huang, X. (2018). One-year Operation of 1000-L Modularized Microbial Fuel Cell for Municipal Wastewater Treatment. *Water Res.* 141, 1–8. doi:10.1016/j.watres.2018.04.066

Lin, W. C., Coppi, M. V., and Lovley, D. R. (2004). *Geobacter Sulfurreducens* Can Grow with Oxygen as a Terminal Electron Acceptor. *Appl. Environ. Microbiol.* 70, 2525–2528. doi:10.1128/aem.70.4.2525-2528.2004

Logroño, W., Ramírez, G., Recalde, C., Echeverría, M., and Cunachi, A. (2015). Bioelectricity Generation from Vegetables and Fruits Wastes by Using Single Chamber Microbial Fuel Cells with High Andean Soils. *Energ. Proced.* 75, 2009–2014. doi:10.1016/j.egypro.2015.07.259

Lopes, P. R., Araújo, K. C. S., Lopes, I. M., Rangel, R. P., Santos, N. F. F., and Kageyama, P. Y. (2014). Uma análise das consequências da agricultura convencional e das opções de modelos sustentáveis de produção –agricultura orgânica e agroflorestal. *REDD –Revista Espaço de Diálogo e Desconexão* 8, 1–38. doi:10.32760/1984-1736/REDD/2014.v8i2.6912

Lovley, R. (1991). Dissimilatory Fe(III) and Mn(IV) Reduction. *Microbiol. Rev.* 55, 259–287. doi:10.1128/mr.55.2.259-287.1991

Lovley, D. R., Holmes, D. E., and Nevin, K. P. (2004). Dissimilatory Fe(III) and Mn(IV) Reduction. *Adv. Microb. Physiol.* 49, 219–286. doi:10.1016/S0065-2911(04)49005-5

Mahdi Mardanpour, M., Nasr Esfahany, M., Behzad, T., and Sedaqatvand, R. (2012). Single Chamber Microbial Fuel Cell with Spiral Anode for Dairy Wastewater Treatment. *Biosens. Bioelectron.* 38, 264–269. doi:10.1016/j.bios.2012.05.046

Mansoorian, H. J., Mahvi, A. H., Jafari, A. J., Amin, M. M., Rajabizadeh, A., and Khanjani, N. (2013). Bioelectricity Generation Using Two Chamber Microbial Fuel Cell Treating Wastewater from Food Processing. *Enzyme Microb. Tech.* 52, 352–357. doi:10.1016/j.enzmictec.2013.03.004

Ministerio de Ambiente y Desarrollo Sostenible (2015). *Resolución 631. Capitulo VI. Artículo 9. Parámetros fisicoquímicos y sus valores límites máximos permisibles en los vertimientos puntuales de aguas residuales no domésticas (ARND) a cuerpos de aguas superficiales. Sector Agroindustria.*

Oon, Y.-L., Ong, S.-A., Ho, L.-N., Wong, Y.-S., Oon, Y.-S., Lehl, H. K., et al. (2015). Hybrid System Up-Flow Constructed Wetland Integrated with Microbial Fuel Cell for Simultaneous Wastewater Treatment and Electricity Generation. *Bioresour. Tech.* 186, 270–275. doi:10.1016/j.biortech.2015.03.014

Palanisamy, G., Jung, H.-Y., Sadhasivam, T., Kurkuri, M. D., Kim, S. C., and Roh, S.-H. (2019). A Comprehensive Review on Microbial Fuel Cell Technologies: Processes, Utilization, and Advanced Developments in Electrodes and Membranes. *J. Clean. Prod.* 221, 598–621. doi:10.1016/j.jclepro.2019.02.172

Pérez, M. (2018). *Nueva Generación de Materiales Plásticos Basados en ABS de Altas Prestaciones Técnicas o más Sostenibles con el Medio Ambiente. Tesis doctoral. Doctorado Industrial en Química*. España: Universidad Autónoma de Barcelona.

Pokusaeva, K., Fitzgerald, G. F., and van Sinderen, D. (2011). Carbohydrate Metabolism in *Bifidobacteria*. *Genes Nutr.* 6, 285–306. doi:10.1007/s12263-010-0206-6

Rabaey, K., Lissenns, G., and Verstraete, W. (2011). "Microbial Fuel Cells: Performances and Perspectives," in *Biofuels for Fuel Cells: Biomass Fermentation towards Usage in Fuel Cells*. Editors P. Lens, P. Westermann, M. Haberbauer, and A. Moreno (London: IWA Publishing).

Rodriguez, N., Sanz, J. R., Oliveros, C., and Ramirez, C. A. (2015). *Beneficio del café en Colombia Prácticas y estrategias para el ahorro, uso eficiente del agua y el control de la contaminación hídrica en el proceso de beneficio húmedo del café*. Manizales, Colombia: Federación Nacional de Cafeteros.

Romero, A., Vásquez, J., and Lugo, A. (2012). Bacterias, fuente de energía para el futuro. *Tecnura* 16, 117–142.

Ryngajłło, M., Kubiak, K., Jędrzejczak-Krzepkowska, M., Jacek, P., and Bielecki, S. (2019). Comparative Genomics of theKomagataeibacterstrains-Efficient Bionanocellulose Producers. *MicrobiologyOpen* 8, e00731. doi:10.1002/mbo3.731

Said, N. S. M., Abdullah, S. R. S., IsmailHasan, N. I. H. A., Hasan, H. A., and Othman, A. R. (2020). Phytoremediation of Real Coffee Industry Effluent through a Continuous Two-Stage Constructed Wetland System. *Environ. Tech. Innovation* 17, 100502. doi:10.1016/j.eti.2019.100502

Samsudeen, N., Radhakrishnan, T. K., and Matheswaran, M. (2015). Bioelectricity Production from Microbial Fuel Cell Using Mixed Bacterial Culture Isolated from Distillery Wastewater. *Bioresour. Tech.* 195, 242–247. doi:10.1016/j.biortech.2015.07.023

Shelobolina, E. S., Nevin, K. P., Blakeney-Hayward, J. D., Johnsen, C. V., Plaia, T. W., Krader, P., et al. (2007). *Geobacter Pickeringii* Sp. nov., *Geobacter Argillaceus* Sp. Nov. And *Pelosinus Fermentans* Gen. nov., Sp. nov., Isolated from Subsurface Kaolin Lenses. *Int. J. Syst. Evol. Microbiol.* 57, 126–135. doi:10.1099/ijs.0.64221-0

Shelobolina, E. S., Vrionis, H. A., Findlay, R. H., and Lovley, D. R. (2008). *Geobacter Uraniireducens* Sp. nov., Isolated from Subsurface Sediment Undergoing Uranium Bioremediation. *Int. J. Syst. Evol. Microbiol.* 58, 1075–1078. doi:10.1099/ijs.0.65377-0

Srivastava, P., Yadav, A. K., and Mishra, B. K. (2015). The Effects of Microbial Fuel Cell Integration into Constructed Wetland on the Performance of Constructed Wetland. *Bioresour. Tech.* 195, 223–230. doi:10.1016/j.biortech.2015.05.072

Varanasi, J. L., Sinha, P., and Das, D. (2017). Maximizing Power Generation from Dark Fermentation Effluents in Microbial Fuel Cell by Selective Enrichment of Exoelectrogens and Optimization of Anodic Operational Parameters. *Biotechnol. Lett.* 39, 721–730. doi:10.1007/s10529-017-2289-2

Voora, V., Bermúdez, S., Larrea, C., and Balinõ, S. (2020). *Global Market Report: Coffee*. Winnipeg, MB: International Institute for Sustainable Development IISD. Availabe at: https://www.iisd.org/system/files/publications/ssi-global-market-report-coffee.pdf (Accessed December 24, 2021).

Walter, X. A., Forbes, S., Greenman, J., and Ieropoulos, I. A. (2016). From Single MFC to cascade Configuration: The Relationship between Size, Hydraulic Retention Time and Power Density. *Sustainable Energ. Tech. Assessments* 14, 74–79. doi:10.1016/j.seta.2016.01.006

Winfield, J., Gajda, I., Greenman, J., and Ieropoulos, I. (2016). A Review into the Use of Ceramics in Microbial Fuel Cells. *Bioresour. Tech.* 215, 296–303. doi:10.1016/j.biortech.2016.03.135

Winfield, J., Greenman, J., Huson, D., and Ieropoulos, I. (2013). Comparing Terracotta and Earthenware for Multiple Functionalities in Microbial Fuel Cells. *Bioproc. Biosyst Eng* 36, 1913–1921. doi:10.1007/s00449-013-0967-6

Yang, P., Peng, Y., Tan, H., Liu, H., Wu, D., Wang, X., et al. (2021). Foaming Mechanisms and Control Strategies during the Anaerobic Digestion of Organic Waste: A Critical Review. *Sci. Total Environ.* 779, 146531. doi:10.1016/j.scitotenv.2021.146531

Yousefi, V., Mohebbi-Kalhori, D., and Samimi, A. (2017). Ceramic-based Microbial Fuel Cells (MFCs): A Review. *Int. J. Hydrogen Energ.* 42, 1672–1690. doi:10.1016/j.ijhydene.2016.06.054

Zang, G.-L., Sheng, G.-P., Li, W.-W., Tong, Z.-H., Zeng, R. J., Shi, C., et al. (2012). Nutrient Removal and Energy Production in a Urine Treatment Process Using Magnesium Ammonium Phosphate Precipitation and a Microbial Fuel Cell Technique. *Phys. Chem. Chem. Phys.* 14, 1978–1984. doi:10.1039/C2CP23402E

Conflict of Interest: The authors declare that the research was conducted in the absence of any commercial or financial relationships that could be construed as a potential conflict of interest.

Publisher's Note: All claims expressed in this article are solely those of the authors and do not necessarily represent those of their affiliated organizations, or those of the publisher, the editors and the reviewers. Any product that may be evaluated in this article, or claim that may be made by its manufacturer, is not guaranteed or endorsed by the publisher.

frontiers | Frontiers in Chemical Engineering

ORIGINAL RESEARCH
published: 17 May 2022
doi: 10.3389/fceng.2022.832505

Bioelectrochemical Treatment Technology—The New Practical Approach for Wastewater Management and GHG Emissions Reduction

Sofia Babanova[1], Jason Jones[1], Kelly Wiseman[1], Jaime Soles[1], Jaime Garcia[2], Pedro Huerta[2], Daniel Barocio[2], Ryoji Naito[2], Orlando Arreola[2], Gerardo Garcia[2] and Orianna Bretschger[1]*

[1]Aquacycl Inc., Escondido, CA, United States, [2]D4C Product Development, San Diego, CA, United States

OPEN ACCESS

Edited by:
Eileen Hao Yu, Loughborough University, United Kingdom

Reviewed by:
Thierry Ribeiro, UniLaSalle, France
Osvaldo Frutos, National University of Asunción, Paraguay

***Correspondence:**
Sofia Babanova
sbabanova@aquacycl.com

Specialty section:
This article was submitted to Sustainable Process Engineering, a section of the journal Frontiers in Chemical Engineering

Received: *09 December 2021*
Accepted: *24 February 2022*
Published: *17 May 2022*

Citation:
Babanova S, Jones J, Wiseman K, Soles J, Garcia J, Huerta P, Barocio D, Naito R, Arreola O, Garcia G and Bretschger O (2022) Bioelectrochemical Treatment Technology—The New Practical Approach for Wastewater Management and GHG Emissions Reduction. Front. Chem. Eng. 4:832505. doi: 10.3389/fceng.2022.832505

This study presents BioElectrochemical Treatment Technology (BETT) as a new wastewater management solution toward the Net-Zero future. The results reported herein were collected from a BETT pilot system installed at a large brewery in Los Angeles, CA, United States processing 0.6 m^3. day^{-1} of raw brewery wastewater with a high content of fruit pulp. Removal of Chemical Oxygen Demand (COD), Total Suspended Solids (TSS) and protein in mg.L^{-1} per day or percentage were evaluated over 2 months of continuous operation of the Demo Unit. The GHG emissions associated with the power consumed, biomass produced, and carbon dioxide emitted were estimated and compared to aerobic and anaerobic solutions. It was demonstrated that BETT can process wastewater with higher organic load than most conventional anaerobic systems. The inflow COD loading varied between 48,550 mg/L to 116,200 mg/L, and BETT achieved up to 33% COD removal in 4-h HRT. The TSS removal reached values as high as 79% with incoming TSS concentrations up to 34,000 mg/L TSS. BETT did not directly generate methane and demonstrated 89 and 49% lower landfill methane emissions than aerobic and anaerobic technologies, respectively. The overall reduction in CO_2 emissions, both direct and indirect, was estimated to be 85–90% compared to existing practices.

Keywords: Wastewater treatment (WWT), Microbial fuel cells (MFC), pilot scale, carbon dioxide emission reduction, Greenhouse gas (GHG) reduction, Aquacycl

INTRODUCTION

Life on Earth is not possible without access to fresh water. Society requires water for survival, daily routines (shower, cooking, hygiene, cleaning, etc.) and industrial processes (manufacturing, clean in place practices, etc.). No part of modern daily life would be possible without water and all daily activities release wastewater.

Wastewater is a valuable resource. However, wastewater requires purification and recovery of useful components to enable water reuse. Many wastewater constituents cannot be released into the environment until properly treated. Thus, the importance of wastewater treatment is two-fold: to restore the water supply and to protect the planet from pollution.

Wastewater management was developed in the 20th century. In 1912 the Eighth Report of the Royal Commission on Sewage Disposal introduced the concept of Biochemical Oxygen Demand (BOD) and established standards and tests to be applied to sewage and sewage effluents which were copied by many other countries (The Eight Report Of The Royal Commission On Sewage Disposal, 1912). Biological wastewater treatment was developed as a concept in 1895 in the form of septic tanks and trickling filters, followed by activated sludge treatment in 1913 (Lofrano and Brown, 2010). The treatment concepts further led to the development of Upward-flow anaerobic sludge blanket (UASB), Membrane biological reactors (MBRs), Sequencing Batch Reactors (SBR) and Moving Bed Biofilm Reactors (MBBRs). Unfortunately, few major advances toward improving wastewater treatment were realized in the 21st century. However, concurrently industrial processes and residential populations continue to grow and produce new, high-strength waste streams that challenge current wastewater practices.

High-Strength Wastewater

Conventional aerobic and anaerobic wastewater treatment technologies are limited in their abilities to remove high concentrations of BOD from wastewater. The main constraint for aerobic systems comes from the limited amount of oxygen that can be dissolved in water (Buchanan and Seabloom, 2004). To maintain efficient treatment conditions in aerobic processes, large quantities of oxygen must be provided and adequately mixed into water. For example if the influent has BOD of 10,000 mg.L^{-1} then 10,000 mg.L^{-1} of dissolved oxygen must be provided in order to satisfy the oxygen demand. Regardless of how creative engineers can be, an oxygen supply at that rate is physically impossible.

Anaerobic technologies have a higher capacity for removing BOD in wastewater and can tolerate higher organic loads (Lier et al., 2008; Evren et al., 2011). However, conventional anaerobic processes also face limitations. The higher BOD of the influent can cause the accumulation of Volatile Fatty Acids (VFAs) in anaerobic digesters (ADs). High VFA concentrations in the wastewater can cause a rapid decrease in pH, which has detrimental effects on the anaerobic microbial community and specifically on the *methanogenic archaea* responsible for biogas production (Franke-Whittle et al., 2014; Moeller and Zehnsdorf, 2016).

Herein we describe a BioElectrochemical Treatment Technology (BETT®) as an industrial pre-treatment strategy for high-BOD wastewaters. BETT systems are the core product of Aquacycl Inc. (https://www.aquacycl.com). Aquacycl is a for-profit entity providing wastewater treatment solutions to address challenging wastewater problems.

BETT systems are based on Microbial Fuel Cell (MFC) principles (Verstraete and Rabaey, 2006; Du et al., 2007). In BETT systems, like MFCs, the organic matter is oxidized at the anode surface. Electrons, protons and carbon dioxide are released during the oxidation process. Protons travel through the solution from the anode to the cathode in a single chamber reactor. Electrons travel through an external circuit also from the anode to the cathode where they combine with protons and oxygen from air to generate new water or hydrogen peroxide. Thus, BETT converts organic pollutants in wastewater to dissolved carbon dioxide, direct electricity and water or hydrogen peroxide.

BETT by nature is a "hybrid" of anaerobic and aerobic biological degradation of organic matter and electrochemical oxidation and reduction reactions. The organic oxidation at the anode is performed under anaerobic conditions. However, oxygen is required at the cathode to complete the electrochemical reactions in the system. Oxygen is supplied via natural diffusion of air through a gas-diffusion electrode (Bidault et al., 2009), but does not penetrate the bulk solution to create an aerobic environment in the system. Using a gas-diffusion electrode as a cathode facilitates high-rate electrochemical reactions and eliminates the need for dissolving oxygen in water for an aerobic treatment process. This enables the processing wastewater with higher organic loads.

Methanogenesis does not occur in BETT systems and so the technology does not suffer from "toxicity" events because of the accumulation of VFAs. To the contrary, VFAs are a desired intermediate product as they are bio-electrochemically oxidized at the anode surface by specific types of bacteria known as electrogenic bacteria (Logan, 2009; Babanova et al., 2020).

The ideal application for BETT systems are small volumes (0.6—600 m^3. day^{-1}) of high-strength wastewater (5,000—150,000 mg.L^{-1}-BOD) or wastewaters that have challenging in compositions organics, for example wastewater from the production, storage and transportation of oil and gas products. Although BETT systems can treat low strength wastewaters (<300 mg.L^{-1}-BOD), they are not economically favorable for these applications when compared to conventional aerobic methods such as membrane bioreactors.

Further, the BOD removal efficiency of BETT systems is significantly reduced when the BOD content in wastewater is less than 150 mg.$L^{-1.}$ Therefore, BETT systems are not considered as a replacement for conventional wastewater treatment technologies, but as a pre-treatment solution to enable downstream technologies to function with less energy consumption, less sludge production, and therefore lower greenhouse gas emissions.

The treatment time in BETT systems varies between 4- and 20-h Hydraulic Retention Times (HRT) under continuous flow conditions. The wide range of time is a function of the composition and/or BOD concentration of the incoming wastewater. Wastewaters with higher BOD and organic solids content will require longer HRTs, such as12-20 h. The same requirement will be applicable for wastewaters with complex or difficult to biodegrade organic compositions. Wastewaters with low BOD and low Total Suspended Solids (TSS) concentrations can be treated in shorter HRTs (4–6 h).

GHG Emissions

All wastewater treatment processes result in the emissions of greenhouse gasses (GHGs) such as carbon dioxide, methane and nitrous oxide (Campos et al., 2016). The majority of the GHG emissions come from the biological degradation of the organic

matter, as a result of the energy demand of the treatment and from the degradation of secondary biomass (Mamais et al., 2015).

According to the Department for Environment Food and Rural Affairs of United Kingdom, in 2008 the GHG emissions associated with wastewater management were between 3.3 $MTCO_2e$ and 4.3 $MTCO_2e$, where 0.2 $MTCO_2e$ were a result of the wastewater pumping/collection, 2.1 $MTCO_2e$ were generated during the wastewater treatment, and 1–2 $MTCO_2e$ came from the landfill application of sludge (Rothausen and Conway, 2011).

Studies have reported that water-related energy use in the US accounts for nearly 5% of total GHG emissions (Rothausen and Conway, 2011)—a figure that is rarely highlighted in climate discussions. However, reduction of greenhouse gas (GHG) emissions throughout the water and wastewater supply chain can be achieved by innovating and optimizing existing practices (Campos et al., 2016).

Aerobic wastewater treatment is extremely energy intensive and generates significant amounts of biomass, carbon dioxide, methane and nitrous oxide emissions (Henze et al., 1995; Campos et al., 2016) with only 1% of the incoming BOD being emitted as methane (Campos et al., 2016). The primary contributor to GHG gases in aerobic technologies is their direct emissions during the treatment process with nitrous oxide being the highest contributor (Mamais et al., 2015; Campos et al., 2016).

The second large contributor to GHG emissions in aerobic treatment is the energy usage. The high energy demand of activated sludge systems typically comes from the requirement of forcing air into water to catalyze the biological consumption of organics. Aeration processes account for 50–60% of the electricity consumption of a given activated sludge plant (Mamais et al., 2015; Chen et al., 2018). Up to 3% of the total US electricity consumption comes from aerobic wastewater treatment plants (McCarty et al., 2011).

Methane and carbon dioxide are emitted when anaerobic digestors are used for wastewater treatment. Biogas generated from ADs can be captured, purified, and sent into a natural gas line or combusted to generate electricity and heat. The latter makes ADs a "cleaner" solution to the GHG problem (Bracmort, 2010; Zaks et al., 2011). Unfortunately, the combustion devices are expensive and inefficient, with the efficiency of the cogeneration processes only reaching 30% (Bracmort, 2010).

In addition to the lower conversion efficiency of methane to electricity, a significant loss of dissolved methane in the effluents was reported as a main contributor of GHG emissions for conventional anaerobic systems (Chen et al., 2018). If methane is not effectively harnessed, or facultative lagoons are used for treatment, carbon dioxide and methane are directly released in the atmosphere contributing to the greenhouse effect.

In BETT processes the anaerobic biological degradation of the organic contaminants does not result in methane generation, and significant reduction in carbon dioxide emissions is realized when compared to current wastewater management practices.

BETT systems consume significantly less power compared to conventional treatment technologies. Low power consumption is due to three major features: i) Passive air supply through the gas-diffusion cathode (no energy input for aeration); ii) Gravity flow and the use of equipment with very low power demands; and iii) BETT generates direct electricity during the treatment process, which can be used to offset the power demand of the system.

The power consumed for the treatment of 1 kg-BOD with BETT systems ranged between 0.1 and 0.2 $kWh.kg\text{-}BOD^{-1}$ (estimated in this study) compared to 0.5–0.7 $kWh.kg\text{-}BOD^{-1}$ for anaerobic digestors and 2.2–6.2 $kWh.kg\text{-}BOD^{-1}$ for aerobic treatment (USDA, 2007; Haas et al., 2018).

The anaerobic conditions and the controlled manner of the oxidation process at the anode in BETT reactors also adds to the benefit of less secondary biomass generation (He et al., 2017). The amount of secondary biomass produced from BETT systems is 5.1% from the BOD removed versus 10% from ADs and 45% from aerobic technologies (Henze et al., 1995). Therefore, BETT contribution to landfill methane emissions is significantly lower than anerobic and anaerobic technologies.

The advantages of a microbial fuel cell approach to wastewater treatment, relative to conventional technologies, are very well described by Gude in his 2016 review (Gude, 2016). Trapero et al. (Trapero et al., 2017) also give some insights into the economic value of MFCs in wastewater treatment and their path to commercialization.

BETT Demonstrations to Date

BETT systems were described and evaluated in previous pilot scale demonstrations (Babanova et al., 2019, 2020; Babanova, 2020). The first BETT pilot was installed in 2015 for the treatment of swine wastewater at a small farm (Babanova et al., 2019). This pilot demonstrated the unique design of BETT systems, the inoculation strategy and principle of BETT operation. The study focused on influent and effluent composition, conversion principles and treatment rates. The microbial composition of the anodic and cathodic microbial populations was also investigated in detail.

The article entitled "New perspectives in sugar industry wastewater treatment" published in International Sugar Journal in 2020 (Babanova, 2020) describes a case study of BETT system treating wastewater from a confectionary plant. The focus on this study was to demonstrate the feasibility of BETT for the treatment of wastewater with extremely high organic content. The Chemical Oxygen Demand (COD) of sugarwater treated was in the range of 100,000–300,000 $mg.L^{-1}$. The biomass generated from BETT pilot was established to be only 0.03–2.5% of the COD removed. The total biomass generated from BETT ranged between 4 and 112 $mg.L^{-1}$ as Volatile Suspended Solids (VSS). The same COD removal realized from anaerobic digestion is anticipated to result in 381 to 4,615 $mg.L^{-1}$ VSS. Aerobic treatment would result in 1,522 to 18,462 $mg.L^{-1}$ VSS (assuming identical COD loading in all cases).

The 2020 study described in Water Environment and Technology focused on the applicability of BETT systems as an industrial pre-treatment step to anaerobic digestion (Babanova et al., 2020). Using BETT to normalize the AD feedstocks can increase biogas production and treatment efficiencies for the AD. BETT reduces the COD load to the AD, enriches the wastewater with VFA, reduces the variability

in feedstock concentration and composition, and reduces or eliminates the effect of nitrate and nitrite as competing reactions in ADs.

This current study further demonstrates the ability of BETT systems to treat high-COD wastewaters. The BETT Demonstration Unit (Demo Unit) was installed at a large brewery in Los Angeles, CA, and processed 0.6 m^3. day^{-1} of brewery wastewater. The brewery wastewater was characterized with high organic (COD of 50,000–100,000 $mg.L^{-1}$), protein (>4,000 $mg.L^{-1}$) and solids content (TSS > 10,000 $mg.L^{-1}$), which makes this specific waste stream impossible for aerobic treatment and very challenging for ADs due to the solids content.

In addition, GHG emissions associated with operations of the BETT system were evaluated to characterize the carbon footprint and compare against existing wastewater management practices. GHG emissions are rarely considered or reported when wastewater treatment solutions are discussed. The GHG emissions associated with the power consumed, biomass produced, and carbon dioxide emitted by BETT units were estimated and compared to aerobic and anaerobic solutions.

MATERIALS AND METHODS

BETT Reactor Design

Each BETT reactor was composed of plastic body, anode assembly, cathodes, and cathode holders (**Supplementary Figure S1**). BETT reactor design was developed by Aquacycl and is covered by non-provisional patent US D875,207.

The plastic body had a rectangular shape with internal dimensions: 25 cm × 19 cm × 16.5 cm, and volume of 7.9 L with an inflow and outflow openings. BETT reactor body was manufactured by injection molding technique using ABS plastic material. The reactor body manufacturing was done by a subcontractor in South Korea and the final reactor assembly was performed at Aquacycl.

The anode assembly had twenty-eight anode units electrically connected in series. Each anode unit had branched electrode structural design in which conductive textile material (Zoltek PW06), having high surface area that provides improved microbial adhesion, was configured around a conductive core. Carbon textile material 15 cm in height and 2.5 cm in diameter was used for microbial adhesion surfaces and Ti-wire (Grade 2 polished titanium wire, diameter 1 mm) was used for the stem. The anode unit design and configuration were also developed and patented by Aquacycl (US2020036029A1). The manufacturing of the anode units was done by a subcontractor in Mexico.

Two gas-diffusion cathodes (19 cm × 28 cm, geometric surface area 532 cm^2) were placed on both sides of the reactor and connected in series. The material composition and design of the gas-diffusion cathodes is an Aquacycl trade secret. The cathodes were manufactured at Aquacycl facility in Escondido, CA, United States.

Demonstration Unit Design

The Demo Unit used in this study was a skid-mounted, automated pilot unit, designed to continuously process 0.6 m^3. day^{-1} of wastewater. The Demo Unit was equipped with equalization, supply, feeder and collection tanks, and twelve BETT reactors connected in hydraulic series with a consecutive flow of the wastewater from Reactor 1 to Reactor 12 (**Figure 1**; **Supplementary Figure S2**). The overall volume of the system was 350 L.

The untreated brewery wastewater was first collected into a storage tank. Sodium bicarbonate was added to the storage tank to improve conductivity and increase pH of the wastewater. The wastewater was then fed into the equalization tank of the Demo Unit. Further pH adjustment was performed in the supply tank using 10 M sodium hydroxide. Bluelab pH controller was used for automatic pH adjustment in the supply tank.

The waste stream was transferred to the elevated feeder tank and gravity-fed into the reactors A peristaltic pump was used to control the outflow rate. Treated effluents from the system were collected in the collection tank and discharged to sanitary sewer.

The hydraulics operation of the Demo Unit was fully automated and controlled by Programmable Logic Controller (PLC) and remotely monitored and controlled via Web User Interface. BETT reactor operation and evaluation was executed by specifically designed firmware able to switch resistors, measure voltage and perform polarization measurements.

Demo Unit Inoculation and Operation

The Demo Unit was installed and operated at brewery facility located in Los Angeles, California and used to continuously process 0.6 m^3. day^{-1} of brewery wastewater with high COD and TSS content. The Demo Unit was inoculated and enriched for 1 month and operated under continuous mode for an additional 2 months. The system was fully exposed to the environment.

Demo Unit Inoculation

The system was inoculated with brewery wastewater, anaerobic activated sludge and lagoon sediment. The chemical composition of the brewery wastewater used for inoculation is shown in **Table 1**.

The system was first filled with 200 L of brewery wastewater. The pH of the wastewater was adjusted to 6.34 with 10 M NaOH. Anaerobic activated sludge (19 L) and lagoon sediment (0.6 L) separately mixed in distilled water were introduced into the feeder tank.

Demo Unit Operation

For the first 30 days, the system was operated in a batch mode with recirculation of the inoculum solution through the equalization tank and BETT reactors at a flow rate of 0.38 L. min^{-1}. The anode and the cathode of each reactor were initially connected to 47,000 Ω resistor. The resistor magnitude was subsequently lowered to 4,000 Ωat day 8; 1,143 Ω at day 15 and 400 Ω at day 21.

After 30 days, the operation was switched from batch to continuous flow mode. For the duration of the continuous

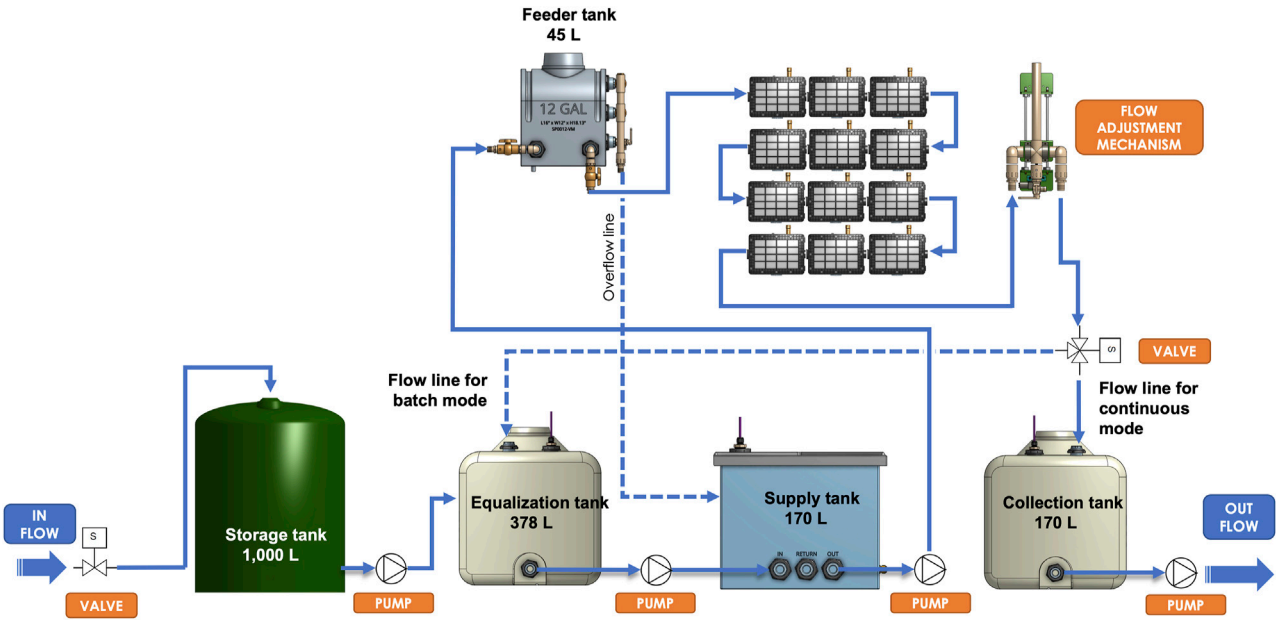

FIGURE 1 | Hydraulic diagram of BETT Demo Unit.

TABLE 1 | Inoculum chemical composition.

Parameter	Unit	Value
Total Chemical Oxygen Demand	mg/L	108,200
Soluble Chemical Oxygen Demand	mg/L	107,600
pH	—	6.34
Conductivity	mS/cm	4.34
Sulfide	mg/L	< LOD
Sulfate	mg/L	75
Nitrate	mg/L	< LOD
Nitrite	mg/L	0.015
Ammonium	mg/L	94
Phosphate	mg/L	520
Volatile Fatty Acids	mg/L	1,990
Protein	mg/L	5,715
Total Suspended Solids	mg/L	2,000

LOD: Limit of Detection.

mode the resistor was predominantly 400 Ω and was lowered to 200 Ωat day 85 and 114 Ω at day 86.

Electrochemical Characterization

The voltage (V) across an external resistor for each reactor was monitored in 30 min intervals using specifically designed automated measurement system. The reactors were periodically disconnected to measure open circuit potential (OCP) of the electrodes and perform polarization measurements.

Polarization measurements were carried out by varying the external resistance from open circuit to 8 Ω in 5 min intervals. The voltage of the reactor as well as the electrodes potentials were measured with each resistor applied. Current (I) and power (P) were calculated using Ohm's law (I = V/R and P=V*I).

The current and power densities of each individual reactor were calculated as the current of the reactor normalized to the cathodes geometric surface area (0.1604 m^2).

Sampling and Chemical Analyses

The Demo Unit was equipped with two sampling ports, for sampling the inflow and outflow of the system. The inflow sampling port was positioned on the feeder box before the wastewater entered BETT reactors. Note that the wastewater had been pH adjusted at that point. The outflow sampling port was positioned after the BETT reactors before the treated wastewater was collected into the collection tank and discharged into sewer. Samples were collected manually, transported under ice and tested at Aquacycl lab facility. Periodically samples were analyzed at an EPA certified lab (Enviromatrix Analytical Inc., San Diego, CA, United States).

During the enrichment phase when the system was operated under batch mode, samples were collected periodically from the inflow sampling port. During continuous mode of operation, samples were collected from the inflow sampling port and 4 h later (representing total hydraulic retention time, HRT, in the system), from the outflow sampling port as representative for influent and effluent samples. Samples were collected at least once a week during continuous mode.

Chemical Oxygen Demand (COD) of influent and effluent samples were periodically analyzed using Hach DR850 and DR900 instruments following Hach Method 8,000. Total Suspended Solids (TSS) was quantified using EPA method 160.2. Protein concentration was measured using.

Pierce™ BCA Protein Assay Kit according to Thermo Scientific Method 23225. Volatile Fatty Acids were analyzed with Hach Volatile Acids TNTplus Vial Test (50–2,500 mg/L) as acetate and

Hach Method 10240. Phosphate was determined with Hach PhosVer® 3 Phosphate Reagent Powder Pillows and Hach Method 8,048. pH and conductivity were measured with Hach HQ40D Portable Multi Meter and IntelliCAL PHC201 Laboratory General Purposes Gel Filled pH Electrode and IntelliCAL CDC401 Laboratory 4-Poles Graphite Conductivity Cell, respectively.

Biological Oxygen Demand (BOD), sulfate, sulfide, nitrite, nitrate and Volatile Suspended Solids (VSS) analyses were outsourced to an EPA certified lab (Enviromatrix Analytical Inc., San Diego, CA, United States).

COD removal rate, COD removal efficiency, TSS removal efficiency TSS loading and biomass produced were calculated as indicated in **Supplemental Material**.

GHG Emissions Calculations

The estimation of GHG emissions of BETT Demo Unit was performed following the methodologies established by the US Environmental Protection Agency (RTI International, 2010). For comparison, the GHG emissions released by aerobic and anaerobic treatment practices treating the same BOD load as BETT system were calculated using the same methodologies. Some assumptions were considered, such as: the power consumed by aerobic treatment varies between 2.2 and 6.2 kWh per kg-BOD removed (Haas et al., 2018); the power consumption of anaerobic technologies is in the range of 0.5–0.7 kWh.kg-BOD^{-1} removed (USDA, 2007; Lier et al., 2008). The power consumption of BETT system was measured as 0.1–0.2 kWh-kg-BOD^{-1} removed depending on the season, where the power consumption is higher during the winter and lower during the summer months. The COD removed was assumed as 24,800 mg.L^{-1}, which was the maximum removal established for BETT Demo Unit in this study.

The biomass produced as a function of the BOD removed was assumed to be 45 and 10% for aerobic and anaerobic techniques, respectively (Henze et al., 1995). The biomass produced by BETT Demo Unit was determined to be 5.1% from BOD removed, sludge recovered, and protein content of secondary sludge.

RESULTS AND DISCUSSION

The treatment capacity and energy recovery capabilities of the BETT system was strongly dependent on the mode of operation, e.g., batch versus continuous mode. The data collected during batch and continuous modes were evaluated and compared separately.

During batch mode the wastewater was cycled through the system and periodically refreshed. This mode was important during the enrichment phase as it did not allow for flushing out the bacteria. Unfortunately, during batch mode accumulation of metabolic compounds can be observed, which can slow down the degradation process due to product inhibition. To avoid product inhibition, continuous mode was the preferred mode of operation of BETT systems.

Under continuous mode, fresh wastewater was constantly flowing through the system at 380 ml.min^{-1}. It has been established by other research that during continuous mode the microbial community structure is uniquely organized because of the different environment in each MFC resulting from sequential passing of products between MFCs in series (Chung and Okabe, 2009).

The natural selection of specific bacteria for the given wastewater composition and degradation processes in each individual MFC within a series enhances the efficiency of the overall MFC treatment train.

Batch Mode (Enrichment Phase)

Batch mode was predominantly used during the enrichment phase when the major goal was the development of stable anodic biofilm. Thus, during batch mode the wastewater was recycled through the system for 15 days and partially refreshed at day 15 and day 21.

The COD removal rates during batch mode were estimated in mg.L^{-1} per day and as percentage removal. A batch cycle was also induced when the wastewater was refreshed and/or when the resistor was changed.

COD and VFA Profiles

The COD removal rate during batch mode fluctuated between 914 mg.L^{-1}. day^{-1} and 2,925 mg.L^{-1}. day^{-1} and between 6 and 22% as shown in **Figures 2A,B**. Cycles 1 and 2 had the same wastewater and the resistor was changed form 40,000 Ω to 4,000 Ω at the beginning of cycle 2. Due to the accumulation of secondary metabolites and therefore reduced biological activity, the COD removal rates during cycle 2 were lower. The wastewater was partially refreshed at the beginning of cycles 3 and 4 along with a resistor change to 1,114 and 400 Ω for cycle 3 and 4, respectively. Partially removing the secondary metabolites by refreshing the wastewater was the reason for the higher removal rates during cycle 3. Unfortunately, the partial replenishment was not able to completely remove the inhibitory effect of metabolites and the removal rates remained in the low range.

As we mentioned before in BETT reactors, the complex organics present in the wastewater are transformed into VFAs, which are subsequently oxidized to carbon dioxide, electrons, and protons at the anode surface. Hence, it is expected that the amount of COD will decrease and the concentration of VFA will increase over time. The described trend can be seen in **Figure 2C**, where for day 15 the COD decreased from 108,200 mg.L^{-1} to 78,900 mg.L^{-1} and the VFA concentration increased from 1,990 mg.L^{-1} to 6,363 mg.L^{-1}. **Figure 2C** also confirmed the statement that the accumulation of metabolites slows down the treatment. The COD removal was higher for the first 4 days of the cycle (16,100 mg.L^{-1} COD removed) and decreased to 6,400 mg.L^{-1} COD removed for the last 7 days.

As the anodic biofilm developed and the microbial community acclimated to the brewery wastewater and the anode as a sole electron acceptor, the COD/VFA conversion efficiency reached 100% after day 15 and remained high for the rest of the batch mode (**Figure 2D**). The high conversion efficiency was an indication of successful fermentation and the reduction of

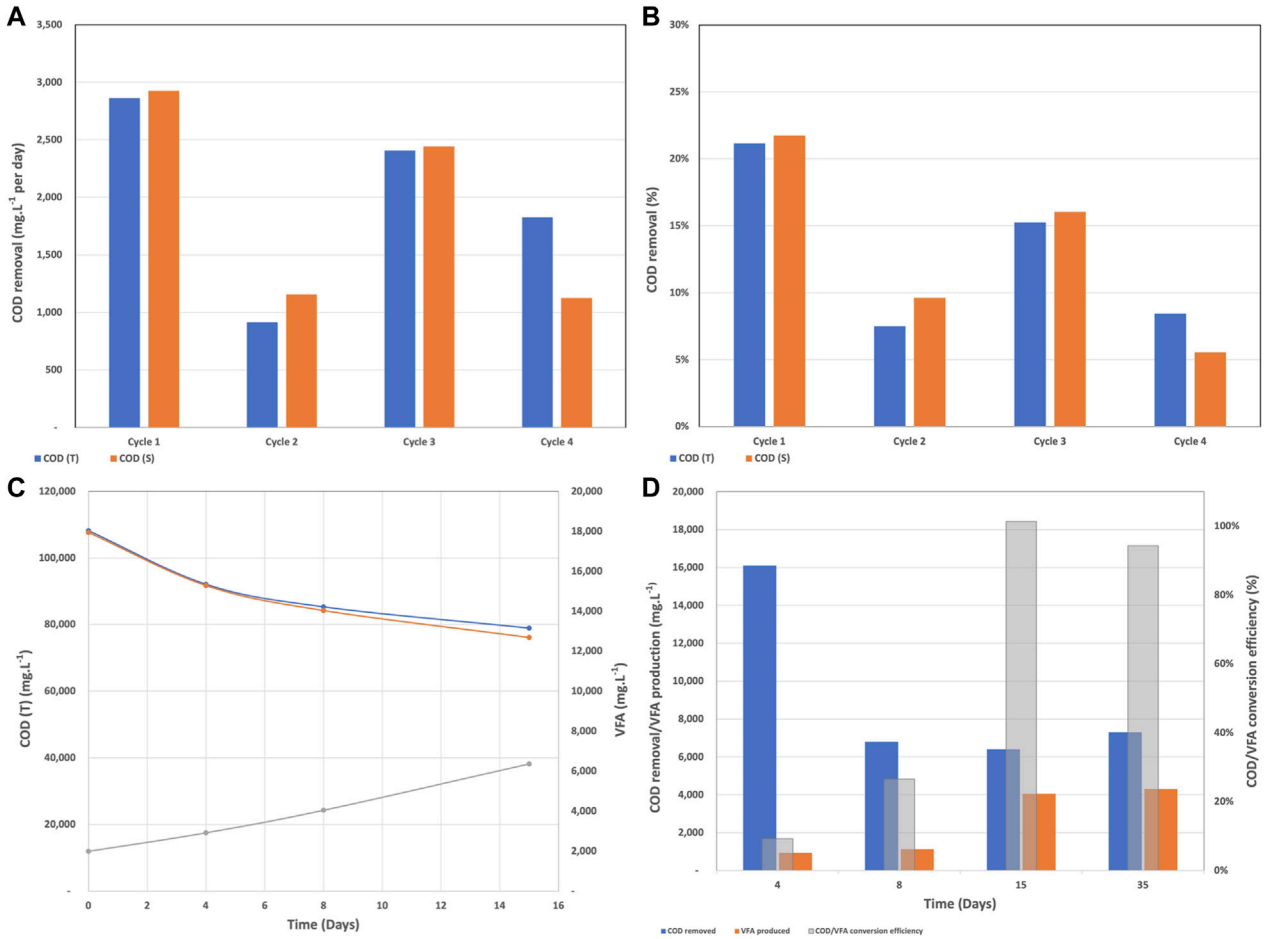

FIGURE 2 | (A) COD removal rate in mg/L per day, **(B)** COD removal rate in percentage, **(C)** COD and VFA trends over the first 15 days, and **(D)** COD to VFA conversion efficiency and removal during batch mode.

COD over time confirmed the bio-electrochemical oxidation at the anode surface.

Electrochemical Characteristics

Periodically, the reactors were disconnected for 1 h and the Open Circuit Potential (OCP) of the anode and the two cathodes were measured versus Ag/AgCl reference electrode. **Figure 3** shows the average OCPs of the anode, left and right cathodes. The average and standard deviation were calculated from the measurements of the twelve BETT reactors.

The electrodes followed the same trend across the twelve BETT reactors, where the cathodic potential decreased rapidly during the first 15 days and remained relatively constant for the rest of the batch mode. The decrease in the cathodic potential may be associated with biofouling of the cathode surface due to the growth of bacteria facilitated by the presence of oxygen (Erable et al., 2012). The high protein content of the wastewater may also have significantly decreased the cathodic potential. Protein molecules are generally hydrophobic and as such can penetrate the hydrophobic pores of the gas-diffusion cathodes and reduce the oxygen transport across the cathode. The reduced oxygen concentration causes decreased cathodic potential similar to biofouling. The brewery wastewater used in this study had high protein content, which for the duration of the batch mode was consistently exceeding 3,000 mg/L (**Supplementary Figure S3**).

The anode was fully developed over the first 15 days as evident by the anodic OCP reaching -527mV *vs.* Ag/AgCl (**Supplementary Figure S4**) for all reactors. It was established that the anodic potential is very sensitive to pH fluctuations with the anodic potential becoming more negative at more neutral pH. Neutral pH values are expected as the optimal pH for microbial communities in MFCs (He et al., 2008).

The daily average current and power densities generated from a single BETT reactor during batch mode are represented in **Supplementary Figure S5**. The maximum current and power densities per BETT reactor reached 4.8 ± 0.9 mA m^{-2} and 9.5 ± 1.7 mW m^{-2}, respectively. Thus, the cumulative current density from the Demo Unit would be 63 mA m^{-2} and 114 mW m^{-2}.

The current and power densities were higher than those recorded by Zhuang at al. treating brewery wastewater with a

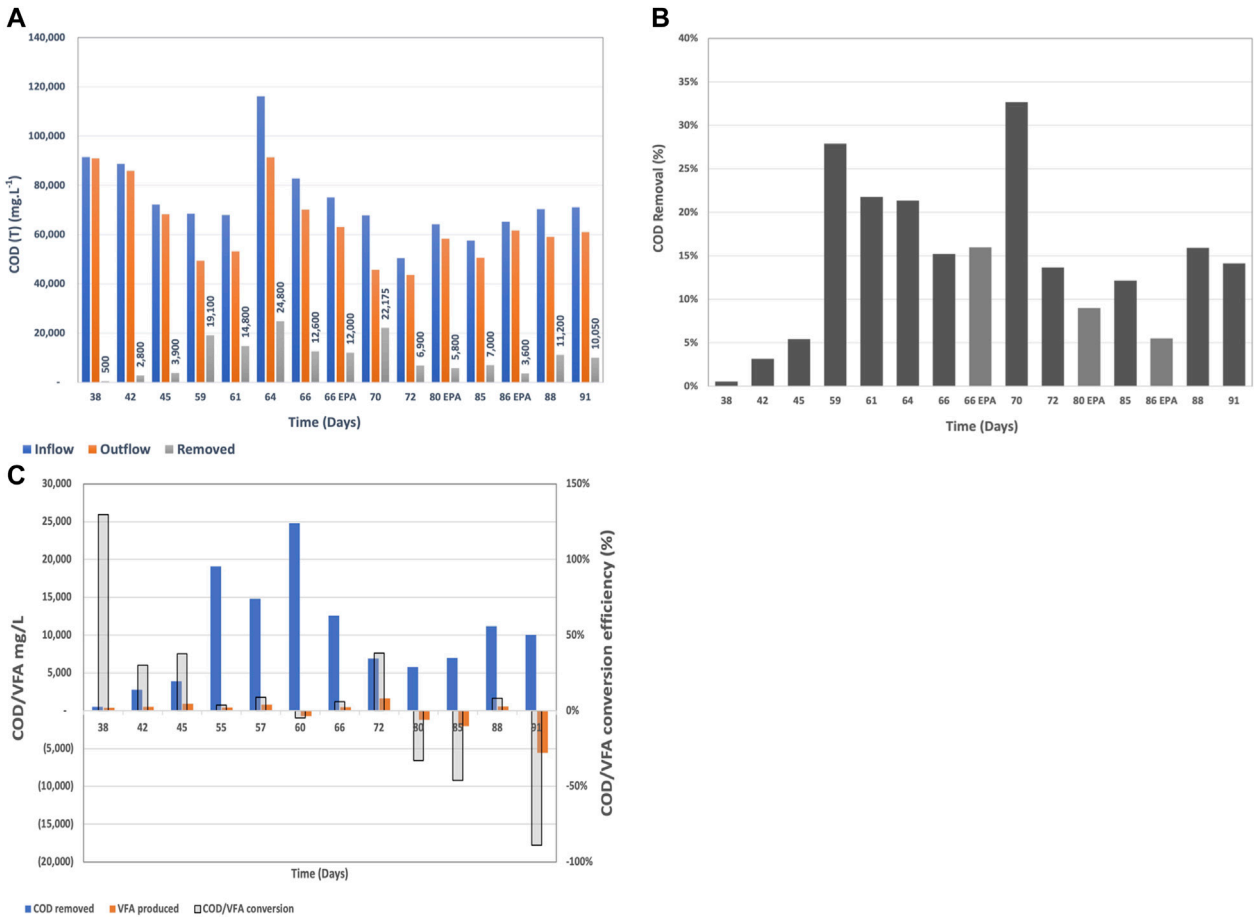

FIGURE 3 | (A) Inflow, outflow COD loading and COD removal rate in mg/L per day, **(B)** COD removal rate in percentage from the inflow COD loading, and **(C)** COD to VFA conversion efficiency and removal during continuous mode.

stack of MFCs (Zhuang et al., 2012). The higher current and power observed with BETT system can be due to the higher organic load for BETT compared to Zhuang (2,120 mg.L^{-1} COD). Feng at al. demonstrated a linear dependence of the generated power from the solution conductivity and Monod dependence of the latter from the substrate concentration (Feng et al., 2008).

Both, the current and power densities followed the same trend of increasing over time as a result of the decreasing resistor load (**Figure 4**). In general, the voltage generated from each BETT reactor was higher along the hydraulic treatment train with reactor 12 showing a higher voltage than reactor 1 (**Supplementary Figure S5**). This is expected given the hypothesis that hydrolysis and fermentation are predominant in the first reactors and the conversion of VFAs to carbon dioxide is carried out mainly within the later subsequent reactors i.e. towards the end of the hydraulic series.

Continuous Mode

On day 35 the system was switched to continuous mode of operation with a constant supply of brewery wastewater and a continuous discharge of the BETT-treated wastewater. The HRT through the twelve BETT reactors was 4 h under continuous flow. Given the short HRT, the small number of reactors in hydraulic series and the high COD concentration of the wastewater, the Demo Unit was targeting a COD removal of 10–15% relative to incoming concentrations.

COD and VFA Profiles

The system required a week to acclimate to the continuous mode, which was reflected by the low COD removal rates until day 45. Once the system was acclimated to the new mode of operation, the COD removal rates were on average 17 ± 8%, which was higher than the targeted COD removal range.

The inflow COD concentration varied between 48,550 mg.L^{-1} and 116,200 mg.L^{-1} depending on the brewing status at the given time. The COD removal varied between 3,600 mg.L^{-1} and 24,800 mg.L^{-1} over the 4 h of residence time and was dependent on the starting COD concentration, pH, temperature and flow rate. Higher inflow COD and neutral pH were associated with higher removal rates. This confirms subsequent studies showing that COD removal (in mg.L^{-1}) is a

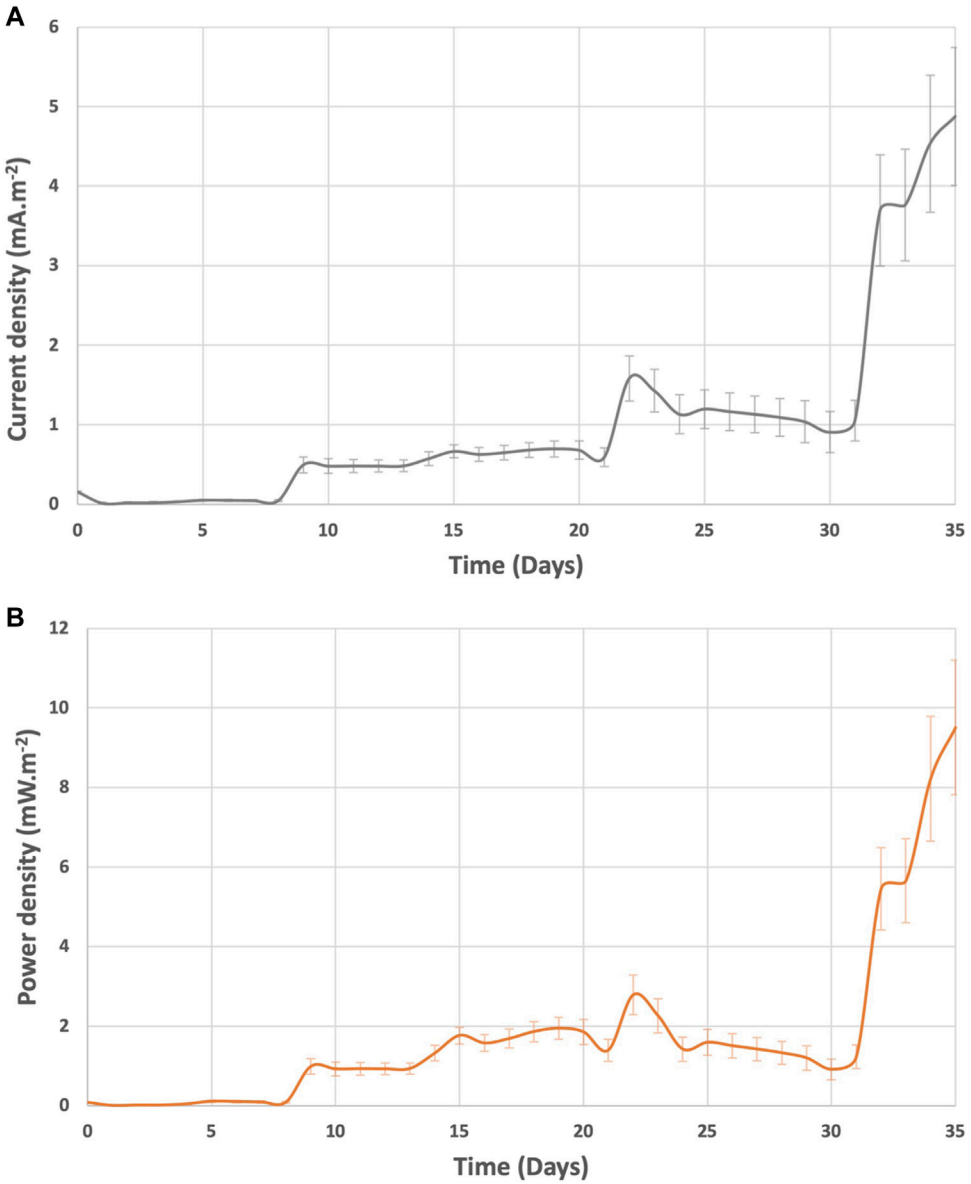

FIGURE 4 | (A) current density and **(B)** power density recorded during batch mode.

function of the incoming COD where higher incoming COD usually induces higher removal rates (Babanova et al., 2019).

The majority of studies involving MFCs for the treatment of brewery wastewater report inflow COD values around 2,000 mg.L^{-1} (Feng et al., 2008; Wang et al., 2008; Zhuang et al., 2012; Dong et al., 2015), which is significantly lower than the COD reported in this study. The highest COD removed from a stack of MFCs under continuous mode treating brewery wastewater was reported to be 989 mg.L^{-1} at a starting inflow concentration of 1,501 mg.L^{-1} (Sun et al., 2010).

To our knowledge, there is no AD that can treat brewery wastewater with COD consistently higher than 45,000 mg.L^{-1} and VFA above 1900 mg.L^{-1}.

The COD to VFA conversion releationship showed a different trend compared to batch mode (**Figure 8**). At the beginning of the continuous mode when the system was still aclimating to the new mode of operation, the COD to VFA conversion efficiency was higher due to the low subsequent oxidation of VFAs to carbon dioxide at the anode surfaces. Thus, VFAs remained in the system and the COD/VFA conversion efficiency appeared higher. Later on, when the VFA removal rates increased due to the acelerated consumption of VFAs at the anode surface, the COD/VFA conversion efficiency appeared as negative. The latter, is a confirmation of the hypothesis that under continuous mode with multiple MFCs connected in hydraulic series, different

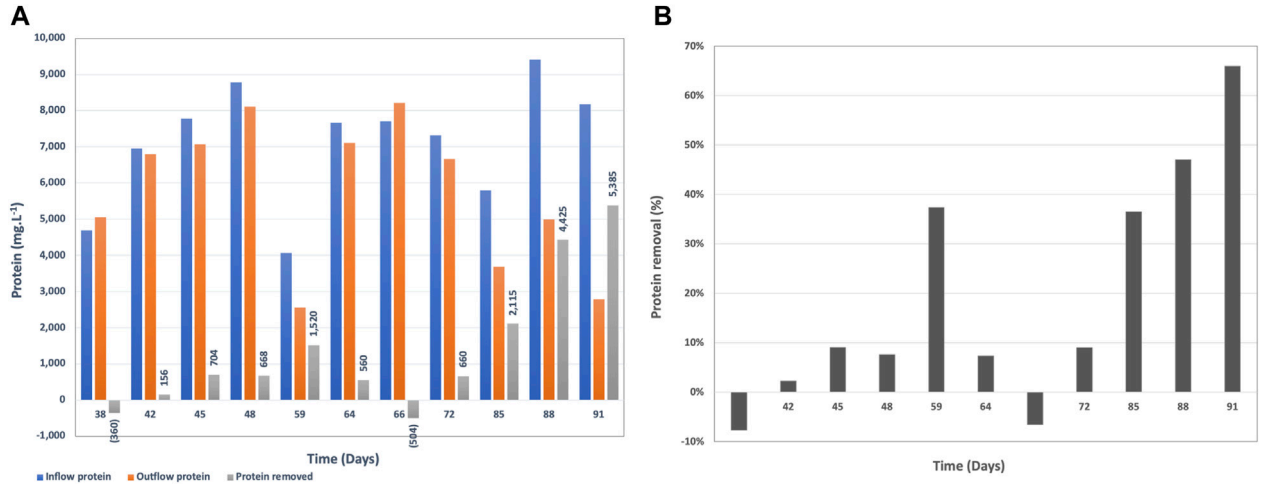

FIGURE 5 | Protein removal rates in **(A)** mg/L and **(B)** percentage during continuous mode.

processes will predominate throught the different reactors within the hydraulic series. Hydrolysis and fermentation will be the dominant processes at the beginning of the reactor series and bioelectrochemical oxidation of VFAs will prevale towards the end of the hydraulic series. This phenomenon has been observed in another Demo Unit also treating brewery wastewater (Babanova et al., 2020).

Protein and TSS Removal

The brewery wastewater in this study contains the centrifugate from the yeast separation after the brewing process. Therefore, it is characterized with high protein content mainly from yeast (**Figure 5A**). This protein is very challenging to break down since it is already a part of the cell structure of yeast. The lowest protein concentration in the inflow wastewater was 4,072 mg.L^{-1} and the highest measured was 9,410 mg.L^{-1}.

The protein removal rate by BETT was in the range of −8–66%, where the negative protein removal was due to biomass growth at the beginning of the continuous mode during the acclimation phase. Removals reached sufficient rates (36–66%) later in the continuous mode (**Figure 5B**).

The high protein concentrations contributed to the reduction of the cathodic performance as indicated by the cathodic OCPs (**Supplementary Figure S4**). A possible solution is to use solids separation or centrifugation prior to wastewater treatment with BETT system. The spent yeast can be used as a feedstock for various industrial applications (Mussatto, 2014). This pre-treatment step can also reduce the amount of solids entering the treatment system.

Total Suspended Solids (TSS) is a regulated parameter for wastewater discharge into sewer, and industries are often facing fees associated with high TSS of the discharged wastewater (United States Environmental Protection Agency, 1992). Therefore, TSS removal is an important parameter in wastewater treatment.

When the TSS is mostly organic, it can be biologically consumed during the treatment process. BETT Demo Unit demonstrated sufficient TSS removal rates after day 72 of system operation (**Figure 6**). TSS removal rates reached up to 26,800 mg.L^{-1} in 4 h HRT, which corresponded to 79% removal. It has to be noted that the incoming TSS was for the most part higher than 10,000 mg.L^{-1} and in some cases was in the range of 20,000 mg.L^{-1} to 34,000 mg.L^{-1} TSS. The high TSS removal rate is partially due to the settling of solids inside the reactors. The solids degradation is usually a slower process compared to the degradation of soluble organics. The accumulated solids ultimately break down but the solids residence time is sufficiently longer than soluble COD.

Electrochemical Characteristics

As noted earlier, the protein molecules can penetrate the hydrophobic channels of the gas-diffusion layer of the cathodes and thus decrease the oxygen supply to the cathode surfaces. The lack of sufficient oxygen at the water-cathode interface allowed for other reduction reactions to take place (sulfate reduction, nitrate reduction, nitrite reduction, etc.), which led to reduced cathodic potential over time (**Supplementary Figure S4**). The cathodic potential was initially reduced during the first 2 weeks of batch mode to approximately -100 mV vs. Ag/AgCl and remained relatively stable until day 60. After day 60, the cathodic potential drastically decreased to—316 mV and -313 mV *vs.* Ag/AgCl for left and right cathodes, respectively. An interesting observation is that the reduction in the cathodic potential correlates with the shift of the anodic potential towards more negative values i.e., more active anode. The authors hypothesize that the accelerated anodic reaction requires faster cathodic reaction that cannot be provided by oxygen reduction reaction (ORR) due to the limited oxygen supply. Thus, the accelerated anodic reaction drives the parasitic reactions at the cathode to a higher rate, which defined the cathodic potential. The same observation was established with other wastewaters in BETT systems (data not included).

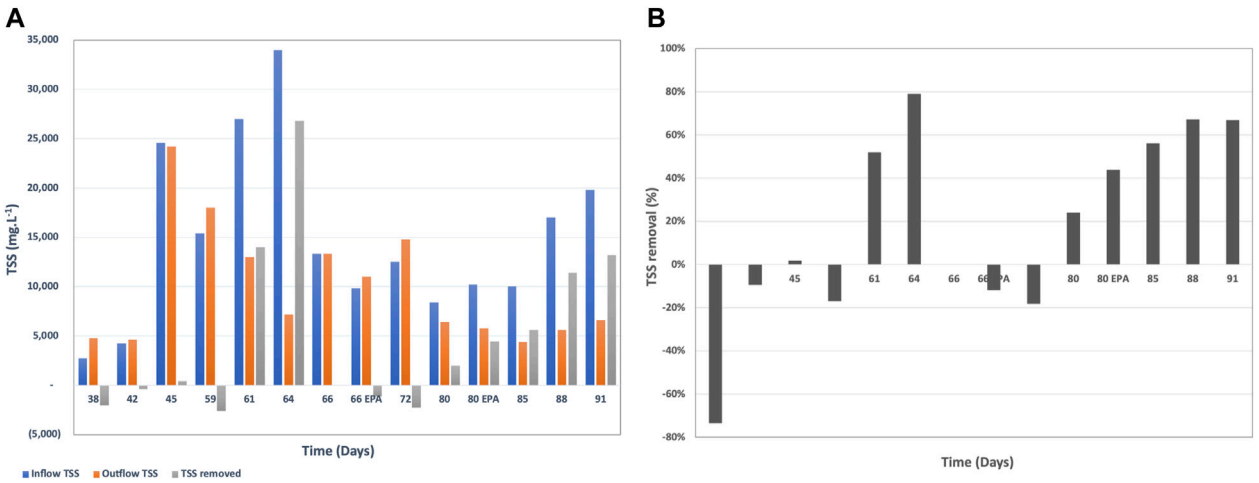

FIGURE 6 | TSS removal rates in **(A)** mg/L and **(B)** percentage during continuous mode.

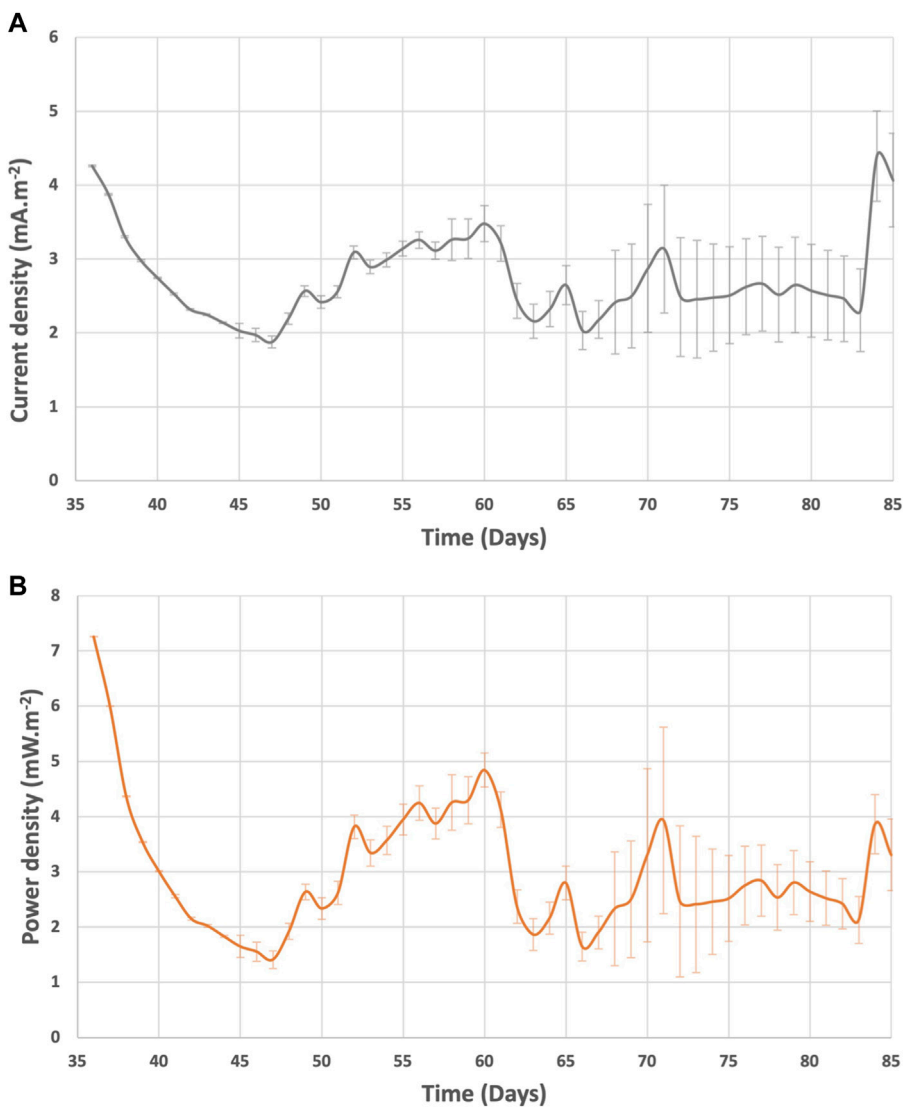

FIGURE 7 | (A) current density and **(B)** power density recorded during continuous mode.

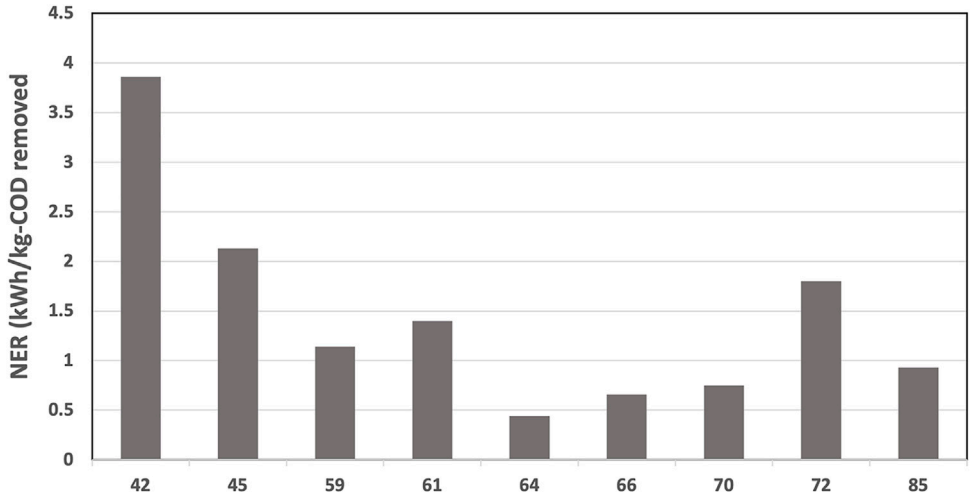

FIGURE 8 | NER estimated for BETT Demo Unit.

The system current and power generation were in the range of 1.9—5.7 mA m^{-2} and 1.4—9.5 mW m^{-2} (**Figure 7**). After day 60, the current and power of BETT Demo Unit were on average 2.9 ± 0.9 mA m^{-2} and 2.8 ± 0.7 mW m^{-2}. Compared to previous BETT Demo Unit treating swine wastewater (current generated was around 2 0 mA m^{-2} during continuous mode (Babanova et al., 2019)), the current and power generated under this study were lower most likely due to the lower cathodic potentials and the interference of parasitic cathodic reactions. Swine wastewater has significantly lower protein content than brewery wastewater, which further confirms the hypothesis.

As expected, the Net Energy Recovery (NER) was higher at the beginning of the continuous mode and was reduced after day 60 due to the decreased cathodic reaction (**Figure 8**). The NER was significantly higher than previously reported data for 12-MFC unit pilot installation treating swine wastewater (0.11 kWh.kg-COD^{-1}) (Babanova et al., 2019) and BETT Demo Unit for brewery wastewater treatment (0.14 kWh.kg-COD^{-1}) (Babanova et al., 2020), The NER in this study was comparable to identical Demo Unit deployed at a confectionary facility (1.6 kWh.kg-COD^{-1}) processing sugarwater (Babanova, 2020).

The reduction in the generated current and power did not have a detrimental effect on treatment rates.

GHG Emissions

The direct CO_2 and CH_4 emissions from biological activity, and indirect CO_2 emissions from electricity consumption and landfill CH_4 emissions for BETT Demo Unit were estimated using the methodologies established by the U.S. Environmental Protection Agency (RTI International, 2010). The calculated values as well as the input parameters for the calculations are presented in **Tables 2**, **3** and the SI. The contribution of nitrous oxide to GHG emissions was not considered in this study. A previous study reporting about BETT systems demonstrated that the predominant denitrification reaction in BETT is the dissimilatory nitrate reduction to ammonium (DNRA) (Babanova et al., 2019). DNRA is also capable of the production of nitrous oxide. A more detailed evaluation is needed for the estimation of GHG emissions from nitrous oxide, which will be a subject to a separate study.

The estimated GHG emissions were compared to aerobic and anerobic wastewater treatment of the same organics' removal e.g. 24,800 mg.L^{-1} COD removed, corresponding to 11,160 mg.L^{-1} BOD. BOD analysis of the brewery wastewater was periodically outsourced to an EPA certified lab to establish the BOD/COD ratio of 0.45. The data related to aerobic and anaerobic technologies was taken from literature (USDA, 2007; Lier et al., 2008; Haas et al., 2018). The data related to BETT Demo Unit were evaluated during the continuous mode of operation of the Demo Unit.

BETT technology provides 100% reduction in methane emissions, no methane is generated during BETT operation. BETT reactions are primarily anaerobic and include fermentation reactions to convert sugars to VFAs; however, unlike anaerobic digestion, the VFAs are oxidized to carbon dioxide using bacteria that naturally reduce solid-phase electron acceptors (Paquete et al., 2014). Further, protons and hydrogen are reacted at the cathode during oxygen reduction to generate hydrogen peroxide and/or molecular water. Due to these favorable reaction chemistries, the carbon dioxide and hydrogen partial pressures in BETT systems are not high enough to support methanogenic growth, Thus, methanogenic archaea are not involved in the process and no methane is generated.

The reduction in carbon dioxide emissions from biological activity were estimated to be 16 to 18% compared to anaerobic and aerobic technologies, respectively. This was a result of the lower biomass production and the higher fraction of COD converted under anaerobic conditions in BETT systems.

As me mentioned earlier, BETT systems have a significantly lower power demand relative to other wastewater treatment technologies due to the gravity feed and slow flow, low

TABLE 2 | Estimation of GHG emissions from power consumption and biological activity for BETT system and aerobic and anaerobic technologies processing identical BOD load.

Technology	COD removed (kg/d)	BOD removed (kg/d)	Energy consumed (kWh/kg-BOD)			Power consumed (kWh/d)			Energy recovered (kWh/kg-BOD)			Power generated (kWh/d)			CO2 emissions from electricity consumption ($kg\text{-}CO_2/d$)			CO2 emissions from biological activity ($kg\text{-}CO_2/d$)	CH4 emissions from biological activity (kg-CH4/d)	$Kg\text{-}CO_2/kg\text{-}BOD$ removed
Activated Sludge	14	6	2.2	–	6.2	14	–	39	NA			NA			10	–	29	0.0082	0.001	0.129%
Anaerobic Digestion	14	6	0.5	–	0.7	3	–	4	1.0	–	1.2	6.4	–	7.6	2	–	3	0.0080	0.003	0.125%
BETT	14	6	0.1	–	0.2	0.6	–	1.3	0.9	–	8.2	5.7	–	52	0.5	–	1	0.007	0.000	0.105%

pressure operations of the system, which leads to low power demand equipment used. Due to the anaerobic nature of the oxidation process, no forced air is needed for the treatment also lowering the energy demand of the system. The power consumption of BETT Demo Unit was determined as 0.1–0.2 $kWh.kg\text{-}BOD^{-1}$ removed depending on the season, where the power consumption was higher during the winter and lower during the summer months. The wastewater was heated to > 10°C during the winter months when needed, which contributes to the higher power consumption during this season. The low power requirements of BETT Demo Unit led to lower CO_2 emissions from electricity consumption i.e. 80% lower emissions than anaerobic digestors and 95% lower emissions compared to aerobic treatment. BETT power requirement does not consider the energy recovered from BETT system since at this stage of BETT development, the voltage generated was used only as an indicator of reactor performance and was not harvested or used to offset the energy demand of the system. In the event of recovering the generated by BETT DC current, the energy demand of the system will be reduced even further by at least 30%.

BETT technology produces significantly lower secondary biomass. The amount of secondary biomass produced is measured as VSS and was 5.1% of the total organics removed. The conversion of the chemical energy, the energy released during the oxidation of organics, into electrical energy in BETT systems reduces the energy available for bacterial growth resulting in a low biomass generation in these systems. Because of the lower biomass production, BETT contribution to landfill methane emissions is 89% lower than aerobic and 49% lower than conventional anaerobic technologies. The landfill CH_4 emissions calculated as $kg\text{-}CH_4.\ d^{-1}$ were estimated to be $0.18\ kg\text{-}CH_4.\ d^{-1}$ for BETT Demo Unit, $0.35\ kg\text{-}CH_4.\ d^{-1}$ for ADs and $1.59\ kg\text{-}CH_4.\ d^{-1}$ for aerobic wastewater treatment plants. In 2015, 16.4% of the total methane emissions in the United States came from landfills (Meegoda et al., 2018).

How BETT Scales

One of the concerns that GWI Magazine expressed about the future of Microbial Fuel Cells as a wastewater treatment solution is the scalability of the technology due to the high cost of the materials and the issues arising with the larger anodes and cathodes (CTO, 2020). To overcome the problem with the electrode scalability, BETT takes advantage of the modularity approach. Instead of scaling up the reactor size, BETT systems rely on connecting multiple reactors in hydraulic series.

BETT Demo Unit is a small-scale pilot installation used for demonstration purposes. The Demo Unit has only 12 BETT reactors operating in hydraulic series, processing $0.6\ m^3.\ day^{-1}$ of wastewater. Due to the small number of reactors and the short HRT (4-h HRT), the wastewater is partially treated.

Commercial BETT systems, abbreviated here as C-BETT, are composed of one or multiple standard shipping containers with up to 640 BETT reactors working in multiple treatment trains. The shipping containers can be 6 m or 12 m depending on the

TABLE 3 | Estimation of landfill GHG emissions for BETT system and aerobic and anaerobic technologies processing identical BOD load.

Technology	COD removed (mg/L)	COD removed (kg/d)	BOD removed (kg/d)	Biomass produced as VSS (mg/L)	Biomass produced (kg/d)	% Biomass/ BOD treated	Volume sludge assuming 8% sludge (gal)	Landfill CH4 emissions (kg-CH4/d)
Activated Sludge	24,800	14	6	11,160	6.4	45.0	20.9	1.59
Anaerobic Digestion	24,800	14	6	2,480	1.4	10.0	4.7	0.35
BETT	24,800	14	6	1,265	0.7	5.1	2.4	0.18

volume of the wastewater to be treated. Each container follows similar to the BETT Demo Unit hydraulic profile. The major difference between the Demo Unit and a C-BETT systems are: 1) the number of BETT reactors connected in hydraulic series composing a "treatment train"; and 2) the number of treatment trains operating in parallel to increase processed volume.

BETT Demo Unit has one partial treatment train with 12 BETT reactors. C-BETT systems typically have 40 BETT reactors in hydraulic series to compose a single treatment train. The number of BETT reactors in a treatment train depends on the composition and concentration of the wastewater (COD loading), and the quality of the effluent to be achieved (targeted COD of the effluent) and can vary between 20 and 80 BETT reactors. Commercial BETT systems treating the wastewater used in this study should have at least 40 BETT reactors in hydraulic series.

Each full-size treatment train can treat roughly between 0.6 and 1.40 m^3 of wastewater. Therefore, to increase the volume of the processed wastewater, C-BETT systems have multiple treatment trains operating in parallel. Thus, a 12-m shipping container with 40 BETT reactors in a treatment train has 16 x treatment trains and can process roughly 9 m^3. day^{-1} of high strength brewery wastewater.

To optimize space, the treatment trains are arranged on rack structures with multiple levels. Each level can have one or multiple treatment trains.

The modulatory of BETT systems allows for easy scale up, maintenance, repair, and expansion to address customer needs when they grow in production.

Figure 9 is showing how multiple BETT reactors are arranged in 12-m C-BETT system installed in February 2021 at a soda manufacturer customer site.

BETT systems might require the addition of a buffer solution such as phosphate or carbonate buffer (Liu et al., 2005; Nam et al., 2010). The buffer solution has a dual role to increase wastewater conductivity and increase pH:

Increasing the wastewater conductivity is needed when the raw wastewater has a conductivity < 1 mS cm^{-1}.

Given the electrochemical nature of the reaction, higher conductivity will facilitate the proton flux from the anode to the cathode and thus enhance the cathodic reaction. Oxygen, protons and electrons combine at the cathode during the oxygen reduction reaction to result in the formation of water or hydrogen peroxide. The higher proton flux and faster proton utilization also helps with maintaining neutral pH around the anode units, which bacteria require.

The addition of buffer solution increases pH and provides buffering capacity. The higher buffering capacity of the solution also keeps the pH stable even at higher VFA concentrations.

BETT systems use sodium bicarbonate to create bicarbonate buffer system. Sodium bicarbonate was specifically selected because the lack of toxicity and low cost.

FIGURE 9 | 12-m C-BETT system installed at a soda manufacturer customer site. **(A)** Outside view of C-BETT and **(B)** BETT reactors arrangement inside C-BETT.

The addition of sodium bicarbonate is not required for all BETT systems. It is defined by the composition of the wastewater and the natural buffering capacity of the raw wastewater. Wastewater with low conductivity (conductivity < 1 ms cm^{-1}) and high organic content (COD > 10,000 mg.L^{-1}) will require the addition of sodium bicarbonate. Wastewater with conductivity > 1 ms cm^{-1} and lower organic content (COD < 10,000 mg.L^{-1}) might not require the addition of sodium bicarbonate.

CONCLUSION

BETT systems are the cleanest and most efficient approach for directly treating high strength wastewater (COD > 25,000 mg.L^{-1}) and are an effective solution for a Net-Zero future.

This study successfully demonstrated the applicability of BETT technology for the treatment of wastewater with high, and highly variable, concentrations of COD, protein and TSS. BETT achieved up to 33% COD removal corresponding to COD of 22,175 mg.L^{-1} in a 4-h HRT. The TSS removal reached values as high as 79% with incoming TSS concentrations up to 34,000 mg.L^{-1} TSS. No other wastewater treatment technology has been reported to efficiently remove such high organic and solids concentrations.

In addition, BETT Demo Unit demonstrated 89 and 49% lower landfill methane emissions than aerobic and anaerobic technologies, respectively. The overall reduction in CO_2 emissions, both direct and indirect, was estimated to be 85–90% lower compared to existing practices.

DATA AVAILABILITY STATEMENT

The original contributions presented in the study are included in the article/**Supplementary Material**, further inquiries can be directed to the corresponding author.

AUTHOR CONTRIBUTIONS

SB and OB designed and managed the study and wrote the manuscript. JJ, KW, and JS collected the data. JG, DB, PH, OA, RN, and GG designed the system. All authors contributed to manuscript revision, read, and approved the submitted version.

SUPPLEMENTARY MATERIAL

The Supplementary Material for this article can be found online at: https://www.frontiersin.org/articles/10.3389/fceng.2022.832505/full#supplementary-material

REFERENCES

Babanova, S., Jones, J., Phadke, S., Lu, M., Angulo, C., Garcia, J., et al. (2019). Continuous Flow, Large-scale, Microbial Fuel Cell System for the Sustained Treatment of Swine Waste. *Water Environ. Res.* 92, 60–7213. doi:10.1002/wer.1183

Babanova, S., Jones, J., Wiseman, K., Soles, J., Garcia, J., Huerta, P., et al. (2020). Electrifying Pretreatment. *Water Environ. Technol.* 31, 35–41.

Babanova, S. (2020). New Perspectives in Sugar Industry Wastewater Treatment. *Int. Sugar J.*, 63–64.

Bidault, F., Brett, D. J. L., Middleton, P. H., and Brandon, N. P. (2009). Review of Gas Diffusion Cathodes for Alkaline Fuel Cells. *J. Power Sourc.* 187, 39–48. doi:10.1016/j.jpowsour.2008.10.106

Bracmort, K. (2010). *Anaerobic Digestion: Greenhouse Gas Emission Reduction and Energy Generation*. Washington D.C: Congressional Research Service, 1–13.

Buchanan, J., and Seabloom, R. (2004). *Aerobic Treatment of Wastewater and Aerobic Treatment Units*. University Curriculum Development for Decentralized Wastewater Management. http://onsite.tennessee.edu/Aerobic%20Treatment%20&%20ATUs.pdf

Campos, J. L., Valenzuela-Heredia, D., Pedrouso, A., Val del Río, A., Belmonte, M., and Mosquera-Corral, A. (2016). Greenhouse Gases Emissions from Wastewater Treatment Plants: Minimization, Treatment, and Prevention. *J. Chem.* 2016, 1–12. doi:10.1155/2016/3796352

Chen, S., Harb, M., Sinha, P., and Smith, A. L. (2018). Emerging Investigators Series: Revisiting Greenhouse Gas Mitigation from Conventional Activated Sludge and Anaerobic-Based Wastewater Treatment Systems. *Environ. Sci. Water Res. Technol.* 4, 1739–1758. doi:10.1039/c8ew00545a

Chung, K., and Okabe, S. (2009). Continuous Power Generation and Microbial Community Structure of the Anode Biofilms in a Three-Stage Microbial Fuel Cell System. *Appl. Microbiol. Biotechnol.* 83, 965–977. doi:10.1007/s00253-009-1990-z

CTO (2020). What Happened to Microbial Fuel Cells? *GWI Mag.*, 41–43.

Dong, Y., Qu, Y., He, W., Du, Y., Liu, J., Han, X., et al. (2015). A 90-liter Stackable Baffled Microbial Fuel Cell for Brewery Wastewater Treatment Based on Energy Self-Sufficient Mode. *Bioresour. Techn.* 195, 66–72. doi:10.1016/j.biortech.2015.06.026

Du, Z., Li, H., and Gu, T. (2007). A State of the Art Review on Microbial Fuel Cells: A Promising Technology for Wastewater Treatment and Bioenergy. *Biotechnol. Adv.* 25, 464–482. doi:10.1016/j.biotechadv.2007.05.004

Erable, B., Féron, D., and Bergel, A. (2012). Microbial Catalysis of the Oxygen Reduction Reaction for Microbial Fuel Cells: A Review. *ChemSusChem* 5, 975–987. doi:10.1002/cssc.201100836

Evren, M., Ozgun, H., Kaan, R., and Ozturk, I. (2011). *Anaerobic Treatment of Industrial Effluents: An Overview of Applications*. Istanbul: Waste Water - Treat. Reutil. doi:10.5772/16032

Feng, Y., Wang, X., Logan, B. E., and Lee, H. (2008). Brewery Wastewater Treatment Using Air-Cathode Microbial Fuel Cells. *Appl. Microbiol. Biotechnol.* 78, 873–880. doi:10.1007/s00253-008-1360-2

Franke-Whittle, I. H., Walter, A., Ebner, C., and Insam, H. (2014). Investigation into the Effect of High Concentrations of Volatile Fatty Acids in Anaerobic Digestion on Methanogenic Communities. *Waste Manage.* 34, 2080–2089. doi:10.1016/j.wasman.2014.07.020

Gude, V. G. (2016). Wastewater Treatment in Microbial Fuel Cells - an Overview. *J. Clean. Prod.* 122, 287–307. doi:10.1016/j.jclepro.2016.02.022

Haas, D. d., Appleby, G., Charakos, G., and Dinesh, N. (2018). Benchmarking Energy Use for Wastewater Treatment Plants. *Water e-Journal* 3, 1–26. doi:10.21139/wej.2018.023

He, L., Du, P., Chen, Y., Lu, H., Cheng, X., Chang, B., et al. (2017). Advances in Microbial Fuel Cells for Wastewater Treatment. *Renew. Sustain. Energ. Rev.* 71, 388–403. doi:10.1016/j.rser.2016.12.069

He, Z., Huang, Y., Manohar, A. K., and Mansfeld, F. (2008). Effect of Electrolyte pH on the Rate of the Anodic and Cathodic Reactions in an Air-Cathode Microbial Fuel Cell. *Bioelectrochemistry* 74, 78–82. doi:10.1016/j.bioelechem.2008.07.007

Henze, M., Harremoes, P., Jansen, J. la. C., and Arvin, E. (1995). in *Wastewater Treatment*. Editors U. Forstner, R. J. Murphy, and W. H. Rulkens Spronger. 3rd ed. (New York: Springer-Verlag Berlin Heidelberg)

Lier, J. B. V., Mahmoud, N., and Zeeman, G. (2008). *Anaerobic Wastewater Treatment*. doi:10.1021/es00154a002

Liu, H., Cheng, S., and Logan, B. E. (2005). Power Generation in Fed-Batch Microbial Fuel Cells as a Function of Ionic Strength, Temperature, and Reactor Configuration. *Environ. Sci. Technol.* 39, 5488–5493. doi:10.1021/es050316c

Lofrano, G., and Brown, J. (2010). Wastewater Management through the Ages: A History of Mankind. *Sci. Total Environ.* 408, 5254–5264. doi:10.1016/j.scitotenv.2010.07.062

Logan, B. E. (2009). Exoelectrogenic Bacteria that Power Microbial Fuel Cells. *Nat. Rev. Microbiol.* 7, 375–381. doi:10.1038/nrmicro2113

Mamais, D., Noutsopoulos, C., Dimopoulou, A., Stasinakis, A., and Lekkas, T. D. (2015). Wastewater Treatment Process Impact on Energy Savings and Greenhouse Gas Emissions. *Water Sci. Technol.* 71, 303–308. doi:10.2166/wst.2014.521

McCarty, P. L., Bae, J., and Kim, J. (2011). Domestic Wastewater Treatment as a Net Energy Producer-Can This Be Achieved? *Environ. Sci. Technol.* 45, 7100–7106. doi:10.1021/es2014264

Meegoda, J., Li, B., Patel, K., and Wang, L. (2018). A Review of the Processes, Parameters, and Optimization of Anaerobic Digestion. *Ijerph* 15, 2224. doi:10.3390/ijerph15102224

Moeller, L., and Zehnsdorf, A. (2016). Process Upsets in a Full-Scale Anaerobic Digestion Bioreactor: Over-acidification and Foam Formation during Biogas Production. *Energ Sustain. Soc.* 6. doi:10.1186/s13705-016-0095-7

Mussatto, S. I. (2014). Brewer's Spent Grain: a Valuable Feedstock for Industrial Applications. *J. Sci. Food Agric.* 94, 1264–1275. doi:10.1002/jsfa.6486

Nam, J.-Y., Kim, H.-W., Lim, K.-H., Shin, H.-S., and Logan, B. E. (2010). Variation of Power Generation at Different Buffer Types and Conductivities in Single Chamber Microbial Fuel Cells. *Biosens. Bioelectron.* 25, 1155–1159. doi:10.1016/j.bios.2009.10.005

Paquete, C. M., Fonseca, B. M., Cruz, D. R., Pereira, T. M., Pacheco, I., Soares, C. u. M., et al. (2014). Exploring the Molecular Mechanisms of Electron Shuttling across the Microbe/metal Space. *Front. Microbiol.* 5, 1–8. doi:10.3389/fmicb.2014.00318

Rothausen, S. G. S. A., and Conway, D. (2011). Greenhouse-gas Emissions from Energy Use in the Water Sector. *Nat. Clim Change* 1, 210–219. doi:10.1038/nclimate1147

RTI International (2010). Greenhouse Gas Emissions Estimation Methodologies for Biogenic Emissions from Selected Source Categories. Available at: http://www3.epa.gov/ttn/chief/efpac/ghg/GHG_Biogenic_Report_draft_Dec1410.pdf.

Sun, Q., Wu, Y., Zhao, L., and Sun, Q. (2010). Production of Electricity from the Treatment of Continuous Brewery Wastewater Using a Microbial Fuel Cell. *Fuel* 89, 1381–13856. doi:10.1016/j.fuel.2009.11.004

The Eight Report Of The Royal Commission On Sewage Disposal (1912). *Lancet* 180, 1530–1531.

Trapero, J. R., Horcajada, L., Linares, J. J., and Lobato, J. (2017). Is Microbial Fuel Cell Technology Ready? an Economic Answer towards Industrial Commercialization. *Appl. Energ.* 185, 698–707. doi:10.1016/j.apenergy.2016.10.109

United States Environmental Protection Agency (1992). Determining Wastewater User Service Charge Rates. Available at: https://nepis.epa.gov/Exe/ZyNET.exe/200041G5.txt?ZyActionD=ZyDocument&Client=EPA&Index=1991 Thru 1994&Docs=&Query=&Time=&EndTime=&SearchMethod=1&TocRestrict=n&Toc=&TocEntry=&QField=&QFieldYear=&QFieldMonth=&QFieldDay=&UseQField=&IntQFieldOp=0&ExtQFieldOp=.

USDA (2007). *An Analysis of Energy Production Costs from Anaerobic Digestion Systems on U . S . Livestock Production Facilities*.

Verstraete, W., and Rabaey, K. (2006). {REW} Microbial Fuel Cells : Methodology and Technology. *Environ. Sci. Technol.* 40, 5181–5192. doi:10.1021/es0605016

Wang, X., Feng, Y. J., and Lee, H. (2008). Electricity Production from Beer Brewery Wastewater Using Single Chamber Microbial Fuel Cell. *Water Sci. Technol.* 57, 1117–1121. doi:10.2166/wst.2008.064

Zaks, D. P. M., Winchester, N., Kucharik, C. J., Barford, C. C., Paltsev, S., and Reilly, J. M. (2011). Contribution of Anaerobic Digesters to Emissions Mitigation and Electricity Generation under U.S. Climate Policy. *Environ. Sci. Technol.* 45, 6735–6742. doi:10.1021/es104227y

Zhuang, L., Yuan, Y., Wang, Y., and Zhou, S. (2012). Long-term Evaluation of a 10-liter Serpentine-type Microbial Fuel Cell Stack Treating Brewery Wastewater. *Bioresour. Techn.* 123, 406–412. doi:10.1016/j.biortech.2012.07.038

Conflict of Interest: SB, JJ, KW, JS, and OB are employed by Aquacycl Inc. JG, PH, DB, RN, OA, and GG are employed by D4C Product Development. Aquacycl Inc. was the leading entity in the research and D4C Product Development was contracted by Aquacycl for the design efforts.The work described in this study is owned by Aquacycl Inc. D4C Product Development was a subcontractor to Aquacycl during this test. The funding for the study was solely provided by Aquacycl Inc. The funder had the following involvement with the study: manufactured, commissioned, operated, and collected and processed the data for the study.

frontiers | Frontiers in Chemical Engineering

ORIGINAL RESEARCH
published: 01 June 2022
doi: 10.3389/fceng.2022.721923

Biodegradation of Herbicide by the Immobilized Microbial Consortium SMC1 in Continuous Packed-Bed Biofilm Reactor

*Satya Sundar Mohanty and Hara Mohan Jena**

Department of Chemical Engineering, National Institute of Technology, Rourkela, India

The present study aimed to investigate the treatment of butachlor and other commonly used herbicides by the synthetically formulated microbial consortium SMC1 immobilized on the ceramic raschig rings in a packed-bed bioreactor (PBBR). The PBBR was operated in continuous mode at various flow rates over a period of 70 days to determine the effect of hydraulic retention time (HRT) and initial butachlor concentration on the removal efficiency and elimination capability of the bioreactor. It was observed that the overall operation of the bioreactor changes from being controlled by the mass transfer limitations to the controlled bio-reaction , thus proposing the range of 270–325 mg/L/d to be the optimum operating range for the efficient removal of butachlor by the PBBR. The bioreactor can reduce up to 90% of the initial chemical oxygen demand (COD) value while treating the mixture of herbicides. The operating parameters were optimized using response surface methodology where the feed flow rate of 2.9 ml/min, initial herbicide concentration of 454.63 mg/L, and concentration of an additional nitrogen source at 1.41 g/L was found to yield maximal COD reduction. To date, a continuous study in the field of butachlor biodegradation is yet to be reported. Hence, the study could be used as a model to design a better herbicide biotreatment technology.

Keywords: biofilm, bioreactor, butachlor, chemical oxygen demand (COD), response surface methodology, bioremediation

OPEN ACCESS

Edited by:
Kun-Yi Andrew Lin,
National Chung Hsing University, Taiwan

Reviewed by:
Jianlong Wang,
Tsinghua University, China
Willian Garcia Birolli,
Barretos Cancer Hospital, Brazil

***Correspondence:**
Hara Mohan Jena
hmjena@nitrkl.ac.in
hara.jena@gmail.com.com

Specialty section:
This article was submitted to Environmental Chemical Engineering, a section of the journal Frontiers in Chemical Engineering

Received: *07 June 2021*
Accepted: *08 April 2022*
Published: *01 June 2022*

Citation:
Mohanty SS and Jena HM (2022) Biodegradation of Herbicide by the Immobilized Microbial Consortium SMC1 in Continuous Packed-Bed Biofilm Reactor. Front. Chem. Eng. 4:721923. doi: 10.3389/fceng.2022.721923

INTRODUCTION

Glyphosates and chloroacetanilide herbicides are the two most widely applied herbicides used extensively in agricultural practices to protect various crops (Choudhury et al., 2016; Atwood and Paisley-Jones 2017; Shuman-Goodier et al., 2021). Butachlor, a synthetic pre-emergent or early post-emergent herbicide belonging to the class of chloroacetanilide, has been widely used for the control of various types of annual grasses and broad-leaved weeds and the submerged freshwater macrophytes (Mohanty et al., 2004; Chattopadhyay et al., 2006; Liu et al., 2008; University of Hertfordshire 2013). Similarly, glyphosate is a broad-spectrum, post-emergent, and non-selective systemic herbicide used in various crops such as soybean, cotton, canola, maize, etc. (Gianessi 2005; Annett et al., 2014). Based on its worldwide usage, the U.S. Environmental Protection Agency has ranked glyphosate as the principal herbicide (Atwood and Paisley-Jones 2017). Asia alone consumes approximately 4.5×10^7 kg of butachlor per year (Kaur and Goyal 2020; Shuman-Goodier et al., 2021). Recent reports on herbicides in Indian agriculture state that butachlor in rice, alachlor in groundnut, and glyphosate in cotton and tea are the highest consumed herbicides in India, with an annual consumption of 6,750

metric tons and 6,003 metric tons, (Choudhury et al., 2016). Evaluating their potential toxicity toward the non-target organisms, studies revealed that the abov mentioned herbicides pose a major concern to aquatic ecosystems especially when applied in the areas near water bodies (Polard et al., 2011; Mohanty and Jena 2019a). Butachlor is reported to be clastogenic, cytotoxic, and carcinogenic in nature and along with alachlor has been enlisted as a B2 group carcinogen by the USEPA and relegated it to be highly toxic to humans (Orme and Kegley 2004; Lauga et al., 2013; Kaur and Goyal 2020). As butachlor is a recalcitrant and highly persistent herbicide having a negative impact on the environment; a number of studies on the removal of buatchlor have been reported previously (Abigail et al., 2015). Several physico-chemical techniques such as adsorption, ozonation, and catalytic degradation have been applied previously. However, these techniques have several shortcomings such as higher opreating cost, generation of secondary toxic wastes, etc (Mohanty and Jena 2019a). Hence, a biological approach for the removal of butachlor has gained focus with time. One such technique is bioremediation where the microbial species can be used for the disintegration of harmful pollutants in to harmless products. However, the major limitation of this alternative is the slower degradation rate which prohibits its application for the treatment of industrial wastewater. Till date, the study of biodegradation of butachlor has been limited to the batch biodegradation of butachlor of low concentrations and the degradation pathways related to it. Hence, these studies are unable to address the limitations such as uneven cell density, mediocre butachlor biodegradation efficiency due to slow microbial growth rate which is due to low substrate utilization, inhibition due to high butachlor concentration, or mass transfer limitations. Thus, to overcome the aforementioned limitations, the potential microbial strains immobilized on the solid support may be used in bioreactors in continuous mode (Yadav et al., 2014). The available body of work on the biodegradation of butachlor supports the scope of in-depth investigation in this topic with a focus on enhancing the butachlor biodegradation efficiency. Biofilm reactors have been designed to maintain a high biomass density to achieve a higher removal rate even under the conditions of slow microbial growth by protecting the microbial cells involved from stressful conditions due to substrate inhibition (Acuna-Askar et al., 2000). Moreover, since the packed-bed biofilm reactors operates at high active biomass concentrations, even reactors with small reactor volume perform exceedingly well at lower substrate concentrations without the necessity for the separation of active biomass from the treated effluent, thus enhancing the stability and productivity of the reactor and making it easier as well as cheaper to operate (Ercan and Demirci 2015). Due to the aforementioned advantages, packed-bed biofilm reactors have been extensively used in the field of bioremediation technology for the treatment of various environmental pollutants (Alfonso-Gordillo et al., 2016a).

Considering the aforementioned specifics, the aim of the present study was to evaluate the performance of a lab-scale packed-bed biofilm reactor packed with immobilized butachlor degrading the microbial consortium at high loading rates. To the very best of our understanding, this is the first-of-its-kind work to report on the biodegradation of butachlor in a continuous packed-bed bioreactor.

MATERIALS AND METHODS

Chemicals and Medium

HPLC-grade methanol, acetonitrile, water, and analytical grade butachlor were procured from Sigma–Aldrich (India). Commercial grade butachlor, alachlor, and glyphosate were obtained from Insecticides India, Ltd., Sinochem India Pvt. Ltd., and Excel Cropcare Ltd., respectively. Other chemicals and reagents used in this study were of analytical grade and were procured from Merck (India) and Himedia (India). The minimal salt medium (MSM) constituted (in g/L) of $(NH_4)_2SO_4$ (1.0), NaCl (1.0), K_2HPO_4 (1.5), KH_2PO_4 (0.5), and $MgSO_4{\cdot}7H_2O$ (0.2) (pH 7.0) (Liu et al., 2012). The medium was sterilized by autoclaving, and the herbicides were added after filter sterilization.

Microorganisms

The synthetic microbial consortium, SMC1, used in this study was formulated from the bacterial strains *Serratia ureilytica* AS1, *Enterobacter cloacae* FP2, and *Pseudomonas putida* G3 isolated previously from the soil samples contaminated with butachlor and other herbicides through the selective enrichment technique (Mohanty and Jena 2018, 2019b, c). The individual strains were grown overnight in a nutrient broth at 32.5°C at 120 RPM in an orbital shaker incubator. The biomass was harvested by centrifugation and resuspended in the nutrient broth prior to the experiment. Equal amount of the cell biomass (approximately 1 g/L of dry cell biomass) was inoculated in the mineral salt medium, and the setup was incubated overnight at 32.5°C, 120 RPM. The mixed bacterial culture obtained by mixing an equal volume of the cell biomass was used for further experiments.

Packed-Bed Bioreactor

The biodegradation of synthetic wastewater containing butachlor and other herbicides in continuous mode was studied in an up-flow packed-bed batch bioreactor of 100 cm length and 8.5 cm internal diameter with a 55-cm-high reactor bed (**Supplementary Figure S1**, **Supplementary Figure S2**). The feed is supplied in to the bioreactor from a feed tank through a peristaltic pump, and the effluent is discharged out of the bioreactor in a collection tank. Sterilized air is supplied in to the system using an air pump having filters at its nozzle through an air sparger at the center of the reactor base with a pore size of 1 mm, and the air feed is controlled by the gas rotameter having a range of 0–30 LPM attached to it. While the outlet for the discharge of exhaust gas was designed at the top of the reactor covered with the lid, the outlet for the effluent was placed above 70 cm from the bottom in the reactor column. To maintain the sterile conditions, the sampling ports were plugged with sterilized silicon tubing and stopper cork. The airflow within the system was regulated by the help of a pressure-regulating valve. The air flow rate was maintained at 2 LPM to maintain the required oxygen level

without creating turbulence within the feedflow. All the experiments were carried out at ambient room temperature. The active reactor bed volume was packed with ceramic raschig rings of 6 mm diameter and 6 mm height as the packing material with a stainless steel wire-mesh at both the ends to prevent their movement. Synthetic wastewater comprising butachlor and other herbicides were used as the feed for the reactor and were fed continuously with the help of peristaltic pump in an up-flow mode of operation.

Surface Immobilization of Bacterial Consortium

The bacterial consortium prepared for this study was inoculated to sterile MSM containing butachlor and incubated for 24–36 h at 32.5°C and 120 RPM. The bacterial biomass was harvested by centrifugation at 5,000 rpm for 10 min and resuspended in 4 L of mineral salt medium containing butachlor (200 mg/L), making the final biomass concentration of the inoculant in the inflow solution to 10^8 CFU/ml (approximate). The cell suspension was transferred into the column packed with previously autoclaved ceramic raschig rings using a peristaltic pump. The raschig rings were washed properly, first with the regular laboratory-grade detergent, followed by 70% ethanol, and finally with sterile double-distilled water repeatedly five times. The raschig rings were vacuum-dried at 45°C for 24 h prior to the immobilization. The biomass washed out of the reactor was recycled back. The reactor was continuously fed with the aforementioned medium containing butachlor and was operated for 15 days until a steady-state performance was achieved. To ensure proper biomass growth; the raschig rings were acclimated for 15 days at the ambient room temperature of 30°C before the commencement of the biodegradation studies. To confirm the formation of bacterial biomass on the support material, a few raschig rings were sampled for ESEM analysis.

ESEM Observation

Formation of the biofilm on the ceramic raschig rings was confirmed by the environmental scanning electron microscope (ESEM). For ESEM sample preparation, the raschig rings were washed with phosphate buffer (pH 7.5) twice and fixed with 2% (w/v) glutaraldehyde for 1 h at 4°C followed by 0.1% tannic acid for 30 min. The fixed samples were washed with PBS and later dehydrated with increasing concentration of ethanol solutions. The samples were washed thrice with 100% ethanol and kept at 37°C for drying. The dried particles were then coated with a gold layer and attached on to the microscope for ESEM analysis.

Continuous Study

The packed-bed bioreactor was operated in continuous mode for 70 days by varying the feed flow rate and inlet butachlor concentration to determine the effect of HRT and inlet loading on the butachlor biodegradation efficiency. The effect of hydraulic retention time on the butachlor removal efficiency of the reactor was determined by keeping the initial butachlor concentration constant at 300 mg/L and gradually increasing the retention time for the operation. Next, the effect of the inlet substrate loading rate was evaluated by keeping the HRT constant and varying the initial butachlor concentration from 500 mg/L to 2000 mg/L. The required nutrient solutions were added separately, and the DO was maintained at the required level. The performance of the PBBR was evaluated in terms of removal efficiency and elimination capacity.

Combined Removal of the Mixture of Herbicides

Approximately 1 g/L each of butachlor, alachlor, and glyphosate was added in a container to prepare the homogenous mixture of the multisubstrate stock solution for the study. The removal efficiency of the bioreactor was evaluated by varying the concentration of the herbicide-mixture (500–2000 mg/L) in the feed keeping all other operating conditions same at a constant HRT of 18 h. The sSamples were collected in the regular interval of 12 h from the outlet and analyzed for COD removal.

Parameter Optimization Using RSM

To evaluate the relationship between the operating parameters on the COD removal efficiency of the packed-bed bioreactor, a statistical optimization technique such as response surface methodology (RSM) was used. Three operational parameters, such as initial substrate concentration, feed flow rate, and additional nitrogen source were considered for the study. To optimize the factors, a 2^3 full factorial central composite design (CCD) for the three parameters was used. A total of 20 experiments were performed, the particulars of which have been enlisted in **Table 1**.

Analytical Methods

The concentration of butachlor in the medium was evaluated as per the protocol discussed in the available literature (Mohanty and Jena 2019b). First, the sample was saturated with sodium chloride and then an equal volume of hexane/ethyl acetate (1:1) was added to it. The organic phase was separated and air-dried at room temperature and resuspended in HPLC-grade methanol. The butachlor concentration in the extracted samples was analyzed by HPLC using a 5 µm, C–18 column of Agilent Technologies (United States) with methanol: water as the mobile phase in a ratio of 70:30. The flow rate was maintained at 1 ml/min, and the peak absorbance was obtained at 225 nm.

The COD value of the synthetic wastewater was determined by the protocol as discussed in the literature (Sung Wang et al., 2017). First, the sample was placed in a container and the digestion solution containing $K_2Cr_2O_7$ was added to it. Then, sulfuric acid was added to the mixture in excess so that an acid layer is created under the mixture. The container was closed tightly and inverted several times for complete mixing of the contents. The containers were placed in a block digester preheated to 150°C and refluxed for 2 h behind a protective shield. Then, the container was cooled to room temperature and one–two drops of Ferroin indicator was added to it. Then, it was stirred rapidly on a magnetic stirrer while titrating with 0.1 M FAS till the color changed from blue-green to reddish

TABLE 1 | Experimental results based on central composite design.

Run order	Feed flow rate (ml/min)	Initial substrate concentration (mg/L)	Biogenic substrate conc. (g/L)	Experimental response (%)	Predicted response (%)
1	4.13	91.75	1	83.59	83.01
2	4.13	908.25	1	54.25	55.95
3	4.13	500	1	77.46	76.32
4	4.13	500	0.6	72.42	75.26
5	1.9	500	1	76.19	79.69
6	4.13	500	1.4	77.93	76.13
7	6.36	500	1	43.42	41.002
8	4.13	500	1	75.93	76.32
9	2.77	750	0.75	76.44	71.84
10	2.77	250	0.75	85.20	83.2
11	2.77	750	1.25	77.29	75.54
12	5.5	250	1.25	63.45	65.26
13	2.77	250	1.25	88.59	86.93
14	5.5	750	1.25	44.32	43.47
15	5.5	750	0.75	47.204	46.13
16	5.5	250	0.75	68.94	67.89
17	4.13	500	1	77.07	76.32
18	4.13	500	1	75.16	76.32
19	4.13	500	1	78.61	76.32
20	4.13	500	1	78.22	76.32

brown. The blank containing only reagents and distilled water equal to the volume of the sample was refluxed and titrated in the same manner, and the COD value was determined using the following formula:

$$COD_{mgO_2/L} = \frac{(A - B) \times M \times 8000}{V_{Sample}},$$

where A is the volume of FAS used for the blank in mL, B is the volume of FAS used for the sample, and M is the molarity of FAS, that is, 0.1.

Statistical Analysis

The performance evaluation of the bioreactor in case of the single-substrate treatment study has been expressed in terms of elimination capacity, removal efficiency, and inlet loading rate calculated by the following formulae (Sonwani et al., 2020):

$$\text{Elimination capacity (EC)} = \frac{Q \times (B_{in} - B_{out})}{V},$$

$$\%\text{Removal efficiency (RE)} = \frac{B_{in} - B_{out}}{B_{in}} \times 100,$$

$$\text{Inlet loading rates (IL)} = \frac{Q \times B_{in}}{V},$$

where B_{in} and B_{out} are the butachlor concentrations at the inlet and outlet of the bioreactor, respectively; Q represents the volumetric feed flow rate; and V represents the reactor volume. However, in case of the multisubstrate biotreatment study, the performance of the bioreactor was expressed in terms of COD removal efficiency which was calculated as per the available literature using the following formulae:

$$\%\text{COD Removal efficiency} = \frac{COD_{in} - COD_{out}}{COD_{in}} \times 100,$$

where COD_{in} and COD_{out} are the COD concentrations at the inlet and outlet of the bioreactor, respectively. All the experiments were conducted in triplicate, and the reported data presented in the graphical form are the mean and standard deviation of these replicates shown as the error bars. Statistical analysis of data was performed using one-way ANOVA at the significance level of 0.05 and Tukey's post-test using the Graph Pad Prism® software version 6.0c.

In case of process parameter optimization to achieve maximal COD removal efficiency, the relationship between the parameters was expressed in terms of a second-order polynomial equation shown below:

$$\mathbf{R} = \mathbf{P_0} + \sum_{i=1}^{n} \mathbf{P_i}\,\mathbf{V_i} + \sum_{i=1}^{n} \mathbf{P_{ii}}\,\mathbf{V2i} + \sum_{i=1}^{n}\sum_{j=1}^{n} \mathbf{P_{ij}}\,\mathbf{V_i V_j}, \quad (1)$$

where R being the predicted response is the COD removal percentage; V is the influencing variables/parameters to be optimized; and P_0, P_i, Pi,i and P_{ij} are the intercept coefficient, linear coefficient, quadratic coefficient, and interaction coefficient, respectively. The three-dimensional plots obtained depict the interaction among the associated variables. Analysis of variance (ANOVA) furnishes the significance of the correlative coefficient value (R^2) and the regression coefficients of the model which in turn defines the quality fit of the model. For designing the experiment and analysis, statistical software Minitab (Version 17.1) has been used.

RESULT AND DISCUSSION

Biofilm Formation on Ceramic Beads

In the present study, ESEM analysis of the immobilized beads in various time frames has been carried out to evaluate the successful biofilm formation of the microbial consortium SMC1 on the

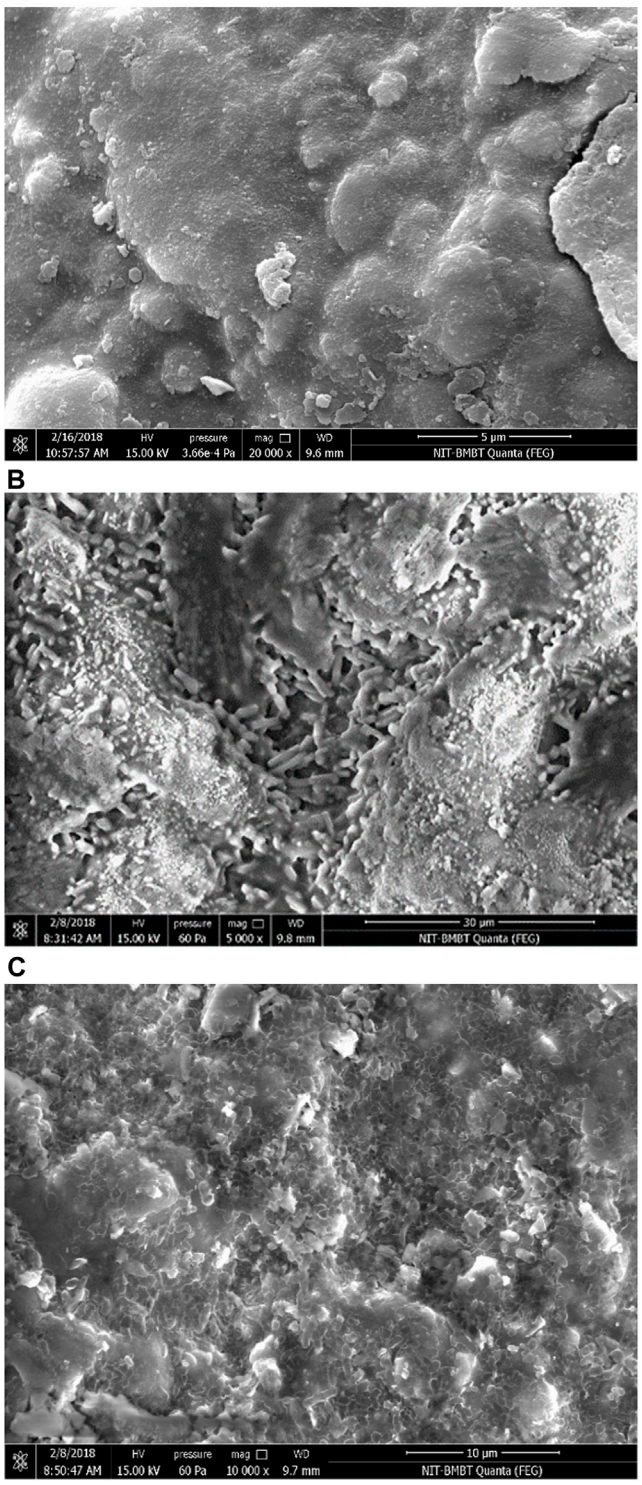

FIGURE 1 | ESEM micrographs of ceramic raschig rings **(A)** without biofilm; **(B)** with biofilm Day 15; **(C)** with biofilm Day 70.

hollow ceramic raschig rings. Microbial cells have reportedly been immobilized on various support materials such as calcium alginate beads, cellulose acetates, ceramics, volcanic rocks etc., (Dzionek et al., 2016). Hollow ceramic raschig rings have been opted for the current study as the support material due to a variety of reasons such as it is non-biodegradable, inert, and has high mechanical strength (Foroughi et al., 2019). After the initial period where the cells were allowed to get acclimatized to the new environment and get adsorbed to the support material, the microbial strains grew rapidly to form a thick layer of biofilm around the beads. **Figure 1A** presents the raschig rings on Day 0 as the control without biomass before the inoculation of the bacterial consortium. The micrograph reveals that the raschig rings have a very rough and porous surface texture with micro-pores scattered randomly throughout the surface, thus providing ample surface area for the immobilization of microbial cells and passage of the medium through the structure (Muter et al., 2017). **Figure 1B** presents the raschig ring on Day 15, which depicts the porous surface of the ceramic raschig rings being colonized with the biofilm and a dense population of rod-shaped bacterial strains. The figure exhibits the biofilm as a complex structure where the abundant extracellular polymeric matrix fortifies the bacterial cells imitating a microbial mat. The micrograph in **Figure 1C** corresponds to the 70th day of operation and is quite similar to the micrograph taken during the commencement of the continuous study, thus indicating the fact that the microbial consortium is capable of withstanding high and variable loading rates of butachlor.

The microporous structure of the ceramic raschig ring posseses high surface area which helps in retaining higher biomass on its surface, thus resulting in a high degradation rate. The hollow raschig ring reduces the channeling of the inlet feed, resulting in even distribution of butachlor within the bioreactor. The micrograph confirms the presence of cells both on the surface and within the hollow structure of the ring. From the batch study, it was evident that the degradation efficiency of the bacterial consortium has enhanced significantly on being immobilized as compared to its freely suspended form. This may be attributed to the increased metabolic activity and tolerance of the microbial cells toward the adverse environment on being immobilized (Shukla et al., 2014). Similar results have previously been reported where immobilizing the bacterial strains on any support materials such as low-density polyethylene enhances the removal efficiency from 78 to 91% of the organic contaminant such as 4-chlorophenol from the wastewater sample (Swain et al., 2021).

Continuous Study

The PBBR was operated in continuous mode for 55 days during which the effect of HRT on biodegradation of butachlor by the microbial consortium SMC1 was studied. The study was carried out by varying the feed flow rates ranging from 1.28 ml/min to 5.5 ml/min at ambient room temperature. The performance of the PBBR was evaluated in terms of removal efficiency (RE) and elimination capacity (EC). **Figure 2** and **Figure 3** represent the variation of the removal efficiency and elimination capacity of the bioreactor system with respect to hydraulic retention time, respectively. After the initial acclimatization period, the PBBR was operated at a low feed flow rate of 1.28 ml/min, which corresponds to the HRT of 36 h and inlet loading rate of

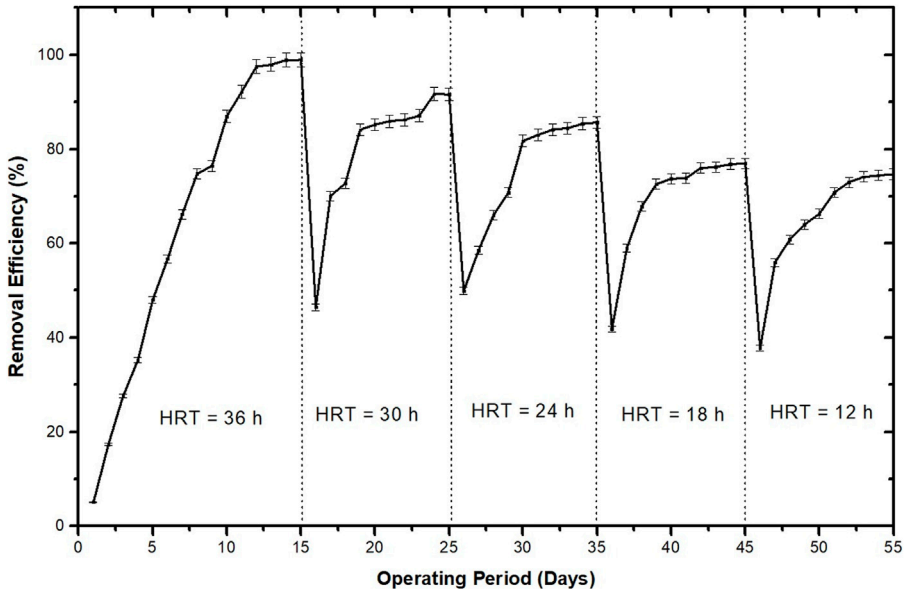

FIGURE 2 | Effect of HRT on butachlor removal efficiencies of the PBBR.

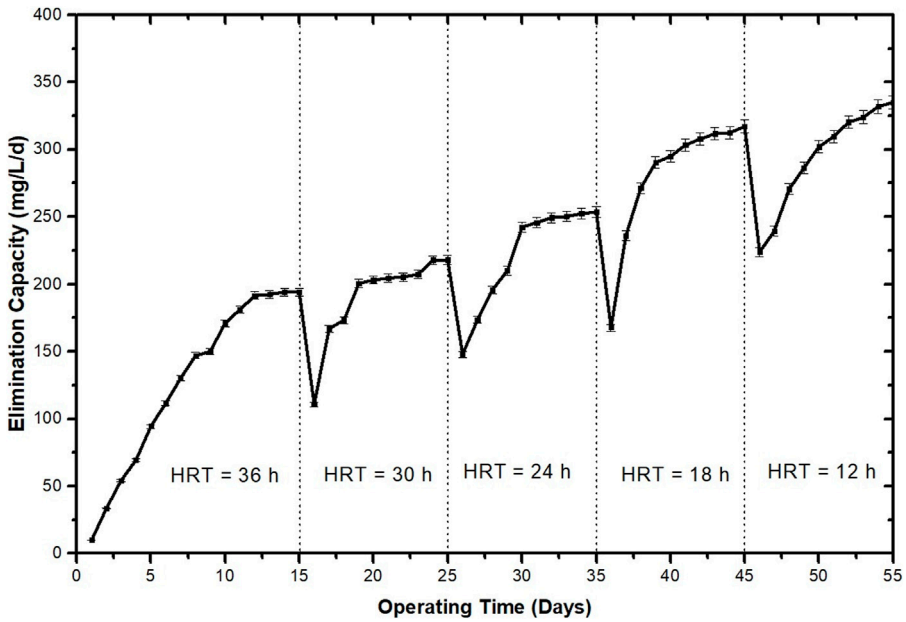

FIGURE 3 | Effect of HRT on butachlor elimination capacity of the PBBR.

133.2 mg/L/d. The steady-state condition was established within 15 days which was evident from the constant RE of 97%. The elimination capacity of the system was found to be 194 mg/L/d of butachlor. On day 16, the feed flow rate was increased to 2.22 ml/min which corresponds to the HRT of 30 h and the inlet loading rate of 159.84 mg/L/d. A sharp dip in both the RE and EC is observed on day 16 with increase in the retention time. However, both RE and EC recovered by day 24 and remained constant at 91% and 217 mg/L/d, respectively, with a very little change. A similar trend was observed with each change in HRT of 24, 18, and 12 h. The effect of retention time on the overall performance of the packed-bed bioreactor has previously been reported for various other organic pollutants where higher contaminant removal efficiency has been obtained on increasing the retention time of the bioreactor system. The contaminant removal efficiency of the packed-bed bioreactor increased from

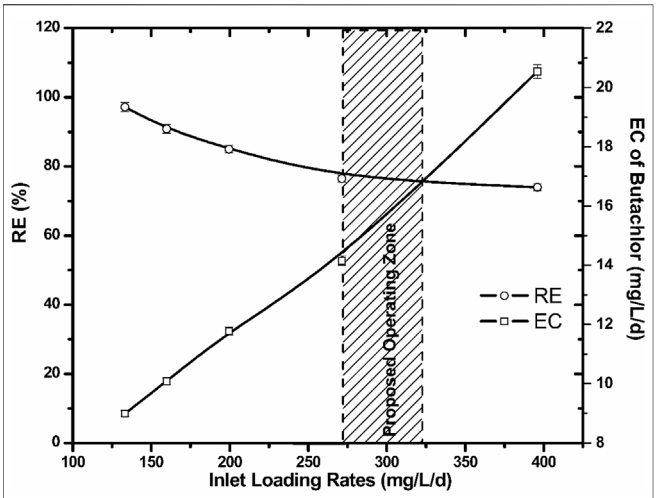

FIGURE 4 | Influence of inlet butachlor loading on the removal efficiency and elimination capacity of the PBBR.

80 to more than 95% on increasing the HRT from 0.25 to 4 days, respectively (Chen et al., 2016; Khalid and Hashmi 2016). The decrease in the removal efficiency (RE) at low retention time may be attributed to the insufficient contact time between the contaminant present in the feed and the immobilized microbial strains, which leads to incomplete or low degradation efficiency of the substrates (Alfonso-Gordillo et al., 2016b).

Since the effective functioning of a bioreactor is dependent upon the inlet loading rate, its effect on the butachlor removal efficiency and elimination capacity has been investigated for the PBBR, and the relationship has been presented in **Figure 4**. From the graph, it is clearly evident that while the removal efficiency of the bioreactor remains almost stable, the elimination capacity increases linearly up to the inlet loading rate of 271.44 mg/L/d beyond which the removal efficiency starts decreasing noticeably and the elimination capacity of the bioreactor tends on increasing. This phenomenon has been discussed in various bioreactor studies carried out previously (Yadav et al., 2014; Briceño et al., 2020). In the present study, the inlet loading rate of 271.44 mg/L/d is the controlling step of the bioreactor that changes operation from mass transfer to bio-reaction controlling. Below the critical rate, diffusion of butachlor into the biomass is low, resulting in mass transfer limitations. Therein, the innermost layer of the biofilm may be depleted of the substrate, thus not utilizing the full potential of the microbial system. However, at higher loading rates, the system overcomes the mass transfer limitations since the diffusional flux is high and under this condition, the butachlor removal efficiency depends on the biodegradation efficiency of the biomass. At higher loading rate, lower removal efficiency may be the result of substrate inhibition or bacterial plugging and channeling due to excess biomass (Patel and Kumar 2016; Kureel et al., 2018). The present study proposes the range of 270–325 mg/L/d to be the optimum operating range for the removal of butachlor by the PBBR.

Effect of Initial Substrate Concentration on RE of the PBBR

In the present study, continuous biodegradation of butachlor fed at a constant flowrate of 2.77 ml/min was assessed for 25 days with the butachlor concentration varying from 500 to 2000 mg/L. Initial substrate concentration plays an important role in determining the performance evaluation of the continuous removal of the contaminant in a bioreactor. Wastewater generated from the industrial applications is prone to have shock loading on the biomass activity due to the inhibitory effect of the contaminants at higher concentrations. Hence, from the practical standpoint, evaluation of the shock loading operation of the PBBR for the treatment of butachlor is highly essential. **Figure 5** demonstrates the effect of initial butachlor concentration on the removal efficiency for different initial butachlor concentrations. For an initial concentration of 500 mg/L of butachlor, the removal efficiency increased from 51 to 92% within 4 days and remained constant. On day 6, increasing the butachlor concentration to 750 mg/L, the removal efficiency sharply decreased to 50% and recovered to 87% by day 9, indicating the effect of shock loading on the bioreactor to be temporary. A similar trend of sharp dip followed by gradual increase in the RE till a steady point was observed when the butachlor concentration was increased to 1,000 mg/L, 1,500 mg/L, and 2000 mg/L. The result obtained in the present investigation indicates that the PBBR can adapt to shock loading pertaining to higher butachlor concentrations. This may be due to the formation of the biofilm on the support material. Formation of biofilm by the bacterial cells has been reported as one of the major adaptation strategies which has been reported for the purpose of bioremediation of various organic contaminants (Sahoo and Panigrahy 2018; Dash and Osborne 2020).

Combined Removal of the Mixture of Herbicides

The previous study refers to the evaluation of the performance of the PBBR using a single-target contaminant, butachlor. However, in most of the cases, more than one contaminant occurs as a mixture in the environment, which may affect the removal efficiency of the bioreactor. Since, COD is a widely used parameter that is measured to assess the magnitude of pollution in any wastewater, in the present study, performance evaluation of the PBBR for the treatment of synthetic wastewater comprising the mixture of herbicides was investigated with respect to its COD removal efficiency (**Figure 6**). The removal efficiency of the PBBR was evaluated for various initial COD concentrations in a continuous mode to evaluate the simultaneous removal of the herbicides. In the present study, percentage of COD reduction was monitored as a function of time. Based on the results of the single-substrate system, the flow rate of the PBBR was maintained at 2.77 ml/min corresponding to the HRT of 24 h for the simultaneous removal of the mixture of pesticides from the wastewater. The figure indicates that at

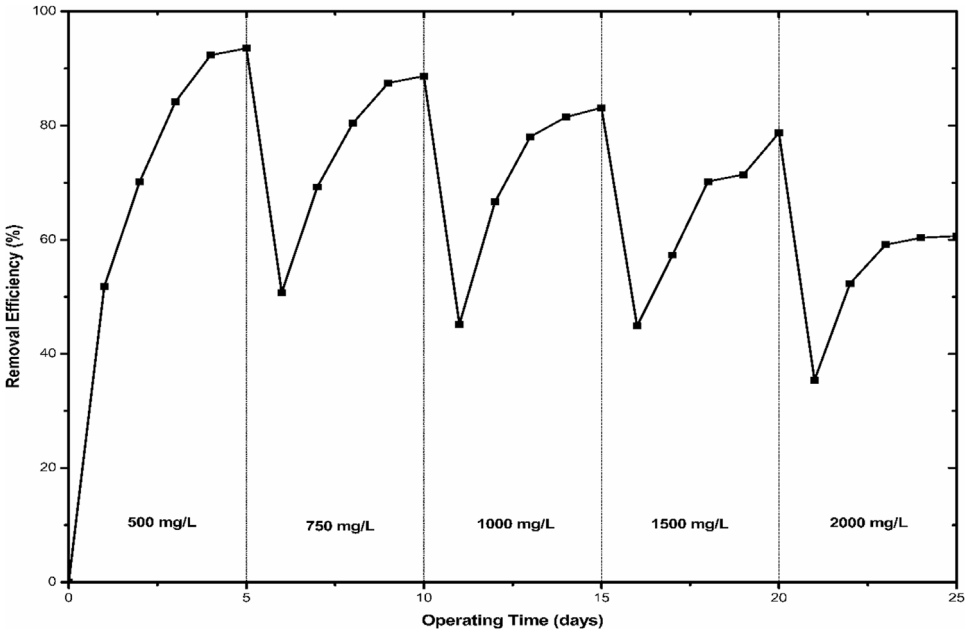

FIGURE 5 | Effect of initial butachlor concentration on the removal efficiencies and elimination capacity of the PBBR.

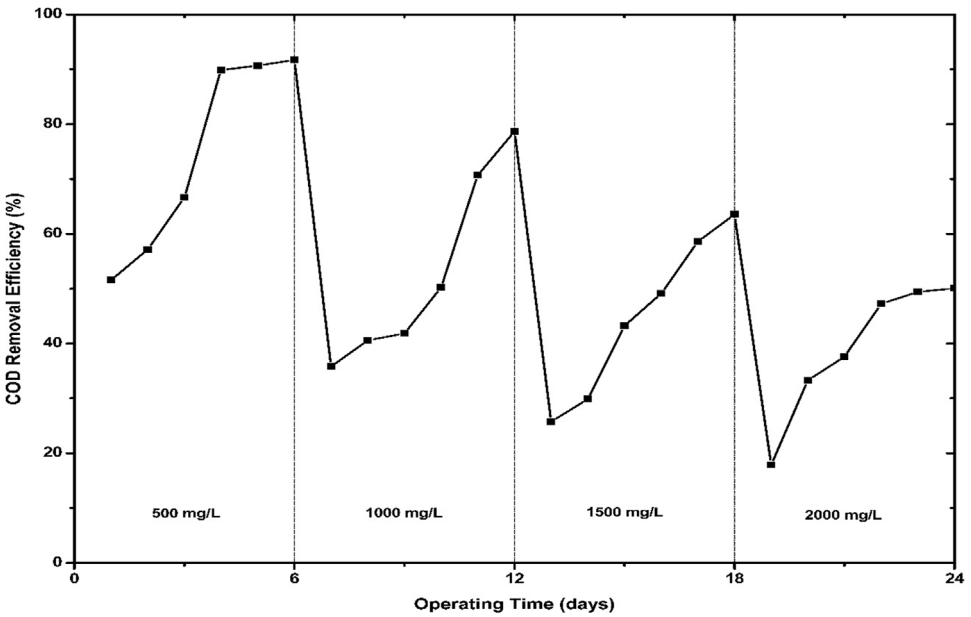

FIGURE 6 | COD level and the corresponding COD removal (%) in the synthetic wastewater by the PBBR.

lower concentration, degradation efficiencies of the PBBR is considerably high, which decreases gradually with increasing concentrations. Though complete removal cannot be achieved, more than 90% removal efficiency is achieved at stage 1, where the COD level of the influent was maintained at 500 mg/L. The COD removal efficiency was further reduced to less than 80% on increasing the COD level of the influent to 1,000 mg/L. A similar trend of gradual decrease in the COD removal efficiency with increasing concentration of the pollutant in the synthetic wastewater was observed previously in various studies (Alfonso-Gordillo et al., 2016b; Arikan et al., 2019). The relative underperformance of the PBBR for the herbicide

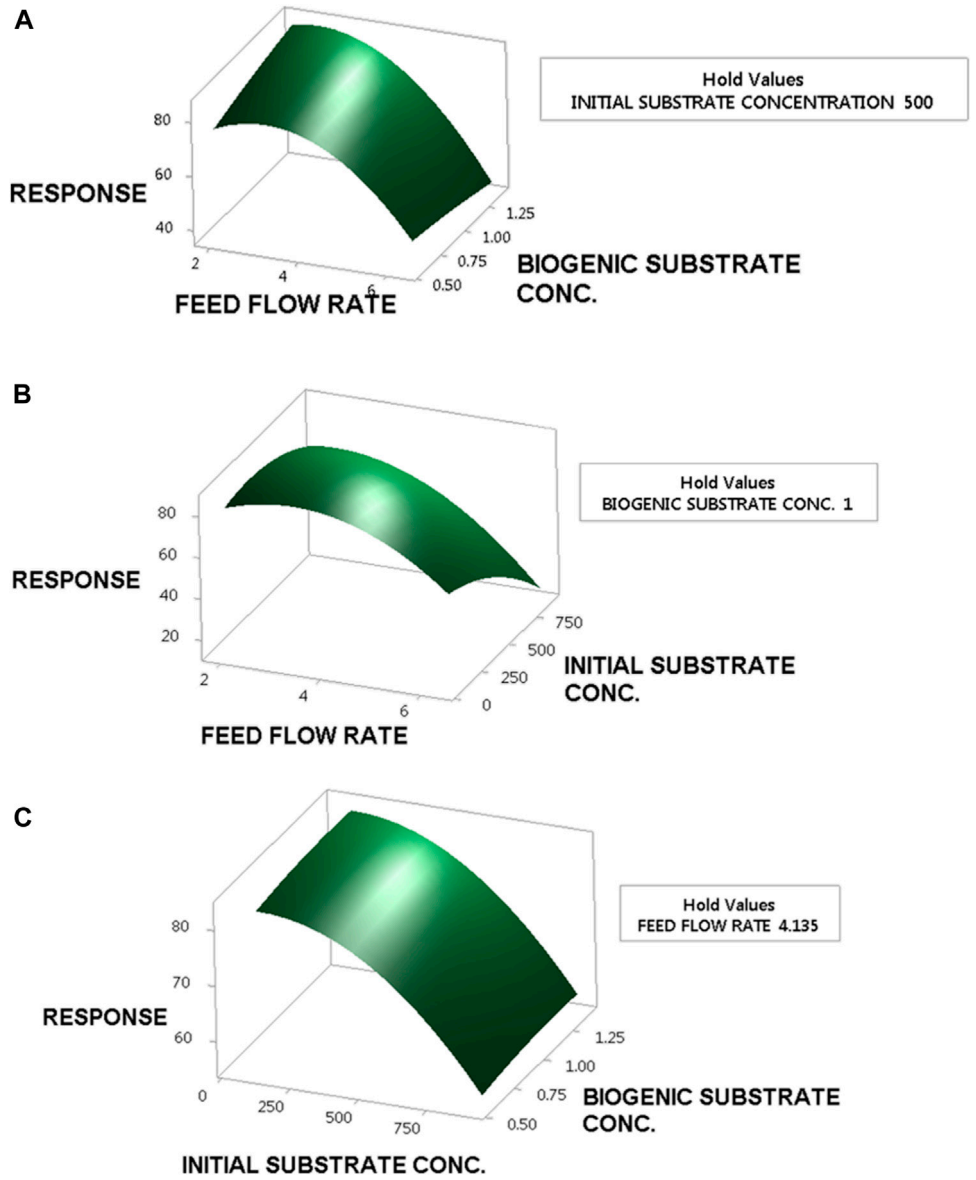

FIGURE 7 | Three-dimensional plot of COD removal efficiency as a function of **(A)** feed flow rate and additional biogenic substrate concentration; **(B)** feed flow rate and initial substrate concentration; **(C)** initial substrate concentration and additional biogenic substrate concentration.

mixture as compared to the single-substrate system may be attributed to the increased toxicity due to the presence of multiple herbicides in the influent that inhibits the normal metabolic activities of the microbial strain (Arikan et al., 2019). However, the PBBR demonstrates excellent COD removal efficiency and projects itself as a potential alternative to treat wastewater generating from the herbicide industries.

Parameter Optimization Using RSM

The available literature survey evidenced that three independent variables, that is, inlet feed flow rate, initial substrate concentration, and additional biogenic substrate concentration have a significant effect on the COD removal efficiency of the bioreactor (Patel and Kumar 2016; Nguyen et al., 2017). Hence, in the present study, the aforementioned parameters were optimized by RSM to yield maximum COD removal by the bioreactor. The design matrix of the subjected variables and the experimental results are being presented in **Table 1**. The significance of each variable and the model was determined by their probability value and the correlation value, respectively (**Supplementary Table ST1**). The results revealed the statistically significant ($p < 0.05$) effects of influent feed flow rate and initial substrate concentration on COD removal efficiency of the PBBR. Regardless of their significance, all the terms (both linear and quadratic) have been included in the following second-order polynomial equation:

$$\mathbf{RE}(\%) = \mathbf{23.7} + \mathbf{26.36}\times\mathbf{FFR} + \mathbf{0.0399}\times\mathbf{ISC} + \mathbf{27.8}\times\mathbf{ABSC} - \mathbf{3.215}\times(\mathbf{FFR}\times\mathbf{FFR}) - \mathbf{0.000041}\times(\mathbf{ISC}\times\mathbf{ISC}) - \mathbf{3.7}\times(\mathbf{ABSC}\times\mathbf{ABSC}) - \mathbf{0.00762}\times(\mathbf{FFR}\times\mathbf{ISC}) - \mathbf{4.66}\times(\mathbf{FFR}\times\mathbf{ABSC}) - \mathbf{0.00013}\times(\mathbf{ISC}\times\mathbf{ABSC}),$$

where RE represents COD removal efficiency; FFR represents feed flow rate; ISC represents initial substrate concentration; and ANS represents additional biogenic substrate concentration.

A regression model is usually considered statistically accurate, highly correlated, and reproducible when the coefficient of correlation (R^2) value is higher than 0.9 (Bakkiyaraj et al., 2016). The R^2 value of 0.9018 indicates a good agreement between the experimental and the predicted values, which can be verified from the normal probability plot of the residual (**Supplementary Figure S3**). The adjusted and predicted R^2 values were found to be 0.9616 and 0.9846, respectively. The "Lack of Fit" of 0.0687 suggests that the Lack of Fit is nonsignificant compared to the pure error. The model is found to be competent for prediction within the range of variables used. The mutual interaction among the variables and their effect on the COD removal efficiency of the PBBR were determined by mapping three-dimensional response surface plots where the function of two variables was observed while retaining the other variable constant at the center point (**Figure 7**). The shape of the plot evidently indicates the prominence of the involved parameters and the significance of the mutual interaction among them. From the figures and from the ANOVA table, it is highly evident that feed flow rate and substrate concentration play a major role in determining the COD removal efficiency of the PBBR. Previous studies pertaining to optimization of the process parameters have reported the significance of substrate concentration and feed flow rate on the COD removal efficiency of the packed-bed bioreactors (Dev et al., 2017; Pandey and Sarkar 2019). It is an established concept that the feed flow rate of the influent has the higest impact in determining the efficiency of the PBBR (Mohanty et al., 2021). The feed flow rate determines the retention time of the pollutant within the bioreactor. The more the retention time, the more opportunities obtained by the to metabolize the pollutant efficiently. However, an exceedingly low feed flow rate may also lead to mass transfer limitations, which may result in lower removal percentage (Yadav et al., 2014). Similarly, up to a certain initial concentration, the substrate may act as the nutrient for the microbial biomass; however, increase in the substrate concentration may confer the toxic effect of the herbicides on the metabolic activity of the microbial biomass, thus resulting in a low removal competency. The desirability function thus predicted that maximum COD removal can be achieved at the optimum range of a feed flow rate of 2.9 ml/min, substrate concentration of 454.63 mg/L, and concentration of additional nitrogen source at 1.41 g/L. The proposed model was validated experimentally, and it was found that the difference between the predicted and actual COD removal rate was less that 3%, thus indicating the adequacy of the model.

CONCLUSION

The present study aims to achieve high butachlor removal efficiency both as a single-substrate system and in a mixture of herbicides from wastewater using microbial consortium SMC1 immobilized on ceramic raschig rings in a continuous vertical flow packed-bed biofilm reactor system. It was observed that both the removal efficiency and the elimination capacity of the system are affected by the retention time, inlet loading rates and the intial substrate concentration of the wastewater. The bioreactor system is also capable of treating the mixture of herbicides efficiently and reduces the overall COD concentration of the wastewater. Optimization of the operating parameters such as feed flow rate, substrate concentrations, and additional biogenic substances that have a major effect on the performance of the bioreactor was successfully carried out using RSM. The removal efficiency obtained in the PBBR system was found to be superior to the previously studied bio-systems. Bioremediation of chloroacetanalide class of herbicides in a continuous-system bioreactor has been one of the least explored fields of study. Hence, the present study demonstrates the feasibility of developing a large-scale biofilm-mediated bioreactor for the effective treatment of wastewater from herbicide industries.

DATA AVAILABILITY STATEMENT

The raw data supporting the conclusion of this article will be made available by the authors, without undue reservation.

AUTHOR CONTRIBUTIONS

SM conceived the presented idea, carried out the experiment, performed the analyses, and wrote the manuscript. HJ supervised the investigation and verified the findings of this work. All authors discussed the results and contributed to the final version of the manuscript.

SUPPLEMENTARY MATERIAL

The Supplementary Material for this article can be found online at: https://www.frontiersin.org/articles/10.3389/fceng.2022.721923/full#supplementary-material

REFERENCES

Abigail, M. E. A., Samuel, S. M., and Ramalingam, C. (2015). Addressing the Environmental Impacts of Butachlor and the Available Remediation Strategies: a Systematic Review. *Int. J. Environ. Sci. Technol.* 12, 4025–4036. doi:10.1007/s13762-015-0866-2

Acuna-Askar, K., Englande, A. J., Hu, C., and Jin, G. (2000). Methyl Tertiary-Butyl Ether (MTBE) Biodegradation in Batch and Continuous Upflow Fixed-Biofilm Reactors. *Water Sci. Technol.* 42, 153–161. doi:10.2166/wst.2000.0509

Alfonso-Gordillo, G., Cristiani-Urbina, E., Flores-Ortiz, C. M., Peralta, H., Cancino-Díaz, J. C., Cruz-Maya, J. A., et al. (2016a). Stenotrophomonas Maltophilia Isolated from Gasoline-Contaminated Soil Is Capable of Degrading Methyl Tert-Butyl Ether. *Electron. J. Biotechnol.* 23, 12–20. doi:10.1016/j.ejbt.2016.06.006

Alfonso-Gordillo, G., Flores-Ortiz, C. M., Morales-Barrera, L., and Cristiani-Urbina, E. (2016b). Biodegradation of Methyl Tertiary Butyl Ether (MTBE) by a Microbial Consortium in a Continuous Up-Flow Packed-Bed Biofilm Reactor: Kinetic Study, Metabolite Identification and Toxicity Bioassays. *PLoS One* 11, e0167494. doi:10.1371/journal.pone.0167494

Annett, R., Habibi, H. R., and Hontela, A. (2014). Impact of Glyphosate and Glyphosate-Based Herbicides on the Freshwater Environment. *J. Appl. Toxicol.* 34, 458–479. doi:10.1002/jat.2997

Arikan, E. B., Isik, Z., Bouras, H. D., and Dizge, N. (2019). Investigation of Immobilized Filamentous Fungi for Treatment of Real Textile Industry Wastewater Using up Flow Packed Bed Bioreactor. *Bioresour. Tech. Rep.* 7, 100197. doi:10.1016/J.BITEB.2019.100197

Atwood, D., and Paisley-Jones, C. (2017). *Pesticides Industry Sales and Usage* https://www.epa.gov/sites/production/files/2017-01/documents/pesticides-industry-sales-usage-2016_0.pdf.

Bakkiyaraj, S., Syed, M. B., Devanesan, M. G., and Thangavelu, V. (2016). Production and Optimization of Biodiesel Using Mixed Immobilized Biocatalysts in Packed Bed Reactor. *Environ. Sci. Pollut. Res.* 23, 9276–9283. doi:10.1007/s11356-015-4583-7

Briceño, G., Levio, M., González, M. E., Saez, J. M., Palma, G., Schalchli, H., et al. (2020). Performance of a Continuous Stirred Tank Bioreactor Employing an Immobilized Actinobacteria Mixed Culture for the Removal of Organophosphorus Pesticides. *3 Biotech.* 10, 252. doi:10.1007/s13205-020-02239-9

Chattopadhyay, A., Adhikari, S., Adhikary, S. P., and Ayyappan, S. (2006). Evaluation of Butachlor for Control of Submerged Macrophytes along with its Impact on Biotic Components of Freshwater System. *Iran J. Environ. Heal Sci. Eng.* 3, 103–108.

Chen, C.-Y., Wang, G.-H., Tseng, I.-H., and Chung, Y.-C. (2016). Analysis of Bacterial Diversity and Efficiency of Continuous Removal of Victoria Blue R from Wastewater by Using Packed-Bed Bioreactor. *Chemosphere* 145, 17–24. doi:10.1016/j.chemosphere.2015.11.061

Choudhury, P. P., Singh, R., Ghosh, D., and Sharma, A. R. (2016). Herbicide Use in Indian Agriculture. Technical report. doi:10.13140/RG.2.2.20822.75848

Dash, D. M., and Osborne, W. J. (2020). Rapid Biodegradation and Biofilm-Mediated Bioremoval of Organophosphorus Pesticides Using an Indigenous Kosakonia Oryzae Strain -VITPSCQ3 in a Vertical-Flow Packed Bed Biofilm Bioreactor. *Ecotoxicology Environ. Saf.* 192, 110290. doi:10.1016/J.ECOENV.2020.110290

Dev, S., Roy, S., and Bhattacharya, J. (2017). Optimization of the Operation of Packed Bed Bioreactor to Improve the Sulfate and Metal Removal from Acid Mine Drainage. *J. Environ. Manage.* 200, 135–144. doi:10.1016/J.JENVMAN.2017.04.102

Dzionek, A., Wojcieszyńska, D., and Guzik, U. (2016). Natural Carriers in Bioremediation: A Review. *Electron. J. Biotechnol.* 23, 28–36. doi:10.1016/j.ejbt.2016.07.003

Ercan, D., and Demirci, A. (2015). Current and Future Trends for Biofilm Reactors for Fermentation Processes. *Crit. Rev. Biotechnol.* 35, 1–14. doi:10.3109/07388551.2013.793170

Foroughi, M., Sarabi Jamab, M., Keramat, J., and Najaf Najafi, M. (2019). The Use ofSaccharomyces Cerevisiaeimmobilized on Activated Alumina, and Alumina Silicate Beads for the Reduction of Aflatoxin M1*In Vitro*. *J. Food Process. Preserv* 43, e13876. doi:10.1111/JFPP.13876

Gianessi, L. P. (2005). Economic and Herbicide Use Impacts of Glyphosate-Resistant Crops. *Pest Manag. Sci.* 61, 241–245. doi:10.1002/ps.1013

Kaur, R., and Goyal, D. (2020). Biodegradation of Butachlor by Bacillus Altitudinis and Identification of Metabolites. *Curr. Microbiol.* 77, 2602–2612. doi:10.1007/s00284-020-02031-1

Khalid, S., and Hashmi, I. (2016). Biotreatment of Chlorpyrifos in a Bench Scale Bioreactor Using Psychrobacter Alimentarius T14. *Environ. Tech.* 37, 316–325. doi:10.1080/09593330.2015.1069406

Kureel, M. K., Geed, S. R., Rai, B. N., and Singh, R. S. (2018). Novel Investigation of the Performance of Continuous Packed Bed Bioreactor (CPBBR) by Isolated Bacillus Sp. M4 and Proteomic Study. *Bioresour. Tech.* 266, 335–342. doi:10.1016/j.biortech.2018.06.064

Lauga, B., Girardin, N., Karama, S., Le Ménach, K., Budzinski, H., and Duran, R. (2013). Removal of Alachlor in Anoxic Soil Slurries and Related Alteration of the Active Communities. *Environ. Sci. Pollut. Res.* 20, 1089–1105. doi:10.1007/s11356-012-0999-5

Liu, H., Cao, L., Lu, P., Ni, H., Li, X. Y., Yan, X., et al. (2012). Biodegradation of Butachlor by Rhodococcus Sp. Strain B1 and Puri Fi Cation of its Hydrolase (ChlH) Responsible for N - Dealkylation of Chloroacetamide Herbicides. *J. Agric. Food Chem.* 60, 12238–12244. doi:10.1021/jf303936j

Liu, Z., He, Y., Xu, J., Huang, P., and Jilani, G. (2008). The Ratio of clay Content to Total Organic Carbon Content Is a Useful Parameter to Predict Adsorption of the Herbicide Butachlor in Soils. *Environ. Pollut.* 152, 163–171. doi:10.1016/j.envpol.2007.05.006

Mohanty, S. R., Nayak, D. R., Babu, Y. J., and Adhya, T. K. (2004). Butachlor Inhibits Production and Oxidation of Methane in Tropical rice Soils under Flooded Condition. *Microbiol. Res.* 159, 193–201. doi:10.1016/j.micres.2004.03.004

Mohanty, S. S., and Jena, H. M. (2019a). A Systemic Assessment of the Environmental Impacts and Remediation Strategies for Chloroacetanilide Herbicides. *J. Water Process Eng.* 31, 100860. doi:10.1016/j.jwpe.2019.100860

Mohanty, S. S., and Jena, H. M. (2019c). Degradation Kinetics and Mechanistic Study on Herbicide Bioremediation Using Hyper Butachlor-Tolerant Pseudomonas Putida G3. *Process Saf. Environ. Prot.* 125, 172–181. doi:10.1016/j.psep.2019.03.014

Mohanty, S. S., and Jena, H. M. (2019b). Evaluation of Butachlor Biodegradation Efficacy of Serratia Ureilytica Strain AS1: a Statistical Optimization Approach. *Int. J. Environ. Sci. Technol.* 16, 5807–5816. doi:10.1007/s13762-018-1958-6

Mohanty, S. S., and Jena, H. M. (2018). Process Optimization of Butachlor Bioremediation by *Enterobacter cloacae* Using Plackett Burman Design and Response Surface Methodology. *Process Saf. Environ. Prot.* 119, 198–206. doi:10.1016/j.psep.2018.08.009

Mohanty, S. S., Reddy, D. K., and Jena, H. M. (2021). Mass Transfer Study of Butachlor Biodegradation Using Immobilized Microbial Consortium SMC1 in a Packed Bed Bioreactor. *Can. J. Chem. Eng.* 100, 1–9. doi:10.1002/cjce.24118

Muter, O., Perkons, I., Svinka, V., Svinka, R., and Bartkevics, V. (2017). Distinguishing the Roles of Carrier and Biofilm in Filtering media for the Removal of Pharmaceutical Compounds from Wastewater. *Process Saf. Environ. Prot.* 111, 462–474. doi:10.1016/j.psep.2017.08.010

Nguyen, P. Y., Carvalho, G., Reis, A. C., Nunes, O. C., Reis, M. A. M., and Oehmen, A. (2017). Impact of Biogenic Substrates on Sulfamethoxazole Biodegradation Kinetics by Achromobacter Denitrificans Strain PR1. *Biodegradation* 28, 205–217. doi:10.1007/s10532-017-9789-6

Orme, S., and Kegley, S. (2004). Alachlor - Toxicity, Ecological Toxicity and Regulatory Information PAN Pestic Database - Chem. AvaliableAt: http://www.pesticideinfo.org/Detail_Chemical.jsp?Rec_Id=PC35160#Toxicity.

Pandey, S., and Sarkar, S. (2019). Performance Evaluation and Substrate Removal Kinetics of an Anaerobic Packed-Bed Biofilm Reactor. *Int. J. Environ. Res.* 13, 223–233. doi:10.1007/S41742-019-00168-X

Patel, B. P., and Kumar, A. (2016). Biodegradation of 2,4-dichlorophenol in Packed-Bed Biofilm Reactor: Effect of Hydraulic Retention Time, Biogenic Substrate, and Loading Rate. *Water Environ. Res.* 88, 2191–2197. doi:10.2175/106143016X14733681695726

Polard, T., Jean, S., Gauthier, L., Laplanche, C., Merlina, G., Sánchez-Pérez, J. M., et al. (2011). Mutagenic Impact on Fish of Runoff Events in Agricultural Areas in South-West France. *Aquat. Toxicol.* 101, 126–134. doi:10.1016/j.aquatox.2010.09.014

Sahoo, N. K., and Panigrahy, N. (2018). Biodegradation and Kinetic Study of 4-Chlorophenol in Bioreactor Packed with Stabilized Bacteria Entrapped in Calcium Alginate Beads System. *Environ. Process.* 5, 287–302. doi:10.1007/S40710-018-0294-7/FIGURES/5

Shukla, S. K., Mangwani, N., Rao, T. S., and Das, S. (2014). "Biofilm-Mediated Bioremediation of Polycyclic Aromatic Hydrocarbons," in *Microbial Biodegradation and Bioremediation*. Editor S. Das (New Delhi, Elsevier: Elsevier BV), 203–232. doi:10.1016/b978-0-12-800021-2.00008-x

Shuman-Goodier, M. E., Singleton, G. R., Forsman, A. M., Hines, S., Christodoulides, N., Daniels, K. D., et al. (2021). Developmental Assays Using Invasive Cane Toads, Rhinella marina, Reveal Safety Concerns of a Common Formulation of the rice Herbicide, Butachlor. *Environ. Pollut.* 272, 115955. doi:10.1016/J.ENVPOL.2020.115955

Sonwani, R. K., Giri, B. S., Jaiswal, R. P., Singh, R. S., and Rai, B. N. (2020). Performance Evaluation of a Continuous Packed Bed Bioreactor: Bio-Kinetics and External Mass Transfer Study. *Ecotoxicology Environ. Saf.* 201, 110860–110868. doi:10.1016/j.ecoenv.2020.110860

Sung Wang, M.-H., Wang, L. K., and De Michele, E. (2017). "Principles, Procedures, and Heavy Metal Management of Dichromate Reflux Method for COD Determination in Laboratories," in *Handbook of Advanced Industrial and Hazardous Wastes Management*. L. K. Wang, M. H. Wang, and Y. T. Hung. (Washington, Taylor & Francis: CRC Press), 809–818. doi:10.1201/9781315117423-24

Swain, G., Sonwani, R. K., Singh, R. S., Jaiswal, R. P., and Rai, B. N. (2021). Removal of 4-Chlorophenol by Bacillus Flexus as Free and Immobilized System: Effect of Process Variables and Kinetic Study. *Environ. Tech. Innovation* 21, 101356. doi:10.1016/J.ETI.2021.101356

University of Hertfordshire (2013). "PPDB: Pesticide Properties DataBase," in *Pestic. Prop. Database Website Database*. Hatfield, Hertfordshire: University of Hertfordshire.

Yadav, M., Srivastva, N., Singh, R. S., Upadhyay, S. N., and Dubey, S. K. (2014). Biodegradation of Chlorpyrifos by Pseudomonas Sp. In a Continuous Packed Bed Bioreactor. *Bioresour. Tech.* 165, 265–269. doi:10.1016/j.biortech.2014.01.098

Conflict of Interest: The authors declare that the research was conducted in the absence of any commercial or financial relationships that could be construed as a potential conflict of interest.

Publisher's Note: All claims expressed in this article are solely those of the authors and do not necessarily represent those of their affiliated organizations, or those of the publisher, the editors, and the reviewers. Any product that may be evaluated in this article, or claim that may be made by its manufacturer, is not guaranteed or endorsed by the publisher.

frontiers | Frontiers in Chemical Engineering

ORIGINAL RESEARCH
published: 26 July 2022
doi: 10.3389/fceng.2022.884451

Fatty Acid Accumulations and Transcriptome Analyses Under Different Treatments in a Model Microalga *Euglena gracilis*

Jiayi He[1,2], *Ming Du*[1], *Yehua Chen*[1], *Yerong Liu*[1], *Jinlin (Kenny) Zhang*[1,3], *Wen Fu*[1], *Anping Lei*[1] *and Jiangxin Wang*[1]*

[1]*Shenzhen Key Laboratory of Marine Bioresource and Eco-Environmental Science, Shenzhen Engineering Laboratory for Marine Algal Biotechnology, Guangdong Provincial Key Laboratory for Plant Epigenetics, College of Life Sciences and Oceanography, Shenzhen University, Shenzhen, China,* [2]*Key Laboratory of Optoelectronic Devices and Systems of Ministry of Education and Guangdong Province, College of Optoelectronic Engineering, Shenzhen University, Shenzhen, China,* [3]*BASIS International School Park Lane Harbour, Shenzhen, China*

With the continuous growth of the world's population and the increasing development of industrialization, the demand for energy by human beings has been expanding, resulting in an increasingly severe energy crisis. Microalgae are considered the most potential alternatives to traditional fossil fuels due to their many advantages, like fast growth rate, strong carbon sequestration capacity, and low growth environment requirements. *Euglena* can use carbon sources such as glucose, ethanol, and others for heterotrophic growth. Moreover, *Euglena* is highly adaptable to the environment and has a high tolerance to various environmental stresses, such as salinity, heavy metals, antibiotics, etc. Different treatments of *Euglena* cells could affect their growth and the accumulation of bioactive substances, especially fatty acids. To expand the industrial application of *Euglena* as a potential biodiesel candidate, we determine the physiological responses of *Euglena* against environmental stresses (antibiotics, heavy metals, salinity) or carbon resources (glucose and ethanol), and evaluate the potential for higher quality and yield of fatty acid with a high growth rate. Adding glucose into the culture media increases cell biomass and fatty acid production with high-quality biodiesel characters. The transcriptome analysis helped explore the possible regulation and biosynthesis of fatty acids under different treatments and exploited in the improvement of biodiesel production. This study provides insights for further improvement and various culture treatments for *Euglena*-based biodiesel and jet fuels.

Keywords: ***Euglena gracilis*, fatty acids, biodiesel, transcriptome, environmental stresses, carbon sources**

OPEN ACCESS

Edited by:
He Huang,
Nanjing Normal University, China

Reviewed by:
Xiao-Jun Ji,
Nanjing Tech University, China
Jingwen Zhou,
Jiangnan University, China

***Correspondence:**
Jiangxin Wang
jxwang@szu.edu.cn

Specialty section:
This article was submitted to Biochemical Engineering, a section of the journal Frontiers in Chemical Engineering

Received: *26 February 2022*
Accepted: *22 June 2022*
Published: *26 July 2022*

Citation:
He J, Du M, Chen Y, Liu Y, Zhang J, Fu W, Lei A and Wang J (2022) Fatty Acid Accumulations and Transcriptome Analyses Under Different Treatments in a Model Microalga Euglena gracilis. Front. Chem. Eng. 4:884451. doi: 10.3389/fceng.2022.884451

1 INTRODUCTION

Environmental problems and energy crises are becoming increasingly severe; therefore, it is imperative to discover novel, renewable, and environmentally friendly energy sources (Xia et al., 2019; Luo et al., 2021). Many microalgae, such as *Chlorella*, *Spirulina*, and *Dunaliella*, are cultured on a large scale and used in industrial applications (Gilmour, 2019). The microalga *Euglena gracilis* has characteristics of both plants and animals, with secondary endosymbiotic chloroplasts without cell

walls. Its cells contain many high-value bioproducts, including vitamins, amino acids, unsaturated fatty acids, and paramylon (Grimm et al., 2015; Zakryś et al., 2017). *E. gracilis* is of considerable environmental importance and biotechnological value: it can survive a variety of carbon resources, toxic chemicals, and adverse environmental conditions such as heavy metals, antibiotics, acid, salinity, and high levels of ionizing radiation, and can be observed in most waters such as ponds, fish farms and small rivers (Rodríguez-Zavala et al., 2007; Kottuparambil et al., 2012; Mukaida et al., 2016; Moreno-Sánchez et al., 2017; He et al., 2021). Indeed, *E. gracilis* exhibits remarkable metabolic diversity, blooming as photosynthetic autotrophy, heterotrophy, and photoheterotrophy (Zakryś et al., 2017). Thus, *Euglena* species are highly flexible to different nutrients and tolerant to adverse environments, which makes *Euglena* a model microorganism for environmental assessments, wastewater remediation, and sources of numerous bioproducts.

Environmental factors such as temperature, nutrients, carbon source, heavy metals, trace elements, antibiotics, and organic matter affect the growth of microalgae (Béchet et al., 2013; Gao et al., 2021; Maltsev et al., 2021). In this study, biomass, fatty acid (FA) contents, compositions, and biodiesel quality under the addition of paromomycin (PRM), ethanol, glucose, $CdCl_2$, and NaCl with continuously light cultivation were evaluated.

In recent years, with the development of next-generation sequencing platforms, transcriptome sequencing (RNA sequencing, RNA-seq) has been gradually applied to microalgae research, with significant results (Khan et al., 2018). The first *de novo* transcriptome study revealed unexpected metabolic capabilities for carbohydrate and natural product biochemistry in *Euglena* (O'neill et al., 2015). Another comparative transcriptome analysis investigated *Euglena*'s response to anaerobic conditions, focusing on paramylon and wax ester metabolic pathways (Yoshida et al., 2016). Five available *E. gracilis* transcriptome data, under fermentative, mixotrophic, heterotrophic, and phototrophic culture conditions, were well summarized (Geimer et al., 2009; Ebenezer et al., 2017, 2019; Cordoba et al., 2021). Thus, research on microalgae transcriptomes helps us characterize microalgal diversity better. The application of this technology will enable us to understand the mechanisms by which *E. gracilis* responds to different carbon sources and environmental stresses. However, no data were collected for transcriptome investigation in *Euglena* under environmental stresses.

In this study, we used RNA-seq technology and *de novo* assembly to perform analysis of the *E. gracilis* transcriptome under selected treatments as addition of ethanol (E1.0, 1.0% vol/vol), glucose (G1.0, 1.0% weight), NaCl (NaCl1, 1.0%) Cd0.5 ($CdCl_2$ 0.5 mM), and PRM5.0 (5 μg/ml). Differential gene expression and related metabolic pathways of *E. gracilis* in response to various treatments were investigated. *Euglena* cells showed both shared and distinct responses to these treatments at the transcriptional level. $CdCl_2$ stress significantly down-regulated thousands of genes, some of them related to amino acid metabolism and N-glycan biosynthesis. NaCl inhibited cell growth but did not change gene expression much at the transcriptional level. Different carbon sources such as ethanol and glucose promoted cell growth and altered the expression of genes related to photosynthesis, carbon fixation, nucleotide biosynthetic processes, component of the plasma membrane, ABC transporters, and the mRNA surveillance pathway. GO and KEGG pathway enrichments provide insights into the mechanisms of differential responses of *E. gracilis* to different treatments, especially the FA contents and composition changes.

2 MATERIALS AND METHODS

2.1 Strain and Cultural Conditions

E. gracilis 1224/5Z was obtained from the Culture Collection of Algae and Protozoa (https://www.ccap.ac.uk/). Aliquots of cells ($1–3 \times 10^5$) were incubated in 5 ml of fresh culture medium. The algal cells were grown in photosynthetic medium (1.8 g/L NH_4Cl, 0.6 g/L KH_2PO_4, 0.6 g/L $MgSO_4$, 60 mg/L urea, 0.02 g/L $CaCl_2$, 0.48 mg/L Na_2EDTA, 2 mg/L $Fe_2(SO_4)_3$, 60 μL HCl, 0.01 mg/L Vb_1, 0.0005 mg/L Vb_{12}, 20 mg/L $CuSO_4{\cdot}5H_2O$, 0.4 g/L $ZnSO_4{\cdot}7H_2O$, 1.3 g/L $Co(NH_3){\cdot}H_2O$, and 1.6 g/L $MnCl_2{\cdot}4H_2O$) under a light intensity of approximately 100 μmol/m^2/s in an illuminating incubator at 26 °C until algal cells reached the stationary phase (Afiukwa et al., 2007; Wang et al., 2018).

2.2 Cultivation and Stress Treatments

E. gracilis cells were cultured for 6 days in a photosynthetic medium, then $1{\times}10^6$ cells/mL were centrifuged at 5,000×g for 3 min and transferred into an equal medium volume. Treatments were applied, including supplementation with PRM (PRM1, 5, 25 as 1, 5, 25 μg/ml), ethanol (E0.5, 1.0, 1.5 as 0.5, 1, 1.5% vol/vol), glucose (G0.5, G1.0, G1.5 as 0.5, 1.0, 1.5% weight), $CdCl_2$ (Cd0.5, 1, 1.5 as $CdCl_2$ of 0.5, 1.0, 1.5 mM), or NaCl1.0 (NaCl as 1% weight); After 6 days, samples were collected and used for future experiments. The concentrations were selected based on previous references (Kirk, 1962; Gonzalez-Moreno et al., 1997; Sánchez-Thomas et al., 2016; Ji et al., 2018) and our primarily experimental results.

2.3 Growth Biomass

The dry weight of $10^7–10^8$ cells was measured using the oven-drying method (Edmunds, 1965). The total algal chlorophyll was extracted with 95% ethanol, and the content was spectrophotometrically assayed according to the method (Harris, 2009). Triplicates of each treatment were conducted.

2.4 Fatty Acids and FAME Analyses

After 6 days' growth, *E. gracilis* samples were taken separately and centrifuged at 3,000 × g for 10 min to collect algal cells. The samples are freeze-dried for 48 h and weighed. Take 10 mg dry algae powder, add C19: 0 fatty acid methyl ester as internal standard, 0.01% butylated hydroxytoluene (BHT) methanol solution as an antioxidant, and refer to Zeng et al. (2016) for processing. The composition and content of fatty acids are detected by gas chromatography-mass spectrometry GC-MS (United States, 7890A-5975C). The column model is VF-23 ms (0.32 mm × 0.15 μm × 60 m), high-purity helium with a purity greater than 99.999% is used as the carrier gas, the injection

volume is 1 μL, the solvent is delayed for 5 min, the inlet temperature is 240°C, constant flow mode, and the split ratio is 10: 1. For calculating the fatty acid content, the internal standard curve method is used to calculate the absolute content and then convert it into the percentage content.

One-way ANOVA is used for the statistics of different treatment samples. The statistical software is SPSS20. The quality of *Euglena* fatty acids derived biodiesels, key indexes like saponification (SN), iodine values (IN), and cetane number (CN) were also investigated (Lu et al., 2012). The saponification value (SN) is the mass of sodium hydroxide required for the complete saponification of 1 g grease, which can reflect the relative molecular weight of grease, and SN = Σ(560 × Pi)/MWi. The iodine value (IN) indicates the degree of grease unsaturation. The iodine value reflects the number of double bonds in FA and IN = Σ(254 × D × Pi)/MWi. CN is a standard to measure the combustion performance of biodiesel in engines, and CN = 46.3 + 5458/SN - 0.225 × IN. This study combines GC-MS component analysis and gets three main performance parameters of FA in *E. gracilis* as biodiesel under different treatments (Lu et al., 2012).

2.5 RNA Isolation and RNA-Seq Analyses

The cDNA library construction and double-ended PE125 Illumina sequencing were performed by Real Omics (Biotech) Co., Ltd (Shenzhen, China). Approximately 10^6–10^7 cells were harvested by centrifugation at 5,000×g for 5 min at 4°C and used for total RNA isolation with a Trizol Kit (Invitrogen, United States). For RNA-seq, triplicates of each sample were used.

Because *E. gracilis* has no reference genome, Trinity software was used to assemble the clean reads, Corset was used to perform hierarchical clustering, and Benchmarking Universal Single-Copy Orthologs (BUSCO) was used to evaluate the completeness and integrity of the transcriptome assembly. Seven NCBI databases were used to annotate the assembled transcripts: NCBI non-redundant protein sequences (Nr), NCBI nucleotide sequences (Nt), Protein family (Pfam), euKaryotic Ortholog Groups (KOG) Clusters of Orthologous Groups of proteins (COG), Swiss-Prot manually annotated and reviewed protein sequence database, Kyoto Encyclopedia of Genes and Genomes (KEGG), and Gene Ontology (GO). The input data for the differential expression analysis were read counts obtained from the analysis of gene expression data. The analysis of samples with biological replicates was performed in DESeq2 based on a negative binomial distribution.

The KEGG Orthology Based Annotation System (KOBAS) was used to perform KEGG pathway enrichment analysis for each comparison with an automatic annotation server e-value of $1e^{-10}$. GO annotations were obtained from the annotations of the top 10 Nr blast hits using Blast2GO (Conesa et al., 2005) and from the Pfam database using InterPro scan (Anders and Huber, 2010; Kimbrel et al., 2011). The Seq method was used to identify pathways enriched in up-regulated and down-regulated differential gene sets for each group. When more genes are up-regulated than down-regulated in a selected pathway, the pathway would be marked up-regulated under this condition (Campanaro et al., 2007).

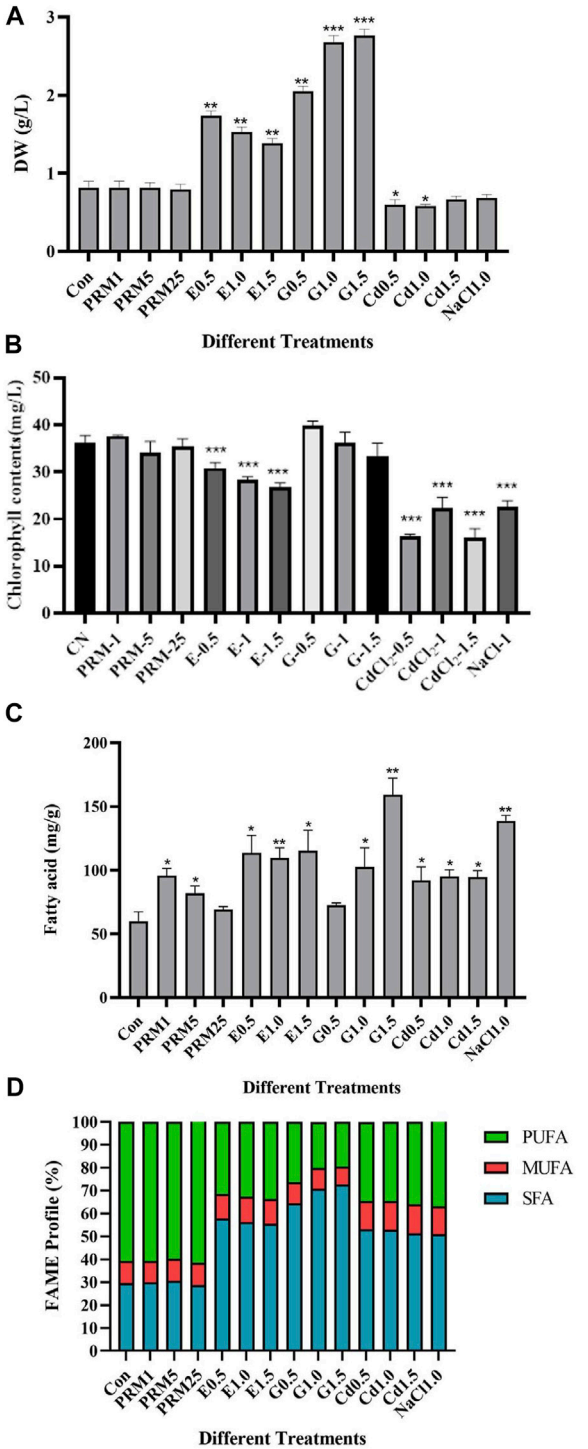

FIGURE 1 | Physiological changes of *E. gracilis* under different treatments. Dried weights **(A)**, chlorophyll contents **(B)**, variations of fatty acids contents **(C)** and FAME profile **(D)** of *E. gracilis* under different treatments. Asterisks "*", "**" indicate significant differences between treatments and control treatment (Con) at $p < 0.05$ and $p < 0.01$, respectively. Treatments include supplementation with paromomycin (PRM1, 5, 25 as 1, 5, 25 μg/ml), ethanol (E0.5, 1.0, 1.5 as 0.5, 1, 1.5% vol/vol), glucose (G0.5, G1.0, G1.5 as 0.5, 1.0, 1.5% weight), CdCl2 (Cd0.5, 1.0, 1.5 as CdCl2 of 0.5, 1.0, 1.5 mM), or NaCl1.0 (NaCl as 1% weight).

2.6 Statistical Analysis

Significant differences in growth biomass, fatty acids, and biodiesel fuel properties were tested using Dunnett's *t*-test. All data were obtained and averaged from at least three independent experiments, and standard errors were calculated and displayed as error bars.

3 RESULTS

3.1 Biomass and Chlorophyll Contents Under Different Treatments

Biomass differed significantly under different environmental treatments (**Figure 1A**). The PRM treatment caused no significant change in biomass, and NaCl and $CdCl_2$ treatment significantly reduced biomass ($p < 0.001$) by 18.18 and 18.72% relative to the control, respectively. All ethanol and glucose concentrations significantly increased biomass ($p < 0.001$) relative to the control by 64.75–107.66% and 216.47%, respectively. Glucose treatments showed higher biomass increases under all current concentrations in this case.

Chlorophylls in microalgae are sensitive to environmental stress. The addition of ethanol (all concentrations) $CdCl_2$ (all doses), and NaCl decreased the chlorophyll content of *E. gracilis* significantly (**Figure 1B**), whereas PRM and Glucose had no significant effect.

3.2 Fatty Acid Contents, Compositions, and FAME

The total fatty acid (TFA) content of *E. gracilis* under all treatments increases to varying degrees compared with the control, and some treated groups showed concentration-dependent manners, such as paromomycin (PRMs) and glucose (G) treatments (**Figure 1C**). The TFA content in PRM groups tends to decrease as the concentration increases. A low concentration of PRM (PRM1) has a higher effect on accumulating total fatty acids. However, in glucose-treated groups (G) TFA tends to increase with concentration, with the highest in G1.5 by about 132% increases compared to the control (Con). The second high TFA content was detected in the NaCl group, around 140 mg/g. The addition of ethanol (E0.5, E1.0, E1.5, as 0.5–1.5% vol/vol) nearly doubled the TFA compared to Con, with no significant difference among different concentrations. This study also showed a similar TFA increase by $CdCl_2$ at different concentrations.

Investigation of FA composition, namely SFA, MUFA, and PUFA, indicated interesting differences under treatments (**Figure 1D** and **Supplementary Table S1**). Compared with the control, the FA composition of *E. gracilis* under paromomycin treatments (PRM1, -5, -25) changed little. In contrast, the FAME profile under $CdCl_2$, ethanol, glucose, and NaCl treatment changed significantly.

The general trend of FA composition changes was almost the same, both which SFA proportion increases and PUFA proportion decreases, indicating more saturated fatty acids under these treatments. MUFA proportion changes little, and the most significant change was observed in the G1.5 treatment, whose SFA proportion increased from 29.51% of the control group to 72.72%. The PUFA proportion decreases from 60.85% of the control group to 19.49%. The change patterns in the other groups, Cd0.5, 1.0, 1.5, E0.5, 1.0, 1.5, and NaCl, were similar with no apparent dose-dependent pattern.

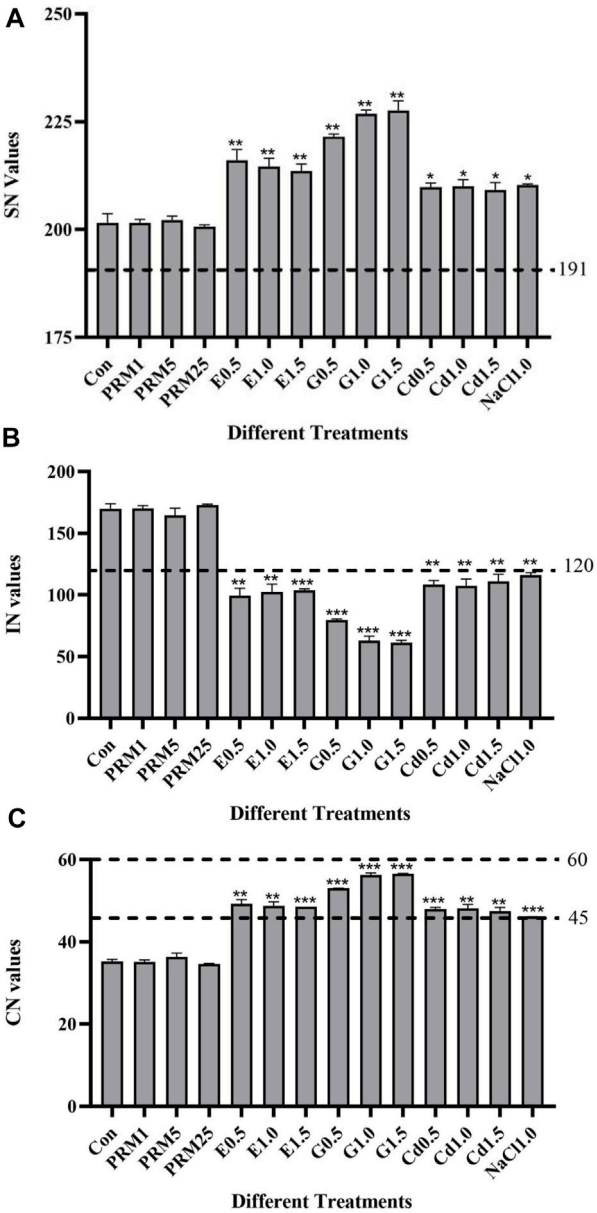

FIGURE 2 | Biodiesel fuel properties of *E. gracilis* TFA under different treatments at the sixth day. **(A)** saponification value (SN), **(B)** iodine value (IN), **(C)** cetane number (CN). Asterisks "*", "**" indicate significant differences between treatments and control treatment (Con) at $p < 0.05$ and $p < 0.01$, respectively. Lines indicate the standard threshold values for each biodiesel fuel property (SN, IN, or CN).

3.3 Evaluation of Biodiesel Fuel Properties of *E. gracilis* TFA

Biodiesel fuel characters were evaluated for *E. gracilis* TFA under different consumption methods. All the data are obtained and averaged from at least three independent experiments. As shown in the figure, compared with the control, the changes of SN (a), IN (b), and CN (c) of *E. gracilis* under different treatments were generally different (**Figure 2**).

The SN value of *E. gracilis* TFA slightly or significantly increased under different treatments than the control, except for no change under antibiotics treatments. The SN value of the G-1.5 treatment is the largest compared with the control, which increases by about 13%. The German EN 14214 standard requires that the SN value of biodiesel should be 187–191 mg/g. The SN value of each group in this study was larger than the standard (**Figure 2A**).

The minimum IN value standard in various countries' biodiesel production standards is <125 g/100 g (Arguelles and Martinez-Goss, 2021). The IN values of *E. gracilis* TFA in the control and paromomycin treated group are higher than the minimum standard by 35.92–36.02%, which is not suitable for direct use as biodiesel feedstock. In addition, the IN values of *E. gracilis* TFA under $CdCl_2$, ethanol, glucose, and NaCl treatments are significantly lower than those in control (**Figure 2B**). With the highest IN level (116.15), NaCl treated group has already met the standards of China, Australia, and the European Union (<120 g/100 g) and could be used as an ideal choice for biodiesel feedstock. The IN values of $CdCl_2$, ethanol, and glucose treatments (107.44–111.03, 99.22–103.62, 61.21–79.63) all reach the strict standards of biodiesel production in various countries, like the biodiesel production standards <115 g/100 g in Germany (EN 14214) and France, with excellent combustibility (Lu et al., 2012; Arguelles and Martinez-Goss, 2021). Among the low IN value treatments, the G1.5 treatment has the lowest compared with the control, with a significant reduction of about 64%.

Compared with the control, CN was improved under all treatments except for PRM (**Figure 2C**). The minimum requirement of CN in biodiesel production standards of various countries is higher than 45. The CN value of control and PRM groups is still 22.87–22.96%, respectively, lower than the minimum production standards of biodiesel. It could not be used directly as the raw material for biodiesel. The CN value of the E0.5 treatment is already 0.04% higher than the Chinese GB/T 20,828 standard and has the potential as a biodiesel feedstock. The CN values of G0.5, G1.0, and G1.5 treatment groups (53.02, 56.22, 56.51) have all reached the most demanding EU 14124 standard (> 51). The ideal treatment is the addition of glucose under different concentrations, about 51–60% higher than the control.

3.4 RNA-Seq Analyses

3.4.1 Summary of RNA-Seq and Differentially Expressed Genes

Our biomass and TFA results showed that treatments of E1.0, G1.0, NaCl1.0, Cd0.5, PRM25 caused significant differences compared to control samples, thus, these conditions were used for further transcriptome analyses. An average of 47,452,424 reads was generated for each sample. After removing low-quality reads, an average of 46,542,906 clean reads was obtained for each sample. The average GC content was less than 60%, the Q20 and Q30 values were 97 and 92%, respectively, and the sequencing error rate was 3%.

TABLE 1 | Differentially expressed genes (DEGs) based on RNA-seq under different treatments compared with the control. Treatments include supplementation with paromomycin (PRM25, 25 μg/ml), ethanol (E1.0, 1.0% vol/vol), glucose (G1.0, 1.0% weight), $CdCl_2$ (Cd0.5, 0.5 mM), or NaCl1.0 (NaCl as 1.0% weight).

Treatments	Total DEGs	Up-regulated	Down-regulated
NaCl1.0	490	280	210
PRM25	209	128	81
Cd0.5	4,324	3,040	1,284
G1.0	1,080	37	1,043
E1.0	1,040	56	984

Compared with the control, overall gene expression changes were the most obvious in the $CdCl_2$ treatment, with 3,040 and 1,284 up-regulated and down-regulated genes. The heavy metal Cd^{2+}, therefore, appeared to have a significant effect on the transcriptome of *E. gracilis* (**Table 1**). The gene expression changes were less evident in the ethanol and glucose treatments. Under ethanol addition (E1.0), there were 56 and 1,040 up- and down-regulated genes, i.e., about 20 times more down-regulated genes than up-regulated ones. Similarly, in the glucose treatment (G1), there were 1,043 down-regulated genes and only 37 up-regulated genes.

Compared with thousands of genes altered under the addition of Cd^{2+}, glucose, and ethanol treatments, PRM and NaCl treatments had relatively modest changes on the overall transcriptome, causing up-regulation of 128–280 genes and down-regulation of 81–210 genes (**Table 1**).

3.4.2 Gene Expression Patterns Related to Reactive Oxygen Species, Fatty Acid Metabolism and Chlorophyll Biosynthesis

Reactive oxygen species (ROS) scavenging genes, such as *APX*, L-ascorbate peroxidase; *FTRC*, Ferredoxin-thioredoxin reductase catalytic chain, chloroplastic; *GPX*, glutathione peroxidase; *SOD1*, Superoxide dismutase [Fe]; *SOD2*, Superoxide dismutase [Mn]; *SOD3*, Superoxide dismutase [Zn]; *CAT1,2*, catalase1, 2; *trxB*, Thioredoxin reductase, were screened for differential gene expression analysis (**Table 2**). Very obviously, 13 of 18 selected genes were induced by addition of $CdCl_2$, while most genes were down-regulated with PRM25 (13/18) and NaCl (11/18) (**Table 2**).

According to FA metabolism, total 31 genes were identified and no significant changes with more than 1.5 or 2 fold. With slightly up-regulation, most FA metabolism related genes were correlated with E1.0 (26/31 genes) and G1.0 (26/31 genes). NaCl treatment did not cause much up-regulation instead (9/31 genes) (**Supplementary Table S2**).

Based on chlorophyll synthesis and metabolism genes, mostly down-regulated gene numbers were identified in treatments of NaCl1.0 (17/24 genes) and Cd0.5 (10/24 genes) (**Table 3**). Again, most changes of these genes were less than 1.0 fold.

TABLE 2 | The Log2FC (fold change) of selected Reactive Oxygen Species (ROS) scavenging genes under different treatments, treatment vs. control.

Gene_ID	KO name	Cd0.5	G1.0	E1.0	PRM25	NaCl1.0
Cluster-31172.42963	*APX*	0.15196	0.25317	-0.051678	0.010221	0.13602
Cluster-31172.42961	*APX*	0.16485	-0.051658	-0.047102	0.038122	-0.084889
Cluster-31172.21483	*FTRC*	0.088081	-0.018337	-0.0071269	0.008834	0.23297
Cluster-31172.21140	*GPX*	-0.067412	0.10687	0.13296	-0.19666	0.17218
Cluster-31172.31278	*GPX*	0.052787	0.25853	0.26442	-0.14531	0.041538
Cluster-31172.24294	*GPX*	0.084417	0.023608	0.0184	-0.16479	-0.11895
Cluster-31172.15664	*GPX*	0.36104	0.13766	0.16633	0.037672	0.067972
Cluster-31172.30627	*SOD1*	-0.23118	0.1078	0.24022	-0.21941	-0.12951
Cluster-31172.19490	*SOD1*	-0.093043	0.13826	-0.11919	-0.014011	-0.094739
Cluster-31172.16822	*SOD1*	0.020231	-0.12859	-0.20322	-0.20549	0.14619
Cluster-31172.17975	*SOD2*	0.089971	-0.013959	-0.19817	-0.38083	-0.24051
Cluster-31172.36115	*SOD2*	0.10199	0.19635	-0.024988	-0.10232	0.21592
Cluster-31172.26831	*SOD3*	0.15103	0.17146	0.30485	-0.12909	-0.0087302
Cluster-31172.22853	*CAT1*	0.17912	0.18002	0.29535	-0.21605	-0.23217
Cluster-31172.31814	*CAT2*	0.63894	0.30887	0.20949	0.12308	-0.088459
Cluster-31172.26383	*trxB*	-0.57939	-0.39629	-0.55989	-0.44473	-0.090589
Cluster-31172.33966	*trxB*	-0.070243	0.12997	0.025197	-0.13855	-0.037955
Cluster-31172.37823	*trxB*	0.077437	0.065051	0.22527	-0.11915	-0.13544

Gene_ID Cluster-31172.XXs were assigned based on our RNA-seq data. APX, *L-ascorbate peroxidase;* FTRC, *ferredoxin-thioredoxin reductase catalytic chain, chloroplastic;* GPX, *glutathione peroxidase;* SOD1, *superoxide dismutase [Fe];* SOD2, *superoxide dismutase [Mn];* SOD3, *superoxide dismutase [Zn];* CAT1,2, *catalase1, 2;* trxB, *thioredoxin reductase. Red color fonts in Cd0.5 indicate up-regulated expression, and green color font in other treatments mean down-regulated expression.*

TABLE 3 | The Log2FC (fold change) of selected chlorophyll related genes under different treatments, treatment vs. control. Gene_ID Cluster-31172.XXs were assigned based on our RNA-seq data.

Gene_ID	KO name	Cd0.5	G1.0	E1.0	PRM25	NaCl1.0
Cluster-31172.33879	CAO	-0.2102	0.1121	0.36737	-0.061843	-0.0086368
Cluster-31172.38450	chlG, bchG	-0.0035863	0.087771	0.036195	-0.68488	-0.10191
Cluster-31172.24557	chlG, bchG	0.20533	0.19798	0.20092	0.11515	0.074355
Cluster-31172.34067	DVR	0.49806	0.22756	0.41184	0.08435	0.22081
Cluster-31172.12419	E1.3.1.33, por	-0.085459	0.31578	-0.039392	-0.1063	-0.2928
Cluster-31172.30226	E1.3.1.33, por	0.36629	-0.016723	0.18033	-0.09283	-0.27796
Cluster-31172.41935	HCAR	0.034584	0.18931	0.19967	-0.078673	-0.16876
Cluster-31172.22139	LHCA1	-0.32772	0.14507	-0.070321	-0.13334	-0.14353
Cluster-31172.34648	LHCA9	0.48159	0.19422	0.47038	0.55464	0.39359
Cluster-31172.32063	LHCB1	-0.50215	0.043473	0.16147	0.26066	0.057025
Cluster-31172.35839	LHCB1	-0.46686	-0.028961	0.13009	0.43923	0.26772
Cluster-31172.27457	LHCB1	0.1813	0.075637	0.24588	0.14815	-0.15394
Cluster-31172.32089	LHCB1	0.23691	0.14142	0.42049	0.24979	-0.041671
Cluster-31172.35597	LHCB1	0.34805	0.11932	0.29077	0.21118	-0.13149
Cluster-31172.28680	LHCB1	0.50319	-0.49634	-0.22636	-0.10685	-0.1687
Cluster-31172.31624	LHCB1	0.98218	0.10297	0.30361	0.3717	-0.097532
Cluster-31172.32503	LHCB1	1.03	0.17016	0.42601	0.34549	-0.097739
Cluster-31172.35322	LHCB2	0.07938	0.13249	0.32385	0.14945	-0.15313
Cluster-31172.33766	LHCB4	-0.46828	-0.098655	0.042181	0.080384	-0.33116
Cluster-31172.31649	LHCB4	-0.2596	0.094778	0.11783	0.092226	-0.2668
Cluster-31172.21282	NOL, NYC1	-0.5075	0.21729	0.036893	-1.1132	-0.18871
Cluster-31172.45925	NOL, NYC1	0.10415	0.1881	-0.008742	0.034387	0.22995
Cluster-31172.24011	PAO, ACD1	-0.35873	0.1644	0.049772	-0.10193	-0.51182
Cluster-31172.21287	psaA	0.85456	-0.84092	-0.65994	0.031673	0.26759

3.4.3 GO and KEGG Pathway Enrichments

GO Pathways enriched under different treatments showed various and similar patterns under our selected treatments. Pathways down-regulated in response to 1.0% ethanol (E1) included several nucleotide biosynthetic or metabolic processes, signal transduction, and cell communication; integral and intrinsic component of the plasma membrane (**Supplementary Figure S1** E1.0 GO). Similarly, adding glucose reduced nucleotide biosynthetic or metabolic processes, signal transduction, and the component of plasma membranes (**Supplementary Figure S1** G1.0 GO). NaCl treatment caused up-regulation of genes associated with the arginine biosynthetic process, argininosuccinate synthase activity, and down-regulation of genes in the monosaccharide binding pathway (**Supplementary Figure S1** NaCl GO). In response to the antibiotic PRM, genes in the pyruvate, proline,

and arginine metabolic processes, sodium ion transmembrane transport, and sodium ion export were up-regulated. Still, genes involved with oxaloacetate decarboxylase activity were down-regulated (**Supplementary Figure S1** PRM GO). The heavy metal treatment is an exception in this case: more pathways were up-regulated than down-regulated. Most significantly, Na + transport, organic transmembrane transports, non-membrane-bounded and plasma membranes, and heterocyclic and organic cyclic compound binding pathways were increased against Cd ions (**Supplementary Figure S1** Cd GO).

KEGG pathways enriched under E1 are involved in the down-regulation of photosynthesis, carbon fixation in photosynthetic organisms, glyoxylate and dicarboxylate metabolism, and ABC transporters. Upregulated pathways like spliceosome, cysteine, and methionine metabolism were detected under E-1 (**Supplementary Figure S2** E-1 KEGG). Photosynthesis, glyoxylate and dicarboxylate metabolism, glycerophospholipid, fatty acid degradation, and lipid metabolism pathways were down-regulated with glucose (G1). In contrast, sulfur metabolism, N-glycan biosynthesis, mRNA surveillance pathway, endocytosis, and cysteine and methionine metabolism were up-regulated (**Supplementary Figure S2** G1 KEGG). Similar changes were also detected in NaCl treatment. Under NaCl treatment, photosynthesis, oxidative phosphorylation, glycerophospholipid, glycerolipid, and ether lipid metabolisms were down-regulated. In contrast, selenocompound metabolism, plant-pathogen interaction, plant hormone signal transduction, endocytosis, and cysteine and methionine metabolism were up-regulated (**Supplementary Figure S2** NaCl KEGG). There are relatively few pathways changed by PRM treatment, with down-regulated purine, porphyrin, chlorophyll metabolisms, and up-regulated glycolysis/gluconeogenesis and endocytosis (**Supplementary Figure S2** PRM KEGG). More complicated changes were disturbed by $CdCl_2$, with many pathways such as down-regulated spliceosome, protein processing, nucleotide excision repair, N-glycan biosynthesis, basal transcription factors, and up-regulated ribosome, glycolysis/gluconeogenesis, and fatty acid biosynthesis and ether lipid metabolism pathways (**Supplementary Figure S2** Cd KEGG).

4 DISCUSSION

Cd^{2+} is a serious environmental pollutant. It is highly toxic to living organisms because it is an unnecessary ion, even at low concentrations. Not only Cd^{2+}accumulates in *Euglena*, but other heavy metals such as Hg^{2+}, Cu^{2+}, Zn^{2+}, Pb^{2+}, Tc^{7+}, and Cr^{6+}, thereby contributing to the remediation of waste and polluted water (Mendoza-Cózatl et al., 2006). *E. gracilis* is considered an efficient and reliable bioremediation microorganism with the potential to remediate heavy metal environments (Sánchez-Thomas et al., 2016). In this study, *E. gracilis* growth was slightly reduced due to a low concentration of 0.5 mM $CdCl_2$. A previous study showed that *Chlorella* also had some tolerance to cadmium. Its growth was unaffected by 0.5 and 1 mg/L $3CdSO_4 \bullet 8H_2O$, although concentrations of 3 and 5 mg/L inhibited growth, and 7 mg/L completely blocked growth (Cheng et al., 2016). Based on the thousands of genes differentially expressed in response to $CdCl_2$ treatment and the observed reductions in biomass, we can conclude that $CdCl_2$ has a significant impact on *Euglena* cells.

NaCl treatment produced similar results, reducing biomass by 18.18%, consistent with previous studies of NaCl in *Scenedesmus* and *E. gracilis* (Ji et al., 2018). This may reflect that NaCl promotes the degradation of chlorophyll a, reduces photosynthetic capacity, and ultimately inhibits microalgae growth. This is verified through our chlorophyll assessments and related gene expression analysis.

The biochemical effects of antibiotics paromomycin (PRM) have seldom been studied in *E. gracilis* and other microalgae. PRM and streptomycin are aminoglycoside antibiotics, and streptomycin has a known inhibitory effect on *E. gracilis* growth (Kirk, 1962). However, this study showed that low concentrations (1–25 μg/ml) of PRM had little effect on *E. gracilis* growth, suggesting that *E. gracilis* is tolerant to low PRM concentrations, consistent with previous reports on *Euglena* antibiotic tolerance (Kirk, 1962; He et al., 2021). *E. gracilis* could grow mixotrophically; that is, it can first use organic carbons in the medium or field waters instead of CO_2 via photosynthesis under the light. Transcriptome analyses indicated down-regulated photosynthesis with the addition of ethanol or glucose. Ethanol has been reported to induce cell division and promote the growth of *E. gracilis* (Horrum and Schwartzbach, 1980; Venugopal et al., 2006). Likewise, studies have shown that adding glucose to the culture medium can promote the growth of *E. gracilis* and *Scenedesmus quadriceps* (Taylor, 1960; Nicolas et al., 1980). Here, we also found out that ethanol and glucose significantly promoted the growth of *E. gracilis*, and the effect of glucose was significant under selected concentrations in this study.

All treatments with low doses of ethanol (all doses), glucose (1.0, 1.5%), $CdCl_2$, NaCl, and PRM (1–5 μg/ml) can promote the accumulation of fatty acids of *E. gracilis*. Also, FA compositions showed some interesting patterns under different treatments.

Coleman's research shows that the fatty acid synthesis rate of *E. gracilis* with an additional carbon source is higher than that of photosynthetic carbon fixation. In this study, adding ethanol and glucose significantly increases the fatty acid contents of *E. gracilis* compared with the control, of which G1.5 treatment has the highest FA content and the total lipid content of *E. gracilis* can reach 16.59% ($p < 0.001$). When *E. gracilis* is cultivated in ethanol-containing media, its total lipid content increases (Coleman et al., 1988; Thuillier-Bruston et al., 1990). When treated with different ethanol concentrations, the total lipid content can also be increased by 82.59–146.96% ($p < 0.01$). The glucose-rich medium can increase the lipid content in *Scenedesmus quadricauda* (Kandimalla et al., 2016), and glucose (35 mM) as a carbon source can promote the accumulation of lipid in *Chromochloris zofingiensis* (Zhang et al., 2019). The addition of carbon sources into *E. gracilis* culture medium alters the FA compositions a lot. The transcriptome data indicated very similar responses to ethanol and glucose. For instance, nucleotide biosynthetic or metabolic processes such as signal transduction, integral and intrinsic components of plasma membrane pathways were down-regulated under both treatments. Characters of plasma membrane depend on the composition of membrane lipids based on the saturated ratio. With the concentrations in this study, glucose increased significantly higher FA contents than ethanol. The reduced fatty acid degradation

detected in the G1.0 treatment may contribute partially to higher FA production under glucose addition.

Our transcriptome analysis showed up-regulated ROS related genes in $CdCl_2$ treatment group. Alho's research shows that Cd has a more significant impact on the biochemical composition of *Raphidocelis subcapitata*, increasing total lipid content (7.2 times), total carbohydrates (3.5 times), and ROS production (3.7 times) (Alho et al., 2019). Addition of $CdCl_2$ into *E. gracilis* culture medium caused the up-regulation of sodium ion and organic transmembrane transports to pump out Cd^{2+}. At the same time, $CdCl_2$ treatment increased glycolysis, fatty acid biosynthesis, and ether lipid metabolism changed non-membrane bound and plasma membranes with increased SFA and reduced PUFA. Thus, increased FA content and changed FA composition of *E. gracilis* might be the defense mechanism of *E. gracilis* when exposed to Cd^{2+}, which helps reduce the metal damage to photosynthesis (Alho et al., 2019).

As we all know, under environmental pressure, FA accumulates as energy reserves, allowing algae to survive (De Carvalho and Caramujo, 2018). Increased intracellular lipid can maintain redox homeostasis because these biomolecules act as electron absorbers and help resist oxidative damage caused by ROS (Sun et al., 2018). Our transcriptome data showed NaCl also inhibited photosynthesis and changed glycerophospholipid, glycerolipid, and ether lipid metabolism. In the end, NaCl treatment resulted in the FA content increasing and FA composition alternating with a high SFA content ratio.

PRM could promote FA accumulation with no change of FA composition under low concentrations. Based on our transcriptome data, porphyrin and chlorophyll metabolisms were down-regulated while glycolysis was up-regulated under PRM treatment. We propose that the decreased chlorophyll inhibits photosynthesis, similar to NaCl, ethanol, or glucose treatments, and promotes FA accumulation. There is no alternation of any membrane metabolism among GO and KEGG pathways enriched from our RNA-seq data. This observation is consistent with no FA composition change under PRM treatment.

Interestingly, FA compositions showed significantly different and similar patterns under different treatments. Except for PRM treatments, all treatments in this study increased saturated rates 1.7~2.4 fold compared to the control. The lipids in green cells of *E. gracilis* grown in the light differ from those in etiolated cells (with no photosynthesis) grown in the dark. The FA of the photosynthesizing green *E. gracilis* cells is mainly of the unsaturated variety (Rosenberg, 1963). An early study showed a complex lipid pattern of *Euglena*: phosphatidylglycerol sulfolipid, and several glycolipids appeared to be the dominant lipids during photosynthesis (Helmy et al., 1967). *E. gracilis* was cultured under heterotrophic or phototrophic growth conditions using ethanol, glucose, or CO_2 as the primary carbon source. TFA analyses indicated that ethanol produced more highly unsaturated acids than glucose (Reitz and Moore, 1972). In *E. gracilis* synthesis, the more significant part of the cellular unsaturated fatty acids accompanies photosynthesis. Although it is not known whether unsaturated fatty acids participate directly in the photosynthetic mechanism, their synthesis is an essential factor in the economy of the photosynthesizing cells. Comparing the relative proportions of fatty acid species in a chloroplast fraction of green *E. gracilis* cells showed a significantly increased ratio of unsaturated to saturated homologs in the chloroplast (Rosenberg, 1963). The effects of ethanol and glucose on fatty acid profile showed significantly higher SFA accumulation (ΣSFA/(ΣMUFA+ΣPUFA) with glucose compared to ethanol (2.5 vs. 0.9) (Barsanti et al., 2000). In our previous report, in fully green photosynthetic *E. gracilis* cells under light conditions, desaturase activity was enhanced to generate a set of MUFAs and PUFAs (Zeng et al., 2016). Transcriptome analyses provide some clues about FA composition changes under treatments. Down-regulated photosynthesis was detected in E1, G1, and NaCl treatments for KEGG enriched pathways, which correlates with the significantly increased saturated FA in these treated cells.

The increase of SFA and the decrease of PUFA proportion mean that the saturation of biodiesel increases. It helps to change some indicators related to the combustion performance, like increasing the CN and lowering IN of biodiesel. This study finds that using suitable conditions to treat *E. gracilis* could improve not only the yield of *E. gracilis* FA can but alsobiodiesel quality. Based on the SN, IN, and CN, *E. gracilis* FA was evaluated as biodiesel. According to the biodiesel production standard, the performance of *E. gracilis* FA in the glucose treatment group is the best. Among them, both IN and CN of *E. gracilis* FA of G1.5 treatment reach the highest standards for biodiesel production in various countries. However, *E. gracilis* FA in all groups has the same shortcoming. The SN is too high to meet biodiesel standards in many countries.

5 CONCLUSION

The total fatty acids and related components of *E. gracilis* have increased under various treatment conditions with various TFA saturated rates and biodiesel fuel properties. Both iodine value and cetane number have reached the highest standard of current international biodiesel production under some treatments. Among them, TFA with glucose treatment is excellent, which can be used as an in-depth research object in biodiesel. The transcriptome analyses indicate that high-quality biodiesel could be achieved in *E. gracilis* by carefully designed cultivation medium and conditions, andbalancing the growth and photosynthesis.

DATA AVAILABILITY STATEMENT

The original contributions presented in the study are publicly available. This data can be found here: https://www.ncbi.nlm.nih.gov/bioproject/, PRJNA714494.

AUTHOR CONTRIBUTIONS

JW conceived the concept, and JH, YC, YL, JZ conducted the experiments and collected the data. MD analyzed the data. JW wrote the manuscript draft. AL and WF helped to collect materials and finish the manuscript. AL, JW, JZ, and MD offered help to this project and/or revised the manuscript. All authors read and approved the final manuscript.

FUNDING

This work was partially supported by China's National Key R&D Programs (2018YFA0902500; 2020YFA0908703; 2021YFA0910800) and the National Natural Science Foundation of China (41876188).

SUPPLEMENTARY MATERIAL

The Supplementary Material for this article can be found online at: https://www.frontiersin.org/articles/10.3389/fceng.2022.884451/full#supplementary-material

Supplementary Figure S1 | Functional categorization of up- (red color) and down-regulated (blue color) genes in E. gracilis under different treatments based on gene ontology (GO) annotations. BP, biological process, CC, cellular components, MP, molecular functions.

Supplementary Figure S2 | Bubble plots of DEGs for visualizing KEGG pathway enrichments. Bubble size indicates the log size of the KEGG term, enrichment of the down-regulated genes (down KEGG), and up-regulated genes (up KEGG).

Supplementary Table S1 | The contents of fatty acids in the unit cell of E. gracilis under different treatment conditions (pg/cell). Treatments include supplementation with paromomycin (PRM1, 5, 25 as 1, 5, 25 μg/mL), ethanol (E0.5, 1.0, 1.5 as 0.5, 1, 1.5% vol/vol), glucose (G0.5, G1.0, G1.5 as 0.5, 1.0, 1.5% weight), CdCl2 (Cd0.5, 1.0, 1.5 as CdCl2 of 0.5, 1.0, 1.5 mM), or NaCl1.0 (NaCl as 1% weight), CN, control.

Supplementary Table S2 | The Log2FC (fold change) of selected fatty acid metabolism genes under different treatments, treatment vs. control.

REFERENCES

Afiukwa, C. A., and Ogbonna, J. C. (2007). Effects of Mixed Substrates on Growth and Vitamin Production by *Euglena gracilis*. *Afr. J. Biotechnol.* 6 (22), 2612–2615.

Alho, L. D. O. G., Gebara, R. C., Paina, K. D. A., Sarmento, H., and Melão, M. D. G. G. (2019). Responses of *Raphidocelis Subcapitata* Exposed to Cd and Pb: Mechanisms of Toxicity Assessed by Multiple Endpoints. *Ecotoxicol. Environ. Saf.* 169, 950–959. doi:10.1016/j.ecoenv.2018.11.087

Anders, S., and Huber, W. (2010). Differential Expression Analysis for Sequence Count Data. *Genome Biol.* 11, R106. doi:10.1186/gb-2010-11-10-r106

Arguelles, E. D. L. R., and Martinez-Goss, M. R. (2021). Lipid Accumulation and Profiling in Microalgae *Chlorolobion Sp.* (BIOTECH 4031) and *Chlorella Sp.* (BIOTECH 4026) during Nitrogen Starvation for Biodiesel Production. *J. Appl. Phycol.* 33, 1–11. doi:10.1007/s10811-020-02126-z

Barsanti, L., Bastianini, A., Passarelli, V., Tredici, M. R., and Gualtieri, P. (2000). Fatty Acid Content in Wild Type and WZSL Mutant of *Euglena Gracilis* - Effects of Carbon Source and Growth Conditions. *J. Appl. Phycol.* 12, 515–520. doi:10.1023/a:1008187514624

Béchet, Q., Shilton, A., and Guieysse, B. (2013). Modeling the Effects of Light and Temperature on Algae Growth: State of the Art and Critical Assessment for Productivity Prediction during Outdoor Cultivation. *Biotechnol. Adv.* 31, 1648–1663.

Campanaro, S., Picelli, S., Torregrossa, R., Colluto, L., Ceol, M., Del Prete, D., et al. (2007). Genes Involved in TGFβ1-Driven Epithelial-Mesenchymal Transition of Renal Epithelial Cells Are Topologically Related in the Human Interactome Map. *BMC Genomics* 8, 383. doi:10.1186/1471-2164-8-383

Cheng, J., Qiu, H., Chang, Z., Jiang, Z., and Yin, W. (2016). The Effect of Cadmium on the Growth and Antioxidant Response for Freshwater Algae *Chlorella Vulgaris*. *Springerplus* 5, 1290. doi:10.1186/s40064-016-2963-1

Coleman, L. W., Rosen, B. H., and Schwartzbach, S. D. (1988). Environmental-control of Carbohydrate and Lipid-Synthesis in *Euglena*. *Plant Cell Physiology* 29, 423–432. doi:10.1016/s0022-2275(20)38565-5

Conesa, A., Gotz, S., Garcia-Gomez, J. M., Terol, J., Talon, M., and Robles, M. (2005). Blast2GO: A Universal Tool for Annotation, Visualization and Analysis in Functional Genomics Research. *Bioinformatics* 21, 3674–3676. doi:10.1093/bioinformatics/bti610

Cordoba, J., Perez, E., Van Vlierberghe, M., Bertrand, A. R., Lupo, V., Cardol, P., et al. (2021). De Novo transcriptome Meta-Assembly of the Mixotrophic Freshwater Microalga *Euglena Gracilis*. *Genes (Basel)* 12. doi:10.3390/genes12060842

De Carvalho, C. C. C. R., and Caramujo, M. J. (2018). The Various Roles of Fatty Acids. *Molecules* 23, 2583. doi:10.3390/molecules23102583

Ebenezer, T. E., Carrington, M., Lebert, M., Kelly, S., and Field, M. C. (2017). *Euglena Gracilis* Genome and Transcriptome: Organelles, Nuclear Genome Assembly Strategies and Initial Features. *Adv. Exp. Med. Biol.* 979, 125–140. doi:10.1007/978-3-319-54910-1_7

Ebenezer, T. E., Zoltner, M., Burrell, A., Nenarokova, A., Novák Vanclová, A. M. G., Prasad, B., et al. (2019). Transcriptome, Proteome and Draft Genome of *Euglena Gracilis*. *BMC Biol.* 17, 11. doi:10.1186/s12915-019-0626-8

Edmunds, L. N., Jr. (1965). Studies on Synchronously Dividing Cultures ofEuglena Gracilis Klebs (Strain Z). II. Patterns of Biosynthesis during the Cell Cycle. *J. Cell. Comp. Physiol.* 66, 159–181. doi:10.1002/jcp.1030660205

Gao, P., Guo, L., Zhao, Y., Jin, C., She, Z., and Gao, M. (2021). Enhancing Microalgae Growth and Product Accumulation with Carbon Source Regulation: New Perspective for the Coordination between Photosynthesis and Aerobic Respiration. *Chemosphere* 278, 130435. doi:10.1016/j.chemosphere.2021.130435

Geimer, S., Belicová, A., Legen, J., Sláviková, S., Herrmann, R. G., and Krajčovič, J. (2009). Transcriptome Analysis of the *Euglena Gracilis* Plastid Chromosome. *Curr. Genet.* 55, 425–438. doi:10.1007/s00294-009-0256-8

Gilmour, D. J. (2019). Microalgae for Biofuel Production. *Adv. Appl. Microbiol.* 109, 1–30. doi:10.1016/bs.aambs.2019.10.001

Gonzalez-Moreno, S., Gomez-Barrera, J., Perales, H., and Moreno-Sanchez, R. (1997). Multiple Effects of Salinity on Photosynthesis of the Protist *Euglena Gracilis*. *Physiol. Plant* 101, 777–786. doi:10.1111/j.1399-3054.1997.tb01063.x

Grimm, P., Risse, J. M., Cholewa, D., Müller, J. M., Beshay, U., Friehs, K., et al. (2015). Applicability of Euglena Gracilis for Biorefineries Demonstrated by the Production of α-tocopherol and Paramylon Followed by Anaerobic Digestion. *J. Biotechnol.* 215, 72–79. doi:10.1016/j.jbiotec.2015.04.004

Harris, E. H. (2009). *The Chlamydomonas Sourcebook: Introduction to Chlamydomonas and its Laboratory Use*. 2nd Edn. San Diego, CA: Academic Press, 119267–158274.

He, J., Liu, C., Du, M., Zhou, X., Hu, Z., Lei, A., et al. (2021). Metabolic Responses of a Model Green Microalga *Euglena Gracilis* to Different Environmental Stresses. *Front. Bioeng. Biotechnol.* 9, 662655. doi:10.3389/fbioe.2021.662655

Helmy, F. M., Hack, M. H., and Yaeger, R. G. (1967). Comparative Lipid Biochemistry-VI. Lipids of Green and Etiolated Euglena Gracilis and of Blastocrithidia Culicis. *Comp. Biochem. Physiology* 23, 565–567. doi:10.1016/0010-406x(67)90408-2

Horrum, M. A., and Schwartzbach, S. D. (1980). Nutritional Regulation of Organelle Biogenesis in Euglena. *Plant Physiol.* 65, 382–386. doi:10.1104/pp.65.2.382

Ji, X., Cheng, J., Gong, D., Zhao, X., Qi, Y., Su, Y., et al. (2018). The Effect of NaCl Stress on Photosynthetic Efficiency and Lipid Production in Freshwater *Microalga-Scenedesmus Obliquus XJ002*. *Sci. Total Environ.* 633, 593–599. doi:10.1016/j.scitotenv.2018.03.240

Kandimalla, P., Desi, S., and Vurimindi, H. (2016). Mixotrophic Cultivation of Microalgae Using Industrial Flue Gases for Biodiesel Production. *Environ. Sci. Pollut. Res.* 23, 9345–9354. doi:10.1007/s11356-015-5264-2

Khan, A. Z., Shahid, A., Cheng, H., Mahboob, S., Al-Ghanim, K. A., Bilal, M., et al. (2018). Omics Technologies for Microalgae-Based Fuels and Chemicals: Challenges and Opportunities. *Ppl* 25, 99–107. doi:10.2174/0929866525666180122100722

Kimbrel, J. A., Di, Y., Cumbie, J. S., and Chang, J. H. (2011). RNA-seq for Plant Pathogenic Bacteria. *Genes* 2, 689–705. doi:10.3390/genes2040689

Kirk, J. T. (1962). Effect of Streptomycin on Greening and Biosynthesis in *Euglena Gracilis*. *Biochimica Biophysica Acta* 56, 139–151. doi:10.1016/0006-3002(62)90534-6

Kottuparambil, S., Shin, W., Brown, M. T., and Han, T. (2012). UV-B Affects Photosynthesis, ROS Production and Motility of the Freshwater Flagellate,

Euglena Agilis Carter. *Aquat. Toxicol.* 122-123, 206–213. doi:10.1016/j.aquatox.2012.06.002

Lu, S., Wang, J., Niu, Y., Yang, J., Zhou, J., and Yuan, Y. (2012). Metabolic Profiling Reveals Growth Related FAME Productivity and Quality of *Chlorella Sorokiniana* with Different Inoculum Sizes. *Biotechnol. Bioeng.* 109, 1651–1662. doi:10.1002/bit.24447

Luo, Y., Zhang, X., Huang, C., Han, X., Jiang, Q., Zhou, T., et al. (2021). Zn0.8Cd0.2S Hollow Spheres with a Highly Dispersed Ni Dopant for Boosting Photocatalytic Hydrogen Generation. *ACS omega* 6, 13544–13553. doi:10.1021/acsomega.0c06038

Maltsev, Y., Maltseva, K., Kulikovskiy, M., and Maltseva, S. (2021). Influence of Light Conditions on Microalgae Growth and Content of Lipids, Carotenoids, and Fatty Acid Composition. *Biology* 10, 1060. doi:10.3390/biology10101060

Mendoza-Cózatl, D. G., Rangel-González, E., and Moreno-Sánchez, R. (2006). Simultaneous Cd^{2+}, Zn^{2+}, and Pb^{2+} Uptake and Accumulation by Photosynthetic *Euglena Gracilis*. *Archives Environ. Contam. Toxicol.* 51, 521–528.

Moreno-Sánchez, R., Rodríguez-Enríquez, S., Jasso-Chávez, R., Saavedra, E., and García-García, J. D. (2017). Biochemistry and Physiology of Heavy Metal Resistance and Accumulation in *Euglena*. *Adv. Exp. Med. Biol.* 979, 91–121.

Mukaida, S., Ogawa, T., Ohishi, K., Tanizawa, Y., Ohta, D., and Arita, M. (2016). The Effect of Rapamycin on Biodiesel-Producing Protist *Euglena Gracilis*. *Biosci. Biotechnol. Biochem.* 80, 1223–1229. doi:10.1080/09168451.2016.1141040

Nicolas, P., Freyssinet, G., and Nigon, V. (1980). Effect of Light on Glucose Utilization by *Euglena Gracilis*. *Plant Physiol.* 65, 631–634. doi:10.1104/pp.65.4.631

O'Neill, E. C., Trick, M., Hill, L., Rejzek, M., Dusi, R. G., Hamilton, C. J., et al. (2015). The Transcriptome of *Euglena Gracilis* Reveals Unexpected Metabolic Capabilities for Carbohydrate and Natural Product Biochemistry. *Mol. Biosyst.* 11, 2808–2820. doi:10.1039/c5mb00319a

Reitz, R. C., and Moore, G. S. (1972). Effects of Changes in the Major Carbon Source on the Fatty Acids ofEuglena Gracilis. *Lipids* 7, 217–220. doi:10.1007/bf02533068

Rodríguez-Zavala, J. S., García-García, J. D., Ortiz-Cruz, M. A., and Moreno-Sánchez, R. (2007). Molecular Mechanisms of Resistance to Heavy Metals in the Protist *Euglena Gracilis*. *J. Environ. Sci. Health A Tox Hazard Subst. Environ. Eng.* 42, 1365–1378.

Rosenberg, A. (1963). A Comparison of Lipid Patterns in Photosynthesizing and Nonphotosynthesizing Cells of Euglena Gracilis*. *Biochemistry* 2, 1148–1154. doi:10.1021/bi00905a042

Sánchez-Thomas, R., Moreno-Sánchez, R., and García-García, J. D. (2016). Accumulation of Zinc Protects against Cadmium Stress in Photosynthetic *Euglena Gracilis*. *Environ. Exp. Bot.* 131, 19–31.

Sun, X.-M., Ren, L.-J., Zhao, Q.-Y., Ji, X.-J., and Huang, H. (2018). Microalgae for the Production of Lipid and Carotenoids: a Review with Focus on Stress Regulation and Adaptation. *Biotechnol. Biofuels* 11, 272. doi:10.1186/s13068-018-1275-9

Taylor, F. J. (1960). The Absorption of Glucose by *Scenedesmus Quadricauda*. I. Some Kinetic Aspects. *Proc. R. Soc. Lond B Biol. Sci.* 151, 400–418. doi:10.1098/rspb.1960.0006

Thuillier-Bruston, F., Briand, J., and Laval-Martin, D. (1990). Effects of a First Exposure to Ethanol on the Compositions of Neutral and Polar Lipids in *Euglena Gracilis Z*, Taken as a Hepatic Cell Model: Equilibration by Citrulline-Malate. *Biochem. Med. Metabolic Biol.* 44, 159–174. doi:10.1016/0885-4505(90)90057-8

Venugopal, V., Prasanna, R., Sood, A., Jaiswal, P., and Kaushik, B. D. (2006). Stimulation of Pigment Accumulation inAnabaena Azollae Strains: Effect of Light Intensity and Sugars. *Folia Microbiol.* 51, 50–56. doi:10.1007/bf02931450

Wang, Y., Seppänen-Laakso, T., Rischer, H., and Wiebe, M. G. (2018). *Euglena gracilis* Growth and Cell Composition Under Different Temperature, Light and Trophic Conditions. *PLoS One* 13 (4), e0195329.

Xia, K., Chi, Y., Fu, J., Zhu, Z., Zhang, H., Du, C., et al. (2019). A Triboelectric Nanogenerator Based on Cosmetic Fixing Powder for Mechanical Energy Harvesting. *Microsyst. Nanoeng.* 5, 26. doi:10.1038/s41378-019-0066-1

Yoshida, Y., Tomiyama, T., Maruta, T., Tomita, M., Ishikawa, T., and Arakawa, K. (2016). De Novo assembly and Comparative Transcriptome Analysis of *Euglena Gracilis* in Response to Anaerobic Conditions. *BMC Genomics* 17, 182. doi:10.1186/s12864-016-2540-6

Zakryś, B., Milanowski, R., and Karnkowska, A. (2017). Evolutionary Origin of *Euglena*. *Adv. Exp. Med. Biol.* 979, 3–17. doi:10.1007/978-3-319-54910-1_1

Zeng, M., Hao, W., Zou, Y., Shi, M., Jiang, Y., Xiao, P., et al. (2016). Fatty Acid and Metabolomic Profiling Approaches Differentiate Heterotrophic and Mixotrophic Culture Conditions in a Microalgal Food Supplement 'Euglena'. *BMC Biotechnol.* 16, 49. doi:10.1186/s12896-016-0279-4

Zhang, Z., Sun, D., Zhang, Y., and Chen, F. (2019). Glucose Triggers Cell Structure Changes and Regulates Astaxanthin Biosynthesis in *Chromochloris Zofingiensis*. *Algal Res.* 39, 101455. doi:10.1016/j.algal.2019.101455

Conflict of Interest: The authors declare that the research was conducted in the absence of any commercial or financial relationships that could be construed as a potential conflict of interest.

Publisher's Note: All claims expressed in this article are solely those of the authors and do not necessarily represent those of their affiliated organizations, or those of the publisher, the editors and the reviewers. Any product that may be evaluated in this article, or claim that may be made by its manufacturer, is not guaranteed or endorsed by the publisher.

frontiers | Frontiers in Chemical Engineering

TYPE Review
PUBLISHED 06 October 2022
DOI 10.3389/fceng.2022.998289

OPEN ACCESS

EDITED BY
Kavitha S,
Anna University Regional Campus Tirunelveli, India

REVIEWED BY
Vinay Kumar Tyagi,
National Institute of Hydrology, India
Yukesh Kannah R,
University at Albany, United States

*CORRESPONDENCE
Lakhan Kumar,
adarsh.lakhan@gmail.com
Navneeta Bharadvaja,
navneetab@dce.ac.in

SPECIALTY SECTION
This article was submitted to Sustainable Process Engineering, a section of the journal Frontiers in Chemical Engineering

RECEIVED 19 July 2022
ACCEPTED 23 September 2022
PUBLISHED 06 October 2022

CITATION
Kumar L, Mohan L, Anand R, Joshi V, Chugh M and Bharadvaja N (2022), A review on unit operations, challenges, opportunities, and strategies to improve algal based biodiesel and biorefinery. *Front. Chem. Eng.* 4:998289. doi: 10.3389/fceng.2022.998289

A review on unit operations, challenges, opportunities, and strategies to improve algal based biodiesel and biorefinery

Lakhan Kumar*, Lalit Mohan, Raksha Anand, Vandana Joshi, Mohita Chugh and Navneeta Bharadvaja*

Plant Biotechnology Laboratory, Department of Biotechnology, Delhi Technological University, Delhi, India

Globally, the demand for energy is increasing with an emphasis on green fuels for a sustainable future. As the urge for alternative fuels is accelerating, microalgae have emerged as a promising source that can not only produce high lipid but many other platform chemicals. Moreover, it is a better alternative in comparison to conventional feedstock due to yearlong easy and mass cultivation, carbon fixation, and value-added products extraction. To date, numerous studies have been done to elucidate these organisms for large-scale fuel production. However, enhancing the lipid synthesis rate and reducing the production cost still remain a major bottleneck for its economic viability. Therefore, this study compiles information on algae-based biodiesel production with an emphasis on its unit operations from strain selection to biofuel production. Additionally, strategies to enhance lipid accumulation by incorporating genetic, and metabolic engineering and the use of leftover biomass for harnessing bio-products have been discussed. Besides, implementing a biorefinery for extracting oil followed by utilizing leftover biomass to generate value-added products such as nanoparticles, biofertilizers, biochar, and biopharmaceuticals has also been discussed.

KEYWORDS

biodiesel, lipid productivity, biorefinery, genetic engineering, algae, carbon dioxide sequestration

Introduction

Over the decade, limitation in availability of fossil fuels and increasing population has resulted in enhanced energy demands. Furthermore, continuous exploitation of non-renewable energy sources has embarked the accumulation of carbon dioxide (CO_2) in the atmosphere from 295 parts per million (ppm) to more than 400 ppm in 2018 leading to global warming and climate change (Tang et al., 2020) (Rosa et al., 2019). According to some studies, it is estimated the current rate of fossil fuel consumption including natural gas, coal, and crude oil will lead to their exhaustion in approximately 50 years. Therefore, the green energy demand is set to increase from 43 billion L/day in 2020 to 55.96 billion L/

day by 2045 (Organization of the Petroleum Exporting Countries - OPEC, 2020). Additionally, reports published by International Energy Agency (IEA) states that the biofuels market was valued at nearly 110 billion USD in 2021 and will increase to 2012 billion USD by 2030 (IEA, 2021). Therefore, current studies are focused on generating alternatives to fabricate green energy. Numerous sources are required which are not only renewable but also environment friendly to develop sustainable carbon neutral fuels. sequestered from CO_2 the atmosphere gets converted into biomass, and upon chemical conversion, into fuel. Therefore, green fuels do not contribute to any further addition or reduction of CO_2 into the atmosphere and lead to carbon neutrality (Kumar et al., 2010). According to several scientific investigations, algae can capture 10–50 times more amount of CO_2 leading to high growth rate (Mondal et al., 2017).

The major cost of fuel is dependent on the biomass which can either be crops like sugarcane or plant seeds but they possess competition with food crops and restrict product yield (first generation); lignocellulosic biomass, kitchen waste, crop residue but the high cost of processing due to lignin and expensive technologies for lipid extraction makes them unsuccessful (second generation); microalgae depict rapid growth and enhanced oil yield but it is still expensive for large scale production (third generation); genetically modified algae with advanced extraction techniques have recently been deployed for large scale production of biofuel but they also imply high initial investment and extensive research (fourth generation) (Yaashikaa et al., 2022). Amongst them, microalgae, chlorophyll harboring photosynthetic microorganism is the best candidate used for green fuel production (Gonçalves et al., 2013). They have the ability to enhance oil yield and marginalize dependence on fossil fuels. Also, they are capable to reduce greenhouse gases (GHG) emissions by 50–70% in comparison to conventional fuels (Liu et al., 2013). The major steps incorporated in the production of microalgae-derived biodiesel are cultivation, harvesting, extraction of oil, and purification followed by biodiesel synthesis from individual cells (Tang et al., 2020). Also, generate carbohydrates, proteins, vitamins, lipids, and pigments depending on species and external growth factors. The downstream processing accounts for 50% of the biodiesel production cost. Hence, novel methodologies are needed to reduce the fuel production cost.

Currently, hybrid models and by-product extractions have been employed with algae to make fuel economically viable. For instance, growing algae in a waste water treatment plant can not only reduce the cultivation cost, but also remove pollutants from it, recover nutrients, and generate high-value commodities (Chandrasekhar et al., 2022). More recently, algal industry has given attention to a diverse variety of algae-based products apart from lipids including carotenoids, proteins, nucleic acids etc., for the production of nutraceutical, cosmeceutical, bio-stimulants, bio-fertilizers, and other environment remediation commodities like biochar. Therefore, implementation of a biorefinery will elucidate the production of such high-value chemicals/products for different industrial interventions (Gondi et al., 2022). While, novel pre-treatment methodologies such as cell wall weakening before cell disintegration *via* nanoparticles may enhance the biogas as well as biofuel yield (Gondi et al., 2022) (Yukesh Kannah et al., 2021). Therefore, valorization of algal biomass for green fuel and using the leftover to extract other industrially important products can compensate the exorbitant fuel prices in the future.

The present article aims to provide an overview on the recent information on unit operations in up and downstream processing for algae-based biofuel as well as high-value chemical/product extraction. Additionally, a detailed study on the life cycle assessment (LCA) framework along with emerging techniques including genetic, metabolomic engineering coupled with omics approach for improving lipid yield and biomass productivity has been discussed. Finally, likelihood of developing an algal biorefinery for high-value products fabrication such as carbohydrates, lipids, carotenoids, amino acids, antioxidants, fatty acids, vitamins etc., for different industrial interventions has also been conferred. Moreover, present challenges and future research directions for integrated algal biorefinery setups are outlined.

Overview to algal biomass-based biodiesel and biochemical production: Unit operations in up and down stream processes

Unit operations in up-stream processes

Algal biodiversity

Microalgae including Cyanophyceae (blue-green algae), Bacillariophyceae (diatoms), Chlorophyceae (green algae), and Chrysophyceae (golden algae) are the most economical and efficient for harboring lipid for biodiesel production, CO_2 fixation and wastewater treatment (Kumar et al., 2010). Numerous bioprocess industries rely on these microorganisms' metabolism to convert carbohydrates to other value-added products such as vitamins, amino acids and organic acids such as acetic acid. However, the cost of carbohydrate feedstock plays a significant role in the total cost of production in such industries. While photosynthetic organisms such as microalgae provide a production alternative and can entirely eliminate the cost associated with carbohydrate feedstock. They employ inexpensive and readily available sunlight as an energy source. Cyanobacteria are known to convert 3–9% of solar energy captured into biomass whereas terrestrial plants can convert only 0.25–3% of the captured solar energy into biomass (Ducat et al., 2011).

Screening and selection of microalgal strain

According to the scientific studies the strain of interest shall have the following features (Chu, 2017).

- Robust with enhanced growth rate and high lipid content.
- Capable to withstand shear stress generated during mixing and tolerate microorganism interference.
- Flexible to adapt according to diverse physiochemical parameters encountered during culturing.
- Genetically manipulable for obtaining high growth rate, lipid productivity, and other related bioproducts.

In order to obtain the above characteristics in the algal strain several techniques have been described for their isolation and screening including gravimetric separation, single-cell isolation by serial dilution, micromanipulation, and atomized cell spray (Mutanda et al., 2011). These conventional methods for strain selection are not only complex but also time-consuming, and labor-intensive (Kwak et al., 2016; Lim et al., 2017). In order to simplify the selection process, Kim et al. reported the advancements in the field of microfluidic systems to study microalgal biotechnology (Kim et al., 2017). Likewise, Challagulla et al. reviewed the applications of various technologies for the analysis of lipid content and biomass productivity of the microalgal cell. These technologies include raman spectroscopy, near-infrared spectroscopy, fluorescent lipid-soluble dye-based detection, nuclear magnetic resonance spectroscopy, and fourier transform techniques (Challagulla et al., 2016). Moreover, flow cytometry, microfluidics, and spectroscopy can either be used alone or in combination with other technologies for screening high lipid and biomass yielding microalgal strains (Shokravi et al., 2020). While there are several strategies for rapid selection of microalgal strains such as bioprospecting is the most prominent approach for screening high biomass producing strains. Also, high throughput techniques including vibrational spectroscopy or flow cytometry which are highly accurate and rapid for characterizing metabolites (Shokravi et al., 2020).

Identification of high lipid yielding strains

Solvent extraction and gravimetric methods are used for identifying high lipid yielding strains. These procedures are not only accurate but also provide reproducible results. However, they are time-consuming, labor intensive, and require a large amount (10–15 mg wet weight) of biomass (Morschett et al., 2016). On the contrary, chromatographic methods procure high reproducibility, require less time, and provide a single report with both qualitative and quantitative estimates of fatty acids. Such methods entail cell disruption to release cellular contents and derivatives of released fatty acids but they comprise highly expensive instrumentation (Dołowy and Pyka, 2015). Another technique is nile red staining, an *in situ* colorimetric detection technique for lipid estimation. Though it is simple, rapid, and highly efficient, still the accuracy of results can be influenced by several factors. Although, these methods are quick, cheap, and simple in nature but cannot detect fatty acid chains having less than 12 carbon atoms (Morschett et al., 2016). Time-domain nuclear magnetic resonance (TD-NMR) an *in situ* technique can be used for estimation as it is highly rapid, simple, and economical but the accuracy of this method depends on cellular lipid content. Therefore, it requires additional analytical equipment (Romel Malapascua, 2012). More recently, inverted fluorescence microscopy has been used for determining lipid content and growth for several microalgal species (Hathwaik and Cushman, 2017). Also, fluorescence-assisted cell sorting (FACS) has been employed for the detection of high lipid yielding cells in *Chlorococcum littorale*. Similarly, a microfluidic cytometer has been applied to quantify lipid accumulation and photosynthetic efficiency in *Phaeodactylum tricornutum*. While fourier-transform infrared spectroscopy (FTIR) has been used for examining both the lipid yield and growth in the case of *Dunaliella salina* (Romel Malapascua, 2012). Similarly, for *Chlamydomonas reinhardtii* mutants, droplet microfluidics-based screening has been applied for analyzing growth and lipid content (Hathwaik and Cushman, 2017).

Microalgae breeding strategies

In comparison to terrestrial plants, microalgae entail several advantages including a short life cycle from hours to days as compared to seasonal cycles seen in plants, are unicellular organisms that can rapidly breed in a confined space thus reducing the setup/land cost, and can do both sexual as well as asexual reproduction and boost the genetic diversity of the species. A variety of species can be screened on the basis of desired phenotypes *via* flow cytometry and other high throughput techniques. According to recent studies, transgenic microalgae are gaining more interest because of efficient phenotype construction (Hallmann, 2007). Novel strains can be developed by targeting specific genes through forward or reverse genetics. The former approach has much to offer by screening the results of random knockout events. Currently, there is a lack of transformation technologies that can be applied to biodiesel-producing algae. However, alternative strategies such as isolation and breeding of highly potent non-genetically modified organism (GMO) strains can be employed. One such method is the screening of libraries produced through UV or chemical mutagen treatment. This method also bypasses the regulatory procedure for GMOs for outdoor systems (Larkum et al., 2012).

Microalgal cultivation

Traditionally, open ponds and land-based photobioreactors (PBRs) have been used for algal cultivation. However, in recent times, the focus has been shifted to ocean-based floating microalgal culture systems due to the availability of large areas and wave energy for continuous mixing. In addition to

this, seawater provides nutrients and impregnates thermoregulation (Park et al., 2018). However, there is still a need for the development of novel and advanced technologies for the harvesting of microalgae biomass, and lipids from the cells. So, to enhance lipid productivity, two-stage microalgal cultivation setups have been proposed 1) Efficient growth stage: either in culture medium or in wastewater effluent medium, and; 2) High lipid accumulation inducing stage: salt stress stage (Hang et al., 2020).

To date several attempts have been made to reduce the production cost of biodiesel, some of them are as follows: (Gong and Jiang, 2011):

- Sequester CO_2 from thermal power plants to enhance biomass productivity
- Use nutrient-enriched wastewater for culturing microalgae
- Design and develop outdoor photobioreactors for large-scale algae cultivation
- Utilize by-products obtained after oil extraction effectively
- Incorporate genetic and metabolic engineering for the optimization of biodiesel production

Common strategies utilized for the cultivation of microalgae are: (Pavithra et al., 2020).

1) Single stage–Cultivation of microalgae using continuous, semi-continuous, or fed-batch system with lower lipid content due to nutrient deprivation in continuous or fed-batch setup.
2) Two-stage–Cultivation of microalgae in nutrient-rich medium followed by subjecting to stressful conditions.

Single-stage cultivation of microalgae

Open pond cultivation system

The operation mode of a cultivation setup not only improves biomass but also lipid yield. Such cultivation setups comprise of artificial ponds, open water bodies, or containers. Besides, on the basis of architecture, they can be shallow raceways, and circular unstirred ponds, out of which, raceway ponds are the most widely implemented. Besides, raceway ponds provide continuous tender agitation, minimal energy requirements, and low cost. Usually, they are cemented/concrete construct divided by baffles arranged in a series to support gentle mixing of nutrients as well as algae biomass. A depth of 1.5 ft promotes efficient sunlight penetration and optimum CO_2 sequestration (Chandra et al., 2020). However, they need an extremely large area and are capable of getting contaminated by microorganisms and birds. Moreover, the productivity quotient of microalgae cultivated in an open pond system is directly proportional to the location of the system, layout, inoculated species, and the prevailing weather conditions. For ponds with water levels higher than 200 mm, the light intensity for ponds, except for the thin upper layer, is below the photo-compensation point and thus, limiting the algal growth (Doucha and Lívanský, 2006). For such cases, thorough mixing can improve light penetration as well as cultivation efficiency. Additionally, such setups are majorly used for synthesizing, lipids, carotenoids (beta-carotene), proteins, carbohydrates and, other industrially important products. Though they are low-cost systems, but variable temperature, high water and weather dependence, and low biomass concentration limits their use for large-scale production.

Photobioreactor system

PBRs are a closed artificial setup which can incorporate both mechanical as well as non-mechanical mixing strategies. Usually, they comprise of a sparger having specialized nozzles to release CO_2 bubbles for non-mechanical agitation. While in some cases impellers can be installed for mechanical mixing in the PBR sets. These systems offer enhanced growth rates, higher cell density, and biomass compared to open pond cultivation systems (Huang et al., 2017). Additionally, CO_2 sequestering PBRs have a high biomass transfer rate due to increased resistance to mass transfer from a gaseous phase to algal cells *via* the lipid phase. Moreover, such setups are composed of glass, polyvinyl chloride (PVC), polyethylene (PE), polycarbonate (PC), plexiglass, or fibre glass and provide appropriate growth conditions with desired amount of carbon, water, light, nutrients, temperature, and pH. Amongst the different bioreactor types, airlift reactors are the most suitable for sequestering flue CO_2. Moreover, they provide uniform mixing, high gas transfer rate, low hydrodynamic stress, and an easy control system (Mondal et al., 2017). The selection of suitable PBR depends on the desired strain, space availability, and the preferred product's nature. Specific advantages of using PBRs are 1) concentration monitoring and control system, 2) minimal or no chances of contamination, 3) no media evaporation, 4) high concentration of microalgal cells, and 5) provides several critical cultural conditions simultaneously such as pH, temperature, CO_2, mixing and others (Pavithra et al., 2020). However, high capital and operational cost owing to complex configuration, an artificial illumination system, cooling, and agitation system, deoxygenation procedures, and other complex operating conditions are some of the limitations that prevent commercial implementation of these setups (Peng et al., 2020). Additionally, biofouling, overheating, and cellular damage due to shear stress are also some drawbacks. The PBRs are further classified into horizontal tubular, stirred tank, airlift, and bubble column PBR. Some advantages and disadvantages of these systems are discussed in Figure 1.

Operational parameters for efficient PBR Working

An effective PBR shall not only allow easy light penetration but also provide equal distribution of it. Besides it shall promote uniform mixing and mass transfer under favorable pH and temperature conditions. Also, cost is an important criterion for a long-term investment. So, it should be cost effective. Some of the aspects are discussed as follows.

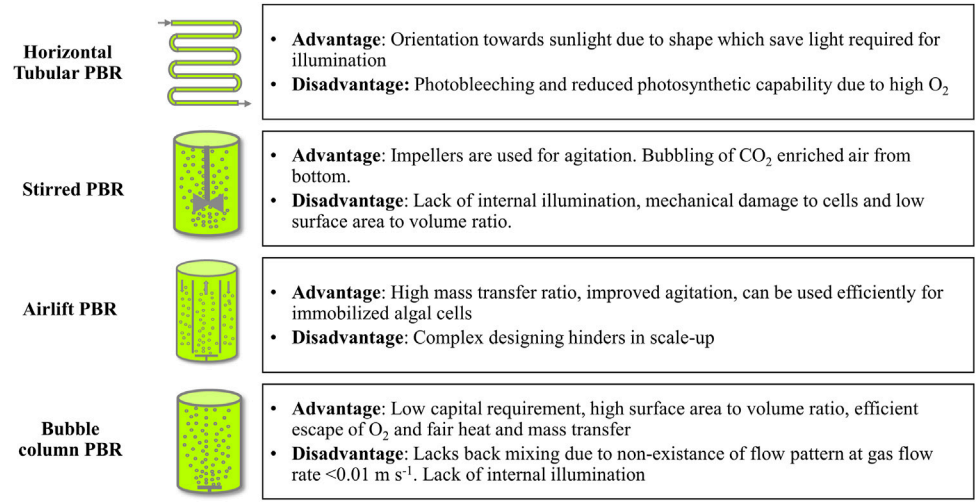

FIGURE 1
Different types of photobioreactors (PBRs) with their advantages and disadvantages.

Light

Intensity of light and UV-Visible spectrum (400–700 nm) are some of the critical factors responsible for improved biomass yield. Usually, distribution of light is non-uniform inside a PBR due to scattering and absorption by individual cells (Quan et al., 2004). The radiation attenuation depends on cell concentration, PBR geometry, distance of light, and visible range. Also, according to studies intensity of light decreases with distance. So, light can penetrate only several millimetres when cell density is more than 10 g/L in a PBR. Additionally, growth decrease as the reactor depth increases. In some cases, investigators revealed that if light is above the critical value so the growth will be inhibited *via* photoinhibition (Richmond, 2004). On the contrary if it is below the necessary level then it will lead to photolimitation and stunned growth. Therefore, based on cell growth, PBR's can be divided into 3 zones namely: strong illuminating zone, light energy fulfils the cell demand; weak illumination zone, light energy just meets the cell demand; and dark zone, cells are unable to grow due to limiting light (Bitog et al., 2011). Hence, for enhanced biomass productivity thickness of a PBR should be minimum.

Mixing

Efficient mixing not only provides uniform distribution of nutrients, gas but also avoids stagnation of cells in dark zones, prevent fouling, and maintain the cultures (Anjos et al., 2013). Additionally, mixing exposes light equally to all the cells and endorse efficient mass transfer. But, excess of mixing might cause cell damage due to shear force. Also, it is recommended to keep the mixing velocity below 1 m/s to prevent micro eddies formation that can damage cells. A velocity of 20–50 cm/s is recommended for good mixing (Lehr & Posten, 2009). Mixing in PBR is induced *via* agitator, impeller, static mixer, or a CO_2 enriched sparger.

Mass transfer

Algae growth can be distributed into three processes including photosynthesis, photorespiration, and dark respiration (Wang et al., 2012). Most of the identified algal species undertake the C3 pathway or Calvin Cycle for CO_2 fixation. An enzyme Ribulose-1,5-bisphosphate carboxylase/oxygenase (RuBisCo) catalyzes the formation of two molecules of the 3-carbon compound from the combination of CO_2 and a 5-carbon containing compound. While, Photosynthesis is carried out in the chloroplast as a result of biophysical and biochemical reactions happening at thylakoid and stroma respectively. Biophysical reactions lead to photon absorption *via* chlorophyll and other accessory photosynthetic pigments. Therefore, water is oxidized and release oxygen. Free electrons from water molecules result in the formation of ATP and NADPH. The energy produced by the splitting of water is used for CO_2 fixation in the dark reaction. Whereas, biochemical reactions lead to the formation of sugar and other organic molecules for cellular functions and metabolism (Raven and Beardall, 2003). Therefore, photosynthesis elucidates light and CO_2 to make ATP and O_2 as a by-product. However, increased amount of dissolved O_2 may cause photoinhibition which is toxic and inhibit algae growth. So, closed PBR's are equipped with a degasser to prevent such condition and mediate smooth mass transfer.

Temperature

Microalgae are capable of growing only under specific temperature range. Exorbitant temperatures lead to growth inhibition followed by cell death. It is seen that Open pond cultivation maintain an approximate temperature of 40°C due to

evaporation (Anto et al., 2020). While closed PBR are well equipped with thermal jackets and cooling water units which prevents desired temperature deviations. However, in tropical regions where the maximum temperature reaches upto 47°C there is a constant need of heat exchangers, IR-radiation, and light dilution is used to enhance biomass productivity. This additional cost can be compensated *via* solar photovoltaic panel setup (SPV) or other bioactive compounds extraction after biofuel production (Stephens et al., 2010) (Gondi et al., 2022).

pH

Optimal pH for algae growth is in the range of 7–9. It greatly affects the CO_2/carbonates solubility, and functioning of intracellular enzymes. Acidic media may enhance nutrition uptake by the cells, produce metabolites and increase metal toxicity. While a basic media interferes with the cell division. Any deviation from the standard pH range will reduce the photosynthetic efficacy. Generally, freshwater algae including cyanobacteria can tolerate altered pH, but marine algae are inflexible to any such deviations and need an optimum value around 8.2. (Lackner, 2003; Kumar et al., 2010).

Carbon dioxide sequestration

Microalgal biodiesel is found to be a carbon-neutral renewable liquid fuel as half of the dry weight of the algal biomass is carbon which is sequestered from the atmosphere. Therefore, cultivation setups are continuously supplied with CO_2 for enhanced biomass production. For instance, approximately 183 tons of CO_2 can produce 100 tons of microalgal biomass (Chisti, 2008). Some sources of CO_2 supply include atmospheric CO_2 (approximately 0.0387% (v/v) in the air), industrial emissions (flue or flaring gases which typically contain approximately 15% (v/v) CO_2 in the exhaust emission), and chemically fixed soluble carbonates (e.g., sodium bicarbonate and sodium carbonate). However, for large-scale setups, industrial emissions have been found to be adequately fulfilling the CO_2 demands (Lackner, 2003; Kumar et al., 2010). Methods for supply and its efficacy vary with the nature of the cultivation system that is either open surface ponds or closed photobioreactors with diverse configurations. So, a closed setup is fortified with membrane transfer, gas injection, and gas exchange which offers fair CO_2 supply, gas transfer, and uniform mixing of nutrients in the cultivation systems (Yamaguchi, 1996; Carvalho et al., 2006). According to the studies extracellular enzyme, carbonic anhydrase (CA)–a zinc metalloenzyme facilitates atmospheric CO_2 uptake by microalgal cells. They are responsible for catalyzing the conversion of CO_2 to bicarbonates. These bicarbonates can easily be taken up by the microalgal cells *via* specialized cell transporters. In addition to this, depending upon the microalgal species, captured CO_2 can be stored in the cells as lipids, proteins, or carbohydrates. (Kumar et al., 2010; Mondal et al., 2017).

Two stage cultivation of microalgae

Microalgae cultivation setup defines fuel quality and quantity extracted from the feedstock (Pavithra et al., 2020). Under ideal cultivation conditions, the algal strain proliferates with a synchronous increase in the lipid content. However, the culture condition required for cellular growth differs from the one required for lipid production. Thus, the culture condition favors biomass production with a lower lipid content (Alishah Aratboni et al., 2019). In order to enhance the lipid content of the microalgal cells, other approaches must be employed, such as inducing nitrogen or phosphate limitation and increased salinity during growth. However, these conditions may reduce the cell growth rate. Therefore, a balance is required so that lipid content and cell growth occur (Qiu et al., 2017). A two-stage cultivation setup provides this balance for microalgae growth. Initially, a nutrient-rich medium is used to maximize biomass production in heterotrophic conditions, followed by inducing stress in the phototrophic mode for enhanced lipid productivity. The most commonly used two-stage strategies are based on: starvation, inducer addition, metabolic switch, and irradiation (Nagappan et al., 2019) (Yap et al., 2021).

Microalgal culturing system

There are two major culturing systems 1) Suspended cell cultivation and 2) Immobilized cell activation system. The suspended cell cultivation system is highly energy intensive and time-consuming. Circular and raceway ponds are preferred for commercial algae cultivation. The commercial ponds should be shallow, with a depth ranging between 0.2 and 0.5 m so that light can penetrate to the bottom of the pond. Microalgae absorb and utilize CO_2 as a carbon source from the atmosphere. A suspended cell cultivation system has an effortless operation, low construction, operational and production cost, and functions under high CO_2 concentration. The significant disadvantages of this cultivation method include a lack of light and temperature control system, and the entire system is prone to contamination. The second method, the immobilized cell activation system, is an alternative cell cultivation method. Biofilm containing microalgal cells are attached to their specific natural surface through effective adsorption, immobilization, semipermeable membrane capture, polymer traps, and covalent joint. Some widely used immobilization methods include cell adhesion, solid surface biofilm formation, and polymer matrix cell entrapment employing polymers such as alginate and carrageenan (Vasilieva et al., 2016; Lin-Lan et al., 2018).

Unit operations in down-stream processes

Harvesting and dewatering

Microalgal biomass harvesting contributes about 20–30% of the total production cost (Molina Grima et al., 2003). A detailed

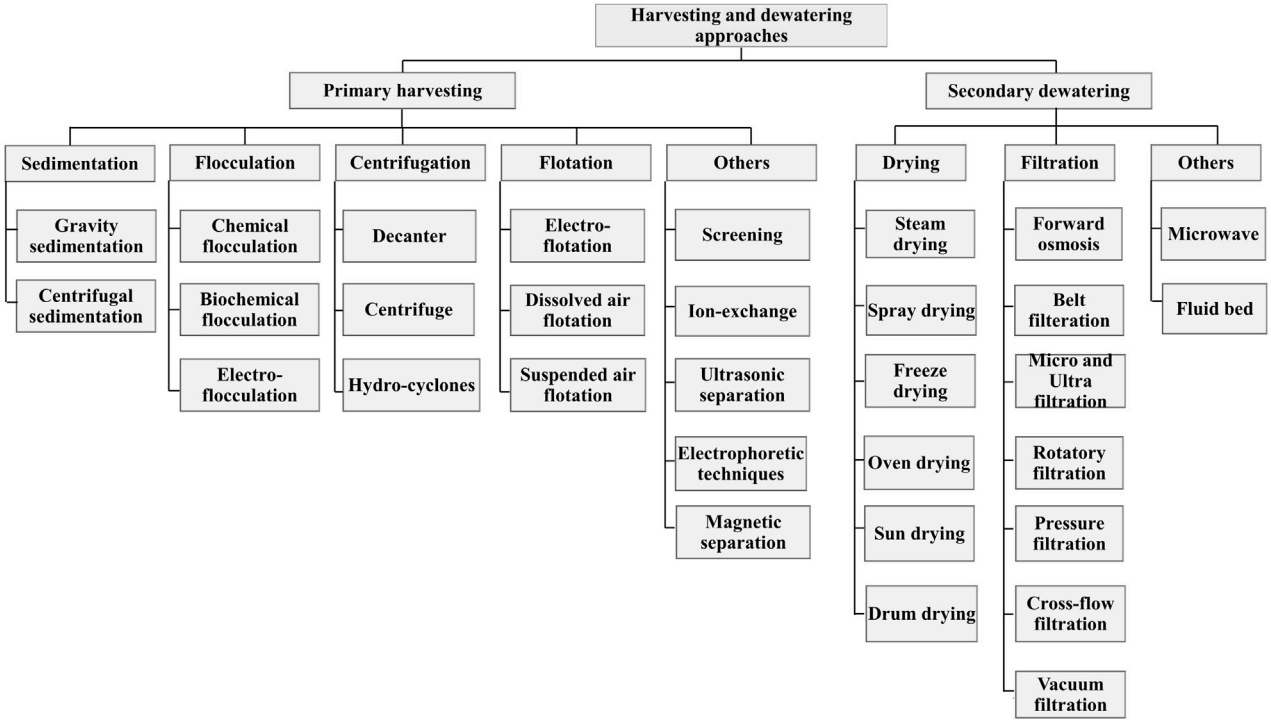

FIGURE 2
Various methodologies of harvesting and dewatering of cultivated microalgal cells.

discussion on the advantages and disadvantages associated with different unit operations adopted in algal biofuels has been presented elsewhere (Kumar et al., 2022a). Since the harvested biomass is highly dilute and contains more than 99.6% of the water on a weight basis, dewatering is required for further downstream processing (Mata et al., 2012). Both harvesting and dewatering are bottlenecks for microalgae-based biofuels as they are energy intensive and incorporate the high cost of production (Peng et al., 2020). Furthermore, these methodologies are categorized as primary harvesting and secondary dewatering, as described in Figure 2.

After the synthesis and accumulation of lipids in microalgal cells, biomass is harvested, followed by lipid extraction and purification before transesterification reaction for biodiesel production. Numerous methods can be sequentially applied in the downstream process or directly to the bioreactors. Additionally, bulk harvesting is performed to separate algal biomass from the bulk suspension, accompanied by thickening protocols further to concentrate the slurry (Das, 2016). Harvesting algae cells are expensive due to their small size, which possesses terminal velocity and hinders mechanical separation. Also, these small-sized cells impart volume reduction and make the water removal process expensive. Algal cells are usually negatively charged, which keeps them in a dispersed state. Therefore, thermal drying and centrifugation can be incorporated to remove water. However, thermal drying is expensive, and centrifugation demands high energy making separation expensive. For economical separation, flocculation, sedimentation, and flotation can be performed before centrifugation or filtration (Jeevanandam and Danquah, 2020).

Cell disruption

It is essential to release the lipid content produced inside the microalgal cell. Many frequently physical, chemical, biological, and mechanical cell disruption methods are incorporated for algal cells as described in Figure 3. Though algae cell walls are sometimes complex, varied chemically, and robust structurally so more energy intensive techniques are required to extract intercellular compounds which are referred as high-value products. Numerous techniques have been studied to break algal cell wall from a variety of species including the use of surfactants, ultrasound, microwave, sonication, bead milling, enzymatic lysis, high-pressure homogenization, and steam treatments (Alhattab et al., 2019). Some disruption techniques with advantages and disadvantages have been discussed below in Table 1.

Microalgal lipid extraction methods

Amongst all the extraction techniques available for the recovery of microalgal oil, an appropriate solvent should be selected to achieve enhanced yield and minimize the

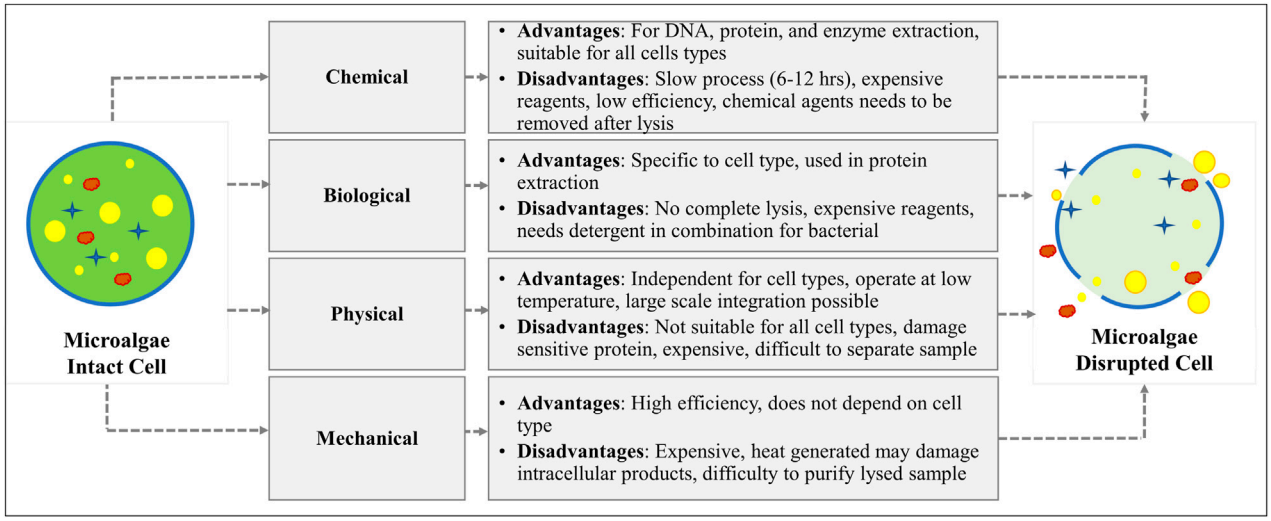

FIGURE 3
Advantages and disadvantages of different cell disruption techniques.

production cost. A comparative analysis of lipid extractions methods is depicted in Figure 4.

Organic solvent extraction

It is a widely applied method for microalgal oil extraction. It involves organic solvent selection on the basis of toxicity, recyclability, and cost. For instance, some common solvents are -hexane, benzene, acetone, cyclohexane, and chloroform. According to some recent studies, the use of Bligh and Dyer's method which amalgamates a mixture of chloroform, methanol, and water to extract microalgal oil is the most efficient process for lipid extraction. Some studies have reported the use of the Folch method for lipid extraction which makes use of a 2:1 ratio of chloroform-methanol by volume. Currently, the Matyash method of lipid extraction is used which is comparatively more rigorous and is a modification to both of the methods. It employs methyl-tert-butyl ether (MTBE) as a solvent for lipid extraction (Kumar et al., 2015). However, their toxicity is a major concern that can be eradicated by employing cell disruption methods preceding the extraction step (Sati et al., 2019). To minimize the toxicity of chloroform, several other solvents such as ethanol, MTBE, hexane, and acetic acid esters can be employed. Recent studies have also suggested the employment of 2-ethoxyethanol (2-EE) for the enhanced extraction of lipids as compared to the traditionally used solvents (Kumar et al., 2015).

Supercritical fluid extraction

Supercritical fluids are compounds that act both as liquid or gas when exposed to varying temperatures and suppress above their critical values. These fluids are an alternative to organic solvents and are used for the extraction of lipids, essential oils, and other functional groups from plants and microalgae (Mata et al., 2012). Based on improved solvation powers of fluids such as CO_2, water, ethane, methanol, and butane above their critical points these fluids have mass transfer properties similar to gases and solvating properties and diffusion coefficient comparable to that of liquids. Most commonly used is supercritical CO_2 ($scCO_2$) for oil extraction due to low critical temperature (31.1 ^{O}C) and pressure (72.9 atm). $scCO_2$ is a green way of oil extraction and it also permits complete characterization of extracted lipid and the resultant biofuel. However, owing to low polarity it is relatively inefficient in the extraction of polar compounds. In order to enhance the extraction capability, modifiers or co-solvents are used. Modifiers are highly polar in nature and when added in small amounts can enhance the solvation properties of $scCO_2$ (Mata et al., 2012). This technique offers several advantages over organic solvent extraction such as no toxicity levels, does not lead to oxidative degradation of extracts, and enabling easy separation of the bioproducts (Li et al., 2014).

Ionic liquid-mediated extraction

Ionic liquids (ILs) are non-volatile, thermally stable, and have high solvation capabilities. They are a promising alternative for toxic and volatile organic solvents. ILs are also referred to as "green" solvents (Gholami et al., 2020). ILs are salts of large asymmetric cations coupled with smaller organic or inorganic anions. ILs can be maintained in a liquid state at temperatures ranging from 0 to 140°C. ILs are the non-aqueous solutions of desirable salts. IL-methanol system has

TABLE 1 Advantages and disadvantages of different cell disruption techniques.

Cell disruption type	Cell disruption technique	Mode of action	Advantages	Disadvantages	References
Chemical	Alkali and detergent lysis	Cell wall degradation *via* different surface chemical reactions	- Easy and simple - Suitable for all cell types	- Expensive -Environment pollution - Chemical contamination - Slow process	Islam et al. (2017)
Biological	Enzymatic	Enzymes hydrolyse the chemical bonds by binding to specific molecules in the cell wall	- Specific to different cell types - No harmful chemical - No harsh physical condition	- Does not do complete lysis - Expensive reagents	Venkata Subhash et al. (2017)
Physical	Ultrasonication	Acoustic streaming, liquid shear stress, cavitation effect	- Less extraction time - Eco-friendly - Enhanced penetration of solvents	- Require energy - Difficult to scale up - High operational cost	Liu et al. (2013)
	Microwave	Temperature, energy increase	- Less solvent used - Less extraction time - Simple, rapid and can be scaled-up	- High temperature cause lipid oxidation - High operational cost - Easy scale up	McMillan et al., (2013)
	Osmotic Shock	Osmotic pressure applied for cell lysis	- For sensitive product extraction	- Long treatment time - Cannot scale up	Karim et al. (2019)
Mechanical	Oil Press	Mechanical pressing and shear force	- Simple process - No requirement of solvent	- Slow/time consuming - Higher quantity of sample needed - Not fit of high moisture content samples	Karim et al. (2019)
	High Speed Homogenization	Turbulent force with hydrodynamic cavitation	- Simple method - Efficient extraction - Less contact time - Solvent free	- Energy intensive - High heat dissipation	Karim et al. (2019)
	Bead Milling	Mechanical pressure and shear force	- No solvent required - Suitable for samples with high moisture content	- May not extract majority of lipid - Low efficiency for rigid cells - May cause lipid degradation - Additional process to remove undesirable products and beads	Suarez Garcia et al. (2019)
	Steam Explosion	Sudden pressure drop	- Do not release any hazardous waste	- Species specific	Lorente et al. (2018)
	Pulse Electric Field	Permeabilization of cell membrane leading to pore formation	- No chemical used - No cell debris - Quick technique - Enhanced yield	- depend on media composition	Vorobiev et al. (2020)

been used as an alternative to imidazolium-based ILs as they are cheap and less toxic to aquatic habitat and thus, prove to be an environment-friendly method of oil extraction from microalgae (Sati et al., 2019). ILs make it possible to use varied combinations of anion and cation which in turn allows for deciding the polarity of the solvent, conductivity, hydrophobicity, and solubility (Kumar et al., 2015).

From algal lipid to biodiesel

Microalgae store excess photosynthetic products as triacylglycerol, a storage lipid. Many microalgal species can be artificially induced to accumulate an increased amount of storage lipids under nutrient deficient conditions. These storage lipids are chemically similar to vegetable oils and can be extracted and converted to fatty acid methyl ester (FAME) for their use as

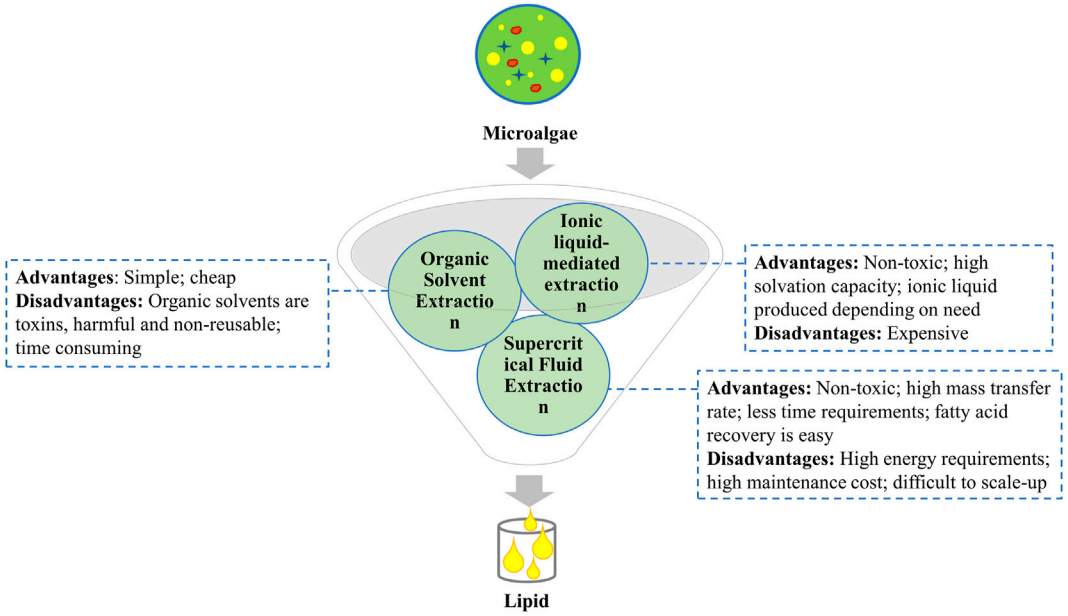

FIGURE 4
Advantages and disadvantages of lipid extraction methods.

biodiesel. Biodiesel has several advantages such as they are renewable, and biodegradable leading to the emission of fewer particulate matter into the environment upon its combustion (Dunahay et al., 1995). Extraction of lipid from biomass requires specific solvents having a high affinity for the microalgal lipids. Most commonly employed extraction methods for microalgal lipids involves the use of organic solvents, supercritical fluids, and ionic liquids (Amaro et al., 2011; Mercer and Armenta, 2011; Taher et al., 2011; Kim et al., 2012). Although these extraction techniques can be applied directly to the dewatered biomass, the efficiency is very less because the cell wall of microalgae prohibits these solvents from reaching the cytoplasm where these lipids are stored (Cravotto et al., 2008; Chen et al., 2009). Thus, in order to increase efficiency, lipid extraction is preceded by cell wall disruption methods (Gonçalves et al., 2013). Additionally, conversion of microalgal lipids to biodiesel is also done chemically by the following methods: 1) micro emulsification of oils; 2) direct use or blending of recovered oil; 3) transesterification/ alcoholysis; 4) thermochemical methods such as thermal cracking, pyrolysis, thermochemical liquefaction, gasification and; 5) biological conversion employing anaerobic digestion, fermentation, and photobiological oxygen production. Amongst all the known conversion methods, transesterification of microalgal oils is the most popularly employed methodology for oil separation (Suali and Sarbatly, 2012; Nandhini et al., 2022).

Transesterification

The most widely used multi-step process which converts triglycerides to low molecular weight alcohols in the presence of a catalyst (homogenous acid or alkali) is termed transesterification. This reaction is carried out in batch mode, stirred reactors. Initially, triglycerides are converted to diglycerides, monoglycerides, and then to glycerol. Such conversion reactions are reversible and each conversion step yields approximately 1 mol fatty acid ester (Quader and Ahmed, 2017). The process constitutes high conversion rates, easy process control, mild reaction temperature, and pressure. In addition to this molar ratio of alcohol, amount of free fatty acids (FFA), type of catalyst, reaction conditions and water content are the factors that affect biomass yield during the reaction (Chozhavendhan et al., 2020). However, prolonged reaction time, complex separation stage after reaction, and batch operation mode limits the use of this method extensively.

Moreover, this reaction is susceptible to the purity of feedstock (water content should be greater than 0.5% w/w and FFA content should be greater than 1% w/w). In order to obtain a pure product, some pre-treatment steps are incorporated with this method. This not only avoids low yield but also saponification. Transesterification can either be applied to the extracted microalgal oil or directly to the biomass, known as *in situ* transesterification. This can reduce the production cost by eliminating the cost involved in the extraction of microalgal oil (Chisti, 2008).

Algal cell components recovery

The multiple product recovery majorly depends on the fractioning ability of several components and maintenance of

the quality and yield of the recovered products. The most crucial step is selecting an appropriate extraction technique and cell wall disruption to release the desired product. Additionally, optimal parameters and gentle extraction of different components manifest multiple product recovery (Gifuni et al., 2019). A large-scale microalgal culturing system currently produces extremely dilute cultures (0.08–3.6 g/L), and weather conditions and light penetration hamper their productivity. In order to minimize energy consumption in harvesting and extraction, a minimum of ~100 g/L cell concentration is required (Gifuni et al., 2019). Microalgae possess an oil yield in the range of 58,700–136,900 L/ha. With 15–77% of oil on a dry basis, making them the best candidate for biodiesel production. The exact percentage of oil content is dependent on the algal species. The average cost of algal biodiesel is USD 0.48 to 2.8 per L, while the average price of conventional biodiesel produced from vegetable oil or palm oil is USD 0.52 per L. The significant expense of algae-based biodiesel depends on cultivation and harvesting techniques. In the current scenario, crude oil prices have exceeded USD 80–100 per 100 L. Therefore, microalgal biodiesel proves to be an economical and sustainable alternative.

Algal lipid synthesis

To obtain microalgae-based fuel, species selection followed by elucidation of lipid metabolism and the connected pathway is crucial. In addition, comprehensive knowledge of carbon flux throughout cellular processes is required. Lipid catabolism plays an integral role in the metabolic processing of lipids throughout cell growth and during nutrition deficiency and is involved in lipid accumulation and homeostasis (Trentacoste et al., 2013). Analysis of various lipid classes, fatty acids, and membrane stability in transgenic strains suggested the role of lipase/phospholipase enzyme in maintaining lipid homeostasis and in membrane lipid turnover. Lipid catabolism provides acyl group for membrane recognition as a change in environmental conditions leads to the synthesis of polar lipids during dark cycles and remobilizes cell membrane when conditions get better. It is hypothesized that the knockdown of the lipase enzyme can lead to high lipid accumulation (Trentacoste et al., 2013). Understanding the microalgal lipid biosynthesis pathway paves the way to accumulate lipids in the microalgal cells, followed by the production of biodiesel and other bio-based products. In addition, genetic engineering, the addition of stimulators or repressors, or changing culture conditions may improve lipid storage inside the cells (Tang et al., 2020).

Genetic engineering approaches

Numerous enzymes inducing biochemical reactions are responsible for synthesizing Triacylglycerol (TAG) and fatty acid (FA) in microalgae cells. It has been reported that over-expression of these enzymes would enhance lipid accumulation (Bajguz and Piotrowska-Niczyporuk, 2013). One of the most exploited enzymes is Acetyl-CoA carboxylase (ACCase), a multi-subunit enzyme found in the chloroplast of algae. According to some studies, overexpression of ACCase alone does not improve lipid accumulation (Ng et al., 2017). However, over-expression of ACCase subunit (accD) in association with malic enzyme (ME) increased lipid productivity in *Dunaliella salina* (Salama et al., 2014). Furthermore, overexpression of ME enhanced 2.5 times the lipid production in *Phaeodactylum tricornutum* without causing any negative impact on biomass productivity. Suppression of the competitive pathways such as lipid and carbohydrate catabolism are an alternative strategy to enhance oil yield (Abomohra et al., 2020). Carbohydrate metabolism is an essential microalgal pathway for storing carbon and producing starch. Therefore, the knockdown of starch metabolism may alter the carbon pathway toward lipid synthesis.

Lipid accumulation strategies

TAG accumulation can remarkably be enhanced by introducing environmental stress such as nitrogen scarcity. Limiting iron, sulfur, zinc, phosphorus, and salt may also trigger lipid and starch synthesis in microalgae. Major steps involved in lipid biosynthesis are: 1) fatty acid production in plastids; 2) glycerol-lipid formation in the endoplasmic reticulum (ER); 3) packaging of glycerol-lipids into oil bodies. Fatty acid synthesis is catalyzed through ACCase, yielding malonyl-coenzyme A from acetyl-coenzyme A and bicarbonate (Maity et al., 2014). ACCase through its two catalytic centers biotin carboxylase (BC) and carboxyl transferase (CT), catalyzes irreversible carboxylation of acetyl-CoA to produce malonyl-CoA, which is essential for fatty acid biosynthesis (Cronan and Waldrop, 2002; Fan et al., 2014).

Nitrogen starvation

Microalgal biomass is initially produced under nitrogen-rich conditions, while TAG accumulation is induced by creating nitrogen deficiency (Peng et al., 2020). Nitrogen limitation reduces metabolism and leads to excess photon dissipation as heat or fluorescence. The percentage reduction in photosynthetic capacity under stressful situations is species-specific and influences the amount of available energy for the synthesis of TAG. Also, it causes a reduction in photosynthetic proteins, pigments, and centers for photosystem reaction in order to minimize overexcitation-associated damage (Chisti, 2008; Kumar et al., 2010). For instance, in *Neochloris oleoabundans* only 8.6% of the generated electrons were used for TAG biosynthesis and the rest of the energy got dissipated in photosystems or utilized in catabolic processes (Trentacoste et al., 2013). Thus, it is highly recommended to choose a species that retains the high photosynthetic capability and

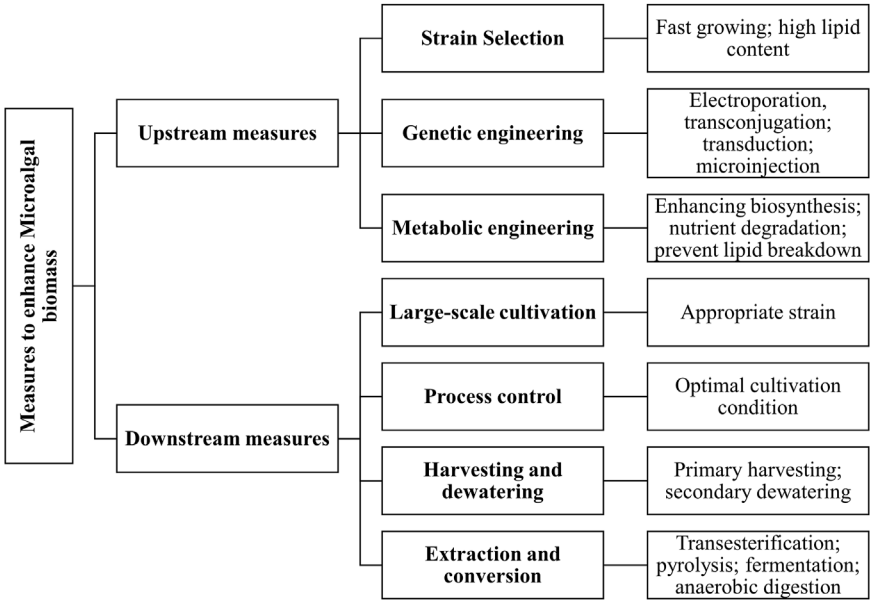

FIGURE 5
Different upstream and downstream measures to enhance microalgal biomass productivity.

TAG productivity under nitrogen depletion (Klok et al., 2014). TAG content can further be improved by employing techniques such as selective cell sorting, targeted engineering, and random mutagenesis (Remmers et al., 2018). It has been studied that the efficiency of bulk lipid production is less due to low solar-lipid conversion. Several attempts have been made to increase solar-lipid conversion efficiencies such as rational strain selection, improvement of selected strain, and process condition optimization (Yamaguchi, 1996; Carvalho et al., 2006; Mondal et al., 2017).

Lipid biosynthesizing enzymes

A variety of enzymes including acetyl-CoA synthetase (ACS), Acetyl-CoA carboxylase (ACCase), acyl-ACP esterase (AAE), diacylglycerol acyltransferase (DGAT), D5-elongase (D5 Elo), D6-elongase (D6 Elo), glycerol-3-phosphate-dehydrogenase (G3PDH), glycerol-3-phosphate acyltransferase (GPAT), lysophosphatidic acid acyltransferase (LPAT), phosphatidic acid phosphatase (PAP) is involved in lipid biosynthesis (Klok et al., 2014). According to some experimental pieces of evidence, overexpression of cytosolic ACCSase in *Chlamydomonas reinhardtii* lead to a 2-fold increase in starch content and a 2.4-fold higher accumulation of TAG (Rengel et al., 2018). Similarly, overexpression of Acetyl-CoA carboxylase (ACCase) in *Chlamydomonas reinhardtii* increased FA synthesis by approximately 56%. It is highly possible that the homeostatic regulation as in the case of redox activation of ACCase under stressful conditions ensures sufficient synthesis of fatty acyl groups (Shahid et al., 2020). Overexpression of AAE, led to fatty acid profile changes in *Phaeodactylum tricornutum* and *Chlamydomonas reinhardtii* whereas an increased lipid content was observed only in *P. tricornutum* (Dunahay et al., 1995; Lin et al., 2018). While, overexpression of type 2 DGAT in *P. tricornutum* leads to only 35% increase in TAG levels (Muñoz et al., 2019) and overexpression of some type 2 DGAT enzymes results in an increased TAG yield in *C. reinhardtii* (Xue et al., 2015; Sharma et al., 2021). In *Chlorella minutisma*, it has been studied that heterologous expression of yeast-derived LPAT, PAP, GPAT, DGAT, and G3PDH enzymes leads to a two-fold increase in TAG content as compared to overexpression of any one of the genes (Han et al., 2021). Heterologous expression of gene D5 Elo and D6 Elo from *Ostreococcus tauri* into *P. tricornutum* resulted in an increase of docosahexaenoic acid (DHA) (Klok et al., 2014).

Challenges to sustainable production of algal biodiesel production

Numerous biological barriers are still present for industrial-scale algal biodiesel production have been discussed. Figure 5 describes various upstream and downstream strategies to enhance microalgal biomass production.

- Organism survival: Current systems have been unable to maintain the best laboratory organisms under field conditions. Laboratory culture when exposed to environmental conditions

gets contaminated by indigenous organisms found in the environment (Gressel, 2007).

- Carbon dioxide enrichment: Carbon dioxide levels above 5% slow the growth of higher plants and animals, yet many algae and cyanobacteria grow happily when "aerated" with 100% carbon dioxide or directly with ca. 14% CO_2 flue gas from power generators. Still, the response of algae to added carbon dioxide is not as good as it could be, and there is a place for improvement of carbon assimilation (Gressel, 2007).

- Light penetration: For autotrophic cultivation of algae light is an important parameter. Its intensity decreases with the increase of water depth. Moreover, the photosynthetic efficacy of the species is highly dependent on the source of light. In open ponds, the shallow depths provide a high surface area with efficient mixing and light penetration. It can be calculated by Beer-Lambert's law (Wang et al., 2015).

- Environmental dependence: The high yields attained in ponds is usually seasonal. Therefore, algal growth is a function of temperature. Some species do not grow well in cold temperatures while some face difficulty at high temperatures. Additionally, they require a special cooling unit (Gressel, 2007).

- Limitations: According to the literature, a major drawback of algae-based biodiesel production is the display of contrasting features such as high biomass productivity accompanied by low lipid accumulation, or high lipid accumulation with low biomass productivity. The growth rate of oleaginous algal species is often slow (Shokravi et al., 2020). It is well established that in order to produce biodiesel economically, a balance is required to be maintained between biomass productivity and lipid accumulation.

- Challenges associated with biomass production:

1) Daily and seasonal variations of sunlight during cultivation.
2) High levels of dissolved oxygen in closed PBRs inhibit photosynthesis in microalgal cells.
3) High oxygen concentration and sunlight intensity cause photo-oxidative damage to microalgal cells.

The maximum tolerance of dissolved oxygen for microalgal cells should not exceed 400% of air saturation in PBRs (Chisti, 2008).

Strategies to make microalgal-based biodiesel economical

The microalgal lipids can be classified into two major groups: polar lipids (phospholipids and glycolipids) which constitute about 41–92% of the total lipid content and non-polar or neutral lipids (sterols and free fatty acids) having 5–51% of lipid content (Tang et al., 2020). Genetic and metabolic engineering can (Chisti, 2008) enhances the photosynthetic efficiency and increase the biomass yield on light, increase biomass growth rate, elevate the oil content in algal biomass, and improve temperature tolerance of algae so that there is a reduced need for cooling consequently reduces the cost of production, and provide tolerance against photoinhibition. Therefore, elucidating the genetic makeup can improve the strain yield.

Abiotic manipulations

Increased levels of polar lipids inside the cell may lead to a reduction in permeability of membranes and also lead to reduced fluidity which limits an excessive flow of sodium and chloride ions into cells. A high concentration of neutral/non-polar lipids enables microalgal cells to resist osmotic pressure by enhancing membrane rigidity. The addition of salts such as sodium bicarbonate increases the lipid content of cells by enhancing the photosynthetic capability and nitrogen utilization by microalgal cells (White et al., 2013). While, ferric, cupric, zinc and chromium salts, have been reported to increase lipid content in some of the algal species (Sharma et al., 2012). However, these salts cannot be used on a large scale due to their extreme harmful environmental impact. Sodium chloride supplementation can be used more effectively and safely for enhancing lipid accumulation in microalgal cells (Xia et al., 2013). Table 2 describes various attempts to enhance algal productivity by employing various abiotic strategies.

Biotic manipulations: GM algae

In recent times, researchers have proposed a number of strategies for increasing lipid content in microalgal cells such as genome manipulation, random mutagenesis, metabolic engineering, blocking carbohydrate metabolism pathways, and lipid degradation which competes with the biosynthesis of lipids. As a result, engineered microalgal strains have high lipid content but slow growth rates. Amongst all the devised strategies, blocking competitive pathways has been recognized as a potential alternative to increase lipid yield (Sun et al., 2019). Researchers have suggested that inhibition of enzymes responsible for converting lipids into free fatty acids may help in improving lipid accumulation. Lipid catabolism provides acyl groups that help in membrane reorganization and acknowledgment of the photosynthetic system. Some recent studies depicted that knockdown of genes associated with lipid catabolism has a lesser impact on the microalgal growth rate as compared to the strains having disrupted carbohydrate pools. Therefore, lipid catabolizing enzymes are the best candidates for improving lipid content through knockout mutations (Nguyen et al., 2020). Table 3

TABLE 2 Abiotic strategies to enhance algal productivity.

Strategies	Algae and growth conditions	Change in biomass productivity (BP)/Cell growth	Change in biochemical components	Possible reasons behind outcome	Remarks	References
Nanoemulsion (NE)-based growth media (1% silicone oil (SE) and 1% paraffin oil (PE) in BG-11)	*Chlorella pyrenoidosa* (LI: 46.5–50 μmol m^{-2} s^{-1}; LP: 12:12 h; T: 25 ± 1°C; shaking at 150 rpm)	3.20 g L^{-1} (PE), 2.75 g L^{-1} (SE) as compared to control 1.03 g L^{-1} in BG-11	Increase in Chlorophyll a synthesis by 76% and 53%; lipid content increased to 23.6% and 26.8% as compared to control 18.05%. Carbohydrates increased from 13.6% to 18.9% and 17.20% for SE and PE respectively.	Effective CO_2 supplementation for microalgal growth media. NE acts as CO_2 delivery agent to algal growth medium.	Biomass productivity and lipid both increased.	Nigam et al. (2021)
Phytohormones- Auxin, Indole-3-acetic acid (IAA) and Brassinosteroids (IAA induced BRs in algal cells)	*Chlorella vulgaris*	—	Increase in total chlorophylls, protein, and carbohydrate.	BRs could prevent loss of photosynthetic pigments by an activation of enzymes participating in chloro- phyll biosynthesis or an induction of their synthesis	BRs promote photosynthesis and growth by positively regulating synthesis and activation of a variety of photosyn-thetic enzymes	Bajguz and Piotrowska-Niczyporuk, (2013)
Phytohormones - Auxin, Indole-3-acetic acid (IAA) and Diethyl aminoethyl hexanoate (DAH)	*Scenedesmus obliquus* GU732418 (BBM media; Shaking at 150 rpm; T- and 27°C; LI-45–50 μmol photon m^2/s)	1.9 and 2.5 fold increase in growth (Cell counts) due to IAA and DAH respectively.	Increase in lipid content was reported for both IAA and DAH.	Phytohormones stimulate algal growth.	At higher concentrations, the proportion of unsaturated fatty acids increased while saturated fatty acids decreased.	Salama et al. (2014)
Phytohormones -Jasmonic acid (JA)	*Chlorella vulgaris* (Trebouxiophyceae) (F/2 medium; T- 24 ± 2°C; 80 μmol $m^{-2}s^{-1}$)	Increase in cell growth	Lipid productivity enhanced.	Phytohormones stimulate algal growth.	Induced production of saturated SFA and MUFA without compensating the production of PUFA.	Jusoh et al. (2015)
Phytohormones, Cytokinin- Kinetin (K) and Zeatin (Z)	*Acutodesmus obliquus* (BG-11 media)	Biomass productivity increased by 50% (K) and 60.7% (Z).	Lipid productivity increased upto 63–65% for both K and Z.	Cytokinin, by enhancing enzymatic activity, improves the photosynthetic efficiency and carbon fixation.	Z was found to be more effective than K for increase in BP.	Renuka et al. (2017)
Phytohormones (PHs), Kinetin, Indole-3-butyric acid (IBA), Methyl jasmonate (MJ), and Antioxidants- Butylated hydroxyanisole (BH)	*Chlorella protothecoides* (Tris-acetate-phosphate (TAP) medium; LP-14:10; T-27°C; LI-4,800 Lux)	Significant increase in biomass productivity for each phytohormone.	Increase in lipid content and alpha-linolenic acid (ALA). An increase of 26.5% and 60.5% in ALA content by kinetin and BH respectively.	PHs (Cytokinin/ Auxin) play a stimulatory role for algal growth.	An increase in biosynthesis of saturated fatty acids and decrease in PUFA was observed.	Parsaeimehr et al. (2017)
Monoethanolamine (MEA)	*Chlorella fusca* LEB 111 (BG-11 growth media)	Increase in Biomass productivity.	Enhanced accumulation in protein and lipid content.	It enhances CO_2 biofixation.	Chemical absorption of CO_2 with MEA solutions is a promising method.	Rosa et al. (2019)
Phytohormones- IAA, and Diethyl		Increase in biomass productivity by 22%	Increase in lipid productivity by 49%	Phytohormones, under N-limitation,	Amount of saturated fatty acid (SFA) and	Giridhar Babu et al. (2017)

(Continued on following page)

TABLE 2 (*Continued*) Abiotic strategies to enhance algal productivity.

Strategies	Algae and growth conditions	Change in biomass productivity (BP)/Cell growth	Change in biochemical components	Possible reasons behind outcome	Remarks	References
aminoethyl hexonate (DA-6) under Nitrogen limitation	*Chlorella sorokiniana* (BG-11 growth media)	and 43% for IAA and DA-6 respectively as compared to control.	and 84% for IAA and DA-6 respectively as compared to control.	cause concurrent increase in biomass and metabolite productivity. IAA and DA-6	monounsaturated fatty acid (MUFA) increased.	
Two stage cultivation; NaCl based lipid induction	*Scenedesmus obtusus* XJ-15 (BG-11 growth media)	Increase in biomass by 52% as compared to the first stage.	Increase in lipid content by 21.6% as compared to the first stage. Final lipid content- 47.7%.	probably induced the activity of antioxidants enzymes, which protect cells from damages caused by abiotic stresses.	Introduction of NaCl enhanced accumulation of polar and neutral lipid or TAGs to counter salinity stress caused by it.	Xia et al. (2013) At increased polar lipid accumulation, the cell membrane permeability and fluidity decrease. It prohibits an excessive flux of NaCl ions into cells.
NaCl based lipid induction	*Monoraphidium dybowskii* LB50	Biomass decreased slightly.	Total lipid and neutral lipid contents increased to 41.7% and 17.48% respectively.	NaCl promote the conversion of Glycolipid into neutral lipids and phospholipids.	NaCl increase the neutral lipid accumulation in algal cells.	Yang et al. (2014)
NaCl-based lipid induction	*Tetraselmis* sp. KCTC12432BP in Saline seawater	At optimum concentration, BP increases by 89 and 152% in closed and open cultures as compared to regular salinity medium.	369% increase in lipid productivity in case of close culture cultivation setup.	Carbon fixation rate enhanced.	At higher salinity, contaminations from other agents were reported to be significantly reduced.	Park et al. (2018)
Phytohormones under N-limitation; Auxin -IAA, gibberellin–gibberellic acid (GA) and Cytokinin-K	*Chlorella sorokiniana*	An increase of 45.55%, 35.94% and 37.37% in BP on supplementation with IAA, GA, and K respectively.	An increase of 56.02%, 37.45% and 53.50% in LP on supplementation with IAA, GA, and K respectively.	IAA and K caused increased cell division and cell elongation resulting into enhanced growth and biomass productivity. N-stress caused enhanced lipid accumulation.	Upregulation of rbcL and accD gene expression was observed for each IAA, GA, and K.	Guldhe et al. (2019)
Synergistic effect of NaCl and $CaCl_2$ stresses	*Chlamydomonas reinhardtii* (C growth medium)	Algal growth rate decreased.	Lipid content increased upto 73.4% as compared to control.	High salinity causes osmotic stress, ion (salt) stress, and oxidative stress leading to enhanced lipid accumulation. Ca^{2+} seems to positively affect lipid synthetic pathways.	Upregulation of GPDH, LPAAT, and DAGAT genes was observed.	Hang et al. (2020)
Salinity stress	*Dunaliella salina* KSA-HS022	Decrease in BP	Enhancement in lipid accumulation.	Oxidative stress results in growth inhibition. High salinity stress positively affected the lipid biosynthesis pathways.	Fatty acid profile varies with salinity of the medium.	Abomohra et al. (2020)
Nitrogen starvation	*Chlorella zofingiensis* (BG-11: LI- 150 l mol m-2 s-1; T- 25 ± 1°C in an airlift reactor)	Decrease in BP (On 10th day of cultivation, BP for N-Starved 0.7 g/L while for N-replete-3.1 g/L)	Increase in synthesis rate of starch (~4-fold) and lipid (~7-fold).	—	Algal cells tend to lower the degree of unsaturation of fatty acids in response to N-starvation.	Zhu et al. (2014)
N/P ratio		Increase in BP.				Choi and Lee, (2015)

(Continued on following page)

TABLE 2 (*Continued*) Abiotic strategies to enhance algal productivity.

Strategies	Algae and growth conditions	Change in biomass productivity (BP)/Cell growth	Change in biochemical components	Possible reasons behind outcome	Remarks	References
	Chlorella vulgaris (Jaworski's medium; LP-16:8; T: 23 ± 1°C)		Increase in lipid accumulation.	Increasing the N/P ratios up to 10 continuously increases the biomass production.	Biomass production is highly dependent on the N/P ratios	

describes various examples of genetic and metabolic engineering that have been carried out to enhance algal lipid productivity.

Metabolic engineering

Metabolic engineering involves the addition or deletion of genes in order to optimize the genetic and regulatory processes of an organism for altering metabolic properties in a predetermined way such as to increase the production of certain metabolites in an organism (Sun et al., 2019). DGAT enzyme involved in TAGs biosynthesis is one of the most crucial enzymes in the pathway as it catalyzes the last step of the lipid synthesis pathway which is the esterification of diacylglycerol yielding triacylglycerol. Overexpression of DGAT can lead to high lipid productivity in GM microalgal cells. Alternative strategies for enhancing microalgal lipid accumulation focus on blocking metabolic pathways competing with lipid production such as starch synthesis, oxaloacetate, or phospholipid biosynthesis pathways. Till now more than 40 microalgal species have been genetically manipulated expressing different stability and efficiencies (Díaz-Santos, 2019).

Enzymes such as glycerol-3-phosphate acyltransferase (GPAT), lysophosphatidic acid acyltransferase (LPAT), and diacylglycerol acyltransferase (DGAT) of the Kennedy pathway are responsible for catalyzing key steps in the formation of TAGs in algal cells. Overexpression of these key enzymes in strains may increase TAG contents in the cells (Muñoz et al., 2019). Overexpression of malic enzyme (ME) also leads an enhanced lipid production in the microalgal cells as ME catalyzes the irreversible oxidative decarboxylation of malate to yield pyruvate, NADH, and CO_2. NADH is required as reducing power for fatty acid biosynthesis. Morphological changes have also been observed in transgenic algae with shorter and thicker cells containing large oil bodies (Xue et al., 2015).

Genetic engineering

Despite all the ideal properties of microalgae, the use of genetic engineering and synthetic biology for genome modification is still a challenge. Genome manipulation helps in improving microalgal strains followed by enhanced biomass yield, productivity, and efficiency of microalgal-based industries. Recently, Clustered Regularly Interspaced Short Palindromic Repeats (CRISPR/Cas9), an advanced genome manipulation technique is gaining importance in manipulating microalgal cells for improved atmospheric CO_2 fixation which eventually would lead to efficient biofuel production. This approach is highly efficient, economical, and environment friendly too (Godbole et al., 2021). The recent methods of genome editing and advancements in metabolic engineering and synthetic biology enable us to combat issues associated with traditional genetic engineering approaches such as instability of transgenes, ineffective expression, and delivery system for effective delivery of genetic material exogenous in nature and selection and screening of recombinants (Sun et al., 2019).

The current strategies employed to improve lipid biosynthesis or to modify the fatty acid profile of microalgal cells includes: 1) fatty acid beta-oxidation elimination, 2) increment in reducing power supply, 3) use of plant-based thioesterase for optimizing fatty acid chain length and 4) thioesterase overexpression to minimize feedback inhibition due to increased levels of acyl-ACP. Genetic engineering tools such as Zinc finger nucleases, CRISPR/Cas9, and chloroplast transfusion should be preferred for overexpressing and blocking the genes of interest (Shahid et al., 2020).

Genetic engineering so far has been applied to the following aspects to increase lipid content in microalgal cells:

1) Overexpressing enzymes responsible for lipid biosynthesis
2) Blocking or inhibiting competitive pathways such as inhibiting beta-oxidation, inhibiting starch synthesis, suppressing the activity of phosphoenolpyruvate carboxylase, and repression of phospholipid biosynthesis.
3) Constitutive expression of lipid biosynthesis transcription regulators in microalgal cells
4) Metabolic engineering to enhance lipid productivity (Morales et al., 2021).

Algae and cyanobacteria for third-generation biodiesel need transgenic manipulation to deal with "weeds", light

TABLE 3 Genetic engineering strategies to enhance algae productivity.

Strategies	Algae	Change in biomass productivity (BP)/Cell growth	Change in biochemical components	Possible reasons behind outcome	Remarks	References
Upregulation in Malic enzyme (ME) gene	*Phaeodactylum tricornutum*	Slight reduction in growth.	Accumulation of neutral lipid increased by 2.5-fold. Total lipid content reached to 57.8% of dry cell weight	Pyruvate metabolism and carbon fixation improved due to overexpression of the targeted gene.	Overexpression of *Phaeodactylum tricornutum* Malic enzyme (PtME) gene along followed by N-stress further enhanced total lipid content.	Xue et al. (2015)
Overexpression of glycerol-3-phosphate acyltransferase (GPAT), lysophosphatidic acid acyltransferase, (LPAT), and diacylglycerol acyltransferase (DGPAT)	*Neochloris oleoabundans*	Insignificant effect on growth in case of single gene overexpression. Simultaneous expression of all three led to reduction in BP and PS activity.	Enhanced lipid production.	These genes are involved in Kennedy pathways catalyzes key TAG synthesis steps in algal cells. Their overexpression leads to higher accumulation of lipids in cells.	Under N-stress, higher lipid accumulation in transformed cells.	Muñoz et al. (2019)
Targeted knockout of gene Cre01.g000300 gene encoding ELT using CRISPR-Cas9	*Chlamydomonas reinhardtii*	Insignificant changes in cell concentration as compared to the wild strain.	Accumulation of lipid increased.	Suppression of catabolic enzymatic activity enhanced cellular growth and lipid productivity.	'Cre01.g000300' gene encodes for Esterase/lipase/thioesterase (ELT) family.	Nguyen et al. (2020)
Knockdown of a multifunctional lipase/ phospholipase/ acyltransferase gene, 'Thaps3_264,297'	*Thalassiosira pseudo- nana*	BP remains unchanged as compared to wild type.	Upto 4.1 folds higher lipid content as compared to wild type.	Disrupting lipid catabolism could increase lipid accumulation without negatively affecting growth.	Lipid catabo- lism involves the release of free fatty acids by lipases and the subsequent breakdown of these fatty acids through β-oxidation.	Trentacoste et al. (2013)
Overexpression of G3PDH, GPAT, LPAAT, PAP, and/or DGAT genes	*Chlorella minutissima*	—	Upto 2 folds higher lipid content as compared to wild type.	Overexpression of G3PDH, GPAT, LPAAT, PAP, and/or DGAT increased the storage lipid content	Multiple-gene ap- proach can yield maximal enzymatic activity and thus maximal lipid synthesis.	Hsieh et al. (2012)
Overexpression of the enzymes thioredoxin reductase (TRXR), aldehyde dehydrogenase (ALDH), glutathione peroxidase (GPO), and glucose-6-phosphate dehydrogenase (ZWF)	*Schizochytrium* sp.	Upto 18.5% increase in dry cell weight as compared to wild type.	Lipid (80.9%) and DHA (114.5%) accumulation increased.	Increased level of Reactive Oxygen Species (ROS) and Reactive Aldehydes led to reduction of cell growth, and increase in lipid accumulation	Increment in generation of ROS and RA was due to oxidation and peroxidation of intracellular lipids.	Han et al. (2021)
Overexpression of diacylglycerol acyltransferase (DGAT) genes	*Phaeodactylum tricornutum*	Slight effect on algal growth.	More than 2 folds increase in TAG and total lipids.	Chloroplast and endoplasmic reticulum-derived diacylglycerol converted into TAGs due to overexpresion of DGAT genes.	Hyper-accumulation of TAGs without any compromise in algal growth.	Zhang et al. (2021)
Overexpression of Carbonic anhydrase (CA)	*Chlorella sorokiniana* (CS) and *Chlorella vulgaris* (CV)	Biomass productivity increased.	2.2 folds increase in lipid accumulation.	CA facilitated enhanced rate of CO_2 sequestration and their fixation.	Carbon flux was diverted, due to reduction in phosphoenolpyruvate carboxylase, towards lipid synthesis.	Lin et al. (2018)

penetration, photoinhibition, carbon assimilation, etc. In order to scale up microalgal production industrially, less than 6 million hectares of land which is less than 0.4% of arable land is required across the world for fulfilling the current demands of fuel (Popp et al., 2014). Recombinant DNA technology can be used to introduce the gene of interest into the host cells through a transformation in order to manipulate physiological pathways or to produce commercially viable compounds. Currently, genetic manipulation of microalgae depends on random

mutagenesis accompanied by screening and selection (Godbole et al., 2021).

Cyclotella cryptica and *Navicula saprophila*, two diatoms were genetically modified by *E. coli* neomycin phosphotransferase gene IZ (nptll) gene. Expression of nptll gene of bacterial origin in diatoms was done by using promoter and terminator sequences of ACC gene from *Cyclotella cryptica* T13L Reimann, Lewin and Guillard. Microprojectile bombardment was used for the introduction of vectors into *Cyclotella cryptica* and *Navicula saprophila* NAVICI L ange-Bertalot and Bonik. Putative transformants were screened and selected G418, and production of neomycin phosphor- based on their ability to grow in the presence of anti-transferase protein by transformed cells was confirmed by western blotting. It was observed that the foreign DNA got integrated into one or more random sites of the transformed algal cells, often in form of tandem repeats. This study was the first study on the reproducible, stable genetic transformation of a chlorophyll-c harboring alga (Dunahay et al., 1995).

In recent studies, it has been demonstrated that genetically engineered cyanobacteria have enhanced carbon-concentrating mechanisms (CCMs) which enables them to secrete heterologous carbonic anhydrases (CAs) (Dunahay et al., 1995). Genetic manipulations in eukaryotic microalgae are difficult due to the lack of stability in the expression of transgenes, the presence of highly efficient endogenous promotors, and the absence of complete genetic information (Lin et al., 2018). Researchers have demonstrated that CGI-58 homolog knockdown in *Thalassiosira pseudonana* resulted in increased polar lipid concentrations and membrane integrity during silicon starvation. This study elucidated the role of the CGI-58 enzyme in the turnover of the membrane during nutrient starvation-induced lipid accumulation. This enzyme is also beneficial for the conversion processes such as hydrothermal liquefaction. Similarly, CGI-58 homolog knockdown in *Arabidopsis thaliana* resulted in an increased concentration of polar lipids (Muñoz et al., 2019). It has been demonstrated recently that although about 60% of the accumulated TAGs under nutrient-deficient conditions are derived from *de novo* lipid synthesis pathways in the case of *Phaeodactylum tricornatum*, a considerable amount of phospholipids turnover also occurs (Xue et al., 2015). Scientists have also proposed a secondary TAG biosynthesis route involving turnover of intracellular membrane employing the enzyme phospholipid diacylglycerol acyltransferase (Han et al., 2021; Sharma et al., 2021). SYTOX staining results indicate that phospholipids of the plasma membrane may also act as a source of acyl groups required for TAG biosynthesis and lipid remodeling may also occur during lipid accumulation (Trentacoste et al., 2013).

Agrobacterium tumefaciens- mediated transformation has shown stability in the case of *Chlorella sorokiniana* as compared to other transformation methods which demonstrate transient stability (Sharma et al., 2021). Overproduction of docosahexaenoic acid (of oxidative defense pathway) by means of genetic engineering in *Schizochytrium* sp. is known to promote DHA production, lipid yield, and cell robustness. Attempts have been made to enhance the oxidative stress defense system of *Schizochytrium* sp. to reduce or lower lipids and DHA oxidation (Han et al., 2021). There have been several attempts to express sequences encoding GPDH, GPAT, LPAT, PAP, DGAT, and PDAT, which can prove to be helpful in the manipulation of metabolic pathways leading to biodiesel production. These methods have been reported to increase storage lipid content by two-fold in *Chlorella minutissma* UTEX 2219 as compared to wild strains (Hsieh et al., 2012).

Drawbacks of GM microalgae

In recent times, there has been a switch towards genetic engineering approaches to escalate lipid and biomass productivity. The possibilities of non-GM approaches should not be forgotten due to strict regulatory procedures over GMOs, environmental safety concerns, commercial, and ethical constraints associated with GMOs. One of the major challenges associated with the use of GM microalgal strains is containment. GM strains must be prevented from their loss into the environment and to mitigate unknown consequences associated with GM strains such as the risk of transgene flow through horizontal gene transfer (HGT) to other species and loss of GM strains caused due to predation or competition with wild strains while mass culturing (Driver et al., 2014).

Biorefinery approach or zero waste approach

A biorefinery is established to produce biofuels and a variety of chemicals from algal biomass *via* bioprocessing and other cost-effective methodologies. It can utilize low energy and produce zero waste. Algal biomass can not only harness biofuel but also other economically viable products including pigments, polyhydroxybutyrate (PHB), and starch which can be used for different interventions (Chandrasekhar et al., 2022). Additionally, investigators have identified the bio-remedial properties of algae. Their capturing capability of heavy metals and toxic chemicals from wastewater makes them a great fit for bioremediation. Algae-based biorefinery has the potential to incorporate numerous technologies to produce green fuel including biodiesel, bioethanol, gasoline, methane, and other high-value compounds like fats, eicosatetraenoic acid and docosahexaenoic acid, dyes/pigments (β-carotene/lutein/astaxanthin), antioxidants and carbohydrates. Theoretically, biorefinery would cultivate algae on a farm followed by biodiesel, bio-oil, bioethanol, biomethane, and biohydrogen

TABLE 4 Biorefinery based algal products.

Algae sp.	Product	Applications	Synthesis/ any other information	Product features	References
Pseudochoricystis ellipsoidea	Fermentation nutrient source	high efficiency as to lactic acid and ethanol production	Hydrolysis (121°C for 20 min) + calcium carbonate. Hydrolysate: 15,000 rpm; 10 min	Sulphuric Acid is used for hydrolysis.	Gao et al. (2012), Rajeswari et al. (2022)
Nannochloropsis salina	Filler in biocomposite fabrication with PVA.	3D printing.	LEA + PVA (Mix at 400 rpm; 5 min) followed by sonication and in the end Heating:90°C at 350 rpm; 1 h.	enhanced the thermal stability	Tran et al. (2018)
Ettlia sp.	nutrient	Growth medium for microalgae	biomass + methanol (1:3 w/w) heated at 90□C. 1% sulfuric acid (v/v) was added, followed by oven dry (60°).	low-cost nutrient; sugar factory waste water and LEA make powerful growth medium	Moon et al. (2014); Mohammadi et al. (2021)
Acutodesmus dimorphus	Ag NP	Antioxidant Activity	10 ml LEA extract: 90 ml AgNO3; Room Temp; 24 h	2–20 nm/ Spherical	Chokshi et al. (2016)
Saccharina japonica	Ag NP	Antimicrobial Activity towards *E. coli and* *S. typhimurium*	50 ml LEA extract: 50 ml $AgNO_3$ (1 mM); 200 rpm	14.77 nm	Sivagnanam et al. (2017)
Micractinium sp., *Scenedesmus* sp., *Chlorella* sp., pennate diatoms and *Chlamydomonas* sp.	Methane	Bioenergy	Anaerobic digestion	Hydrothermal pre-treatment and co-digestion enhance methane production	Bohutskyi et al. (2019)
Chlorella sp.	Antibiotic	Bioremediation	For Non-living biomass: light and air source is removed	71.19% removal efficiency for Cephalexin	Angulo et al. (2018)
Auxenochlorella protothecoides	Methane and Nutrients	Bioenergy and fertilizer	Semi-continuous Anaerobic digestion	Reduce the fertilizer cost up to 45% and enhances biofuel production	Bohutskyi et al. (2015)
Scenedesmus obliquus	levulinic acid	Chemical used for microalgae feedstocks and thermochemical conversion.	Acid-catalyzed thermochemical conversion	—	Jeong and Kim, (2020)
Dunaliella tertiolecta	Bioethanol	Bioenergy	Chemo-enzymatic saccharification and fermentation	Enzymatic saccharification: AMG 300L	Lee et al. (2013)
Chlorella variabilis and *Lyngbya majuscule*	Fertilizer	Biofertilizer	Ovendried de-oiled biomass in a muffle furnace at 575 ± 25°C	Fertilizer for *Zea mays L.*	Maurya et al. (2016a)
Chlorella vulgaris	Growth media and Lipid production.	Nutrient and Biofuel production	Cell disruption: cellulose Hydrolysis; 55°C for 10 h	Enhances productivity of lipid as well as Chlorella vulgaris	Ma et al. (2014)
Lyngbya majuscula	Growth Media for Chlorella vulgaris	Growth stimulating supplement	Residual biomass: Drying (80°C)	Replaces nutrient media BG-11; Enhances biomass productivity, lipid and pigments	Maurya et al. (2016b)
Monoraphidium sp. KMC4	Growth promoter and feedstock for bioenergy production	Bioremediation and Biorefinery	—	High-value bioenergy feedstocks	Mishra and Mohanty, (2019)
Botryococcus braunii	Gaseous product (CO + CO2 + CH4)	Renewable source of syngas or hydrogen.	Catalytic gasification	higher contents of CO and H2; Maximum hydrogen yield of 74.7 mmol g-biomass1	Watanabe et al. (2015)
Chlorella vulgaris, *Nannochloropsis* sp. and *Nanofrustulum* sp. *Phaeodactylum tricornutum*	Methane	Bioenergy	—	—	Zhao et al. (2014)
Chlorella sp.	Lipid and Nutrient Production	Biodiesel Feedstock and Growth media.	—	Mixture of Lipid-extracted microalgal and molasses	Zheng et al. (2015)

(Continued on following page)

TABLE 4 (*Continued*) Biorefinery based algal products.

Algae sp.	Product	Applications	Synthesis/ any other information	Product features	References
				enhances Lipid (335 mg/L/day) and Chlorella sp. (5.58 g/L) production	
Chlorella vulgaris	Lipid and Nutrient Production	Biodiesel Feedstock and Growth media	enzymatic hydrolysates and 5% CO2	Biomass: 3.83 g/L and Lipid: 157 mg/L/d	Zheng et al. (2012)
Chlorella vulgaris	Microbial fuel cell	Power generation	Dual chamber MFC reactors: Graphite felt (Anode and Cathode)	(LEA) used as an anodic substrate; Power density of 2.7 W m -3 (260% Increase as compared to MFC)	Khandelwal et al. (2018)
Thraustochytrid sp.	Lipid and algal Biomass	Nutrient recycling strategy	—	Enhances thraustochytrid biomass and Lipid production	Lowrey et al. (2016)

extraction from the harvested biomass. While, the leftover biomass can be processed to harness other value-added products including livestock feed, organic fertilizer due to the presence of high N:P ratio, food additives, bio-adsorbents, growth regulators, and bioactive compounds for pharmaceutical industries (Chugh et al., 2022; Wang et al., 2008; Karpanai Selvan et al., 2022). Some of the biorefinery-based products are discussed in Table 4 below.

Lipid extracted algal biomass-based fertilizers, nanomaterials, biochar and other products for various agricultural, biomedical, and environmental applications

LEA based fertilizers and bio-stimulants

Modern agriculture is totally dependent on the use of fertilizers for the desired growth. Therefore, extensive research is going on in this field to develop sustainable fertilizers that are non-toxic to the environment. According to some recent investigations, a variety of algae species act as bio-stimulants and enhance crop yield (Win et al., 2018; Abusweireh et al., 2022). Blue-green algae (cyanobacteria) are the most promising source due to their nitrogen metabolizing capability. Additionally, they solubilize phosphates and fix nitrogen anaerobically (Chittora et al., 2020). The nitrogen fixation mechanism is switched on during the deprived conditions that are below 40 ppm. Besides, reduced fertility along with rice-mustard-mung crop rotation was preferable for cyanobacteria-based nitrogen fixation in comparison to rice-wheat-maize rotation (Jha et al., 2001). Recently, *Chlorella variabilis* and *Lyngbya majuscula* were investigated as potential biofertilizers for *Zea mays L*. The pot experiments were successful in reproducing recommended rate for fertilizer by algae-based biofertilizer which was nearly 65.16 g per plant.

LEA based nanomaterials

Nano-based products have dimensions in the range of 1–100 nm and are classified as natural, incidental, or engineered. Due to the presence of hydrophilic surface groups, such as sulfate, carboxyl, and hydroxyl nano-based materials are successful in the fabrication of products possessing antioxidant, antimicrobial, antibacterial, cell imaging, and dye degradation properties. Parameters include pH, temperature, incubation time, intensity of light, and precursor effects the synthesis rate (Rahman et al., 2020; Kumar et al., 2022b). For instance, *Acutodesmus dimorphus* synthesized silver nanoparticles depict 79% ROS scavenging at 25 µg/ml concentration making it antioxidant (Chokshi et al., 2016). Similarly, *Gracilaria corticata* based ZnSe nanoparticles showed 77.9% oxidant activity. Additionally, ZnSe NPs possess an anticancer effect on the lung as well as breast cell lines (Mirzaei et al., 2021). *Trichodesmium erythraeum* was also studied to depict 77.1% of antioxidant activity. Most of these algae-derived NPs are successful against bacteria. Such as, ZnSe NPs elucidated antibacterial effect on *S. aureus* (gram-positive) and *K. pneumoniae* (gram-negative) bacteria. Similarly, *Botryococcus braunii* extract was also effective against *S. aureus* and *K. pneumonia.* While *Chlorella sp.*-based nanoparticles have been inhibiting *E. coli, Klebsiella pneumonia, B. sphaericus,* and *P. mirabilis* respectively (Mirzaei et al., 202; Borah et al., 2020; Kashyap et al., 2019; Sathishkumar et al., 2019). Moreover, AgNPs can do dye degradation and doped NPs can be of use in imaging root and guard cells (Zhang et al., 2017; Borah et al., 2020). Therefore, nanotechnology has the ability to not only revolutionize human health but also offer detection and disease prevention products. Some of the

TABLE 5 Green synthesis of Nanomaterials from Algae and lipid extracted algal (LEA) biomass.

Nanomaterials	Algae sp.	Morphological Features Size/shape	Synthesis conditions	Applications	References
Ag NP	*Acutodesmus dimorphus*	2–20 nm/	10 ml LEA extract:	Antioxidant Activity:	Chokshi et al. (2016)
			0 ml $AgNO_3$;		
	(LEA)	Spherical	Room Temp; 24 h	79% ROS scavenging at 25 μg/ml conc.	
Ag NP	*Saccharina japonica*	14.77 nm	50 ml LEA extract	Antimicrobial Activity:	Sivagnanam et al. (2017)
				MIC value:	
				(5 μg/ml AgNP)	
				E. coli- 6 ± 1.5 μL/ml	
			: 50 ml $AgNO_3$ (1 mM);	*S. typhimurium*:	
	(LEA)		200 rpm	14 ± 4.2 μL/ml	
Ag NP	*Chlorella ellipsoidea*	17.7 nm/ Quasispherical	1 g extract powder:	Dye Degradation:	Borah et al. (2020)
				MB: blue to colorless in 30 min s	
				MO: orange to pale yellow in 30 min s	
				Antimicrobial	
				Activity:	
				ZoI:	
			100 ml $AgNO_3$ (0.001 M);	*E. coli*: 9 mm at 5 μg ml^{-1} conc. Of AgNP	
			Room Temp; 12 h	*Klebsiella pneumonia*: 10 mm at 20 μg ml^{-1} conc. Of AgNP	
ZnSe NP	*Gracilaria corticata*	50–250 nm/	30 ml algae extract:	Antioxidant activity:	Mirzaei et al. (2021)
				DPPH Assay: 30 μg/ml of ZnSe NP showed 77.97%	
				Antibacterial activity:	
				MIC: *K. pneumoniae*—150 μg/ml	
		spherical	10 ml sodium selenite, 10 ml zinc nitrate;	and *S. aureus* 125 μg/ml	
			Constant stirring;	Antitumor activity:	
			Room temp;	MTT assay: ZnSe NP	
			48 h	28.42 mg/ml IC50 epithelial kB cell line.	
Ag/AgCl Hybrid NP	*Chlorella sp.*	10–20 nm	10 ml extract:	Antimicrobial Activity:	Kashyap et al. (2019)
				ZoI:	
				B. sphaericus -4.9 mm	
			90 ml $AgNO_3$ (0.5 mM);	*B. subtilis*-8.6 mm	
			5 h	*B. pasteurii*-11.25 mm	
Ag NP	*Trichodesmium erythraeum*	26.5 nm	:100 ml $AgNO_3$	Antioxidant Activity:	Sathishkumar et al. (2019)
			pH-7;	DPPH assay: 77.01% at 500 μg AgNP	
			Sunlight irradiation;	Antibacterial Activity:	
			Constant stirring	100 μg/ml AgNP –	
				S. aureus-11 mm ZoI	
				P. mirabilis- 10 mm ZoI	
N-S doped Carbon dot	*Nannochloropsis*	2.5–6 nm/spherical	80°C; pH 7;	Root and guard cell imaging:	Zhang et al. (2017)
			30 min	Blue light emitted at 450 nm.	
Cu NP	*Botryococcus braunii*	10–70 nm	5 ml extract: 50 ml	Antimicrobial Activity:	Arya et al. (2018)
			Cu $(CH_3COO)_2$:	*Staphylococcus aureus*	
			Constant stirring;	ZoI-22 mm	
			1 day incubation;	*Klebsiella pneumoniae*	

(Continued on following page)

TABLE 5 (*Continued*) Green synthesis of Nanomaterials from Algae and lipid extracted algal (LEA) biomass.

Nanomaterials	Algae sp.	Morphological Features Size/shape	Synthesis conditions	Applications	References
Ag NP		40–100 nm	100°C 5 ml extract: 45 ml $AgNO_3$; Constant stirring; 25°C; 3 h	ZoI-19 mm *Staphylococcus aureus* ZoI-22 mm *Klebsiella pneumoniae* ZoI-21 mm	

applications of nanoparticles have been discussed in Table 5 below.

LEA based biochar

Biochar is defined as a carbon enriched material usually produced *via* thermochemical decomposition of biomass at extremely high temperatures (500–1,000°C) in an O_2 deficient environment. It is prominently produced from the leftover biomass after bio-oil extraction. Recently, different strategies are developed to produce biochar including conventional techniques like slow and microwave-assisted pyrolysis as well as some newly developed methodologies like hydrothermal carbonization and torrefaction (Yu et al., 2017). It is charcoal that can adsorb heavy metal impurities from wastewater, pharmaceutical metabolites, phenols, and chemical intermediates, perform dye degradation, reduce soil erosion as well as improve crop yield. Due to high nutrition content and ion-exchange capacity, they are successful in replenishing soil (Karthik et al., 2021). Moreover, recent investigations reveal that biochar can enhance soil productivity, prevent greenhouse gas emissions and enhance the degradation speed of organic matter in the soil making it an ideal solution for composting (Wu et al., 2019). More recently, N-doped biochar has been utilized as an energy absorbent and promotes energy conservation. Super capacitors, batteries, fuel cells, and biochar-based composites are a successful result of this N-type doping (Xia et al., 2020). Therefore, for over a decade the algae-derived biochar can be of great importance in energy storage as well as carbon sequestration.

LEA based biomedical applications

Carotenoids are the bioactive compounds extracted from algal biomass and are of great importance for drug preparation. According to the investigators, pigments including β-carotene, lutein, fucoxanthin, violaxanthin, astaxanthin, and phycobiliproteins possess antitumor potential. Besides, they are also a promising source of antioxidants. For instance, *Haematococcus pluvialis* extracted astaxanthin provides UV protection, improves immune response, and reduces tumor formation as well as inflammation (Mota et al., 2022). Phycocyanin obtained from *Spirulina* possesses fluorescence and is utilized for labeling antibodies, receptors, and other biological molecules for diagnostics. Numerous brown algae including Wakame, Kombu, Mozuki are a rich source of fucoxanthin which has anti-cancer as well as anti-obesity effects. It also improves lipid metabolism (Das, 2016). Additionally, algae machinery can be used for recombinant protein production due to the easy transformation of both plastids as well as nuclear genomes and offers advantages such as cheap production, easy scale-up, lack of pathogens, and easy assembling of complex proteins (Rosales-Mendoza et al., 2012). Hence, chloroplast can be a site for antibiotics fabrication (Purton et al., 2013). The pure algal extract also possesses some antimicrobial effects on gram-positive and gram-negative species such as *Staphylococcus aureus, Bacillus subtilis, Pseudomonas aeruginosa, Salmonella typhimurium,* and *Proteus mirabilis* (Soltani et al., 2011).

LEA based other products

Apart from biodiesel, bioethanol, biohydrogen, biomethane, and bio-oil synthesis leftover biomass can be used to reproduce products including food, feed, natural colors, and polymers. Microalgae such as *Spirulina, Chlorella, Scenedesmus, Dunaliella salina*, and *Aphanizomenon flos-aquae* have promising nutrients for not only humans but also animals. For instance, *Chlorella pyrenoidosa* comprise of 65% protein, 5–10% lipid, 10–20% hydrocarbons, 200–500 mg kg/L vitamin C, 120–300 mg kg/L of vitamin A and antioxidants (Shen et al., 2008). *Dunaliella*-based proteins are used in the baking industry while its biomass is utilized for fish and animal feed (Das, 2016). Several vitamins (vitamins A, B1, B2, B6, B12, C, E, nioctinate, folic acid, and pantothenic acid) and minerals are also enriched in species (Koyande et al., 2019). Some freshwater species have a higher prebiotic index and modulate intestinal microbiota by increasing *Lactobacillus–Enterococcus* and *Bifidobacterium*

(desired bacteria) while inhibiting *Prevotellaceae-Bacteroidaceae, Clostridium histolyticum,* and *Eubacterium rectale Clostridium coccoides* (undesired bacteria) (de Medeiros et al., 2021). Algae-derived protein not only has essential amino acids (isoleucine, valine, lysine, tryptophan, methionine, threonine, and histidine) but is higher than conventional sources such as meat, fish, and dairy products. For instance, 7 g dried biomass of *Spirulina maxima* contains 4 g of protein, 1 g of fat (omega-3 and omega-6 fatty acids) 11% Vitamin B1, 15% vitamin B2 and 4% vitamin B3, 21% copper, and 11% iron of required daily allowance (RDA) (Milledge, 2011). While, magnesium, manganese and potassium are reported in trace amounts (Christaki et al., 2011). The inclusion of microalgae biomass in the animal feedstock can improve meat quality in ruminants, pigs, poultry, and rabbits (Madeira et al., 2017). For example, the addition of *Arthrospira platensis* in poultry diets increases average daily gain but negatively affects the feed conversion ratio. Similarly, *Schizochytrium sp*., improve fatty acid composition in poultry animals, due to the presence of a high amount of DHA. Therefore, adding algae biomass into the feed can be a cost-effective measure of fuel production. Due to the presence of chlorophylls, carotenoids, xanthophylls, and phycobiliproteins in several algal species natural colors can be harnessed as additives in ice-creams, candies, non-alcoholic beverages, and dietary foods as well as clothes (Azeem et al., 2019) (Das, 2016). According to some recent studies, species of algae are also capable of producing bioplastic which can be harnessed to produce numerous products including biodegradable plastic bags, slippers, buckets, etc. Additionally, red algae can produce some gelling polysaccharides like agar, agarose, and carrageenan possessing sulphated galactans. For instance, *Hydropuntia cornea*-produced agar can be blended at different concentrations with polyvinyl alcohol to produce biodegradable films for the packaging industry (Das, 2016). Therefore, numerous applications of algal species are possible by implementing a biorefinery.

Conclusion

Over the decade, genetic and metabolomic engineering coupled with omics has played a prominent role in improving lipid yield. While, more recently integrating biomass-based biorefinery with a waste-water treatment setup has proved to reduce the production cost of algae-based fuel. However, more innovation is required to overcome the issues of strain selection, cultivation, harvesting, drying and fuel conversion methodologies. Additionally, environmental risk assessment, resource organization, and life cycle assessment (LCA) of algal strain to biofuels is required. More recently biorefineries have been established that not only helps to produce biofuel but also several high-value-low-yield biomolecules for pharmaceutical and nutraceutical interventions. Additionally, several environmentally important products such as biofertilizers, biochar, bio-stimulants, nanomaterials, etc., are also generated. However, research on various aspects of algal-based bioactive compound extraction is in nascent phase and requires bioprospecting of high yielding native algal species, development and deployment of mass cultivation strategies, process optimization for harvest and cell disruption techniques followed by efficient biomolecule extraction procedures to make algal biorefinery sustainable and commercially viable in nature.

Author contributions

LK, LM, and RA- wrote the original draft, Concept. VJ and MC- Review and edited the manuscript. NB- Concept, and Supervise.

Conflict of interest

The authors declare that the research was conducted in the absence of any commercial or financial relationships that could be construed as a potential conflict of interest.

Publisher's note

All claims expressed in this article are solely those of the authors and do not necessarily represent those of their affiliated organizations, or those of the publisher, the editors and the reviewers. Any product that may be evaluated in this article, or claim that may be made by its manufacturer, is not guaranteed or endorsed by the publisher.

References

Abomohra, A. E.-F., El-Naggar, A. H., Alaswad, S. O., Elsayed, M., Li, M., and Li, W. (2020). Enhancement of biodiesel yield from a halophilic green microalga isolated under extreme hypersaline conditions through stepwise salinity adaptation strategy. *Bioresour. Technol.* 310, 123462. doi:10.1016/j.biortech.2020.123462

Abusweireh, R. S., Rajamohan, N., and Vasseghian, Y. (2022). Enhanced production of biodiesel using nanomaterials: A detailed review on the mechanism and influencing factors. *Fuel* 319, 123862. doi:10.1016/J.FUEL.2022.123862

Alhattab, M., Kermanshahi-Pour, A., and Brooks, M. S. L. (2019). Microalgae disruption techniques for product recovery: Influence of cell wall composition. *J. Appl. Phycol.* 31, 61–88. doi:10.1007/s10811-018-1560-9

Alishah Aratboni, H., Rafiei, N., Garcia-Granados, R., Alemzadeh, A., and Morones-Ramírez, J. R. (2019). Biomass and lipid induction strategies in microalgae for biofuel production and other applications. *Microb. Cell Fact.* 18, 178–195. doi:10.1186/s12934-019-1228-4

Amaro, H. M., Guedes, A. C., and Malcata, F. X. (2011). Advances and perspectives in using microalgae to produce biodiesel. *Appl. Energy* 88, 3402–3410. doi:10.1016/J.APENERGY.2010.12.014

Angulo, E., Bula, L., Mercado, I., Montaño, A., and Cubillán, N. (2018). Bioremediation of Cephalexin with non-living Chlorella sp., biomass after lipid extraction. *Bioresour. Technol.* 257, 17–22. doi:10.1016/J.BIORTECH.2018.02.079

Anjos, M., Fernandes, B. D., Vicente, A. A., Teixeira, J. A., and Dragone, G. (2013). Optimization of CO2 bio-mitigation by Chlorella vulgaris. *Bioresour. Technol.* 139, 149–154. doi:10.1016/j.biortech.2013.04.032

Anto, S., Mukherjee, S. S., Muthappa, R., Mathimani, T., Deviram, G., Kumar, S. S., et al. (2020). Algae as green energy reserve: Technological outlook on biofuel production. *Chemosphere* 242, 125079. doi:10.1016/j.chemosphere.2019.125079

Arya, A., Gupta, K., Chundawat, T. S., and Vaya, D. (2018). Biogenic synthesis of copper and silver nanoparticles using green alga Botryococcus braunii and its antimicrobial activity. *Bioinorganic Chem. Appl.*, 1–9. doi:10.1155/2018/7879403

Azeem, M., Iqbal, N., Mir, R. A., Adeel, S., Batool, F., Khan, A. A., et al. (2019). Harnessing natural colorants from algal species for fabric dyeing: A sustainable eco-friendly approach for textile processing. *J. Appl. Phycol.* 31. doi:10.1007/s10811-019-01848-z

Bajguz, A., and Piotrowska-Niczyporuk, A. (2013). Synergistic effect of auxins and brassinosteroids on the growth and regulation of metabolite content in the green alga Chlorella vulgaris (Trebouxiophyceae). *Plant Physiol. biochem.* 71, 290–297. doi:10.1016/J.PLAPHY.2013.08.003

Bitog, J. P., Lee, I. B., Lee, C. G., Kim, K. S., Hwang, H. S., Hong, S. W., et al. (2011). Application of computational fluid dynamics for modeling and designing photobioreactors for microalgae production: A review. *Comput. Electron. Agric.* 76, 131–147. doi:10.1016/J.COMPAG.2011.01.015

Bohutskyi, P., Ketter, B., Chow, S., Adams, K. J., Betenbaugh, M. J., Allnutt, F. C. T., et al. (2015). Anaerobic digestion of lipid-extracted Auxenochlorella protothecoides biomass for methane generation and nutrient recovery. *Bioresour. Technol.* 183, 229–239. doi:10.1016/J.BIORTECH.2015.02.012

Bohutskyi, P., Phan, D., Spierling, R. E., Kopachevsky, A. M., Bouwer, E. J., Lundquist, T. J., et al. (2019). Production of lipid-containing algal-bacterial polyculture in wastewater and biomethanation of lipid extracted residues: Enhancing methane yield through hydrothermal pretreatment and relieving solvent toxicity through co-digestion. *Sci. Total Environ.* 653, 1377–1394. doi:10.1016/J.SCITOTENV.2018.11.026

Borah, D., Das, N., Das, N., Bhattacharjee, A., Sarmah, P., Ghosh, K., et al. (2020). Alga-mediated facile green synthesis of silver nanoparticles: Photophysical, catalytic and antibacterial activity. *Appl. Organomet. Chem.* 34, e5597. doi:10.1002/AOC.5597

Carvalho, A. P., Meireles, L. A., and Malcata, F. X. (2006). Microalgal reactors: A review of enclosed system designs and performances. *Biotechnol. Prog.* 22, 1490–1506. doi:10.1002/bp060065r

Challagulla, V., Nayar, S., Walsh, K., and Fabbro, L. (2016). Advances in techniques for assessment of microalgal lipids. *Crit. Rev. Biotechnol.* 37, 566–578. doi:10.1080/07388551.2016.1206058

Chandra, R., Vishal, G., Sánchez, C. E. G., and Uribe, J. A. G. (2020). Bioreactor for algae cultivation and biodiesel production. *Bioreact. Sustain. Des. Industrial Appl. Mitig. GHG Emiss.*, 289–307. doi:10.1016/B978-0-12-821264-6.00015-2

Chandrasekhar, K., Raj, T., Ramanaiah, S. V., Kumar, G., Banu, J. R., Varjani, S., et al. (2022). Algae biorefinery: A promising approach to promote microalgae industry and waste utilization. *J. Biotechnol.* 345, 1–16. doi:10.1016/j.jbiotec.2021.12.008

Chen, W., Zhang, C., Song, L., Sommerfeld, M., and Hu, Q. (2009). A high throughput Nile red method for quantitative measurement of neutral lipids in microalgae. *J. Microbiol. Methods* 77, 41–47. doi:10.1016/J.MIMET.2009.01.001

Chisti, Y. (2008). Biodiesel from microalgae beats bioethanol. *Trends Biotechnol.* 26, 126–131. doi:10.1016/j.tibtech.2007.12.002

Chittora, D., Meena, M., Barupal, T., Swapnil, P., and Sharma, K. (2020). Cyanobacteria as a source of biofertilizers for sustainable agriculture. *Biochem. Biophysics Rep.* 22, 100737. doi:10.1016/j.bbrep.2020.100737

Choi, H. J., and Lee, S. M. (2015). Effect of the N/P ratio on biomass productivity and nutrient removal from municipal wastewater. *Bioprocess Biosyst. Eng.* 38, 761–766. doi:10.1007/s00449-014-1317-z

Chokshi, K., Pancha, I., Ghosh, T., Paliwal, C., Maurya, R., Ghosh, A., et al. (2016). Green synthesis, characterization and antioxidant potential of silver nanoparticles biosynthesized from de-oiled biomass of thermotolerant oleaginous microalgae: Acutodesmus dimorphus. *RSC Adv.* 6, 72269–72274. doi:10.1039/C6RA15322D

Chozhavendhan, S., Vijay Pradhap Singh, M., Fransila, B., Praveen Kumar, R., and Karthiga Devi, G. (2020). A review on influencing parameters of biodiesel production and purification processes. *Curr. Res. Green Sustain. Chem.* 1 (2), 1–6. doi:10.1016/J.CRGSC.2020.04.002

Christaki, E., Florou-Paneri, P., and Bonos, E. (2011). Microalgae: A novel ingredient in nutrition. *Int. J. Food Sci. Nutr.* 62, 794–799. doi:10.3109/09637486.2011.582460

Chu, W. L. (2017). Strategies to enhance production of microalgal biomass and lipids for biofuel feedstock. *Eur. J. Phycol.* 52, 419–437. doi:10.1080/09670262.2017.1379100

Chugh, M., Kumar, L., Shah, D. M. P., and Bharadvaja, D. N. (2022). Algal bioremediation of heavy metals: An insight into removal mechanisms, recovery of by-products, challenges, and future opportunities. *Energy Nexus* 7, 10012. doi:10.1016/J.NEXUS.2022.100129

Cravotto, G., Boffa, L., Mantegna, S., Perego, P., Avogadro, M., and Cintas, P. (2008). Improved extraction of vegetable oils under high-intensity ultrasound and/or microwaves. *Ultrason. Sonochemistry* 15, 898–902. doi:10.1016/J.ULTSONCH.2007.10.009

Cronan, J. E., and Waldrop, G. L. (2002). Multi-subunit acetyl-CoA carboxylases. *Prog. Lipid Res.* 41, 407–435. doi:10.1016/S0163-7827(02)00007-3

Das, D., Mazumdar, P., Maity, A., Tripathy, S., Roy, S., Chattopadhyay, D., et al. (2016). Algal biorefinery: An integrated approach. *J. Photochem. Photobiol. B* 156, 1–10. doi:10.1016/j.jphotobiol.2016.01.003

de Medeiros, V. P. B., de Souza, E. L., de Albuquerque, T. M. R., da Costa Sassi, C. F., dos Santos Lima, M., Sivieri, K., et al. (2021). Freshwater microalgae biomasses exert a prebiotic effect on human colonic microbiota. *Algal Res.* 60, 102547. doi:10.1016/J.ALGAL.2021.102547

Díaz-Santos, E. (2019). Towards the genetic manipulation of microalgae to improve the carbon dioxide fixation and the production of biofuels: Present status and future prospect. *Microalgae Biotechnol. Dev. Biofuel Wastewater Treat.*, 135–146. doi:10.1007/978-981-13-2264-8_7

Dołowy, M., and Pyka, A. (2015). Chromatographic methods in the separation of long-chain mono- and polyunsaturated fatty acids. *J. Chem.*, 1–20. doi:10.1155/2015/120830

Doucha, J., and Lívanský, K. (2006). Productivity, CO2/O2 exchange and hydraulics in outdoor open high density microalgal (Chlorella sp.) photobioreactors operated in a Middle and Southern European climate. *J. Appl. Phycol.* 18 (18), 811–826. doi:10.1007/S10811-006-9100-4

Driver, T., Bajhaiya, A., and Pittman, J. K. (2014). Potential of bioenergy production from microalgae. *Curr. Sustain. Renew. Energy Rep.* 1, 94–103. doi:10.1007/s40518-014-0011-8

Ducat, D. C., Way, J. C., and Silver, P. A. (2011). Engineering cyanobacteria to generate high-value products. *Trends Biotechnol.* 29, 95–103. doi:10.1016/J.TIBTECH.2010.12.003

Dunahay, T. G., Jarvis, E. E., and Roessler, P. G. (1995). Genetic transformation of the diatoms cyclotella cryptica and navicula saprophila. *J. Phycol.* 31, 1004–1012. doi:10.1111/J.0022-3646.1995.01004.X

Fan, J., Cui, Y., Wan, M., Wang, W., and Li, Y. (2014). Lipid accumulation and biosynthesis genes response of the oleaginous Chlorella pyrenoidosa under three nutrition stressors. *Biotechnol. Biofuels* 7, 17–14. doi:10.1186/1754-6834-7-17

Gao, M. T., Shimamura, T., Ishida, N., and Takahashi, H. (2012). Investigation of utilization of the algal biomass residue after oil extraction to lower the total production cost of biodiesel. *J. Biosci. Bioeng.* 3, 330–333. doi:10.1016/J.JBIOSC.2012.04.002

Gholami, A., Pourfayaz, F., and Maleki, A. (2020). Recent advances of biodiesel production using ionic liquids supported on nanoporous materials as catalysts: A review. *Fron. Energy Res.* 8, 144. doi:10.3389/FENRG.2020.00144/BIBTEX

Gifuni, I., Pollio, A., Safi, C., Marzoc++ chella, A., and Olivieri, G. (2019). Current bottlenecks and challenges of the microalgal biorefinery. *Trends Biotechnol.* 37, 242–252. doi:10.1016/J.TIBTECH.2018.09.006

Giridhar Babu, A., Wu, X., Kabra, A. N., and Kim, D.-P. (2017). Cultivation of an indigenous Chlorella sorokiniana with phytohormones for biomass and lipid production under N-limitation. *Algal Res.* 23, 178–185. doi:10.1016/j.algal.2017.02.004

Godbole, V., Pal, M. K., and Gautam, P. (2021). A critical perspective on the scope of interdisciplinary approaches used in fourth-generation biofuel production. *Algal Res.* 58, 102436. doi:10.1016/J.ALGAL.2021.102436

Gonçalves, A. L., Pires, J. C. M., and Simões, M. (2013). Green fuel production: Processes applied to microalgae. *Environ. Chem. Lett.* 11, 315–324. doi:10.1007/S10311-013-0425-3

Gondi, R., Kavitha, S., Yukesh Kannah, R., Kumar, G., and Rajesh Banu, J. (2022). Wastewater based microalgae valorization for biofuel and value-added products recovery. *Sustain. Energy Technol. Assess.* 53, 102443. doi:10.1016/J.SETA.2022.102443

Gong, Y., and Jiang, M. (2011). Biodiesel production with microalgae as feedstock: From strains to biodiesel. *Biotechnol. Lett.* 33, 1269–1284. doi:10.1007/s10529-011-0574-z

Gressel, J. (2007). Transgenics are imperative for biofuel crops. *Plant Sci.* 174. doi:10.1016/j.plantsci.2007.11.009

Guldhe, A., Renuka, N., Singh, P., and Bux, F. (2019). Effect of phytohormones from different classes on gene expression of Chlorella sorokiniana under nitrogen limitation for enhanced biomass and lipid production. *Algal Res.* 40, 101518. doi:10.1016/j.algal.2019.101518

Hallmann, A. (2007). Algal transgenics and biotechnology. *Transgenic Plant J.* 1, 82–96.

Han, X., Li, Z., Wen, Y., and Chen, Z. (2021). Overproduction of docosahexaenoic acid in Schizochytrium sp. through genetic engineering of oxidative stress defense pathways. *Biotechnol. Biofuels* 14, 70–10. doi:10.1186/s13068-021-01918-w

Hang, L. T., Mori, K., Tanaka, Y., Morikawa, M., and Toyama, T. (2020). Enhanced lipid productivity of Chlamydomonas reinhardtii with combination of NaCl and CaCl2 stresses. *Bioprocess Biosyst. Eng.* 43, 971–980. doi:10.1007/S00449-020-02293-W

Hathwaik, L. T., and Cushman, J. C. (2017). Strain selection strategies for improvement of algal biofuel feedstocks. *Biofuels Bioenergy* 1, 173–189. doi:10.1002/9781118350553.ch11

Hsieh, H. J., Su, C. H., and Chien, L. J. (2012). Accumulation of lipid production in Chlorella minutissima by triacylglycerol biosynthesis-related genes cloned from *Saccharomyces cerevisiae* and Yarrowia lipolytica. *J. Microbiol.* 50, 526–534. doi:10.1007/S12275-012-2041-5

Huang, Q., Jiang, F., Wang, L., and Yang, C. (2017). Design of photobioreactors for mass cultivation of photosynthetic organisms. *Engineering* 3, 318–329. doi:10.1016/J.ENG.2017.03.020

IEA (2021a). *Renewables 2021*. Paris, France: International Energy Agency (IEA) Publications International, 167.

Islam, M. S., Aryasomayajula, A., and Selvaganapathy, P. R. (2017). A review on macroscale and microscale cell lysis methods. *Micromachines* 8 (3). doi:10.3390/mi8030083

Jeevanandam, J., and Danquah, M. K. (2020). "Dewatering and drying of algal cultures," in *Handbook of microalgae-based processes and products: Fundamentals and advances in energy, food, feed, fertilizer, and bioactive compounds*, 207–224. doi:10.1016/B978-0-12-818536-0.00009-9

Jeong, G. T., and Kim, S. K. (2020). Valorization of thermochemical conversion of lipid-extracted microalgae to levulinic acid. *Bioresour. Technol.* 313, 123684. doi:10.1016/J.BIORTECH.2020.123684

Jha, M. N., Prasad, A. N., Sharma, S. G., and Bharati, R. C. (2001). Effects of fertilization rate and crop rotation on diazotrophic cyanobacteria in paddy field. *World J. Microbiol. Biotechnol.* 17, 463–468. doi:10.1023/A:1011913316988

Jusoh, M., Loh, S. H., Chuah, T. S., Aziz, A., and Cha, T. S. (2015). Elucidating the role of jasmonic acid in oil accumulation, fatty acid composition and gene expression in Chlorella vulgaris (Trebouxiophyceae) during early stationary growth phase. *Algal Res.* 9, 14–20. doi:10.1016/J.ALGAL.2015.02.020

Karim, A., Amirul Islam, M., Khalid, Z. B., Faizal, C. K. M., Khan, M. M. R., and Yousuf, A. (2019). Microalgal cell disruption and lipid extraction techniques for potential biofuel production. *Microalgae Cultiv. Biofuels Prod.* 2020. doi:10.1016/B978-0-12-817536-1.00009-6

Karpanai Selvan, B., Das, S., Chandrasekar, M., Girija, R., John Vennison, S., Jaya, N., et al. (2022). Utilization of biodiesel blended fuel in a diesel engine–Combustion engine performance and emission characteristics study. *Fuel* 311, 122621. doi:10.1016/J.FUEL.2021.122621

Karthik, V., Senthil Kumar, P., Dai, V., Vo, N., Sindhu, J., Sneka, D., et al. (2021). Hydrothermal production of algal biochar for environmental and fertilizer applications: A review. *Environ. Chem. Lett.* 19, 1025–1042. doi:10.1007/s10311-020-01139-x

Kashyap, M., Samadhiya, K., Ghosh, A., Anand, V., Shirage, P. M., and Bala, K. (2019). Screening of microalgae for biosynthesis and optimization of Ag/AgCl nano hybrids having antibacterial effect. *RSC Adv.* 9, 25583–25591. doi:10.1039/C9RA04451E

Khandelwal, A., Vijay, A., Dixit, A., and Chhabra, M. (2018). Microbial fuel cell powered by lipid extracted algae: A promising system for algal lipids and power generation. *Bioresour. Technol.* 247, 520–527. doi:10.1016/J.BIORTECH.2017.09.119

Kim, H. S., Hsu, S. C., Han, S. I., Thapa, H. R., Guzman, A. R., Browne, D. R., et al. (2017). High-throughput droplet microfluidics screening platform for selecting fast-growing and high lipid-producing microalgae from a mutant library. *Plant Direct* 1, e00011. doi:10.1002/PLD3.11

Kim, Y. H., Choi, Y. K., Park, J., Lee, S., Yang, Y. H., Kim, H. J., et al. (2012). Ionic liquid-mediated extraction of lipids from algal biomass. *Bioresour. Technol.* 109, 312–315. doi:10.1016/J.BIORTECH.2011.04.064

Klok, A. J., Lamers, P. P., Martens, D. E., Draaisma, R. B., and Wijffels, R. H. (2014). Edible oils from microalgae: Insights in TAG accumulation. *Trends Biotechnol.* 32, 521–528. doi:10.1016/J.TIBTECH.2014.07.004

Koyande, A. K., Chew, K. W., Rambabu, K., Tao, Y., Chu, D. T., and Show, P. L. (2019). Microalgae: A potential alternative to health supplementation for humans. *Food Sci. Hum. Wellness* 8, 16–24. doi:10.1016/J.FSHW.2019.03.001

Kumar, A., Ergas, S., Yuan, X., Sahu, A., Zhang, Q., Dewulf, J., et al. (2010). Enhanced CO2 fixation and biofuel production via microalgae: Recent developments and future directions. *Trends Biotechnol.* 28, 371–380. doi:10.1016/J.TIBTECH.2010.04.004

Kumar, L., Anand, R., Shah, M. P., and Bharadvaja, N. (2022). Microalgae biodiesel: A sustainable source of energy, unit operations, technological challenges, and solutions. *J. Hazard. Mater. Adv.* 8, a100145. doi:10.1016/J.HAZADV.2022.100145

Kumar, L., Mohan, L., Anand, S., Bhardwaj, D., and Bharadvaja, N. (2022b). Phyconanoremediation: A sustainable approach to deal with environmental pollutants heavy metals and dyes. *Vegetos*. doi:10.1007/s42535-022-00399-y

Kumar, R. R., Rao, P. H., and Arumugam, M. (2015). Lipid extraction methods from microalgae: A comprehensive review. *Front. Energy Res.* 3, 61. doi:10.3389/fenrg.2014.00061

Kwak, H. S., Kim, J. Y. H., Woo, H. M., Jin, E. S., Min, B. K., and Sim, S. J. (2016). Synergistic effect of multiple stress conditions for improving microalgal lipid production. *Algal Res.* 19, 215–224. doi:10.1016/J.ALGAL.2016.09.003

Lackner, K. S. (2003). A guide to CO2 sequestration. *Science* 300, 1677–1678. doi:10.1126/science.1079033

Larkum, A. W. D., Ross, I. L., Kruse, O., and Hankamer, B. (2012). Selection, breeding and engineering of microalgae for bioenergy and biofuel production. *Trends Biotechnol.* 30, 198–205. doi:10.1016/j.tibtech.2011.11.003

Lee, O. K., Kim, A. L., Seong, D. H., Lee, C. G., Jung, Y. T., Lee, J. W., et al. (2013). Chemo-enzymatic saccharification and bioethanol fermentation of lipid-extracted residual biomass of the microalga, Dunaliella tertiolecta. *Bioresour. Technol.* 132, 197–201. doi:10.1016/J.BIORTECH.2013.01.007

Lehr, F., and Posten, C. (2009). Closed photo-bioreactors as tools for biofuel production. *Curr. Opin. Biotechnol.* 20, 280–285. doi:10.1016/J.COPBIO.2009.04.004

Li, Y., Ghasemi Naghdi, F., Garg, S., Adarme-Vega, T. C., Thurecht, K. J., Ghafor, W. A., et al. (2014). A comparative study: The impact of different lipid extraction methods on current microalgal lipid research. *Microb. Cell Fact.* 13, 14–19. doi:10.1186/1475-2859-13-14

Lim, D. K. Y., Schenk, P. M., Lim, D. K. Y., and Schenk, P. M. (2017). Microalgae selection and improvement as oil crops: GM vs non-GM strain engineering. *AIMS Bioeng.* 2017, 151–161. doi:10.3934/BIOENG.2017.1.151

Lin, W. R., Lai, Y. C., Sung, P. K., Tan, S. I., Chang, C. H., Chen, C. Y., et al. (2018). Enhancing carbon capture and lipid accumulation by genetic carbonic anhydrase in microalgae. *J. Taiwan Inst. Chem. Eng.* 93, 131–141. doi:10.1016/J.JTICE.2018.10.010

Lin-Lan, Z., Jing-Han, W., and Hong-Ying, H. (2018). Differences between attached and suspended microalgal cells in ssPBR from the perspective of physiological properties. *J. Photochem. Photobiol. B Biol.* 181, 164–169. doi:10.1016/j.jphotobiol.2018.03.014

Liu, X., Saydah, B., Eranki, P., Colosi, L. M., Greg Mitchell, B., Rhodes, J., et al. (2013). Pilot-scale data provide enhanced estimates of the life cycle energy and emissions profile of algae biofuels produced via hydrothermal liquefaction. *Bioresour. Technol.* 148, 163–171. doi:10.1016/j.biortech.2013.08.112

Lorente, E., Hapońska, M., Clavero, E., Torras, C., and Salvadó, J. (2018). Steam explosion and vibrating membrane filtration to improve the processing cost of microalgae cell disruption and fractionation. *Processes* 6(4). doi:10.3390/pr6040028

Lowrey, J., Brooks, M. S., and Armenta, R. E. (2016). Nutrient recycling of lipid-extracted waste in the production of an oleaginous thraustochytrid. *Appl. Microbiol. Biotechnol.* 100, 4711–4721. doi:10.1007/S00253-016-7463-2

Ma, X., Zheng, H., Huang, H., Liu, Y., and Ruan, R. (2014). Effects of temperature and substrate concentration on lipid production by Chlorella vulgaris from enzymatic hydrolysates of lipid-extracted microalgal biomass residues (LMBRs). *Appl. Biochem. Biotechnol.* 174, 1631–1650. doi:10.1007/S12010-014-1134-5

Madeira, M. S., Cardoso, C., Lopes, P. A., Coelho, D., Afonso, C., Bandarra, N. M., et al. (2017). Microalgae as feed ingredients for livestock production and meat quality: A review. *Livest. Sci.* 205, 111–121. doi:10.1016/J.LIVSCI.2017.09.020

Mata, T. M., Martins, A. A., and Caetane, N. S. (2012). Microalgae processing for biodiesel production. *Adv. Biodiesel Prod. Process. Technol.*, 204–231. doi:10.1016/B978-0-85709-117-8.50009-5

Maurya, R., Chokshi, K., Ghosh, T., Trivedi, K., Pancha, I., Kubavat, D., et al. (2016a). Lipid extracted microalgal biomass residue as a fertilizer substitute for Zea mays L. *Front. Plant Sci.* 6, 1266. doi:10.3389/fpls.2015.01266

Maurya, R., Paliwal, C., Chokshi, K., Pancha, I., Ghosh, T., Satpati, G. G., et al. (2016b). Hydrolysate of lipid extracted microalgal biomass residue: An algal growth promoter and enhancer. *Bioresour. Technol.* 207, 197–204. doi:10.1016/J.BIORTECH.2016.02.018

McMillan, J. R., Watson, I. A., Ali, M., and Jaafar, W. (2013). Evaluation and comparison of algal cell disruption methods: Microwave, waterbath, blender, ultrasonic and laser treatment. *Appl. Energy* 103, 128–134. doi:10.1016/J.APENERGY.2012.09.020

Mercer, P., and Armenta, R. E. (2011). Developments in oil extraction from microalgae. *Eur. J. Lipid Sci. Technol.* 113, 539–547. doi:10.1002/EJLT.201000455

Milledge, J. J. (2011). Commercial application of microalgae other than as biofuels: A brief review. *Rev. Environ. Sci. Biotechnol.* 10, 31–41. doi:10.1007/s11157-010-9214-7

Mirzaei, S. Z., Ahmadi Somaghian, S., Lashgarian, H. E., Karkhane, M., Cheraghipour, K., and Marzban, A. (2021). Phyco-fabrication of bimetallic nanoparticles (zinc–selenium) using aqueous extract of Gracilaria corticata and its biological activity potentials. *Ceram. Int.* 47, 5580–5586. doi:10.1016/J.CERAMINT.2020.10.142

Mishra, S., and Mohanty, K. (2019). Comprehensive characterization of microalgal isolates and lipid-extracted biomass as zero-waste bioenergy feedstock: An integrated bioremediation and biorefinery approach. *Bioresour. Technol.* 273, 177–184. doi:10.1016/J.BIORTECH.2018.11.012

Mohammadi, M., Sedighi, M., Natarajan, R., Hassan, S. H. A., and Ghasemi, M. (2021). Microbial fuel cell for oilfield produced water treatment and reuse: Modelling and process optimization. *Korean J. Chem. Engin.* 38 (1), 72–80. doi:10.1007/S11814-020-0674-3

Molina Grima, E., Belarbi, E. H., Acién Fernández, F. G., Robles Medina, A., and Chisti, Y. (2003). Recovery of microalgal biomass and metabolites: Process options and economics. *Biotechnol. Adv.* 20, 491–515. doi:10.1016/S0734-9750(02)00050-2

Mondal, M., Goswami, S., Ghosh, A., Oinam, G., Tiwari, O. N., Das, P., et al. (2017). Production of biodiesel from microalgae through biological carbon capture: A review. *3 Biotech.* 7, 99–21. doi:10.1007/s13205-017-0727-4

Moon, M., Kim, C. W., Farooq, W., Suh, W. I., Shrivastav, A., Park, M. S., et al. (2014). Utilization of lipid extracted algal biomass and sugar factory wastewater for algal growth and lipid enhancement of Ettlia sp. *Bioresour. Technol.* 163, 180–185. doi:10.1016/J.BIORTECH.2014.04.033

Morales, M., Aflalo, C., and Bernard, O. (2021). Microalgal lipids: A review of lipids potential and quantification for 95 phytoplankton species. *Biomass Bioenergy* 150, 106108. doi:10.1016/J.BIOMBIOE.2021.106108

Morschett, H., Wiechert, W., and Oldiges, M. (2016). Automation of a Nile red staining assay enables high throughput quantification of microalgal lipid production. *Microb. Cell Fact.* 15, 34–11. doi:10.1186/s12934-016-0433-7

Mota, G. C. P., Moraes, L. B. S. de, Oliveira, C. Y. B., Oliveira, D. W. S., Abreu, J. L. de, Dantas, D. M. M., et al. (2022). Astaxanthin from *Haematococcus pluvialis* : Processes, applications, and market. *Prep. Biochem. Biotechnol.* 52, 598–609. doi:10.1080/10826068.2021.1966802

Muñoz, C. F., Weusthuis, R. A., D'Adamo, S., and Wijffels, R. H. (2019). Effect of single and combined expression of lysophosphatidic acid acyltransferase, glycerol-3-phosphate acyltransferase, and diacylglycerol acyltransferase on lipid accumulation and composition in Neochloris oleoabundans. *Front. Plant Sci.* 10, 1573. doi:10.3389/FPLS.2019.01573

Mutanda, T., Ramesh, D., Karthikeyan, S., Kumari, S., Anandraj, A., and Bux, F. (2011). Bioprospecting for hyper-lipid producing microalgal strains for sustainable biofuel production. *Bioresour. Technol.* 102, 57–70. doi:10.1016/J.BIORTECH.2010.06.077

Nagappan, S., Devendran, S., Tsai, P. C., Dahms, H. U., and Ponnusamy, V. K. (2019). Potential of two-stage cultivation in microalgae biofuel production. *Fuel* 252, 339–349. doi:10.1016/j.fuel.2019.04.138

Nandhini, R., Berslin, D., Sivaprakash, B., Rajamohan, N., and Vo, D. V. N. (2022). Thermochemical conversion of municipal solid waste into energy and hydrogen: a review. *Environ. Chem. Let.* 20 (3), 1645–1669. doi:10.1007/S10311-022-01410-3

Ng, I. S., Tan, S. I., Kao, P. H., Chang, Y. K., and Chang, J. S. (2017). Recent developments on genetic engineering of microalgae for biofuels and bio-based chemicals. *Biotechnol. J.* 12, 1600644. doi:10.1002/BIOT.201600644

Nguyen, T. H. T., Park, S., Jeong, J., Shin, Y. S., Sim, S. J., and Jin, E. S. (2020). Enhancing lipid productivity by modulating lipid catabolism using the CRISPR-Cas9 system in Chlamydomonas. *J. Appl. Phycol.* 32, 2829–2840. doi:10.1007/S10811-020-02172-7

Nigam, H., Malik, A., and Singh, V. (2021). A novel nanoemulsion-based microalgal growth medium for enhanced biomass production. *Biotechnol. Biofuels* 14, 111–118. doi:10.1186/s13068-021-01960-8

Organization of the Petroleum Exporting Countries - OPEC (2020). *2020 world oil outlook 2045*.

Park, H., Jung, D., Lee, J., Kim, P., Cho, Y., Jung, I., et al. (2018). Improvement of biomass and fatty acid productivity in ocean cultivation of Tetraselmis sp. using hypersaline medium. *J. Appl. Phycol.* 30, 2725–2735. doi:10.1007/S10811-018-1388-3

Parsaeimehr, A., Mancera-Andrade, E. I., Robledo-Padilla, F., Iqbal, H. M. N., and Parra-Saldivar, R. (2017). A chemical approach to manipulate the algal growth, lipid content and high-value alpha-linolenic acid for biodiesel production. *Algal Res.* 26, 312–322. doi:10.1016/j.algal.2017.08.016

Pavithra, K. G., Kumar, P. S., Jaikumar, V., Vardhan, K. H., and SundarRajan, P. S. (2020). Microalgae for biofuel production and removal of heavy metals: A review. *Environ. Chem. Lett.* 18, 1905–1923. doi:10.1007/S10311-020-01046-1

Peng, L., Fu, D., Chu, H., Wang, Z., and Qi, H. (2020). Biofuel production from microalgae: A review. *Environ. Chem. Lett.* 18, 285–297. doi:10.1007/S10311-019-00939-0

Popp, J., Lakner, Z., Harangi-Rákos, M., and Fári, M. (2014). The effect of bioenergy expansion: Food, energy, and environment. *Renew. Sustain. Energy Rev.* 32, 559–578. doi:10.1016/J.RSER.2014.01.056

Purton, S., Szaub, J. B., Wannathong, T., Young, R., and Economou, C. K. (2013). Genetic engineering of algal chloroplasts: Progress and prospects. *Russ. J. Plant Physiol.* 60, 491–499. doi:10.1134/S1021443713040146

Qiu, R., Gao, S., Lopez, P. A., and Ogden, K. L. (2017). Effects of pH on cell growth, lipid production and CO2 addition of microalgae Chlorella sorokiniana. *Algal Res.* 28, 192–199. doi:10.1016/j.algal.2017.11.004

Quader, M. A., and Ahmed, S. (2017). Bioenergy with carbon capture and storage (BECCS): Future prospects of carbon-negative technologies. *Clean Energy for Sustainable Development: Comparisons and Contrasts of New Approaches* Amsterdam, Netherlands: Elsevier Inc, 91–140. doi:10.1016/B978-0-12-805423-9.00004-1

Quan, Y., Pehkonen, S. O., and Ray, M. B. (2004). Evaluation of three different lamp emission models using novel application of potassium ferrioxalate actinometry. *Ind. Eng. Chem. Res.* 43, 948–955. doi:10.1021/ie0304210

Rahman, A., Kumar, S., and Nawaz, T. (2020). Biosynthesis of nanomaterials using algae. *Microalgae Cultiv. Biofuels Prod.*, 265–279. doi:10.1016/B978-0-12-817536-1.00017-5

Rajeswari, S., Baskaran, D., Saravanan, P., Rajasimman, M., Rajamohan, N., and Vasseghian, Y. (2022). Production of ethanol from biomass–Recent research, scientometric review and future perspectives. *Fuel* 317, 123448. doi:10.1016/J.FUEL.2022.123448

Raven, J. A., and Beardall, J. (2003). *Carbohydrate metabolism and respiration in algae*, 205–224. doi:10.1007/978-94-007-1038-2_10

Remmers, I. M., Wijffels, R. H., Barbosa, M. J., and Lamers, P. P. (2018). Can we approach theoretical lipid yields in microalgae? *Trends Biotechnol.* 36, 265–276. doi:10.1016/J.TIBTECH.2017.10.020

Rengel, R., Smith, R. T., Haslam, R. P., Sayanova, O., Vila, M., and León, R. (2018). Overexpression of acetyl-CoA synthetase (ACS) enhances the biosynthesis of neutral lipids and starch in the green microalga Chlamydomonas reinhardtii. *Algal Res.* 31, 183–193. doi:10.1016/j.algal.2018.02.009

Renuka, N., Guldhe, A., Singh, P., Ansari, F. A., Rawat, I., and Bux, F. (2017). Evaluating the potential of cytokinins for biomass and lipid enhancement in microalga Acutodesmus obliquus under nitrogen stress. *Energy Convers. Manag.* 140, 14–23. doi:10.1016/J.ENCONMAN.2017.02.065

Richmond, A. (2004). Principles for attaining maximal microalgal productivity in photobioreactors: An overview. *Hydrobiologia* 512 (Table 1), 33–37. doi:10.1023/B:HYDR.0000020365.06145.36

Romel Malapascua, J. (2012). Development of an indirect method of microalgal lipid quantification using a lysochrome dye, Nile red. *Afr. J. Biotechnol.* 11, 13518–13527. doi:10.5897/ajb12.1142

Rosa, G. M., Morais, M. G., and Costa, J. A. V. (2019). Fed-batch cultivation with CO2 and monoethanolamine: Influence on Chlorella fusca LEB 111 cultivation, carbon biofixation and biomolecules production. *Bioresour. Technol.* 273, 627–633. doi:10.1016/J.BIORTECH.2018.11.010

Rosales-Mendoza, S., Paz-Maldonado, L. M. T., and Soria-Guerra, R. E. (2012). Chlamydomonas reinhardtii as a viable platform for the production of recombinant proteins: Current status and perspectives. *Plant Cell Rep.* 31, 479–494. doi:10.1007/s00299-011-1186-8

Salama, E. S., Kabra, A. N., Ji, M. K., Kim, J. R., Min, B., and Jeon, B. H. (2014). Enhancement of microalgae growth and fatty acid content under the influence of phytohormones. *Bioresour. Technol.* 172, 97–103. doi:10.1016/J.BIORTECH.2014.09.002

Sathishkumar, R. S., Sundaramanickam, A., Srinath, R., Ramesh, T., Saranya, K., Meena, M., et al. (2019). Green synthesis of silver nanoparticles by bloom forming marine microalgae Trichodesmium erythraeum and its applications in antioxidant, drug-resistant bacteria, and cytotoxicity activity. *J. Saudi Chem. Soc.* 23, 1180–1191. doi:10.1016/J.JSCS.2019.07.008

Sati, H., Mitra, M., Mishra, S., and Baredar, P. (2019). Microalgal lipid extraction strategies for biodiesel production: A review. *Algal Res.* 38, 101413. doi:10.1016/j.algal.2019.101413

Shahid, A., Rehman, A., Usman, M., Ashraf, M. U. F., Javed, M. R., Khan, A. Z., et al. (2020). Engineering the metabolic pathways of lipid biosynthesis to develop robust microalgal strains for biodiesel production. *Biotechnol. Appl. Biochem.* 67, 41–51. doi:10.1002/BAB.1812

Sharma, K. K., Schuhmann, H., and Schenk, P. M. (2012). High lipid induction in microalgae for biodiesel production. *Energies* 5 (5), 15321532–15531553. doi:10.3390/EN5051532

Sharma, P. K., Goud, V. V., Yamamoto, Y., and Sahoo, L. (2021). Efficient Agrobacterium tumefaciens-mediated stable genetic transformation of green microalgae, Chlorella sorokiniana. *3 Biotech.* 311, 196–207. doi:10.1007/s13205-021-02750-7

Shen, G., Schluchter, W. M., and Bryant, D. A. (2008). Biogenesis of phycobiliproteins: I. cpcS-I and cpcU mutants of the cyanobacterium synechococcus sp. pcc 7002 define a heterodimeric phyococyanobilin lyase specific for β-phycocyanin and allophycocyanin subunits. *J. Biol. Chem.* 283, 7503–7512. doi:10.1074/JBC.M708164200

Shokravi, Z., Shokravi, H., Chyuan, O. H., Lau, W. J., Koloor, S. S. R., Petrů, M., et al. (2020). Improving 'lipid productivity' in microalgae by bilateral enhancement of biomass and lipid contents: A review. *Sustainability* 12, 9083. doi:10.3390/SU12219083

Sivagnanam, S. P., Tilahun Getachew, A., Choi, J. H., Park, Y. B., Woo, H. C., and Chun, B. S. (2017). Green synthesis of silver nanoparticles from deoiled Brown algal extract via Box-Behnken based design and their antimicrobial and sensing properties. *Green Process. Synthesis* 6, 147–160. doi:10.1515/GPS-2016-0052/ASSET/GRAPHIC/J_GPS-2016-0052_FIG_009.JPG

Soltani, S., Saadatmand, S., Khavarinejad, R., and Nejadsattari, T. (2011). Antioxidant and antibacterial activities of cladophora glomerata (L.) kütz. In caspian sea coast, Iran. *Afr. J. Biotechnol.* 10, 7684–7689. doi:10.5897/AJB11.491

Stephens, E., Ross, I. L., Mussgnug, J. H., Wagner, L. D., Borowitzka, M. A., Posten, C., et al. (2010). Future prospects of microalgal biofuel production systems. *Trends Plant Sci.* 15 (10), 554–564. doi:10.1016/J.TPLANTS.2010.06.003

Suali, E., and Sarbatly, R. (2012). Conversion of microalgae to biofuel. *Renew. Sustain. Energy Rev.* 16, 4316–4342. doi:10.1016/j.rser.2012.03.047

Sun, X. M., Ren, L. J., Zhao, Q. Y., Ji, X. J., and Huang, H. (2019). Enhancement of lipid accumulation in microalgae by metabolic engineering. *Biochimica Biophysica Acta (BBA) - Mol. Cell Biol. Lipids* 1864, 552–566. doi:10.1016/J.BBALIP.2018.10.004

Suarez Garcia, E., Lo, C., Eppink, M. H. M., Wijffels, R. H., and van den Berg, C. (2019). Understanding mild cell disintegration of microalgae in bead mills for the release of biomolecules. *Chem. Eng. Sci.* 203, 380–390. doi:10.1016/J.CES.2019.04.008

Taher, H., Al-Zuhair, S., Al-Marzouqi, A. H., Haik, Y., and Farid, M. M. (2011). A review of enzymatic transesterification of microalgal oil-based biodiesel using supercritical technology. *Enzyme Res.*, 1–25. doi:10.4061/2011/468292

Tang, D. Y. Y., Yew, G. Y., Koyande, A. K., Chew, K. W., Vo, D. V. N., and Show, P. L. (2020). Green technology for the industrial production of biofuels and bioproducts from microalgae: A review. *Environ. Chem. Lett.* 18, 1967. doi:10.1007/S10311-020-01052-3

Tran, D. T., Lee, H. R., Jung, S., Park, M. S., and Yang, J. W. (2018). Lipid-extracted algal biomass based biocomposites fabrication with poly(vinyl alcohol). *Algal Res.* 31, 525–533. doi:10.1016/J.ALGAL.2016.08.016

Trentacoste, E. M., Shrestha, R. P., Smith, S. R., Glé, C., Hartmann, A. C., Hildebrand, M., et al. (2013). Metabolic engineering of lipid catabolism increases microalgal lipid accumulation without compromising growth. *Proc. Natl. Acad. Sci. U. S. A.* 110, 19748–19753. doi:10.1073/PNAS.1309299110

Vasilieva, S. G., Lobakova, E. S., Lukyanov, A. A., and Solovchenko, A. E. (2016). Immobilized microalgae in biotechnology. *Mosc. Univ. Biol. Sci. Bull.* 71, 170–176. doi:10.3103/S0096392516030135

Venkata Subhash, G., Rajvanshi, M., Navish Kumar, B., Govindachary, S., Prasad, V., and Dasgupta, S. (2017). Carbon streaming in microalgae: extraction and analysis methods for high value compounds. *Biores. Technol.* 244, 1304–1316. doi:10.1016/J.BIORTECH.2017.07.024

Vorobiev, E., Lebovka, N. I., Redondo, L. M., Pataro, G., Carullo, D., Donsì, F., et al. (2020). Pulsed electric fields-assisted extraction of valuable compounds from Arthrospira Platensis: Effect of pulse polarity and mild heating *Front. Bioeng. Biotechnol.* 8, 551272. doi:10.3389/fbioe.2020.551272

Wang, B., Li, Y., Wu, N., and Lan, C. Q. (2008). CO2 bio-mitigation using microalgae. *Appl. Microbiol. Biotechnol.* 79, 707–718. doi:10.1007/s00253-008-1518-y

Wang, C., Guo, L., Li, Y., and Wang, Z. (2012). Systematic comparison of C3 and C4 plants based on metabolic network analysis. *BMC Syst. Biol.* 6, S9. doi:10.1186/1752-0509-6-S2-S9

Wang, J., Liu, J., and Liu, T. (2015). The difference in effective light penetration may explain the superiority in photosynthetic efficiency of attached cultivation over the conventional open pond for microalgae. *Biotechnol. Biofuels* 8, 49–12. doi:10.1186/s13068-015-0240-0

Watanabe, H., Li, D., Nakagawa, Y., Tomishige, K., and Watanabe, M. M. (2015). Catalytic gasification of oil-extracted residue biomass of Botryococcus braunii. *Bioresour. Technol.* 191, 452–459. doi:10.1016/J.BIORTECH.2015.03.034

White, D. A., Pagarette, A., Rooks, P., and Ali, S. T. (2013). The effect of sodium bicarbonate supplementation on growth and biochemical composition of marine microalgae cultures. *J. Appl. Phycol.* 25, 153–165. doi:10.1007/s10811-012-9849-6

Win, T. T., Barone, G. D., Secundo, F., and Fu, P. (2018). Algal biofertilizers and plant growth stimulants for sustainable agriculture. *Ind. Biotechnol.* 14, 203–211. doi:10.1089/ind.2018.0010

Wu, P., Ata-Ul-Karim, S. T., Singh, B. P., Wang, H., Wu, T., Liu, C., et al. (2019). A scientometric review of biochar research in the past 20 years (1998–2018). *Biochar* 1, 23–43. doi:10.1007/s42773-019-00002-9

Xia, H., Riaz, M., Zhang, M., Liu, B., El-Desouki, Z., and Jiang, C. (2020). Biochar increases nitrogen use efficiency of maize by relieving aluminum toxicity and improving soil quality in acidic soil. *Ecotoxicol. Environ. Saf.* 196, 110531. doi:10.1016/J.ECOENV.2020.110531

Xia, L., Ge, H., Zhou, X., Zhang, D., and Hu, C. (2013). Photoautotrophic outdoor two-stage cultivation for oleaginous microalgae Scenedesmus obtusus XJ-15. *Bioresour. Technol.* 144, 261–267. doi:10.1016/J.BIORTECH.2013.06.112

Xue, J., Niu, Y. F., Huang, T., Yang, W. D., Liu, J. S., and Li, H. Y. (2015). Genetic improvement of the microalga Phaeodactylum tricornutum for boosting neutral lipid accumulation. *Metab. Eng.* 27, 1–9. doi:10.1016/J.YMBEN.2014.10.002

Yaashikaa, P. R., Keerthana Devi, M., Senthil Kumar, P., and Pandian, E. (2022). A review on biodiesel production by algal biomass: Outlook on lifecycle assessment and techno-economic analysis. *Fuel* 324, 124774. doi:10.1016/J.FUEL.2022.124774

Yamaguchi, K. (1996). Recent advances in microalgal bioscience in Japan, with special reference to utilization of biomass and metabolites: A review. *J. Appl. Phycol.* 8, 487–502. doi:10.1007/BF02186327

Yang, H., He, Q., Rong, J., Xia, L., and Hu, C. (2014). Rapid neutral lipid accumulation of the alkali-resistant oleaginous Monoraphidium dybowskii LB50 by NaCl induction. *Bioresour. Technol.* 172, 131–137. doi:10.1016/j.biortech.2014.08.066

Yap, J. K., Sankaran, R., Chew, K. W., Halimatul Munawaroh, H. S., Ho, S. H., Rajesh Banu, J., et al. (2021). Advancement of green technologies: A comprehensive review on the potential application of microalgae biomass. *Chemosphere* 281, 130886. doi:10.1016/J.CHEMOSPHERE.2021.130886

Yu, K. L., Lau, B. F., Show, P. L., Ong, H. C., Ling, T. C., Chen, W. H., et al. (2017). Recent developments on algal biochar production and characterization. *Bioresour. Technol.* 246, 2–11. doi:10.1016/J.BIORTECH.2017.08.009

Yukesh Kannah, R., Kavitha, S., Parthiba Karthikeyan, O., Rene, E. R., Kumar, G., Rajesh Banu, J., et al. (2021). A review on anaerobic digestion of energy and cost effective microalgae pretreatment for biogas production. *Bioresour. Technol.* 332, 125055. doi:10.1016/J.BIORTECH.2021.125055

Zhang, C., Xiao, Y., Ma, Y., Li, B., Liu, Z., Lu, C., et al. (2017). Algae biomass as a precursor for synthesis of nitrogen-and sulfur-co-doped carbon dots: A better probe in Arabidopsis guard cells and root tissues. *J. Photochem. Photobiol. B Biol.* 174, 315–322. doi:10.1016/J.JPHOTOBIOL.2017.06.024

Zhang, Y., Pan, Y., Ding, W., Hu, H., and Liu, J. (2021). Lipid production is more than doubled by manipulating a diacylglycerol acyltransferase in algae. *GCB Bioenergy* 13, 185–200. doi:10.1111/GCBB.12771

Zhao, B., Ma, J., Zhao, Q., Laurens, L., Jarvis, E., Chen, S., et al. (2014). Efficient anaerobic digestion of whole microalgae and lipid-extracted microalgae residues for methane energy production. *Bioresour. Technol.* 161, 423–430. doi:10.1016/J.BIORTECH.2014.03.079

Zheng, H., Gao, Z., Yin, F., Ji, X., and Huang, H. (2012). Effect of CO2 supply conditions on lipid production of Chlorella vulgaris from enzymatic hydrolysates of lipid-extracted microalgal biomass residues. *Bioresour. Technol.* 126, 24–30. doi:10.1016/J.BIORTECH.2012.09.048

Zheng, H., Ma, X., Gao, Z., Wan, Y., Min, M., Zhou, W., et al. (2015). Lipid production of heterotrophic Chlorella sp. from hydrolysate mixtures of lipid-extracted microalgal biomass residues and molasses. *Appl. Biochem. Biotechnol.* 177, 662–674. doi:10.1007/S12010-015-1770-4

Zhu, S., Huang, W., Xu, J., Wang, Z., Xu, J., and Yuan, Z. (2014). Metabolic changes of starch and lipid triggered by nitrogen starvation in the microalga Chlorella zofingiensis. *Bioresour. Technol.* 152, 292–298. doi:10.1016/j.biortech.2013.10.092

frontiers | Frontiers in Chemical Engineering

TYPE Review
PUBLISHED 29 November 2022
DOI 10.3389/fceng.2022.1066027

OPEN ACCESS

EDITED BY
Le Han,
Chongqing University, China

REVIEWED BY
Enrico Drioli,
Department of Chemical Sciences and Materials Technologies, Institute for Membrane Technology (CNR), Italy
Qingyao He,
Huazhong Agricultural University, China

*CORRESPONDENCE
Heidi Richards,
Heidi.richards@wits.ac.za

SPECIALTY SECTION
This article was submitted to Separation Processes,
a section of the journal
Frontiers in Chemical Engineering

RECEIVED 10 October 2022
ACCEPTED 18 November 2022
PUBLISHED 29 November 2022

CITATION
Chimanlal I, Nthunya LN, Quist-Jensen C and Richards H (2022), Membrane distillation crystallization for water and mineral recovery: The occurrence of fouling and its control during wastewater treatment.
Front. Chem. Eng. 4:1066027.
doi: 10.3389/fceng.2022.1066027

Membrane distillation crystallization for water and mineral recovery: The occurrence of fouling and its control during wastewater treatment

Indira Chimanlal[1,2], Lebea N. Nthunya[1,2], Cejna Quist-Jensen[2] and Heidi Richards[1]*

[1]Molecular Sciences Institute, School of Chemistry, University of Witwatersrand, Johannesburg, South Africa, [2]Center for Membrane Technology, Department of Chemistry and Bioscience, Aalborg University, Aalborg, Denmark

Membrane distillation crystallization (MDC) is an emerging technology envisaged to manage challenges affecting the desalination industry. This technology can sustainably treat concentrated solutions of produced water and industrially discharged saline wastewater. Simultaneous recovery of clean water and minerals is achieved through the integration of crystallization to membrane distillation (MD). MDC has received vast research interest because of its potential to treat hypersaline solutions. However, MDC still faces challenges in harnessing its industrial applications. Technically, MDC is affected by fouling/scaling and wetting thereby hindering practical application at the industrial level. This study reviews the occurrence of membrane fouling and wetting experienced with MDC. Additionally, existing developments carried out to address these challenges are critically reviewed. Finally, prospects suggesting the sustainability of this technology are highlighted.

KEYWORDS

water recovery, mineral mining, fouling, wetting, membrane distillation crystallization

Introduction

Presently, about four billion people are affected by water scarcity (Mekonnen and Hoekstra, 2016). Water scarcity is influenced by an increase in urbanization and industrialization, population growth, and climate change (Ahmed et al., 2020). Additionally, mineral resource depletion is emerging as an industrial problem. Thus, the decline in raw materials results in energy and financial challenges in several industries (Quist-Jensen et al., 2016). The shortage of raw materials consequently minimizes industrial production required to meet the market demand. Therefore, recycling mineral resources from waste streams while recovering freshwater is imperative. This avenue circumvents the

search for freshwater sources due to their steady depletion. A progressively attractive technique addressing the issues of mineral and freshwater shortages is membrane distillation crystallization (MDC). Interestingly, MDC affords simultaneous recovery of both mineral crystals and freshwater from high saline wastewater (Quist-Jensen et al., 2016). Technically, MDC is a hybrid process consisting of membrane distillation (MD) and a crystallization reactor wherein the feed solution is concentrated in the MD system to reach supersaturation, followed by crystallization to recover the minerals (Quist-Jensen et al., 2017). Particularly, MDC can overcome challenges associated with common wastewater treatment options such as reverse osmosis (RO) and nanofiltration (NF) (Pramanik et al., 2017). Additionally, MDC operates at low temperatures and pressures, uses simple configuration, and consumes less energy compared to other thermal processes (Bouchrit et al., 2017; Pramanik et al., 2017). This review aims to unpack the principles and process characteristics of MDC for mineral and water recovery. Secondly, membrane fouling, and scale control measures are highlighted. Furthermore, process parameter optimization towards permeate flux, and crystal growth and selectivity are discussed. Additionally, membrane fabrication and modification strategies are reviewed to provide further insight into the development of more efficient and competitive membranes. Lastly, the latest developments towards MDC application are reported.

Principles of membrane distillation crystallization

Membrane distillation (MD) has been extensively evaluated for the desalination of seawater and the treatment of high saline industrially discharged wastewater. During desalination processes, concentrated brines are generated and discharged to the environment. However, these brines could be treated further to recover mineral resources. Drioli et al. (2015) regard mineral resources to be more economically valuable compared to fresh water produced from MD processes. In their study, the researchers presented a proof-of-concept to extract mineral resources from MD desalination plants (Drioli et al., 2015). In this regard, MDC emerged as a new technology with similar mechanisms to MD. The MDC saturates the feed solution to recover mineral crystals. The feed solution is concentrated through the MD process while recovering fresh water (Pramanik et al., 2016). In this process, the feed solution becomes concentrated towards super-saturation, thus enabling nucleation and mineral crystallization while simultaneously recovering freshwater on the permeate side of the membrane (Figure 1) (Quist-Jensen et al., 2016). To facilitate selective passage of water in vapour state while exclusively retaining liquid, this technique requires the use of hydrophobic membrane (Das et al., 2021). This process operates in various MD modes namely, direct contact membrane distillation (DCMD), air gap membrane distillation (AGMD), sweep gas membrane distillation (SGMD) and vacuum membrane distillation (VMD) (Pramanik et al., 2016; Quist-Jensen et al., 2016). The detailed description of each mode is reported elsewhere (Nthunya et al., 2019a). Interestingly, the water recovery in MDC ranges from 50%–90%, thus emerging as an alternative water desalination technology (Quist-Jensen et al., 2019). According to Quist-Jensen et al. (2019), MDC can increase water production, mineral recovery and advance zero-liquid discharge (Quist-Jensen et al., 2019). The advantages and disadvantages of this technique are summarized in Table 1.

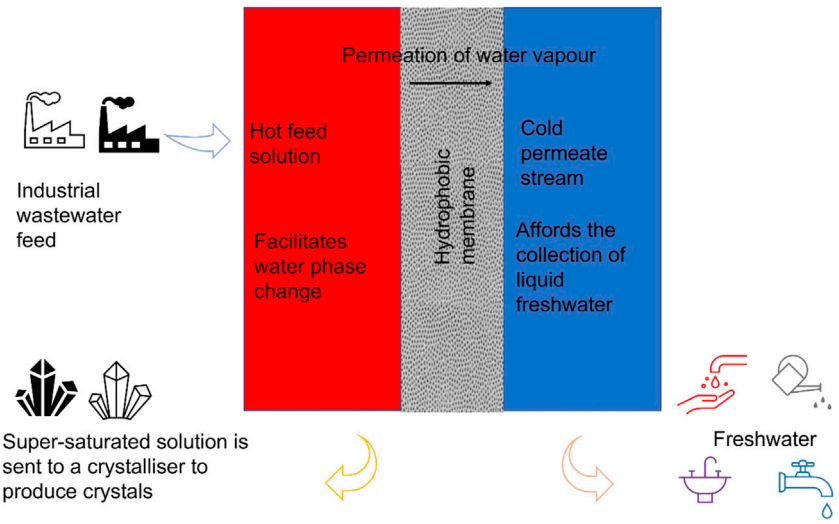

FIGURE 1
Schematic representation of MDC for recovery of freshwater and minerals from industrial wastewater.

TABLE 1 Summary of the advantages and disadvantages associated with MDC.

Advantages	Disadvantages	References
Independent of the feed concentration. Not affected by osmotic pressures from concentrated brines	Membranes are susceptible to fouling due to the contaminant deposition in membrane pores, resulting in clogging among other consequences	(Drioli et al., 2012; Pramanik et al., 2016; Ali et al., 2018)
Can be utilized for salt separation processes to circumvent salt co-crystallization. Also, crystal growth and nucleation are controlled	May suffer from scaling which is due to the collection of inorganic salts on the membrane surface	(Drioli et al., 2012; Bouchrit et al., 2017; Ruiz Salmón and Luis, 2018)
Lower energy consumption and can make use of alternative energy sources such as solar power	Membrane performance may deteriorate due to membrane wetting	(Ruiz Salmón and Luis, 2018; Das et al., 2021)
Provides sustainable and simultaneous water and mineral salt recovery	—	Pramanik et al. (2016)

Parameter optimization to enhance membrane distillation crystallization

The development of a viable MDC process requires optimization to prevent undesired crystallization inside the module and tubing. For this reason, the selection of appropriate MD and crystallization operating conditions are imperative. These parameters include process temperature, solution supersaturation, flow rates and duration of crystallization. Moreover, the temperatures and flow rates affect the crystal size distribution. Therefore, analysis of these parameters provides a better understanding of the MDC process and requirements to realize the maximum performance while ensuring zero liquid discharge to the environment.

Process temperature

The effect of process temperature on permeate flux is best described by Antoine equation, where α, β, and γ are constants relating to the specific substance and P_i is the vapour pressure (Pa) and T is the temperature (K).

$$P_i(T) = e^{\left(\alpha - \frac{\beta}{\gamma + T}\right)}$$

According to Antoine equation, vapour pressure exponentially increases with temperature (Choudhury et al., 2019). Furthermore, water flux is directly proportional to feed temperature (Banat and Simandl, 1998). However, flux increments are limited by the process temperature and declines once an optimum has been attained (Banat and Simandl, 1998). Moreover, Attia et al. (2017) evaluated the effect of temperature using synthetic electrospun PVDF, superhydrophobic alumina, and commercial PVDF membranes in a comparative AGMD process. A direct relationship between permeate flux and feed temperature was established (Attia et al., 2017). Liu et al. (2022) assessed the effect of temperature and flow velocity to obtain lithium chloride from air-conditioning systems *via* DCMD. Reportedly, an increase in feed temperature improved solute generation although the membrane's hydrophobicity was altered. However, the increase in solute concentration reduced the water flux due to a decreased partial vapour pressure (Liu et al., 2022). Although high water fluxes are obtained at higher temperatures, the water recovery factor is reduced due to salt precipitation (Zhu et al., 2021). The effect of feed temperature on process operation is summarized in Table 2.

Solution supersaturation

The capability of the MD technique to progressively concentrate a feed solution to supersaturation gave rise to MDC (Yadav et al., 2022). The gradual passage of water vapor from the feed stream to the distillate results in the eventual concentration of the feed solution to its critical saturation. Further increase in feed supersaturation enables the recovery of crystal salts from the crystallization reactor (Das et al., 2021). Importantly, this process facilitates the recovery of higher quality mineral crystals in terms of size and purity. Other benefits include controlled rate of supersaturation and nucleation (Yadav et al., 2022). However, the increase in feed concentration towards solution supersaturation induces temperature and concentration polarization, thus reducing the permeate flux (Martínez, 2004). Moreover, pore blockage occurs due to the formation of crystals on the surface of membrane (Yadav et al., 2022). Martínez (2004) investigated the effect of feed concentration on the permeate flux using a flat sheet PTFE membrane and feed solutions of pure water, sodium chloride, and sucrose. Notably, the pure water flux remained stable towards supersaturation. However, the deposition of sodium chloride and sucrose crystal on the membrane surface resulted in a decrease in the permeate flux (Martínez, 2004). When supersaturation is attained in the bulk feed solution, nucleation is then induced which is succeeded by crystallization (Yadav et al., 2022). Moreover, a higher feed temperature increases rate of solvent evaporation, thus facilitating an increased rate of supersaturation compared to that experienced at low feed temperatures (Edwie and Chung, 2013).

TABLE 2 Summary of the effect of varying the feed temperature on the permeate flux.

Membrane type	MD process type	Feed temperature variation (°C)	Flow rate (L min^{-1})	Permeate flux (L m^{-2} h^{-1})	Reference
Electrospun PVDF	AGMD	30–70	1.5	Increased from 9.17 to 26.22	Attia et al. (2017)
Flat sheet PVDF membrane	ADMD	25–80	5.5	Increased from 0.5 to 9.1	Banat and Simandl, (1998)
Commercial polypropylene (PP) membrane	Integrated FO—MD process	40–70	0.4	Increased from 8.1 to 35.4	Husnain et al. (2015)
PTFE	DCMD	55–65	0.4–1.0	Significant increase in flux	Liu et al. (2022)
PTFE	AGMD	50–80	0.03–0.06	3.06	Kargari and Yousefi, (2021)
Polyimide fibrous membrane (PI FM)	DCMD	30–50	0.24	Increased from 26.12 to 64.15	Zhu et al. (2021)
Commercial PTFE	DCMD	40–60	1.0	Increased from 4 to 12	Ramos et al. (2022)

Duration of crystallization

The formation and crystal growth are influenced by the solubility of the salt, rate of water recovery and process temperature. For instance, feed solutions with low concentration containing extremely soluble solutes requires a lengthy period to form crystals (Rudolph, 2010; Liu et al., 2021). Additionally, slow crystal growth rate facilitates formation of large crystals. Therefore, longer crystallization periods give rise to larger crystals (Alvarez et al., 2020). In their study, Wagstaff et al. (1964) evaluated the impact of crystallization duration to the size of cristobalite. Based on their findings, the size of the crystals increased quadratically upon increase in duration of process crystallization (Wagstaff et al., 1964). Essentially, the rate of crystal growth is governed by the various factors including flow of latent heat from the growing crystal, diffusion and reactions occurring at the crystal interface (Rudolph, 2010). In MDC processes, the inclusion of the membrane provides a site for heterogeneous nucleation. The Gibbs free energy is lower at the membrane-solution interface, thus favoring heterogeneous nucleation rather than homogenous nucleation (Ruiz Salmón and Luis, 2018). According to Edwie and Chung (2013), a high feed temperature encourages a higher rate of evaporation resulting in a lower average crystal size. Once nucleation has been established, the nuclei begin to grow until the critical cluster size has been achieved. Thereafter, crystals form and grow in saturation zones (i.e., metastable and unstable growth zones) (Yadav et al., 2022). Technically, rate of supersaturation and nucleation affect crystal network growth, consequently the duration of crystallization (Das et al., 2021).

Recirculation rate

High recovery rates of MDC processes are realized at higher recirculation rates (Swaminathan and Lienhard, 2018). For an efficient and high performing MDC process, the overall recovery factor should be greater than that of a single pass process (Lokare et al., 2018). To achieve high recovery factors, the retentate is mixed with the new feed solution prior to crystallization (Lokare et al., 2018). In addition to high recoveries, an increase in the recirculation rate enhances the heat transfer coefficient. Consequently, this minimizes the boundary layer thus improving the permeate flux (Srisurichan et al., 2006). Due to the improvement of water turbulence, a high recirculation rate reduces temperature polarization and membrane fouling, thus ensuring the stable water flux (Lokare et al., 2018).

Fouling of MDC membranes

Occurrence of fouling in MDC is a common problem affecting process performance. To minimize fouling, its developments and successions should be established. Briefly, fouling occurs due to the deposition of microbial, colloidal, organic, or inorganic constituents on the surface or inner pores of the membrane, thus causing blockages (Choudhury et al., 2019; Mpala et al., 2022). Due to changes in the membrane physicochemical properties, fouling reduces permeate water flux, salt rejections and also increases the operating expenditure (OPEX) of the process (Nthunya et al., 2022). Additionally, fouling reduces membrane hydrophobicity leading to membrane wetting (Wang and Lin, 2017). Reduced membrane hydrophobicity encourages the passage of water in liquid state, thus reducing mineral salt rejection (Wang and Lin, 2017; Choudhury et al., 2019). Moreover, fouling is not limited to the membrane surface, but can also occur within the membrane pores. This was evident in a study conducted by Kim et al. (2018) reporting deposition of foulants within the membrane pores in conjunction with reduced water recoveries and permeate flux. Usually, permeate flux reduction is caused by partial and

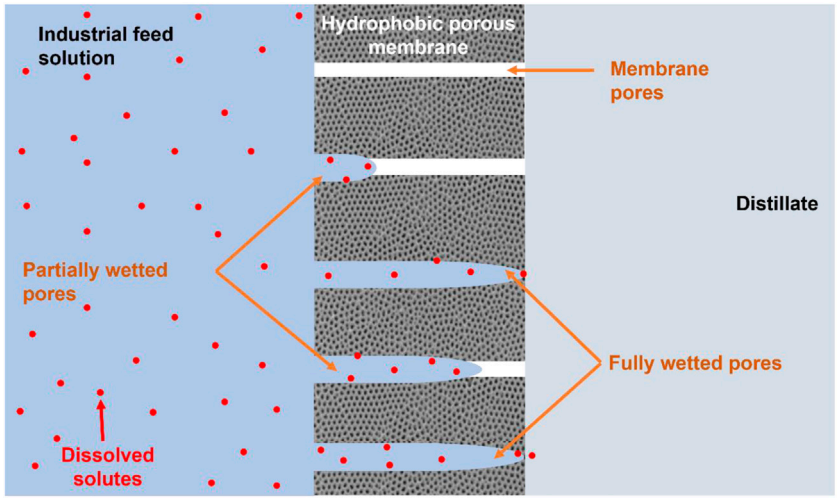

FIGURE 2
Graphical representation of membrane pore wetting experienced in MDC.

complete wetting while the latter is true for water quality deterioration (Figure 2) (Yao et al., 2020). Technically, the membrane is partially wetted by process conditions with limited passage of water in both liquid and vapour state. However, during full pore wetting, the water carrying salt ions passes through the membrane in liquid state, thus reducing the quality of the distillate.

Common factors influencing fouling include feed solution properties, hydrodynamic conditions, and membrane characteristics (Yao et al., 2020). The most prevalent form of fouling in MDC is scaling caused by sparingly soluble salts (Pramanik et al., 2016; Char et al., 2021). Inorganic scaling occurs *via* two mechanisms, namely; 1) nucleation and precipitate growth on the surface or pores of the membrane and 2) the build-up of precipitates materializing in the bulk solution (Horseman et al., 2021). Common scalants causing membrane damage include calcium sulfate and calcium carbonate (Alkhatib et al., 2021). Fouling can be classified into porous and non-porous where the former causes thermal resistance and the latter results in both thermal and hydraulic resistance (Abdel-Karim et al., 2021; Alkhatib et al., 2021). Therefore, to maintain high MDC process performance, operational challenges associated with a high concentration of salts and a complex feed solution should be overcome. Fouling and its implications are presented in Table 3 below.

Fouling control

Membrane fouling is inevitable and therefore requires strategic measures to minimize its effects on process performance. Fouling control increases the membrane lifespan and maintains the performance of MDC processes (Laqbaqbi et al., 2017). Membrane fouling is controlled through several measures including pre-treatments, backwashing, and chemical cleaning. These processes lengthen membrane longevity. Chemical cleaning and backwashing are employed post membrane fouling to recover flux and salt rejection. To increase water recoveries, fouling control is optimized to minimize cost and damage of membranes.

Pre-treatment

Flux decline caused by membrane fouling requires frequent membrane cleaning and possibly replacement, consequently increasing operating and maintenance costs (OPEX). Therefore, wastewater pre-treatment integrated to MDC improves process performance. Primarily, pre-treatment strategies limit fouling by reducing foulants concentration in the feed water. The choice of pre-treatment depends on the feed water. Typically, a combination of pre-treatment strategies is required to improve efficiency of foulant removal from the feed solution. These combinations involve physical and chemical processes such as low-pressure membrane filtration, coagulation and flocculation, adsorption, pH adjustments and the addition of anti-scalants.

Mechanical pre-treatments consist of membrane processes such as microfiltration (MF), ultrafiltration (UF), and nanofiltration (NF). Particularly, NF is used for water softening and reduction of natural organic matter (NOM). The UF and MF reduces colloidal, suspended and biological matter (Alkhatib et al., 2021). These pre-treatment methods have been evaluated in water processing of various complexities

TABLE 3 Implications of fouling during experimental procedures.

Membrane type	Fouling classification	Implications	References
Commercial PP hollow-fiber	Calcium carbonate and sodium scaling	Reduced water recovery and permeate flux	Kim et al. (2018)
Synthesised PVDF hollow-fiber	Organic fouling (dyes)	Decreased flux with long term operation	Shi et al. (2022)
Commercial PVDF	Scaling	Rapid flux decline	Choi et al. (2020)
PTFE/PP	Calcium sulphate scaling	Permeate flux decreased almost to zero	Nghiem and Cath, (2011)
PTFE and PE	Organic fouling (from petrochemical wastewater) and scaling	Decreased permeate flux	Venzke et al. (2021)
Commercial PTFE	Organic fouling	Reduced water recovery rate and permeate flux	Ramos et al. (2022)
Synthesised PVDF/PSF hollow fiber	Organic (ginseng) and inorganic fouling	Reduced overall flux and rejection factor	Zou et al. (2022)
Commercial PP	Organic and inorganic fouling	40% flux decline	Gryta (2020)

(Nthunya et al., 2021). El-Abbassi et al. (2013) studied coagulation-flocculation and MF pre-treatment of olive mill wastewater in DCMD. Coagulation-flocculation pre-treatment reduced the concentration of TDS and phenolic compounds by 23% and 18%, respectively. The TDS removal was improved to 30% while that of phenolic compounds was reduced to 4.8% upon the MF treatment (El-Abbassi et al., 2013). In another study, Karakulski and Gryta (2005) investigated NF pre-treatment of tap water for use in MD. Reportedly, untreated feed water caused membrane scaling leading to rapid flux decay. However, NF pre-treatment removed scalants thus ensuring high process performance (Karakulski and Gryta, 2005). Additionally, adsorption has been proven to effectively remove organic matter prior to MD water purification. Nthunya et al. (2019c) reported removal of phenolic compounds from feed wastewater using a candle filter (pore size ~100 μm) equipped with polyethyleneimine-functionalized polyacrylonitrile nanofibre membranes. The membranes presented 39.9 mg g^{-1} adsorption capacity (Nthunya et al., 2019b). Notably, MD process performance remained relatively stable upon feeding with pre-treated wastewater. Coagulation-flocculation is another process proven to effectively remove foulants prior to MD water processing. In this process, foulant particles are converted into larger flocs, thus reducing their adhesive interaction with the membranes. Moreover, coagulation-flocculation coupled with conventional treatment or membrane filtration processes remove the flocs from the feed water (Alkhatib et al., 2021). Li et al. (2016) investigated the purification of biologically treated coking wastewater using MD coupled with coagulation pre-treatment. A poly-aluminium chloride (PACl) flocculant reduced the foulants thus promoting the stable performance in MD (Li et al., 2016). Lastly, pH-adjustments have been extensively used to treat feed solutions in membrane processes. The increase in feed pH promotes formation of metal precipitates which are removed as insoluble metal hydroxides prior to MDC. Similarly, the feed solution is acidified to dissolve the foulant, thus impeding their interaction with the membranes (Karakulski and Gryta, 2005). A summary of MDC pre-treatment processes is presented in Figure 3.

Use of anti-scalants

Anti-scalants are precipitation-inhibiting chemicals impeding nucleation or crystal growth of scalants on membrane surfaces. Anti-scalants adsorb on the nuclei surface to obstruct the rate of crystal growth and agglomeration (Lin and Singer, 2005; Gloede and Melin, 2008; Abdel-Karim et al., 2021). The anti-scaling mechanism of action takes place through ligand exchange or electrostatic interactions (Horseman et al., 2021). Commonly used anti-scalants include organophosphates, polyelectrolytes and polyphosphates (Ketrane et al., 2009). Yin et al. (2021) evaluated gypsum anti-scaling in reverse osmosis (RO) coupled with MD using Poly (acrylic) acid (PAA). A 1,300 min test recorded 95% water flux decay in the absence of an antiscalant. However, the decay was reduced by 30% upon addition of anti-scalant, thus corresponding to 40% water recovery (Yin et al., 2021). Lin and Singer (2005) utilized polyphosphates to minimize calcite crystal growth in MD. The process performance remained stable with minimal flux decay recorded. Though anti-scalants improve MDC processes, their addition beyond maximum threshold promote membrane biofouling (Tijing et al., 2015). Therefore, the anti-scalant dosage should be optimized to meet the process requirement upon treatment of a specific feed solution.

Membrane flushing and gas bubbling

Membrane flushing and gas bubbling are classified as physical fouling mitigation strategies. Flushing is often carried out to remove adsorbed solutes from the membrane surface using deionized water. Nonetheless, flushing fails to remove solutes

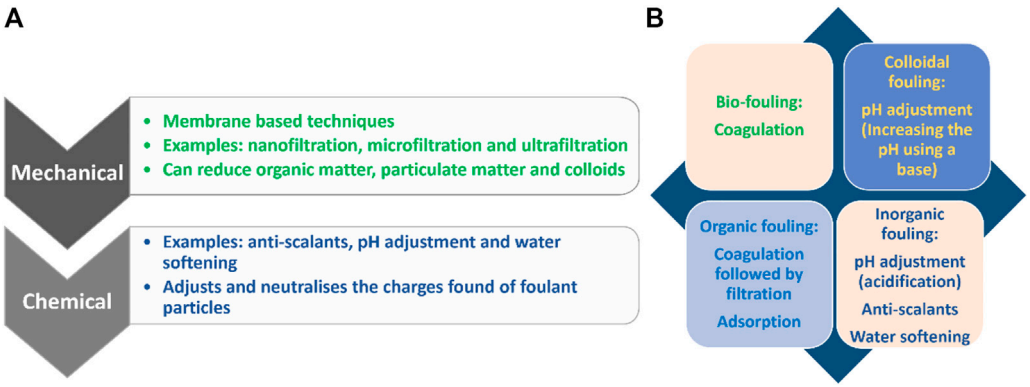

FIGURE 3
A summary of pretreatment processes in MDC **(A)** pre-treatment classifications and **(B)** process selection for specific foulant.

within the membrane pores (Alkhatib et al., 2021). Flushing is often operated in two modes namely, forward and backwashing. Technically, deionized water is pumped in a forward direction during forward flushing while the reverse is true for backflushing (Alkhatib et al., 2021). Gas bubbling enhances shear rate and fluid dynamics thus reducing temperature and concentration polarization (Alkhatib et al., 2021). Reportedly, finely dispersed bubbles are more efficient compared to course bubbles (Lu et al., 2008). Choi et al. (2020) assessed the recovery of sodium sulfate from seawater brine using a hollow fiber PVDF membrane in fractionally submerged MD crystallization. Two cleaning procedures were used, namely air backwashing and deionized water flushing in the presence of ammonium sulfate. Air backwashing enabled 90% flux recovery. Similarly, flushing recovered 82% water flux from the original level. However, multiple air backwashing caused progressive permeate flux decline (Choi et al., 2020). To reduce scaling of a commercial PTFE membrane supported on polypropylene (PP), Nghiem and Cath (2011) used MilliQ water. Five cycles of membrane flushing recovered 30% of the original flux (Nghiem and Cath, 2011). Though flushing is more efficient for removal of inorganic foulants, it can also be used for removal of organic foulants upon treatment of an oil-contaminated feed (Gryta, 2020).

Temperature adjustments and backflow

Temperature and flow reversal (backflow) techniques are novel methods used to mitigate fouling in MD/MDC. This experimental procedure was evaluated by Hickenbottom and Cath (2014) to minimize scaling while ensuring stable process performance. The temperature swap between the feed and distillate effectively reversed the driving force across the membrane, thus reducing the surface interactions between the membrane and scalants. Water flux and rejection efficiencies were recovered to 95%. Remarkably, both methods minimized scaling, thus ensuring stable fluxes and maintaining high salt rejection (Hickenbottom and Cath, 2014). Notably, these mitigation strategies avoid the use of expensive and toxic chemicals. Therefore, temperature and flow reversal are attractive alternative measures to control membrane fouling. However, extensive research is required to ascertain their sustainability at an industrial scale.

Chemical cleaning

Chemical cleaning is the most evaluated reactive measure used to control membrane fouling. The mechanism of action involves breaking foulant-membrane interactions (Alkhatib et al., 2021). Chemical reagents include acids, bases, surfactants, chelating agents, enzymes, and oxidants (Al-Amoudi and Lovitt, 2007; Porcelli and Judd, 2010). Typically, bases and surfactants are used to address organic and biofouling (Alkhatib et al., 2021; Char et al., 2021) while acids and chelating agents are true for inorganic fouling (Alkhatib et al., 2021; Gryta, 2021). To ensure a synergistic cleaning process, a combination of chemicals is generally used during the treatment of complex feed solutions characterized by various foulants (Alkhatib et al., 2021). Charfi et al. (2021) optimized cleaning procedures of the MD process during treatment of anaerobic digestate. Reportedly, deionized water flushing was followed by 0.2% NaOCl and 3% citric acid for 60 min. NaOCl and citric acid were effective for organic and inorganic foulant removal, respectively thus ensuring 75.5% flux recovery. Furthermore, the cleaning process recovered 87% of membrane hydrophobicity with minimal membrane wetting (Char et al., 2021). In another study Guillen-Burrieza et al. (2014) evaluated a variety of

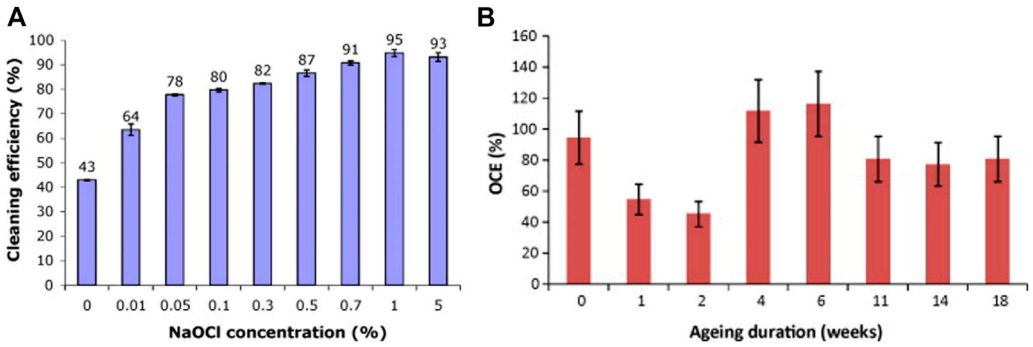

FIGURE 4
(A) Average cleaning efficiencies as a function of varying NaOCl concentrations, **(B)** overall cleaning efficiencies (OCE) observed for aged, fouled membranes (Puspitasari et al., 2010).

cleaning agents in long-term scaling control in MD processes. As per reported findings, a combination of 0.1 wt% oxalic acid and 0.8 wt% citric acid recovered 97% of the membrane WCA. Furthermore, formic, and sulfuric acid recovered 96.7% and 94.6% of the membrane WCA respectively. Although these processes restored WCA, the integrity and mechanical strength of the membranes were affected (Guillen-Burrieza et al., 2014). The destruction of membrane integrity depends on cleaning conditions including the concentration of reagents, duration, and cleaning frequency. To understand the impact of chemical cleaning pertaining to physicochemical properties, various characterization techniques should be employed. These include chemical, morphological, topological, hydrophobic/hydrophilic, and mechanical analysis of the membrane. Puspitasari et al. (2010) investigated the cleaning and ageing of PVDF membranes using oxidative sodium hypochlorite (NaOCl). The effect of chemical concentration on the cleaning and ageing of the membrane is presented in Figure 4A. The cleaning efficiency improved with an increase in NaOCl. The same trend was observed for cyclical membrane cleaning. However, following the cleaning protocol, SEM micrographs showed presence of foulants on the membrane surface. Moreover, FTIR results presented changes in the chemical functional groups of membrane, thus alluding to an ageing effect. Furthermore, higher concentrations NaOCl damaged the integrity of the membrane (Figure 4B) (Puspitasari et al., 2010). To minimize the damage, a combination of cleaning reagents and anti-scalants is commonly used. This was evaluated by Peng et al. (2015) during the MD treatment of RO concentrated brine. A series of chemicals namely, NaCl, NaOH, KCOOH, citric acid, and EDTA-4Na were used. While operating at elevated temperatures, EDTA-4Na enabled highest flux recovery. Improved recovery was associated to chelation of calcium ions, thus reducing their interactions with the membranes (Peng et al., 2015). In another study, Zhang J et al. (2021) used a combination of organic phosphoric acid and hexamethylene diamine tetra (methylene phosphonic acid) (HDTMPA) during treatment of landfill leachate in FO/MD system. A combination of these chemicals reduced the foulant-membrane interactions, thus improving the process performance. Although 90% of flux was recovered in the first cycle, continuous cleaning did not show significant increase in performance recovery (Zhang P et al., 2021).

Some foulants bind strongly on membrane surfaces, thus causing irreversible fouling. This phenomenon was reported by Naidu et al. (2015) upon NaOH cleaning MD membranes fouled by humic substances. Partial regeneration of the membrane with 19% hydrophobicity recovery was reported (Naidu et al., 2015). Further improvements in chemical cleaning involves the use of 3D spacers. Spacers amplify flow turbulence, thus reducing foulant-membrane interaction. In their study, Castillo et al. (2019) investigated a step-wise cleaning of MD membrane using citric acid and water in the presence of spacers. Upon cleaning, 87% of membrane WCA was recovered (Castillo et al., 2019). The effect of various cleaning strategies is presented in Table 4.

Membrane modification

Membrane modification improves resistance to fouling and wetting. Typically, modification is achieved through systematic manipulation. Currently, superhydrophobic membranes characterized by self-cleaning properties are explored with low success rate. To improve membrane resistance to fouling while retaining high salt rejection, omniphobic and Janus membranes are also reported (Wang and Lin, 2017; Yao et al., 2020; Tjale et al., 2022). These membranes are characterized by asymmetric wettability to minimize fouling while retaining process stability (Afsari

TABLE 4 Summary of the cleaning strategies used in various studies.

Cleaning strategy	Cleaning duration	Frequency	Effect on flux	Effect on WCA	Comments	Reference
60 min rinsing with deionized water followed by 0.2% NaOCl and 3% citric acid		Every 2 days	87% water flux was recovered	75.5% WCA was restored	Membrane was resistant to wetting	Charfi et al. (2021)
30 min rinsing with deionized water followed by 0.1 wt% oxalic acid and 0.8 wt% citric acid		—	—	126.4° compared to 129°for the unused membrane	Mechanical integrity of the membrane was reduced	Guillen-Burrieza et al. (2014)
1% NaOCl followed by 10 min rinsing with deionized		—	—	—	95% cleaning efficiency was recorded	Puspitasari et al. (2010)
60 min washing with NaOH, absolute ethanol, and pure water		—	—	—	Combined cleaning strategy was effective	Shi et al. (2022)
EDTA-4Na	—	—	—	—	Higher flux recoveries achieved at higher temperatures	Peng et al. (2015)
2.5 wt% HCl	30–70 h	—	—	—	100% flux recovery was recorded	Gryta (2007)
Deionized water rinsing and NaOH	—	—	—	Average hydrophobicity was reduced by 19%	Fouling was irreversible	Naidu et al. (2015)
Membrane modification using SiO_2-PNIPAM particles, and thermal actuation	5 and 10 min	—	—		Membrane surface free energy was reduced, thus restoring hydrophobicity	Lyly et al. (2021)
Hydraulic rinsing	—		Flux recovery of >90%	—	HDTMPA facilitated antiscaling	Zhang P et al. (2021)
0.1 wt% citric acid and deionized wate. Also, 3D Gyroid spacer was used	24 h	—	—	WCA of membranes was reduced by 13%	Acid improved cleaning process	Castillo et al. (2019)

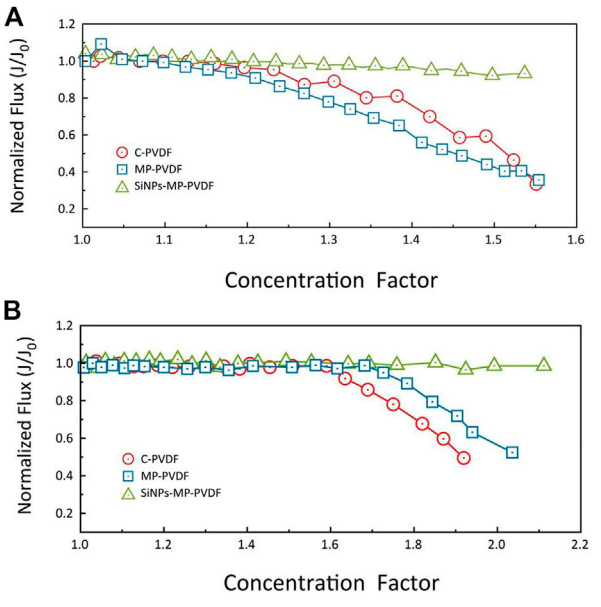

FIGURE 5
Normalized water flux (J/J_o) vs. concentration factor for the individual membranes upon evaluation of **(A)** $CaSO_4$ scaling, **(B)** casein protein organic fouling (Xiao et al., 2020).

et al., 2021). Xiao et al. (2020) prepared omniphobic membranes through incorporation of silica nanoparticles (SiNPs)-coated micropillars (MP) to PVDF. Reportedly, SiNPs-MP-PVDF membrane reduced scaling and fouling, thus maintaining the process performance over a longer period. Figure 5 1) and 2) present the role of membrane modification towards preventing flux decay.

In another study, Toh et al. (2019) modified PVDF-co-hexafluropropylene membranes using silica nanoparticles to improve their resistance to wetting and fouling. The modified membranes were characterized by high WCA and low surface energy (Toh et al., 2019). Zhang J et al. (2021) reported hydrophilic surface modification of PVDF hollow fibre membrane through co-deposition of polydopamine (PDA) and poly (MPC-co-2-aminoethyl methacrylate hydrochloride) (MPC-co-AEMA). The smooth hydrophilic thin layer reduced the foulant-membrane interaction (Zhang P et al., 2021). In addition to hydrophilic coating, antimicrobial nanoparticles are embedded on hydrophobic membranes to combat organic, inorganic and biofouling. These additives include silver nanoparticles, cellulose nanocrystals and carbon nanotubes (Nthunya et al., 2019a; Nthunya et al., 2020). Membrane modifications processes addressing fouling are presented in Table 5.

TABLE 5 Summary of various membrane modification strategies and their effects on membrane properties.

Membrane type	Membrane modification	Physical properties			Findings	Reference
		WCA (°)	LEP (bar)	Flux (kg m^{-2} h^{-1})		
Omniphobic PVDF membrane	Incorporation of silica nanoparticles	Improved from 130.1 to 175.6	—	—	Fouling resistant	Xiao et al. (2020)
Superhydrophobic PVDF-HFP)	Incorporation of silica nanoparticles	Improved from 135 to 151	—	—		Toh et al. (2019)
PVDF hollow fiber membrane	Modified with PDA and AEMA-HCl	—	Improved from 1.13 to 1.15	—	Improved fouling resistance	Zhang P et al. (2021)
Two-layer superhydrophobic PVDF membrane	Surface fluorination coating	Increased from 123.1 to 154.5	—	18% flux increase	Fouling resistant	Kharraz and An, (2020)
Superhydrophobic electrospun PVDF membrane	Electrosprayed with PDMS and silica fumes	170	—	—	Anti-abrasive and fouling resistant	Liao et al. (2020)
PFPE/PVDF	Prepared by UV-curing	162.6	—	34.2	No flux and salt rejection decay	Pan et al. (2022a)
PVDF-PDMS Janus membrane	AgNP deposition on membrane surface	Top surface: 85.62, and bottom surface: 119.7	—	Flux increased from 11.5 to 20	Improved vaporiz-ation and flux	Yue et al. (2021)
PVDF membrane	Modified with TNTs	—	—	Water flux increased by 38.7%	Improved porosity, thermal and mechanical properties	Rahmaniyan et al. (2021)
PVDF	Blended with Hyflon and PFPE	Hyflon/PV: 138.4 and PFPE/PV: 157.7	—	Hyflon/PVDF: > 28 L PFPE/ PVDF: 21	Improved permeate quality and resistant to flux decay	Pan et al. (2022b)
PVDF/PSF hollow fiber	Fluorinated	132	—	~6.0	Improved mechanical strength, anti-wettability, and water permeability	Zou et al. (2022)

Application in wastewater treatment

Membrane distillation crystallization (MDC) emerged as a promising innovation in response to the global shortage of fresh water and mineral resources. Owing to the challenges associated with industrial application, MDC is extensively tested at laboratory-scale. Various applications of MDC are summarized in Table 6. Nonetheless, process optimization with sound findings has motivated its industrial use for treatment of wastewater. For instance, Hamzah et al. (2019) reported a flux of 11.0 kg m^{-2}·hr^{-1} during the treatment of a phenolic-rich feed solution using a PVDF/TiO_2/SiO_2 composite membrane. Remarkably, TiO_2-modification improved process resistance to organic fouling (Hamzah et al., 2019). Although fouling is minimized to some extent, it remains critically challenging (Kim et al., 2017). Notably, fouled membranes attract scaling and wetting (Kim et al., 2017). Despite all these challenges, MDC is relatively versatile towards treatment of complex feed solutions. In their study, Lu et al. (2017), reported 99% water purity recovered from oil-processing wastewater. Moreover, MDC is used as a finishing process to recover minerals and freshwater (90% water recovery and 99% salt rejection) from the RO concentrate (Venzke et al., 2021). Nonetheless, treatment of the RO concentrate causes concentration polarization and scaling (Venzke et al., 2021). Interestingly, MDC does not only treat industrial wastewater but also biological waste including human urine (Zhao et al., 2013). During this treatment, 31.9%–48.6% water recovery was reported along with ammonia-nitrogen recovery and COD reduction (Zhao et al., 2013). Among other factors related to the economics of the process, MDC is driven by renewable energy sources. The use of solar energy was evaluated by Li et al. (2020) in a pilot-scale where photothermal membrane was used. Although high flux (21.99 kg m^{-2}·hr^{-1}) was reported, water recovery factors were low and production of photothermal membrane was costly (Li et al., 2020). The successes achieved at lab scale supports the implementation of this technology toward pilot and industrial scale. Memstill ® reported first pilot testing of MD technology implemented at an incineration plant in Singapore in 2006 (Dotremont et al., 2010). Other pilot studies were established at BASF in Antwerp, Belgium in 2011 (Camacho et al., 2013).

TABLE 6 Various application of MDC towards treatment of wastewater and mineral recovery.

Membrane type	Mode of application	Feed solution used	Process temperature (feed/permeate/ crystallizer) (°C)	Process flow rates	Permeate flux	Products	Reference
Commercial hollow fiber PVDF	Fractional submerged MDC	RO brine	50.0/20.1/ -	0.8 L min^{-1}	—	72% water recovery, 223.73 g Na_2SO_4	Choi et al. (2020)
Commercial hollow fiber PP	MDC	Shale gas produced water	60/20/ -	—	—	84% water recovery, salt production 2.72 kg m^{-2}·day^{-1}	Kim et al. (2018)
Hollow fiber PP	VMD-crystallization	Wastewater from oil extraction	55–75/10/ -	—	—	99% water purity, NaCl and ethylene glycol	Lu et al. (2017)
Commercial PVDF	DCMD - MDC	2 M concentrated Na_2SO_4	40–70/25/variable	2 L h^{-1}	—	80% water recovery, 100 kg m^{-3} Na_2SO_4	Bouchrit et al. (2017)
PTFE	MD/MDC	Synthetic shale gas produced water	60/20/40	25 cm s^{-1}	—	62.5% water recovery and NaCl, $BaCl_2$, and $CaCO_3$	Kim et al. (2017)
Microporous PTFE plate membrane	VMD	Human urine	50–70/ -/ -	30 L h^{-1}	—	31.9–48.6% water recovery	Zhao et al. (2013)
Fe_3O_4—PVDF—co-hexafluoropropylene nanofibers	Solar driven MD	Synthetic NaCl solution	-/20/ -	20 ml min^{-1}	0.97 kg m^{-2} h^{-1}	Salt rejection of 99.99%	Li et al. (2020)
Cloisite 15 -modified PVDF hollow fiber membrane	MDC	26.4 wt% NaCl solution	70/ -/25	—	—	34 kg NaCl was produced per m^3 of feed	Edwie and Chung (2013)
PTFE, standard PE (PE—S) and oleophobic PE (PE—O)	DCMD	RO concentrates from petrochemical wastewater	60/20	—	PE—O = 5.0 kg m^{-2}·h^{-1}, PE—S = 2.1 kg m^{-2}·h^{-1} and PTFE reduced by 30% of initial flux after 250 h	Recoveries close to 90% and rejection rates >99.5%	Venzke et al. (2021)
PVDF blended with multi-walled carbon nanotubes	DCMD	35 g L^{-1} synthetic NaCl solution	82/20/ -	48 ml min^{-1}	9.5×10^{-3} kg m^{-2} s^{-1}	Salt rejection of 100% after 60 min	Silva et al. (2015)
PVDF/TiO_2/SiO_2	DCMD	A phenolic-rich solution containing surfactant	40/20/-	300 ml min^{-1}	11.0 kg m^{-2}·h^{-1} after 8 h	99.9% gallic acid rejection with a flux decay resistance	Hamzah et al. (2019)
Commercial PP and hollow fiber PVDF	DCMD	Wastewater produced from oil and gas production	35,45,55/10/-	Feed: 150 ml min^{-1} and permeate: 70 ml min^{-1}	Increased flux as a function of temperature	NaCl purity: > 99.9%, water and NaCl recovery: 37% and 16 kg m^{-3} respectively	Ali et al. (2015)

Conclusion and future perspectives

MDC addresses financial challenges affecting developing countries. Various literature reports have documented the successes of this technique in effectively recovering freshwater and mineral salts from a myriad of wastewater feed sources (Quist-Jensen et al., 2016, 2017; Kim et al., 2017; Choi et al., 2020). In conjunction to emerging laboratory-scale studies, implementation of pilot studies at an industrial platform provides a promising trajectory for the future of this technology. Nevertheless, membrane fouling, and wetting requires special attention. Membrane fouling can be classified into organic, inorganic (i.e., scaling), biofouling, and/or colloidal fouling. In some circumstances, a combination of foulants may exist in the feed solutions thus resulting in more complex membrane fouling scenarios. To circumvent these issues, various fouling control measures have been registered including mechanical pre-treatment options such as microfiltration (MF) and nanofiltration

(NF). Other pre-treatment strategies include anti-scalants, temperature adjustments, and membrane flushing. Moreover, chemical cleaning has been extensively evaluated to restore MDC performance. While commercial membranes have be used for MDC processes, further research has been directed towards synthesis and modification of various fouling resistant membranes. This includes incorporation of nanoparticles to induce self-cleaning through superhydrophicity enhancement (i.e., improving the lotus effect of the membrane). Similarly, Janus membranes characterized by asymmetric wettability have been evaluated to mitigate membrane fouling. The steady development in this technique and its accompanying components has probed further interest into its applicative potential. Promising feedback established with the use of this technique pave the way towards further implementation in an industrial setting for mineral and water recycling. Future perspectives include, though not limited to:

- Production of membranes using environmentally friendly reagents in addressing membrane fouling and wetting.
- Optimization of membrane cleaning strategies towards a feasible industrial application.
- Further research and implementation of pilot-scale studies to provide a realistic MDC suitability in industrial application.
- Further research establishing fouling mechanism is required to understand membrane longevity and process performance.

Author contributions

IC: Investigation; Methodology; Validation; Roles/Writing—original draft. LN: Conceptualization; Data curation; Formal analysis; Funding acquisition; Resources; Writing—review and editing. HR: Conceptualization; Funding acquisition; Project administration; Resources; Supervision; Writing—review and editing. CQ-J: Software; Visualization; Writing—review, editing and funding acqusition.

Funding

The authors would like to thank the University of the Witwatersrand, Aalborg University, Danish International Development Agency (Grant number: DANIDA1) and National Research Foundation (NRF-grant number: 132724) for funding this research work.

Conflict of interest

The authors declare that the research was conducted in the absence of any commercial or financial relationships that could be construed as a potential conflict of interest.

Publisher's note

All claims expressed in this article are solely those of the authors and do not necessarily represent those of their affiliated organizations, or those of the publisher, the editors and the reviewers. Any product that may be evaluated in this article, or claim that may be made by its manufacturer, is not guaranteed or endorsed by the publisher.

References

Abdel-Karim, A., Leaper, S., Skuse, C., Zaragoza, G., Gryta, M., and Gorgojo, P. (2021). Membrane cleaning and pretreatments in membrane distillation – A review. *Chem. Eng. J.* 422, 129696. doi:10.1016/j.cej.2021.129696

Afsari, M., Shon, H. K., and Tijing, L. D. (2021). Janus membranes for membrane distillation: Recent advances and challenges. *Adv. Colloid Interface Sci.* 289, 102362. doi:10.1016/j.cis.2021.102362

Ahmed, F. E., Hashaikeh, R., and Hilal, N. (2020). Hybrid technologies: The future of energy efficient desalination – a review. *Desalination* 495, 114659. doi:10.1016/j.desal.2020.114659

Al-Amoudi, A., and Lovitt, R. W. (2007). Fouling strategies and the cleaning system of NF membranes and factors affecting cleaning efficiency. *J. Membr. Sci.* 303 (1–2), 4–28. doi:10.1016/j.memsci.2007.06.002

Ali, A., Quist-Jensen, C. A., Drioli, E., and Macedonio, F. (2018). Evaluation of integrated microfiltration and membrane distillation/crystallization processes for produced water treatment. *Desalination* 434, 161–168. doi:10.1016/j.desal.2017.11.035

Ali, A., Quist-Jensen, C., Macedonio, F., and Drioli, E. (2015). Application of membrane crystallization for minerals' recovery from produced water. *Membranes* 5, 772–792. doi:10.3390/membranes5040772

Alkhatib, A., Ayari, M. A., and Hawari, A. H. (2021). Fouling mitigation strategies for different foulants in membrane distillation. *Chem. Eng. Process. - Process Intensif.* 167, 108517. doi:10.1016/j.cep.2021.108517

Alvarez, R., Nievergelt, P. P., Slyshkina, E., Muller, P., Alberto, R., and Spingler, B. (2020). Single crystal growth of water-soluble metal complexes with the help of the nano-crystallization method. *Dalton Trans.* 49 (28), 9632–9640. doi:10.1039/d0dt01236j

Attia, H., Osman, M. S., Johnson, D. J., Wright, C., and Hilal, N. (2017). Modelling of air gap membrane distillation and its application in heavy metals removal. *Desalination* 424, 27–36. doi:10.1016/j.desal.2017.09.027

Banat, F. A., and Simandl, J. (1998). Desalination by membrane distillation: A parametric study. *Sep. Sci. Technol.* 33 (2), 201–226. doi:10.1080/01496399808544764

Bouchrit, R., Boubakri, A., Mosbahi, T., Hafiane, A., and Bouguecha, S. A. T. (2017). Membrane crystallization for mineral recovery from saline solution: Study case Na2SO4 crystals. *Desalination* 412, 1–12. doi:10.1016/j.desal.2017.02.021

Camacho, L. M., Dumee, L., Zhang, J., Li, J. d., Duke, M., Gomez, J., et al. (2013). Advances in membrane distillation for water desalination and purification applications. *Water* 5 (1), 94–196. doi:10.3390/w5010094

Castillo, E. H. C., Thomas, N., Al-Ketan, O., Rowshan, R., Abu Al-Rub, R. K., Nghiem, L. D., et al. (2019). 3D printed spacers for organic fouling mitigation in membrane distillation. *J. Membr. Sci.* 581, 331–343. doi:10.1016/j.memsci.2019.03.040

Char, A., Kim, S., Yoon, Y., and Cho, J. (2021). Optimal cleaning strategy to alleviate fouling in membrane distillation process to treat anaerobic digestate. *Chemosphere* 279, 130524. doi:10.1016/j.chemosphere.2021.130524

Choi, Y., Naidu, G., Lee, S., and Vigneswaran, S. (2020). Recovery of sodium sulfate from seawater brine using fractional submerged membrane distillation crystallizer. *Chemosphere* 238, 124641. doi:10.1016/j.chemosphere.2019.124641

Choudhury, M. R., Anwar, N., Jassby, D., and Rahaman, M. S. (2019). Fouling and wetting in the membrane distillation driven wastewater reclamation process – a review. *Adv. Colloid Interface Sci.* 269, 370–399. doi:10.1016/j.cis.2019.04.008

Das, P., Dutta, S., and Kumar, K. (2021). Insights into membrane crystallization : A sustainable tool for value added product recovery from effluent streams. *Sep. Purif. Technol.* 257, 117666. doi:10.1016/j.seppur.2020.117666

Dotremont, C., Kregersman, B., Sih, R., Lai, K. C., Koh, K., and Seah, H. (2010). Seawater desalination with memstill technology - a sustainable solution for the industry. *Water Pract. Technol.* 5 (2), 1–7. doi:10.2166/wpt.2010.026

Drioli, E., Ali, A., and Macedonio, F. (2015). Membrane distillation: Recent developments and perspectives. *Desalination* 356, 56–84. doi:10.1016/j.desal.2014.10.028

Drioli, E., Profio, G. D., and Curcio, E. (2012). Progress in membrane crystallization. *Curr. Opin. Chem. Eng.* 1 (2), 178–182. doi:10.1016/j.coche.2012.03.005

Edwie, F., and Chung, T.-S. (2013). Development of simultaneous membrane distillation–crystallization (SMDC) technology for treatment of saturated brine. *Chem. Eng. Sci.* 98, 160–172. doi:10.1016/j.ces.2013.05.008

El-Abbassi, A., Hafidi, A., Khayet, M., and Garcia-Payo, M. (2013). Integrated direct contact membrane distillation for olive mill wastewater treatment. *Desalination* 323, 31–38. doi:10.1016/j.desal.2012.06.014

Gloede, M., and Melin, T. (2008). Physical aspects of membrane scaling. *Desalination* 224 (1–3), 71–75. doi:10.1016/j.desal.2007.02.081

Gryta, M. (2007). Influence of polypropylene membrane surface porosity on the performance of membrane distillation process. *J. Membr. Sci.* 287 (1), 67–78. doi:10.1016/j.memsci.2006.10.011

Gryta, M. (2020). Separation of saline oily wastewater by membrane distillation. *Chem. Pap.* 74 (7), 2277–2286. doi:10.1007/s11696-020-01071-y

Gryta, M. (2021). Surface modification of polypropylene membrane by helium plasma treatment for membrane distillation. *J. Membr. Sci.* 628, 119265. doi:10.1016/j.memsci.2021.119265

Guillen-Burrieza, E., Ruiz-Aguirre, A., Zaragoza, G., and Arafat, H. A. (2014). Membrane fouling and cleaning in long term plant-scale membrane distillation operations. *J. Membr. Sci.* 468, 360–372. doi:10.1016/j.memsci.2014.05.064

Hamzah, N., Leo, C. P., and Ooi, B. S. (2019). Superhydrophobic PVDF/TiO2-SiO2 membrane with hierarchical roughness in membrane distillation for water recovery from phenolic rich solution containing surfactant. *Chin. J. Polym. Sci.* 37, 609–616. doi:10.1007/s10118-019-2235-y

Hickenbottom, K. L., and Cath, T. Y. (2014). Sustainable operation of membrane distillation for enhancement of mineral recovery from hypersaline solutions. *J. Membr. Sci.* 454, 426–435. doi:10.1016/j.memsci.2013.12.043

Horseman, T., Yin, Y., Christie, K. S., Wang, Z., and Tong, T. (2021). Wetting, scaling, and fouling in membrane distillation: State-of-the-Art insights on fundamental mechanisms and mitigation strategies. *ACS Est. Eng.* 1 (1), 117–140. doi:10.1021/acsestengg.0c00025

Husnain, T., Liu, Y., Riffat, R., and Mi, B. (2015). Integration of forward osmosis and membrane distillation for sustainable wastewater reuse. *Sep. Purif. Technol.* 156, 424–431. doi:10.1016/j.seppur.2015.10.031

Karakulski, K., and Gryta, M. (2005). Water demineralisation by NF/MD integrated processes. *Desalination* 177, 109–119. doi:10.1016/j.desal.2004.11.018

Kargari, A., and Yousefi, A. (2021). Process intensification through magnetic treatment of seawater for production of drinking water by membrane distillation process: A novel approach for commercialization membrane distillation process. *Chem. Eng. Process. - Process Intensif.* 167, 108543. doi:10.1016/j.cep.2021.108543

Ketrane, R., Saidani, B., Gil, O., Leleyter, L., and Baraud, F. (2009). Efficiency of five scale inhibitors on calcium carbonate precipitation from hard water: Effect of temperature and concentration. *Desalination* 249 (3), 1397–1404. doi:10.1016/j.desal.2009.06.013

Kharraz, J. A., and An, A. K. (2020). Patterned superhydrophobic polyvinylidene fluoride (PVDF) membranes for membrane distillation: Enhanced flux with improved fouling and wetting resistance. *J. Membr. Sci.* 595, 117596. doi:10.1016/j.memsci.2019.117596

Kim, J., Kim, J., and Hong, S. (2018). Recovery of water and minerals from shale gas produced water by membrane distillation crystallization. *Water Res.* 129, 447–459. doi:10.1016/j.watres.2017.11.017

Kim, J., Kwon, H., Lee, S., Lee, S., and Hong, S. (2017). Membrane distillation (MD) integrated with crystallization (MDC) for shale gas produced water (SGPW) treatment. *Desalination* 403, 172–178. doi:10.1016/j.desal.2016.07.045

Laqbaqbi, M., Sanmartino, J., Khayet, M., Garcia-Payo, C., and Chaouch, M. (2017). Fouling in membrane distillation, osmotic distillation and osmotic membrane distillation. *Appl. Sci.* 7 (4), 334. doi:10.3390/app7040334

Li, J., Wu, J., Sun, H., Cheng, F., and Liu, Y. (2016). Advanced treatment of biologically treated coking wastewater by membrane distillation coupled with pre-coagulation. *Desalination* 380, 43–51. doi:10.1016/j.desal.2015.11.020

Li, W., Chen, Y., Yao, L., Ren, X., Li, Y., and Deng, L. (2020). Fe3O4/PVDF-HFP photothermal membrane with *in-situ* heating for sustainable, stable and efficient pilot-scale solar-driven membrane distillation. *Desalination* 478, 114288. doi:10.1016/j.desal.2019.114288

Liao, Y., Zheng, G., Huang, J. J., Tian, M., and Wang, R. (2020). Development of robust and superhydrophobic membranes to mitigate membrane scaling and fouling in membrane distillation. *J. Membr. Sci.* 601, 117962. doi:10.1016/j.memsci.2020.117962

Lin, Y. P., and Singer, P. C. (2005). Inhibition of calcite crystal growth by polyphosphates. *Water Res.* 39 (19), 4835–4843. doi:10.1016/j.watres.2005.10.003

Liu, G., Liu, J., Dunn, A. S., Nadazdy, P., Siffalovic, P., Resel, R., et al. (2021). Directional crystallization from the melt of an organic p-type and n-type semiconductor blend. *Cryst. Growth & Des.* 21 (9), 5231–5239. doi:10.1021/acs.cgd.1c00570

Liu, J., Albdoor, A. K., Lin, W., Hai, F. I., and Ma, Z. (2022). Membrane fouling in direct contact membrane distillation for liquid desiccant regeneration: Effects of feed temperature and flow velocity. *J. Membr. Sci.* 642, 119936. doi:10.1016/j.memsci.2021.119936

Lokare, O. R., Tavakkoli, S., Khanna, V., and Vidic, R. D. (2018). Importance of feed recirculation for the overall energy consumption in membrane distillation systems. *Desalination* 428, 250–254. doi:10.1016/j.desal.2017.11.037

Lu, D., Li, P., Xiao, W., He, G., and Jiang, X. (2017). Simultaneous recovery and crystallization control of saline organic wastewater by membrane distillation crystallization. *AIChE J.* 63, 2187–2197. doi:10.1002/aic.15581

Lu, Y., Ding, Z., Liu, L., and Wang, Z. (2008). The influence of bubble characteristics on the performance of submerged hollow fiber membrane module used in microfiltration. *Sep. Purif. Technol.* 61, 89–95. doi:10.1016/j.seppur.2007.09.019

Lyly, L. H. T., Chang, Y., Ng, W., Lim, J., Derek, C., and Ooi, B. (2021). Development of membrane distillation by dosing SiO2-PNIPAM with thermal cleaning properties via surface energy actuation. *J. Membr. Sci.* 636, 119193. doi:10.1016/j.memsci.2021.119193

Martínez, L. (2004). Comparison of membrane distillation performance using different feeds. *Desalination* 168 (1–3), 359–365. doi:10.1016/j.desal.2004.07.022

Mekonnen, M. M., and Hoekstra, A. Y. (2016). Four billion people facing severe water scarcity. *Sci. Adv.* 2 (2), e1500323–e1500327. doi:10.1126/sciadv.1500323

Mpala, T. J., Etale, A., Richards, H., and Nthunya, L. N. (2022). Biofouling phenomena in membrane distillation : Mechanisms and mitigation strategies. *Environ. Sci. Adv.* doi:10.1039/d2va00161f

Naidu, G., Jeong, S., and Vigneswaran, S. (2015). Interaction of humic substances on fouling in membrane distillation for seawater desalination. *Chem. Eng. J.* 262, 946–957. doi:10.1016/j.cej.2014.10.060

Nghiem, L. D., and Cath, T. (2011). A scaling mitigation approach during direct contact membrane distillation. *Sep. Purif. Technol.* 80 (2), 315–322. doi:10.1016/j.seppur.2011.05.013

Nthunya, L. N., Bopape, M. F., Mahlangu, O. T., Mamba, B. B., Van der Bruggen, B., Quist-Jensen, C. A., et al. (2022). Fouling, performance and cost analysis of membrane-based water desalination technologies: A critical review. *J. Environ. Manag.* 301, 113922. doi:10.1016/j.jenvman.2021.113922

Nthunya, L. N., Gutierrez, L., Derese, S., Edward, N., Verliefde, A. R., Mamba, B. B., et al. (2019a). A review of nanoparticle-enhanced membrane distillation membranes : Membrane synthesis and applications in water treatment. *J. Chem. Technol. Biotechnol.* 94 (9), 2757–2771. doi:10.1002/jctb.5977

Nthunya, L. N., Gutierrez, L., Derese, S., Mamba, B. B., Verliefde, A. R., and Mhlanga, S. D. (2019b). Adsorption of phenolic compounds by polyacrylonitrile nano fibre membranes : A pretreatment for the removal of hydrophobic bearing compounds from water. *J. Environ. Chem. Eng.* 7, 103254. doi:10.1016/j.jece.2019.103254

Nthunya, L. N., Gutierrez, L., Lapeire, L., Verbeken, K., Zaouri, N., Nxumalo, E. N., et al. (2019c). Fouling resistant PVDF nanofibre membranes for the desalination of brackish water in membrane distillation. *Sep. Purif. Technol.* 228, 115793. doi:10.1016/j.seppur.2019.115793

Nthunya, L. N., Gutierrez, L., Nxumalo, E. N., Verliefde, A. R., Mhlanga, S. D., and Onyango, M. S. (2020). f-MWCNTs/AgNPs-coated superhydrophobic PVDF nanofibre membrane for organic, colloidal, and biofouling mitigation in direct contact membrane distillation. *J. Environ. Chem. Eng.* 8 (2), 103654. doi:10.1016/j.jece.2020.103654

Nthunya, L. N., Mbakop, S., and Mhlanga, S. D. (2021). "Emerging nanoenhanced membrane-based hybrid processes for complex industrial wastewater treatment," in *Membrane-based hybrid processes for wastewater treatment* (Netherlands: Elsevier B.V), 633–656. doi:10.1016/B978-0-12-823804-2.00024-0

Pan, J., Chen, M., Xu, X., Sun, S. P., Wang, Z., Cui, Z., et al. (2022a). Enhanced anti-wetted PVDF membrane for pulping RO brine treatment by vacuum membrane distillation. *Desalination* 526, 115533. doi:10.1016/j.desal.2021.115533

Pan, J., Zhang, F., Wang, Z., Sun, S. P., Cui, Z., Jin, W., et al. (2022b). Enhanced anti-wetting and anti-fouling properties of composite PFPE/PVDF membrane in vacuum membrane distillation. *Sep. Purif. Technol.* 282, 120084. doi:10.1016/j.seppur.2021.120084

Peng, Y., Ge, J., Li, Z., and Wang, S. (2015). Effects of anti-scaling and cleaning chemicals on membrane scale in direct contact membrane distillation process for RO brine concentrate. *Sep. Purif. Technol.* 154, 22–26. doi:10.1016/j.seppur.2015.09.007

Porcelli, N., and Judd, S. (2010). Chemical cleaning of potable water membranes: A review. *Sep. Purif. Technol.* 71 (2), 137–143. doi:10.1016/j.seppur.2009.12.007

Pramanik, B. K., Shu, L., and Jegatheesan, V. (2017). A review of the management and treatment of brine solutions. *Environ. Sci. Water Res. Technol.* 3, 625–658. doi:10.1039/C6EW00339G

Pramanik, B. K., Thangavadivel, K., Shu, L., and Jegatheesan, V. (2016). A critical review of membrane crystallization for the purification of water and recovery of minerals. *Rev. Environ. Sci. Biotechnol.* 15, 411–439. doi:10.1007/s11157-016-9403-0

Puspitasari, V., Granville, A., Le-Clech, P., and Chen, V. (2010). Cleaning and ageing effect of sodium hypochlorite on polyvinylidene fluoride (PVDF) membrane. *Sep. Purif. Technol.* 72 (3), 301–308. doi:10.1016/j.seppur.2010.03.001

Quist-Jensen, C. A., Ali, A., Drioli, E., and Macedonio, F. (2019). Perspectives on mining from sea and other alternative strategies for minerals and water recovery – the development of novel membrane operations. *J. Taiwan Inst. Chem. Eng.* 94, 129–134. doi:10.1016/j.jtice.2018.02.002

Quist-Jensen, C. A., Ali, A., Mondal, S., Macedonio, F., and Drioli, E. (2016). A study of membrane distillation and crystallization for lithium recovery from high-concentrated aqueous solutions. *J. Membr. Sci.* 505, 167–173. doi:10.1016/j.memsci.2016.01.033

Quist-Jensen, C. A., Macedonio, F., Horbez, D., and Drioli, E. (2017). Reclamation of sodium sulfate from industrial wastewater by using membrane distillation and membrane crystallization. *Desalination* 401, 112–119. doi:10.1016/j.desal.2016.05.007

Rahmaniyan, B., Mohammadi, T., and Tofighy, M. A. (2021). Development of high flux PVDF/modified TNTs membrane with improved properties for desalination by vacuum membrane distillation. *J. Environ. Chem. Eng.* 9 (6), 106730. doi:10.1016/j.jece.2021.106730

Ramos, R. L., Lebron, Y. A., Moreira, V. R., Martins, M. F., Santos, L. V., and Amaral, M. C. (2022). Direct contact membrane distillation as an approach for water treatment with phenolic compounds. *J. Environ. Manag.* 303, 114117. doi:10.1016/j.jenvman.2021.114117

Rudolph, P. (2010). "Defect Formation during crystal growth from the melt," in *Springer handbook of crystal growth*. 1st edn. (Berlin: Springer), 159–201. doi:10.1007/978-3-540-74761-1_6

Ruiz Salmón, I., and Luis, P. (2018). Membrane crystallization via membrane distillation. *Chem. Eng. Process. - Process Intensif.* 123, 258–271. doi:10.1016/j.cep.2017.11.017

Shi, W., Tian, Y., Li, H., Fan, M., Zhang, H., et al. (2022). An innovative hollow fiber vacuum membrane distillation-crystallization (VMDC) coupling process for dye house effluent separation to reclaim fresh water and salts. *J. Clean. Prod.* 337, 130586. doi:10.1016/j.jclepro.2022.130586

Silva, T. L. S., Morales-Torres, S., Figueiredo, J. L., and Silva, A. M. (2015). Multi-walled carbon nanotube/PVDF blended membranes with sponge- and finger-like pores for direct contact membrane distillation. *Desalination* 357, 233–245. doi:10.1016/j.desal.2014.11.025

Srisurichan, S., Jiraratananon, R., and Fane, A. G. (2006). Mass transfer mechanisms and transport resistances in direct contact membrane distillation process. *J. Membr. Sci.* 277 (1–2), 186–194. doi:10.1016/j.memsci.2005.10.028

Swaminathan, J., and Lienhard, J. H. (2018). Design and operation of membrane distillation with feed recirculation for high recovery brine concentration. *Desalination* 445, 51–62. doi:10.1016/j.desal.2018.07.018

Tijing, L. D., Woo, Y. C., Choi, J. S., Lee, S., Kim, S. H., and Shon, H. K. (2015). Fouling and its control in membrane distillation-A review. *J. Membr. Sci.* 475, 215–244. doi:10.1016/j.memsci.2014.09.042

Tjale, L., Richards, H., Mahlangu, O., and Nthunya, L. N. (2022). Silica nanoparticle modified polysulfone/polypropylene membrane for separation of oil-water emulsions. *Results Eng.* 16, 100623. doi:10.1016/j.rineng.2022.100623

Toh, M. J., Oh, P. C., Chew, T. L., and Ahmad, A. L. (2019). Antiwettability enhancement of PVDF-HFP membrane via superhydrophobic modification by SiO2 nanoparticles. *Comptes Rendus Chim.* 22 (5), 369–372. doi:10.1016/j.crci.2019.05.004

Venzke, C. D., Rizzana, D., Giacobbo, A., Rodrigues, M., and Bernardes, A. (2021). Membrane distillation treating a real petrochemical reverse osmosis concentrate: Influence of membrane characteristics on the process performance. *J. Water Process Eng.* 39, 101722. doi:10.1016/j.jwpe.2020.101722

Wagstaff, F. E., Brown, S. D., and Cutler, I. (1964). The influence of H2O and O2 atmospheres on the crystallisation of vitreous silica. *Phys. Chem. Glasses* 5 (3), 76–81.

Wang, Z., and Lin, S. (2017). Membrane fouling and wetting in membrane distillation and their mitigation by novel membranes with special wettability. *Water Res.* 112, 38–47. doi:10.1016/j.watres.2017.01.022

Xiao, Z., Guo, H., He, H., Liu, Y., Li, X., Zhang, Y., et al. (2020). Unprecedented scaling/fouling resistance of omniphobic polyvinylidene fluoride membrane with silica nanoparticle coated micropillars in direct contact membrane distillation. *J. Membr. Sci.* 599, 117819. doi:10.1016/j.memsci.2020.117819

Yadav, A., Labhasetwar, P. K., and Shahi, V. K. (2022). Membrane distillation crystallization technology for zero liquid discharge and resource recovery: Opportunities, challenges and futuristic perspectives. *Sci. Total Environ.* 806, 150692. doi:10.1016/j.scitotenv.2021.150692

Yao, M., Tijing, L. D., Naidu, G., Kim, S. H., Matsuyama, H., Fane, A. G., et al. (2020). A review of membrane wettability for the treatment of saline water deploying membrane distillation. *Desalination* 479, 114312. doi:10.1016/j.desal.2020.114312

Yin, Y., Kalam, S., Livingston, J. L., Minjarez, R., Lee, J., et al. (2021). The use of anti-scalants in gypsum scaling mitigation: Comparison with membrane surface modification and efficiency in combined reverse osmosis and membrane distillation. *J. Membr. Sci.* 643, 120077. doi:10.1016/j.memsci.2021.120077

Yue, D., Wang, Y., Zhang, H., Sun, D., Ye, X., et al. (2021). A novel silver/activated - polyvinylidene fluoride - polydimethyl siloxane hydrophilic-hydrophobic Janus membrane for vacuum membrane distillation and its anti-oil-fouling ability. *J. Membr. Sci.* 638, 119718. doi:10.1016/j.memsci.2021.119718

Zhang, J., Wang, D., Chen, Y., Gao, B., and Wang, Z. (2021). Scaling control of forward osmosis-membrane distillation (FO-MD) integrated process for pre-treated landfill leachate treatment. *Desalination* 520, 115342. doi:10.1016/j.desal.2021.115342

Zhang, P., Liu, W., Rajabzadeh, S., Jia, Y., Shen, Q., Fang, C., et al. (2021). Modification of PVDF hollow fiber membrane by co-deposition of PDA/MPC-co-AEMA for membrane distillation application with anti-fouling and anti-scaling properties. *J. Membr. Sci.* 636, 119596. doi:10.1016/j.memsci.2021.119596

Zhao, Z. P., Xu, L., Shang, X., and Chen, K. (2013). Water regeneration from human urine by vacuum membrane distillation and analysis of membrane fouling characteristics. *Sep. Purif. Technol.* 118, 369–376. doi:10.1016/j.seppur.2013.07.021

Zhu, Z., Tan, G., Lei, D., Yang, Q., Tan, X., Liang, N., et al. (2021). Omniphobic membrane with process optimization for advancing flux and durability toward concentrating reverse-osmosis concentrated seawater with membrane distillation. *J. Membr. Sci.* 639, 119763. doi:10.1016/j.memsci.2021.119763

Zou, D., Kim, H. W., Jeon, S. M., and Lee, Y. M. (2022). Fabrication and modification of PVDF/PSF hollow-fiber membranes for ginseng extract and saline water separations via direct contact membrane distillation. *J. Membr. Sci.* 644, 120101. doi:10.1016/j.memsci.2021.120101

frontiers | Frontiers in Chemical Engineering

TYPE Mini Review
PUBLISHED 29 November 2022
DOI 10.3389/fceng.2022.1059305

OPEN ACCESS

EDITED BY
Rafael Luque,
University of Cordoba, Spain

REVIEWED BY
Guoyong Song,
Beijing Forestry University, China

*CORRESPONDENCE
Hemant Choudhary,
hchoudhary@lbl.gov

SPECIALTY SECTION
This article was submitted to Sustainable Process Engineering, a section of the journal Frontiers in Chemical Engineering

RECEIVED 01 October 2022
ACCEPTED 31 October 2022
PUBLISHED 29 November 2022

CITATION
Jassal V, Dou C, Sun N, Singh S, Simmons BA and Choudhary H (2022), Finding values in lignin: A promising yet under-utilized component of the lignocellulosic biomass.
Front. Chem. Eng. 4:1059305.
doi: 10.3389/fceng.2022.1059305

Finding values in lignin: A promising yet under-utilized component of the lignocellulosic biomass

Vidhisha Jassal[1], Chang Dou[2,3], Ning Sun[2,3], Seema Singh[4,5], Blake A. Simmons[4,3] and Hemant Choudhary[4,5]*

[1]BASIS.ed Texas, Pflugerville, TX, United States, [2]Advanced Biofuels and Bioproducts Process Development Unit (ABPDU), Lawrence Berkeley National Laboratory, Emeryville, CA, United States, [3]Biological Systems and Engineering Division, Lawrence Berkeley National Laboratory, Berkeley, CA, United States, [4]Deconstruction Division, Joint BioEnergy Institute, Emeryville, CA, United States, [5]Department of Bioresource and Environmental Security, Sandia National Laboratories, Livermore, CA, United States

This article outlines the technical and economic potentials of lignin in unlocking sustainable biorefineries. The benefits of using this highly functionalized biopolymer for the growth of sustainable economy have been highlighted. But practically, the possibility of commercially substituting petroleum oil with lignin is still not very high as the estimated biofuel production cost is 2–3 times higher than the former one. However, with the advancement in technology and more efficient measures by biorefineries such as storing and processing the biomass near the field so as to reduce the transportation cost, it is possible to gain higher profits. Companies like Domtar, Stora Enso, Borregaard's LignoTech, VITO, and Chemelot InSciTe have been promoting commercial value of lignin. The growth of lignin market after the start-up production at various sites has been discussed in this review. Combining the complete "start-to-finish" analysis with economic evaluation gives a pragmatic overview of the possibilities whether lignin will join petroleum oil as an efficient and cost-effective renewable source.

KEYWORDS

ligno cellulose, valorization, commercial and industrial, biorefinery and bioeconomy, material and process optimization, biofuel, bioproduct

Introduction

The past decade has been quite interesting in terms of dealing with chemicals, energy and renewable resources—especially lignocellulosic biomass. The major raw materials for transportation, energy and chemicals in the latter half of the 20th century has been mainly the "crude" or "petroleum" oil. Processing crude oil has always been a chief task and technologies have been developing since 1860s for the same. Currently, several refineries/industrial plants have been developed that are highly advanced including hi-tech integrated devices (Babich and Moulijn 2003; Rana et al., 2007). Due to limited

technical maturity of lignocellulosic biomass-based processes thus far, the chemical industries were obligated to depend on petroleum, coal, or natural gas feedstocks as the carbon source to produce nearly 90% carbon containing plastics, paints, adhesives, fertilizers, pesticides, among others. The reliance on fossil fuel to accomplish every single need of the modern industrialized society could be attractive until "peak-oil" is reached, as indicated by Hubbert's in 1956 that the petroleum oil will not last forever (Hubbert 1956; Sorrell et al., 2010; Aleklett et al., 2010; de Almeida and Silva 2009). Studies have anticipated over 60% energy demand by 2030 owing to the increasing world population (Kumarasamy et al., 2017). This raises an alarming question of how are we going to meet this additional energy requirement when we have already been struggling with depleting fossil fuel resources today? In order to meet these huge energy requirements throughout the world, nearly 85 million barrels of crude oil is being processed currently, which are expected to increase to 116 million barrels in the next decade (IEA 2007). It is only after the public awareness about the depletion of crude oil reserves that federal agencies around the globe paid significant attention to find substitutes for fossil fuels (Maggio and Cacciola 2012). This change is highly imperative for the development of sustainable economy. In order to achieve this target, "biorefineries" are envisaged as highly significant since they convert biomass into biodiesel, bioethanol, and value-added chemicals (Sun and Cheng 2002; Kiss et al., 2006). So, is it true that we are shifting gears from petroleum refineries to biorefineries? This move towards biorefineries is "born from necessity" as we did not have many options but to switch to alternative source of energy due to the limited available reserves of non-renewable sources. Worldwide, renewable resources contributed to nearly 19% of the total energy consumption in 2014 (compared to ~38%, 21%, 20%, and 2% from oil, coal, natural gas, and nuclear, respectively) and is expected to increase dramatically in the coming decades (World Bioenergy Statistics, 2017).

Remarkably, in this revolutionizing world, not only the growth of bio-economy (involving natural feedstocks) has been a great achievement, but also the society's attitude towards the utilization of renewables such as lignocellulosic biomass as source of energy has changed significantly (UNECE, 2021). For instance, in contrast to the fossil resources, lignocelluloses have lower carbon footprints in addition to its abundance and rapid rate of growth under varied climatic conditions (Therasame, et al., 2022; Awosusi, et al., 2022, Hadj 2021). The holocellulosic component of lignocelluloses have been successfully converted into fuels and commodities, but lignin, on the other hand, has been underutilized (Tuck et al., 2012). In order to attain a sustainable bio-refinery, lignin must be processed and valorized through a biorefining process that is cost-effective and environment friendly (Zakzeski et al., 2010). Typically, bio-economy aims to (a) decrease dependency on fossil fuels that are non-renewable, (b) prevent deprivation of ecosystems, (c) promote economic development of the country, and (d) create new jobs.

Lignin: Emerging petroleum-substitute?

Lignin is an untouched natural gem—at least from the bio-economy point of view, representing about 10-35% of lignocellulose biomass consisting of various phenylpropanoids (aromatic building blocks), thereby a potential source of fuel, energy, and chemicals including pharmaceuticals, paints, and plastics (Dossier, 2017).

Lignin being a highly complex polymer with variable structures (like molecular weight distribution, chemical functionalities, etc. depending upon the biomass source and fractionation process), the valorization of lignin into value-added products is still challenging (Cateto et al., 2008; Sun et al., 2018). It is more reasonable and economical that instead of defunctionalizing lignin completely into fine chemicals, i.e., BTX (benzene, toluene and xylene), we should defunctionalize to alkanes, arenes, and mixture of products that together can be used as feedstocks for the production of chemicals and biofuels (Zmierczak and Miller 2006; Kleinert and Barth 2008). Its high abundance and wide opportunities for defunctionalization has motivated scientists to carry out extensive research into catalytic valorization of lignin and thereby developing economical methods for its use as a feedstock (Chio et al., 2019; Liao et al., 2020; Wener et al., 2020; Abu-Omar et al., 2021).

Valorization or processing of lignin is mainly targeted to obtain a product (either pure or mixture) that fits into a particular purpose, and the by-products obtained are regarded as residue. But this is not in accordance with the "atom economy" principle of Green Chemistry (Anastas and Warner, 1998), as no by-products should be left behind and the matter should be processed completely. Scarce information is available on the complete valorization of lignin and its by-products. Borges da Silva et al., 2009, anticipated that during the valorization of lignin into vanillin, its by-products can be utilized for the production of polyurethanes (de Almedia and Silva, 2009).

An understanding of all of the interconnected stages starting from the extraction of lignocellulose from its source (mainly trees), its transportation to the bio-refineries and finally the conversion of the initial biomass feedstock into intended lignin-derived product (with no by-products) is very important. In spite of the high potential of lignin to be used as an alternative to petroleum or crude oil, it can only be made commercially available if it is easily affordable by the common people. In this article, we aim to present an analysis on the potential of lignin as an emerging petroleum alternative and current efforts/hurdles in commercialization process.

Isolation of lignin

The isolation of lignin from lignocellulosic biomass is targeted from high lignin containing sources such as woody biomass, i.e., hardwoods and softwoods in the bio-refineries producing "biofuel" along with lignin (Strassberger et al., 2014; Abu-Omar et al., 2021). Most of the lignin is obtained as a by-product of the pulp and paper industry. Also, it is separated from linked wood components either by preferentially dissolving lignin or by preferentially dissolving non-lignin components (Glennie and McCarthy 1962). Several methods are employed for the purpose, such as, ball milling, milled wood lignin (MWL), Brauns or Native Lignin, Organosolv processes, etc. Chemical pulping is employed in order to separate native lignins from wood in the form of MWL. In this process, various by-products that possess industrial applications are also formed such as dioxane lignin and enzymically liberated lignin. Kraft, sulfite and soda-AQ pulping of wood yield Kraft lignin, lignosulfonates and soda lignin (or alkali lignin), respectively (Stenius 2000); the first two being the major lignin types available commercially. During the isolation of lignin from black liquor, carbon dioxide is used to reduce the pH of the liquor while precipitating lignin from the black liquor, followed by the addition of sulfuric acid (Tamminen at al., 1995). A brown amorphous lignin powder is obtained from such processes where the lignin structure, molecular weight, and color is process severity dependent. Low grade lignin production in 2010 by pulp and paper industry was estimated to be 50 MT (metric tons). Out of this, just 2% was pure enough for further commercial use, rest of the amount was employed to generate energy through combustion (Higson and Smith, 2011). The conversion of such lignin to value-added chemicals have been an Achilles's heel but success stories utilizing lignin in the production of specialty or performance materials in terms of heat and water resistance, lower weight, higher durability and toughness and fire retardancy have been demonstrated by various ventures (Graichen et al., 2017).

Storage and transportation

The production of biofuels in biorefineries are economically unfeasible unless a maximum yield of fermentable sugars followed by maximum bioconversion is achieved (Periyasamy et al., 2018). Also, for the economic operation of a biorefinery, it is essential that it is located within 50 miles from the feedstock location. This is because the bulk density of biomass is very low and should not be stored at centers with high moisture content as the feedstock decomposes on exposure to the microbes present in the moisture (Audsley and Annetts 2003; Annetts and Audsley 2003; Baral et al., 2019). Keeping in view the continuous feedstock supply throughout the year, it becomes more reasonable if we store and process the biomass near the field (You and Wang 2011; Kurian et al., 2013). Transportation of the feedstock to the biorefinery becomes easier in this case since the field is very near and thus uninterrupted supply is possible. Such centers or facilities operated by farmers for processing the biomass are named as "regional biomass processing depots (RBPDs)." This concept was first given by the researchers at Michigan State University (Carolan et al., 2007) and then studied by the University of Tennessee Biofuel Initiative and benefited Dupont Cellulosic Ethanol (DCE) and the Idaho National Laboratory (INL) (Sharma et al., 2013). These RBPDs are not only storage centers for the feedstock, but also helps in creating new job opportunities and improvement of infrastructure in the rural areas. Biomass is mainly transported *via* trucks to the biorefinery located nearby. But this adds on to the overall production cost of the biofuel as nearly 88 trips per day will be required to achieve the target of 2,000 tons. Furthermore, transportation cost will increase with the increase in distance from the field (Sultana et al., 2010).

Cost reduction strategies

To gain market access, several developments have been carried out to cut short the processing cost and prove its credentials to compete with petroleum-based counterparts. One of the best strategies to gain wide-ranging economic benefits is by carrying out "genetic engineering." It aims at reducing the energy intake for breaking down the biomass and thereby, making the whole process more cost-effective. Scientists at Scion, New Zealand, in collaboration with the University of Wisconsin, have successfully engendered pine trees genetically containing syringyl units (mostly occurring in hardwoods). These genetically engineered species now comprise more labile linkages in the lignin backbone, thus, making its processing far easier (Wagner et al., 2015). It has been reported that genetic reduction of lignin content successfully overcame the resistance of cell wall for bioconversion. The current prototype for the production of ethanol involves costly pretreatment of the biomass for making the cell walls easily accessible to enzymes. Whereas, the untreated genetically modified plants such as HCT and C3H alfalfa lines produced much higher amounts of sugar than those obtained from the natural plants after the pretreatment process (Hiroshi et al., 2009). Hence, such genetic manipulations in plants can be helpful in reducing the overall cost of biofuel production. Voelker et al., 2010 demonstrated the positive effects of lignin reduction practically by conducting field trials (Voelker et al., 2010). The authors synthesized a hybrid with lower lignin content in cell walls and high growth rate, thus, proving to be a worthy feedstock for pulp and paper industries. In view of this, it can be concluded that "genetic engineering" can be considered as a game changer in the way tress are cultivated for cost and energy reductions.

Commercial development

World's first investigations into commercial development and application of lignin were performed in 1934 at Rothschild, Wisconsin, USA. After 1971, there was a significant increase in the sale of lignin, hence, new grades of purified lignin products started fabricating. Over the recent 10 years, the industry has observed several successful attempts in developing and expanding commercially relevant lignin processes. The world's first large-scale lignin manufacturing plant started at Domtar's Plymouth mill (NC, United States) in 2013, where LignoBoost®, a patented lignin extraction process, was employed in a kraft pulp mill is employed to produce high-quality lignin. This plant has an annual capacity of 25,000 MT of lignin along with 466,000 ADMT (Air Dry Metric Ton) of softwood kraft pulp from South Pinewood and now markets the lignin as BioChoice™ lignin (Björk et al., 2015). In 2015, the second LignoBoost® plant was deployed at Stora Enso's Sunila mill (Kotka, Finland). Sunila plant has an annual capacity of 50,000 MT of lignin and produces 370,000 ADMT of bleached softwood Kraft pulp from pine and spruce. The existing lignin market has grown significantly since the start-up of lignin production at these sites. For example, UPM signed an agreement with Domtar to acquire all BioChoice™ lignin from Domtar's Plymouth Mill (UPM, 2020). Most supply will be used for manufacturing UPM BioPiva™ products, which are substitutes to fossil-based phenol in phenolic-type resins (UPM, 2022). Borregaard's LignoTech, a biorefinery operated in Norway for over 70 years, is an exclusive company where 90% of the woody biomass input exits as marketable products (Martin Lersch, 2009). It reported an annual sales of lignin-based products 366,000 metric tons in 2021 (Borregaard, 2022) including its flagship wood/lignin-based vanillin. Recently, Avantium (2022) demonstrated the use of its lignin product as asphalt, which is normally derived from crude oil, for road pavement. Vertoro, a spin-off of Chemelot InSciTe (Chemelot Institute for Science and Technology), developed a technology platform where lignin is processed into the form of "oil" (Kouris et al., 2019). Through partnering with companies such as Shell and Maersk, the oil will be hydro-processed and used as a fuel for boats and ships (InSciTe, 2017a; Vertoro, 2022). Pure Lignin Environmental Technology Ltd. (Kelowna, British Columbia, Canada) aims at producing superior grade lignin and cellulose from any biomass following a cost-effective strategy. The company produces a unique "water-soluble lignin," which is now

TABLE 1 Commercial and pre-commercial lignin-based technologies.

Ventures	Lignin type	Technology	Major product	Commercialization level and scale (dry metric ton)
Domtar[a] (Valmet, 2022)	Kraft	LignoBoost[b]	BioChoice™ lignin	Commercial, 25 k
Stora Enso (Valmet, 2022)	Kraft	LignoBoost	BioChoice™ lignin	Commercial, 50 k
Ingevity (Ingevity, 2022)	Kraft	—	Indulin® AT	Commercial, —
Borregaard LignoTech (Borregaard, 2022)	Lignosulfonate		Vanillin and other biopolymers	Commercial, 366 k (2021 sales volume)
UPM (UPM, 2020; UPM, 2022)	BioChoice™ lignin (Liedberg, 2014)	—	BioPiva™, Phenolic-type resin	Commercial, >20 k
Suzano Papel e Cellulose (Suzano, 2022)	Kraft	—	Ecolig	Commercial, 20 k
Avantium (Avantium, 2022)	Acid hydrolysis (HCl) lignin	Dawn Technology™	Bio-asphalt	Pilot, —
Independent Flemish Research Organization (VITO) (Bioplastics News, 2018)	—	—	Bio-aromatics	Pilot, —
Vertoro (Vertoro, 2022)	Biorefinery and technical lignins (Kouris et al., 2019)	—	Marine fuel	Technology licensing
Pure Lignin Environmental Technology Ltd. (PLET)	Acid hydrolysis (dilute nitric acid) (DiVA, 2010)	—	Water-soluble lignin	Technology licensing
BENANOVA (BENANOVA, 2022)	—	—	Colloidal- and nano-particles	—
Spero Renewables LLC (Spero Renewables, 2022)	—	—	Thermoset polymers	—
RenFuel AB (Renfuel AB, 2022)	—	—	Bio-oil and bio-plastics	—
Bloom Biorenewables Ltd (Bloom Biorenewables, 2022)	—	Aldehyde-assisted fractionation	Variety of bio-products	—

[a]Currently a paper excellence subsidiary.
[b]LignoBoost is process patented by Valmet (Espoo, Finland).

attracting customers worldwide (PLET 2012). A Belgium based company named VITO (Independent Flemish Research Organization) co-financed by the European Regional Development Fund (ERDF) aims to convert lignin and wood into bio-aromatics in close collaboration with Scion, a Crown Research Institute in New Zealand (Bioplastics News, 2018). It is worthwhile mentioning that more and more lignin is now available in the market with continuously improving technologies; some other start-up companies are not discussed here but listed in Table 1.

Large quantities of lignin are expected to be produced from paper and pulp industries in the coming years. According to the international lignin institute (ILI), about 40–50 million MT of lignin is being produced worldwide, currently (www.ili-lignin.com). But, in order to meet the ambitious goal of replacing 30% of fossil fuels with biofuel by 2030, this production should shoot up to 225 million MT (Sahoo et al., 2011). This is only possible if the biorefineries are able to successfully utilize the complete feedstock and convert all its components into value-added bioproducts (Gowen and Fong, 2011; Rabinovitch-Deere et al., 2013). The US Department of Agriculture (USDA) and the US Department of Energy (DOE) have made mandatory that by 2022, 20% of liquid transportation fuel, 5% of heat and power energy, and 25% of chemicals and materials should come from biomass (Perlack et al., 2005). However, achieving this target is highly challenging, as it is evident from the recent estimates of biofuel production cost which is 2–3 times higher than its petroleum/crude oil counterparts on an energy equivalent basis (Carriquiry et al., 2011). Yet, with the advancement in technology the total production cost is expected to decrease. Few measures must be followed by biorefineries in order to gain high profits. This includes producing high value products such as chemical precursors, human food or medicinal materials in low volume, managing their own needs and finally producing high volumes of low value products like animal feed and fuels (Balan 2014).

Conclusion

This review highlighted the need, potential, and emergence of underutilized biopolymer, i.e., lignin, since it is the nature's prime reserve of functional groups and aromatics. Owing to its high abundance and functionalization, lignin can be considered as the best substituent in tomorrow's energy, fuel and chemical sectors. Lignin can be used in diverse applications, depending on its original source and method of extraction. However, commercialization of the biofuel production for the economic development is still a challenge mainly because of its complex nature and scarce information on extraction protocols. Moreover, the bio-refining processes for the extracted of lignin are economically infeasible. In order to compete with the cost of petrol or diesel, energy efficient technologies must be employed to reduce the biofuel processing cost. Biorefineries should focus on the complete conversion of feedstock into valuable products. Based on public awareness and extraordinary efforts by companies like Borregaard LignoTech, VITO and Chemelot (InSciTe, 2017b), it looks like lignin-derived biofuel the market soon, though, some delay is also expected due to the challenges discussed in this paper.

Present and future scope

Inspite of the high natural abundance and polyaromatic nature, lignocellulosic biomass is still not a commercially available feedstock for biofuel production. Methods for the extraction and purification of lignin are complex and expensive, consequently, cannot be employed at large-scales. The advancement in technology along with intensive collaboration among teams of different disciplines such as catalysis, chemical engineering and processing, analytics, etc. and boundaries is the key to solving problem. Big companies should establish commercial grade biorefineries that could produce several million gallons of fuel per year. The location of the biorefinery is very important for the economic transportation of the feedstock. In the coming years, biorefineries can be designed to utilize energy from renewable resources like solar, wind and geothermal, or we can even collocate them near thermal plants (coal or nuclear). This will help in preserving other non-renewable sources of energy such as natural gas. In view of above discussion about the pros and cons of using a sustainable biofuel, should not lignin be given the same chance as petroleum or crude oil?

Licenses and permission statement

Author contributions

HC and BAS conceptualized; VJ wrote the original draft; All authors edited the manuscript.

Funding

This work was part of the DOE Joint BioEnergy Institute (https://www.jbei.org) supported by the U.S. Department of Energy, Office of Science, Office of Biological and Environmental Research, through contract DE-AC02-05CH11231 between Lawrence Berkeley National Laboratory and the U.S. Department of Energy.

Author Disclaimer

The views expressed in the article do not necessarily represent the views of the DOE or the U.S. Government.

Acknowledgments

ABPDU would also like to thank the support from The Bioenergy Technologies Office (BETO) within the US DOE's Office of Energy Efficiency and Renewable Energy. Authors also thank Xiao Jiang of North Carolina State University in scouting the lignin technologies.

Conflict of interest

Author SS and HC were employed by company Sandia National Laboratories.

The remaining authors declare that the research was conducted in the absence of any commercial or financial relationships that could be construed as a potential conflict of interest.

Publisher's note

All claims expressed in this article are solely those of the authors and do not necessarily represent those of their affiliated organizations, or those of the publisher, the editors and the reviewers. Any product that may be evaluated in this article, or claim that may be made by its manufacturer, is not guaranteed or endorsed by the publisher.

References

Abu-Omar, M. M., Bara, K., Beackham, G. T., Luterbacher, J. S., Ralph, J., Rinaldi, R., et al. (2021). Guidelines for performing lignin-first biorefining. *Energy Environ. Sci.* 14, 262–292. doi:10.1039/d0ee02870c

Aleklett, K., Jakobsson, K., Lardelli, M., Snowden, S., and Soderbergh, B. (2010). The peak of the oil age – analyzing the world oil production reference scenario in world energy outlook. *Energy Policy* 38, 1398–1414. doi:10.1016/j.enpol.2009.11.021

Anastas, P. T., and Warner, C. J. (1998). *Green Chemistry: Theory and practice*. Oxford University Press.

Annetts, J. E., and Audsley, E. (2003). Modelling the value of a rural biorefinery—part II: Analysis and implications. *Agric. Syst.* 76, 61–76. doi:10.1016/s0308-521x(02)00039-2

Audsley, E., and Annetts, J. E. (2003). Modelling the value of a rural biorefinery—part I: The model description. *Agric. Syst.* 76, 39–59. doi:10.1016/s0308-521x(02)00038-0

Avantium (2022). Dawn technology. Available at: https://www.avantium.com/technologies/dawn/(Accessed: October 28, 2022).

Awosusi, A. A., Adebayo, A. A., Altuntas, M., Agyekum, E. B., Zawbaa, H. M., and Kamel, S. (2022). The dynamic impact of biomass and natural resources on ecological footprint in brics economies: A quantile regression evidence. *Energy Rep.* 8, 1979–1994. doi:10.1016/j.egyr.2022.01.022

Babich, I. V., and Moulijn, J. A. (2003). Science and technology of novel processes for deep desulfurization of oil refinery streams: A review. *Fuel* 82, 607–631. doi:10.1016/s0016-2361(02)00324-1

Balan, V. (2014). Current challenges in commercially producing biofuels from lignocellulosic biomass. *ISRN Biotechnol.*, 463074. doi:10.1155/2014/463074

Baral, N. R., Sundstrom, E. R., Das, L., Gladden, J. M., Eudes, A., Mortimer, J. C., et al. (2019). Approaches for more efficient biological conversion of lignocellulosic feedstocks to biofuels and bioproducts. *ACS Sustain. Chem. Eng.* 7 (10), 9062–9079. doi:10.1021/acssuschemeng.9b01229

Bioplastics News (2018). Belgium will build plant to convert lignin and wood into bio-aromatics. Available at: https://bioplasticsnews.com/2018/07/29/belgium-pilot-plant-convert-lignin-wood-bio-aromatics/(Accessed October 28, 2022).

BENANOVA (2022). BENANOVA - Benign innovations. Available at: https://benanova.com/ (Accessed October 28, 2022)

Björk, M., Rinne, J., Nikunen, K., Kotilainen, A., Korhonen, V., Christiansen, G., et al. (2015). "Valmet, Important lessons learned during the commercialization of the LignoBoost process," in International Bioenergy and Bioproducts Conference, Atlanta, GA, October 28–30. Available at: https://www.valmet.com/media/articles/up-and-running/new technology/PEERS1stLignoBoostPlants/.

Borges da Silva, E. A., Zabkova, M., Araújo, J. D., Cateto, C. A., Barreiro, M. F., an Belgacem, M. N., et al. (2009). An integrated process to produce vanillin and lignin-based polyurethanes from Kraft lignin. *Chem. Eng. Res. Des.* 87, 1276–1292. doi:10.1016/j.cherd.2009.05.008

Borregaard (2022). 2nd quarter 2022 results - borregaard. Available at: https://www.borregaard.com/investors/ir-news/2nd-quarter-2022-results/ (Accessed: October 28, 2022).

Carolan, J. E., Joshi, S. V., and Dale, B. E. (2007). Technical and financial feasibility analysis of distributed bioprocessing using regional biomass pre-processing centers. *J. Agric. Food Ind. Organ.* 5 (2), 1–29. doi:10.2202/1542-0485.1203

Carriquiry, M. A., Du, X., and Timilsina, G. R. (2011). Second generation biofuels: Economics and policies. *Energy Policy* 39, 4222–4234. doi:10.1016/j.enpol.2011.04.036

Cateto, C. A., Barreiro, M. F., Rodrigues, A. E., Brochier-Salon, M. C., Thielemans, W., and Belgacem, M. N. (2008). Lignins as macromonomers for polyurethane synthesis: A comparative study on hydroxyl group determination. *J. Appl. Polym. Sci.* 109, 3008–3017. doi:10.1002/app.28393

Chio, C., Sain, M., and Qin, W. (2019). Lignin utilization: A review of lignin depolymerization from various aspects. *Renew. Sustain. Energy Rev.* 107, 232–249. doi:10.1016/j.rser.2019.03.008

de Almeida, P., and Silva, P. D. (2009). The peak of oil production--Timings and market recognition. *Energy Policy* 37, 1267–1276. doi:10.1016/j.enpol.2008.11.016

DiVA (2010). Available at: https://www.diva-portal.org/smash/record.jsf?pid=diva2%3A1308186&dswid=5491 (Accessed: October 28, 2022).

Dossier (2017). Juliette irmer, BIOPRO baden-württemberg GmbH lignin- a natural resource with huge potential. available at: https://www.biooekonomie-bw.de/en/articles/dossiers/lignin-a-natural-resource-with-huge-potential/.15.

Glennie, D. W., and McCarthy, J. L. (1962). "Chemistry of lignin," in *Pulp and paper science and technology*. Editor C. E. Libby (New York: McGraw-Hill Book Company, Inc), 82–107.

Gowen, C. M., and Fong, S. S. (2011). Applications of systems biology towards microbial fuel production. *Trends Microbiol.* 19 (10), 516–524. doi:10.1016/j.tim.2011.07.005

Graichen, F. H. M., Grigsby, W. J., Hill, S. J., Raymond, L. G., Sanglard, M., Smith, D. A., et al. (2017). Y es, we can make money out of lignin and other bio-based resources. *Ind. Crops Prod.* 106, 74–85. doi:10.1016/j.indcrop.2016.10.036

Higson, A., and Smith, C. (2011). Lignin. Fact sheet. NNFCC. Available at http://www.nnfcc.co.uk/publications/nnfcc-renewable-chemicals-factsheet-lignin.A.

Hubbert, M. K. (1956). *Nuclear energy and the fossil fuels*. San Antonio: American Petroleum InstituteProceedings of Spring Meeting, 7–25.

Ingevity (2022). Indulin® at - ingevity. Available at: https://www.ingevity.com/products/indulin-at-agricultural-chemicals/(Accessed: October 28, 2022).

InSciTe (2017a). InSciTe. https://medium.com/@BrightlandsIF/inscite-comes-with-the-worlds-first-lignin-refinery-for-marine-fuel-3da8b0e89186 (Accessed October 28, 2022).

InSciTe (2017b). InSciTe. Available at: https://medium.com/@BrightlandsIF/inscite-comes-with-the-worlds-first-lignin-refinery-for-marine-fuel-3da8b0e89186.

International Energy Agency (IEA) (2007). *World energy outlook world energy outlook*. Paris, France: International Energy Agency.

Kiss, A. A., Omota, F., Dimian, A. C., and Rothenberg, G. (2006). The heterogeneous advantage: Biodiesel by catalytic reactive distillation. *Top. Catal.* 40, 141–150. doi:10.1007/s11244-006-0116-4

Kleinert, M., and Barth, T. (2008). Towards a lignincellulosic biorefinery: Direct one-step conversion of lignin to hydrogen-enriched biofuel. *Energy fuels.* 22, 1371–1379. doi:10.1021/ef700631w

Kouris, P., Boot, M. D., Hensen, E. J. M., and Oevering, H. (2019). *A method for obtaining a stable lignin: Polar organic solvent composition via mild solvolytic modifications. WO 2019/053287 A1.*

Kumarasamy, R., Uthandi, S., and Thangappan, S. (2017). Lignin depolymerization route derived commodities towards tangible bio-economy. *Madras Agric. J.* 104 (7-9), 207–217. doi:10.29321/maj.2017.000046

Kurian, J. K., Nair, G. R., Hussain, A., and Raghavan, G. S. V. (2013). Feedstocks, logistics and pre-treatment processes for sustainable lignocellulosic biorefineries: A comprehensive review. *Renew. Sustain. Energy Rev.* 25, 205–219. doi:10.1016/j.rser.2013.04.019

Lersch, Martin (2009). 'Creating value from wood-The Borregaard Biorefinery', *bioref-integ.eu*. Solihull, UK. Available at: https://www.bioref-integ.eu/fileadmin/bioref-integ/user/documents/Martin_Lersch__Borregaard_-_Creating_value_from_wood_-_The_Borregaard_biorefinery.pdf (Accessed October 28, 2022).

Liao, Y., Koelewijn, S. F., Van den Bossche, G., Van Aelst, J., Van den Bosch, S., Renders, T., et al. (2020). A sustainable wood biorefinery for low–carbon footprint chemicals production. *Science* 367 (6484), 1385–1390. doi:10.1126/science.aau1567

Liedberg, A. (2014). Valmet's new LignoBoost technology gaining foothold. Available at: https://valmetsites.secure.force.com/solutionfinderweb/sfc/servlet.shepherd/version/download/06858000000qgfXAAQ (Accessed October 28, 2022).15.

Maggio, G., and Cacciola, G. (2012). When will oil, natural gas, and coal peak? *Fuel* 98, 111–123. doi:10.1016/j.fuel.2012.03.021

Periyasamy, K., Santhalembi, L., Mortha, G., Aurousseau, M., Boyer, A., and Subramanian, S. (2018). Bioconversion of lignocellulosic biomass to fermentable sugars by immobilized magnetic cellulolytic enzyme cocktails. *Langmuir* 34 (22), 6546–6555. doi:10.1021/acs.langmuir.8b00976

Perlack, R. D., Wright, L. L., Turhollow, A. F., Graham, R. L., Stokes, B. J., and Erbach, D. C. (2005). *Biomass as feedstock for a Bioenergy and bioproducts industry: The technical feasibility of a billion-ton annual supply*. Oak Ridge, Tenn, USA: U.S. Department of Energy & U.S. Department of Agriculture.

PLET (2012). Pure lignin environmental technology. Available at: http://purelignin.com/ (Accessed October 28, 2022).

Rabinovitch-Deere, C. A., Oliver, J. W. K., Rodriguez, G. M., and Atsumi, S. (2013). Synthetic biology and metabolic engineering approaches to produce biofuels. *Chem. Rev.* 113 (7), 4611–4632. doi:10.1021/cr300361t

Rana, M. S., S`amano, V., Ancheyta, J., and Diaz, J. A. I. (2007). A review of recent advances on process technologies for upgrading of heavy oils and residua. *Fuel* 86, 1216–1231. doi:10.1016/j.fuel.2006.08.004

Renfuel, A. B. (2022). RenFuel. Available at: https://renfuel.se/(Accessed: October 28, 2022).

Sahoo, S., Seydibeyoglu, M. O., Mohanty, A. K., and Misra, M. (2011). Characterization of industrial lignins for their utilization in future value added applications. *Biomass Bioenergy* 35, 4230–4237. doi:10.1016/j.biombioe.2011.07.009

Sharma, B., Ingalls, R. G., Jones, C. L., and Khanchi, A. (2013). Biomass supply chain design and analysis: Basis, overview, modeling, challenges, and future. *Renew. Sustain. Energy Rev.* 24, 608–627. doi:10.1016/j.rser.2013.03.049

Sorrell, S., Speirs, J., Bentley, R., Brandt, A., and Miller, R. (2010). Global oil depletion: A review of the evidence. *Energy Policy* 38, 5290–5295. doi:10.1016/j.enpol.2010.04.046

Spero Renewables, L. L. C. (2022). *SperoSET™ recyclable*. Available at: https://www.sperorenewables.com/(Accessed October 28, 2022).

Stenius, P. (2000). *Forest products Chemistry*. Helsinki: Fapet Oy.

Strassberger, Z., Tanase, S., and Rothenberg, G. (2014). The pros and cons of lignin valorisation in an integrated biorefinery. *RSC Adv.* 4, 25310–25318. doi:10.1039/c4ra04747h

Sultana, A., Kumar, A., and Harfield, D. (2010). Development of agri-pellet production cost and optimum size. *Bioresour. Technol.* 101 (14), 5609–5621. doi:10.1016/j.biortech.2010.02.011

Sun, Y., and Cheng, J. (2002). Hydrolysis of lignocellulosic materials for ethanol production: A review. *Bioresour. Technol.* 83, 1–11. doi:10.1016/s0960-8524(01)00212-7

Sun, Z., Fridrich, B., De Santi, A., Elangovan, S., and Barta, K. (2018). Bright side of lignin depolymerization: Toward new platform chemicals. *Chem. Rev.* 118, 614–678. doi:10.1021/acs.chemrev.7b00588

Suzano (2022). Suzano ecolig: A universe of biopossibilities. Available at: https://www.suzanoecolig.com.br/en-home/(Accessed: October 28, 2022).

Tamminen, T., Vuorinen, T., Tenkanen, M., Hausalo, T., and Hortling, B. (1995). "Analysis of lignin and lignin- carbohydrate complexes isolated from black liquor," in *The 8th International Symposium on Wood and Pulping Chemistry: Poster presentations* vol. 2, Gummerus, and Jyväskylä (Helsinki, Finland: 8th International Symposium on Wood and Pulping Chemistry), 297–302.

Thersasme, O., Volk, T. A., Fortier, M. O., Kim, Y., Wood, C. D., Ha, H., et al. (2022). Carbon footprint of biofuels production from forest biomass using hot water extraction and biochemical conversion in the Northeast United States. *Energy* 241, 122853. doi:10.1016/j.energy.2021.122853

Tuck, C. O., Pérez, E., Horváth, I. T., Sheldon, R. A., and Poliakoff, M. (2012). Valorization of bio- mass: Deriving more value from waste. *Science* 337, 695–699. doi:10.1126/science.1218930

UNECE (2021). "Circularity concepts in forest-based industries," in *United nations economic commission for europe (UNECE) or the food and agriculture organization of the united nations* (Geneva: FAO).

UPM (2022). About UPM biochemicals | UPM biochemicals. Available at: https://www.upmbiochemicals.com/lignin-solutions/products/(Accessed: October 28, 2022).

UPM (2020) UPM Biochemicals grows lignin business with new Domtar supply agreement | Available at: https://www.upm.com/about-us/for-media/releases/2020/12/upm-biochemicals-grows-lignin-business-with-new-domtar-supply-agreement/(Accessed: 28 October 2022).

Valmet (2022). Valmet LignoBoost - lignin extraction. Available at: https://www.valmet.com/pulp/other-value-adding-processes/lignin-extraction/(Accessed: October 28, 2022).

Vertoro (2022). Projects & partners. Available at: https://vertoro.com/projectspartners/(Accessed: October 28, 2022).

Voelker, S. L., Lachenbruch, B., Meinzer, F. C., Jourdes, M., Ki, C., Patten, A. M., et al. (2010). Antisense down-regulation of *4CL* expression alters lignification, tree growth, and saccharification potential of field-grown poplar. *Plant Physiol.* 154, 874–886. doi:10.1104/pp.110.159269

Wagner, A., Tobimatsu, Y., Phillips, L., Flint, H., Geddes, B., Lu, F., et al. (2015). Syringyl lignin production in conifers: Proof of concept in a pine tracheary element system. *Proc. Natl. Acad. Sci. U. S. A.* 112, 6218–6223. doi:10.1073/pnas.1411926112

Wener, J., Haas, V., and Stern, T. (2020). Why can we make anything from lignin except money? Towards a broader economic perspective in lignin research. *Curr. For. Rep.* 6, 294–308. doi:10.1007/s40725-020-00126-3

World Bioenergy Statistics (2017). Available at: https://worldbioenergy.org/uploads/WBA%20GBS%202017_lq.pdf.

You, F., and Wang, B. (2011). Life cycle optimization of biomass-to- liquid supply chains with distributed-centralized processing networks. *Ind. Eng. Chem. Res.* 50, 10102–10127. doi:10.1021/ie200850t

Zakzeski, J., Bruijnincx, P. C. A., Jongerius, A. L., and Weckhuysen, B. M. (2010). The catalytic va- lorization of lignin for the production of renewable chemicals. *Chem. Rev.* 110, 3552–3599. doi:10.1021/cr900354u

Zmierczak, W. W., and Miller, J. D. (2006). Processes for catalytic conversion of lignin to liquid bio-fuels. International Patent WO/2006/119357.

frontiers | Frontiers in Chemical Engineering

TYPE Mini Review
PUBLISHED 05 January 2023
DOI 10.3389/fceng.2022.1087435

OPEN ACCESS

EDITED BY
Ghulam Yasin,
Beijing University of Chemical Technology, China

REVIEWED BY
Sajjad Ali,
University of Electronic Science and Technology of China, China
Saira Ajmal,
Shenzhen University, China

*CORRESPONDENCE
Adrian Cesar Cavazos Sepulveda,
adrian.cavazossepulveda@aramco.com

SPECIALTY SECTION
This article was submitted to Electrochemical Engineering, a section of the journal Frontiers in Chemical Engineering

RECEIVED 02 November 2022
ACCEPTED 19 December 2022
PUBLISHED 05 January 2023

CITATION
Velazquez-Rizo M and Cavazos Sepulveda AC (2023), Low-temperature direct electrochemical splitting of H_2S.
Front. Chem. Eng. 4:1087435.
doi: 10.3389/fceng.2022.1087435

Low-temperature direct electrochemical splitting of H_2S

Martin Velazquez-Rizo[1] and Adrian Cesar Cavazos Sepulveda[2]*

[1]Electrical and Computer Engineering Program, Computer, Electrical and Mathematical Sciences and Engineering Division, King Abdullah University of Science and Technology (KAUST), Thuwal, Saudi Arabia, [2]Exploration and Petroleum Engineering Center-Advanced Research Center (EXPEC ARC), Saudi Aramco, Dhahran, Saudi Arabia

Hydrogen is considered one of the most promising decarbonized fuels. However, its applicability is limited due to the ecological constraints of its production. Hydrogen sulfide (H_2S) is widely available in oil and gas reservoirs and has the potential of becoming an energetically favorable source of hydrogen. Nevertheless, its electrochemical separation into H_2 and elemental sulfur has not been successfully achieved at the industrial scale, due to sulfur poisoning of the electrodes at the sulfur oxidation half-reaction. This review highlights the progress of the direct electrolytic separation of H_2S below the sulfur dew point, where the sulfur poisoning effect becomes more prominent. The article discusses the different technologies and approaches explored to improve the energy efficiency and stability of H_2S electrolytic systems, including the recent use of nanostructured electrodes and novel sulfur solvents as electrolytes.

KEYWORDS

hydrogen sulfide, electrolysis, H_2 generation, sulfur generation, ionic liquids

1 Introduction

Current environmental conditions call for the development of ecological energy sources (Sekimoto et al., 2015; Raziq et al., 2022a; Ali et al., 2022b; Raziq et al., 2022b; Ali et al., 2022c; Ali et al., 2022d; Iqbal et al., 2022; Wahid et al., 2023). Among the candidates, H_2 is one of the most attractive alternatives to fossil fuels. Its direct combustion or fuel cells oxidation release no pollutant byproducts. However, the industrial production of H_2 is mainly carried out by energy-intensive hydrocarbon reformation process (Kalamaras and Efstathiou, 2013). This aspect overshadows the ecological qualities of H_2 and hinders its usage as a standard fuel. Research towards finding scalable, efficient, and environmentally friendly methods to produce H_2 has been relentless, focusing primarily on catalytic water splitting (Ahmad et al., 2015; Chen et al., 2016; Shiva Kumar and Himabindu, 2019; Iqbal et al., 2021; Ali et al., 2022a; Yasin et al., 2022a; Yasin et al., 2022b; Ibraheem et al., 2022), due to its worldwide availability. Currently, the most economically and environmentally viable option to drive this reaction is *via* electrolysis. H_2 generation systems based on this method are already commercially available. Nevertheless, water electrolysis, a longstanding known phenomenon (Trasatti, 1999), still has constraints such as high-cost electrodes, electrolytes, and catalysts, as well as long-term stability issues (Li et al., 2016).

An alternative source of H_2 is hydrogen sulfide, although it is conventionally overlooked. Gaseous H_2S is recognized for its characteristic rotten egg odor and its health hazards at concentrations as low as 10 ppm (Li et al., 2022). H_2S is found concurrently in gas and oil reservoirs. It is conventionally considered a burden in processing fossil fuels, as it requires strict handling safety measures and costly remedial treatments. H_2S is helpful in diverse industrial applications, nevertheless it is primarily oxidized in the Claus process (Zhang et al., 2015). Its byproducts are mostly sulfur and water, as indicated by the overall reaction found in Eq. 1.

$$2H_2S + O_2 \rightarrow 2S + 2H_2O \quad (1)$$

An unwanted byproduct of the Claus process is SO_x. Its emission is reduced to acceptable standards using tail-gas treatments, which achieve more than 99% sulfur recovery (de Crisci et al., 2019). Sulfur is the only valuable byproduct of this process, although it is not a high value commodity. Therefore, the Claus process is considered a convenient H_2S mitigation method rather than a sulfur production process. In this regard, finding cost-effective and scalable methods to generate H_2 from H_2S is essential to unlocking the ecological and economic benefits of H_2. Furthermore, such a process would bring value to the oil and gas industry.

The different explored approaches to achieve efficient and stable H_2S splitting include high-temperature catalysis, thermochemical methods (Bandermann and Harder, 1982; Noring and Fletcher, 1982), photolysis, photocatalysis (Oladipo et al., 2021), plasma (Nunnally et al., 2009), and electrolysis. However, several challenges have hindered the development of a practical and economically viable splitting method. In the case of heterogeneous catalysis, the most common obstacle is the passivation of the electrocatalyst by elemental sulfur. This phenomenon has forced the development of specialized techniques to inhibit it, e. g., stirring the electrolyte, and using porous electrodes, organic solvents, and high operational temperatures (Jangam et al., 2021). The last technique is common in current Claus H_2S treatment units. They are operated above the dew temperature of sulfur (180°C) to avoid precipitation (Li et al., 2022). However, its implementation becomes more delicate when the purpose of the reaction is to obtain H_2 (Lim and Winnick, 1984; Weaver and Winnick, 1987). Additionally, operating at sustained high temperatures requires a continuous heat supply, which increases the reactor's operational cost and promotes the components' degradation. Thus, low-temperature dissociation methods would be preferable from an economic and environmental perspective. This review intends to highlight, from a technological and chronological perspective, the progress towards the decomposition of H_2S into H_2 and elemental sulfur by direct electrolysis at temperatures below the dew point of sulfur. The electrochemical conditions of the reactions, the electrocatalyst materials, and the available techniques to diminish the electrocatalyst passivation by sulfur precipitation are discussed, including novel techniques involving nanostructured electrodes and specialized sulfur solvents.

2 Electrochemical separation of H_2S

Low-temperature electrochemical methods have gained interest in splitting H_2S due to its scalability and promising overall energetic requirements. The former is due to the relatively simple electrochemical cell setup, especially when compared to complex photoelectrochemical methods. The latter attribute is a consequence of the minimal energy required for heating and relatively favorable thermodynamics of the H_2S decomposition reaction. The potential difference between the H_2 evolution reaction (HER) and sulfur oxidation reaction (SOR) is only 0.14 V (Kelsall and Thompson, 1993), substantially lower than the theoretical 1.23 V necessary to drive water splitting (Kay et al., 2006). However, the overall energy required to drive H_2S splitting depends not only on its thermodynamics but also on the electrochemical setup, given that it is largely affected by the ohmic and mass transport losses as well as kinetic overpotentials on the electrocatalysts (Obata et al., 2019). Proper selection of the electrochemical conditions is a crucial step for optimizing the energy expenditure of the process.

In general, the electrolytic splitting of H_2S is conducted *via* direct and indirect electrolysis. In direct electrolysis, H_2S is oxidized straightforwardly into elemental sulfur and free protons, whereas indirect electrolysis is a two-step process. First, an intermediate is used to react chemically with H_2S and precipitate or separate sulfur. Subsequently, the intermediate is regenerated by electrolytic oxidization. The advantage of the indirect electrolysis method is that the sulfur extraction is facilitated since the initial H_2S reaction is decoupled from the electrolytic process. Nevertheless, this method requires a higher voltage to electrolyze the intermediate, and in some cases, the intermediate can degrade over time or migrate from the anodic to the cathodic chamber (Huang et al., 2019). On the other hand, the advantage of the direct electrolysis method is that it requires less energy because the potential necessary to drive the reaction is close to the HER and SOR potential difference. However, these systems suffer from sulfur passivation on the electrocatalyst surface or struggle to separate the sulfur from the electrolyte during the reaction. The sections below describe the advances in the field, and a summary of the mentioned works is found in Table 1.

2.1 Early developments on H_2S splitting

One of the crucial steps in direct electrolysis of H_2S at low temperatures is their absorption by a suitable electrolyte. This fluid should be chemically stable and thermodynamically inactive within the electrolysis potential difference. Early works demonstrated the possibility of using alkaline solutions for this purpose, particularly solutions containing NaOH (Anani et al., 1990; Mao et al., 1991). In those works, attention was shifted from the material composition of the SOR electrocatalyst, as their primary objective was to find the optimal H_2S processing conditions. This involves splitting H_2S with minimal sulfur deposition on the electrocatalysts at ~80°C. Anani et al. (Anani et al., 1990) used graphite, nickel, nickel-chromium, and titanium as SOR electrodes. However, they did not present a meaningful comparison of their electrocatalytic activity as they only mentioned a worse passivation effect in the metallic electrodes. Indeed, at that time, the deactivation of electrocatalysts by sulfur precipitation during the electrolysis of polysulfide solutions was a well-known problem (Fetzer, 1928; Hodes et al., 1980; Buckley et al., 1987), and several attempts to palliate it are documented, including the use of organic solvents to remove it from the electrocatalyst (Shih and Lee, 1986).

Research towards optimizing the H_2S splitting continued, looking for better SOR electrocatalysts and more practical methods to avoid their deactivation. Subsequent works expanded the list of SOR electrocatalytic materials, adding $LaSrMnO_3$ and Raney-nickel. Petrov and Srinivasan (Petrov and Srinivasan, 1996) demonstrated that $LaSrMnO_3$ had better SOR electrocatalytic performance than graphite, CoS, Raney-nickel, and Pt/C electrodes. They reached a current density of 300 $mAcm^{-2}$ at a cell potential of only 1 V. Their process scrubbed H_2S in a NaOH solution, then alkalinized the solution to pH 14, and electrolyzed it. All those steps were done in separate chambers, as Anani et al. (Anani et al., 1990) had previously proposed. Petrov and Srinivasan improved Anani et al.'s method by

TABLE 1 Direct electrolysis systems used for simultaneous SOR and HER at low temperature.

SOR electrode	HER electrode	Anolyte (and temperature)	Electrical conditions	SOR electrode passivation	Reference
Pt	Pt	H_2S/NaOH @ 20°C	J > 35 $mAcm^{-2}$	Yes	Fetzer, (1928)
Cu_2S, CoS, PbS, Pt, C, brass and RuS_2	Pt	KOH/S/$Na_2S{\cdot}9H_2O$ @ 25°C–65°C	J < 45 $mAcm^{-2}$	Yes	Hodes et al. (1980)
Pt	Pt	Toluene/Na_2S/NaOH @ 20°C–60°C	J < 3 $mAcm^{-2}$ @ 1.8–4.8 V	In some conditions	Shih and Lee, (1986)
Au	Au	$H_2B_4O_7$/$Na_2B_4O_7$/Na_2SO_4, $Na_2B_4O_7$ and NaOH, mixed with $Na_2S{\cdot}9H_2O$ @ 23°C	~50 μAcm^{-2} @ ~1 V vs. SHE	Yes	Buckley et al. (1987)
Graphite, Ni, Ni-Cr, Ti	Graphite, Ni	H_2S/NaOH, Na_2S_4, @ 80°C	J = 20 $mAcm^{-2}$	In some conditions	Anani et al. (1990)
N/D	N/D	H_2S/NaOH, Na_2S_4, @ 80°C	J = 200 $mAcm^{-2}$ @ 0.9 V	Yes	Mao et al. (1991)
Graphite, CoS, $LaSrMnO_3$ Raney-Ni, Pt/C	Raney-Ni	H_2S/NaOH @ 80°C	J = 300 $mAcm^{-2}$ @ 1 V (using $LaSrMnO_3$)	Yes, in Raney-Ni and Pt/C anodes	Petrov and Srinivasan, (1996)
Co phthalocyanine	Pt	Na_2S/KNO_3- H_3BO_3/NaOH/KCl @ 20°C	J < 6.4 μAcm^{-2}	N/D	Komorsky-Lovrić et al. (1997)
Ti/Ta_2O_5-IrO_2	Pt	$Na_2S{\cdot}9H_2O$ @ 20°C–60°C	J < 200 $mAcm^{-2}$	Yes	Chen and Miller (2004); Miller and Chen (2005)
Carbon felt	Pt	Na_2S/NaCl @ 25°C–80°C	J < 300 $mAcm^{-2}$	Yes	Ateya et al. (2005)
MoS_2	Pt	$Na_2S{\cdot}9H_2O$/artificial sea water/KOH @ 22°C–90°C	J < 3.6 $mAmg^{-1}$	N/D	Sanli et al. (2014)
N/D	N/D	Gaseous phase electrolysis, using a PEME of $CsHSO_4$ @ 150 °C, 0.8 MPa	70 kW @ 100 H_2S kg/h	N/D	Karapekmez and Dincer, (2018)
Graphene encapsulated CoNi	Graphite	Na_2S/NaOH @ 25°C	I = 30 $mAcm^{-2}$ @ 0.4 V vs. RHE	No	Zhang et al. (2020)
Pt	Pt	H_2S/[C_3OHmim]- BF_4/TGDE/MEA @ 50°C	J~10.5 $mAcm^{-2}$ @ 1.63 V	No	Ma et al. (2020)
$CoFeS_2$	Graphite	H_2S/NaOH	J~55 $mAcm^{-2}$ @ 0.3 V vs. RHE (using $Co_{0.75}Fe_{0.25}S_2$)	Partial	Kumar and Nagaiah (2022)

The voltage values indicated correspond to the cell voltage, unless otherwise indicated. N/D: Not described; RHE: reversible hydrogen electrode; SCE: saturated calomel electrode.

doing the final sulfur precipitation in a separate chamber, preventing sulfur precipitation in the graphite, CoS, and $LaSrMnO_3$ electrodes but not in the Raney-nickel, Ni, and Pt/C electrodes.

2.2 Sulfide electrooxidation mechanisms

Concomitantly, other researchers focused in understanding the reaction mechanism of sulfide electrooxidation. Cobalt phthalocyanine traces, used previously to catalyze the electroreduction of oxygen in KNO_3 aqueous solutions (Komorsky-Lovrić, 1995), were studied as electrocatalysts for the oxidation of sulfide ions by Komorsky-Lovrić et al. (Komorsky-Lovrić et al., 1997) *via* cyclic voltammetry (CV). Under the chemical conditions of their experiments, the CV measurements were consistent with a two-step oxidation of HS^- ions:

$$2HS^- + OH^- + K^+ \rightarrow (KHS_2)_{ads} + 2e^- + H_2O \quad (2)$$

$$2HS^- + OH^- \rightarrow HS_2^- + 2e^- + H_2O \quad (3)$$

In the case of a low sulfide ion concentration (<10^{-4} M), the KHS_2 adsorbed species would dissociate following the reaction shown in Eq. 4.

$$(KHS_2)_{ads} \rightarrow S_{ads} + HS^- + K^+ \quad (4)$$

Komorsky-Lovrić et al. (1997) stated that the adsorbed sulfur stays on the surface of the electrocatalyst and works as a bridge for the charge transfer process between the electrode and HS^- ions. However, it is essential to note that the proposed reaction mechanism does not yield free elemental sulfur as a final byproduct and that there were no analytical measurements of the species in the electrolyte after the redox reaction. Moreover, there was no description of gas evolution in electrodes, so it is unclear whether cobalt phthalocyanine-based SOR electrodes can perform the corresponding electrooxidation reaction to produce elemental sulfur.

Chen and Miller (Chen and Miller, 2004; Miller and Chen, 2005) performed further studies related to the mechanism of the electrochemical oxidation of sulfide ions. The SOR electrode used in their experiments was Ti/Ta_2O_5-IrO_2, and they performed different electrochemical characterizations under different conditions, including variations in temperature and sulfide concentration in the aqueous electrolyte. In their experiments, temporal oscillations of the SOR electrode potential (vs. a reference electrode) were present in specific galvanostatic conditions and at specific current intervals during linear galvanic voltammograms. The analysis of their chronopotentiometry observations indicates that the origin of the

oscillations was the alternation of the dominant oxidation reaction performed by the electrode. In the lower part of the potential oscillation, the dominant reaction is the oxidation of sulfide into sulfur, causing the sulfur deposition on the electrode and therefore inducing an increase of the electrode potential to keep the current at the set value. However, this increment in potential favors the oxygen evolution reaction (OER) from the aqueous electrolyte, making water oxidation the dominant reaction in the oscillation peak potential. The shift towards OER increases the availability of HS^- and S^{2-} ions as sulfur oxidation is minimized, increasing the dissolution of sulfur through the reactions displayed in Eq. 5 and Eq. 6.

$$S + HS^- + OH^- \rightarrow S_2^{2-} + H_2O \quad (5)$$

$$S + S^{2-} \rightarrow S_3^{2-} \quad (6)$$

The enhanced sulfur solubility and the increased mass transfer rate generated by the oxygen evolution led to the removal of sulfur deposits from the SOR electrode, promoting the rebound of the electrode potential at the lower bound of the oscillation. The continuous formation and removal of sulfur deposits on the surface of the electrode were observed during those measurements. This further supports the proposed reaction mechanism. These results highlight the importance of the selection of electrode materials, electrolytes, and electrical conditions of the electrolysis. The latter encompasses current density and potential, which influence the preferred chemical reactions. Such observation becomes even more relevant when there is great interest in applying these electrolytic processes at an industrial scale, where it is necessary to use high currents and voltages to obtain a higher yield of desired products.

2.3 H_2S splitting beyond fossil fuels

Subsequent works explored the possibility of using electrolysis for H_2S splitting in applications beyond the discussed cases of fossil fuel and natural gas scenarios. Sanli et al. (Sanli et al., 2014) researched the attainability of oxidizing sulfide ions contained in artificial seawater with chemical conditions like the ones found in the Black Sea. Their investigations used MoS_2 as the SOR electrode, which exhibited electrocatalytic activity towards the oxidation of HS^- into elemental sulfur. However, the final purpose of their work was to use the SOR electrode in H_2S fuel cells, where the catalytic HS^- oxidation must occur spontaneously to generate electricity besides elemental sulfur. The idea of oxidizing sulfide from brines was also explored by Ateya et al. (Ateya et al., 2005). They used carbon-felt SOR electrodes to drive H_2S splitting from wastewater brines. Alternatively, Karapekmez and Dincer (Karapekmez and Dincer, 2018) presented an H_2S abatement system using a proton exchange membrane electrolyzer (PEME). The H_2S PEME had a $CsHSO_4$ electrolyte and operated at 150°C. Their system was designed to treat the H_2S generated in geothermal power plants, and its practical implementation led to a substantial decrease in H_2S emissions.

2.4 Avoiding the passivation of SOR electrodes

The passivation of SOR electrodes had been the bottleneck in the development of low-temperature H_2S splitting systems. Recently, two research approaches, shown schematically in Figure 1, demonstrated

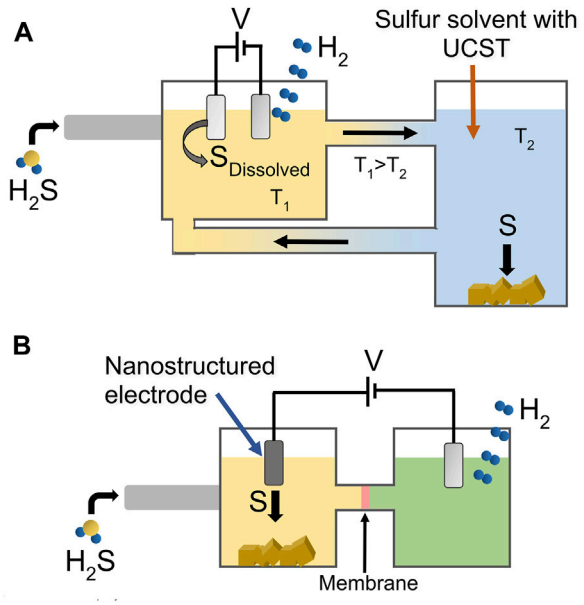

FIGURE 1
Current approaches to solve the SOR electrode passivation by sulfur deposition by using either **(A)** a sulfur solvent with a upper critical solution temperature (UCST), where sulfur solubility drastically depends on the solvent temperature; and **(B)** a nanostructured electrode with high sulfur-deposition resistance.

the possibility of avoiding the passivation of SOR electrodes, one through the design of nanostructured electrocatalysts and the other using a novel organic sulfur solvent. In the case of nanostructured electrodes, Zhang et al. (Zhang et al., 2020) reported the fabrication of a SOR electrode consisting of CoNi nanoparticles encapsulated in graphene shells and supported in Ni foam. Three-electrode measurements showed that using this electrode, the onset potential of sulfide oxidation was only ~0.25 V vs. reversible hydrogen electrode (RHE), 1.24 V lower than the onset potential of water oxidation. Additionally, the electrode exhibited a stable performance during a 500 h chronoamperometry test using a Na_2S/NaOH aqueous solution with a current density of around 30 $mAcm^{-2}$. These results showcase the possibility of generating H_2 reliably, with a Faradaic efficiency of about 98% and using significantly less energy than water splitting. The chronopotentiometry analysis of the nanostructured electrode in more realistic conditions was also reported, where it was tested for 1,200 h in a 1 M NaOH solution saturated with 2% H_2S/Syngas (50% CO and 50% H_2) at a current density of 20 $mAcm^{-2}$. In such conditions, the electrode's potential was maintained at around 0.5 V vs. RHE with minimal variations. Density functional theory calculations showed that the free adsorption energy of the sulfide oxidation intermediate is minimized in graphene-encapsulated CoNi nanoparticles compared with pure graphene or CoNi nanoparticles alone. This characteristic is generally accepted as an indicator of good catalytic material (Nørskov et al., 2009), thus explaining the excellent activity of the electrode towards the SOR and its capacity to avoid sulfur deposition on its surface.

Nanostructured electrodes exhibited further advantages in the work led by Kumar and Nagaiah (Kumar and Nagaiah, 2022). They used $CoFeS_2$ nanograins conjugated with nitrogen-containing carbon as a SOR electrode. They tested several stoichiometries of the

sulfide material, finding a better electrocatalytic activity towards the SOR using an electrode with a Co:Fe ratio of 3:1. Linear sweep voltammograms of this electrode showed a SOR onset potential of just 0.23 V vs. RHE. The current of the electrode in chronopotentiometry measurements for 120 h was about 55 $mAcm^{-2}$ at only 0.3 V vs. RHE, a better performance than the nanostructured SOR electrode from the work of Zhang et al. (Zhang et al., 2020) with a comparable Faradaic efficiency for H_2 generation (~97%). The electrode's current during the 120-h characterization was relatively stable, with a slight decrease over time due to a reduction of the electrochemically active area to 81% of its initial value, demonstrating a minor passivation effect suffered by the electrode.

Ma et al. (2020) proposed another approach to suppress the passivation of the SOR electrode. They electrolyzed H_2S in a mixture of an ionic liquid (IL) [C_3OHmim]- BF_4, tetraethylene glycol dimethyl ether (TGDE), and monoethanolamide (MEA). The IL, TGDE, and MEA mixture exhibited a superior sulfur solubility above 20°C when compared with a mixture of IL and TGDE. This is ascribed to the protonation of MEA by H_2S, as indicated in Eq. 7.

$$MEA + H_2S \rightarrow MEAH^+ + HS^- \quad (7)$$

They took advantage of the gradient of the sulfur solubility as a function of temperature to propose a cyclic electrolytic process. A Pt microdisk was used as a SOR electrode and the temperature was modified at different stages of the cycle. During H_2S electrolysis, the temperature of the electrolyte is kept at 50°C. As the electrolysis process continues, the electrolyte's color shifts from transparent to yellow, indicating the presence of elemental sulfur dissolved in the electrolyte. The electrolysis is stopped, and the electrode is removed before the electrolyte saturates with dissolved sulfur to avoid its precipitation on the surface of the Pt microdisk. Next, the electrolyte is cooled down to room temperature, which decreases its sulfur solubility, enhancing the precipitation of sulfur. Then the solid sulfur is separated from the electrolyte, which can be used to absorb H_2S again and start a new electrolytic cycle. The electrode's endurance test consisted of three 7-h electrolytic cycles with a current density in the range of 10–13 $mAcm^{-2}$. The Faraday efficiency of the H_2 evolution presented a slight decrease from 90.5% to 89.3% from the first to the third electrolytic cycles. These relatively low values were attributed to the formation of polysulfides. The "shuttling mechanism," could explain the large overpotential (~1.63 V at ~10.5 $mAcm^{-2}$) in comparison to the nanostructured electrode proposed by Zhang et al. (0.4 V at ~30 $mAcm^{-2}$) (Zhang et al., 2020). The report does not discuss the origin of the large overpotential or if it originates in the oxidation or reduction side. However, the cyclic voltammograms suggest that the electrocatalytic activity of the Pt microdisk is larger when using the electrolyte containing MEA. The origin of the overpotential is likely related to the slower kinetics of this amine, for example, in the reduction of the protonated MEA species formed by the reaction shown in Eq. 7.

3 Conclusion and perspectives

The direct electrolysis of H_2S into H_2 and elemental sulfur has proven to be a laborious task. The challenge of driving the reaction at low temperatures adds a new dimension to this conversion pathway. However, the research done so far in this field has brought several promising achievements, particularly regarding the avoidance of the passivation of SOR electrodes by using novel nanostructured electrodes or novel sulfur solvents. At this point, there is no feasible method that can be taken to an industrial scale, and there is room for improvement and research on low-temperature H_2S splitting systems. For example, it is cumbersome to evaluate the actual capability of a SOR electrode when its electrocatalytic activity is immediately blocked by sulfur deposition. Thus, with the development of novel sulfur solvents, it might be worth revisiting the performance of the SOR electrode materials studied so far in conditions where they are not affected by sulfur passivation. From Table 1, the variety of materials used as SOR electrocatalysts is not as diverse as it might be expected after almost a century of research. Possibly the electrode passivation and H_2S toxicity discouraged researchers from dedicating their effort and resources to the topic. Further research may also include sustainable regeneration techniques, where the electrocatalysts can be subjected to chemical or thermal treatment to reactivate their catalytic sites (Ledoux et al., 2000).

Author contributions

MV-R and AC contributed to the discussion of the topic and the structuring of the manuscript. MV-R wrote the first draft of the manuscript and AC revised the final version. All the authors approved the submitted version of the manuscript.

Funding

This research was internally funded by Saudi Aramco. The funder was not involved in the study design, collection, analysis, interpretation of data, the writing of this article, or the decision to submit it for publication.

Conflict of interest

The authors declare that the research was conducted in the absence of any commercial or financial relationships that could be construed as a potential conflict of interest.

Publisher's note

Supplementary material

The Supplementary Material for this article can be found online at: https://www.frontiersin.org/articles/10.3389/fceng.2022.1087435/full#supplementary-material

References

Ahmad, H., Kamarudin, S. K., Minggu, L. J., and Kassim, M. (2015). Hydrogen from photo-catalytic water splitting process: A review. *Renew. Sustain. Energy Rev.* 43, 599–610. doi:10.1016/j.rser.2014.10.101

Ali, S., Ali, S., Ismail, P. M., Shen, H., Zada, A., Ali, A., et al. (2022a). Synthesis and bader analyzed cobalt-phthalocyanine modified solar UV-blind β-Ga2O3 quadrilateral nanorods photocatalysts for wide-visible-light driven H2 evolution. *Appl. Catal. B* 307, 121149. doi:10.1016/J.APCATB.2022.121149

Ali, S., Iqbal, R., Wahid, F., Ismail, P. M., Saleem, A., Ali, S., et al. (2022b). Cobalt coordinated two-dimensional covalent organic framework a sustainable and robust electrocatalyst for selective CO2 electrochemical conversion to formic acid. *Fuel Process. Technol.* 237, 107451. doi:10.1016/j.fuproc.2022.107451

Ali, S., Ismail, P. M., Wahid, F., Kumar, A., Haneef, M., Raziq, F., et al. (2022c). Benchmarking the two-dimensional conductive Y3(C6X6)2 (Y = Co, Cu, Pd, Pt; X = NH, NHS, S) metal-organic framework nanosheets for CO2 reduction reaction with tunable performance. *Fuel Process. Technol.* 236, 107427. doi:10.1016/j.fuproc.2022.107427

Ali, S., Yasin, G., Iqbal, R., Huang, X., Su, J., Ibraheem, S., et al. (2022d). Porous aza-doped graphene-analogous 2D material a unique catalyst for CO2 conversion to formic-acid by hydrogenation and electroreduction approaches. *Mol. Catal.* 524, 112285. doi:10.1016/j.mcat.2022.112285

Anani, A. A., Mao, Z., White, R. E., Srinivasan, S., and Appleby, A. J. (1990). Electrochemical production of hydrogen and sulfur by low-temperature decomposition of hydrogen sulfide in an aqueous alkaline solution. *J. Electrochem Soc.* 137, 2703–2709. doi:10.1149/1.2087021

Ateya, B. G., Al-Kharafi, F. M., Abdallah, R. M., and Al-Azab, A. S. (2005). Electrochemical removal of hydrogen sulfide from polluted brines using porous flow through electrodes. *J. Appl. Electrochem* 35, 297–303. doi:10.1007/s10800-004-7273-6

Bandermann, F., and Harder, K. B. (1982). Production of H2 via thermal decomposition of H2S and separation of H2 and H2S by pressure swing adsorption. *Int. J. Hydrogen Energy* 7, 471–475. doi:10.1016/0360-3199(82)90103-3

Buckley, A. N., Hamilton, I. C., and Woods, R. (1987). An investigation of the sulphur(-II)/sulphur(0) system on bold electrodes. *J. Electroanal. Chem.* 216, 213–227. doi:10.1016/0022-0728(87)80208-5

Chen, A., and Miller, B. (2004). Potential oscillations during the electrocatalytic oxidation of sulfide on a microstructured Ti/Ta2O5-IrO2 electrode. *J. Phys. Chem. B* 108, 2245–2251. doi:10.1021/jp036639h

Chen, S., Thind, S. S., and Chen, A. (2016). Nanostructured materials for water splitting - state of the art and future needs: A mini-review. *Electrochem Commun.* 63, 10–17. doi:10.1016/j.elecom.2015.12.003

de Crisci, A. G., Moniri, A., and Xu, Y. (2019). Hydrogen from hydrogen sulfide: Towards a more sustainable hydrogen economy. *Int. J. Hydrogen Energy* 44, 1299–1327. doi:10.1016/j.ijhydene.2018.10.035

Fetzer, W. R. (1928). The electrolysis of sodium sulphide solutions. *J. Phys. Chem.* 32, 1787–1807. doi:10.1021/j150294a002

Hodes, G., Manassen, J., and Cahen, D. (1980). Electrocatalytic electrodes for the polysulfide redox system. *J. Electrochem Soc.* 127, 544–549. doi:10.1149/1.2129709

Huang, H., Shang, J., Yu, Y., and Chung, K. H. (2019). Recovery of hydrogen from hydrogen sulfide by indirect electrolysis process. *Int. J. Hydrogen Energy* 44, 5108–5113. doi:10.1016/j.ijhydene.2018.11.010

Ibraheem, S., Yasin, G., Kumar, A., Mushtaq, M. A., Ibrahim, S., Iqbal, R., et al. (2022). Iron-cation-coordinated cobalt-bridged-selenides nanorods for highly efficient photo/electrochemical water splitting. *Appl. Catal. B* 304, 120987. doi:10.1016/J.APCATB.2021.120987

Iqbal, R., Akbar, M. B., Ahmad, A., Hussain, A., Altaf, N., Ibraheem, S., et al. (2022). Exploring the synergistic effect of novel Ni-Fe in 2D bimetallic metal-organic frameworks for enhanced electrochemical reduction of CO2. *Adv. Mater Interfaces* 9, 2101505. doi:10.1002/admi.202101505

Iqbal, R., Yasin, G., Hamza, M., Ibraheem, S., Ullah, B., Saleem, A., et al. (2021). State of the art two-dimensional covalent organic frameworks: Prospects from rational design and reactions to applications for advanced energy storage technologies. *Coord. Chem. Rev.* 447, 214152. doi:10.1016/J.CCR.2021.214152

Jangam, K., Chen, Y. Y., Qin, L., and Fan, L. S. (2021). Perspectives on reactive separation and removal of hydrogen sulfide. *Chem. Eng. Sci. X* 11, 100105. doi:10.1016/j.cesx.2021.100105

Kalamaras, C. M., and Efstathiou, A. M. (2013). Hydrogen production technologies: Current state and future developments. *Conf. Pap. Energy* 2013, 1–9. doi:10.1155/2013/690627

Karapekmez, A., and Dincer, I. (2018). Modelling of hydrogen production from hydrogen sulfide in geothermal power plants. *Int. J. Hydrogen Energy* 43, 10569–10579. doi:10.1016/j.ijhydene.2018.02.020

Kay, A., Cesar, I., and Grätzel, M. (2006). New benchmark for water photooxidation by nanostructured α-Fe 2O3 films. *J. Am. Chem. Soc.* 128, 15714–15721. doi:10.1021/ja064380l

Kelsall, G. H., and Thompson, I. (1993). Redox chemistry of H2S oxidation by the British gas Stretford process part V: Aspects of the process chemistry. *J. Appl. Electrochem* 23, 427–434. doi:10.1007/BF00707618

Komorsky-Lovrić, Š. (1995). Voltammetry of microcrystals of cobalt and manganese phthalocyanines. *J. Electroanal. Chem.* 397, 211–215. doi:10.1016/0022-0728(95)04194-5

Komorsky-Lovrić, Š., Lovrić, M., and Scholz, F. (1997). Sulfide ion electrooxidation catalysed by cobalt phthalocyanine microcrystals. *Mikrochim. Acta* 127, 95–99. doi:10.1007/bf01243171

Kumar, M., and Nagaiah, T. C. (2022). Efficient production of hydrogen from H2S via electrolysis using a CoFeS2 catalyst. *J. Mater Chem. A Mater* 10, 7048–7057. doi:10.1039/d1ta09888h

Ledoux, M. J., Pham-Huu, C., Keller, N., Nougayrède, J. B., Savin-Poncet, S., and Bousquet, J. (2000). Selective oxidation of H2S in Claus tail-gas over SiC supported NiS2 catalyst. *Catal. Today* 61, 157–163. doi:10.1016/S0920-5861(00)00365-5

Li, F., Laaksonen, A., Zhang, X., and Ji, X. (2022). Rotten eggs revaluated: Ionic liquids and deep eutectic solvents for removal and utilization of hydrogen sulfide. *Ind. Eng. Chem. Res.* 61, 2643–2671. doi:10.1021/acs.iecr.1c04142

Li, X., Hao, X., Abudula, A., and Guan, G. (2016). Nanostructured catalysts for electrochemical water splitting: Current state and prospects. *J. Mater Chem. A Mater* 4, 11973–12000. doi:10.1039/c6ta02334g

Lim, H. S., and Winnick, J. (1984). Electrochemical removal and concentration of hydrogen sulfide from coal gas. *J. Electrochem Soc.* 131, 562–568. doi:10.1149/1.2115627

Ma, Y., Jin, X., Hu, Y., Huang, Q., and Wang, Z. (2020). Recovery of hydrogen and sulfur by electrolysis of ionized H2S in an amine-containing organic electrolyte with highly temperature-dependent sulfur solubility. *Energy Fuels* 34, 7756–7762. doi:10.1021/acs.energyfuels.0c01161

Mao, Z., Anani, A., White, R. E., Srinivasan, S., and Appleby, A. J. (1991). A modified electrochemical process for the decomposition of hydrogen sulfide in an aqueous alkaline solution. *J. Electrochem Soc.* 138, 1299–1303. doi:10.1149/1.2085775

Miller, B., and Chen, A. (2005). Effect of concentration and temperature on electrochemical oscillations during sulfide oxidation on Ti/Ta2O5-IrO2 electrodes. *Electrochim Acta* 50, 2203–2212. doi:10.1016/j.electacta.2004.10.002

Noring, J. E., and Fletcher, E. A. (1982). High temperature solar thermochemical processing-hydrogen and sulfur from hydrogen sulfide. *Energy* 7, 651–666. doi:10.1016/0360-5442(82)90002-0

Nørskov, J. K., Bligaard, T., Rossmeisl, J., and Christensen, C. H. (2009). Towards the computational design of solid catalysts. *Nat. Chem.* 1, 37–46. doi:10.1038/nchem.121

Nunnally, T., Gutsol, K., Rabinovich, A., Fridman, A., Starikovsky, A., Gutsol, A., et al. (2009). Dissociation of H2S in non-equilibrium gliding arc "tornado" discharge. *Int. J. Hydrogen Energy* 34, 7618–7625. doi:10.1016/j.ijhydene.2009.07.045

Obata, K., Shinohara, Y., Tanabe, S., Waki, I., Kotsovos, K., Ohkawa, K., et al. (2019). A stand-alone module for solar-driven H2 production coupled with redox-mediated sulfide remediation. *Energy Technol.* 7, 1900575. doi:10.1002/ente.201900575

Oladipo, H., Yusuf, A., al Jitan, S., and Palmisano, G. (2021). Overview and challenges of the photolytic and photocatalytic splitting of H2S. *Catal. Today* 380, 125–137. doi:10.1016/j.cattod.2021.03.021

Petrov, K., and Srinivasan, S. (1996). Low temperature removal of hydrogen sulfide from sour gas and its utilization for hydrogen and sulfur production. *Int. J. Hydrogen Energy* 21, 163–169. doi:10.1016/0360-3199(95)00003-8

Raziq, F., Aligayev, A., Shen, H., Ali, S., Shah, R., Ali, S., et al. (2022a). Exceptional photocatalytic activities of rGO modified (B, N) Co-doped WO3, coupled with CdSe QDs for one photon Z-scheme system: A joint experimental and dft study. *Adv. Sci.* 9, 2102530. doi:10.1002/advs.202102530

Raziq, F., Khan, K., Ali, S., Ali, S., Xu, H., Ali, I., et al. (2022b). Accelerating CO2 reduction on novel double perovskite oxide with sulfur, carbon incorporation: Synergistic electronic and chemical engineering. *Chem. Eng. J.* 446, 137161. doi:10.1016/j.cej.2022.137161

Sanli, A. E., Aytaç, A., and Mat, M. (2014). Investigation of the electro-oxidation of artificial Black Sea water by cyclic voltammetry on molybdenum (II). *Int. J. Hydrogen Energy* 39, 9221–9229. doi:10.1016/j.ijhydene.2014.03.047

Sekimoto, T., Shinagawa, S., Uetake, Y., Noda, K., Deguchi, M., Yotsuhashi, S., et al. (2015). Tandem photo-electrode of InGaN with two Si p-n junctions for CO2 conversion to HCOOH with the efficiency greater than biological photosynthesis. *Appl. Phys. Lett.* 106, 073902–073910. doi:10.1063/1.4910510

Shih, Y.-S., and Lee, J.-L. (1986). Continuous solvent extraction of sulfur from the electrochemical oxidation of a basic sulfide solution in the CSTER system. *Industrial Eng. Chem. Process Des. Dev.* 25, 834–836. doi:10.1021/i200034a041

Shiva Kumar, S., and Himabindu, V. (2019). Hydrogen production by PEM water electrolysis – a review. *Mater Sci. Energy Technol.* 2, 442–454. doi:10.1016/j.mset.2019.03.002

Trasatti, S. (1999). Water electrolysis: Who first? *J. Electroanal. Chem.* 476, 90–91. doi:10.1016/S0022-0728(99)00364-2

Wahid, F., Ali, S., Ismail, P. M., Raziq, F., Ali, S., Yi, J., et al. (2023). Metal single atom doped 2D materials for photocatalysis: Current status and future perspectives. *Prog. Energy* 5, 012001. doi:10.1088/2516-1083/ac9eff

Weaver, D., and Winnick, J. (1987). Electrochemical removal of H2S from hot gas streams: Nickel/Nickel-sulfide cathode performance. *J. Electrochem Soc.* 134, 2451–2458. doi:10.1149/1.2100220

Yasin, G., Ibraheem, S., Ali, S., Arif, M., Ibrahim, S., Iqbal, R., et al. (2022a). Defects-engineered tailoring of tri-doped interlinked metal-free bifunctional catalyst with lower gibbs free energy of OER/HER intermediates for overall water splitting. *Mater Today Chem.* 23, 100634. doi:10.1016/J.MTCHEM.2021.100634

Yasin, G., Ibrahim, S., Ajmal, S., Ibraheem, S., Ali, S., Nadda, A. K., et al. (2022b). Tailoring of electrocatalyst interactions at interfacial level to benchmark the oxygen reduction reaction. *Coord. Chem. Rev.* 469, 214669. doi:10.1016/J.CCR.2022.214669

Zhang, M., Guan, J., Tu, Y., Chen, S., Wang, Y., Wang, S., et al. (2020). Highly efficient H2 production from H2S: Via a robust graphene-encapsulated metal catalyst. *Energy Environ. Sci.* 13, 119–126. doi:10.1039/c9ee03231b

Zhang, X., Tang, Y., Qu, S., Da, J., and Hao, Z. (2015). H2S-selective catalytic oxidation: Catalysts and processes. *ACS Catal.* 5, 1053–1067. doi:10.1021/cs501476p

frontiers | Frontiers in Chemical Engineering

TYPE Perspective
PUBLISHED 11 April 2023
DOI 10.3389/fceng.2023.1140953

OPEN ACCESS

EDITED BY
Bita Bayatsarmadi,
Commonwealth Scientific and Industrial Research Organisation (CSIRO), Australia

REVIEWED BY
Jaewon Byun,
Chonnam National University, Republic of Korea

*CORRESPONDENCE
Soheil Shayegh,
soheil.shayegh@eiee.org

SPECIALTY SECTION
This article was submitted to Environmental Chemical Engineering, a section of the journal Frontiers in Chemical Engineering

RECEIVED 09 January 2023
ACCEPTED 30 March 2023
PUBLISHED 11 April 2023

CITATION
Shayegh S (2023), The prospect of direct air capture for energy security and climate stability.
Front. Chem. Eng. 5:1140953.
doi: 10.3389/fceng.2023.1140953

The prospect of direct air capture for energy security and climate stability

Soheil Shayegh*

RFF-CMCC European Institute on Economics and the Environment (EIEE), Centro Euro-Mediterraneo Sui Cambiamenti Climatici, Milano, Italy

Energy policies aim at securing energy supply through domestic production or imports have significant consequences for climate change and its long-term impacts on the economy. Recent European energy crisis as a result of extensive reliance on imported Russian natural gas has highlighted the European Union (EU) energy vulnerability and has challenged its climate change commitments. While switching to alternative domestic fossil fuel sources such as coal in some member states has put the EU climate ambitions in jeopardy, it has also provided new opportunities for up-scaling renewable technologies as well as climate stability measures such as direct air capture (DAC). This paper examines the interaction between energy policy and climate stability by considering imported natural gas, domestic coal production, and possible DAC deployment in the EU under two scenarios of full cooperation and full competition among the EU member states. The results suggest that while cooperation induces higher reliance on imported energy, it also provides a strong incentive for DAC uptake. Competition on the other hand, may result in more reliance on domestic coal production and worse climate change outcomes despite the availability of DAC. Therefore, as the EU is striving for a more perfect union, it should consider better alignment of its short-term energy security policies with long-term climate stability ambitions.

KEYWORDS

energy policy, direct air capture, climate change, energy security, climate stability, negative emission technologies

1 Introduction

The widespread adoption of innovative technologies often can be contributed to a convolution of multiple social, behavioral, political, and economic factors (Urmee and Md, 2016). Similarly, the uptake of climate change solutions such as carbon removal (CDR) technologies depends on not only their technological readiness but also on an array of socioeconomic factors facilitating or obstructing their development and deployment (Buck, 2016). In the last few months and after the Russian invasion of Ukraine, growing energy security concerns in Europe (Żuk and Żuk, 2022), combined with unequivocal commitments for decarbonization (Buschle and Westphal, 2019), have provided a unique opportunity for large scale deployment of innovative climate solutions that can play a key role in shaping the future of European energy-climate ecosystem.

In the latest assessment report by intergovernmental panel on climate change (IPCC), CDR has been acknowledged as a "necessary element" in keeping global warming well- 2°C and even more essential in staying below 1.5°C (IPCC, 2022). Although there is no consensus among the researchers, policymakers, climate activist, and the general public on the best

approach to removing existing carbon dioxide emissions from the atmosphere (Cox et al., 2020), Direct Air Capture (DAC) in particular, has increasingly been considered as a viable solution for achieving net-zero and net-negative climate objectives (Bednar et al., 2021).

There are several technical and economic reasons for the growing interest in commercialization and early adoption of DAC technologies (McQueen et al., 2021)[1]. First, DAC technology is flexible in the sense that unlike carbon capture and storage (CCS) that applies to stationary sources of highly concentrated emissions such as fossil fuel power plants, DAC process is not limited to an specific location as long as it is in close proximity to reliable energy sources and CO_2 storage sites (Erans et al., 2022). Furthermore, it can use either solid sorbents or liquid solvents (McQueen et al., 2021). Second, the capture units are modular and their annual capacity can be scaled up from a few tons to megatons of captured carbon (Hanna et al., 2021). Third, the DAC operation is an industrial process with controllable and verifiable input and output quantities which can potentially alleviate concerns about verification and certification of the DAC plants (Sovacool et al., 2023). Finally, and compared to other CDR approaches, DAC has a relatively small physical footprint and it requires far less land and water resources for its operation while there is no direct threat to existing food or biodiversity systems (Beuttler et al., 2019). Nevertheless, there are still large uncertainties about optimization of the DAC processes at large scale, their integration into renewable energy systems, and the permanent sequestration of the captured carbon which requires further research and investigation

In the past few years, multiple studies have assessed the techno-economic potentials of DAC technologies (Fasihi et al., 2019; National Academies of Sciences Engineering and Medicine, 2019), their limitations (Smith et al., 2016; Erans et al., 2022), and their future prospect (Nemet et al., 2018; Shayegh et al., 2021). However, the integration of DAC into energy-climate system models is still limited and the results are largely dependent on critical assumptions about the cost and the deployment rate of DAC technologies (Chatterjee and Huang, 2020).

This paper, however, takes a different approach by framing the question of DAC deployment against a broader backdrop of energy transition and energy security from an European perspective. It develops an analytical model for energy policy making mechanism in a representative EU member state economy who has a significant dependence on an insecure foreign energy source (e.g., Russian natural gas), and a controversial reliance on domestic fossil fuel production (e.g., coal industry). Furthermore, the European Union (EU), in line with its member states, has set out an ambitious program (i.e., the European Green Deal) to make the EU climate neutral in 2050 (Commission and for Communication, 2021). As a result, a complex array of such climate ambitions and energy security incentives, in addition to Energy Union considerations (Pérez et al., 2019), has created national policies within the EU member states, which are largely misaligned and are hard to navigate through (Maris and Flouros, 2021; Osička and Černoch, 2022).

On the other hand, delayed deployment of CDR initiatives including DAC, would be costly for the EU and would substantially undermine the removal potential to meet the 2100 targets (Galán-Martín et al., 2021). Therefore, there is an urgent need for the alignment of national energy policies with carbon removal up-scaling strategies in a way that both provide energy security and achieve the long-term climate stability objectives. This paper attempts to revisit energy security considerations and priorities in light of climate change commitments by developing and analysing a simple economic model of a major importer and exporter of natural gas (i.e., the EU member states and Russia, respectively) with differentiated climate change preferences under two scenarios: cooperation between the importing entities and competition among them. The results highlight the interconnection of the imported energy price and the incentive to develop and deploy a reliable carbon removal option such as DAC to offset the negative impacts of domestic and imported fossil fuel consumption.

TABLE 1 List of variables and parameters used in the model.

Name	Definition	Type
i	Importing country	index
e	Exporting country	index
$coop$	Cooperation case	index
$comp$	Competition case	index
m	Share of coal in total energy demand (%)	Decision variable
R	DAC level	Decision variable
U	Utility of importing	Auxiliary variable
E	Total energy demand	Auxiliary variable
$\Delta\ T$	Change in global mean temperature	Auxiliary variable
N	Number of importing countries	Parameter
η_c	Price of coal	Parameter
η_g	Price of natural gas	Parameter
η_e	Cost of natural gas extraction	Parameter
η_r	Price of DAC	Parameter
θ_c	Warming potential of coal	Parameter
θ_g	Warming potential of natural gas	Parameter
δ_r	Cooling potential of DAC	Parameter
$\theta\theta$	Climate change damage cost	Parameter
T_x	Exogenous temperature change	Parameter

2 Modeling energy security and climate stability

We investigate the interaction between energy security and climate stability efforts through the development of an importer-

1 It is worth noting that there are already a dozen commercial applications of DAC in Europe and North America with pioneering companies such as Climeworks (Switzerland), Global Thermostat (United States), and Carbon Engineering (Canada) among others leading the way (McQueen et al., 2021).

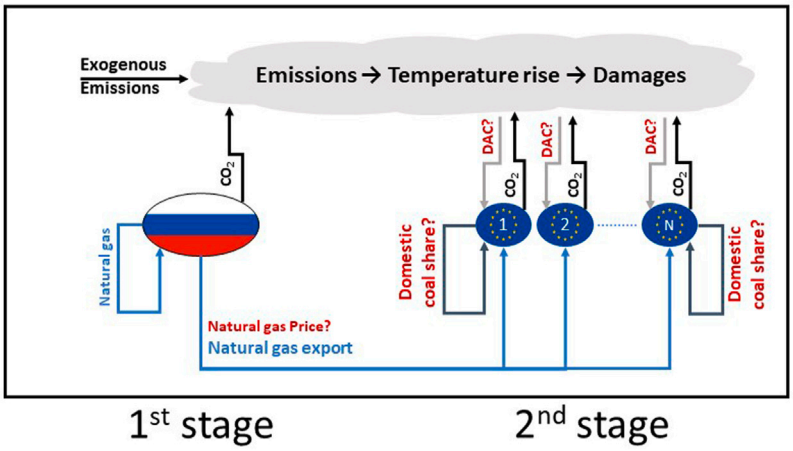

FIGURE 1
Energy security and climate stability dynamics. In the first stage, Russia decides about the price of exported natural gas. In the second stage, the EU countries decide about the share of domestic coal to secure their energy demand, and the level of direct air capture (DAC) to stabilize the climate.

exporter two-actor model. In this simple model, a group of countries (e.g., the EU member states) represents the *importer* actor as they are the main importer of the Russian natural gas. On the other hand, Russia whose economy is heavily dependent on the export of fossil fuel energy commodities (and in particular natural gas to Europe), represents the *exporter* actor. In addition, we distinguish between two types of fossil fuel as primary sources of energy: coal and natural gas. The importer countries like Germany and Poland produce coal domestically but import natural gas from Russia. Consuming either types of fossil fuel generates an economic value but causes climate change damages due to the CO_2 emissions resulting from their combustion in energy generation during economic activities. Russia on the other hand, has an abundance of natural gas which is not only sufficient for its domestic consumption but can sufficiently meet the demand of the importer actors. It is important to note that the equations used in the following sections, are highly simplified and only used to demonstrate the high-level associations among different parameters and variables. Therefore, the scope of this study is limited to analyzing the relationship among the key variables and not presenting any quantitative results. Table 1 provides the list of variables and parameters used in this model along with a brief description of each item.

2.1 Sequence of actions

We model the European energy security and climate stability as a sequential game in two stages: In the first stage, the exporter country (i.e., Russia) sets the price of natural gas and then, in the second stage, the importer countries (i.e., the EU member states) decide on the share of domestic production of coal (as a complement to imported natural gas), and the level of DAC deployment, simultaneously. Besides economic value associated with energy consumption, both the exporter and the importer countries suffer from climate damages linked to rising temperatures as a result of greenhouse gas emissions from fossil fuel consumption. Such damages are however, not equal and among other factors, depend on the geographic location and socioeconomic structure of each country's economy. As a result, the advanced economies of the importer countries have an incentive to opt for the deployment of DAC as a reliable carbon dioxide removal option to alleviate the negative consequence of global warming. Therefore, in the second stage, the importer countries face two choices: 1) the portion of their energy demand to be supplied domestically (i.e., the energy security indicator), and 2) the level of DAC deployment (i.e., the climate stability indicator). Figure 1 shows the dynamics of this game considering energy security and climate stability. For simplicity, we assume the importer actor comprises N identical entities (e.g., the 27 member states of the EU). Further we assume that information about the energy price and quantities, in addition to the level of DAC deployments are publicly available and shared among all actors. This allows us to use the backward induction technique (Aliprantis, 1999) to solve this sequential game with perfect information.

2.1.1 Importer's problem

In this paper we develop and use a conceptual model of energy economics which assumes that countries benefit from energy consumption but they incur energy expenditures and climate change damage costs. In other words, energy consumption increases their utility while energy acquisition and climate change decrease it. The aim of each country is to maximise their utility by setting the optimal share of energy import and DAC deployment. We start from the second stage, assuming that the price of natural gas (η_g) is known to the importer actor. The utility of each importer entity can be expressed as

$$U_i(m_i, R_i) = E_i - \eta_c\ (m_i\ E_i) - \eta_g\ ((1-m_i)\ E_i) - \frac{1}{2}\ \eta_r\ R_i^2 - \frac{1}{2}\ \delta_i\ (\Delta T)^2 \quad (1)$$

with the change in global mean temperature (ΔT) calculated as

$$\Delta T = \sum_{i=1}^{N} \underbrace{\left(\theta_c\ m_i\ E_i + \theta_g\ (1-m_i)\ E_i - \theta_r\ R_i\right)}_{T_i} + T_x \quad (2)$$

where m_i is the share of coal in total energy demand (E_i) of an importing entity, and R_i is the carbon removal level through DAC deployment. Parameters η_c, η_g, and η_r reflect the price of coal, natural gas, and DAC respectively. The quadratic DAC cost function is used to account for the required up-scaling investments in carbon removal technologies. Furthermore, the climate damage cost is linked to global mean temperature change and follows a conventional quadratic form (Richard, 1995; Nordhaus, 2017) with parameter δ_i. In the temperature Eq. 2, parameters θ_c and θ_g are used to translate emissions from energy consumption to temperature change for coal and natural gas, respectively. Parameter θ_r represents the effect of carbon removal on reducing carbon concentration and global mean temperature, subsequently. Finally, T_i represents the contribution of each entity i to global mean temperature change while T_x is the exogenous temperature change due to emissions and other factors beyond the scope of the energy trade between the two actors in this model. To maximize the utility of the importer's energy consumption, we can derive the optimal values of m_i and R_i from the first-order conditions of Eq. 1.

$$\frac{\partial U_i}{\partial m_i} = 0 \rightarrow m_i = \frac{\Delta\eta - \delta_i\ \Delta\theta\ \left(\theta_g\ E_i - \theta_r\ R_i + \sum_{j\neq i} T_j + T_x\right)}{\delta_i\ (\Delta\theta)^2\ E_i} \quad (3)$$

$$\frac{\partial U_i}{\partial R_i} = 0 \rightarrow R_i = \frac{\delta_i\ \theta_r\ \left(m_i\ \Delta\theta\ E_i + \theta_g\ E_i + \sum_{j\neq i} T_j + T_x\right)}{\eta_r + \delta_i\ \theta_r^2} \quad (4)$$

Where $\Delta\eta = \eta_g - \eta_c$ (i.e., the price difference between imported natural gas and domestic coal) and $\Delta\theta = \theta_c - \theta_g$ (i.e., the warming potential difference between domestic coal emissions and imported natural gas emissions). Solving these two equations simultaneously will provide the optimal values:

$$m_i^* = \frac{\Delta\eta\ (\eta_r + \delta_i\ \theta_r^2) - \delta_i\ \eta_r\ \Delta\theta\ \left(\theta_g\ E_i + \sum_{j\neq i} T_j + T_x\right)}{\eta_r\ \delta_i\ (\Delta\theta)^2\ E_i} \quad (5)$$

$$R_i^* = \frac{\Delta\eta\ \theta_r}{\eta_r\ \Delta\theta} \quad (6)$$

If the DAC technology proved to be inefficient (i.e., $\theta_r \rightarrow 0$), there will be no incentive to deploy it (i.e., $R_i^* \rightarrow 0$) and the optimal share of domestic coal will be independent of the DAC price η_r:

$$m_i^* \rightarrow \frac{\Delta\eta - \delta_i\ \Delta\theta\ \left(\theta_g\ E_i + \sum_{j\neq i} T_j + T_x\right)}{\delta_i\ (\Delta\theta)^2\ E_i} \quad (7)$$

2.1.2 Exporter's problem

In the first stage, the exporter benefits from domestic consumption of natural gas and its export's revenue while incurring the extraction and climate change damage costs. Therefore, the exporter's utility can be expressed as

$$U_e\left(\eta_g\right) = E_e + \left(\eta_g - \eta_e\right)\ (1 - m_i)\ E_i - \eta_e\ E_e - \delta_e\ (\Delta T) \quad (8)$$

where E_e is the domestic energy demand in the exporting country and η_e is the extraction unit cost. We use a linear climate damage function in the exporter's utility to reflect the potential benefits of rising temperatures for Russia which moderates the climate change damages.

Taking the first-order condition, the optimal price of natural gas can be obtained from plugging back the results of the second stage into this equation:

$$\frac{\partial U_e}{\partial \eta_g} = 0 \rightarrow (1 - m_i)\ E_i - \left(\eta_g - \eta_e\right)\frac{\partial m_i}{\partial \eta_g}\ E_i - \delta_e\left(\Delta\theta\ \frac{\partial m_i}{\partial \eta_g}\ E_i - \theta_r\ \frac{\partial R_i}{\partial \eta_g}\right) = 0$$
$$\rightarrow \eta_g^\star = \frac{\eta_c + \eta_e}{2} + \frac{\eta_r\ \Delta\theta(-\delta_e + \delta_i\ (\theta_c\ E_i + T_x))}{2\ (\eta_r + \delta_i\ \theta_r^2)} \quad (9)$$

This result shows that minimum price of exported natural gas is the average of its extraction cost and the price of coal in the importing countries. In order to gain a better understanding of the market mechanism and its impact on energy security and climate stability efforts, we consider two cases of *cooperation* and *competition* among the N importing players. We then compare the optimal share of domestic coal production and DAC deployment between these two cases.

2.2 Cooperation

In the case of full cooperation, the N importing entities act as a block (e.g., the EU negotiates the gas import from Russia on behalf of all its member states). We formulate the utility optimization problem of the importing actor (i.e., the block of N importing entities) as follows:

$$U_{coop}(m_i, R_i) = N\ E_i - N\ \eta_c\ m_i\ E_i - N\ \eta_g\ (1 - m_i)\ E_i - N\ \frac{1}{2}\ \eta_r\ R_i^2 - N\ \frac{1}{2}\ \delta_i\ (\Delta T)^2 \quad (10)$$

where the change in global mean temperature (ΔT) is calculated as

$$\Delta T = N\ \theta_c\ m_i\ E_i + N\ \theta_g\ (1 - m_i)\ E_i - N\ \theta_r\ R_i + T_x \quad (11)$$

The optimization of Eq. 10 with respect to decision variables m_i (the share of domestic coal) and R_i (the carbon removal through DAC) provides the following two firs-order conditions:

$$\frac{\partial U_{coop}}{\partial m_i} = 0 \rightarrow m_i = \frac{\Delta\eta - N\ \delta_i\ \Delta\theta\ \left(N\ \theta_g\ E_i - N\ \theta_r\ R + T_x\right)}{N^2\ \delta_i\ (\Delta\theta)^2\ E_i} \quad (12)$$

$$\frac{\partial U_{coop}}{\partial R_i} = 0 \rightarrow R_i = \frac{N\ \delta_i\ \theta_r\ \left(N\ m\ \Delta\theta\ E_i + N\ \theta_g\ E_i + T_x\right)}{\eta_r + N^2\ \delta_i\ \theta_r^2} \quad (13)$$

Solving these equations simultaneously will provide the optimal levels of m_i and R_i in this case.

$$m_{i-coop}^\star = \frac{\Delta\eta\ (\eta_r + N^2\ \delta_i\ \theta_r^2) - N\ \delta_i\ \eta_r\ \Delta\theta\ \left(N\ \theta_g\ E_i + T_x\right)}{N^2\ \eta_r\ \delta_i\ (\Delta\theta)^2\ E_i} \quad (14)$$

$$R_{i-coop}^\star = \frac{\Delta\eta\ \theta_r}{\eta_r\ \Delta\theta} \quad (15)$$

In this case, the price of natural gas in the first stage will be calculated as

$$\eta_{g-coop}^\star = \frac{\eta_c + \eta_e}{2} + \frac{\eta_r\ \Delta\theta(-\delta_e + N\ \delta_i\ (N\ \theta_c\ E_i + T_x))}{2\ (\eta_r + N^2\ \delta_i\ \theta_r^2)} \quad (16)$$

Next, we investigate the case when the N importing countries act independently in a competitive market.

2.3 Competition

In this case, every importing entity decides on the level of domestic coal production and DAC deployment independently, bearing in mind that other importing entities are doing the same. We formulate the utility optimization problem of each importing actor as follows:

$$U_{comp}(m_i, R_i) = E_i - \eta_c\ m_i\ E_i - \eta_g\ (1 - m_i)\ E_i - \frac{1}{2}\ \eta_r\ R_i^2 - \frac{1}{2}\ \delta_i\ (\Delta T)^2 \tag{17}$$

where the change in global mean temperature (ΔT) is calculated as

$$\Delta T = \theta_c\ m_i\ E_i + \theta_g\ (1 - m_i)\ E_i - \theta_r\ R_i + \sum_{j \neq i} T_j + T_x \tag{18}$$

The optimization of Eq. 17 with respect to decision variables m_i (the share of domestic coal) and R_i (the carbon removal through DAC) provides firs-order conditions similar to those shown in Eqs 3, 4. However, since all N importing entities are similar, the solution should be the same for everyone and therefore, we have $T_i = T_j$ for all $i, j \in \{1, \ldots, N\}$.

$$\frac{\partial U_{comp}}{\partial m_i} = 0 \rightarrow m_i = \frac{\Delta\eta - \delta_i\ \Delta\theta\ \left(N\ \theta_g\ E_i - N\ \theta_r\ R + T_x\right)}{N\ \delta_i\ (\Delta\theta)^2\ E_i} \tag{19}$$

$$\frac{\partial U_{comp}}{\partial R_i} = 0 \rightarrow R_i = \frac{\delta_i\ \theta_r\ \left(N\ m\ \Delta\theta\ E_i + N\ \theta_g\ E_i + T_x\right)}{\eta_r + N\ \delta_i\ \theta_r^2} \tag{20}$$

As a result the optimal levels of m_i and R_i in this case will be.

$$m^{\star}_{i-comp} = \frac{\Delta\eta\ \left(\eta_r + N\ \delta_i\ \theta_r^2\right) - \delta_i\ \eta_r\ \Delta\theta\ \left(N\ \theta_g\ E_i + T_x\right)}{N\ \eta_r\ \delta_i\ (\Delta\theta)^2\ E_i} \tag{21}$$

$$R^{\star}_{i-comp} = \frac{\Delta\eta\ \theta_r}{\eta_r\ \Delta\theta} \tag{22}$$

In this case, the price of natural gas in the first stage will be calculated as

$$\eta^{\star}_{g-comp} = \frac{\eta_c + \eta_e}{2} + \frac{\eta_r\ \Delta\theta(-\delta_e + \delta_i\ (N\ \theta_c\ E_i + T_x))}{2\ \left(\eta_r + N\ \delta_i\ \theta_r^2\right)} \tag{23}$$

3 Results

The derivation of optimal natural gas price in the first stage, and energy security (m) and climate stability measures (R) in the second stage for a given number of importing entities (N) allows us to infer important comparisons between the two extreme cases of full cooperation and full competition. To do so, we first consider a case where the natural gas price is exogenously determined by the exporter, and then we investigate the full endogenous case where the price is set in the first stage foreseeing the market conditions in the second stage.

3.1 Exogenous natural gas prices

We evaluate the performance of each case along the energy security dimension by comparing the share of domestic coal in final energy consumption in both cases under the assumption that the all prices are exogenous and therefore, we only focus on the implications of a fixed price of natural gas on the performance of both markets. Proposition 1 unveils the important implication of the well-know free-riding phenomenon in the competition case. While competition disincentives lowering emissions and therefore, encourages the consumption of the dirtier domestic coal, cooperation induces higher imports of (relatively cleaner) natural gas to lower emissions. In other words, cooperation, unintentionally, leads to higher reliance on foreign energy which undermines energy security within the EU.

Proposition 1. *For a given $N > 1$ and an exogenous natural gas price higher than coal price ($\eta_g > \eta_c$), the share of imported natural gas is always (strictly) higher in the full cooperation case compared to the full competition case regardless of the availability of any climate stability measure (e.g., DAC).*

Proof. To prove this proposition, we compare the share of domestic coal in both cases using Eq. 21 and Eq. 14. If we can show that the difference between the two shares for any given N and η_m is strictly positive, it means that the EU imports less natural gas in the competition case and therefore, the theorem is proved. Let's define $\Delta_m = m^{\star}_{i-comp} - m^{\star}_{i-coop}$. We want to show that $\Delta_m > 0$ for all N:

$$\begin{aligned}\Delta^{ex}_m &= m^{\star}_{i-comp} - m^{\star}_{i-coop} \\ &= \frac{\Delta\eta\left(\eta_r + N\delta_i\theta_r^2\right) - \delta_i\eta_r\Delta\theta\ \left(N\theta_g E_i + T_x\right)}{N\ \eta_r\ \delta_i\ (\Delta\theta)^2\ E_i} \\ &\quad - \frac{\Delta\eta\left(\eta_r + N^2\delta_i\theta_r^2\right) - N\delta_i\eta_r\Delta\theta\left(N\theta_g E_i + T_x\right)}{N^2\ \eta_r\ \delta_i(\Delta\theta)^2\ E_i} \\ &= \frac{(N-1)\ \Delta\eta}{N^2\ \delta_i\ (\Delta\theta)^2\ E_i} > 0 \qquad \text{for } N > 1\end{aligned} \tag{24}$$

Since all of its components are positive, Δ^{ex}_m is positive.

3.2 Endogenous natural gas prices

So far we have analysed energy security and climate stability implications of exogenous imported natural gas rices in cooperative and competitive markets. Now, we allow for the natural gas price to be determined endogenously through Eq. 16 and Eq. 23 for any given number of importing entities (N). Proposition below asserts that in the first stage, the natural gas exporter foreseeing the market conditions in the second stage, always sets the natural gas price higher in the cooperation case compared to the competition case.

Proposition 2. *For a given $N > 1$, the price of natural gas in the full cooperation case is (strictly) higher than the full competition case regardless of the availability of any climate stability measure such as DAC.*

Proof. To prove this proposition, we compare the natural gas price in both cases using Eq. 16 and Eq. 23. If we can show that for a given N, the difference between the two prices is strictly positive, the theorem is proved. Let's define $\Delta_g = \eta_{g-coop} - \eta_{g-comp}$. We want to show that $\Delta_g > 0$ for all N:

$$\begin{aligned}\Delta_g^{en} &= \eta_{g-coop} - \eta_{g-comp} \\ &= \frac{\eta_r\ \Delta\theta(-\delta_e + N\ \delta_i\ (N\ \theta_c\ E_i + T_x))}{2\ (\eta_r + N^2\ \delta_i\ \theta_r^2)} - \frac{\eta_r\ \Delta\theta(-\delta_e + \delta_i\ (N\ \theta_c\ E_i + T_x))}{2\ (\eta_r + N\ \delta_i\ \theta_r^2)} \\ &= \frac{(N-1)\ \delta_i\ \eta_r\ \Delta\theta\ (N\ \delta_e\ \theta_r^2 + \eta_r\ (N\ \theta_c\ E_i + T_x))}{2\ (\eta_r + N^2\ \delta_i\ \theta_r^2)\ (\eta_r + N\ \delta_i\ \theta_r^2)} > 0 \qquad \text{for } N > 1\end{aligned} \tag{25}$$

Since all the components are positive, Δ_g is positive. In the special case when $\theta_r = 0$ (i.e., DAC is ineffective or more generally, in the no-DAC case) the difference will be simplified to:

$$\Delta_{g-no\ DAC} = \frac{(N-1)\ \Delta\theta\ \delta_i\ (N\ \theta_c\ E_i + T_x)}{2} > 0 \qquad \text{for } N > 1 \tag{26}$$

which again is positive and therefore, the theorem holds regardless of the availability of any climate stability measure such as DAC.

The comparison between the optimal share of domestic coal in the cooperative case and competitive case is less straightforward since it both depends on the number of importers and the price of natural gas as shown in equation below.

$$\begin{aligned}\Delta_m^{en} &= m_{i-comp}^{\star} - m_{i-coop}^{\star} \\ &= \frac{\Delta\eta^{comp}\left(\eta_r + N\delta_i\theta_r^2\right) - \delta_i\eta_r\Delta\theta\left(N\theta_g E_i + T_x\right)}{N\ \eta_r\ \delta_i\ (\Delta\theta)^2\ E_i} \\ &\quad - \frac{\Delta\eta^{coop}\left(\eta_r + N^2\delta_i\theta_r^2\right) - N\delta_i\eta_r\Delta\theta\left(N\theta_g E_i + T_x\right)}{N^2\ \eta_r\ \delta_i\ (\Delta\theta)^2\ E_i} \\ &= \frac{-\left(\eta_{g-coop} - N\ \eta_{g-comp}\right)\eta_r - \left(\eta_{g-coop} - \eta_{g-comp}\right)N^2\ \eta_r\ \delta_i\ \theta_r - (N-1)\ \eta_c\ \eta_r}{N^2\ \delta_i\ (\Delta\theta)^2\ E_i} \\ &= \frac{-\left(\eta_{g-coop} - N\ \eta_{g-comp}\right)\eta_r - \Delta_g^{en}\ N^2\ \eta_r\ \delta_i\ \theta_r - (N-1)\ \eta_c\ \eta_r}{N^2\ \delta_i\ (\Delta\theta)^2\ E_i}\end{aligned} \tag{27}$$

We know from Eq. 25 that $\Delta_g^{en} > 0$, therefore the sign of Δ_m^{en} only depends on the value of the first term in the numerator, $\eta_{g-coop} - N\ \eta_{g-comp}$. If the natural gas price in the cooperation case is at least N times larger than the price in the competition case then $\Delta_m^{en} < 0$ which means the share of domestic coal will be higher in the cooperation case. Otherwise, the price difference Δ_m^{en} may or may not be negative depending on other factors including the climate damage costs in importing and exporting countries.

4 Numerical example

Figure 2 shows the result of a hypothetical model with the following parameter values: $E_i = 150$, $E_e = 80$, $\eta_c = 0.25$, $\eta_r = 0.001$, $\eta_e = 0.4$, $\theta_c = 0.003$, $\theta_g = 0.00012$, $\theta_r = 0.001$, $\delta_i = 400$, $\delta_e = 75$, and $T_x = 0.15$.

The first 2 rows of this figure correspond to the case with exogenous gas price while the last row is related to the results of the case with endogenous gas price. In Figures 2A,C we assume that the number of importing countries is fixed at $N = 10$. In Figures 2B,D we assume that the natural gas price is fixed at $\eta_g = 0.76$.

Using this set of numerical values, we are able to make a quantitative comparison between the two cases of full cooperation and competition.

4.1 Exogenous natural gas prices

Keeping the number of importing countries constant at $N = 10$, in the cooperation case, from Eqs 14, 15 we get.

$$m_{i-coop}^{\star} = -0.282 + 0.824\ \eta_g \tag{28}$$

$$R_{i-coop}^{\star} = -87 + 347\ \eta_g \tag{29}$$

Similarly, in the competition case, from Eqs 21, 22 we get.

$$m_{i-comp}^{\star} = -0.328 + \eta_g \tag{30}$$

$$R_{i-comp}^{\star} = -87 + 347\ \eta_g \tag{31}$$

As price increases, there is more incentive for importing entities to rely on their domestic energy production in both cases. However, as stated in Proposition 1, such reliance on domestic production is always higher in the competition case compared to the cooperation case. Therefore, the red continuous line corresponding to optimal import share in the competition case cooperation stays above the blue dashed line (Figure 2A).

Alternatively, keeping the natural gas price constant at $\eta_g = 0.76$, in the cooperation case, from Eqs 14, 15 we get.

$$m_{i-coop}^{\star} = \frac{51 - 17\ N + 18\ N^2}{50\ N^2} \tag{32}$$

$$R_{i-coop}^{\star} = 177 \tag{33}$$

Similarly, in the competition case, from Eqs 21, 22 we get.

$$m_{i-comp}^{\star} = \frac{34 - 18\ N}{50\ N} \tag{34}$$

$$R_{i-comp}^{\star} = 177 \tag{35}$$

In this case, the optimal domestic coal shares follow a reciprocal form and converge in the limit case where $N \to \infty$ (i.e., a large number of countries import natural gas from Russia). In this situation, the difference between the two cases will approaches zero and the cooperative share of domestic coal nears the competitive share ($m^* \to 0.36$) implying that every country imports the same share of their energy consumption from Russia regardless of the market structure. Therefore, and similar to the previous case, by following Proposition 1 we have the red continuous curve corresponding to optimal import share in the competition case cooperation staying above the blue dashed curve corresponding to optimal import share in the cooperation case (Figure 2B).

Optimal deployment of DAC however, is always the same in both cooperation and competition cases according to Eq. 15 and Eq. 22 and only depends on the price of imported natural gas. Therefore, when the natural gas price increases the optimal DAC deployment level increases (Figure 2C) while it stays constant when the natural gas price is fixed (Figure 2D). Nevertheless, since the optimal level of DAC deployment is the same in both cases of cooperation and competition, climate change outcomes such as global mean temperature will be worse off under the competitive market conditions due to higher rates of domestic coal consumption.

Finally, as shown in Eq. 24, the difference in the optimal share of domestic coal between the cooperation and competition cases do not depend on the DAC's effectiveness (θ_r) or cost (η_r). Therefore, if a reliable DAC technology is not available (e.g., $\theta_r = 0$), Proposition 1 still holds and the free-riding phenomenon discussed above, still applies to a limit case without DAC.

4.2 Endogenous natural gas prices

Figure 2E shows the schematic comparison of natural gas prices between the two cases of cooperation and competition by changing

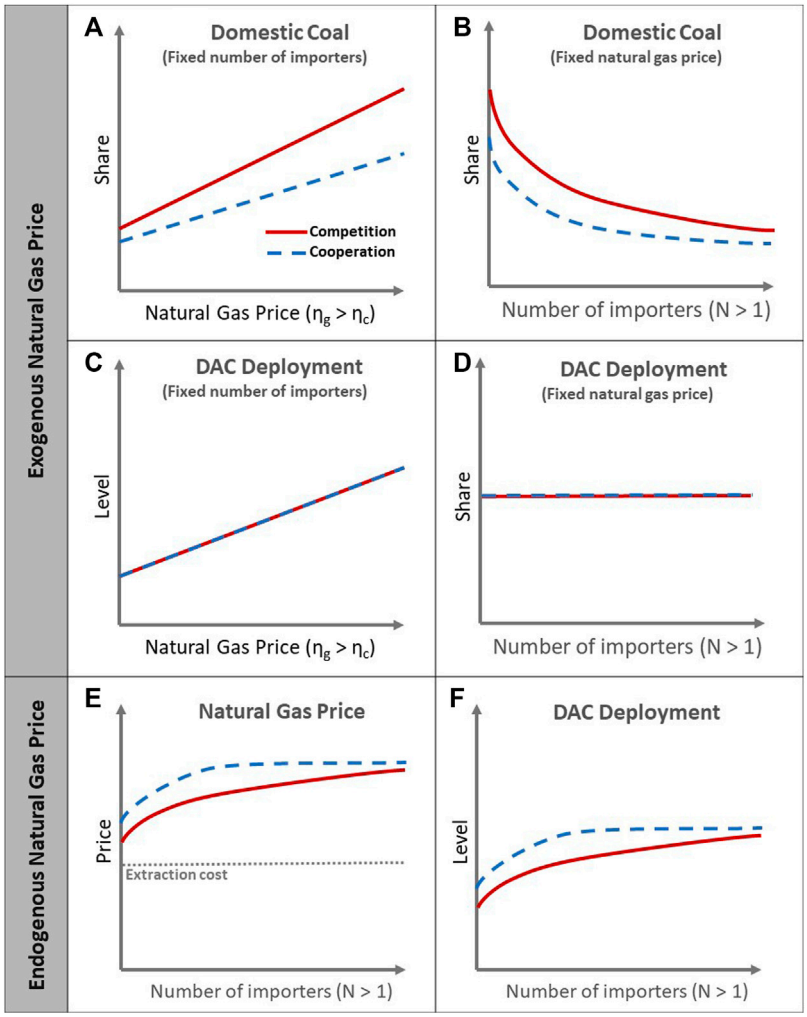

FIGURE 2
Natural gas prices impact in two cases of *cooperation* and *competition* with exogenous natural gas prices **(A–D)** or endogenous natural gas prices **(E,F)**: **(A)** optimal share of domestic coal with a fixed number of importers, **(B)** optimal share of domestic coal with a fixed natural gas price, **(C)** optimal level of DAC deployment with a fixed number of importers, **(D)** optimal level of DAC deployment with a fixed natural gas price, **(E)** natural gas price with varying number of importing entities, and **(F)** DAC deployment levels with varying number of importing entities.

the number of importing entities. The natural gas price can be obtained from Eq. 16 in the cooperation case and Eq. 23 in the competition case:

$$\eta^{\star}_{g-coop} = 0.325 + \frac{-270 + 216\ N + 648\ N^2}{2500 + 1000\ N^2} \tag{36}$$

$$\eta^{\star}_{g-comp} = 0.325 + \frac{-54 + 648\ N}{2500 + 1000\ N} \tag{37}$$

As shown in Figure 2E and according to Proposition 2, the red continuous curve corresponding to optimal import share in the competition case cooperation stays below the blue dashed curve corresponding to optimal import share in the cooperation case. As N increases, the imported natural gas price grows slowly in both cases while the price in cooperative case is always dominating the price in the competitive case. In the limit case where $N \to \infty$ (i.e., a large number of countries import natural gas from Russia), the natural gas price in both cases approaches. $\eta^{\star}_{g} \to 0.973$

Similarly, for the optimal DAC level, from Eq. 15 and Eq. 22 we get.

$$R^{\star}_{i-coop} = 26 + \frac{-93750 + 75000\ N + 225000\ N^2}{2500 + 1000\ N^2} \tag{38}$$

$$R^{\star}_{i-comp} = 26 + \frac{-18750 + 225000\ N}{2500 + 1000\ N} \tag{39}$$

The results of this case are shown in Figure 2F similar to the natural gas price, the red continuous curve corresponding to optimal DAC level in the competition case cooperation stays below the blue dashed curve corresponding to optimal import share in the cooperation case. As N increases, the imported natural gas price grows slowly in both cases while the price in cooperative case is always dominating the DAC levels in the competitive case. In the limit case where $N \to \infty$, the DAC level in both cases approaches $R^{\star} \to 251$.

This has a significant implications for energy security and climate stability. As the optimal share of domestic coal and the

optimal level of DAC deployment both directly depend on the natural gas price, an increase in the price of natural gas induce more reliance on domestic coal for energy security and DAC for climate stability. For any given number of importers, $N > 1$, since the natural gas price is higher in the cooperative case, the optimal level of DAC deployment will also be higher in the cooperative case compared to the competitive case.

5 Discussion

The topic of energy security cannot and should not be addressed without climate change considerations. In particular, and in the case of the EU, the European Green Deal and the Climate law have already provided legal frameworks for the member states to achieve the collective objective of reaching climate neutrality by 2050 while ensuring their energy security (Claeys et al., 2019). Nevertheless, the recent developments in energy markets due to the invasion of Ukraine by Russia has revealed growing vulnerability of the EU energy market to foreign actions beyond its jurisdiction (Mišík, 2022).

This paper has provided an analytical framework for assessing the implications of cooperation and competition among the members of a union such as the EU, for their energy security and climate stability. Despite many simplifying assumptions in this model, it provides several findings which shed light on some less-discussed mechanisms shaping energy markets and climate change solutions.

First, when the natural gas prices are exogenous meaning that they are determined globally and are not affected by the coordination decisions of importing entities at the local level, the optimal level of climate intervention through carbon removal technologies such as DAC is independent of the market conditions (e.g., cooperation or competition). It only depends on the properties of the removal technology (e.g., cost and effectiveness) and the degree that imported and domestic fossil fuels differ in costs and warming potentials. In other words, while energy security considerations yield an optimal combination of imported natural gas and domestic coal to meet the energy demand in any member state, carbon removal measures such as DAC are deployed to offset the emissions rising from such energy portfolio and provide better climate stability.

Furthermore, cooperation among importing entities result in more reliance on imported natural gas in the case of exogenous natural gas prices. This is due to the fact that cooperation induces a coordinated and aggressive emission cuts which implies lowering the consumption of domestic coal and relying on cleaner but more expensive natural gas. Therefore, while cooperation may undermine energy security, competition threatens climate stability despite the availability of DAC.

Finally, if the natural gas price is sensitive to the market conditions, cooperation among importers sends a strong signal about their climate ambitions to curb emissions by reducing domestic coal consumption. The natural gas exporter in this case, is likely to increase the price. If the price increase is significant enough (i.e., if the price in the cooperation case is at least N times the price in the competition case), then the cooperative importers are forced to reduce their import and rely more on their domestic coal. However, higher natural gas price in the cooperation case will also results in higher DAC deployment to offset the emissions resulting from such energy policy switch.

This paper only considered two extreme cases of full cooperation and full competition among identical entities assuming a simple linear form of energy cost and benefit. In reality, the EU countries have very different social, political, and economic characteristics and the energy cost structures are far from being linear. The level of coordination among the EU member states varies significantly over time and over different issues ranging from cooperation to competition side of the spectrum. Furthermore, significant differences in energy system and climate damage cost among the EU member countries or any other economic or political block of cooperating countries can lead to very different outcomes in terms of optimal level of energy import or CDR deployment. Nevertheless, this paper tried to provide an analytical framework for investigating the issues at the intersection of climate security and climate stability. Future research may extend this analysis by incorporating other players and other energy options as well more sophisticated climate change models. A full assessment of energy policies at the national and the EU levels require deeper understanding of domestic energy needs and ambitions as well as potential climate change damages that affect local communities and can translate into political demand for action in the realm of climate change intervention.

Data availability statement

The original contributions presented in the study are included in the article/Supplementary Materials, further inquiries can be directed to the corresponding author.

Author contributions

SS carried out the research and wrote the manuscript solely.

Funding

This project has received funding from the European Union's Horizon 2020 research and innovation programme under grant agreements No. 101036458—LOCALISED—Localised decarbonisation pathways for citizens, local administrations and businesses to inform for mitigation and adaptation action.

Acknowledgments

I acknowledge the full LOCALISED project team for their support.

Conflict of interest

The author declares that the research was conducted in the absence of any commercial or financial relationships that could be construed as a potential conflict of interest.

Publisher's note

References

Aliprantis, C. D. (1999). On the backward induction method. *Econ. Lett.* 64, 125–131. doi:10.1016/s0165-1765(99)00068-3

Bednar, J., Obersteiner, M., Baklanov, A., Thomson, M., Wagner, F., Geden, O., et al. (2021). Operationalizing the net-negative carbon economy. *Nature* 596, 377–383. doi:10.1038/s41586-021-03723-9

Beuttler, C., Charles, L., and Wurzbacher, J. (2019). The role of direct air capture in mitigation of anthropogenic greenhouse gas emissions. *Front. Clim.* 1, 10. doi:10.3389/fclim.2019.00010

Buck, H. J. (2016). Rapid scale-up of negative emissions technologies: Social barriers and social implications. *Clim. Change* 139, 155–167. doi:10.1007/s10584-016-1770-6

Buschle, D., and Westphal, K. (2019). A challenge to governance in the eu: Decarbonization and energy security. *Eur. Energy & Clim. J.* 8, 53–64. doi:10.4337/eecj.2019.03-04.04

Chatterjee, S., and Huang, K.-W. (2020). Unrealistic energy and materials requirement for direct air capture in deep mitigation pathways. *Nat. Commun.* 11, 3287–3293. doi:10.1038/s41467-020-17203-7

Claeys, G., Tagliapietra, S., and Zachmann, G. (2019). *How to make the European Green Deal work (JSTOR)* Brussels: Bruegel.

Commission, E., and for Communication, D. G. (2021). *European green deal: Delivering on our targets.* Publications Office. doi:10.2775/595210

Cox, E., Spence, E., and Pidgeon, N. (2020). Public perceptions of carbon dioxide removal in the United States and the United Kingdom. *Nat. Clim. Change* 10, 744–749. doi:10.1038/s41558-020-0823-z

Erans, M., Sanz-Pérez, E. S., Hanak, D. P., Clulow, Z., Reiner, D. M., and Mutch, G. A. (2022). Direct air capture: Process technology, techno-economic and socio-political challenges. *Energy Environ. Sci.* 15, 1360–1405. doi:10.1039/d1ee03523a

Fasihi, M., Efimova, O., and Breyer, C. (2019). Techno-economic assessment of co2 direct air capture plants. *J. Clean. Prod.* 224, 957–980. doi:10.1016/j.jclepro.2019.03.086

Galán-Martín, Á., Vázquez, D., Cobo, S., Mac Dowell, N., Caballero, J. A., and Guillén-Gosálbez, G. (2021). Delaying carbon dioxide removal in the European Union puts climate targets at risk. *Nat. Commun.* 12, 6490–6512. doi:10.1038/s41467-021-26680-3

Hanna, R., Abdulla, A., Xu, Y., and Victor, D. G. (2021). Emergency deployment of direct air capture as a response to the climate crisis. *Nat. Commun.* 12, 368. doi:10.1038/s41467-020-20437-0

IPCC (2022). *Climate change 2022: Mitigation of climate change. Contribution of working group III to the sixth assessment report of the intergovernmental panel on climate change*. Cambridge, UK and New York, NY, USA: Cambridge University Press. doi:10.1017/9781009157926

Maris, G., and Flouros, F. (2021). The green deal, national energy and climate plans in Europe: Member states' compliance and strategies. *Adm. Sci.* 11, 75. doi:10.3390/admsci11030075

McQueen, N., Gomes, K. V., McCormick, C., Blumanthal, K., Pisciotta, M., and Wilcox, J. (2021). A review of direct air capture (dac): Scaling up commercial technologies and innovating for the future. *Prog. Energy* 3, 032001. doi:10.1088/2516-1083/abf1ce

Mišík, M. (2022). The eu needs to improve its external energy security. *Energy Policy* 165, 112930. doi:10.1016/j.enpol.2022.112930

National Academies of Sciences Engineering and Medicine (2019). *Negative emissions technologies and reliable sequestration: A research agenda*. National Academies Press.

Nemet, G. F., Callaghan, M. W., Creutzig, F., Fuss, S., Hartmann, J., Hilaire, J., et al. (2018). Negative emissions—Part 3: Innovation and upscaling. *Environ. Res. Lett.* 13, 063003. doi:10.1088/1748-9326/aabff4

Nordhaus, W. D. (2017). Revisiting the social cost of carbon. *Proc. Natl. Acad. Sci.* 114, 1518–1523. doi:10.1073/pnas.1609244114

Osička, J., and Černoch, F. (2022). European energy politics after Ukraine: The road ahead. *Energy Res. Soc. Sci.* 91, 102757. doi:10.1016/j.erss.2022.102757

Pérez, M. d. l. E. M., Scholten, D., and Stegen, K. S. (2019). The multi-speed energy transition in Europe: Opportunities and challenges for eu energy security. *Energy Strategy Rev.* 26, 100415. doi:10.1016/j.esr.2019.100415

Richard, S. (1995). The damage costs of climate change toward more comprehensive calculations. *Environ. Resour. Econ.* 5, 353–374. doi:10.1007/bf00691574

Shayegh, S., Bosetti, V., and Tavoni, M. (2021). Future prospects of direct air capture technologies: Insights from an expert elicitation survey. *Front. Clim.* 46. doi:10.3389/fclim.2021.630893

Smith, P., Davis, S. J., Creutzig, F., Fuss, S., Minx, J., Gabrielle, B., et al. (2016). Biophysical and economic limits to negative co2 emissions. *Nat. Clim. change* 6, 42–50. doi:10.1038/nclimate2870

Sovacool, B. K., Baum, C. M., and Low, S. (2023). Reviewing the sociotechnical dynamics of carbon removal. *Joule* 7, 57–82. doi:10.1016/j.joule.2022.11.008

Urmee, T., and Md, A. (2016). Social, cultural and political dimensions of off-grid renewable energy programs in developing countries. *Renew. Energy* 93, 159–167. doi:10.1016/j.renene.2016.02.040

Żuk, P., and Żuk, P. (2022). National energy security or acceleration of transition? Energy policy after the war in Ukraine. *Joule* 6, 709–712. doi:10.1016/j.joule.2022.03.009

frontiers | Frontiers in Chemical Engineering

TYPE Review
PUBLISHED 07 September 2023
DOI 10.3389/fceng.2023.1228510

OPEN ACCESS

EDITED BY
Oisik Das,
Luleå University of Technology, Sweden

REVIEWED BY
Hugo Olvera-Vargas,
National Autonomous University of Mexico, Mexico
Arvind Kumar Mungray,
Sardar Vallabhbhai National Institute of Technology, India
Rhoda Afriyie Mensah,
Luleå University of Technology, Sweden

*CORRESPONDENCE
Prabhu Saravanan,
psaravanan@udec.cl
Cristian H. Campos,
ccampos@udec.cl

RECEIVED 24 May 2023
ACCEPTED 22 August 2023
PUBLISHED 07 September 2023

CITATION
Elangovan K, Saravanan P, Campos CH, Sanhueza-Gómez F, Khan MMR, Chin SY, Krishnan S and Viswanathan Mangalaraja R (2023), Outline of microbial fuel cells technology and their significant developments, challenges, and prospects of oxygen reduction electrocatalysts.
Front. Chem. Eng. 5:1228510.
doi: 10.3389/fceng.2023.1228510

Outline of microbial fuel cells technology and their significant developments, challenges, and prospects of oxygen reduction electrocatalysts

Kavery Elangovan[1], Prabhu Saravanan[2,3]*, Cristian H. Campos[2]*, Felipe Sanhueza-Gómez[3], Md. Maksudur Rahman Khan[4], Sim Yee Chin[5], Santhana Krishnan[6] and Ramalinga Viswanathan Mangalaraja[7]

[1]Department of Chemistry, N.K.R. Government Arts College for Women, Namakkal, India, [2]Department of Physical-Chemistry, Faculty of Chemical Sciences, University of Concepcion, Concepción, Chile, [3]Electrochemical Technologies and Green Energies Laboratory, Department of Materials Engineering, Faculty of Engineering, University of Concepcion, Concepción, Chile, [4]Petroleum and Chemical Engineering Programme Area, Faculty of Engineering, Universiti Teknologi Brunei, Gadong, Brunei, [5]Faculty of Chemical and Process Engineering Technology, Universiti Malaysia Pahang Al-Sultan Abdullah, Gambang, Malaysia, [6]Department of Civil and Environmental Engineering, Faculty of Engineering, Prince of Songkla University, Hat Yai, Songkhla, Thailand, [7]Faculty of Engineering and Sciences, Adolfo Ibáñez University, Santiago, Chile

The microbial fuel cells (MFCs) which demonstrates simultaneous production of electricity and wastewater treatment have been considered as one of the potential and greener energy production technology among the available bioelectrochemical systems. The air-cathode MFCs have gained additional benefits due to using air and avoiding any chemical substances as catholyte in the cathode chamber. The sluggish oxygen reduction reaction (ORR) kinetics at the cathode is one of the main obstacles to achieve high microbial fuel cell (MFC) performances. Platinum (Pt) is one of the most widely used efficient ORR electrocatalysts due to its high efficient and more stable in acidic media. Because of the high cost and easily poisoned nature of Pt, several attempts, such as a combination of Pt with other materials, and using non-precious metals and non-metals based electrocatalysts has been demonstrated. However, the efficient practical application of the MFC technology is not yet achieved mainly due to the slow ORR. Therefore, the review which draws attention to develop and choosing the suitable cathode materials should be urgent for the practical applications of the MFCs. In this review article, we present an overview of the present MFC technology, then some significant advancements of ORR electrocatalysts such as precious metals-based catalysts (very briefly), non-precious metals-based, non-metals and carbon-based, and biocatalysts with some significant remarks on the corresponding results for the MFC applications. Lastly, we also discussed the challenges and prospects of ORR electrocatalysts for the practical application of MFCs.

KEYWORDS

microbial fuel cells (MFCs), oxygen reduction reaction (ORR), electrocatalysts, electricity production, wastewater treatment

1 Introduction

The shrinking of non-renewable energy sources and environmental pollution are the main critical issues the world has been facing in recent years. Therefore, the research area of energy generation by the alternative renewable sources is increasing drastically. Converting organic or inorganic waste materials into useful products and energy can better address energy and environmental problems (Babanova et al., 2022; Díaz-Vázquez et al., 2022; Gargalo et al., 2022; Kamali et al., 2023). Bioelectrochemical systems (BES) can be an effective potential candidate for the waste materials conversion and energy production (Agudelo-Escobar et al., 2022). BES is one of the emerging bioengineering technologies which show the process of electrochemical reactions, such as the conversion of chemical energy into electrical energy or *vice versa*, in the presence of microorganisms or biomaterials (Zheng et al., 2020). In the BES, the microorganism can exchange electrons with the electrodes directly or indirectly via a chemical compound that acts as an electron carrier (E. Logan et al., 2006). The BES can be categorized based on the task as (i) microbial fuel cells (MFCs), (ii) plant MFCs (P-MFC), (iii) constructed wetlands MFCs (CW-MFC) (iv) benthic MFCs (B-MFC), (v) microbial electrolysis cells (MEC), (vi) anaerobic digestion coupled MEC (AD-MEC), (vii) microbial electrosynthesis cells (MES), (viii) microbial desalination cells (MDC), and (ix) microbial electro-Fenton (MEF) (Zou and He, 2018; Mier et al., 2021). MFCs and P-MFC will generate electricity from an organic substrate using microorganisms and living plants with microorganisms, respectively as a catalyst. In the CW-MFC, the electricity generation and wastewater treatment occurs in MFCs integrated with constructed wetlands. In B-MFC, the electricity will be generated using sea's inorganic and organic matter in the presence of bacterial catalysis. In MEC, the hydrogen (H_2) can be produced in its cathode part by reducing H^+ using small external voltage and the ammonia recovery from wastewater. By reducing carbon dioxide, the MES can generate value-added chemical products, such as formic acid, acetate, ethanol, and butanol. Besides, methane can be produced by the degradation of a substrate from the AD-MEC system. The MDC produces fresh water from seawater or brackish water with the help of self-produced electricity or applying the external electricity (Wang and Ren, 2013). In MEF, the electricity will be generated at the anode microbial chamber, and H_2O_2 will be generated at the cathode chamber (Mier et al., 2021). The BES has several advantages, such as the clean process, lower operational cost, flux of electrons, and the energy level can be adjusted and maintained constant. The electrical signal can be used for monitoring and high selectivity towards the target compounds. Besides, there are disadvantages of BES, such as the challenge of scale-up, the cathodic reaction in MFC may limit the anodic reaction, pH changes of the system may affect the electrochemical process and the formation of chlorine gas from marine environment (Daghio et al., 2017).

Among the above bioelectrochemical systems, microbial fuel cell (MFC) is considered one of the potential renewable energy devices where microorganisms used as biocatalysts to convert organic substrates into electricity (E. Logan et al., 2006; Slate et al., 2019; Priya et al., 2022; Abubackar et al., 2023). An MFC requires about three times less potential difference compared to a conventional electrochemical cell for the H_2 production (Rozendal et al., 2006). The simultaneous treatment of wastewater during the electricity generation and the removal of metals such as chromium, copper, nickel, and zinc has gained additional importance regarding the environmental benefits (Nancharaiah et al., 2015; Hidayat et al., 2022). There are several review articles available very recently which include the focusing on functional materials (Zhu Q. et al., 2022), graphene-based materials (Aiswaria et al., 2022), carbonaceous materials (Dhilllon et al., 2022), nanomaterials (Chen et al., 2022b; Kamali et al., 2022; Dey et al., 2023; Kausar et al., 2023), anodic modification materials (Ma et al., 2023), and different types of MFCs (Gupta et al., 2023). Because the sluggish oxygen reduction reaction (ORR) kinetics is one of the main obstacles, the review which draws attention to choosing the suitable cathode materials should be urgent for the practical applications of the MFC technology. Therefore, here we present an overview of the present MFC technology, then some significant advancements of ORR electrocatalysts such as precious metals-based catalysts (very briefly), non-precious metals-based, non-metals and carbon-based, and biocatalysts with some significant remarks on the corresponding results for the MFC applications. Lastly, we also discussed the challenges and prospects of ORR electrocatalysts for the practical application of MFCs.

2 Microbial fuel cells (MFCs)

In the early 20th century, Potter reported the first bioelectrochemical reaction to generate electricity with some live microbial cultures such as *Escherichia coli* and *Saccharomyces* spp. and Pt macro-electrodes in a battery style system (Potter M. C., 1911). Later in 1931, Cohen confirmed this reaction by generating 0.2 mA current and 35 V voltage with a stacked bacterial fuel cell arrangement (Cohen, 1931). Interestingly after a few years, in 1963, electricity generated using human waste during space flight was demonstrated by the National Aeronautics and Space Administration (NASA) space program (Canfield et al., 1963; Slate et al., 2019). Recently, the MFC technology has been one of the best emerging eco-friendly research areas, as can be witnessed from the extensive reports (Gude, 2016; Zhang Y. et al., 2019; Kaur et al., 2020; Huang et al., 2021; Munoz-Cupa et al., 2021). A typical MFC contains anodic and cathodic chambers, which are separated by a proton exchange membrane (PEM). In the anodic chamber, microbes degrade the organic substances and produce electrons, protons (H^+), and carbon dioxide (CO_2). Then, the produced electrons and H^+ are transported through an external circuit and PEM, respectively to the cathodic chamber and react with oxygen (O_2) to form water.

Typical electrode reactions of MFC with acetic acid (CH_3COOH) as a model organic substance are shown below:

$$\text{Anodic reaction: } CH_3COOH + 2H_2O \xrightarrow{microbe} 2CO_2 + 8H^+ + 8e^- \quad (1)$$

$$\text{Cathodic reaction: } 8H^+ + 8e^- + 2O_2 \rightarrow 4H_2O \quad (2)$$

$$\text{Overall reaction: } 2CH_3COOH + 2O_2 \xrightarrow{microbe} 2H_2O + 2CO_2 \quad (3)$$

The potentials of −0.300, 0.805, and 1.105 V (vs. NHE) correspond to the anode, cathode, and the cell, respectively, for the production of electricity from the above electrochemical cell reaction (Obileke et al., 2021).

The main classification of MFC includes double-chamber MFC, single-chamber MFC, and stacked MFC. The double chamber MFC will consist of two chambers separated by a cation exchange membrane (CEM) to separate the different electrolytes in the compartments and only to allow H^+. The distance between the two electrodes and the small surface area of the membrane causes high internal resistance of these types of MFCs, hence limiting the output power density. Chemical substances like permanganate, ferricyanides, and dichromates act as oxidizing agents, and no catalysts are needed for cathodic reactions in double-chamber MFCs (Yu et al., 2017; Fang and Achal, 2019; Hidayat et al., 2022). Double-chamber MFCs are suitable for laboratory research as these are run in batch mode. Different double-chamber MFCs are available such as H-type MFC, cube-type MFC, flate-type MFC, tubular upflow MFC, and miniature MFC, which have decreased internal resistance and therefore increasing power generation(Kun et al., 2012). In a single chamber MFC, the cathode can be in direct contact with air and with the presence or absence of a membrane(Logan and Regan, 2006). The anode and cathode in a single-chamber MFCs are separated by a PEM in a single compartment and it is not necessary that the cathode part have to be filled with catholyte (electrolyte on the cathode part) when O_2 was used at the cathode. Single-chamber MFC is also called air-cathode MFC since the cathode is directly exposed to air. The single chamber MFC has emerged into several variants, such as cube-type MFC (Liu and Logan, 2004), horizontal tube-type MFC (Wang and Ren, 2013), side-arm bottle MFC (Logan et al., 2007), and upflow-type MFC (You et al., 2007). The single-chamber MFCs have several advantages over the double-chamber MFCs, such as cost-effective, simple construction, sustainable sources, and better performance. Directly harvesting electricity from the biodegradable organic substances using a single MFC is lower. This problem can be addressed by using another type of MFC called stacked MFCs, in which the MFCs are stacked in series or parallel or a combination of series and parallel (Aelterman et al., 2006; Oh and Logan, 2007; An et al., 2015; Santoro et al., 2019; Dziegielowski et al., 2021; Mukherjee et al., 2022). There are 4-module sedimentMFC (Prasad and Tripathi, 2021), 6-cell stacked MFC (Aelterman et al., 2006), bipolar type of stacked MFC (Shin et al., 2006), stacked MFCs bridged internally through an extra CEM (Liu et al., 2008) and the MFC stack assembled from two single MFCs (Oh and Logan, 2007).

3 Air-cathode MFC

The single-chamber or air-cathode MFCs demonstrated higher efficiency than double-chamber MFCs. However, the efficiency of air-cathode MFCs can be fine-tuned by controlling many factors such as substrates, inoculums, electrodes materials, PEMs, and operating conditions (Bagchi and Behera, 2019; Merino-Jimenez et al., 2019; Vilas Boas et al., 2019). The structures and the types of single-chamber MFCs were discussed earlier in Section 2.

3.1 Limitations of air-cathode MFCs performances

The limitations of the MFC technology for the industrial and social applications include using high-cost materials such as electrodes and proton exchange membranes (PEMs), low life spans, and low energy outputs.

3.1.1 Thermodynamic factors

Generally, the cathodic reactions take place in the aerobic or anaerobic conditions. The anaerobic cathodic reactions will have occurred in double-chamber MFCs where a chemical substance acts as an oxidizing agent. The aerobic condition usually occurs in the cathodic part of air-cathode MFCs. The potential generated from an MFC can be thermodynamically derived using the Nernst equation (Eq. 4) given below (Rismani-Yazdi et al., 2008),

$$E_{thermo} = E^o - \frac{RT}{n_e F}\ln(\pi) \tag{4}$$

Where, E^o, R, T, n_e, F, and π are the standard cell potential (V), ideal gas constant (8.314 J/mol K), temperature (K), number of electrons transferred in the reaction, Faraday's constant (96,485 C/mol), and the chemical activity of products divided by those of reactants, respectively.

The potential of an ideal MFC is always higher than the actual MFC because of irreversible losses such as activation losses, ohmic losses, and transport losses (Rabaey and Verstraete, 2005). The potential required for redox (oxidation-reduction) reactions to occur is the activation loss, also known as activation over potential. The overpotential is a limiting step, and this can be reduced by increasing operating temperature, efficient electrocatalysts, electrode surface area, the concentration of redox shuttles, etc. The electrical resistance between anode and cathode, solution and electrode interfaces, and the electrolyte and membrane interfaces cause ohmic losses. Ohmic losses can be avoided by using appropriate electrolyte and electrode materials which are having high electrical conductivity. Generally, at high current densities, mass transport losses occur due to the limited mass transport of species from or to the electrode. This limited mass transport causes product depletion or accumulation. These losses can be minimized by maintaining high bulk concentrations and distribution of oxidants such as O_2 at the cathode compartment (Oguz Koroglu et al., 2019).

3.1.2 Other factors

In addition to the above thermodynamic factors, several other factors such as biofouling, catalyst inactivation (if existing), and excessive biofilm growth are the main obstacles to the real-world applications of the technology (Sun M. et al., 2016; Li et al., 2023). The factors such as microbial electron transfer, supply of oxygen, fuel oxidation, circuit resistance, proton transfer via the PEM, pH, concentration, and reduction at the cathode influenced the MFCs' performances (Woodward et al., 2010; Jatoi et al., 2021). The crossover of electron acceptors or organic compounds from the cathode compartment to the anode compartment and *vice versa* also decreases the efficiency of the MFCs (Harnisch et al., 2009; Winfield et al., 2013). The biofouling involves the generation of insulating materials such as polymeric and/or dead cells, which can separate the dynamic biofilm from the surface of the electrode or blockage the porous electrode surface. This results in the reduction of efficiently active sites of the electrodes and ultimately decrease the overall performance of MFCs (Amirul Islam et al., 2016; Sun M. et al., 2016; Blanchet et al., 2016).

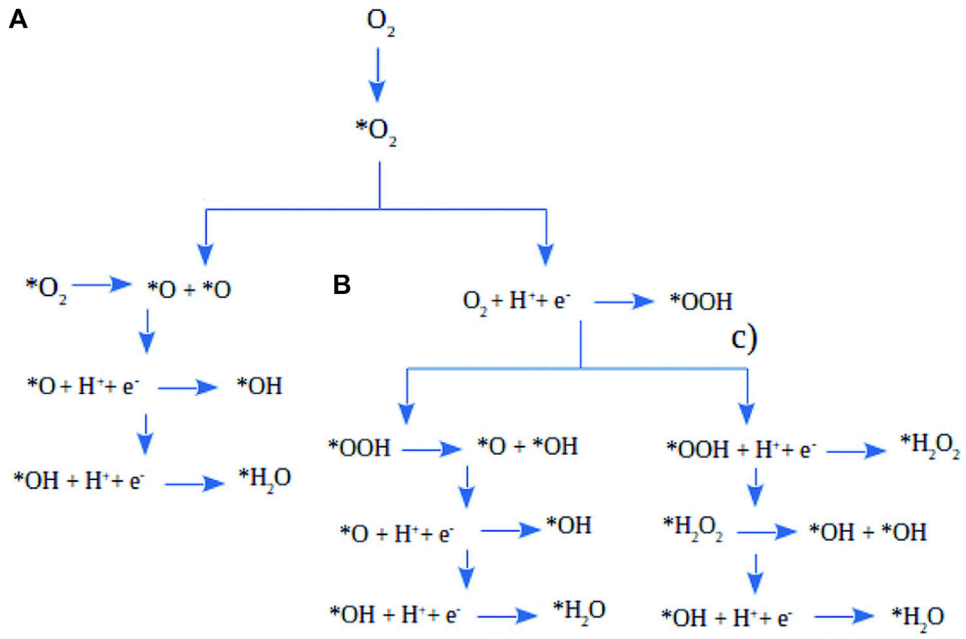

FIGURE 1
Possible mechanisms of ORR: **(A)** dissociation of O_2, **(B)** dissociation of OOH, and **(C)** dissociation of H_2O_2 (Haile et al., 2020).

4 Mechanisms of oxygen reduction reaction (ORR)

The ORR is an essential reaction in many systems, such as biological respiration, fuel cells, and metal-air batteries. In an aqueous solution, the ORR occurs mainly by two pathways which are a) direct four-electron transfer from O_2 to H_2O (Equations 5–9) and b) the two-electron transfer from O_2 to hydrogen peroxide (H_2O_2) (Equations 10–12). The one-electron transfer pathway from O_2 to superoxide (O^{2-}) could also occur in alkaline solutions and/or in non-aqueous aprotic solvents (Oguz Koroglu et al., 2019).

$$O_2 + [H^+ + e^-] \rightarrow {}^{\bullet}OOH \quad (5)$$
$${}^{\bullet}OOH + [H^+ + e^-] \rightarrow {}^{\bullet}O + H_2O \quad (6)$$
$${}^{\bullet}O + [H^+ + e^-] \rightarrow {}^{\bullet}OH \quad (7)$$
$${}^{\bullet}OH + [H^+ + e^-] \rightarrow H_2O \quad (8)$$

$$O_2 + 4H^+ + 4e^- \rightarrow 2H_2O\left(E^0 = 0.816\,V\right) \quad (9)$$

$$O_2 + [H^+ + e^-] \rightarrow {}^{\bullet}OOH \quad (10)$$
$${}^{\bullet}OOH + [H^+ + e^-] \rightarrow H_2O_2 \quad (11)$$

$$2O_2 + 4H^+ + 4e^- \rightarrow 2H_2O_2\ \left(E^0 = 0.295\,V\right) \quad (12)$$

The ORR occurs in the cathodic part under ambient temperature and pH, involving complicated interfacial electron and mass transfer processes. The kinetics of the ORR is generally sluggish and result in a high overpotential at the cathode which decreases the MFC efficiency (Gao et al., 2020). Platinum (Pt) is one of the most widely used and the efficient ORR electrocatalysts. The ORR can occur through three possible mechanistic pathways such as dissociation of O_2, dissociation of OOH, and dissociation of H_2O_2, as shown in Figure 1 (Haile et al., 2020). The ORR in the presence of a Pt catalyst takes place predominately through a four-electron transfer pathway as shown below (Equations 13–17) (Si et al., 2014),

$$Pt + O_2 \leftrightarrow Pt - O_{2(abs)} \quad (13)$$
$$Pt - O_{2(abs)} + H^+ + e^- \rightarrow Pt - O_2H_{(abs)}\left(Rate - determining\ step\right) \quad (14a)$$
$$x\left(Pt - O_2H_{(abs)} + H^+ + e^- \rightarrow Pt - O_2H_{2(abs)}\right) \quad (14b)$$
$$x\left(Pt - O_2H_{2(abs)} \rightarrow Pt + H_2O_2\right) \quad (15)$$
$$(1-x)\left(Pt + Pt - O_2H_{(abs)} + H^+ + e^- \rightarrow 2Pt + OH_{(abs)}\right) \quad (16)$$
$$2(1-x)\left(Pt - O_2H_{(abs)} + H^+ + e^- \rightarrow Pt + H_2O\right) \quad (17)$$

In the case of other electrocatalysts such as carbon based, transition metal oxides and hybrid nanomaterials may follow two-electron transfer or a combination of two- and four-electron transfer pathways. The pH (acidic or basic) also influences the ORR pathway as given below (Equations 18–25), In acidic pH,

$$\text{Four} - \text{electron pathway: } O_2 + 4H^+ + 4e^- \rightarrow 2H_2O\ \left(E^0 = 1.229\,V\ \text{vs SHE}\right) \quad (18)$$
$$\text{Two} + \text{two} - \text{electron pathway: } O_2 + 2H^+ + 2e^- \rightarrow H_2O_2\ \left(E^0 = 0.695\,V\ \text{vs SHE}\right) \quad (19)$$
$$H_2O_2 + 2H^+ + 2e^- \rightarrow 2H_2O\ \left(E^0 = 1.770\,V\ \text{vs SHE}\right) \quad (20)$$
$$2H_2O_2 \rightarrow 2H_2O + O_2 \quad (21)$$

In basic pH,

$$\text{Four} - \text{electron pathway: } O_2 + 2H_2O + 4e^- \rightarrow 2OH^- \left(E^0 = 0.401\ \text{V vs SHE}\right) \quad (22)$$

$$\text{Two} + \text{two} - \text{electron pathway: } O_2 + H_2O + 2e^- \rightarrow HO_2^- + OH^- \left(E^0 = -0.065\ \text{V vs SHE}\right) \quad (23)$$

$$HO_2^- + H_2O + 2e^- \rightarrow 3OH^- \left(E^0 = 0.867\ \text{V vs SHE}\right) \quad (24)$$

$$2HO_2^- \rightarrow 2OH^- + O_2 \quad (25)$$

The formation of OH^- in the basic media accumulated at the cathode may result in a lower kinetic performance of ORR. Therefore, the effective elimination of OH^- at the catalyst active sites is a central challenge in the ORR. Besides, the functional groups on the surface of the catalyst (if present) can assist in the elimination of OH^- for ease of ORR (Hou et al., 2016). The electrocatalysts' performance for the ORR is generally studied by rotating ring disc electrode (RRDE). The Koutecky-Levich equation can be used to measure the number of electron transfers in ORR as given below (Eq. 26),

$$\frac{1}{j} = \frac{1}{j_k} + \frac{1}{B\omega^{1/2}} \quad (26)$$

Where j, j_k and ω are the total current density, kinetic current density, and electrode rotation rate (rpm) respectively. The coefficient, B, can be obtained from the Levich equation (Eq. 27) and the slope of the Koutecky-Levich plots.

$$B = 0.2nF\left(D_{O2}\right)^{\frac{2}{3}}\nu^{-\frac{1}{6}}C_{O2} \quad (27)$$

Where n, F, D_{O2}, ν, and C_{O2} are the number of electron transfer per O_2 molecule, Faraday constant (96,485 C/mol), the diffusion coefficient of O_2 in 0.1 M KOH (1.9×10^{-5} cm^2/s), kinetic viscosity (0.01 cm^2/s) and bulk concentration of O_2 (1.2×10^{-6} mol/cm^3) respectively. The constant 0.2 in the above equation is assumed when the rotation speed is mentioned in rpm (Gautam and Verma, 2019).

5 Importance of ORR electrocatalysts

However, the infinite source of O_2 makes the air-cathode MFCs a potential eco-friendly technology; incomplete reduction of O_2 at the cathodic part produces some destructive reactive intermediates and free radicals. The performance of the MFC for the current generation depends on the ORR at the surface of the cathode, which is restricted by the activation barrier (Sawant et al., 2017; Liu et al., 2022). The large activation energy loss due to the sluggish ORR results in high overpotential at the cathode. The use of mediators, optimization of MFC operating conditions, and cathode modification with catalysts are adopted to enhance the ORR kinetics. Among these, using the ORR electrocatalysts is the most feasible way to facilitate the fast ORR kinetics (Kamali et al., 2022). The ORR electrocatalyst should possess excellent catalytic activity (including good electrical conductivity, high surface area, functional groups, and surface morphology), cost-effectiveness, and higher stability. Pt has been proven to be the most widely used conventional electrocatalyst for ORR activity due to the superior activity, and highly stable in acidic media when compared to other non-precious ORR electrocatalysts (Sui et al., 2017; Ma et al., 2020). The high cost and easily poisoned by anions such as carbon monoxide and sulphide limits its large-scale applications (Chaturvedi and Kundu, 2021). The fabrication cost of a Pt cathode is more than half of the total cost of a lab-scale MFC. Therefore, the research on cost-effective, efficient ORR electrocatalysts has become an attractive and vital research field (Chaturvedi and Kundu, 2021; Peera et al., 2021). There are several types of electrocatalysts have been reported to decrease and/or to replace the usage of Pt for the ORR activity which include Pt-based, non-precious metals-based, and carbon-based electrocatalysts (Chaturvedi and Kundu, 2021; Peera et al., 2021; Priyadarshini et al., 2021; Kamali et al., 2022).

6 Types of ORR electrocatalysts

The types of ORR electrocatalysts can be broadly categorized as (i) precious metals-based ORR electrocatalysts, (ii) non-precious metals-based ORR electrocatalysts, (iii) non-metals and/or carbon based ORR electrocatalysts and (iv) biocatalysts.

6.1 Precious metals-based ORR electrocatalysts

Due to the high-cost nature and aim toward the practical applications of the MFC technology, the precious metal-based catalysts are reviewed very briefly in this section. Pt is the most widely used and potential electrocatalyst for ORR applications. The Pt loaded on carbon cathode in MFC generated a maximum of 1,553 mW cm^{-2} power with simultaneously treating piggery waste (Chandrasekhar and Ahn, 2017). The carbon paper electrode contains lower loading of Pt fabricated using an e-beam evaporation technique performed 2.5 times higher than the commercial Pt catalyst in MFC applications (Park et al., 2007). Similarly, the lower loading of Pt on carbon cloth using electrodeposition showed superior performances in the MFC applications (Yen et al., 2013). Zerrouki et al. demonstrated the Pt-PANI composite catalyst showed better ORR activity and a maximum power density of 1,510 mW cm^{-2} with 88% of COD removal efficiency in MFC. The enhanced activity was ascribed to the presence of conducting polymer PANI, which enhanced the electron cloud on the catalyst (Zerrouki et al., 2022). The Pt-boron-nitride-carbon electrocatalyst recently showed superior stable MFC performances over 2 months with 936.31 mW cm^{-2} of maximum power density. The superior performance was due to the availability of more and uniformly dispersed active sites as well as the strong coordination structure of Pt-N_4 (Shixuan et al., 2023).

The palladium (Pd) on the Si nanowire exhibited 84.5% methyl orange degradation with simultaneous generation of 0.119 W/m^2 of maximum output power density (Han et al., 2017). The Pd supported on stainless steel fiber felt prepared by simple water bath method having macropores showed a higher power density of 390.79 mW m^{-2}, comparable to the efficiency of conventional Pt/C ORR electrocatalyst (405.47 mW m^{-2}) (Chen et al., 2019). Wang et al. demonstrated around 1.8 times enhanced MFC performance of 901 mW m^{-2} maximum power density using Pd/GO-C catalyst than the other Pd catalysts. They used a novel method to prepare the Pd/GO-C catalyst by simply mixing GO, carbon block, and $PdCl_2$ as

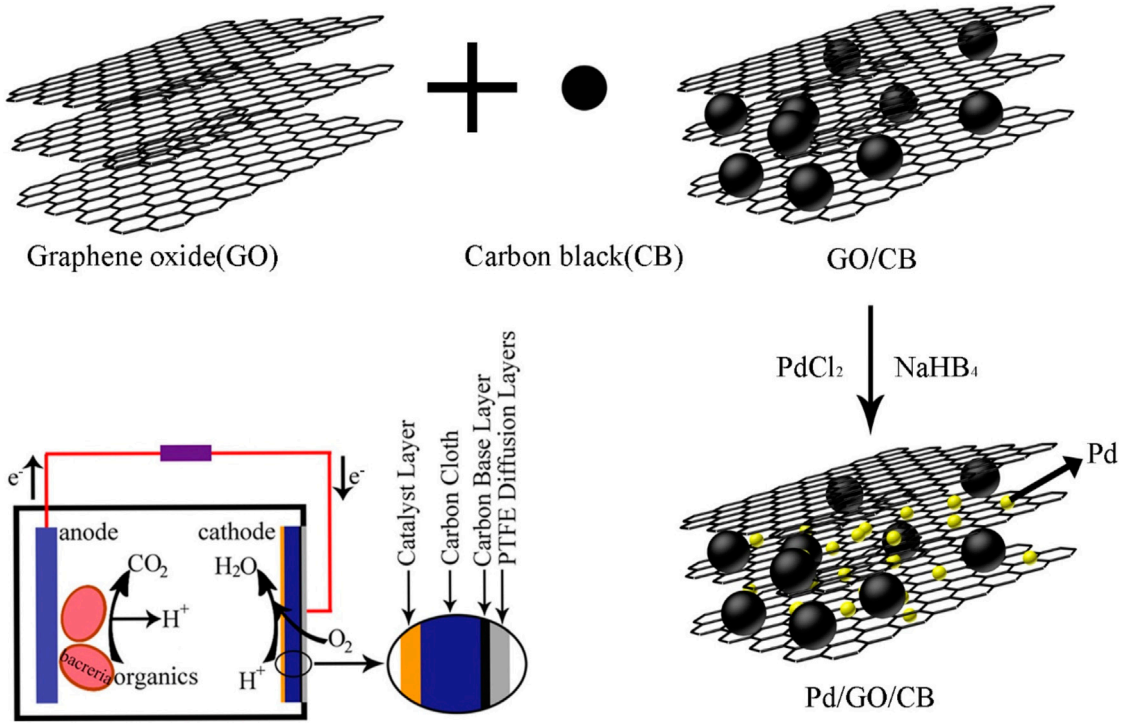

FIGURE 2
Schematic diagram of the preparation and application of Pd/GO-C in microbial fuel cells (MFCs) (Wang et al., 2021).

shown in Figure 2 (Wang et al., 2021). Remarkably, beyond 100 days, the MFC performance was demonstrated using sub-5nm Pd nanocrystals in FeN_3-Pd@NC NBs composite ORR catalyst. The active sites of Fe and Pd, and the structural properties of the catalyst resulted the higher MFC performances (Lin et al., 2022). The silver (Ag) based electrocatalysts show the good performances in the MFC applications (Dai et al., 2017). Ag_2O/Ag cathode showed stable maximum power output of 1.796 W m^{-3} in MFC applications (Dai et al., 2017). The Ag performance in MFC was also enhanced by hybridizing with tungsten carbide, which showed better efficiency than the commercial Pt/C electrocatalyst (Gong et al., 2013). The Ag–Fe–N/C ORR catalyst derived from a zeolitic imidazole framework displayed a higher power density of 523 mW m^{-2} than the commercial Pt/C (358 mW m^{-2}) owing to the synergistic effects of Ag nanoparticles, Fe and N-doped porous carbon (Lai et al., 2022). Recently, Sun et al. reported CNFs-Ag/Fe based catalyst derived using metal organic framework material showed a higher maximum power density of 737.45 mW m^{-2} than the commercial Pt/C (457.99 mW m^{-2}), which was due to the incorporation of Fe in the catalyst (Sun et al., 2023).

The combination of different transition and/or non-precious metals with Pt and forming alloys provides high surface area by decreasing particle size and, thus, more active sites for ORR in MFCs. The Pt-Co alloy supported on carbon demonstrated more elevated and more stable MFC performances when compared with the commercial Pt/C ORR electrocatalyst due to the presence of Co with optimized composition (Yan et al., 2014b). The Pt-Ni alloy showed higher power generation efficiency of 0.637 W m^{-2} in MFC than that of the Pt cathode of 0.180 W m^{-2} due to its increased oxygen adsorption and reduction on the more active sites (Cetinkaya et al., 2015). The optimized Pt-Pd alloy coated on carbon paper via the electrodeposition method demonstrated 1,274 m Wm^{-2} of maximum power density comparable to that of commercial Pt/C catalyst in air-cathode MFC application (Quan et al., 2015). The PtSn/C ORR electrocatalyst showed a maximum power density of 336 mW m^{-2} in MFC application, while the commercial Pt/C catalyst showed lower efficiency of 307 mW m^{-2}. The modification of the electronic structure of the Pt by the introduction of Sn enhanced the MFC performances of the catalyst (Li et al., 2017). The Pt_3-Fe/C ORR electrocatalyst showed a 18% enhanced performance of 1,680 mW m^{-2} power generation with outstanding durability compared with the commercial Pt/C (1,422 mW m^{-2}) in MFC application (Yan et al., 2014a). The Pt coated onto carbon paper (CP) as cathode generated the maximum power density of 84.01 mW/m^2 in the MFC, which is approximately two times higher than neat CP (44.7 mW/m^2). The performance of the MFC was then increased to about 147 mW/m^2 by incorporating carbon nanotube (CNT) with Pt electrocatalyst, which was attributed to the high surface area of the CNT(Halakoo et al., 2015). The summary of maximum power density, wastewater, and cell configuration with significant remarks corresponding to a few essential precious metals-based ORR electrocatalysts for the MFC applications are given in Table 1.

6.2 Non-precious metals-based ORR electrocatalysts

Several non-precious metals-based materials have been studied as the ORR electrocatalysts in air-cathode MFC. The main concern

TABLE 1 Summary of substrates or wastewater, cell configuration, and maximum power density with significant remarks corresponds to a few essential precious metals-based ORR electrocatalysts for the MFC applications.

Type	ORR catalysts	Substrate/ wastewater	Cell configuration	Maximum power density (MPD)	Significant remarks	Reference
Pt	Pt	Raw piggery wastewater	Carbon brush anode and carbon cloth cathode in 28 mL single chamber type cell	1,553 mW m^{-2}	93% removal of piggery waste	Chandrasekhar and Ahn (2017)
	Pt	Sludge from municipal wastewater plant	Carbon paper with and without Pt as electrodes in two chamber type cell	2,500 mW m^{-2}	performed 2.5 times higher than that of commercial Pt catalyst in MFC applications	Park et al. (2007)
	Pt	Synthetic wastewater with *Escherichia coli*	Carbon cloth anode electrodes with Pt in single chamber type cell	59 mW m^{-2}		Yen et al. (2013)
Pd	Pd on Si nanowire (NW)	Synthetic wastewater	Carbon felt electrodes in 400 mL two chamber type cell	119 mW m^{-2}	84.5% removal of methyl orange	Han et al. (2017)
	Pd	Sodium acetate	Carbon fiber brush anode and stainless steel (SS) fiber felt cathode in 28 mL single chamber type cell	390.79 mW m^{-2}	comparable efficiency as that of Pt/C	Chen et al. (2019)
	FeN_3-Pd@ NC NBs	Artificial wastewater	Carbon felt anode and carbon fiber cathode cloth in 28 mL single chamber type cell	831.2 mW m^{-2}	Stable MFC performance over 100 days	Lin et al. (2022)
Ag	Ag_2O/Ag	Sodium acetate	Carbon felt anode and Ag_2O/Ag cathode in 90 mL single chamber type cell	1,800 mW m^{-2}	Relatively stable current	Dai et al. (2017)
	Ag–WC/C	Activated sludge	Carbon cloth anode and SS mesh cathode in two chamber type cell	20.62 W m^{-3}	comparable efficiency as that of Pt/C	Gong et al. (2013)
	Ag–Fe–N/C	Artificial wastewater	Carbon cloth electrodes in 28 mL single chamber type cell	523 mW m^{-2}	Higher MPD than Pt/C (358 mW m^{-2})	Lai et al. (2022)
	CNFs-Ag/Fe	Artificial wastewater	Carbon cloth electrodes in 50 mL single chamber type cell	737.45 mW m^{-2}	Higher MPD than Pt/C (457.99 mW m^{-2}) with 72% COD removal	Sun et al. (2023)
Alloys/ composites	Pt-Co/C	Artificial wastewater	Carbon cloth electrodes in 27 mL single chamber type cell	1,730 mW m^{-2}	Better stability than Pt/C	Yan et al. (2014b)
	Pt-Ni	Dairy based wastewater	Carbon cloth cathode and carbon brush anode in 123 mL two chamber type cell	637 mW m^{-2}	Higher efficiency than Pt (180 mW m^{-2})	Cetinkaya et al. (2015)
	Pt-Pd	Synthetic wastewater	Carbon cloth anode and carbon paper cathode in 27 mL two chamber type cell	1,274 mW m^{-2}	Comparable efficiency as that of commercial Pt/C	Quan et al. (2015)
	PtSn/C	Municipal wastewater	Carbon cloth electrodes in 28 mL single chamber type cell	336 mW m^{-2}	Higher MPD than Pt/C (307 mW m^{-2})	Li et al. (2017)
	Pt_3-Fe/C	Synthetic wastewater	Carbon cloth anode and carbon paper cathode in 27 mL single chamber type cell	1,680 mW m^{-2}	18% enhanced performance than commercial Pt/C	Yan et al. (2014a)
	Pt-CNT	Palm oil mill effluent and anaerobic sludge	Carbon paper electrodes in two chamber type cell	147 mW m^{-2}	enhanced performance than neat Pt (84.01 mW m^{-2})	Halakoo et al. (2015)
	PANI-Pt	Medicinal plant wastes	Carbon cloth electrodes in two chamber type cell	1,510 mW m^{-2}	88% COD removal	Zerrouki et al. (2022)
	Pt-boron-nitride-carbon	Synthetic wastewater	Carbon fiber anode and carbon cloth cathode in 28 mL single chamber type cell	936.31 mW m^{-2}	Stable performance for 2 months	Shixuan et al. (2023)

of using non-precious metals is to reduce the cost of electrocatalysts and aim for the future potential of scaling-up applications. The transition metal compounds were found to have higher activity as ORR electrocatalysts. Plentiful research articles displayed that properly designed non-precious metal-based ORR electrocatalysts can perform comparable to, or even higher than, the commercial Pt/C in MFC applications with high stability. The summary of maximum power density, wastewater, and cell configuration with

TABLE 2 Summary of the MFC configurations and performances of some significant non-precious metals-based ORR electrocatalysts.

Types	Catalysts	Substrate/ wastewater	Cell configuration	Maximum power density (MPD)	Significant remarks	Reference
Metal oxides	Co_3O_4	Activated sludge	Graphite felts electrodes in 604 mL each of six plant-sediment microbial fuel cells	75.12 mW m^{-2}	99.76% Cr(VI) removal efficiency	Cheng et al. (2019)
	MnO_2	Synthetic wastewater	Carbon cloth electrodes in 28 mL single chamber type cell	213 mW m^{-2}	44% efficiency compared with Pt/C	Alireza et al. (2019)
	Mesoporous MnO_2	Synthetic wastewater	Carbon felt anode and stainless steel (SS) mesh cathode in 28 mL single chamber type cell	1,671 mW m^{-2}	88% higher power density than the control	Zhang et al. (2018b)
	V_2O_5 nanorod	Fish market wastewater	Carbon cloth anode and SS mesh cathode in 90 mL single chamber type cell	384 mW m^{-2}	Enhanced to 533 mW m^{-2} when rGO introduced	Noori et al. (2017)
	$Cu_{1.5}Mn_{1.5}O_4$	Artificial wastewater	Carbon felt anode and SS cathode in 28 mL single chamber type cell	1,928 mW m^{-2}	1.53 times higher power generation than the bare electrode	Wang et al. (2016)
	$CaFe_{0.9}Cu_{0.1}O_3$	Synthetic wastewater	Carbon felt anode and carbon cloth cathode in 350 mL single chamber type cell	1,090 mW m^{-3}	Higher MPD than Pt/C (970 mW m^{-3})	Zhang et al. (2022a)
	SnO_2	Synthetic wastewater	Carbon felt anode and carbon plate cathode in 1,300 mL baffled microbial fuel cell	13.70 mW m^{-2}	2.48 times higher MPD than bare C-plate	Yap et al. (2023)
Alloy	$FeMn_2$	Synthetic wastewater	Carbon brush anode and SS mesh cathode in single chamber type cell	1940 mW m^{-2}	24% higher MPD than Pt/C	Guo et al. (2019)
MnO_x based	MnO_2/f-CNT	Municipal wastewater	Carbon paper electrodes in 380 mL dual chamber type cell	520 mW m^{-2}	86.6% COD removal efficiency	Liew et al. (2015)
	Graphite:γ-MnO_2:MoS_2	Data not available	SS cathode in single chamber type cell	183 mW m^{-2}	Improved from 120 mW m^{-2} by ultrasonic treatment	Jiang et al. (2017)
	MnO_2-rGO	Artificial wastewater	Carbon felt anode and SS mesh cathode in 100 mL single chamber type cell	5.06 W m^{-3}	Higher MPD than pure MnO_2 (3.96 W/m^3)	Rout et al. (2018)
	α-MnO_2 nanowires	Domestic wastewater	Graphite brush anode and carbon cloth cathode in 28.84 mL of single chamber type cell	180 mW m^{-2}	Improved MPD from 111 mW m^{-2} using carbon Vulcan	Majidi et al. (2019)
	MnO_2@Co_3O_4	Activated sludge	Carbon felt anode and SS mesh cathode in two chamber type cell	475 mW m^{-2}	~2 times higher MPD than the control	Chen et al. (2022a)
	$Cs_3PMo_{12}O_{40}$	Artificial wastewater	Graphite plate electrodes in two chamber (190 mL each) type cell	64.73 mW m^{-2}	~86% COD removal efficiency	Rezaei et al. (2023)
Metals based composites	Co_3O_4/$NiCo_2O_4$	Domestic wastewater	Carbon felt anode and stainless steel mesh cathode in 28 mL single chamber type cell	1,810 mW m^{-2}	104% higher MPD than the control	Zhang et al. (2018a)
	Fe_3O_4@ NiFe-LDH	Synthetic wastewater	Carbon felt anode and stainless steel cathode in 50 mL of single chamber type cell	211.40 mW m^{-2}	34-fold higher and stable MPD than the control	Jiang et al. (2020a)
	CoNiAl-LDH@ $NiCo_2O_4$	Synthetic wastewater	Graphite plate elecctrodes in 700 mL two chamber type cell	85.28 mW m^{-2}	Stable performances for 93.66 h	Tajdid Khajeh et al. (2020)
	NiFe-LDH@ Co_3O_4	Activated sludge	Graphite felt anode and stainless steel mesh cathode in single chamber type cell	467.35 mW m^{-2}	stability and durability over 8 days	Jiang et al. (2020b)
	Co-Ni/ TiO_2-NTs	Mixed activated sludge	Carbon cloth electrodes in 250 mL single chamber type cell	104 mW m^{-2}	Higher MPD than Pt/C (64 mW m^{-2})	Chaturvedi et al. (2022)
	Co-Zeolite/GO	Activated sludge	Membrane electrode assembly in single chamber 50 mL type cell	416.78 mW m^{-2}	306% higher MPD than Pt/C	Chaturvedi and Kundu (2022)

(Continued on following page)

TABLE 2 (*Continued*) Summary of the MFC configurations and performances of some significant non-precious metals-based ORR electrocatalysts.

Types	Catalysts	Substrate/ wastewater	Cell configuration	Maximum power density (MPD)	Significant remarks	Reference
	Zn/Co-S-3DHFLM	Wastewater (wastewater treatment plant)	Carbon felt anode and carbon cloth cathode in 200 mL two chamber type cell	172.8 mW m^{-2}	Higher MPD than the control and 93% COD removal	Lu et al. (2023)
	$NiCo_2S_4$/ $NiCo_2O_4$@NSC	Activated sludge	Carbon fiber anode and stainless steel cathode in 50 mL single chamber type cell	831.74 mW m^{-2}	~1.2 and 1.7 times higher MDP than $NiCo_2O_4$@NSC, and NC respectively	Dhillon and Kundu (2023)
	N-MnO_2@ NiAl-LDH	Activated sludge	Carbon felt anode and stainless steel cathode in single chamber type cell	698 mW m^{-2}	4.59 times higher MPD than NiAl-LDH (152.1 mW m^{-2})	Xu et al. (2023)

important remarks corresponding to some significant non-precious metals-based ORR electrocatalysts for the MFC applications are given in Table 2.

The transition metal oxide ORR electrocatalysts such as Co_3O_4 (maximum power density of 75.12 mW m^{-2} with 99.76% Cr(VI) removal efficiency) (Cheng et al., 2019), MnO_2 (maximum power density of 213 mW m^{-2}) (Alireza et al., 2019) (maximum power density of 1,671 mW m^{-2}) (Zhang et al., 2018b), V_2O_5 (maximum power density of 384 mW/m^2) (Noori et al., 2017), TiO_2 nanotubes (15.16 mWm^{-2}) (Yahia et al., 2016), TiO_2 nanoparticles (15.2 Wm^{-3}) (Kumar A. et al., 2023), SnO_2 (Yap et al., 2023), etc., showed better activity in MFC applications. Among these metal oxides, manganese oxides (MnO_x) are a potential candidate for ORR due to their high chemical stability, low cost, and environmental benignity. However, they showed relatively less activity (Gao et al., 2020). The performance of MnOx was improved by adopting several ways, such as introducing oxygen vacancies, doping with other metals, combining with carbon-based materials, etc. The oxygen-deficient nest-like $Cu_{1.5}Mn_{1.5}O_4$ ORR electrocatalyst showed 1.53 times higher power generation of 1,928 mW m^{-2} than that of the bare electrode. The enhanced activity with the four electron transfer oxygen reduction mechanism was due to the presence of oxygen deficient in the catalyst (Wang et al., 2016). The MnO_2/functionalized carbon nanotubes (f-CNT) exhibited a 86.6% of COD removal efficiency and a higher power density of 520 mW m^{-2} than the individual components (Liew et al., 2015). The mixture of graphite, γ-MnO_2, and MoS_2 can achieve a higher maximum power density of up to 183 mW m^{-2} due to the high surface area and porous structural properties of the catalyst(Jiang et al., 2017). Rout et al. reported that the higher charge transfer property of rGO was enhanced the power density of 5.06 W/m^3 of MnO_2-reduced graphene oxide (rGO) ORR electrocatalysts than that of pure MnO_2 (3.96 W m^{-3}) (Rout et al., 2018). The α-MnO_2 nanowires showed a power density of 111 mW m^{-2}, which was increased to 180 mW/m^2 when supported on carbon Vulcan which provides high surface area and surface structure (Majidi et al., 2019). The MnO_2@Co_3O_4 composite catalyst showed more than 2-fold higher maximum power generation efficiency than that of the individual components in MFC due to their multiple active sites, high surface area, and high conductivity (Chen et al., 2022a). The $Cs_3PMo_{12}O_{40}$ ORR electrocatalyst showed a maximum power density of 64.73 mW m^{-2} with around 86% COD removal efficiency in MFC application which was higher than that of the bare graphite electrode. The higher efficiency of the catalyst was due to the mesoporous structure, good electrochemical active sites, electron and proton sink ability, and the presence of Mo (Rezaei et al., 2023). Likewise, the other mixed metal oxide $CaFe_{0.9}Cu_{0.1}O_3$ catalyst showed a higher maximum power density of 1,090 mW m^{-3} than the commercial Pt/C (970 mW m^{-3}). The Fe^{3+} content was increased by introducing Cu in the catalyst which resulted in the higher MFC performances (Zhang H. et al., 2022). Besides, Pema et al. very recently reported $BiFe_{1-x}Li_xO_3$-graphene (G) composite as a low-cost catalyst. They achieved a higher ORR activity of 8.1 W/m^3 compared with GO in MFC applications, with a more stable COD removal efficiency of 78.5%. The $BiFe_{1-x}Li_xO_3$-G composite favors mainly the four electron pathway for ORR in the single chamber MFC as shown in Figure 3 (Pema et al., 2023).

The ORR performance of several other metal oxide electrocatalysts was significantly enhanced by adopting some modifications, especially the formation of composites. The Co_3O_4/$NiCo_2O_4$ double-shelled nanocage ORR electrocatalyst showed a 104% higher maximum power density of 1,810 mW m^{-2} than the control. This catalyst showed improved ORR activity due to its nanocage structure and the presence of Co^{2+}/Co^{3+} and Ni^{2+}/Ni^{3+} redox couples (Zhang et al., 2018a). The Fe_3O_4 supported nickel-iron layered double hydroxides (LDH) showed 34 times higher and more stable (for 110 h) power generation efficiency of about 211.40 mW/m^2 than the blank control components in the MFC. The enhanced efficiency was due to its high electrochemical active sites and the excellent conductivity of Fe_3O_4 (Jiang et al., 2020a). The CoNiAl-LDH@$NiCo_2O_4$ composite exhibited a stable output power density of 85.28 mW m^{-2} for 93.66 h due to the hierarchical core-shell structure of the catalyst (Tajdid Khajeh et al., 2020). In another study, Jiang et al. displayed a remarkable stability and durability over 8 days with a maximum power density of 467.35 mW m^{-2} by the NiFe-LDH@Co_3O_4 composite due to its rich active sites and high conductivity (Jiang et al., 2020b). Besides, Guo et al. demonstrated a 39% and 24% higher power density when employing the bimetallic $FeMn_2$ nanocatalysts than the plain AC cathode and Pt/C cathode, respectively due to the synergistic effect between Fe and Mn catalyst(Guo et al., 2019). The Co and Ni doped TiO_2 nanotubes (NTs) showed enhanced ORR activity and produced ~104 mW m^{-2} current density, which was higher than the commercial Pt/C catalyst. The higher performance was due to the higher specific

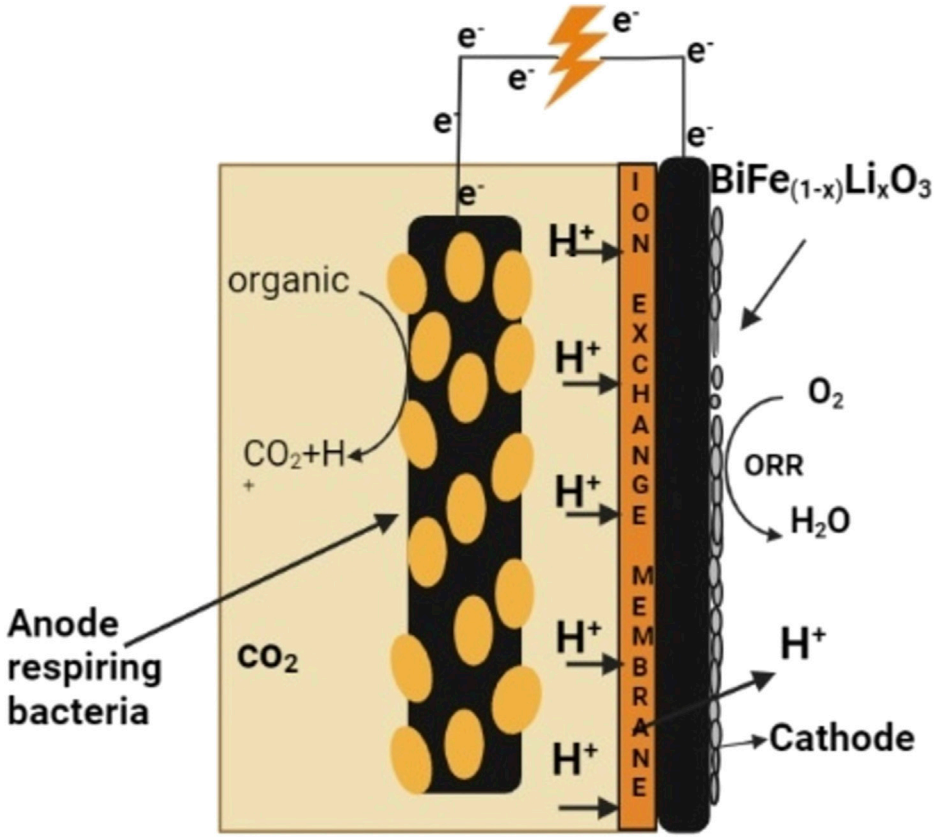

FIGURE 3
Schematic illustration of a single chamber microbial fuel cell (MFC) processes using $BiFe_{1-x}Li_xO_3$-graphene (G) composite as ORR catalyst (Pema et al., 2023).

surface area of TiO_2 NTs and active sites of the catalyst (Chaturvedi et al., 2022). Recently, a 3D flower-like metal organic material (3DHFLM), Zn/Co-S-3DHFLM showed enhanced ORR activity in MFC with 172.8 maximum power density and 93% COD removal efficiency 467.35 mW m^{-2}. The synergistic effect of the bimetallic active center and the sulfur has greatly enhanced the ORR activity of the Zn/Co-S-3DHFLM catalyst (Lu et al., 2023). Besides, the $NiCo_2S_4/NiCo_2O_4$@NSC electrocatalyst showed excellent ORR performances in MFC application which showed around 1.2 and 1.7 times the enhanced maximum power density of 831.74 mW m^{-2} compared to the $NiCo_2O_4$@NSC, and N-C catalysts, respectively. The enhanced performance of the catalyst resulted from the synergistic effect between heteroatoms and metal species, optimized amount of N and S, and better active surface area (Dhillon and Kundu, 2023). Besides, the excellent properties such as unique Ping-pong chrysanthemum-like structure, pore size distribution and electrochemical active sites of N-MnO_2@NiAl-LDH ORR catalyst showed a maximum power density of 698 mW m^{-2} (Xu et al., 2023). Gosh et al. reported the CeO_2-gC_3N_4 catalyst showed excellent ORR activity and a power density of 12.53 W m^{-3} in MFC application. The high surface area, Ce^{3+} content, oxygen defects, and pyridinic N of the catalyst contributed to better MFC performances (Ghosh et al., 2023). Xie et al. reported a novel MXene@NiCoP ORR electrocatalyst and achieved a maximum power density of 732 W m^{-3} in MFC application which was due to the presence of active NiCoP species on the MXene (Xie et al., 2023).

The carbon-based composite materials have attracted significant attention as ORR electrocatalysts in MFC applications due to their excellent physicochemical and electrical properties. Ge et al. reported the total resistance was reduced when doping activated carbon into the ortho-hexagon spinel nano Co_3O_4 which generated the maximum power density of 1,500 mW m^{-2} in the MFC application, which was 97.36% and 41.24% higher when compared to the bare activated carbon and the commercial Co_3O_4 cathodes, respectively (Ge et al., 2015). Mecheri et al. demonstrated the oxygen adsorption and ORR rate was increased by increasing the ZrO_2 content on carbon which showed a maximum power generation efficiency of 600 mW m^{-2}, which was 15 times lower in cost as compared with the commercial Pt/C catalyst in the MFC application (Mecheri et al., 2016). Zhang et al. reported a Cu_2O doped activated carbon ORR electrocatalyst which showed a 59% higher power generation efficiency of 1,390 mW m^{-2} than that of the bare activated carbon. The lattice (111) plane and surface oxygen defects of the catalyst was enhanced the ORR performances (Zhang et al., 2015). The $CoFe_2O_4$ (CFO) supported on nitrogen doped activated carbon (N-AC) performed 2.39 times higher maximum power density of 1770.8 mW m^{-2} than pure activated carbon cathode catalyst in

the MFC application, which was due to the synergistic effect between N-AC and CFO (Huang et al., 2017). The $MnCo_2O_4$ nanoparticles in the carbon block exhibited 545 mW m^{-2} of maximum power density in MFC application which was comparable to the Pt/C catalyst (689 mW m^{-2}) and higher than the bare cathode (214 mW m^{-2}) (Hu et al., 2015). Ge et al. reported the activated carbon modified with $NiCo_2O_4$ exhibited a maximum power generation efficiency of 1730 mW m^{-2}, which was comparable with that of the commercial Pt/C catalyst in MFC applications (Ge et al., 2016). Noori et al. displayed the enhancement of the maximum power density of bare V_2O_5 of 384 mW/m^2 to 533 mW m^{-2} by the incorporation of rGO (Noori et al., 2017). The MnO_2/TiO_2/g-C_3N_4 supported on granular activated carbon exhibited a maximum power density of 1,176.47 mW m^{-3} while simultaneous efficient industrial wastewater treatment of 17.77 kg COD $m^{-3}d^{-1}$ COD removal capacity (Zhang and Liu, 2020). The iron phthalocyanine (FePc) and nitrogen-doped graphene oxide ORR electrocatalyst showed the better waste treatment and power generation performances (Mecheri et al., 2018). Liu et al. reported the Fe-N derived from FePc supported on activated carbon (AC) performed for MFC of 1,092 mW m^{-2} maximum current density due to its porous structures and high N content (Liu et al., 2019). The Co and FePc supported in carbon derived from SiC generated 1.57 W m^{-2} of power with up to 86% of COD removal efficiency of wastewater. The graphitic and high mesoporous properties of the catalyst promote the good four-electron ORR pathway (Noori and Verma, 2019). Huang et al. reported the $CoFe_2O_4$ NPs/N-doped AC composite electrocatalyst generated a maximum power density in MFC of 1770.8 mW m^{-2}, which was much greater than the AC of 741.5 mW m^{-2} due to its large surface area and conductivity (Huang et al., 2017). Yang et al. reported Fe(III)-chitosan hydrogel derived Fe-N-C low-cost ORR electrocatalyst exhibited a 33% higher power generation efficiency of 2.4 W m^{-2} than the AC control due to the improved ORR activity by higher electron transfer number of 3.4 (Yang et al., 2020b). The Fe, N co-doped graphene with CNTs generated a maximum power density of 1,210 mW m^{-2} which was higher than the Pt catalyst performance of 1,080 mW m^{-2} (Wang et al., 2018). Liang et al. achieved a maximum power density of 1,738 mW m^{-2} when using the N-doped carbon incorporated with cobalt (Co) nanoparticle ORR electrocatalyst, which was higher than the commercial Pt/C (1,203 mW m^{-2}). The higher performance of the catalyst was attributed to the high surface area and the porous carbon structure(Liang et al., 2020). The N and Co or Fe co-doped multi-walled carbon nanotubes (MWCNTs) exhibited an output power density of 5.1 W m^{-3} and 6 W m^{-3}, respectively which was due to the nitrogen-metal center active sites formation in the catalysts (Türk et al., 2018). The square-like cobalt oxide nanostructures on N-doped graphene showed a higher ORR activity and exhibited a 24.9% higher power density of 713.6 mW m^{-2} than the commercial Pt/C (571.3 mW m^{-2}), which was due to the synergistic effect of N-G and Co nanostructures (Cao et al., 2016). Yang et al. reported a novel N-doped molybdenum sulfide combined with CNTs and carbon atoms (N-MoS_2/CNTs/C) composite showed a higher maximum power density of 987.4 mW m^{-2} than that of commercial Pt/C of 601.96 mW m^{-2} which was due to the excellent electrical properties of the CNT and N present in the catalyst (Yang et al., 2018). Jing et al. demonstrated that the porous structure, defects, heterojunctions, and N atoms in the Fe_3Se_4/FeSe heterojunctions in N-doped carbon achieved a higher 1,003 mW m^{-2} power density with good stability for 105 days of operation of air cathode MFC (Jing et al., 2019). The Co_2P incorporated in a N-doped carbon nanoframework (Co_2PNC-NF) composite electrocatalyst showed 2001 mW m^{-2} of maximum power density, which was 123% higher than the bare active carbon. The higher activity resulted from the double Co site of 001 face present in the catalyst (Lin et al., 2021). The NiCo alloy on N-doped carbon showed excellent ORR activity and showed a 2.16 times higher maximum power density of 2,325.60 mW m^{-2} than that of the Pt/C catalyst which was due to the synergistic effect of NiCo active sites, and graphitic and pyridinic N (Huang et al., 2022). Similarly, a novel Co/Ni@GC/NCNTs/CNFs catalyst displayed a splendid performance than the commercial Pt/C in MFC which was due to the abundant active sites and 3D structure of the catalyst(Li J. et al., 2022). Besides, a 4.5 times higher maximum power density than that of bare carbon felt was obtained by FeCoO/Go composite owing to its higher ORR activity(Zheng et al., 2022). The Co nanoparticles on zeolite-GO showed a 306% higher maximum power density of 416.78 mW m^{-2} than the Pt/C in the MFC application (Chaturvedi and Kundu, 2022). The N and S co-doped carbon based composite, Co_9S_8@HN/S-C, showed better ORR and COD removal activities in MFC application (Ding et al., 2022). Metal and N co-doped porous carbon, such as Fe-NpC (atomically dispersed Fe-N_4 moieties), showed superior performances than Pt/C in MFC (Wang et al., 2023b). Liang et al. reported Fe, N codoped carbon ORR electrocatalysts derived from different Fe ligands showed a maximum power density of 2,041 mW m^{-2}. The improved ORR and MFC activity of the catalysts was ascribed to the graphitization degree and different amounts of Fe^{2+} and Fe^{3+} of the catalysts (Liang et al., 2023). Similarly, single atom Fe sites in the N-C showed a higher MFC performance of 3,323 mW m^{-2} than that of the Pt/C catalyst. The higher performance was due to the optimized Fe-N-C with porous structure and efficient electron transfer properties of the catalyst (Zhao et al., 2023). Long et al. reported CoFe-LDH on partially reduced GO (p-rGO) showed 30 times higher MFC performance than the blank due to more the active sites, structural and interlayer diffusion properties of the catalyst (Long et al., 2023). Remarkably, the fantastic ORR activity in the MFC applications of carbon based composites such as Cu_2O@Co/N-C (Chen et al., 2023), Fe-N-C (Kumar D. et al., 2023; Zhang et al., 2023), FeCoNi@N-C (Kaur Dhillon and Paban Kundu, 2023), Fe/Co-N-C (Liu et al., 2023; Zhuang et al., 2023), Co/CoS_2@N-CNF (Guo et al., 2023), Co/CoFe NAs@NCNFs (Wang et al., 2023a), etc., were witnessed in several recent reports. The maximum power density, wastewater, and cell configuration with important remarks corresponding to some significant non-precious carbon-based ORR electrocatalysts for the MFC applications are summarized in Table 3.

The metal organic framework (MOF) composites exhibited the excellent performances in MFCs (Priyadarshini et al., 2021). The iron-based MOF, Fe-*t*-MOF/PANI synthesized by a sustainable route using terephthalic acid monomer (*t*) derived from plastic waste showed a power density of 680 mW m^{-2} (Kaur et al., 2021). The Ni-MOF-74, the another cost-effective ORR electrocatalyst, exhibited a maximum power density of 446 mW m^{-2} with

TABLE 3 Summary of the MFC configurations and performances of some significant non-precious carbon-based ORR electrocatalysts.

Catalysts	Substrate/ wastewater	Cell configuration	Maximum power density (MPD)	Significant remarks	Reference
Co_3O_4 doped into activated carbon (AC)	Domestic wastewater	Carbon felt anode and SS mesh cathode in 28 mL single chamber type cell	1,500 mW m^{-2}	97.36% and 41.24% higher MPD compared to the bare AC and commercial Co_3O_4, respectively	Ge et al. (2015)
ZrO_2 supported on carbon	Domestic wastewater	Graphite fiber brush anode and carbon cloth cathode in single chamber type cell	600 mW m^{-2}	15 times low-cost than Pt/C	Mecheri et al. (2016)
Cu_2O doped AC	Domestic wastewater	Carbon felt anode and SS mesh cathode in 28 mL single chamber type cell	1,390 mW m^{-2}	59% higher MPD compared to the bare AC	Zhang et al. (2015)
$CoFe_2O_4$ supported on nitrogen doped (N-) AC	Artificial wastewater	Carbon felt anode and SS mesh cathode in 28 mL single chamber type cell	1,770.8 mW m^{-2}	2.39-fold higher MPD compared to the bare AC	Huang et al. (2017)
$MnCo_2O_4$ nanoparticles in carbon block (CB)	Artificial wastewater	Carbon cloth electrodes in two chamber (2 × 654 mL) type cell	545 mW m^{-2}	comparable MPD to Pt/C (689 mW m^{-2}) and ~2.5 times higher than the bare cathode	Hu et al. (2015)
AC modified with $NiCo_2O_4$	Synthetic wastewater	Carbon felt anode and SS mesh cathode in 28 mL single chamber type cell	1,730 mW m^{-2}	comparable MPD to Pt/C	Ge et al. (2016)
$MnO_2/TiO_2/g\text{-}C_3N_4$ on AC	Organic acid industrial wastewater	Carbon rod anode and granular activated carbon cathode in two chamber type cell	1,176.47 mW m^{-3}	simultaneous efficient industrial wastewater treatment	Zhang and Liu (2020)
FePc/N-graphene oxide (GO)	Artificial wastewater	Carbon cloth electrodes in 28 mL single chamber type cell	260 mW m^{-2}	More stable MFC performances	Mecheri et al. (2018)
Fe-N/AC	Artificial wastewater	Carbon brush anode and carbon dloth cathode in dual chamber type cell	1,092 mW m^{-2}	63.23% higher and comparable MPD than AC and Pt/C, respectively	Liu et al. (2019)
Co-FePc/C	Artificial wastewater	Activated carbon fiber electrodes in 100 mL two chamber type cell	1,570 mW m^{-2}	86% COD removal efficiency	Noori and Verma (2019)
$CoFe_2O_4$ NPs/N-AC	Artificial wastewater	Carbon felt anode and SS mesh cathode in 28 mL single chamber type cell	1,770.8 mW m^{-2}	much greater MPD than AC (741.5 mW m^{-2})	Huang et al. (2017)
Fe–N–C	Synthetic wastewater	Graphitic fiber brush anode and SS mesh cathode in single chamber type cell	2,400 mW m^{-2}	33% higher MPD compared to AC	Yang et al. (2020b)
Fe–N/G with CNTs	Activated sludge from municipal wastewater	Carbon fiber brush anode and carbon cloth cathode in 28 mL single chamber type cell	1,210 mW m^{-2}	much higher MPD than Pt/C (1,080 mW m^{-2})	Wang et al. (2018)
Co/N-C	Municipal wastewater	Carbon felt anode and SS mesh cathode in single chamber 28 mL type cell	1738 mW m^{-2}	44.5% higher MPD than Pt/C	Liang et al. (2020)
Co-N-CNT	Anaerobic sludge collected from septic tank bottom	Carbon felt electrodes in 80 mL single chamber type cell	5.1 W m^{-3}	Superior organic matter removal efficiency	Türk et al. (2018)
Fe-N-CNT			6 W m^{-3}		
Cobalt oxide on N-G	Artificial wastewater	Graphite felt anode and carbon cloth cathode in 27 cm^3 single chamber type cell	713.6 mW m^{-2}	24.9% higher MPD than Pt/C	Cao et al. (2016)
$N–MoS_2$/CNTs/C	Synthetic wastewater	Graphite fiber brush anode and SS mesh cathode in 28 mL single chamber type cell	987.4 mW m^{-2}	Higher MPD than Pt/C (601.96 mW m^{-2})	Yang et al. (2018)
Fe_3Se_4/FeSe/N-C	Artificial wastewater	Carbon fiber brush anode and SS mesh cathode in single 28 mL chamber type cell	1,003 mW m^{-2}	good MFC stability for 105 days	Jing et al. (2019)
Co_2P/N-C	Domestic wastewater		2,001 mW m^{-2}	123% higher MPD than AC	Lin et al. (2021)

(Continued on following page)

TABLE 3 (*Continued*) Summary of the MFC configurations and performances of some significant non-precious carbon-based ORR electrocatalysts.

Catalysts	Substrate/ wastewater	Cell configuration	Maximum power density (MPD)	Significant remarks	Reference
		Carbon felt anode and SS mesh cathode in 28 mL single chamber type cell			
NiCo/N-C	Synthetic wastewater	Carbon fiber brush electrodes in 28 mL single chamber type cell	2,325.60 mW m^{-2}	2.16 times higher MPD than Pt/C	Huang et al. (2022)
Co/Ni@GC/NCNTs/ CNFs	Domestic sewage	Carbon brush anode and carbon cloth cathode in 28 mL single chamber type cell	2,100 mW m^{-2}	Higher MPD than Pt/C (1,334 mW m^{-2})	Li et al. (2022b)
Co_9S_8@HN/S-C	Artificial wastewater	Carbon fiber anode and carbon paper cathode in single chamber 28 mL type cell	1,436.5 mW m^{-2}	80% COD removal activity	Ding et al. (2022)
FeCoO/GO	Artificial wastewater	Carbon fiber electrodes in two chamber 118 mL type cell	461.2 mW m^{-2}	4.5-fold higher MPD than CF	Zheng et al. (2022)
FeCo/Co/Co2P/ NPGC	Synthetic wastewater	Graphite fiber brush anode and SS mesh cathode in 28 mL single chamber type cell	997.74 mW m^{-2}	Stable MFC activity over 90 days	Xu et al. (2022)
Fe, N codoped carbon	Artificial wastewater	Carbon felt anode and stainless steel cathode in 28 mL single chamber type cell	2,041 mW m^{-2}	Stable MFC performance over 20 days	Liang et al. (2023)
Fe-N-C	5% Luria–Bertani (LB) with 18 mM lactate	Carbon paper electrodes in two chamber type cell	3,323 mW m^{-2}	Higher MPD than Pt/C (2,760 mW m^{-2})	Zhao et al. (2023)
Cu_2O@Co/N-C	Synthetic wastewater	Titanium mesh electrodes in two chamber type cell	1,100 mW m^{-2}	Slightly higher than Pt/C (1,067 mW m^{-2})	Chen et al. (2023)
Fe–N–C	Activated sludge	Carbon brush fiber anode and SS mesh cathode in 50 mL single chamber type cell	736.06 mW m^{-2}	Higher MPD than the control	Kumar et al. (2023b)
Fe-N-C	Artificial wastewater	Carbon felt anode and carbon cloth cathode in 252 mL single chamber type cell	184 mW m^{-2}	86.6% COD removal efficiency	Zhang et al. (2023)
FeCoNi@N-C	Activated sludge	Carbon fiber brush anode and SS mesh cathode in 50 mLsingle chamber type cell	963.5 mW m^{-2}	66.84% COD removal efficiency	Kaur Dhillon and Paban Kundu (2023)
Fe/Co-N-C	Artificial wastewater	Graphite felt electrodes in two chamber 1 L type cell	1,059.62 mW m^{-2}	Higher MPD than Pt/C (957.33 mW m^{-2})	Liu et al. (2023)
FeCo–N–C	Domestic wastewater	Carbon cloth electrodes in 28 mL single chamber type cell	1,425 mW m^{-2}	10.5% higher MPD than Pt/C	Zhuang et al. (2023)
Fe-NpC	Municipal effluent derivatives	Carbon cloth electrodes in 28 mL single chamber type cell	1,793 mW m^{-2}	90% COD removal and high MPD than Pt/C	Wang et al. (2023b)
Co/CoS_2@N-CNF	Activated sludge	Carbon cloth electrodes in 100 mL dual chamber type cell	400.06 mW m^{-2}	Higher MPD than Pt/C (333.70 mW m^{-2}) and high stability	Guo et al. (2023)
CoFe-LDH@p-rGO	Synthetic wastewater	Carbon brush anode and carbon cloth cathode in 140 mL single chamber type cell	204 mW m^{-2}	30 times higher MPD than the blank	Long et al. (2023)

sulfamethoxazole degradation of 84% COD removal (Li S. et al., 2021). The Ni-catecholate-based MOF grown on NiCoAl-LDH/ MWCNTs showed an enhanced maximum power density of 448.5 mW m^{-2} in MFC, which also attributed to the high conductivity and more active sites (Chen et al., 2021). Cheng et al. reported the Co_3O_4-ZIF/Zn composite showed a highly stable power generation efficiency of 656.9 mW m^{-2} for up to 30 days compared to the commercial Pt/C catalyst (Chang et al., 2021). The ZIF-67/CNFs showed higher power generation efficiency of 1.191 W m^{-2}, which was higher than that of Pt and CNF due to the porous structure and lower internal resistance of the catalyst (Jiang et al., 2021). Recently, Chen et al. reported the ZIF-67@Ti_3AlC_2/ ZnAl-LDH, which exhibited a 2-fold higher maximum power density of 587 mW m^{-2} than that of their components, owing to the multiple active sites, high electrical conductivity, and high surface area of the catalyst (Chen et al., 2022d). The covalent organic frameworks (COFs) based composites and their derivatives showed good efficiency in MFCs. For example, the

cobalt oxides incorporated COF-derived carbon (Co/N-C-COPs) ORR electrocatalyst showed higher efficiency of 1,817 mW m^{-2} than the Pt/C catalyst (1,622 mW m^{-2}) in the MFC applications (Yang et al., 2020a). Recently, Chen et al. prepared a highly stable COF-300@NiAl-LDH/GO catalyst showed the enhanced ORR activity in MFC with a maximum power density of 481.69 mW m^{-2}. The high conductivity, catalytic activity, and high electron transfer properties of the catalyst improved the MFC performances of the catalyst(Chen et al., 2022c). Similarly, the MOF derivatives also demonstrated the excellent ORR performances in the MFC applications(Zhang Y. et al., 2018; Wang X. et al., 2022). Tang et al. reported the dual metal (Ni, Co) and N-doped carbon ORR electrocatalysts derived from MOF generated a higher maximum power density of 4,335.6 mW m^{-2} with outstanding durability over 755 h. This excellent performance of the catalyst resulted from the high surface area and uniform distribution of N and metal species in the graphite structure(Tang et al., 2015). The zeolitic imidazolate framework-67 (ZIF-67) derived Co-N-C composite exhibited a maximum output power density of 399.7 mW m^{-2} (Li J. C. et al., 2018). Xue et al. reported the Fe, Co, and N-doped carbon derived from ZIF-67 generated a higher maximum power density of 1769.95 mW m^{-2} than the Pt/C catalyst of 1,410.3 mW m^{-2}. The higher performance was achieved by the optimum pyrolysis temperature of 900°C, which resulted from the higher graphitization and corrosion resistance along with the higher conductivity and active sites of the catalysts (Xue et al., 2020). The N-doped CNT-embedded Co nanoparticles derived from bimetallic MOF produced a much higher power density than Pt/C and 2.54 times higher than the pure AC. The N and metal combination with CNT enhanced the ORR activity, and the reduced total and charge transfer resistance resulted in the higher MFC performances (Zhang S. et al., 2019). The hierarchical porous Fe-N-C nanofibers developed using MOF and bacterial cellulose exhibited high power generation than the commercial Pt/C catalysts of 640.56 mW m^{-2} with 66.6% COD removal performance which was attributed to its more active sites and porous structure (Li H. et al., 2021). in another report, Li et al. prepared ZIF-67-derived CoNi-LDH@CNFs, which exhibited long durability in MFC and showed a higher maximum power density of 1,390.37 mW m^{-2} compared to the Pt/C. The higher four-electron transfer ORR was promoted by CoNi active sites and the nanoflower structure of the catalyst (Li H. et al., 2022). The MFC performance of the Fe-N-C catalyst prepared from Fe-doped ZIF-8 was optimized for cost-effective and stable activity using pyrolyzing at different temperature (Wang D. et al., 2022). Similarly, the $Co_{0.7}Fe_{0.3}$@Co-NC-1 catalyst derived from different MOF precursors showed good ORR activity with 2,486 mW m^{-2} maximum power density due to the optimized electronic structure and porous carbon (Zhang X. et al., 2022). Recently, Huang et al. demonstrated the 1.45 times higher maximum power generation of 1974 mW m^{-2} by Fe/Fe_3C/NC catalyst derived from MOF than the Pt/C catalyst due to the mesoporous structure and the presence of N in the catalyst (Huang et al., 2023). Ding et al. prepared Co encapsulated in hierarchical porous N-C (Co/HNC) derived from ZIF based MOF, which showed good ORR activity and a maximum power density of 1324 mW m^{-2} in MFC application (Ding et al., 2023). Qin et al. reported a novel hybrid porous CoCu@N-CNFs ORR catalysts which showed a slightly higher maximum power density of 543 mW m^{-2} than Pt/C due to the synergistic effect of CoCu alloy (Qin et al., 2023). Table 4 summarizes the maximum power density, wastewater, and cell configuration with important remarks corresponding to some significant non-precious MOFs- and COFs-based ORR electrocatalysts for the MFC applications.

6.3 Non-metals and/or carbon-based ORR electrocatalysts

The carbon-based materials without any metals have attracted scientists to discover the high-efficiency ORR electrocatalysts due to their chemical inertness, high electrical conductivity, high stability, high surface area and porosity, good mechanical properties, and inexpensive (Pötschke et al., 2022). The chemically modified carbon block (Vulcan XC-72R) showed the comparable ORR performance in the MFC applications (Duteanu et al., 2010; Yang et al., 2014). The nitrogen doped carbon block performed 2.2 times higher than the pure carbon block in the MFC applications (Kumar et al., 2017). The AC as ORR electrocatalyst on nickel foam as a current collector showed comparable power generation efficiency as that of commercial Pt/C in air-cathode MFC application. The cathode cost was very cheaper (1/30th) when compared with the commercial Pt/C electrocatalyst (Cheng and Wu, 2013). The chemically treated P-doped or non-doped AC showed enhanced performances in MFC applications (Chen Z. et al., 2014; Liu et al., 2015; Wang et al., 2017). Similarly, the low-cost N-doped carbon materials showed 11.3% higher(Feng et al., 2012) and comparable(Shi et al., 2012) performances as the commercial Pt/C catalyst in the MFC applications. The pretreated N-doped AC showed higher maximum power density in the air-cathode MFCs when compared with the commercial Pt/C and the pure AC (Zhang et al., 2014). The surface structural modification of AC also enhanced the ORR performance in MFC applications (Li et al., 2014; Liu et al., 2016). The porous structural modification of AC generated 2.4 times higher power density than that of the unmodified one in the air-cathode MFCs (Li et al., 2014). A large-scale MFC of 85 L was constructed with an AC-based air cathode of 0.62 m^2 exposed area and a graphite fiber-based anode of 5.1 cm diameter, 61 cm long. A maximum power density of 0.101 W m^{-2} was achieved in static flow conditions. The maximum power density was further increased by recirculating the anolyte (domestic wastewater) over the electrodes in a diagonal direction by 17% to 0.118 W m^{-2} at a hydraulic retention time (HRT) of 33 min (Rossi et al., 2019).

The graphite in the cathode activated using H_3PO_4 and HNO_3 generated 7.9 W m^{-3} and 6.5 W m^{-3}, respectively of maximum power densities which were 2.4 and 1.8 times greater than that of the bare graphite in the MFC applications (Zhang et al., 2016). The porous structure and high crystallinity of graphite were proven to have a high surface area and, thus, better performance in MFC (Xing et al., 2017). The 3D graphite particle showed as a potential cathode for the generation of H_2O_2 in the MFC application with 84% COD removal efficiency (Fu et al., 2010; Chen J. Y. et al., 2014). Interestingly, an ultra-low cost MFC fabricated with pencil trace demonstrated excellent performance for portable applications of MFCs (Lee et al., 2016). The three dimensional (3D) graphene nanosheets exhibited a maximum power density of 2.059 W m^{-2} in the MFC

TABLE 4 The MFC configurations and performances of some significant non-precious metal-organic frameworks (MOFs) and covalent organic frameworks (COFs) based ORR electrocatalysts.

Types	Catalysts	Substrate/ wastewater	Cell configuration	Maximum power density (MPD)	Significant remarks	Reference
MOF based Composites	Fe-*t*-MOF/PANI	Synthetic wastewater	SS mesh electrodes in dual chamber type cell	680 mW m^{-2}	Low-cost materials from plastic waste	Kaur et al. (2021)
	Ni-MOF-74	Synthetic wastewater	Carbon cloth electrodes in 28 mL single chamber type cell	446 mW m^{-2}	84% COD removal	Li et al. (2021b)
	NiCoAl-LDH/ MWCNTs	Anaerobic activated sludge	Carbon felt anode and SS mesh cathode in single chamber type cell	448.5 mW m^{-2}	Stability over 8 days	Chen et al. (2021)
	Co_3O_4-ZIF/Zn	Domestic sewage (20%) and culture medium (80%) from treatment plant	Graphitic brush anode and carbon fiber cloth cathode in 28 mL single chamber type cell	656.9 mW m^{-2}	Stability over 30 days	Chang et al. (2021)
	ZIF-67/CNFs	Simulated wastewater and sewage treatment plant effluent	Carbon felt fiber electrodes in two chamber (300 mL each) type cell	1,191 mW m^{-2}	Higher MPD than Pt	Jiang et al. (2021)
COF-based/ derivatives	Co/N-C-COPs	Artificial wastewater	Graphite fiber brush anode and carbon cloth cathode in 28 mL single chamber type cell	1,817 mW m^{-2}	Higher MPD than the Pt/C (1,622 mW m^{-2})	Yang et al. (2020a)
	COF-300@NiAl-LDH/GO	-	-	481.69 mW m^{-2}	Stable MFC activity for 8 days	Chen et al. (2022c)
MOF derivatives	Ni, Co, and N doped carbon (C)	Synthetic wastewater	Carbon cloth anode and carbon paper cathode in single chamber type cell	4,335.6 mW m^{-2}	Outstanding durability	Tang et al. (2015)
	Co-N-C composite	Activated sludge	Carbon cloth electrodes in 28 mL single chamber type cell	399.7 mW m^{-2}	Low-cost and high efficiency catalysts	Li et al. (2018a)
	Fe–N–C	Domestic wastewater	SS mesh electrodes in 28 mL single chamber type cell	2,229 mW m^{-2}	257% higher MPD than AC	Zhang et al. (2018c)
	Fe, Co, and N-C	Artificial wastewater	Carbon cloth electrodes in single chamber 28 mL type cell	1769.95 mW m^{-2}	Higher than the Pt/C (1,410.3 mW m^{-2})	Xue et al. (2020)
	N-doped CNT-embedded Co nanoparticles	Domestic wastewater	Carbon felt anode and SS mesh cathode in 28 mL single chamber type cell	2,252 mW m^{-2}	154% higher MPD than the control	Zhang et al. (2019a)
	Fe–N–C nanofibers	Activated sludge	Carbon cloth electrodes in 118 mL single chamber type cell	640.56 mW m^{-2}	Higher MPD than Pt/C with 66.6% COD removal efficiency	Li et al. (2021a)
	CoNi-LDH@CNFs	Activated sludge	Carbon cloth electrodes in single chamber type cell	1,390.37 mW m^{-2}	Higher than the Pt/C (843.67 mW m^{-2})	Li et al. (2022a)
	Fe-N-C	Artificial wastewater	Carbon fiber brush anode and carbon cloth cathode in 28 mL single chamber type cell	1,508 mW m^{-2}	Stable MFC activity and one step synthesis	Wang et al. (2022a)
	$Co_{0.7}Fe_{0.3}$@Co-NC-1	Domestic sewage	Carbon felt anode and SS mesh cathode in 28 mL single chamber type cell	2,486 mW m^{-2}	A novel strategy using dual MOF	Zhang et al. (2022b)
	Fe-FeNx@N-CNT/CNFs	*Shewanella putrefaciens* CN32 cells	Carbon cloth electrodes in single chamber 28 mL type cell	742.26 mW m^{-2}	Comparable MFC activity to Pt/C	Wang et al. (2022c)
	Fe/Fe_3C/NC	Artificial wastewater	Carbon brush anode and carbon cloth cathode in single chamber type cell	1,974 mW m^{-}	1.45 times higher MPD than the Pt/C (1,366 mW m^{-2})	Huang et al. (2023)
	Co/HNC	Synthetic wastewater	Carbon brush anode and carbon paper cathode in 28 mL single chamber type cell	1,324 mW m^{-2}	Stable performance in a wide pH range	Ding et al. (2023)

application which was higher than that of activated carbon (Santoro et al., 2017). Dong et al. reported the oxidized graphene in MFC application and achieved 131% more generation of H_2O_2 than that of pure graphene cathode which was due to the oxygen containing functional groups present in the catalyst (Dong et al., 2018).

The N is one of the most widely used heteroatoms doped with carbon to enhance the ORR activity due to its electronegativity, close atomic radius to carbon, and facilitate easy oxidant adsorption (Dhilllon et al., 2022). The N-doped carbon aerogel (CA) was developed for ORR activity, and its performance was further increased by activating the CA with KOH. The activation of KOH increased the surface area, hierarchically porous structure, reduced C-O-C and COOH, higher pyridinic N content, and decreased pyrrolic N content, thus the enhanced MFC performance than that of non-activated CA (Tian et al., 2018). In another report, Yang et al. demonstrated the improvement of active sites by N doping in the N-CA, which generated 1,048 mW m^{-2} of power density in the MFC application, which was comparable with the efficiency of the commercial Pt/C (1,051 mW m^{-2}) catalyst (Yang et al., 2019). Wang et al. reported the N-doped carbon derived from isoreticular MOF-3 modified with g-C_3N_4, which showed a maximum output power density of 1,402.8 mW m^{-2} in MFC application. This performance was higher than the Pt (1,292.8 mW m^{-2}) and attributed to the introduction of more active N and mesoporous structure when using g-C_3N_4 as the template for the catalyst synthesis (Wang et al., 2020).

The carbon materials derived from different organic precursors and/or biomass showed excellent performances in MFC applications. The porous AC derived from different sources such as Arhar stalks(Om Prakash et al., 2021), Bamboo(Yang et al., 2017), corncob (Li M. et al., 2018), and coconut shell (Sekhon et al., 2021) showed higher thermal stability and high surface area which results in better MFC performances. The other carbon materials derived from different biomass, such as cornstalk (Sun Y. et al., 2016), sewage sludge (Mian et al., 2019), bacterial cellulose (Wu et al., 2016), hemoglobin (Maruyama et al., 2007), etc., showed excellent ORR performance. Zhou et al. prepared the carbon nanofibers (CNFs) from spider silk exhibited 1800 mW m^{-2} power density in the MFC, which was higher than the commercial Pt/C electrocatalyst (704 mW m^{-2}). The higher MFC performances were attributed to the increased surface area and more active sites by N and S doping in the catalyst (Zhou et al., 2016). The carbon derived from chitosan having high surface area by high temperature KOH activation showed an increased MFC performance of 1,435 mW m^{-2}, which was 101% higher than the pure AC in the medium of domestic wastewater and nutrient solution (1:1) (Liu et al., 2018). Linget al. demonstrated the MFC performance of the carbon material derived from chitosan was again enhanced by five times from 322.4–1,603.6 mW m^{-2} by co-doping of N and P. The C-O bond, N, and P existence resulted in a large surface area, lower total resistance, more oxygen transfer, and abundant active sites in the catalyst, which enhanced the ORR and MFC performance (Liang et al., 2019). The P-doped carbon derived from cellulose showed 1,312 mW m^{-2} of maximum power density in the air-cathode MFC application, which was three-fold higher than the pure carbon and also higher than that of Pt/C electrocatalyst (Liu et al., 2014). The N and F co-doped carbon black obtained from the polytetrafluoroethylene and BP-2000 mixture by pyrolysis under an ammonium atmosphere showed a maximum power density of 672 mW m^{-2}. At the same time, the commercial Pt/C achieved a lesser of 572 mW m^{-2} (Meng et al., 2015). Ye et al. reported the carbon electrocatalyst obtained from the lotus leaf which showed a maximum power density of 511.5 mW m^{-2}. This hierarchically structured carbon catalyst was stable and showed four-electron transfer performance comparable to the commercial Pt/C catalyst due to the large surface area and porous structure (Ye et al., 2019). The N self-doped porous carbon derived from duckweed provided more active sites for ORR reaction in MFC, which resulted in 625.9 mW m^{-2} of power density and higher stability than the commercial Pt/C electrocatalyst (Gong et al., 2020). Pepè Sciarria et al. reported the biochar obtained from Olive mill waste and pistachio nutshell which showed a high surface area and O and N functionalities. The MFC performance of the biochar was 271 mWm^{-2} of maximum output power density, which was 15 times higher than the commercial carbon black (Pepè Sciarria et al., 2020). The N-doped carbon ORR electrocatalysts derived from pomelo peel showed MFC performance of 907.2 mW m^{-2} power generation, which was comparable to the Pt/C (1,022.9 mW m^{-2}) electrocatalyst (Zhang et al., 2020). Carbon materials derived from watermelon as ORR catalysts showed the good performances in the MFC applications (Zhong et al., 2019; Jiang et al., 2022). The biochar materials derived from different sources such as microalgae, pomelo peel, and eggplant performed well as low-cost and durable materials compared to the commercial Pt/C (Chakraborty et al., 2020; Zhang et al., 2020; Zha et al., 2021; Wang K. et al., 2022; Dhanda et al., 2023). Zhu et al. developed the porous Co and N doped carbon using tea residue showed excellent MFC efficiencies, such as higher maximum power density than Pt/C with COD removal activity. The excellent activity was attributed to the pyridinic-N, and pore structure of the catalyst (Zhu H. et al., 2022). Yang et al. prepared N-doped biochar from microalgae residue by single-step pyrolysis method, which showed a maximum power density of 843.6 mW m^{-2} and comparable MFC performances with commercial Pt/C. The optimized pyrolysis process resulted in porous structure and improved N content in the catalyst, which promoted the better four-electron pathway ORR in MFC (Yang et al., 2023). In addition, the activated carbon from areca nut husk demonstrated a maximum power density of 590 mW m^{-2} with good COD removal activity. The better MFC performances was attributed to the porous structure, graphitic nature, and N content present in the catalyst (Subran et al., 2023). Several significant non-metals and/or carbon-based ORR electrocatalysts with their maximum power density, wastewater, cell configuration, and important remarks in the MFC applications are given in Table 5.

6.4 Biocatalysts

Besides exploring the chemically fabricated ORR electrocatalysts, several biomaterials, such as enzymes, living microbial cells, etc., are used as ORR catalysts at the cathode of MFCs (He and Angenent, 2006). The construction of the biocathode was done by growing electroactive bacteria on carbon felt materials or stainless steel mesh and demonstrated a maximum stable power generation of 12.3 μW cm^{-2} (De Schamphelaire et al., 2010). The laccase immobilized on graphite cathode utilized in MFC showed

TABLE 5 Several significant non-metals and/or carbon-based ORR electrocatalysts with their maximum power density, MFC configurations, and important remarks in the MFC applications.

Types	Catalysts	Substrate/ wastewater	Cell configuration	Maximum power density (MPD)	Significant remarks	Reference
Carbon based	N-C powder	Mixed anaerobic sludge	Carbon felt anode and stainless steel (SS) mesh cathode in 300 mL single chamber type cell	66 mW m^{-2}	Only 12.5% were lost in MPD after 40 days	Kumar et al. (2017)
	AC on nickel foam	Synthetic wastewater	Carbon fiber brush anode and nickel foam cathode in 26 mL single chamber type cell	1,190 mW m^{-2}	Low-cost (1/30th) compared with the Pt/C	Cheng and Wu (2013)
	Chemically treated AC	Partial domestic water	Carbon felt anode and SS mesh cathode in 28 mL single chamber type cell	1,546 mW m^{-2}	115% higher MPD than the pristine AC	Wang et al. (2017)
	Chemically treated N-AC	Synthetic wastewater	Carbon brush anode and carbon cloth cathode in two (140 mL each) chamber type cell	580 mW m^{-2}	Higher MPD than the control and Pt/C	Zhang et al. (2014)
	Porous AC	20% domestic wastewater	Carbon fiber brush anode and SS mesh cathode in 28 mL single chamber type cell	892 mW m^{-2}	33% higher MPD than the control	Li et al. (2014)
	AC	Effluent wastewater	Graphite fiber anode and SS mesh cathode in 28 mL single chamber type cell	118 mW m^{-2}	Large scale setup	Rossi et al. (2019)
	Acid treated graphite	Artificial wastewater	Graphite rod electrodes in two (110 mL each) chamber type cell	7.9 W m^{-3}	2.4 times higher MPD than the bare graphite	Zhang et al. (2016)
	Pencil-traced graphite	*Shewanella Oneidensis* MR-1	Graphite electrodes in all-paper microbial-activated air cathode battery	8.33 mW m^{-2}	Ultra-low cost material	Lee et al. (2016)
	3D graphene (G) nanosheets	Activated sludge	Carbon brush anode and SS mesh cathode in single chamber supercapacitive MFC	2,059 mW m^{-2}	Higher MPD than AC (1.017 mW m^{-2})	Santoro et al. (2017)
	Oxidized-G	Synthetic wastewater	Carbon brush anode and SS mesh cathode in two chamber type cell	378 mW m^{-2}	131% higher H_2O_2 generation than G in MFC	Dong et al. (2018)
	AC fiber	Artificial wastewater	SS mesh electrodes in 12.4 L in continuous-flow MFC system	169 mW m^{-2}	Stable wastewater treatment for 400 days	Long et al. (2019)
	N-doped carbon aerogel (CA)	Synthetic wastewater	Carbon cloth electrodes in 28 mL single chamber type cell	1,048 mW m^{-2}	Comparable MPD with the Pt/C (1,051 mW m^{-2})	Yang et al. (2019)
	N-doped carbon	Synthetic wastewater	Carbon felt anode and carbon cloth cathode in 350 mL single chamber type cell	1,402.8 mW m^{-2}	Higher MPD than the Pt (1,292.8 mW m^{-2})	Wang et al. (2020)
Organic or biomass derived carbon catalysts	carbon nanofibers (CNFs) from spider silk	Synthetic wastewater	Graphite brush fiber anode and carbon nanofiber cathode in single chamber type cell	1800 mW m^{-2}	Higher MPD than the Pt/C (704 mW m^{-2})	Zhou et al. (2016)
	C from chitosin	Domestic wastewater	Carbon felt anode and SS mesh cathode in 28 mL single chamber type cell	1435	101% higher MPD than the pure AC	Liu et al. (2018)
	Biochar derived from corncob	Synthetic wastewater	Carbon felt anode and carbon cloth cathode in single chamber 350 mL type cell	458.85 mW m^{-3}	Low-cost biochar material	Li et al. (2018a)
	N & P-C from chitosan	Domestic wastewater	Carbon felt anode and SS mesh cathode in 28 mL single chamber type cell	1,603.6 mW m^{-2}	5 times higher MPD than non-doped C	Liang et al. (2019)
	P-C from cellulose	Wastewater from wastewater treatment plant	Graphite fiber brush anode and SS mesh cathode in single chamber type cell	1,312 mW m^{-2}	3 fold higher MPD than the pure carbon	Liu et al. (2014)

(Continued on following page)

TABLE 5 (*Continued*) Several significant non-metals and/or carbon-based ORR electrocatalysts with their maximum power density, MFC configurations, and important remarks in the MFC applications.

Types	Catalysts	Substrate/ wastewater	Cell configuration	Maximum power density (MPD)	Significant remarks	Reference
	N & F-CB from an organic mixture	Artificial wastewater	Carbon fiber brush anode and carbon cloth cathode in single chamber type cell	672 mW m^{-2}	Higher MPD than Pt/C (572 mW m^{-2})	Meng et al. (2015)
	C from lotus leaf	Anaerobic sludge	Graphite plate electrodes in single chamber 28 mL type cell	515.5 mW m^{-2}	Higher MPD than Pt/C (486.7 mW m^{-2})	Ye et al. (2019)
	N-porous C from duckweed	Activated sludge	Carbon fiber anode and SS cathode in 28 mL single chamber type cell	625.9 mW m^{-2}	Low-cost and more stability than Pt/C	Gong et al. (2020)
	Biochar from Olive mill waste and pistachio nutshell	Synthetic wastewater	Carbon cloth electrodes in 28 mL single chamber type cell	271 mW m^{-2}	15 times higher MPD than the commercial CB	Pepè Sciarria et al. (2020)
	Biochar from microalgae	Mixed anaerobic sludge	Carbon felt electrodes in two chamber type cell	13.52 W m^{-3}	Low-cost (0.3%) than Pt/C and 73% COD removal	Chakraborty et al. (2020)
	N-biochar from pomelo peel	Synthetic wastewater	Carbon cloth electrodes in 28 mL single chamber type cell	907.2 mW m^{-2}	Long (90 days) durability and comparableMPD than Pt/C (1,022.9 mW m^{-2})	Zhang et al. (2020)
	Biochar from eggplant	Anaerobic sludge from wastewater treatment plant	Carbon felt anode and carbon cloth cathode in single chamber type cell	667 mW m^{-2}	Higher MPD than Pt/C (621 mW m^{-2})	Zha et al. (2021)
	Fe/Mn-biochar from watermelon	Wastewater from wastewater treatment plant	Carbon fiber mesh anode and carbon cloth cathode in single chamber 28 mL type cell	399 mW m^{-2}	97% COD removal	Jiang et al. (2022)
	Co, N-C from the tea residue	Activated sludge	Carbon felt anode and carbon cloth cathode in 20 mL single chamber type cell	748.9 mW m^{-2}	Higher MPD than Pt/C (588.7 mW m^{-2}) and 81% COD removal	Zhu et al. (2022a)
	N-C from microalgae	Artificial wastewater	Carbon brush anode and carbon cloth cathode in 28 mL single chamber type cell	412.85 mW m^{-2}	Higher MPD than the control	Wang et al. (2022b)
	N-doped biochar from microalgae residue	Artificial wastewater	Carbon brush anode and carbon cloth cathode in 28 mL single chamber type cell	843.6 mW m^{-2}	Comparable MFC activity with Pt/C	Yang et al. (2023)
	AC from areca nut husk	Synthetic wastewater	Carbon cloth electrodes in 200 mL single chamber type cell	590 mW m^{-2}	78% COD removal	Subran et al. (2023)

enhanced decolorization of the organic contaminant and generated higher power density (Savizi et al., 2012). The microorganism on the CNT-deposited stainless steel mesh cathode played an essential role in enhancing the power generation efficiency in the MFC applications (Zhang et al., 2013). The cathode choosing was a limiting factor in the MFC application while using the biomaterials as the ORR electrocatalysts. In a comparative study, the graphite felt biocathode demonstrated the better power generation efficiency in the MFC application among graphite felt, carbon paper, and stainless steel mesh biocathodes (Zhang et al., 2012). The low-cost biocathode materials such as semicoke and activated carbon also showed better performance in MFC application, costing just 2.8% and 22.7% compared to graphite and carbon felt biocathode, respectively (Wei et al., 2011). Besides, the carbon materials such as graphite granules, activated carbon granules, and activated carbon powder in the cathodic part played a significant role to enhance the MFC performances. Among the above, activated carbon granules have greatly enhanced the biocathode's efficiency by increasing the active microbes for ORR, which resulted in higher MFC performances (Tursun et al., 2016). The biocathode developed with CNT/chitosan exhibited 130% higher electricity generation efficiency when compared with the carbon paper biocathode in MFC application due to the decreased energy loss at the electrode/bacteria interface (Liu et al., 2011). The bacterial cellulose doped with Cu and P showed the maximum output current density of 1,177.31 mW m^{-2}, which was attributed to their more active sites of Cu and P present in the electrocatalyst(Li et al., 2019). Interestingly, Izadi et al. demonstrated highly enhanced power generation efficiency over gas diffusion biocathode consisting of iron-oxidizing bacteria (IOB) of 1.1 W m^{-2} maximum power density compared to Pt catalyst in MFC application. The mechanism of the MFC process involves oxidation of Fe^{2+} by IOB and regeneration at the cathode as shown in Figure 4 (Izadi et al., 2019). Very recently, sarma et al. reported the *Chlorella sorokiniana,* and *Philodendron erubescens* in the cathodic part of the MFCs showed significantly increased power generation efficiency. The enhanced activity was attributed to the presence of *C. sorokiniana,* which improved the ORR rate and dissolved

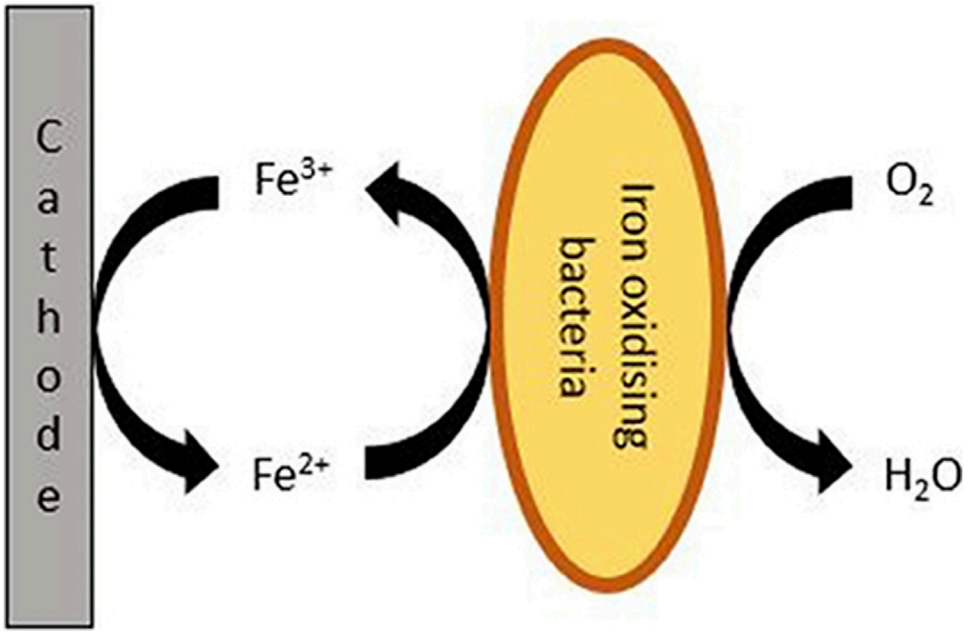

FIGURE 4
Mechanism of biocathode reactions using iron-oxidizing bacteria in microbial fuel cell (MFC) application (Izadi et al., 2019).

oxygen concentration (Sarma et al., 2023). The summary of several significant biomaterials-based ORR electrocatalysts with their maximum power density, wastewater, cell configuration, and essential remarks in the MFC applications are given in Table 6.

7 Durability of the ORR electrocatalysts

The long-term stability of the ORR electrocatalysts is a major challenging factor of the MFCs for real-time applications. The researchers have intensively focused on improving the durability along with the higher activity of the ORR electrocatalysts. Several methodologies, such as optimizing structural and chemical composition (Li J. C. et al., 2018), using support materials (Mecheri et al., 2018)., obtaining from other materials (e.g.,: derivatives of MOFs, COFs, and biomaterials) (Yang et al., 2020a), introducing interface with other components (Zhang and Liu, 2020), etc., are demonstrated improved stability and durability of the ORR electrocatalysts. Here are some significant achievements in improving the durability of the ORR electrocatalysts for MFC applications. The FePc stability was increased by less than 1% loss when the introduction of N-GO, which increased the OH group density, and the interaction between FePc and N-GO (Mecheri et al., 2018). Li et al. demonstrated the chemical composition and structural optimization of Co-N-C composite derived from MOF could achieve higher and more stable MFC performance for 1,200 h (Li J. C. et al., 2018). The activated carbon fiber on the stainless-steel ring electrode was used as an air cathode for a continuous-flow MFC system to treat azo dye wastewater for 400 days. This long-term efficiency was attributed to the abundance of microorganisms during the MFC operation. However, the removal efficiency remained stable, and the power output of 169 mW m^{-2} decreased slowly on the 400th day (Long et al., 2019). The stability of Fe_3O_4@NiFe in MFC operation was enhanced by introducing LDH, which improved the rate capability, electroactive sites, and cycling stability (Jiang et al., 2020a). Yang et al. demonstrated a high stable MFC performance over 200 h when using COF-derived Co/N-C-COPs ORR electrocatalyst than the Pt/C catalyst, which was due to the high ORR activity and poison tolerance properties of the catalyst (Yang et al., 2020a). Zhang and Liu demonstrated a stable and durable MFC activity by a novel $MnO_2/TiO_2/g\text{-}C_3N_4$ ORR electrocatalyst when supported on granular activated carbon for more than 6 months which enhanced the ORR rate and decreased the activation energy of the reaction (Zhang and Liu, 2020). Zhang et al. demonstrated that the high degree of graphitization, good electrical conductivity, and higher specific surface area of the N-C OOR electrocatalyst derived from pomelo peel enhanced the long-term durability in MFC operation for 90 days (Zhang et al., 2020). The mesoporous structure, high N content, and abundant active sites of the Co_3O_4-ZIF/Zn composite catalyst played a significant role in stable performance for up to 30 days in the MFC operation compared to the commercial Pt/C catalyst (Chang et al., 2021). The improved stability of MnO_2@Co_3O_4 composite catalyst in MFC was achieved by tuning its structural properties, such as high surface area and high ion flow efficiency (Chen et al., 2022a). The $CaFe_{0.9}Cu_{0.1}O_3$ porous perovskite catalyst stability was increased due to the presence of Cu, which increased the amount of Fe^{3+} and resulted in the higher adsorption of oxygen (Zhang H. et al., 2022). Interestingly, N-doped partially graphitized carbon (NPGC) based composite, FeCo/Co/Co_2P/NPGC showed superior stable MFC performance over 90 days with a maximum power density of 997.74 mW m^{-2}, which was due to the different metallic active sites and N-doping of the catalyst (Xu et al., 2022). The combined action of Ti_3AlC_2, ZnAl-LDH, and ZIF-67 in the ZIF-67@Ti_3AlC_2/ZnAl-LDH ORR electrocatalyst

TABLE 6 The summary of several significant biomaterials-based ORR electrocatalysts with their maximum power density, MFC configurations, and essential remarks in the MFC applications.

Types	Catalysts	Substrate/ wastewater	Cell configuration	Maximum power density (MPD)	Significant remarks	Reference
Enzymes based	Laccase	Sludge from diary wastewater treatment plant	Carbon brush anode and graphite bar cathode in two (250 mL each) chamber type cell	58.8 mW m^{-2}	65% higher MPD than simple graphite and 74% decolorization efficiency for azo dye	Savizi et al. (2012)
	Glucose and vitamin solution with CNT-stainless steel mesh	Anaerobic sludge from sewage treatment plant	Graphite felt anode and carbon paper cathode in 40 mL single chamber type cell	147 mW m^{-2}	49 times higher MPD than bare stainless steel electrode	Zhang et al. (2013)
Microorganism based	*Proteobacterium* (electroactive bacteria)	Freshwater and brackish sediment	Carbon felt electrodes in two cylindrical reactors of sediment MFCs	12.3 μW cm^{-2}	Stable power generation	De Schamphelaire et al. (2010)
	Bacteria with CNT/ chitosan	Anaerobic sludge	Carbon cloth anode and carbon paper cathode in single chamber 40 mL type cell	189 mW m^{-2}	130% higher MPD than carbon paper biocathode	Liu et al. (2011)
	Bacteria with semicoke and AC	Synthetic wastewater	Granular graphite and carbon felt cathode in two chamber 100 mL type cell	24.3 W m^{-3}	much more cost-effective than graphite	Wei et al. (2011)
	Microbes with AC granules	Synthetic wastewater (CH_3COONa)	carbon fiber brush electrodes in two chamber (28 mL each) type cell	736 mW m^{-2}	166.1% MPD enhancement while adding AC granules	Tursun et al. (2016)
	P & Cu doped bacterial cellulose	Activated sludge	Carbon felt electrodes in single chamber type cell	1,177.31 mW m^{-2}	Higher MPD than Pt (1,044.93 mW m^{-2})	Li et al. (2019)
	Iron-oxidizing bacteria	Synthetic wastewater	Carbon felt anode and carbon paper cathode in two (60 mL each) chamber type cell	1.1 W m^{-2}	Higher MPD than Pt (0.5 W m^{-2})	Izadi et al. (2019)
	Chlorella sorokiniana, Philodendron erubescens	Artificial wastewater	Carbon fiber electrodes in plant based MFC	32.21 mW m^{-2}	31% increase concerning other bacterial biocathode	Sarma et al. (2023)

improved the stability and durability in the MFC operation for 8 days (Chen et al., 2022d). The single-atom structure Phen-Fe MFC demonstrated highly stable and durable performance over 20 days due to the excellent ORR property of the catalyst (Liang et al., 2023). The stable performance of N-MnO_2@NiAl-LDH in the MFC application over 7 days was attributed to its excellent porosity, electrochemical active sites, and the presence of N and MnO_2 in the catalyst (Xu et al., 2023).The Co/HNC catalyst showed good stable ORR activity with a wide pH range owing to the strong interaction of Co and N-C, hierarchical porous structure, and presence of N in the catalyst (Ding et al., 2023). Therefore, the proper design and development of the ORR electrocatalyst for MFCs could still be explored using an appropriate methodology for efficient practical applications.

8 Challenges and prospects for the practical application

The design and development of highly efficient ORR electrocatalysts are one of the major challenging factors in achieving the practical applications of MFCs. However, Pt is a benchmark ORR electrocatalyst, and its high cost is challenging. In the case of precious metal-based ORR electrocatalysts such as precious metal-based alloys, composites, etc., again, their high cost comes into the picture of challenges. Thus, the alternative highly efficient ORR electrocatalysts contain significantly lower Pt content are should still be explored.

The most common challenge of non-precious metal-based ORR electrocatalysts is the leaching of corresponding metal ions during the reaction, which results in performance loss and environmental issues. The methods such as incorporating or forming composites with other suitable materials have been adopted to overcome the leaching issues. Still, the ORR electrocatalysts' efficiency is lower and involves complex synthetic processes.

Pure graphite or carbon as ORR electrocatalysts in MFCs are limited due to their low performance. Doping of metals or non-metals increased the above catalysts' performances in the MFCs. However, the durability and the insight mechanism of ORR activity of the effect of doping should be further explored for a better understanding of the reaction. Besides, high N content in the graphite or carbon catalyst decreases the conductivity, which results in lowering the performance of the electrocatalyst.

The challenges involved in the biocatalysts are poor electron transfer and oxygen diffusion at the interface of the cathode and microbial metabolism, and growth utilizes organic carbon, which

decreases the ORR performances. In addition to the above, the careful design and development of ORR electrocatalysts of any kind with suitable phase, crystalline, and surface morphological structure is the real challenge for the practical applications of MFCs.

Besides the performances of the air cathode MFC being quite good on the laboratory scale, the ORR electrocatalysts' stability still needs to be achieved at the peak. Thus, more experimental and theoretical studies for the development of alternative cost-effective, highly efficient, and durable ORR electrocatalysts should be done for the real-time applications. The development of alternative efficient ORR electrocatalysts may be explored for the practical applications of MFCs by using several methodologies include, formation of potential heterojunction by integrating two or more different materials, the introduction of more multifunctional metals (e.g., Fe, Co, Ni, Cu, etc.), and or heteroatoms (e.g., C, N, P, F, etc.) active sites, porous structure, and surface defects, and preparation from inexpensive or waste materials.

9 Conclusion

In conclusion, the air-cathode MFC has been considered a potential technology due to the usage of air as a catholyte in the cathode chamber. The key hindrances to achieving better performances are the factors such as thermodynamic factors, which include activation losses, ohmic losses, and transport losses, and other factors, such as biofouling, catalyst inactivation, and excessive biofilm growth. The development of highly efficient and durable ORR electrocatalysts is one of the main challenges for their practical applications. The high cost of Pt is the main hindrance to large-scale applications. Several attempts have been made to develop alternative ORR electrocatalysts, such as the combination of Pt with other non-precious metals, carbon-based materials, and metal oxides. The non-precious metals based and non-metals and/or carbon based electrocatalysts were also extensively studied as potential ORR electrocatalysts in the MFCs. In addition to the above, the biocatalysts also showed good performances in the MFC applications. Based on the current review, metal-free ORR electrocatalysts such as carbon-based catalysts have been considered as one of the potential alternatives due to their excellent physicochemical properties. However, the stability and efficiency of the ORR electrocatalysts still need to improve for the practical applications of the MFCs. Besides, the quite good performances of the air-cathode MFCs on the lab-scale should be further extended to real-time applications by adopting several experimental and theoretical research.

Author contributions

KE: Prepare original draft of the manuscript; PS: Prepare and review the original draft of the manuscript and supervision; CC: Review of the manuscript and supervision; FS-G, MRK, SYC, SK, and RVM: Review of the manuscript. All authors contributed to the article and approved the submitted version.

Funding

The Government of Chile, Santiago through FONDECYT/ANID Post-doctoral Project No. 3220357.

Acknowledgments

The author PS grateful to the Government of Chile, Santiago for the financial assistance through FONDECYT/ANID Post-doctoral Project No. 3220357.

Conflict of interest

The author SC declared that they were an editorial board member of Frontiers, at the time of submission. This had no impact on the peer review process and the final decision.

The remaining authors declare that the research was conducted in the absence of any commercial or financial relationships that could be construed as a potential conflict of interest.

Publisher's note

References

Abubackar, H. N., Biryol, İ., and Ayol, A. (2023). Yeast industry wastewater treatment with microbial fuel cells: effect of electrode materials and reactor configurations. *Int. J. Hydrogen Energy* 48, 12424–12432. doi:10.1016/j.ijhydene.2022.05.277

Aelterman, P., Rabaey, K., The Pham, H., Boon, N., and Verstraete, W. (2006). Continuous electricity generation at high voltages and currents using stacked microbial fuel cells. *Environ. Sci. Technol.* 40, 3388–3394. doi:10.1021/es0525511

Agudelo-Escobar, L. M., Cabrera, S. E., and Avignone Rossa, C. (2022). A bioelectrochemical system for waste degradation and energy recovery from industrial coffee wastewater. *Front. Chem. Eng.* 4, 814987. doi:10.3389/fceng.2022.814987

Aiswaria, P., Naina Mohamed, S., Singaravelu, D. L., Brindhadevi, K., and Pugazhendhi, A. (2022). A review on graphene/graphene oxide supported electrodes for microbial fuel cell applications: challenges and prospects. *Chemosphere* 296, 133983. doi:10.1016/j.chemosphere.2022.133983

Alireza, A. A., Hamnabard, N., Meshkati, S. M. H., Pakan, M., and Ahn, Y. H. (2019). Effectiveness of phase- and morphology-controlled MnO 2 nanomaterials derived from flower-like δ-MnO 2 as alternative cathode catalyst in microbial fuel cells. *Dalt. Trans.* 48, 5429–5443. doi:10.1039/c9dt00520j

Amirul Islam, M., Wai Woon, C., Ethiraj, B., Kui Cheng, C., Yousuf, A., and Maksudur Rahman Khan, M. (2016). Ultrasound driven biofilm removal for stable power generation in microbial fuel cell. *Energy & Fuels* 31, 968–976. doi:10.1021/acs.energyfuels.6b02294

An, J., Kim, B., Chang, I. S., and Lee, H.-S. (2015). Shift of voltage reversal in stacked microbial fuel cells. *J. Power Sources* 278, 534–539. doi:10.1016/j.jpowsour.2014.12.112

Babanova, S., Jones, J., Wiseman, K., Soles, J., Garcia, J., Huerta, P., et al. (2022). Bioelectrochemical treatment technology—the new practical approach for wastewater management and GHG emissions reduction. *Front. Chem. Eng.* 4, 832505. doi:10.3389/fceng.2022.832505

Bagchi, S., and Behera, M. (2019). Methanogenesis suppression in microbial fuel cell by aluminium dosing. *Bioelectrochemistry* 129, 206–210. doi:10.1016/j.bioelechem.2019.05.019

Blanchet, E., Erable, B., De Solan, M.-L., and Bergel, A. (2016). Two-dimensional carbon cloth and three-dimensional carbon felt perform similarly to form bioanode fed with food waste. *Electrochem. Commun.* 66, 38–41. doi:10.1016/j.elecom.2016.02.017

Canfield, J. H., Goldner, B. H., and Lutwack, R. (1963). Utilization of human wastes as electrochemical fuels. *NASA Tech. Rep. Magna Corp. Anaheim CA* 63, 615–616.

Cao, C., Wei, L., Su, M., Wang, G., and Shen, J. (2016). Enhanced power generation using nano cobalt oxide anchored nitrogen-decorated reduced graphene oxide as a high-performance air-cathode electrocatalyst in biofuel cells. *RSC Adv.* 6, 52556–52563. doi:10.1039/c6ra11095a

Cetinkaya, A. Y., Ozdemir, O. K., Koroglu, E. O., Hasimoglu, A., and Ozkaya, B. (2015). The development of catalytic performance by coating Pt-Ni on CMI7000 membrane as a cathode of a microbial fuel cell. *Bioresour. Technol.* 195, 188–193. doi:10.1016/j.biortech.2015.06.064

Chakraborty, I., Bhowmick, G. D., Ghosh, D., Dubey, B. K., Pradhan, D., and Ghangrekar, M. M. (2020). Novel low-cost activated algal biochar as a cathode catalyst for improving performance of microbial fuel cell. *Sustain. Energy Technol. Assessments* 42, 100808. doi:10.1016/j.seta.2020.100808

Chandrasekhar, K., and Ahn, Y. H. (2017). Effectiveness of piggery waste treatment using microbial fuel cells coupled with elutriated-phased acid fermentation. *Bioresour. Technol.* 244, 650–657. doi:10.1016/J.BIORTECH.2017.08.021

Chang, J., Wang, W., Wang, Y., Su, C., Pan, J., Wang, H., et al. (2021). Fabrication of bimetallic Co/Zn leaf blade structure template derived Co3O4-ZIF/Zn and its ORR catalytic performance for MFC. *J. Taiwan Inst. Chem. Eng.* 129, 144–153. doi:10.1016/J.JTICE.2021.09.027

Chaturvedi, A., Dhillon, S. K., and Kundu, P. P. (2022). 1-D semiconducting TiO2 nanotubes supported efficient bimetallic Co-Ni cathode catalysts for power generation in single-chambered air-breathing microbial fuel cells. *Sustain. Energy Technol. Assessments* 53, 102479. doi:10.1016/j.seta.2022.102479

Chaturvedi, A., and Kundu, P. P. (2022). Co-doped zeolite–GO nanocomposite as a high-performance ORR catalyst for sustainable bioelectricity generation in air-cathode single-chambered microbial fuel cells. *ACS Appl. Mat. Interfaces* 14, 33219–33233. doi:10.1021/acsami.2c07638

Chaturvedi, A., and Kundu, P. P. (2021). Recent advances and perspectives in platinum-free cathode catalysts in microbial fuel cells. *J. Environ. Chem. Eng.* 9, 105662. doi:10.1016/J.JECE.2021.105662

Chen, H., Jiang, D., Xie, H., Liu, Y., Li, S., and Wang, Y. (2023). Cu 2 O@Co/N-doped carbon as antibacterial catalysts for oxygen reduction in microbial fuel cells. *Environ. Sci. Nano* 10, 158–165. doi:10.1039/D2EN00980C

Chen, J., Liu, Y., Yang, J., Wang, H., Liu, H., Cao, S., et al. (2022a). The potential of Co3O4 nanoparticles attached to the surface of MnO2 nanorods as cathode catalyst for single-chamber microbial fuel cell. *Bioresour. Technol.* 346, 126584. doi:10.1016/j.biortech.2021.126584

Chen, J., Yang, J., Jiang, L., Wang, X., Yang, D., Wei, Q., et al. (2021). Improved electrochemical performances by Ni-catecholate-based metal organic framework grown on NiCoAl-layered double hydroxide/multi-wall carbon nanotubes as cathode catalyst in microbial fuel cells. *Bioresour. Technol.* 337, 125430. doi:10.1016/J.BIORTECH.2021.125430

Chen, J., Yang, J., Wang, R., Yang, Y., and Liu, Y. (2022b). Design and research progress of nano materials in cathode catalysts of microbial fuel cells: A review. *Int. J. Hydrogen Energy* 47, 18098–18108. doi:10.1016/j.ijhydene.2022.04.020

Chen, J., Yang, J., Wang, X., Yang, D., Yang, M., Tian, J., et al. (2022c). Cathode catalyst selection for enhancing oxygen reduction reactions of microbial fuel cells: COF-300@NiAl-LDH/GO and Ti3AlC2/NiCoAl-LDH. *Int. J. Hydrogen Energy* 47, 16179–16188. doi:10.1016/j.ijhydene.2022.03.107

Chen, J., Yang, J., Wu, Y., Zhao, Y., Wang, X., Wang, J., et al. (2022d). Three-dimensional ZIF-67 attached lamellar Ti3AlC2 combined with ZnAl-LDH as cathode catalyst for enhancing oxygen reduction reaction of microbial fuel cells. *Int. J. Hydrogen Energy* 47, 16262–16271. doi:10.1016/j.ijhydene.2022.03.133

Chen, J. Y., Li, N., and Zhao, L. (2014a). Three-dimensional electrode microbial fuel cell for hydrogen peroxide synthesis coupled to wastewater treatment. *J. Power Sources* 254, 316–322. doi:10.1016/J.JPOWSOUR.2013.12.114

Chen, W., Liu, Z., Li, Y., Jiang, K., Hou, J., Lou, X., et al. (2019). A novel stainless steel fiber felt/Pd nanocatalysts electrode for efficient ORR in air-cathode microbial fuel cells. *Electrochim. Acta* 324, 134862. doi:10.1016/J.ELECTACTA.2019.134862

Chen, Z., Li, K., and Pu, L. (2014b). The performance of phosphorus (P)-doped activated carbon as a catalyst in air-cathode microbial fuel cells. *Bioresour. Technol.* 170, 379–384. doi:10.1016/j.biortech.2014.07.114

Cheng, C., Hu, Y., Shao, S., Yu, J., Zhou, W., Cheng, J., et al. (2019). Simultaneous Cr(VI) reduction and electricity generation in Plant-Sediment Microbial Fuel Cells (P-SMFCs): synthesis of non-bonding Co3O4 nanowires onto cathodes. *Environ. Pollut.* 247, 647–657. doi:10.1016/J.ENVPOL.2019.01.084

Cheng, S., and Wu, J. (2013). Air-cathode preparation with activated carbon as catalyst, PTFE as binder and nickel foam as current collector for microbial fuel cells. *Bioelectrochemistry* 92, 22–26. doi:10.1016/j.bioelechem.2013.03.001

Cohen, B. (1931). The bacterial culture as an electrical half-cell. *J. Bacteriol.* 21, 18–19. Available at: https://www.scopus.com/inward/record.uri?eid=2-s2.0-0002906445&partnerID=40&md5=bfcdc2eb3fcc88f839a3083f277efb6f.

Daghio, M., Aulenta, F., Vaiopoulou, E., Franzetti, A., Arends, J. B. A., Sherry, A., et al. (2017). Electrobioremediation of oil spills. *Water Res.* 114, 351–370. doi:10.1016/j.watres.2017.02.030

Dai, H. Y., Yang, H. M., Jian, X., Liu, X., and Liang, Z. H. (2017). Performance of Ag2O/Ag electrode as cathodic electron acceptor in microbial fuel cell. *Acta Metall. Sin. Engl. Lett.* 30, 1243–1248. doi:10.1007/s40195-017-0616-1

De Schamphelaire, L., Boeckx, P., and Verstraete, W. (2010). Evaluation of biocathodes in freshwater and brackish sediment microbial fuel cells. *Appl. Microbiol. Biotechnol.* 87, 1675–1687. doi:10.1007/s00253-010-2645-9

Dey, N., Samuel, G. V., Raj, D. S., and Gajalakshmi, B. (2023). Nanomaterials as potential high performing electrode materials for microbial fuel cells. *Appl. Nanosci.* 13, 2625–2640. doi:10.1007/s13204-022-02371-3

Dhanda, A., Raj, R., Sathe, S. M., Dubey, B. K., and Ghangrekar, M. M. (2023). Graphene and biochar-based cathode catalysts for microbial fuel cell: performance evaluation, economic comparison, environmental and future perspectives. *Environ. Res.* 231, 116143. doi:10.1016/j.envres.2023.116143

Dhilllon, S. K., Kundu, P. P., and Jain, R. (2022). Catalytic advancements in carbonaceous materials for bio-energy generation in microbial fuel cells: A review. *Environ. Sci. Pollut. Res.* 1, 24815–24841. doi:10.1007/s11356-021-17529-9

Dhillon, S. K., and Kundu, P. P. (2023). Transition metal sulfide/oxide nanoflowers decorated on poly (aniline-2-sulfonic acid) modified polyacrylamide derived carbon cathode catalyst for bioenergy generation in microbial fuel cells. *Electrochim. Acta* 461, 142697. doi:10.1016/j.electacta.2023.142697

Díaz-Vázquez, D., Garibay, M. V., Fernández del Castillo, A., Orozco-Nunnelly, D. A., Senés-Guerrero, C., and Gradilla-Hernández, M. S. (2022). Yeast community composition impacts on tequila industry waste treatment for pollution control and waste-to-product synthesis. *Front. Chem. Eng.* 4, 1013873. doi:10.3389/fceng.2022.1013873

Ding, F., Liu, H., Jiang, X., Jiang, Y., Cheng, J., Tu, Y., et al. (2023). Bimetallic zeolite imidazolium framework derived multiphase Co/HNC as pH-universal catalysts with efficient oxygen reduction performance for microbial fuel cells. *Electrochim. Acta* 438, 141548. doi:10.1016/j.electacta.2022.141548

Ding, F., Liu, H., Jiang, X., Jiang, Y., Tu, Y., Xiao, W., et al. (2022). Co9S8 nanoparticles encapsulated in N,S co-doped hierarchical carbon as an efficient oxygen reduction electrocatalyst for microbial fuel cells. *J. Electroanal. Chem.* 909, 116130. doi:10.1016/j.jelechem.2022.116130

Dong, H., Liu, X., Xu, T., Wang, Q., Chen, X., Chen, S., et al. (2018). Hydrogen peroxide generation in microbial fuel cells using graphene-based air-cathodes. *Bioresour. Technol.* 247, 684–689. doi:10.1016/j.biortech.2017.09.158

Duteanu, N., Erable, B., Senthil Kumar, S. M., Ghangrekar, M. M., and Scott, K. (2010). Effect of chemically modified Vulcan XC-72R on the performance of air-breathing cathode in a single-chamber microbial fuel cell. *Bioresour. Technol.* 101, 5250–5255. doi:10.1016/j.biortech.2010.01.120

Dziegielowski, J., Metcalfe, B., and Di Lorenzo, M. (2021). Towards effective energy harvesting from stacks of soil microbial fuel cells. *J. Power Sources* 515, 230591. doi:10.1016/j.jpowsour.2021.230591

Fang, C., and Achal, V. (2019). The potential of microbial fuel cells for remediation of heavy metals from soil and water—review of application. *Microorganisms* 7, 697. doi:10.3390/microorganisms7120697

Feng, Y., Shi, X., Wang, X., Lee, H., Liu, J., Qu, Y., et al. (2012). Effects of sulfide on microbial fuel cells with platinum and nitrogen-doped carbon powder cathodes. *Biosens. Bioelectron.* 35, 413–415. doi:10.1016/j.bios.2011.08.030

Fu, L., You, S. J., Yang, F. L., Gao, M. M., Fang, X. H., and Zhang, G. Q. (2010). Synthesis of hydrogen peroxide inmicrobial fuel cell. *J. Chem. Technol. Biotechnol.* 85, 715–719. doi:10.1002/jctb.2367

Gao, M., Lu, J.-Y., and Li, W.-W. (2020). "Oxygen reduction reaction electrocatalysts for microbial fuel cells," in *Novel catalyst materials for bioelectrochemical systems: Fundamentals and applications*. Editors L. Singh, D. M. Mahapatra, and H. Liu (ACS Publications), 73–96. doi:10.1021/bk-2020-1342.ch004

Gargalo, C. L., Rapazzo, J., Carvalho, A., and Gernaey, K. V. (2022). Optimal conversion of organic wastes to value-added products: toward a sustainable integrated biorefinery in Denmark. *Front. Chem. Eng.* 4, 837105. doi:10.3389/fceng.2022.837105

Gautam, R. K., and Verma, A. (2019). "Electrocatalyst materials for oxygen reduction reaction in microbial fuel cell," in *Microbial electrochemical technology sustainable platform for fuels, chemicals and remediation*. Editors S. Venkata Mohan, S. Varjani, and A. Pandey (Elsevier B.V), 451–483. doi:10.1016/B978-0-444-64052-9.00018-2

Ge, B., Li, K., Fu, Z., Pu, L., Zhang, X., Liu, Z., et al. (2016). The performance of nano urchin-like NiCo2O4 modified activated carbon as air cathode for microbial fuel cell. *J. Power Sources* 303, 325–332. doi:10.1016/j.jpowsour.2015.11.003

Ge, B., Li, K., Fu, Z., Pu, L., and Zhang, X. (2015). The addition of ortho-hexagon nano spinel Co3O4 to improve the performance of activated carbon air cathode microbial fuel cell. *Bioresour. Technol.* 195, 180–187. doi:10.1016/J.BIORTECH.2015.06.054

Ghosh, D., Chakraborty, I., Ghangrekar, M. M., and Pradhan, D. (2023). Precious-metal-free solvothermally synthesized CeO 2 nanosphere-graphitic carbon nitride sheet composites for oxygen reduction reaction. *ACS Appl. Energy Mat.* 6, 4570–4583. doi:10.1021/acsaem.2c03959

Gong, X. B., You, S. J., Wang, X. H., Gan, Y., Zhang, R. N., and Ren, N. Q. (2013). Silver-tungsten carbide nanohybrid for efficient electrocatalysis of oxygen reduction reaction in microbial fuel cell. *J. Power Sources* 225, 330–337. doi:10.1016/j.jpowsour.2012.10.047

Gong, X., Peng, L., Wang, X., Wu, L., and Liu, Y. (2020). Duckweed derived nitrogen self-doped porous carbon materials as cost-effective electrocatalysts for oxygen reduction reaction in microbial fuel cells. *Int. J. Hydrogen Energy* 45, 15336–15345. doi:10.1016/J.IJHYDENE.2020.03.177

Gude, V. G. (2016). Wastewater treatment in microbial fuel cells – An overview. *J. Clean. Prod.* 122, 287–307. doi:10.1016/j.jclepro.2016.02.022

Guo, S., Liu, Y., Sun, Y., and Li, C. (2023). Heterostructure-induced enhanced oxygen catalysis behavior based on metal cobalt coupled with compound anchored on N-doped carbon nanofiber for microbial fuel cell. *J. Colloid Interface Sci.* 636, 305–316. doi:10.1016/j.jcis.2023.01.013

Guo, X., Jia, J., Dong, H., Wang, Q., Xu, T., Fu, B., et al. (2019). Hydrothermal synthesis of FeMn bimetallic nanocatalysts as high-efficiency cathode catalysts for microbial fuel cells. *J. Power Sources* 414, 444–452. doi:10.1016/J.JPOWSOUR.2019.01.024

Gupta, S., Patro, A., Mittal, Y., Dwivedi, S., Saket, P., Panja, R., et al. (2023). The race between classical microbial fuel cells, sediment-microbial fuel cells, plant-microbial fuel cells, and constructed wetlands-microbial fuel cells: applications and technology readiness level. *Sci. Total Environ.* 879, 162757. doi:10.1016/j.scitotenv.2023.162757

Haile, A. S., Yohannes, W., and Mekonnen, Y. S. (2020). Oxygen reduction reaction on Pt-skin Pt 3 V(111) fuel cell cathode: A density functional theory study. *RSC Adv.* 10, 27346–27356. doi:10.1039/D0RA02972F

Halakoo, E., Khademi, A., Ghasemi, M., Yusof, N. M., Gohari, R. J., and Ismail, A. F. (2015). Production of sustainable energy by carbon nanotube/platinum catalyst in microbial fuel cell. *Procedia CIRP* 26, 473–476. doi:10.1016/J.PROCIR.2014.07.034

Han, H. X., Shi, C., Yuan, L., and Sheng, G. P. (2017). Enhancement of methyl orange degradation and power generation in a photoelectrocatalytic microbial fuel cell. *Appl. Energy* 204, 382–389. doi:10.1016/J.APENERGY.2017.07.032

Harnisch, F., Wirth, S., and Schröder, U. (2009). Effects of substrate and metabolite crossover on the cathodic oxygen reduction reaction in microbial fuel cells: platinum vs. iron(II) phthalocyanine based electrodes. *Electrochem. Commun.* 11, 2253–2256. doi:10.1016/j.elecom.2009.10.002

He, Z., and Angenent, L. T. (2006). Application of bacterial biocathodes in microbial fuel cells. *Electroanalysis* 18, 2009–2015. doi:10.1002/elan.200603628

Hidayat, A. R. P., Widyanto, A. R., Asranudin, A., Ediati, R., Sulistiono, D. O., Putro, H. S., et al. (2022). Recent development of double chamber microbial fuel cell for hexavalent chromium waste removal. *J. Environ. Chem. Eng.* 10, 107505. doi:10.1016/j.jece.2022.107505

Hou, Y., Chen, J., He, Z., Yuan, H., and Abu-Reesh, I. M. (2016). Oxygen reduction reaction catalysts used in microbial fuel cells for energy-efficient wastewater treatment: A review. *Mat. Horiz.* 3, 382–401. doi:10.1039/c6mh00093b

Hu, D., Zhang, G., Wang, J., and Zhong, Q. (2015). Carbon-supported spinel nanoparticle MnCo2O4 as a cathode catalyst towards oxygen reduction reaction in dual-chamber microbial fuel cell. *Aust. J. Chem.* 68, 987. doi:10.1071/CH14516

Huang, Q., Zhou, P., Yang, H., Zhu, L., and Wu, H. (2017). *In situ* generation of inverse spinel CoFe 2 O 4 nanoparticles onto nitrogen-doped activated carbon for an effective cathode electrocatalyst of microbial fuel cells. *Chem. Eng. J.* 325, 466–473. doi:10.1016/j.cej.2017.05.079

Huang, S., Geng, Y., Chen, D., Li, N., Xu, Q., Li, H., et al. (2023). Metal-organic framework-derived Fe/Fe3C embedded in N-doped carbon as a highly efficient oxygen reduction catalyst for microbial fuel cells. *Chem. Eng. Sci.* 278, 118906. doi:10.1016/j.ces.2023.118906

Huang, S., Geng, Y., Xia, J., Chen, D., and Lu, J. (2022). NiCo alloy nanoparticles on a N/C dual-doped matrix as a cathode catalyst for improved microbial fuel cell performance. *Small* 18, 2106355. doi:10.1002/smll.202106355

Huang, X., Duan, C., Duan, W., Sun, F., Cui, H., Zhang, S., et al. (2021). Role of electrode materials on performance and microbial characteristics in the constructed wetland coupled microbial fuel cell (CW-MFC): A review. *J. Clean. Prod.* 301, 126951. doi:10.1016/j.jclepro.2021.126951

Izadi, P., Fontmorin, J.-M., Fernández, L. F. L., Cheng, S., Head, I., and Yu, E. H. (2019). High performing gas diffusion biocathode for microbial fuel cells using acidophilic iron oxidizing bacteria. *Front. Energy Res.* 7, 00093. doi:10.3389/fenrg.2019.00093

Jatoi, A. S., Akhter, F., Mazari, S. A., Sabzoi, N., Aziz, S., Soomro, S. A., et al. (2021). Advanced microbial fuel cell for waste water treatment—A review. *Environ. Sci. Pollut. Res.* 28, 5005–5019. doi:10.1007/s11356-020-11691-2

Jiang, B., Muddemann, T., Kunz, U., Silva e Silva, L. G., Bormann, H., Niedermeiser, M., et al. (2017). Graphite/MnO 2 and MoS 2 composites used as catalysts in the oxygen reduction cathode of microbial fuel cells. *J. Electrochem. Soc.* 164, E519–E524. doi:10.1149/2.0801714jes

Jiang, J., Zhang, S., Li, S., Zeng, W., Li, F., and Wang, W. (2022). Magnetized manganese-doped watermelon rind biochar as a novel low-cost catalyst for improving oxygen reduction reaction in microbial fuel cells. *Sci. Total Environ.* 802, 149989. doi:10.1016/j.scitotenv.2021.149989

Jiang, L., Chen, J., An, Y., Han, D., Chang, S., Liu, Y., et al. (2020a). Enhanced electrochemical performance by nickel-iron layered double hydroxides (LDH) coated on Fe3O4 as a cathode catalyst for single-chamber microbial fuel cells. *Sci. Total Environ.* 745, 141163. doi:10.1016/j.scitotenv.2020.141163

Jiang, L., Chen, J., Han, D., Chang, S., Yang, R., An, Y., et al. (2020b). Potential of core-shell NiFe layered double hydroxide@Co3O4 nanostructures as cathode catalysts for oxygen reduction reaction in microbial fuel cells. *J. Power Sources* 453, 227877. doi:10.1016/J.JPOWSOUR.2020.227877

Jiang, N., Huang, M., Li, J., Song, J., Zheng, S., Gao, Y., et al. (2021). Enhanced bioelectricity output of microbial fuel cells via electrospinning zeolitic imidazolate framework-67/polyacrylonitrile carbon nanofiber cathode. *Bioresour. Technol.* 337, 125358. doi:10.1016/J.BIORTECH.2021.125358

Jing, B., You, S., Ma, Y., Xing, Z., Chen, H., Dai, Y., et al. (2019). Fe3Se4/FeSe heterojunctions in cornstalk-derived N-doped carbon framework enhance charge transfer and cathodic oxygen reduction reaction to boost bio-electricity generation. *Appl. Catal. B Environ.* 244, 465–474. doi:10.1016/J.APCATB.2018.11.074

Kamali, M., Aminabhavi, T. M., Abbassi, R., Dewil, R., and Appels, L. (2022). Engineered nanomaterials in microbial fuel cells – recent developments, sustainability aspects, and future outlook. *Fuel* 310, 122347. doi:10.1016/j.fuel.2021.122347

Kamali, M., Guo, Y., Aminabhavi, T. M., Abbassi, R., Dewil, R., and Appels, L. (2023). Pathway towards the commercialization of sustainable microbial fuel cell-based wastewater treatment technologies. *Renew. Sustain. Energy Rev.* 173, 113095. doi:10.1016/j.rser.2022.113095

Kaur Dhillon, S., and Paban Kundu, P. (2023). Transitional trimetallic alloy embedded polyacrylamide hydrogel derived nitrogen-doped carbon air-cathode for bioenergy generation in microbial fuel cell. *Sustain. Energy Technol. Assessments* 55, 103001. doi:10.1016/j.seta.2022.103001

Kaur, R., Marwaha, A., Chhabra, V. A., Kim, K.-H., and Tripathi, S. K. (2020). Recent developments on functional nanomaterial-based electrodes for microbial fuel cells. *Renew. Sustain. Energy Rev.* 119, 109551. doi:10.1016/j.rser.2019.109551

Kaur, R., Singh, S., Chhabra, V. A., Marwaha, A., Kim, K. H., and Tripathi, S. K. (2021). A sustainable approach towards utilization of plastic waste for an efficient electrode in microbial fuel cell applications. *J. Hazard. Mat.* 417, 125992. doi:10.1016/J.JHAZMAT.2021.125992

Kausar, A., Ahmad, I., Zhao, T., Maaza, M., and Bocchetta, P. (2023). Green nanocomposite electrodes/electrolytes for microbial fuel cells—cutting-edge technology. *J. Compos. Sci.* 7, 166. doi:10.3390/jcs7040166

Kumar, A., Siddiqui, T., Pandit, S., Roy, A., Gacem, A., Souwaileh, A. A, et al. (2023a). Application of biogenic TiO2 nanoparticles as ORR catalysts on cathode for enhanced performance of microbial fuel cell. *Catalysts* 13, 937. doi:10.3390/catal13060937

Kumar, D., Geetanjali,, and Kundu, P. P. (2023b). Poly (acrylamide-co-acrylonitrile) hydrogel-derived iron-doped carbon foam electrocatalyst for enhancing oxygen reduction reaction in microbial fuel cell. *Int. J. Hydrogen Energy* 48, 7884–7895. doi:10.1016/j.ijhydene.2022.11.109

Kumar, P., Chatterjee, P., and Ghangrekar, M. M. (2017). Fouling resistant nitrogen doped carbon powder with amino-trimethylene-phosphate cathode for microbial fuel cell. *Mat. Renew. sustain. Energy* 6, 9. doi:10.1007/s40243-017-0093-5

Kun, G., Hassett, D., Gu, T., and Arora, R. (2012). *Microbial fuel cells: electricity generation from organic wastes by microbes*. CABI International.

Lai, B., Xiao, Z., Jiang, P., Xie, Y., Li, N., and Liu, Z. (2022). Two-dimensional Ag–Fe–N/C nanosheets as efficient cathode catalyst to improve power-generation performance of microbial fuel cells. *ChemElectroChem* 9, e202101699. doi:10.1002/celc.202101699

Lee, S. H., Ban, J. Y., Oh, C. H., Park, H. K., and Choi, S. (2016). A solvent-free microbial-activated air cathode battery paper platform made with pencil-traced graphite electrodes. *Sci. Rep.* 6, 28588. doi:10.1038/srep28588

Li, B., He, Z., Wang, M., and Wang, X. (2017). PtSnP/C and PtSn/C as efficient cathode catalysts for oxygen reduction reaction in microbial fuel cells. *Int. J. Hydrogen Energy* 42, 5261–5271. doi:10.1016/j.ijhydene.2017.01.087

Li, C., Yi, K., Hu, S., and Yang, W. (2023). Cathodic biofouling control by microbial separators in air-breathing microbial fuel cells. *Environ. Sci. Ecotechnology* 15, 100251. doi:10.1016/j.ese.2023.100251

Li, D., Qu, Y., Liu, J., He, W., Wang, H., and Feng, Y. (2014). Using ammonium bicarbonate as pore former in activated carbon catalyst layer to enhance performance of

air cathode microbial fuel cell. *J. Power Sources* 272, 909–914. doi:10.1016/j.jpowsour.2014.09.053

Li, H., Ma, H., Liu, T., Ni, J., and Wang, Q. (2019). An excellent alternative composite modifier for cathode catalysts prepared from bacterial cellulose doped with Cu and P and its utilization in microbial fuel cell. *Bioresour. Technol.* 289, 121661. doi:10.1016/J.BIORTECH.2019.121661

Li, H., Sun, Y., Wang, J., Liu, Y., and Li, C. (2022a). Nanoflower-branch LDHs and CoNi alloy derived from electrospun carbon nanofibers for efficient oxygen electrocatalysis in microbial fuel cells. *Appl. Catal. B Environ.* 307, 121136. doi:10.1016/j.apcatb.2022.121136

Li, H., Zhang, X., Qin, Y., Liu, Y., Wang, J., Peng, L., et al. (2021a). Crafting controllable Fe-based hierarchically organic-frameworks from bacterial cellulose nanofibers for efficient electrocatalysts in microbial fuel cells. *J. Power Sources* 512, 230522. doi:10.1016/J.JPOWSOUR.2021.230522

Li, J. C., Wu, X. T., Chen, L. J., Li, N., and Liu, Z. Q. (2018a). Bifunctional MOF-derived Co-N-doped carbon electrocatalysts for high-performance zinc-air batteries and MFCs. *Energy* 156, 95–102. doi:10.1016/J.ENERGY.2018.05.096

Li, J., Qian, J., Chen, X., Zeng, X., Li, L., Ouyang, B., et al. (2022b). Three-dimensional hierarchical graphitic carbon encapsulated CoNi alloy/N-doped CNTs/carbon nanofibers as an efficient multifunctional electrocatalyst for high-performance microbial fuel cells. *Compos. Part B Eng.* 231, 109573. doi:10.1016/j.compositesb.2021.109573

Li, M., Zhang, H., Xiao, T., Wang, S., Zhang, B., Chen, D., et al. (2018b). Low-cost biochar derived from corncob as oxygen reduction catalyst in air cathode microbial fuel cells. *Electrochim. Acta* 283, 780–788. doi:10.1016/j.electacta.2018.07.010

Li, S., Zhu, X., Yu, H., Wang, X., Liu, X., Yang, H., et al. (2021b). Simultaneous sulfamethoxazole degradation with electricity generation by microbial fuel cells using Ni-MOF-74 as cathode catalysts and quantification of antibiotic resistance genes. *Environ. Res.* 197, 111054. doi:10.1016/J.ENVRES.2021.111054

Liang, B., Li, K., Liu, Y., and Kang, X. (2019). Nitrogen and phosphorus dual-doped carbon derived from chitosan: an excellent cathode catalyst in microbial fuel cell. *Chem. Eng. J.* 358, 1002–1011. doi:10.1016/J.CEJ.2018.09.217

Liang, B., Su, M., Zhao, Z., He, H., Lin, S., and Liang, S. (2023). Fe, N-codoped carbon derived from different ligands for oxygen reduction reaction in air-cathode microbial fuel cells: performance comparison and the associated mechanism. *Electrochim. Acta* 462, 142779. doi:10.1016/j.electacta.2023.142779

Liang, B., Zhao, Y., Li, K., and Lv, C. (2020). Porous carbon codoped with inherent nitrogen and externally embedded cobalt nanoparticles as a high-performance cathode catalyst for microbial fuel cells. *Appl. Surf. Sci.* 505, 144547. doi:10.1016/J.APSUSC.2019.144547

Liew, K. B., Wan Daud, W. R., Ghasemi, M., Loh, K. S., Ismail, M., Lim, S. S., et al. (2015). Manganese oxide/functionalised carbon nanotubes nanocomposite as catalyst for oxygen reduction reaction in microbial fuel cell. *Int. J. Hydrogen Energy* 40, 11625–11632. doi:10.1016/j.ijhydene.2015.04.030

Lin, Z., Su, W., Zhang, S., Zhang, M., Li, K., and Liu, J. (2021). Co2P embedded in nitrogen-doped carbon nanoframework derived from Co-based metal-organic framework as efficient oxygen reduction reaction electrocatalyst for enhanced performance of activated carbon air-cathode microbial fuel cell. *J. Electroanal. Chem.* 895, 115355. doi:10.1016/J.JELECHEM.2021.115355

Lin, Z., Yang, A., Zhang, B., Liu, B., Zhu, J., Tang, Y., et al. (2022). Coupling the atomically dispersed Fe-N 3 sites with sub-5 nm Pd nanocrystals confined in N-doped carbon nanobelts to boost the oxygen reduction for microbial fuel cells. *Adv. Funct. Mat.* 32, 2107683. doi:10.1002/adfm.202107683

Liu, H., and Logan, E. B. (2004). Electricity generation using an air-cathode single chamber microbial fuel cell in the presence and absence of a proton exchange membrane. *Environ. Sci. Technol.* 38, 4040–4046. doi:10.1021/es0499344

Liu, J., Chu, C., Wei, L., Feng, J., and Shen, J. (2023). Iron/cobalt-decorated nitrogen-rich 3D layer-stacked porous biochar as high-performance oxygen reduction air-cathode catalyst in microbial fuel cell. *Biosens. Bioelectron.* 222, 114926. doi:10.1016/j.bios.2022.114926

Liu, Q., Chen, S., Zhou, Y., Zheng, S., Hou, H., and Zhao, F. (2014). Phosphorus-doped carbon derived from cellulose phosphate as efficient catalyst for air-cathode in microbial fuel cells. *J. Power Sources* 261, 245–248. doi:10.1016/j.jpowsour.2014.03.060

Liu, X. W., Sun, X. F., Huang, Y. X., Sheng, G. P., Wang, S. G., and Yu, H. Q. (2011). Carbon nanotube/chitosan nanocomposite as a biocompatible biocathode material to enhance the electricity generation of a microbial fuel cell. *Energy Environ. Sci.* 4, 1422–1427. doi:10.1039/c0ee00447b

Liu, Y., Fan, Y. S., and Liu, Z. M. (2019). Pyrolysis of iron phthalocyanine on activated carbon as highly efficient non-noble metal oxygen reduction catalyst in microbial fuel cells. *Chem. Eng. J.* 361, 416–427. doi:10.1016/J.CEJ.2018.12.105

Liu, Y., Guo, S., Wang, J., and Li, C. (2022). Fundamental development and research of cathodic compartment in microbial fuel cells: A review. *J. Environ. Chem. Eng.* 10, 107918. doi:10.1016/j.jece.2022.107918

Liu, Y., Li, K., Ge, B., Pu, L., and Liu, Z. (2016). Influence of micropore and mesoporous in activated carbon air-cathode catalysts on oxygen reduction reaction in microbial fuel cells. *Electrochim. Acta* 214, 110–118. doi:10.1016/j.electacta.2016.08.034

Liu, Y., Li, K., Liu, Y., Pu, L., Chen, Z., and Deng, S. (2015). The high-performance and mechanism of P-doped activated carbon as a catalyst for air-cathode microbial fuel cells. *J. Mat. Chem. A* 3, 21149–21158. doi:10.1039/c5ta04595a

Liu, Y., Zhao, Y., Li, K., Wang, Z., Tian, P., Liu, D., et al. (2018). Activated carbon derived from chitosan as air cathode catalyst for high performance in microbial fuel cells. *J. Power Sources* 378, 1–9. doi:10.1016/J.JPOWSOUR.2017.12.019

Liu, Z., Liu, J., Zhang, S., and Su, Z. (2008). A novel configuration of microbial fuel cell stack bridged internally through an extra cation exchange membrane. *Biotechnol. Lett.* 30, 1017–1023. doi:10.1007/s10529-008-9658-9

Logan, B., Cheng, S., Watson, V., and Estadt, G. (2007). Graphite fiber brush anodes for increased power production in air-cathode microbial fuel cells. *Environ. Sci. Technol.* 41, 3341–3346. doi:10.1021/es062644y

Logan, B. E., and Regan, J. M. (2006). Microbial fuel cells - challenges and applications. *Environ. Sci. Technol.* 40, 5172–5180. doi:10.1021/es0627592

Logan, E. B., Hamelers, B., Rozendal, R., Schröder, U., Keller, J., Freguia, S., et al. (2006). Microbial fuel cells: methodology and technology. *Environ. Sci. Technol.* 40, 5181–5192. doi:10.1021/es0605016

Long, P., Qin, M., Zhang, B., Liu, Q., Zhao, F., Wu, Z., et al. (2023). Nano-flower like CoFe-layered double hydroxide@reduced graphene oxide with efficient oxygen reduction reaction for high-power air-cathode microbial fuel cells. *Carbon N. Y.* 212, 118088. doi:10.1016/j.carbon.2023.118088

Long, X., Cao, X., Song, H., Nishimura, O., and Li, X. (2019). Characterization of electricity generation and microbial community structure over long-term operation of a microbial fuel cell. *Bioresour. Technol.* 285, 121395. doi:10.1016/J.BIORTECH.2019.121395

Lu, J., Ren, L., Li, C., and Liu, H. (2023). Three-dimensional hierarchical flower-like bimetallic–organic materials *in situ* grown on carbon cloth and doped with sulfur as an air cathode in a microbial fuel cell. *New J. Chem.* 47, 2068–2078. doi:10.1039/D2NJ05476K

Ma, J., Zhang, J., Zhang, Y., Guo, Q., Hu, T., Xiao, H., et al. (2023). Progress on anodic modification materials and future development directions in microbial fuel cells. *J. Power Sources* 556, 232486. doi:10.1016/j.jpowsour.2022.232486

Ma, Z., Cano, Z. P., Yu, A., Chen, Z., Jiang, G., Fu, X., et al. (2020). Enhancing oxygen reduction activity of Pt-based electrocatalysts: from theoretical mechanisms to practical methods. *Angew. Chem. Int. Ed.* 59, 18334–18348. doi:10.1002/anie.202003654

Majidi, M. R., Shahbazi Farahani, F., Hosseini, M., and Ahadzadeh, I. (2019). Low-cost nanowired α-MnO2/C as an ORR catalyst in air-cathode microbial fuel cell. *Bioelectrochemistry* 125, 38–45. doi:10.1016/j.bioelechem.2018.09.004

Maruyama, J., Okamura, J., Miyazaki, K., and Abe, I. (2007). Two-step carbonization as a method of enhancing catalytic properties of hemoglobin at the fuel cell cathode. *J. Phys. Chem. C* 111, 6597–6600. doi:10.1021/jp071451+

Mecheri, B., Ficca, V. C. A., Costa de Oliveira, M. A., D'Epifanio, A., Placidi, E., Arciprete, F., et al. (2018). Facile synthesis of graphene-phthalocyanine composites as oxygen reduction electrocatalysts in microbial fuel cells. *Appl. Catal. B Environ.* 237, 699–707. doi:10.1016/J.APCATB.2018.06.031

Mecheri, B., Iannaci, A., D'Epifanio, A., Mauri, A., and Licoccia, S. (2016). Carbon-supported zirconium oxide as a cathode for microbial fuel cell applications. *Chempluschem* 81, 80–85. doi:10.1002/cplu.201500347

Meng, K., Liu, Q., Huang, Y., and Wang, Y. (2015). Facile synthesis of nitrogen and fluorine co-doped carbon materials as efficient electrocatalysts for oxygen reduction reactions in air-cathode microbial fuel cells. *J. Mat. Chem. A* 3, 6873–6877. doi:10.1039/c4ta06500j

Merino-Jimenez, I., Gonzalez-Juarez, F., Greenman, J., and Ieropoulos, I. (2019). Effect of the ceramic membrane properties on the microbial fuel cell power output and catholyte generation. *J. Power Sources* 429, 30–37. doi:10.1016/J.JPOWSOUR.2019.04.043

Mian, M. M., Liu, G., and Fu, B. (2019). Conversion of sewage sludge into environmental catalyst and microbial fuel cell electrode material: a review. *Sci. Total Environ.* 666, 525–539. doi:10.1016/j.scitotenv.2019.02.200

Mier, A. A., Olvera-Vargas, H., Mejía-López, M., Longoria, A., Verea, L., Sebastian, P. J., et al. (2021). A review of recent advances in electrode materials for emerging bioelectrochemical systems: from biofilm-bearing anodes to specialized cathodes. *Chemosphere* 283, 131138. doi:10.1016/j.chemosphere.2021.131138

Mukherjee, A., Patel, V., Shah, M. T., Jadhav, D. A., Munshi, N. S., Chendake, A. D., et al. (2022). Effective power management system in stacked microbial fuel cells for onsite applications. *J. Power Sources* 517, 230684. doi:10.1016/j.jpowsour.2021.230684

Munoz-Cupa, C., Hu, Y., Xu, C., and Bassi, A. (2021). An overview of microbial fuel cell usage in wastewater treatment, resource recovery and energy production. *Sci. Total Environ.* 754, 142429. doi:10.1016/j.scitotenv.2020.142429

Nancharaiah, Y. V., Venkata Mohan, S., and Lens, P. N. L. (2015). Metals removal and recovery in bioelectrochemical systems: A review. *Bioresour. Technol.* 195, 102–114. doi:10.1016/j.biortech.2015.06.058

Noori, M. T., Mukherjee, C. K., and Ghangrekar, M. M. (2017). Enhancing performance of microbial fuel cell by using graphene supported V2O5-nanorod catalytic cathode. *Electrochim. Acta* 228, 513–521. doi:10.1016/J.ELECTACTA.2017.01.016

Noori, M. T., and Verma, N. (2019). Cobalt - iron phthalocyanine supported on carbide - derived carbon as an excellent oxygen reduction reaction catalyst for microbial fuel cells. *Electrochim. Acta* 298, 70–79. doi:10.1016/J.ELECTACTA.2018.12.056

Obileke, K., Onyeaka, H., Meyer, E. L., and Nwokolo, N. (2021). Microbial fuel cells, a renewable energy technology for bio-electricity generation: a mini-review. *Electrochem. Commun.* 125, 107003. doi:10.1016/j.elecom.2021.107003

Oguz Koroglu, E., Civelek Yoruklu, H., Demir, A., and Ozkaya, B. (2019). "Chapter 3.9 - scale-up and commercialization issues of the MFCs: challenges and implications," in Microbial electrochemical technology *biomass, biofuels and biochemicals*. Editors S. V. Mohan, S. Varjani, and A. Pandey (Elsevier), 565–583. doi:10.1016/B978-0-444-64052-9.00023-6

Oh, S.-E., and Logan, B. E. (2007). Voltage reversal during microbial fuel cell stack operation. *J. Power Sources* 167, 11–17. doi:10.1016/j.jpowsour.2007.02.016

Om Prakash, M., Raghavendra, G., Ojha, S., and Panchal, M. (2021). Characterization of porous activated carbon prepared from arhar stalks by single step chemical activation method. *Mat. Today Proc.* 39, 1476–1481. doi:10.1016/J.MATPR.2020.05.370

Park, H. I, Mushtaq, U., Perello, D., Lee, I., Cho, S. K., Star, A., et al. (2007). Effective and low-cost platinum electrodes for microbial fuel cells deposited by electron beam evaporation. *Energy Fuels* 21, 2984–2990. doi:10.1021/ef070160x

Peera, S. G., Maiyalagan, T., Liu, C., Ashmath, S., Lee, T. G., Jiang, Z., et al. (2021). A review on carbon and non-precious metal based cathode catalysts in microbial fuel cells. *Int. J. Hydrogen Energy* 46, 3056–3089. doi:10.1016/J.IJHYDENE.2020.07.252

Pema, T., Kumar, A., Tripathi, B., Pandit, S., Chauhan, S., Singh, S., et al. (2023). Investigating the performance of lithium-doped bismuth ferrite [BiFe1−xLixO3]-graphene nanocomposites as cathode catalyst for the improved power output in microbial fuel cells. *Catalysts* 13, 618. doi:10.3390/catal13030618

Pepè Sciarria, T., de Oliveira, M. A. C., Mecheri, B., D'Epifanio, A., Goldfarb, J. L., and Adani, F. (2020). Metal-free activated biochar as an oxygen reduction reaction catalyst in single chamber microbial fuel cells. *J. Power Sources* 462, 228183. doi:10.1016/J.JPOWSOUR.2020.228183

Pötschke, L., Huber, P., Stegschuster, G., Schriever, S., Kroppen, N., Schmatz, J., et al. (2022). Customized woven carbon fiber electrodes for bioelectrochemical systems—a study of structural parameters. *Front. Chem. Eng.* 4, 765682. doi:10.3389/fceng.2022.765682

Potter, M. C. (1911). Electrical effects accompanying the decomposition of organic compounds. *Proc. R. Soc. Lond. Ser. B, Contain. Pap. a Biol. Character* 84, 260–276. doi:10.1098/rspb.1911.0073

Prasad, J., and Tripathi, R. K. (2021). Effect of sediment microbial fuel cell stacks on 9 V/12 V DC power supply. *Int. J. Hydrogen Energy* 46, 14628–14638. doi:10.1016/j.ijhydene.2020.07.187

Priya, A. K., Subha, C., Kumar, P. S., Suresh, R., Rajendran, S., Vasseghian, Y., et al. (2022). Advancements on sustainable microbial fuel cells and their future prospects: A review. *Environ. Res.* 210, 112930. doi:10.1016/j.envres.2022.112930

Priyadarshini, M., Ahmad, A., Das, S., and Ghangrekar, M. M. (2021). Metal organic frameworks as emergent oxygen-reducing cathode catalysts for microbial fuel cells: A review. *Int. J. Environ. Sci. Technol.* 19, 11539–11560. doi:10.1007/s13762-021-03499-5

Qin, Y., Li, H., Sun, Y., Guo, S., Liu, Y., Zhai, Z., et al. (2023). Directional assembly of multi-catalytic sites CoCu-MOFs with porous carbon nanofiber templates as efficient catalyst for microbial fuel cells. *J. Environ. Chem. Eng.* 11, 109662. doi:10.1016/j.jece.2023.109662

Quan, X., Mei, Y., Xu, H., Sun, B., and Zhang, X. (2015). Optimization of Pt-Pd alloy catalyst and supporting materials for oxygen reduction in air-cathode microbial fuel cells. *Electrochim. Acta* 165, 72–77. doi:10.1016/j.electacta.2015.02.235

Rabaey, K., and Verstraete, W. (2005). Microbial fuel cells: novel biotechnology for energy generation. *Trends Biotechnol.* 23, 291–298. doi:10.1016/j.tibtech.2005.04.008

Rezaei, A., Karami, Z., Feli, F., and Aber, S. (2023). Oxygen reduction reaction enhancement in microbial fuel cell cathode using cesium phosphomolybdate electrocatalyst. *Fuel* 352, 129040. doi:10.1016/j.fuel.2023.129040

Rismani-Yazdi, H., Carver, S. M., Christy, A. D., and Tuovinen, O. H. (2008). Cathodic limitations in microbial fuel cells: an overview. *J. Power Sources* 180, 683–694. doi:10.1016/j.jpowsour.2008.02.074

Rossi, R., Evans, P. J., and Logan, B. E. (2019). Impact of flow recirculation and anode dimensions on performance of a large scale microbial fuel cell. *J. Power Sources* 412, 294–300. doi:10.1016/J.JPOWSOUR.2018.11.054

Rout, S., Nayak, A. K., Varanasi, J. L., Pradhan, D., and Das, D. (2018). Enhanced energy recovery by manganese oxide/reduced graphene oxide nanocomposite as an air-cathode electrode in the single-chambered microbial fuel cell. *J. Electroanal. Chem.* 815, 1–7. doi:10.1016/J.JELECHEM.2018.03.002

Rozendal, R. A., Hamelers, H. V. M., Euverink, G. J. W., Metz, S. J., and Buisman, C. J. N. (2006). Principle and perspectives of hydrogen production through biocatalyzed electrolysis. *Int. J. Hydrogen Energy* 31, 1632–1640. doi:10.1016/j.ijhydene.2005.12.006

Santoro, C., Kodali, M., Kabir, S., Soavi, F., Serov, A., and Atanassov, P. (2017). Three-dimensional graphene nanosheets as cathode catalysts in standard and supercapacitive microbial fuel cell. *J. Power Sources* 356, 371–380. doi:10.1016/J.JPOWSOUR.2017.03.135

Santoro, C., Kodali, M., Shamoon, N., Serov, A., Soavi, F., Merino-Jimenez, I., et al. (2019). Increased power generation in supercapacitive microbial fuel cell stack using FeNC cathode catalyst. *J. Power Sources* 412, 416–424. doi:10.1016/j.jpowsour.2018.11.069

Sarma, P. J., Malakar, B., and Mohanty, K. (2023). Self-sustaining bioelectricity generation in plant-based microbial fuel cells (PMFCs) with microalgae-assisted oxygen-reducing biocathode. *Biomass Convers. Biorefinery*. doi:10.1007/s13399-023-03848-z

Savizi, I. S. P., Kariminia, H.-R., and Bakhshian, S. (2012). Simultaneous decolorization and bioelectricity generation in a dual chamber microbial fuel cell using electropolymerized-enzymatic cathode. *Environ. Sci. Technol.* 46, 6584–6593. doi:10.1021/es300367h

Sawant, S. Y., Han, T. H., and Cho, M. H. (2017). Metal-free carbon-based materials: promising electrocatalysts for oxygen reduction reaction in microbial fuel cells. *Int. J. Mol. Sci.* 18, 25. doi:10.3390/ijms18010025

Sekhon, S. S., Kaur, P., and Park, J. S. (2021). From coconut shell biomass to oxygen reduction reaction catalyst: tuning porosity and nitrogen doping. *Renew. Sustain. Energy Rev.* 147, 111173. doi:10.1016/J.RSER.2021.111173

Shi, X., Feng, Y., Wang, X., Lee, H., Liu, J., Qu, Y., et al. (2012). Application of nitrogen-doped carbon powders as low-cost and durable cathodic catalyst to air-cathode microbial fuel cells. *Bioresour. Technol.* 108, 89–93. doi:10.1016/j.biortech.2011.12.078

Shin, S. H., Choi, Y., Na, S. H., Jung, S., and Kim, S. (2006). Development of bipolar plate stack type microbial fuel cells. *Bull. Korean Chem. Soc.* 27, 281–285. doi:10.5012/bkcs.2006.27.2.281

Shixuan, Z., Donghao, L., Jiwei, J., Li, F., and Hua, T. (2023). Oxygen reduction activity of a Pt-N4 single-atom catalyst prepared by electrochemical deposition and its bioelectrochemical application. *Electrochim. Acta* 437, 141543. doi:10.1016/j.electacta.2022.141543

Si, F., Zhang, Y., Yan, L., Zhu, J., Xiao, M., Liu, C., et al. (2014). "4 - electrochemical oxygen reduction reaction," in *Rotating electrode methods and oxygen reduction electrocatalysts*. Editors W. Xing, G. Yin, and J. Zhang (Amsterdam: Elsevier), 133–170. doi:10.1016/B978-0-444-63278-4.00004-5

Slate, A. J., Whitehead, K. A., Brownson, D. A. C., and Banks, C. E. (2019). Microbial fuel cells: an overview of current technology. *Renew. Sustain. Energy Rev.* 101, 60–81. doi:10.1016/j.rser.2018.09.044

Subran, N., Ajit, K., Krishnan, H., Pachiyappan, S., and Ramaswamy, P. (2023). Synthesis and performance of a cathode catalyst derived from areca nut husk in microbial fuel cell. *Chemosphere* 312, 137303. doi:10.1016/j.chemosphere.2022.137303

Sui, S., Wang, X., Zhou, X., Su, Y., Riffat, S., and Liujun, C. (2017). A comprehensive review of Pt electrocatalysts for the oxygen reduction reaction: nanostructure, activity, mechanism and carbon support in PEM fuel cells. *J. Mat. Chem. A* 5, 1808–1825. doi:10.1039/C6TA08580F

Sun, M., Zhai, L.-F., Li, W.-W., and Yu, H.-Q. (2016a). Harvest and utilization of chemical energy in wastes by microbial fuel cells. *Chem. Soc. Rev.* 45, 2847–2870. doi:10.1039/C5CS00903K

Sun, Y., Duan, Y., Hao, L., Xing, Z., Dai, Y., Li, R., et al. (2016b). Cornstalk-derived nitrogen-doped partly graphitized carbon as efficient metal-free catalyst for oxygen reduction reaction in microbial fuel cells. *ACS Appl. Mat. Interfaces* 8, 25923–25932. doi:10.1021/acsami.6b06895

Sun, Y., Li, H., Wang, J., Liu, Y., Guo, S., Xie, H., et al. (2023). Enhanced oxygen reduction upon Ag-Fe-doped polyacrylonitrile@UiO-66-NH2 nanofibers to improve power-generation performance of microbial fuel cells. *J. Colloid Interface Sci.* 648, 654–663. doi:10.1016/j.jcis.2023.05.166

Tajdid Khajeh, R., Aber, S., and Zarei, M. (2020). Comparison of NiCo2O4, CoNiAl-LDH, and CoNiAl-LDH@NiCo2O4 performances as ORR catalysts in MFC cathode. *Renew. Energy* 154, 1263–1271. doi:10.1016/J.RENENE.2020.03.091

Tang, H., Cai, S., Xie, S., Wang, Z., Tong, Y., Pan, M., et al. (2015). Metal-organic-framework-derived dual metal-and nitrogen-doped carbon as efficient and robust oxygen reduction reaction catalysts for microbial fuel cells. *Adv. Sci.* 3, 1500265. doi:10.1002/advs.201500265

Tian, X., Zhou, M., Tan, C., Li, M., Liang, L., Li, K., et al. (2018). KOH activated N-doped novel carbon aerogel as efficient metal-free oxygen reduction catalyst for microbial fuel cells. *Chem. Eng. J.* 348, 775–785. doi:10.1016/J.CEJ.2018.05.007

Türk, K. K., Kruusenberg, I., Kibena-Põldsepp, E., Bhowmick, G. D., Kook, M., Tammeveski, K., et al. (2018). Novel multi walled carbon nanotube based nitrogen impregnated Co and Fe cathode catalysts for improved microbial fuel cell performance. *Int. J. Hydrogen Energy* 43, 23027–23035. doi:10.1016/J.IJHYDENE.2018.10.143

Tursun, H., Liu, R., Li, J., Abro, R., Wang, X., Gao, Y., et al. (2016). Carbon material optimized biocathode for improving microbial fuel cell performance. *Front. Microbiol.* 7, 6. doi:10.3389/fmicb.2016.00006

Vilas Boas, J., Oliveira, V. B., Marcon, L. R. C., Simões, M., and Pinto, A. M. F. R. (2019). Optimization of a single chamber microbial fuel cell using lactobacillus pentosus: influence of design and operating parameters. *Sci. Total Environ.* 648, 263–270. doi:10.1016/j.scitotenv.2018.08.061

Wang, D., Liu, H., Cao, Z., Cai, T., Han, P., Song, J., et al. (2022a). Ordered porous nitrogen-doped carbon with atomically dispersed FeN4 for efficient oxygen reduction reaction in microbial fuel cell. *Sci. Total Environ.* 838, 156186. doi:10.1016/j.scitotenv.2022.156186

Wang, D., Ma, Z., Xie, Y., Zhang, M., Zhao, N., and Song, H. (2018). Fe/N-doped graphene with rod-like CNTs as an air-cathode catalyst in microbial fuel cells. *RSC Adv.* 8, 1203–1209. doi:10.1039/c7ra11613f

Wang, H., and Ren, Z. J. (2013). A comprehensive review of microbial electrochemical systems as a platform technology. *Biotechnol. Adv.* 31, 1796–1807. doi:10.1016/j.biotechadv.2013.10.001

Wang, J., Mu, K., Zhao, X., Luo, D., Yu, X., Li, W., et al. (2021). Uniform distribution of Pd on GO-C catalysts for enhancing the performance of air cathode microbial fuel cell. *Catalysts* 11, 888. doi:10.3390/catal11080888

Wang, J., Tian, P., Li, K., Ge, B., Liu, D., Liu, Y., et al. (2016). The excellent performance of nest-like oxygen-deficient Cu1.5Mn1.5O4 applied in activated carbon air-cathode microbial fuel cell. *Bioresour. Technol.* 222, 107–113. doi:10.1016/J.BIORTECH.2016.09.126

Wang, K., Yang, J., Liu, W., Yang, H., Yi, W., Sun, Y., et al. (2022b). Self-nitrogen-doped carbon materials derived from microalgae by lipid extraction pretreatment: highly efficient catalyst for the oxygen reduction reaction. *Sci. Total Environ.* 821, 153155. doi:10.1016/j.scitotenv.2022.153155

Wang, X., Xu, H., Huang, S., Zeng, X., Li, L., Zhao, X., et al. (2023a). CoFe alloy nanoparticles embedded in vertically grown nanosheets on N-doped carbon nanofibers as a trifunctional electrocatalyst for high-performance microbial fuel cells. *Appl. Surf. Sci.* 609, 155452. doi:10.1016/j.apsusc.2022.155452

Wang, X., Yuan, T., Liang, J., Yang, J., Xie, Y., Li, L., et al. (2022c). FeNx nanoparticles embedded in three-dimensional N-doped carbon nanofibers as efficient oxygen reduction reaction electrocatalyst for microbial fuel cells in alkaline and neutral media. *Int. J. Hydrogen Energy* 47, 23608–23617. doi:10.1016/j.ijhydene.2022.05.176

Wang, X., Zhang, H., Ye, J., and Li, B. (2023b). Atomically dispersed Fe–N4 moieties in porous carbon as efficient cathode catalyst for enhancing the performance in microbial fuel cells. *J. Power Sources* 556, 232434. doi:10.1016/j.jpowsour.2022.232434

Wang, Y., Zhong, K., Huang, Z., Chen, L., Dai, Y., Zhang, H., et al. (2020). Novel g-C3N4 assisted metal organic frameworks derived high efficiency oxygen reduction catalyst in microbial fuel cells. *J. Power Sources* 450, 227681. doi:10.1016/J.JPOWSOUR.2019.227681

Wang, Z., Liu, Y., Li, K., Liu, D., Yang, T., Wang, J., et al. (2017). The influence and mechanism of different acid treatment to activated carbon used as air-breathing cathode catalyst of microbial fuel cell. *Electrochim. Acta* 246, 830–840. doi:10.1016/j.electacta.2017.05.086

Wei, J., Liang, P., Cao, X., and Huang, X. (2011). Use of inexpensive semicoke and activated carbon as biocathode in microbial fuel cells. *Bioresour. Technol.* 102, 10431–10435. doi:10.1016/J.BIORTECH.2011.08.088

Winfield, J., Ieropoulos, I., Rossiter, J., Greenman, J., and Patton, D. (2013). Biodegradation and proton exchange using natural rubber in microbial fuel cells. *Biodegradation* 24, 733–739. doi:10.1007/s10532-013-9621-x

Woodward, L., Perrier, M., Srinivasan, B., Pinto, R. P., and Tartakovsky, B. (2010). Comparison of real-time methods for maximizing power output in microbial fuel cells. *AIChE J.* 56, 2742–2750. doi:10.1002/aic.12157

Wu, Z. Y., Liang, H. W., Chen, L. F., Hu, B. C., and Yu, S. H. (2016). Bacterial cellulose: a robust platform for design of three dimensional carbon-based functional nanomaterials. *Acc. Chem. Res.* 49, 96–105. doi:10.1021/acs.accounts.5b00380

Xie, H., Jiang, D., Chen, H., Ma, X., Liu, X., Qi, Q., et al. (2023). Electron transfer and surface activity of NiCoP-wrapped MXene: cathodic catalysts for the oxygen reduction reaction. *Nanoscale* 15, 7430–7437. doi:10.1039/D3NR00192J

Xing, Z., Gao, N., Qi, Y., Ji, X., and Liu, H. (2017). Influence of enhanced carbon crystallinity of nanoporous graphite on the cathode performance of microbial fuel cells. *Carbon N. Y.* 115, 271–278. doi:10.1016/j.carbon.2017.01.014

Xu, X., Xie, J., Dai, Y., Yang, L., Cai, Z., Jing, B., et al. (2022). FeCo alloys *in-situ* formed in Co/Co2P/N-doped carbon as a durable catalyst for boosting bio-electrons-driven oxygen reduction in microbial fuel cells. *Int. J. Hydrogen Energy* 47, 3063–3074. doi:10.1016/j.ijhydene.2021.10.199

Xu, Y., Zhang, X., Liu, Y., Wei, Y., Lan, F., Wang, R., et al. (2023). Trace N-doped manganese dioxide cooperated with Ping-pong chrysanthemum-like NiAl-layered double hydroxide on cathode for improving bioelectrochemical performance of microbial fuel cell. *Bioresour. Technol.* 381, 129139. doi:10.1016/j.biortech.2023.129139

Xue, W., Zhou, Q., and Li, F. (2020). The feasibility of typical metal–organic framework derived Fe, Co, N co-doped carbon as a robust electrocatalyst for oxygen reduction reaction in microbial fuel cell. *Electrochim. Acta* 355, 136775. doi:10.1016/J.ELECTACTA.2020.136775

Yahia, S. A. A., Hamadou, L., Salar-García, M. J., Kadri, A., Ortiz-Martínez, V. M., Hernández-Fernández, F. J., et al. (2016). TiO 2 nanotubes as alternative cathode in microbial fuel cells: effect of annealing treatment on its performance. *Appl. Surf. Sci.* 387, 1037–1045. doi:10.1016/j.apsusc.2016.07.018

Yan, Z., Wang, M., Liu, J., Liu, R., and Zhao, J. (2014a). Glycerol-stabilized NaBH4 reduction at room-temperature for the synthesis of a carbon-supported PtxFe alloy with superior oxygen reduction activity for a microbial fuel cell. *Electrochim. Acta* 141, 331–339. doi:10.1016/j.electacta.2014.06.137

Yan, Z., Wang, M., Lu, Y., Liu, R., and Zhao, J. (2014b). Ethylene glycol stabilized NaBH4 reduction for preparation carbon-supported Pt-Co alloy nanoparticles used as oxygen reduction electrocatalysts for microbial fuel cells. *J. Solid State Electrochem.* 18, 1087–1097. doi:10.1007/s10008-013-2361-3

Yang, G., Sun, Y., Yuan, Z., Lü, P., Kong, X., Li, L., et al. (2014). Application of surface-modified carbon powder in microbial fuel cells. *Chin. J. Catal.* 35, 770–775. doi:10.1016/s1872-2067(14)60023-1

Yang, J., Yang, H., Wang, S., Wang, K., Sun, Y., Yi, W., et al. (2023). Importance of pyrolysis programs in enhancing the application of microalgae-derived biochar in microbial fuel cells. *Fuel* 333, 126244. doi:10.1016/j.fuel.2022.126244

Yang, L., Cai, Z., Hao, L., Ran, L., Xu, X., Dai, Y., et al. (2018). Increase of structural defects by N doping in MoS2 cross-linked with N-doped CNTs/carbon for enhancing charge transfer in oxygen reduction. *Electrochim. Acta* 283, 448–458. doi:10.1016/J.ELECTACTA.2018.06.152

Yang, W., Li, J., Lan, L., Zhang, Y., and Liu, H. (2020a). Covalent organic polymers derived carbon incorporated with cobalt oxides as a robust oxygen reduction reaction catalyst for fuel cells. *Chem. Eng. J.* 390, 124581. doi:10.1016/J.CEJ.2020.124581

Yang, W., Li, J., Ye, D., Zhu, X., and Liao, Q. (2017). Bamboo charcoal as a cost-effective catalyst for an air-cathode of microbial fuel cells. *Electrochim. Acta* 224, 585–592. doi:10.1016/J.ELECTACTA.2016.12.046

Yang, W., Peng, Y., Zhang, Y., Lu, J. E., Li, J., and Chen, S. (2019). Air cathode catalysts of microbial fuel cell by nitrogen-doped carbon aerogels. *ACS Sustain. Chem. Eng.* 7, 3917–3924. doi:10.1021/acssuschemeng.8b05000

Yang, W., Wang, X., Rossi, R., and Logan, B. E. (2020b). Low-cost Fe–N–C catalyst derived from Fe (III)-chitosan hydrogel to enhance power production in microbial fuel cells. *Chem. Eng. J.* 380, 122522. doi:10.1016/J.CEJ.2019.122522

Yap, K.-L., Ho, L.-N., Guo, K., Liew, Y.-M., Lutpi, N. A., Azhari, A. W., et al. (2023). Role of tin (IV) oxide as cathodic catalyst on wastewater treatment and bioelectricity generation in a baffled microbial fuel cell. *IOP Conf. Ser. Earth Environ. Sci.* 1135, 012007. doi:10.1088/1755-1315/1135/1/012007

Ye, W., Tang, J., Wang, Y., Cai, X., Liu, H., Lin, J., et al. (2019). Hierarchically structured carbon materials derived from lotus leaves as efficient electrocatalyst for microbial energy harvesting. *Sci. Total Environ.* 666, 865–874. doi:10.1016/J.SCITOTENV.2019.02.300

Yen, S. J., Tsai, M. C., Wang, Z. C., Peng, H. L., Tsai, C. H., and Yew, T. R. (2013). The improvement of catalytic efficiency by optimizing Pt on carbon cloth as a cathode of a microbial fuel cell. *Electrochim. Acta* 108, 241–247. doi:10.1016/j.electacta.2013.06.019

You, S., Zhao, Q., Zhang, J., Jiang, J., Wan, C., Du, M., et al. (2007). A graphite-granule membrane-less tubular air-cathode microbial fuel cell for power generation under continuously operational conditions. *J. Power Sources* 173, 172–177. doi:10.1016/j.jpowsour.2007.07.063

Yu, D., Bai, L., Zhai, J., Wang, Y., and Dong, S. (2017). Toxicity detection in water containing heavy metal ions with a self-powered microbial fuel cell-based biosensor. *Talanta* 168, 210–216. doi:10.1016/j.talanta.2017.03.048

Zerrouki, A., Kameche, M., Ait Amer, A., Tayeb, A., Moussaoui, D., and Innocent, C. (2022). Platinum nanoparticles embedded into polyaniline on carbon cloth: improvement of oxygen reduction at cathode of microbial fuel cell used for conversion of medicinal plant wastes into bio-energy. *Environ. Technol.* 43, 1359–1369. doi:10.1080/09593330.2020.1829088

Zha, Z., Zhang, Z., Xiang, P., Zhu, H., Zhou, B., Sun, Z., et al. (2021). One-step preparation of eggplant-derived hierarchical porous graphitic biochar as efficient oxygen reduction catalyst in microbial fuel cells. *RSC Adv.* 11, 1077–1085. doi:10.1039/D0RA09976G

Zhang, B., Wen, Z., Ci, S., Mao, S., Chen, J., and He, Z. (2014). Synthesizing nitrogen-doped activated carbon and probing its active sites for oxygen reduction reaction in microbial fuel cells. *ACS Appl. Mat. Interfaces* 6, 7464–7470. doi:10.1021/am5008547

Zhang, H., Shi, H., You, H., Su, M., Huang, L., Zhou, Z., et al. (2022a). Cu-doped CaFeO3 perovskite oxide as oxygen reduction catalyst in air cathode microbial fuel cells. *Environ. Res.* 214, 113968. doi:10.1016/j.envres.2022.113968

Zhang, L., Lu, Z., Li, D., Ma, J., Song, P., Huang, G., et al. (2016). Chemically activated graphite enhanced oxygen reduction and power output in catalyst-free microbial fuel cells. *J. Clean. Prod.* 115, 332–336. doi:10.1016/j.jclepro.2015.12.067

Zhang, Q., and Liu, L. (2020). A microbial fuel cell system with manganese dioxide/titanium dioxide/graphitic carbon nitride coated granular activated carbon cathode successfully treated organic acids industrial wastewater with residual nitric acid. *Bioresour. Technol.* 304, 122992. doi:10.1016/J.BIORTECH.2020.122992

Zhang, S., Su, W., Li, K., Liu, D., Wang, J., and Tian, P. (2018a). Metal organic framework-derived Co3O4/NiCo2O4 double-shelled nanocage modified activated carbon air-cathode for improving power generation in microbial fuel cell. *J. Power Sources* 396, 355–362. doi:10.1016/J.JPOWSOUR.2018.06.057

Zhang, S., Su, W., Wang, X., Li, K., and Li, Y. (2019a). Bimetallic metal-organic frameworks derived cobalt nanoparticles embedded in nitrogen-doped carbon nanotube nanopolyhedra as advanced electrocatalyst for high-performance of activated carbon air-cathode microbial fuel cell. *Biosens. Bioelectron.* 127, 181–187. doi:10.1016/J.BIOS.2018.12.028

Zhang, S., Su, W., Wei, Y., Liu, J., and Li, K. (2018b). Mesoporous MnO2 structured by ultrathin nanosheet as electrocatalyst for oxygen reduction reaction in air-cathode microbial fuel cell. *J. Power Sources* 401, 158–164. doi:10.1016/J.JPOWSOUR.2018.08.102

Zhang, S., Zhang, S., Liu, H., Li, L., and Guo, R. (2023). Fe-N-C-based cathode catalyst enhances redox reaction performance of microbial fuel cells: azo dyes degradation accompanied by electricity generation. *J. Environ. Chem. Eng.* 11, 109264. doi:10.1016/j.jece.2023.109264

Zhang, X., Li, K., Yan, P., Liu, Z., and Pu, L. (2015). N-type Cu2O doped activated carbon as catalyst for improving power generation of air cathode microbial fuel cells. *Bioresour. Technol.* 187, 299–304. doi:10.1016/j.biortech.2015.03.131

Zhang, X., Liang, B., Lin, Z., Zhong, M., Li, K., Wang, H., et al. (2022b). Engineering heterostructured Co0.7Fe0.3@Co doped leaf-like carbon nanoplates from dual metal-organic frameworks for high-efficiency oxygen reduction reaction in microbial fuel cell. *J. Power Sources* 520, 230799. doi:10.1016/j.jpowsour.2021.230799

Zhang, Y., Deng, L., Hu, H., Qiao, Y., Yuan, H., Chen, D., et al. (2020). Pomelo peel-derived, N-doped biochar microspheres as an efficient and durable metal-free ORR catalyst in microbial fuel cells. *Sustain. Energy Fuels* 4, 1642–1653. doi:10.1039/c9se00834a

Zhang, Y., Sun, J., Hu, Y., Li, S., and Xu, Q. (2012). Bio-cathode materials evaluation in microbial fuel cells: A comparison of graphite felt, carbon paper and stainless steel mesh materials. *Int. J. Hydrogen Energy* 37, 16935–16942. doi:10.1016/j.ijhydene.2012.08.064

Zhang, Y., Sun, J., Hu, Y., Li, S., and Xu, Q. (2013). Carbon nanotube-coated stainless steel mesh for enhanced oxygen reduction in biocathode microbial fuel cells. *J. Power Sources* 239, 169–174. doi:10.1016/j.jpowsour.2013.03.115

Zhang, Y., Tian, P., Li, K., Liu, Y., and Zhang, Z. (2018c). C3N4 coordinated metal-organic-framework-derived network as air-cathode for high performance of microbial fuel cell. *J. Power Sources* 408, 74–81. doi:10.1016/j.jpowsour.2018.10.036

Zhang, Y., Zhao, Y., and Zhou, M. (2019b). A photosynthetic algal microbial fuel cell for treating swine wastewater. *Environ. Sci. Pollut. Res.* 26, 6182–6190. doi:10.1007/s11356-018-3960-4

Zhao, C., Luo, W., Tian, H., Lu, T., Yi, L., Zhang, Y., et al. (2023). Single-atomic Fe sites decorated N-doped carbon toward oxygen reduction in MFCs. *Chem. Commun.* 59, 6749–6752. doi:10.1039/D3CC01415K

Zheng, L., Lin, X., Liu, Y., Li, H., Sun, Y., and Li, C. (2022). Synergistically enhanced oxygen reduction reaction and oxytetracycline mineralization by FeCoO/GO modified cathode in microbial fuel cell. *Sci. Total Environ.* 808, 151873. doi:10.1016/j.scitotenv.2021.151873

Zheng, T., Li, J., Ji, Y., Zhang, W., Fang, Y., Xin, F., et al. (2020). Progress and prospects of bioelectrochemical systems: electron transfer and its applications in the microbial metabolism. *Front. Bioeng. Biotechnol.* 8, 10. doi:10.3389/fbioe.2020.00010

Zhong, K., Li, M., Yang, Y., Zhang, H., Zhang, B., Tang, J., et al. (2019). Nitrogen-doped biochar derived from watermelon rind as oxygen reduction catalyst in air cathode microbial fuel cells. *Appl. Energy* 242, 516–525. doi:10.1016/j.apenergy.2019.03.050

Zhou, L., Fu, P., Cai, X., Zhou, S., and Yuan, Y. (2016). Naturally derived carbon nanofibers as sustainable electrocatalysts for microbial energy harvesting: A new application of spider silk. *Appl. Catal. B Environ.* 188, 31–38. doi:10.1016/J.APCATB.2016.01.063

Zhu, H., Zhang, Z., Zhou, Y., Jiang, X., Cai, F., Bai, Y., et al. (2022a). Porous Co, N co-doped carbon derived from tea residue as efficient cathode catalyst in microbial fuel cells for swine wastewater treatment and the microbial community analysis. *J. Water Process Eng.* 45, 102471. doi:10.1016/j.jwpe.2021.102471

Zhu, Q., Hu, J., Liu, B., Hu, S., Liang, S., Xiao, K., et al. (2022b). Recent advances on the development of functional materials in microbial fuel cells: from fundamentals to challenges and outlooks. *ENERGY Environ. Mat.* 5, 401–426. doi:10.1002/eem2.12173

Zhuang, S., Li, B., and Wang, X. (2023). Engineering the electronic structure of high performance FeCo bimetallic cathode catalysts for microbial fuel cell application in treating wastewater. *Environ. Res.* 216, 114542. doi:10.1016/j.envres.2022.114542

Zou, S., and He, Z. (2018). Efficiently "pumping out" value-added resources from wastewater by bioelectrochemical systems: A review from energy perspectives. *Water Res.* 131, 62–73. doi:10.1016/j.watres.2017.12.026

frontiers | Frontiers in Chemical Engineering

TYPE Original Research
PUBLISHED 02 October 2023
DOI 10.3389/fceng.2023.1235125

OPEN ACCESS

EDITED BY
Santhana Krishnan,
Prince of Songkla University, Thailand

REVIEWED BY
Mullai Pandian,
Annamalai University, India
Abirami Balakrishnan,
Hindustan University, India

*CORRESPONDENCE
Chitra Murugan,
chitramurugan.g@gmail.com

RECEIVED 05 June 2023
ACCEPTED 21 August 2023
PUBLISHED 02 October 2023

CITATION
Subbian S, Natarajan P and Murugan C (2023), Circular economy-based multi-objective decentralized controller for activated sludge wastewater treatment plant.
Front. Chem. Eng. 5:1235125.
doi: 10.3389/fceng.2023.1235125

Circular economy-based multi-objective decentralized controller for activated sludge wastewater treatment plant

Sutha Subbian[1], Pappa Natarajan[1] and Chitra Murugan[2]*

[1]Bioprocess Laboratory, Department of Instrumentation Engineering, Anna University, Chennai, India, [2]Rajalakshmi Institute of Technology, Chennai, India

Introduction: Water scarcity and water pollution are two major issues in India. Circular economy-based wastewater treatment technology provides the most sustainable solutions for solving these issues. In this paper, a novel multi-objective decentralized controller (MODC) is proposed for benchmarking a multi-input multi-output (MIMO) activated sludge wastewater treatment plant (WWTP) to achieve maximum effluent quality with minimum cost. WWTPs with conventional control schemes consume more energy to achieve the desired effluent quality.

Methods: In this study, a MIMO model is developed for the activated sludge process (ASP) from a physics-based model, and relative gain array (RGA) analysis are carried out to determine the interaction between the loops to identify a suitable control scheme for the MIMO process. In addition, a multi-objective decentralized control problem is formulated to achieve the conflicting multiple objectives of improving effluent quality and minimizing operational costs by efficient usage of energy.

Results and discussion: The desired quality and cost reduction are verified by comparing the integral square error (ISE) and control effort (CE) values of a closed-loop WWTP. A multi-objective evolutionary algorithm (MOEA), namely, the non-dominated sorting genetic algorithm (NSGA)-II, successfully solves the multi-objective control problem. NSGA-II provides several optimal solutions in the Pareto front. In order to demonstrate the feasibility of the proposed controller, three optimal solutions are selected from the Pareto-optimal front, and their closed-loop performances are evaluated qualitatively and quantitatively for both servo and regulatory operations. Improving the quality of effluent enhances active sludge production, which in turn increases the methane production in the anaerobic digester.

KEYWORDS

circular economy, activated sludge process, MODC, WWTP, MIMO, MOEA, RGA, NSGA-II

1 Introduction

Wastewater treatment plays a major role in developing countries like India due to water scarcity and environmental pollution. The population rise in major cities leads to more water consumption and wastewater discharge into natural water bodies. According to the Central Ground Water Authority, Government of India report, an average individual utilizes 150–200 L of water per day. Only 10 L is consumed for cooking and drinking; 40 L per day is spent on

washing dishes, washing clothes, and floor cleaning; and the remaining 85 L is utilized for toilet flushing and bathing. In general, the 80 L of wastewater used for washing and bathing could be reused for gardening, toilet flushing, and other useful applications with proper treatment. Many cities in India have centralized wastewater treatment plants (WWTPs) with conventional treatment techniques. However, most of them are less effective because they require underground pipe lining, pumping stations, and extensive maintenance. In contrast, a WWTP with advanced technologies would improve the quality of water and reduce maintenance costs (Grobelak et al., 2019). These technologies could lead to the design of decentralized WWTPs that deploy sophisticated techniques closer to the water generation point to enable more effective reuse of water. Two types of treatment plants, namely, sewage treatment plants (STPs) and effluent treatment plants (ETPs), are used to treat sewage and industrial wastewater, respectively (Negi et al., 2022). In a WWTP, wastewater undergoes three stages: primary treatment, secondary treatment, and tertiary treatment.

Generally, untreated sewage has biological oxygen demand (BOD) and total solid substrate (TSS) values in the range of 250–350 mg/L and 150–200 mg/L, respectively. The characteristics of the effluent are predominantly influenced by its levels of BOD and TSS. A considerable proportion of sewage treatment plants (STPs) yield effluent containing BOD concentrations lower than 20 mg/L and TSS concentrations lower than 10 mg/L. In order to improve the quality of effluent, ETP requires conventional biological wastewater treatment techniques like the activated sludge process (ASP) to control dissolved oxygen concentration and substrate concentration in the effluent. The ASP is an effective secondary treatment process that uses an aeration tank and a sludge-settling tank. Organic matter in the sewage is digested by aerobic bacteria in the aeration tank. Aerobic bacteria within the aeration tank facilitate the digestion of organic substances present in sewage. Ensuring the growth of these aerobic bacteria necessitates an effective control system. According to Malaysia (2011), there's a notable need for advanced control strategies to enhance or uphold the effluent quality of wastewater treatment plants (WWTPs). As a result, the processes of modeling, control variable selection, and designing control structures assume crucial importance in the pursuit of optimizing control objectives.

Hodasz et al. (2016) developed a linear model to estimate the unmeasured process parameters of an activated sludge model (ASM1). They also suggested that good control of a WWTP leads to better water quality and an efficient use of energy. Castro-Amoedo et al. (2022) presented an overview of energy potentials present in a WWTP and demonstrated the concepts for local energy supply based on integrated perspectives. The control of dissolved oxygen levels in WWTPs has considerably reduced the energy required for aeration purposes in aerobic-activated sludge plants. de Araujo et al. (2013) discussed the application of sensitivity analysis for the selection of economic controlled variables for the optimal operation of a WWTP. Samuelsson et al. (2005) analyzed the cross coupling between loops in a bioreactor model using the relative gain array (RGA) and Hankel interaction index array (HIIA) methods. In addition, they compared the performances of a decentralized control scheme and a multivariable control scheme. Vilanova and Alfaro (2009) proposed a multi-loop decentralized control strategy for the control of a WWTP based on an ASP. Vinayak and Narayanan (2017) attempted a centralized nonlinear state feedback proportional integral (PI) controller for an ASP and compared its performance with a centralized linear state feedback controller. Nor'Azlan et al. (2017) developed a centralized controller for a linear system using the Davison, Penttinen–Koivo, and Maciejowski methods. They have also tuned the centralized controller parameters using single objective optimization techniques, such as a genetic algorithm (GA), particle swarm optimization (PSO), and the bat algorithm. Holenda et al. (2007, 2008) applied a model predictive controller for an activated sludge wastewater treatment process to control the dissolved oxygen level in the reactor and optimize the effluent quality and aeration energy cost against the number of aeration cycles required per day using a GA. Sweetapple et al. (2014) demonstrated the potential of multi-objective optimization of WWTP control strategies for the reduction of greenhouse gas emissions. Chen et al. (2014) optimized benchmark simulation model 1 (BSM1) parameters to achieve the percentage of effluent violation (PEV), overall cost index (OCI), total volume (TV), and total solid substrate (TSS) using a non-dominated sorting genetic algorithm (NSGA)-II.

A multi-objective optimization is a valuable tool in control engineering for controller design and process optimization. Hu et al. (2014) proposed a multi-objective nonlinear PID controller parameter for greenhouse systems to minimize cost and maximize performance using NSGA-II. Tian et al. (2023) recently proposed that the installation position parameters of a submersible mixer can be optimized using multi-input multi-output (MIMO) for improved performance.

Compromising the performance and cost becomes a critical issue in WWTP. In recent years, applications of multi-objective optimization have played a major role in WWTP for control and process optimization. Reynoso-Meza and Carreño-Alvarado (2019) designed a multi-objective controller for a multivariable active sludge process with nitrification and denitrification. Qiao and Zhang (2018) developed a multi-objective control scheme for the Benchmark Simulation Model 1 (BSM1) MIMO process. Ghimire et al. (2021) reviewed two routes for developing more sustainable and circular economy-based wastewater treatment systems and challenges in those approaches. Kaur (2023) applied multi-objective optimization to improve the quality of WWTP effluent based on a data-driven model. The ASP utilizes suspended growth microorganisms to effectively remove organic matter and nutrients from wastewater, but it demands substantial energy and land resources and generates sludge. Trickling filters, in contrast, employ attached growth microorganisms and offer simpler operations with lower energy requirements but may not efficiently remove nutrients and face potential media clogging issues. Membrane bioreactors (MBRs) combine biological treatment with membrane filtration, producing high-quality effluent with reduced sludge, yet they come with higher capital and operational costs and are susceptible to membrane fouling. Sequential batch reactors (SBRs) feature flexible operation and good nutrient removal but may cause variations due to intermittent operation and require longer treatment time. Constructed wetlands provide an eco-friendly and aesthetically pleasing approach with low operating costs but necessitate larger land areas and may not be suitable for high-strength industrial wastewater. Advanced oxidation processes (AOPs) utilize chemical reactions to effectively remove recalcitrant pollutants without producing sludge,

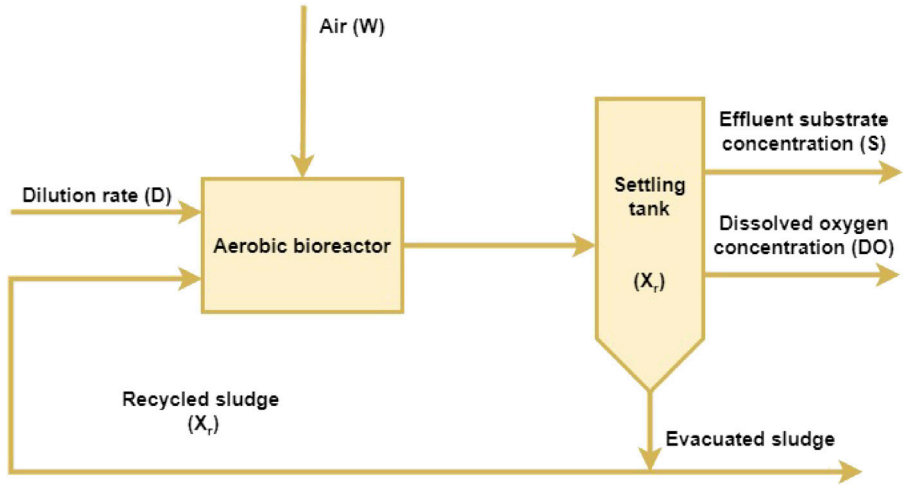

FIGURE 1
Schematic diagram of activated sludge process.

but their high cost and potential secondary waste generation remain drawbacks. Ultimately, the choice of the wastewater treatment model depends on the specific characteristics of the wastewater, treatment goals, available resources, and environmental considerations. Often, a combination of different treatment processes is adopted to optimize efficiency and achieve the desired effluent quality.

Much literature has been reported on circular-economy-based wastewater treatments (Neczaj and Grosser, 2018; Spreafico, 2022; Zhang and Liu, 2022). These studies have reported on circular economics in WWTPs and challenges, barriers that prevent the implementation of circular economics, and analysis and design for circular economics.

To our knowledge, using a multi-objective decentralized controller (MODC) for WWTP with ASM1 to control effluent substrate concentration and DO concentration by maximizing effluent quality and minimizing production cost has not yet been explored. MIMO systems allow for better control performance by considering multiple variables simultaneously. They can take into account cross-coupling effects between inputs and outputs, which often exist in interconnected processes. By controlling multiple variables concurrently, MIMO models can achieve tighter control and improved overall system stability. The main aim of this paper is to design a multi-objective decentralized PI controller for an ASP to achieve the conflicting multi-objectives of maximizing the performance of effluent quality and minimizing the production cost.

The main contributions of the proposed work are i) identifying inputs and outputs and developing an ASM1 model for a WWTP, ii) identification of a suitable controller (centralized/decentralized) for a MIMO process, iii) multi-objective control problem formulation for a decentralized controller, and iv) design of a circular economy-based MODC for WWTP using NSGA-II.

The paper is organized as follows: the modeling of benchmark ASP is described in Section 2. RGA analysis and multi-objective problem formulation are elucidated in Section 3. The design of the proposed MODC is discussed in Section 4. Section 5 presents closed-loop simulation studies of ASP. The concluding remarks are presented at the end.

TABLE 1 Steady-state operating points.

Variable	Steady-state value	Unit
Biomass (X)	565.5	[mg/L]
Substrate (s)	42.35	[mg/L]
Dissolved oxygen (DO)	6.442	[mg/L]
Recycled biomass (X_r)	1244	[mg/L]
Dissolved oxygen concentration (DO_i)	0.5	[mg/L]
Influent substrate (S_{in})	765	[mg/L]
Model constant (K_0)	0.46	—
Affinity constant (K_s)	181	—
Saturation constant (K_{DO})	0.2	—
Ratio of waste flow to influent flow (β)	0.015	—
Ratio of recycled flow to influent flow (r)	0.8	—
Oxygen mass transfer coefficient (α)	0.017	—
Biomass production factor (γ)	0.54	—
Air flow rate (W)	340	[m^3/h]
Dilution rate (D)	0.0638	[h−1]
Biomass growth rate (μ_{max})	0.229	[h−1]

2 Modeling of activated sludge process

2.1 Benchmark ASP

Secondary treatment plays a major role in treating wastewater in STPs. Secondary treatment consists of an aerobic bioreactor for aeration purposes and a settling tank, which is used to settle the sludge at the bottom while effluent is collected at the top of the tank. The schematic diagram of the ASP is given in Figure 1.

The aerator is taken to be a well-stirred tank for complete mixing in which microorganisms start reacting with organic pollutants in the

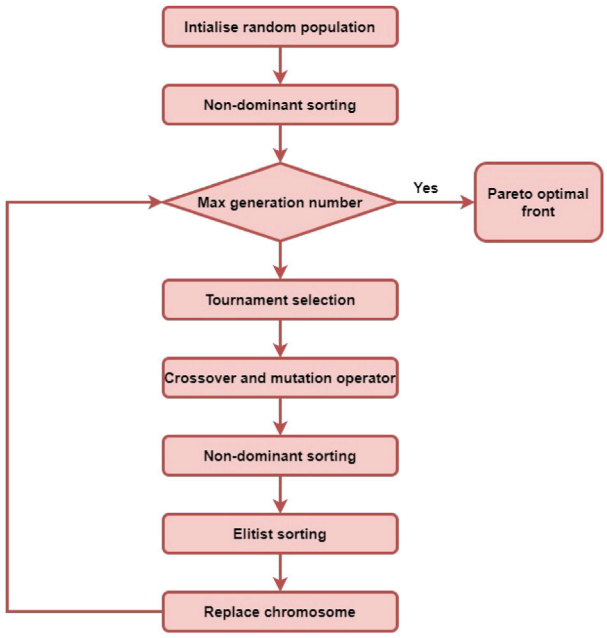

FIGURE 2
Flow chart of NSGA-II.

TABLE 2 Parameters of NSGA-II.

Point	Process loop	K_C	K_i
K1	LOOP 1	0.4833	0.9666
	LOOP 2	120.8256	241.6513
K2	LOOP 1	0.2534	0.5068
	LOOP 2	63.3575	126.7151
K3	LOOP 1	0.0796	0.1593
	LOOP 2	19.9158	39.8316

wastewater. Six major groups of microorganisms, namely, bacteria, protozoa, metazoa, filamentous bacteria, algae, and fungi, are generally found in the aeration basin of the ASP. Microorganisms take the organic pollutants as food material and start growing; they collide to form sludge. Then, the suspended microorganisms are given to the settling tank (gravitational settling tank). In order to maintain the microorganism level in the tank, a part of the concentrated biomass is recycled back to the bioreactor, and the remaining material is removed from the settling tank. This study assumes that there is no microorganism growth in the settling tank.

2.2 Modeling of ASP

Modeling and control of an ASP is more complex due to biological reactions and variations in the influent characteristics. The ASM1 model is developed from the real-time ASP under the following assumptions: i) complete mixing takes place in the aeration tank, ii) the substrate concentration of influent wastewater is constant, iii) all reactions take place only in the aeration basin, and iv) no reaction takes place in the settling tank. Hence, the concentration of substrate in the aerobic bioreactor is the same as the concentration of substrate in the settling tank. Hodasz et al. (2016) reported the dynamic model of the ASP, which is given in Eqs 1–5.

Mass balance equation of biomass in aeration tank:

$$\frac{dX(t)}{dt} = \mu(t) - D(t)(1 + r(t))X(t) + r(t)D(t)X_r(t) - bX(t). \tag{1}$$

Mass balance equation of substrate present in aeration tank:

$$\frac{dS(t)}{dt} = -\frac{\mu(t)}{Y}X(t) - D(t)(1 + r(t)S(t) + D(t)S_{in}(t). \tag{2}$$

Mass balance equation of dissolved oxygen concentration:

$$\frac{dDO(t)}{dt} = -K_0\frac{\mu(t)}{Y}X(t) - D(t)(1 + r(t))DO(t) + D(t)DO_i + \alpha W(t)[DO_{max} - DO(t)]. \tag{3}$$

Mass balance equation in the activated sludge in the settling tank:

$$\frac{dX_r(t)}{dt} = D(t)(1 + r(t))X(t) - D(t)(\beta + r(t))X_r(t). \tag{4}$$

Biomass growth rate in aeration tank:

$$\mu = \mu_{max}\frac{S(t)}{K_s + S(t)}\ \frac{DO(t)}{K_{DO} + DO(t)}, \tag{5}$$

where $X(t), S(t), DO(t), X_r(t)$ are the state variables. In the ASP, the dilution rate (D) and the air flow rate $W(t)$ are taken as manipulated variables to control the substrate (S) and dissolved oxygen (DO), and the biomass production factor (Y) is taken to be the disturbance variable.

The transfer function plays a pivotal role in wastewater treatment plant and significantly impacts its performance. It represents the relationship between input variables, such as influent characteristics or control actions, and the corresponding output variables, usually effluent quality or process variables. Understanding the transfer function allows process engineers and operators to gain insight into the dynamic behavior of the WWTP and its response to changes in influent conditions or operational parameters. With this knowledge, they can design effective control strategies, optimize process conditions, and enhance treatment efficiency. Additionally, transfer functions are vital for process modeling and simulation, aiding in predicting system behavior under different scenarios and facilitating process optimization. They also play a crucial role in control system design and performance evaluation, enabling the WWTP to achieve stable operation, comply with regulatory standards, and consistently deliver high-quality effluent while minimizing environmental impact.

The transfer function model for MIMO is developed by linearizing the dynamic equations given in Eq. 1–4 around the steady-state operating points tabulated in Table 1 (Hodasz et al., 2016). The transfer function model is presented in Eq. 6:

$$[S(s); DO(s)] = [G_{11}\ G_{12};\ G_{21}\ G_{22}][D(s); W(s)], \tag{6}$$

where

$$G_{11}(s) = \frac{S(s)}{D(s)} = \frac{688.8s^3 + 4261s^2 + 680.9s + 0.4246}{s^4 + 7.651s^3 + 7.277s^2 + 1.136s + 0.01056},$$

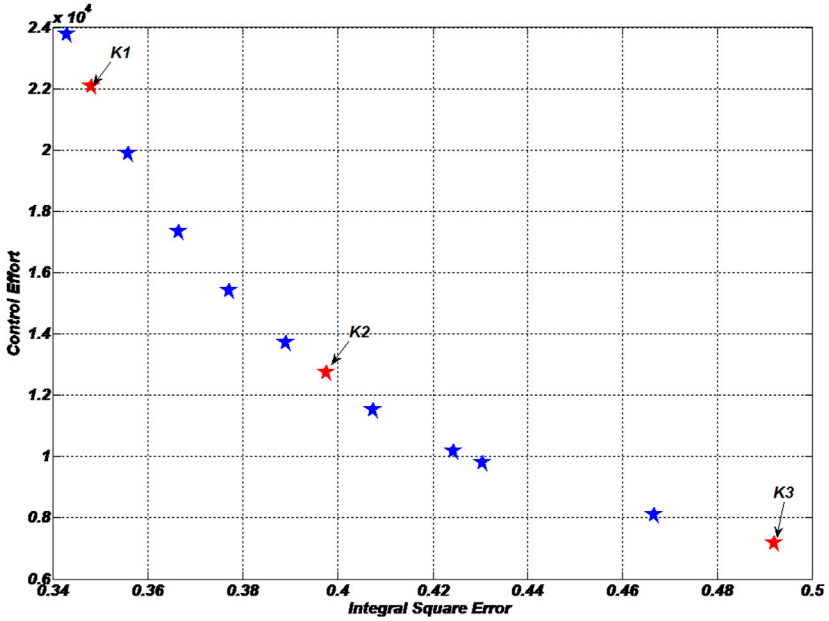

FIGURE 3
Pareto optimal front of NSGA-II.

TABLE 3 Controller parameters for the selected three points.

Point	Process loop	K_C	K_i
K1	LOOP 1	0.4833	0.9666
	LOOP 2	120.8256	241.6513
K2	LOOP 1	0.2534	0.5068
	LOOP 2	63.3575	126.7151
K3	LOOP 1	0.0796	0.1593
	LOOP 2	19.9158	39.8316

$$G_{12}(s) = \frac{S(s)}{W(s)} = \frac{-0.01268s^2 - 0.002405s - 2.457\times10^{-5}}{s^4 + 7.651s^3 + 7.277s^2 + 1.136s + 0.01056},$$

$$G_{21}(s) = \frac{DO(s)}{D(s)} = \frac{-11.1s^3 - 278.7s^2 - 52.54s - 0.5329}{s^4 + 7.651s^3 + 7.277s^2 + 1.136s + 0.01056},$$

$$G_{22}(s) = \frac{DO(s)}{W(s)} = \frac{-0.06151s^3 + 0.06734s^2 + 0.01078s + 0.0001004}{s^4 + 7.651s^3 + 7.277s^2 + 1.136s + 0.01056}.$$

The aforementioned transfer function model is used for RGA analysis to identify a suitable control scheme for the ASP in the subsequent section.

3 Identification of control strategy and multi-objective control problem formulation

In this section, RGA analysis is applied to the WWTP transfer function model, and the multi-objective control problem formulation is discussed.

3.1 RGA analysis

RGA is used to determine the best input (u)–output (y) pairing for multivariable systems. It quantifies the change in steady-state gain between an input–output pair that occurs when other control loops are closed. It provides a measure of steady-state interactions from gain. The relative gain between input j and output i is given by Eq. 7:

$$\lambda_{ij} = \frac{\left(\partial y_i / \partial u_j\right)_u}{\left(\partial y_i / \partial u_j\right)_y}, \tag{7}$$

where $(\partial y_i/\partial u_j)_u$ is the open-loop gain with all other control loops open, and $(\partial y_i/\partial u_j)_y$ is the closed-loop gain with all other control loops closed.

The ASP is a 2 × 2 system; its RGA structure is presented in Eq. 8:

$$\wedge = [\lambda_{11}\,\lambda_{12};\,\lambda_{21}\,\lambda_{22}] = \left[\frac{1}{1-\frac{K_{12}K_{21}}{K_{22}K_{11}}}\;\frac{1}{1-\frac{K_{11}K_{22}}{K_{12}K_{21}}};\frac{1}{1-\frac{K_{11}K_{22}}{K_{12}K_{21}}}\;\frac{1}{1-\frac{K_{12}K_{21}}{K_{22}K_{11}}}\right]. \tag{8}$$

The steady-state gain matrix of the ASP is computed from Eq. 6 given in Eq. 9:

$$[K_{11}\,K_{12}\,;K_{21}\,K_{22}] = [40.20833 - 0.00232670; -50.4640\;0.0095075]. \tag{9}$$

Using the gain matrix given in Eq. 9, the RGA matrix is developed using Eq. 10:

$$[\lambda_{11}\,\lambda_{12}\,;\lambda_{21}\,\lambda_{22}] = [1.443293 - 0.443293\,;-0.443293\;1.443293]. \tag{10}$$

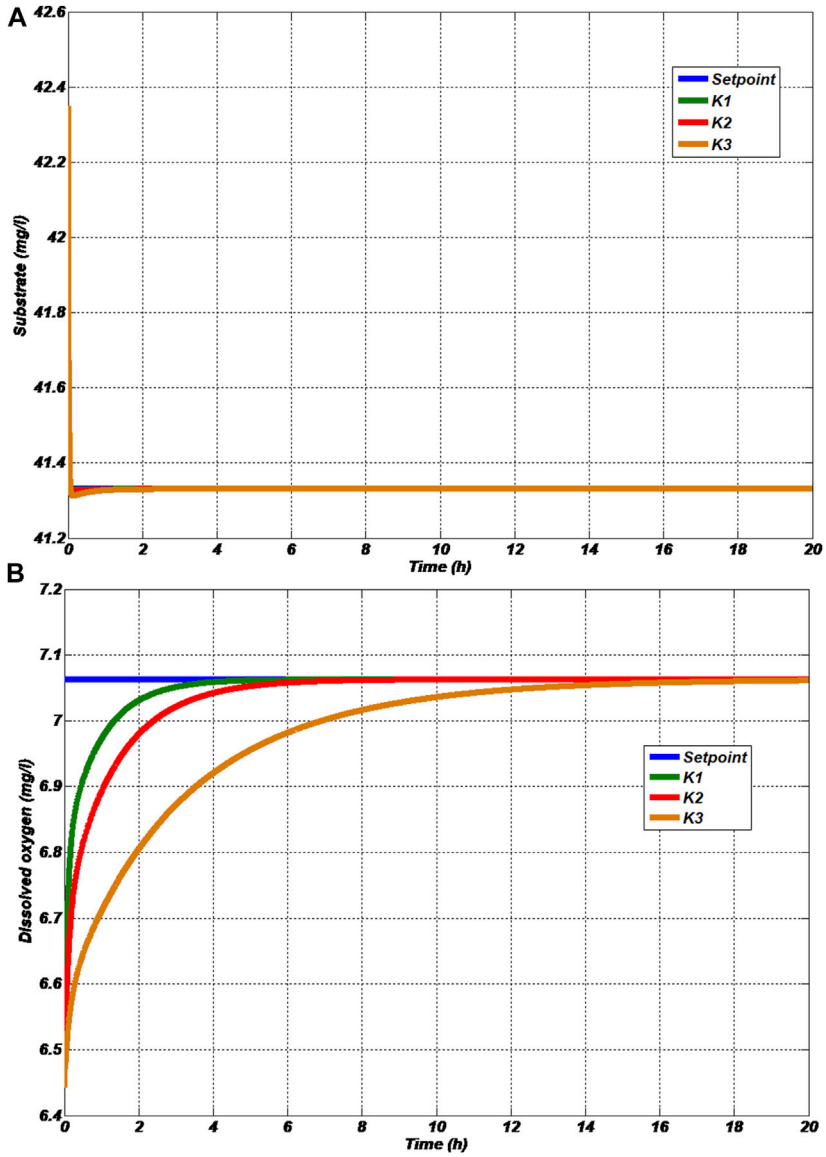

FIGURE 4
Servo response of Activated Sludge Process **(A)** Substrate **(B)** Dissolved oxygen.

From the obtained RGA matrix, it is recommended that u_1 be paired with y_1 and u_2 be paired with y_2. The obtained RGA matrix shows that there is a minimum interaction between the process loops. Hence, a decentralized control scheme is preferred for an ASP. Muntean et al. (2015) also carried out RGA analysis for the WWTP process with recycled sludge flow to influent flow and aeration rate from the bioreactor as manipulated variables and used the substrate and dissolved oxygen as controlled variables and reported that a decentralized control scheme is more suitable for the WWTP process with the identified model due to fewer interactions between the loops.

3.2 Decentralized PI controller

As stated earlier, the interaction between inputs and outputs is weak; hence, a decentralized control architecture with a PI controller is proposed. The decentralized control is given in Eq. 11:

$$G_c(s) = \begin{bmatrix} G_{c11}(s) & 0 \\ 0 & G_{c22}(s) \end{bmatrix}, \tag{11}$$

where $G_{c11}(s) = K_{c1} + \frac{K_{i1}}{s}$ and

$$G_{c22}(s) = K_{c2} + \frac{K_{i2}}{s}.$$

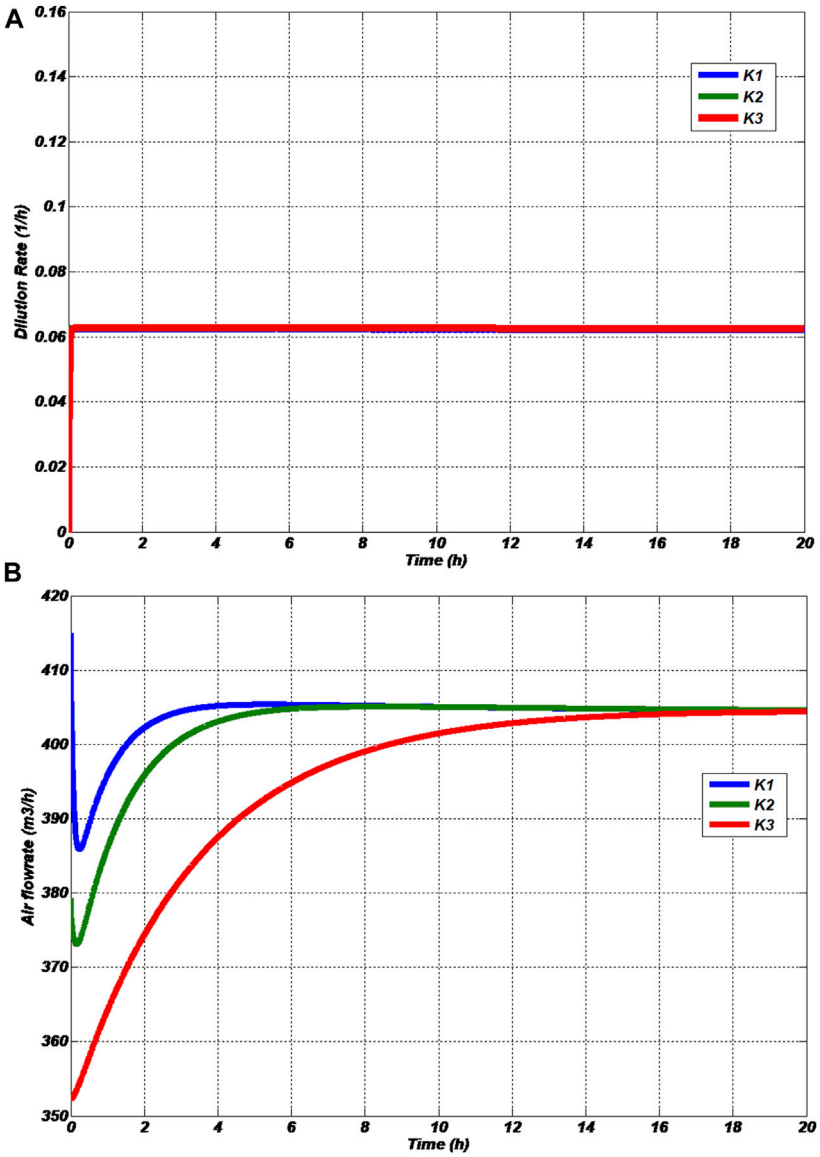

FIGURE 5
Variations in manipulated variables under servo operation **(A)** Dilution rate **(B)** Airflow rate.

TABLE 4 Performance measures of MODC.

Point	Servo		Regulatory	
	Operation		Operation	
	ISE	CE	ISE	CE
K1	0.0715	1.978×10^{6}	0.0878	1.19×10^{6}
K2	0.0817	9.947×10^{5}	0.1026	5.979×10^{5}
K3	0.09451	2.558×10^{5}	0.1152	1.56×10^{5}

To tune the PI controller parameters, a multi-objective control problem is formulated in the next subsection.

3.3 Multi-objective problem formulation (MOO)

The multi-objective control problem is formulated by identifying the PI control structure to improve the quality of effluent by minimizing the integral square error (ISE) and reducing production costs by minimizing control effort (CE). The

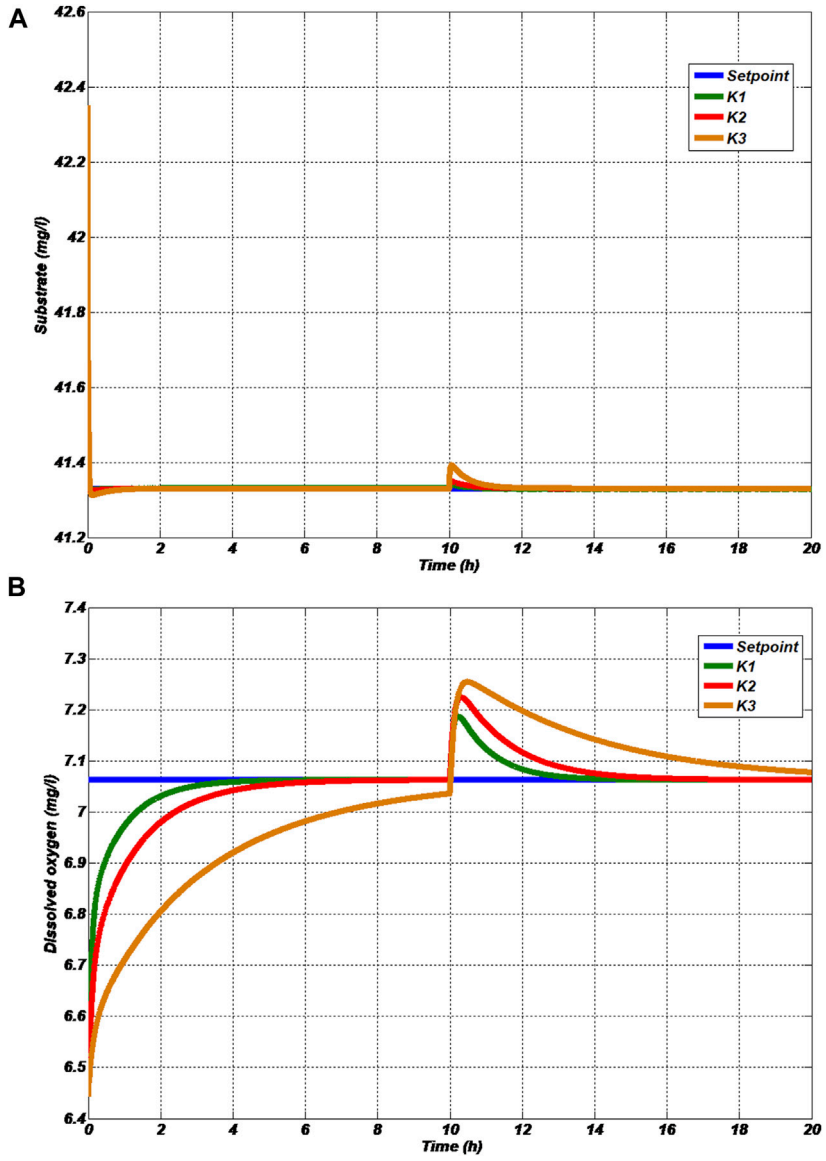

FIGURE 6
Regulatory response of activated sludge process **(A)** Substrate **(B)** Dissolved oxygen.

conflicting objective functions of the multi-objective control problem are given in Equations (12) and (13):

$$\min f_1(ISE) = \int_0^\infty (\alpha_1 {e_1}^2 + \alpha_2 {e_2}^2)\, dt = f(K_{C1}, K_{i1}, K_{C2}, K_{i2}, \alpha_1, \beta_1, \alpha_2, \beta_2), \quad (12)$$

$$\min f_2(CE) = \int_0^\infty (\beta_1 {c_1}^2 + \beta_2 {c_2}^2)\, dt = f(K_{C1}, K_{i1}, K_{C2}, K_{i2}, \alpha_1, \beta_1, \alpha_2, \beta_2). \quad (13)$$

The aforementioned two objective functions are optimized using eight decision variables. K_{C1} and K_{i1} are proportional gain and integral gain of the substrate (loop 1), respectively.K_{C2} and K_{i2} are proportional gain and integral gain of dissolved oxygen (loop 2), respectively.α_1 and α_2 are weighting factors for loop 1 and loop 2, respectively.β_1 and β_2 are weighting factors for loop 1 and loop 2, respectively.e_1 and e_2 are errors in loop 1 and loop 2, respectively.c_1 and c_2 are control efforts of loop 1 and loop 2, respectively.

4 Design of a multi-objective decentralized controller

Multi-objective optimization involves more than one objective function, and the functions must be optimized simultaneously. The multi-objective control problem is commonly solved by evolutionary algorithms (EAs). The primary reason for using EAs is their ability to find multiple Pareto-optimal solutions in one single simulation run. Deb

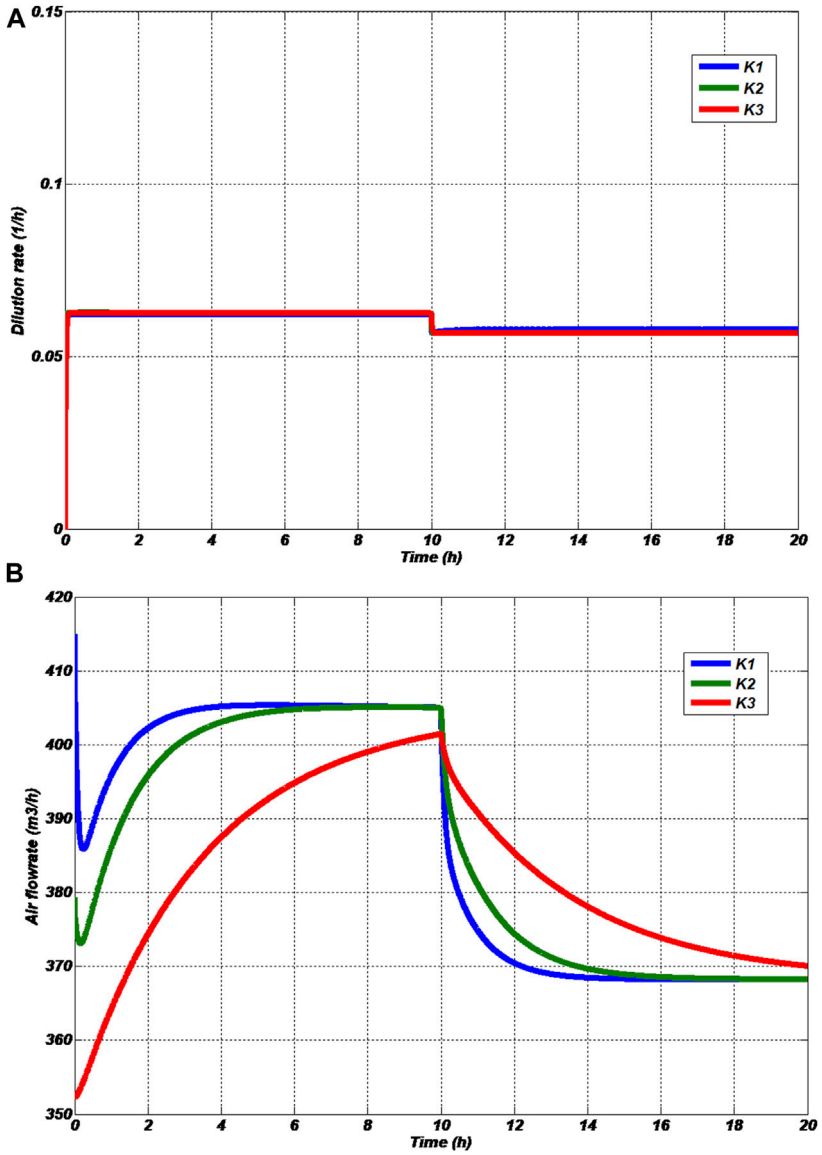

FIGURE 7
Variations in manipulated variables under regulatory operation **(A)** Dilution rate **(B)** Airflow rate.

et al. (2002) reported the performance comparisons of various multi-objective evolutionary algorithms (MOEAs) such as a niched Pareto genetic algorithm (NPGA), a Pareto-archived evolution strategy (PAES), a strength Pareto evolutionary algorithm (SPEA) and a non-dominant sort genetic algorithm-II (NSGA-II) for different test problems. Most EAs have been successfully applied for design optimization and controller optimization over the past two decades. However, NSGA-II outperforms other EAs for most multi-objective problems. It can provide a better spread of solutions and better convergence near the true Pareto-optimal front. In this paper, NSGA-II is selected to solve the multi-objective control problem of ASP.

4.1 Non-dominant sort genetic algorithm-II

Deb et al. (2002) proposed NSGA-II, which alleviates the difficulty of NSGA. The important features of NSGA-II are as follows:

- NSGA-II is based upon a GA.
- It is an extended version of NSGA.
- It overcomes the difficulties faced in NSGA, which are complexity, lack of elitism, and choosing the optimal parameter for the sharing parameter.
- The main aim of NSGA-II is to preserve elitism and diversity.
- NSGA-II gives a Pareto-optimal front, which consists of a set of optimal solutions for conflicting objective functions.

The algorithm and detailed implementation procedure of NSGA-II are found in Kalyanmoy Deb (2002). The flowchart of NSGA-II is shown in Figure 2.

4.2 Implementation of NSGA-II

The parameters of NSGA-II used for execution are given in Table 2. The Pareto-optimal front provides the optimal solutions for the conflicting objective functions, and it is shown in Figure 3.

To study the trade-off between the performance and cost of production, three controller parameters at points K1, K2, and K3 are selected from the Pareto-optimal front and are tabulated in Table 3.

5 Closed-loop simulation studies of ASP

5.1 Servo response

The ASP is simulated using the set of differential equations given in the modeling section. Then, the closed-loop servo responses are obtained for the selected controllers and qualitatively compared in Figure 4, and associated manipulated variables are shown in Figure 5. For quantitative comparison, the performance measures are given in Table 4.

The servo responses with controller gains at the K_1 point do not provide significant variation in the substrate concentration. However, the responses show the variation in the dissolved oxygen concentration in the effluent. From Figures 4B,5B, it is observed that the process with controller gains at the K_1 point takes less retention time and settles very quickly at the steady-state value due to large CE (refer Table 4). It is observed from Table 4 that controller gains at the K_1 point give a much smaller integral square error. Hence, in order to improve the performance, the closed-loop system must compromise on CE.

The process with controller gains at the K_2 point gives the trade-off between the performance and CE (refer Table 4). The retention time of the process with controller gains at the K_2 point shown in Figures 4B, 5B is larger than the controller gains at the K_1 point; meanwhile, it takes a smaller CE than a process with controller gains at the K_1 point.

The closed-loop servo response with controller gains at K_3 shown in Figures 4B, 5B exhibited a longer retention time than other controllers. The controller gains at the K_3 point have less CE (refer Table 4). At the same time, it should compromise on the performance of the system.

5.2 Regulatory response

To study the regulatory operation of the ASP, biomass production factor (Y) is selected as a disturbance and is changed from 0.54 to 0.594 at the tenth hour. The simulated regulatory responses of loop 1 and loop 2 are shown in Figure 6, and the corresponding manipulated variables are shown in Figure 7. The quantitative comparison of the regulatory operation with various controllers is tabulated in Table 4.

It is found from Figures 6A, B that the effect of disturbance on substrate concentration and dilution rate is less than the effect on dissolved oxygen concentration and air flow rate. In quantitative comparison, it is noted that the CE required for regulatory operation is less than the CE required by the servo operation. However, the ISEs provided by the regulatory operation are larger than those of the servo operation. Hence, minimization of CE will affect the performance of the process. Meanwhile, minimization of CE reduces the production cost of freshwater.

The circular economy in wastewater treatment leads to freshwater, nutrient, and energy recovery from wastewater. Improvement in effluent water quality leads to the reuse of water for domestic applications, which will reduce water stress. Furthermore, nutrients recovered from active sludge can be used as fertilizers. Energy recovery can also be done by producing biogas from active sludge.

6 Conclusion

In this work, a novel circular economy-based MODC design is proposed for the MIMO ASP. The transfer function model is developed from nonlinear differential equations to select an appropriate control scheme to control dissolved oxygen concentration and substrate concentration in the effluent of the ASP. Then, RGA analysis is performed to determine the interactions between the loops. From the interaction analysis, it is concluded that a decentralized controller is the best control scheme for the ASP due to less interaction between the loops. A multi-objective control problem is formulated to improve effluent quality and reduce costs. The multi-objective control problem is successfully solved by the MOEA NSGA-II. Some of the conventional wastewater treatment techniques are simple and have low production costs; however, they require a long treatment time and result in poor effluent quality. Whereas sophisticated treatment techniques are more expensive due to high production costs but can provide good-quality effluent. The advantage of the proposed multi-objective controller is that it can provide a number of optimal solutions in the Pareto-optimal front. The users can select their own solutions according to the applications from the Pareto-optimal front. The feasibility of the proposed controller is demonstrated by selecting three controller parameters from the Pareto-optimal front, and their closed-loop servo and regulatory performances are compared qualitatively as well as quantitatively. The proposed circular economy-based multi-objective controller will be very useful for the reuse of wastewater, nutrients, and energy.

Data availability statement

The original contributions presented in the study are included in the article/Supplementary material; further inquiries can be directed to the corresponding author.

Author contributions

SS: writing—original draft, conceptualization, methodology, and software. CM: writing—review, editing, conceptualization, methodology, and software. PN: writing and conceptualization. All authors contributed to the article and approved the submitted version.

Acknowledgments

The authors gratefully acknowledge the Department of Instrumentation, Madras Institute of Technology, for their support with conducting the experiments.

Conflict of interest

The authors declare that the research was conducted in the absence of any commercial or financial relationships that could be construed as a potential conflict of interest.

Publisher's note

All claims expressed in this article are solely those of the authors and do not necessarily represent those of their affiliated organizations, or those of the publisher, the editors, and the reviewers. Any product that may be evaluated in this article, or claim that may be made by its manufacturer, is not guaranteed or endorsed by the publisher.

References

Castro-Amoedo, R., Morisod, N., Granacher, J., and Maréchal, F. (2021). The role of biowaste: A multi-objective optimization platform for combined heat, power and fuel. *Front. Energy Res.* 9, 718310. doi:10.3389/fenrg.2021.718310

Chen, W., Yao, C., and Lu, X. (2014). Optimal design activated sludge process by means of multi-objective optimization: case study in benchmark simulation model 1 (BSM1). *Water Sci. Technol.* 69 (10), 2052–2058. doi:10.2166/wst.2014.119

de Araujo, A. C., Gallani, S., Mulas, M., and Skogestad, S. (2013). Sensitivity analysis of optimal operation of an activated sludge process model for economic controlled variable selection. *Industrial Eng. Chem. Res.* 52 (29), 9908–9921. doi:10.1021/ie4006673

Deb, K., Pratap, A., Agarwal, S., and Meyarivan, T. A. M. T. (2002). A fast and elitist multiobjective genetic algorithm: NSGA-II. *IEEE Trans. Evol. Comput.* 6 (2), 182–197. doi:10.1109/4235.996017

Ghimire, U., Sarpong, G., and Gude, V. G. (2021). Transitioning wastewater treatment plants toward circular economy and energy sustainability. *ACS omega* 6 (18), 11794–11803. doi:10.1021/acsomega.0c05827

Grobelak, A., Grosser, A., Kacprzak, M., and Kamizela, T. (2019). Sewage sludge processing and management in small and medium-sized municipal wastewater treatment plant-new technical solution. *J. Environ. Manag.* 234, 90–96. doi:10.1016/j.jenvman.2018.12.111

Hodasz, N. I., Brădilă, V. I., Nascu, I., and Lendek, Z. "Modeling and parameter estimation for an activated sludge wastewater treatment process," in Proceedings of the 2016 IEEE International Conference on Automation, Quality and Testing, Robotics (AQTR), Cluj-Napoca, Romania, 2016, May, 1–6.

Holenda, B., Domokos, E., Rédey, A., and Fazakas, J. (2007). Aeration optimization of a wastewater treatment plant using genetic algorithm. *Optim. control Appl. methods* 28 (3), 191–208. doi:10.1002/oca.796

Holenda, B., Domokos, E., Redey, A., and Fazakas, J. (2008). Dissolved oxygen control of the activated sludge wastewater treatment process using model predictive control. *Comput. Chem. Eng.* 32 (6), 1270–1278. doi:10.1016/j.compchemeng.2007.06.008

Hu, H., Xu, L., Goodman, E. D., and Zeng, S. (2014). NSGA-II-based nonlinear PID controller tuning of greenhouse climate for reducing costs and improving performances. *Neural Comput. Appl.* 24, 927–936. doi:10.1007/s00521-012-1312-8

Kaur, N. (2023). "Modeling and multi-objective optimization of wastewater treatment process,". Doctoral dissertation (Canada: The University of Western Ontario).

Malaysia, M. (2011). Control strategies of wastewater treatment plants. *Aust. J. Basic Appl. Sci.* 5 (8), 446–455.

Muntean, I., Both, R., Crisan, R., and Nascu, I. "RGA analysis and decentralized control for a wastewater treatment plant," in Proceedings of the 2015 IEEE International Conference on Industrial Technology (ICIT), Seville, Spain, March 2015.

Neczaj, E., and Grosser, A. (2018). Circular economy in wastewater treatment plant–challenges and barriers. *Proceedings* 2 (11), 614. doi:10.3390/proceedings2110614

Negi, P., Verma, H., Singh, S. P., Mahapatra, B. S., and Jatav, H. S. (2022). "Global scenario of sewage-sludge management," in *Sustainable management and utilization of sewage sludge* (Berlin, Germany: Springer), 383–401.

Nor'Azlan, N. A., Selamat, N. A., and Yahya, N. M. (2018). Multivariable PID controller design tuning using bat algorithm for activated sludge process IOP Conference Series: materials science and engineering. *IOP Conf. Ser. Mater. Sci. Eng.* 342 (1), 012030. doi:10.1088/1757-899x/342/1/012030

Qiao, J., and Zhang, W. (2018). Dynamic multi-objective optimization control for wastewater treatment process. *Neural Comput. Appl.* 29, 1261–1271. doi:10.1007/s00521-016-2642-8

Reynoso-Meza, G., and Carreño-Alvarado, E. P. (2019). November). PI tuning of a multivariable activated sludge process with nitrification and denitrification with multi-objective optimization. *Proceedings* 48 (1), 4. doi:10.3390/ECWS-4-06434

Samuelsson, P., Halvarsson, B., and Carlsson, B. (2005). Interaction analysis and control structure selection in a wastewater treatment plant model. *IEEE Trans. Control Syst. Technol.* 13 (6), 955–964. doi:10.1109/tcst.2005.854322

Spreafico, C. (2022). An analysis of design strategies for circular economy through life cycle assessment. *Environ. Monit. Assess.* 194 (3), 180. doi:10.1007/s10661-022-09803-1

Sweetapple, C., Fu, G., and Butler, D. (2014). Multi-objective optimisation of wastewater treatment plant control to reduce greenhouse gas emissions. *Water Res.* 55, 52–62. doi:10.1016/j.watres.2014.02.018

Tian, F., Yang, C., Zhang, E., Sun, D., Shi, W., and Chen, Y. (2023). A study on the multi-objective optimization method and characteristic analysis of installation locations of submersible mixer for sewage. *Front. Energy Res.* 11, 1180607. doi:10.3389/fenrg.2023.1180607

Vilanova, R., and Alfaro, V. "Multi-loop PI-based control strategies for the activated sludge process," in Proceedings of the 2009 IEEE Conference on Emerging Technologies & Factory Automation, Palma de Mallorca, Spain, 2009, September, 1–8.

Vinayak, J. R., and Narayanan, S. "Nonlinear PI with state feedback control for activated sludge process," in Proceedings of the 2017 International Conference on Information, Communication, Instrumentation and Control (ICICIC), Indore, India, 2017, August, 1–7.

Zhang, X., and Liu, Y. (2022). Circular economy is game-changing municipal wastewater treatment technology towards energy and carbon neutrality. *Chem. Eng. J.* 429, 132114. doi:10.1016/j.cej.2021.132114

Frontiers in
Chemical Engineering

Explores all scales of chemical engineering in theory, computation and practice

A multidisciplinary journal that explores the opportunities for chemical engineering to address some of the key challenges we face - energy, health, food, manufacturing and the environment.

Discover the latest Research Topics

See more →

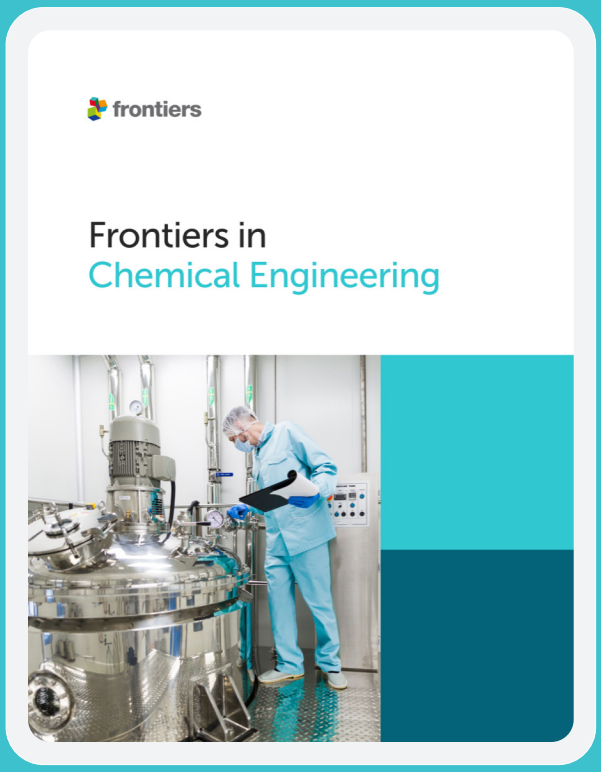

Frontiers

Avenue du Tribunal-Fédéral 34
1005 Lausanne, Switzerland
frontiersin.org

Contact us

+41 (0)21 510 17 00
frontiersin.org/about/contact